AD NUMBER
AD865949
LIMITATION CHANGES

TO:

Approved for public release; distribution is unlimited. Document partially illegible.

FROM:

Distribution authorized to U.S. Gov't. agencies and their contractors; Critical Technology; JAN 1970. Other requests shall be referred to Air Force Rome Air Development Center, EMCRC, Griffiss AFB, NY 13440. Document partially illegible. This document contains export-controlled technical data.

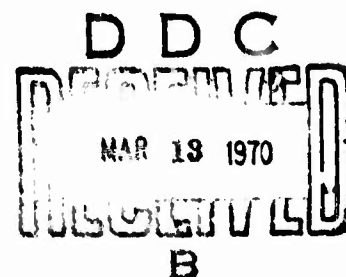| AUTHORITY |
|---|
| radc, usaf ltr, 27 aug 1973 |

AD 865949

RADC-TR-69-424, Volume II
Final Technical Report
January 1970

INTEGRATED FUNCTION (CNI) WAVEFORM STUDY

Magnavox Research Laboratories
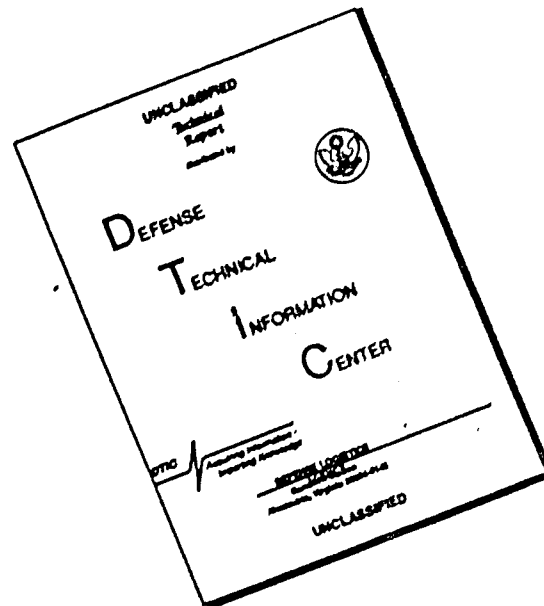
D D C

MAR 13 1970

B

Rome Air Development Center
Air Force Systems Command
Griffiss Air Force Base, New York

DISCLAIMER NOTICE

THIS DOCUMENT IS BEST QUALITY AVAILABLE. THE COPY FURNISHED TO DTIC CONTAINED A SIGNIFICANT NUMBER OF PAGES WHICH DO NOT REPRODUCE LEGIBLY.

When US Government drawings, specifications, or other data are used for any purpose other than a definitely related government procurement operation, the government thereby incurs no responsibility nor any obligation whatsoever, and the fact that the government may have formulated, furnished, or in any way supplied the said drawings, specifications, or other data is not to be regarded, by implication or otherwise, as in any manner licensing the holder or any other person or corporation, or conveying any rights or permission to manufacture, use, or sell any patented invention that may in any way be related thereto.

Do not return this copy. Retain or destroy.

ABSTRACT

This Final Report, presented in three volumes, describes a comparison of candidate spread spectrum waveforms and the selection of a preferred waveform to perform integrated communication, navigation, and identification (CNI) functions. Satellites are presumed available in appropriate orbits for global communication and navigation. A coordinated frequency/hop/pseudonoise/time hop (FH/PN/TH) waveform is made considering such factors as efficient use of satellite ERP in the remote mode, multiple access of wide dynamic range signals in the direct mode, range and range rate measurement accuracy, initial synchronization, and equipment complexity for full capacity implementation in a nominal 100 MHz bandwidth.

Since CNI system requirements are not presently known, the waveform choice has been made considering a postulated worst case environment based on future air traffic control requirements.

Implementation of the preferred CNI waveform will depend on certain technology developments particularly in the areas of wide dynamic range receivers, phase coherent frequency hopping, high peak power pulse transmitters, and LSI digital devices. However, a demonstration concept can be advanced within the present state-of-the-art to illustrate the preferred waveform with scaled parameters.

Volume I covers the concept formulation studies leading to the preferred waveform and demonstration concept while Volume II summarizes the detailed performance and operational analysis. Volume III presents navigation considerations for the enroute case.

INTEGRATED FUNCTION (CNI) WAVEFORM STUDY

Charles R. Cahn
Stanley E. Kosowski
Magnavox Research Laboratories

FOREWORD

This Final Report was submitted by Magnavox Research Laboratories, 2829 Maricopa Street, Torrence, California, under Contract F30602-69-C-0186, Project 4519, Task 451911, with Rome Air Development Center, Griffiss Air Force Base, New York. Contractor's report number is R-1959. Dean Baerwald, EMCRR, was the RADC Project Engineer for the effort.

To facilitate the dissemination of unclassified information, subsections 7.7.1.1 and 7.7.1.2 of Section 7.7 were removed from Volume II and printed as a separate Volume III. Volume III, Confidential, contains the only classified material in this document.

Distribution of the report is restricted under the provisions of the U.S. Mutual Security Acts of 1949.

This technical report has been reviewed and is approved.

Approved:

DEAN L. BAERWALD
Project Engineer

Approved;

RICHARD M. COSEL, Colonel, USAF
Chief, Communications & Navigation Division

FOR THE COMMANDER,

IRVING J. GABELMAN
Chief, Plans Office

ii

SECTION VII
PERFORMANCE ANALYSIS AND SIMULATION

This section in Volume II of the Final Report for Integrated Function (CNI) Waveform Study presents the performance analyses conducted in support of the concept formulation and comparison of candidate waveforms described in Volume I. The studies cover channel modeling and detailed performance tradeoff evaluations of various techniques that were considered during the program.

For a user terminal involving an essentially omnidirectional antenna, multipath becomes a particularly important problem area. The multipath modeling employed for the study is, accordingly discussed first.

7.1 MULTIPATH MODELING

Significant evidence indicates substantial multipath can exist for satellite-to-aircraft links as well as links with similar geometry, such as aircraft-to-aircraft and satellite-to-satellite. Under a recent study conducted by NASA[*], satellite-to-satellite multipath intensity was evaluated and found to be significant (approaching desired signal level) when a user satellite was at altitudes between 100 and 1000 miles above the earth and was attempting to relay information through a synchronous satellite. It is contemplated that satellite-to-satellite multipath measurements will be made in the near future, in support of this Data Relay Satellite System Program.

Substantial multipath has been measured by K. L. Jordan[**] of Lincoln Laboratory, in support of the TACSAT Program. These measurements were conducted at 250 MHz and showed significant multipath for the satellite-to-aircraft link, wherein the aircraft was a C135 flying in altitudes in excess of 25,000 feet. Using correlation techniques, Jordan was able to measure the intensity of the reflected signal off the earth as well as the direct path signal level and such statistical parameters as the fading bandwidth of the received signal. His measurements have indicated that when

---

[*] Wachsman and Ghais, "Multipath and RFI Characteristics of a Data Relay Satellite System," ITC/USA/'69, September 1969.

[**] K. L. Jordan, "Measurement of Multipath Effects in a Satellite-Aircraft UHF Link, pp. 1117-1118, Proc. IEEE, June 1967.

the reflecting surface is a calm sea, specular reflection will occur at angles below 10 degrees (at 230 MHz) and that the reflection will be primarily diffuse when the grazing angle is in excess of 20 degrees. Furthermore, the intensity of the reflected energy can be equal to, or in some instances greater than, that associated with the direct path, depending upon the variations in the receiver antenna pattern. Receiver antenna patterns have variations of up to 6 db when observed in various planes of polarization; thus, while theory would indicate that the multipath should be equal to or less than the direct signal, such anomalous antenna behavior can cause the reflected signal to appear larger than the indirect signal.

Multipath is of concern to such agencies as the FAA because of its deleterious effects on the conventional traffic control beacon (ATC) system. Measurements conducted by Joseph Hermann, * in the late 50's, at the Indianapolis Airport, indicated that in such an environment multipath between aircraft and conventional air traffic control ground stations, as well as between aircraft, can be quite significant, normally on the order of 6 db below the direct signal path, but in some instances can be equal to the direct signal path strength. To combat the effects of multipath, the FAA initiated studies into broadband coding techniques, such as truncated Reed-Solomon coding, to provide signal immunity in the presence of multipath.

This discussion describing the existence of multipath on various types of links that are similar to those in a CNI system, serves to point out the fact that multipath can in fact exist and that it can be a significant factor in the determination of the final performance of any CNI system. If full coverage service is to be provided by a CNI waveform, then this waveform must combat its own multipath during the entire mission.

7.1.1 MULTIPATH MODEL FOR CNI TRANSMISSION CHANNEL

Prior to any in-depth analysis to determine the effects of multipath on various types of candidate waveform, it is advisable to determine the nature of the transmission channel associated with the user-to-satellite link. What follows is a description of this channel in terms of its statistical time varying parameters. The transmission link between any ground station with a directive antenna and a satellite is rather conventional and for that reason need not be treated.

---

* Private communication.

Shown in Figure 7-1 is the transmission link between a potential user and the satellite. The channel consists of a direct path and a potential indirect path resulting from reflection of the satellite signal from the earth and received by the user. This link is symmetrical and the same multipath situation arises when the user is transmitting to a satellite. The user antenna is assumed to be almost omnidirectional, possessing antenna pattern irregularities on the order of ± 5 decibels with respect to omnidirectional characteristics. The antenna on board an aircraft will also vary in performance depending upon aircraft shadowing, etc. Thus, we can expect varying degrees of multipath energy as seen by an aircraft depending upon the aircraft's attitude relative to the earth and a particular member of the satellite system.

The direct path is characterized by a signal that is nonfading. This is only approximately true since atmospheric effects and antenna irregularities will cause the direct path to fade to some extent. For the purpose of this analysis, however, we will not consider the direct path as a fading channel. The direct path does, however, have associated with it Doppler, and therefore, Doppler rate variations. These are dependent upon the frequency of operation, the vector velocity, and the vector velocity rate of change between the user aircraft and a particular satellite. In addition to the direct Doppler path there is a multiplicity of indirect signals that result from energy
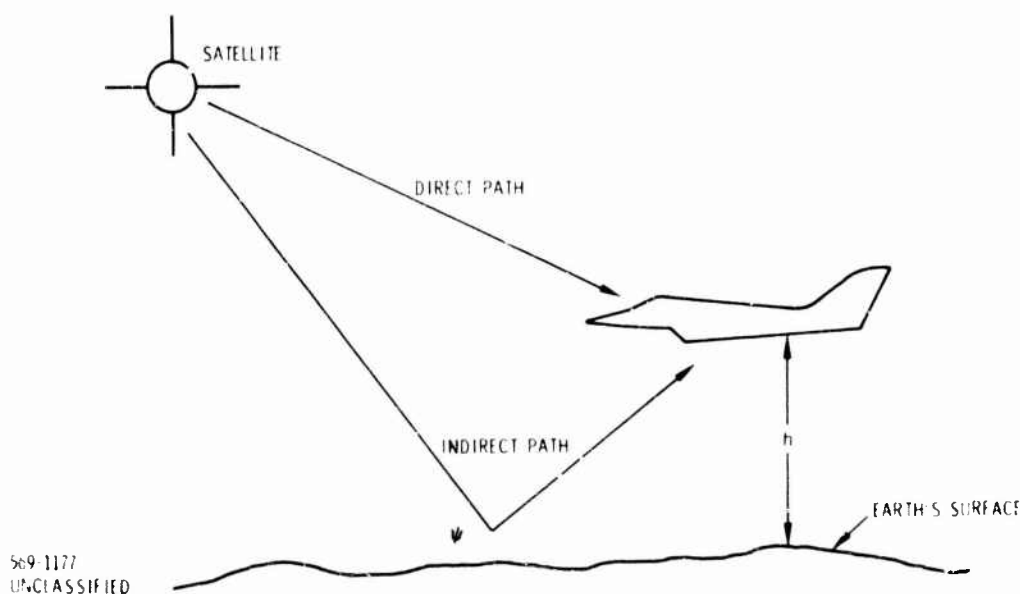

SATELLITE

DIRECT PATH

INDIRECT PATH

h

EARTH'S SURFACE

569-1177
UNCLASSIFIED

Figure 7-1. Satellite to User Link

-201-

reflected from the earth's surface and arrive at the user aircraft delayed with respect to the direct path. This indirect path is characterized by its dispersive nature; that is, a time spread in energy and a fading bandwidth is associated with the indirect path. The indirect path is also characterized by the type of reflection from the earth's surface. This reflection is bounded by the two extremes of completely diffuse scat- tering or completely specular scattering. In some instances, the indirect path is correctly synthesized by a combination of diffuse and specular paths depending upon the complex nature of the reflecting surface.

Such a complex transmission channel can be replaced by its equivalent band- pass linear filter representation as shown in Figure 7-2. The direct path is character- ized by an impulse response that is essentially time invariant with the exception of Doppler, and the indirect path can be characterized by a time varying dispersive impulse response. An electrical analog that can be used as a simulator for such a transmission channel is illustrated in Figure 7-2. The simulator consists of a number
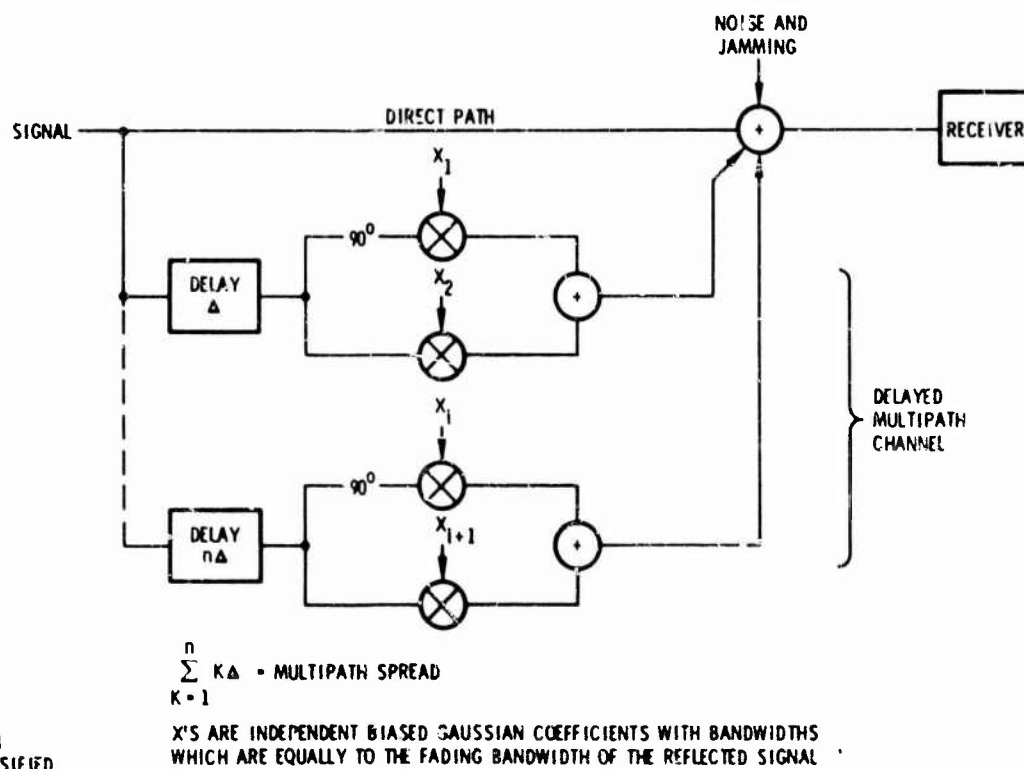
Figure 7-2. Electronic Simulator of the Multipath Channel

-202-

of fixed delays relative to the direct path and situations of complex multipliers and Doppler frequency synthesizers.

Depending upon the wavelength of operation relative to the Rayleigh criteria, the reflected path will be either specular or diffuse, or a combination of the two. Therefore, we can expect that the multiplicative coefficients associated with the respective delayed signal replicas may be either Gaussian or non-Gaussian in nature. The Rayleigh criteria, or roughness factor, Δh, is given in Equation (1) and represents a rule-of-thumb for the dividing line between specular and diffuse scattering from a surface.

$$\Delta h < \lambda/8 \sin \psi$$
$$\text{(for specular reflection)} \tag{1}$$

In general, the power associated with the indirect path will be constrained to be equal to or less than the power associated with the direct path, although in practice it is possible for the total energy in the reflected path to exceed that associated with the direct path. This is primarily true because of antenna gain irregularities as a function of angle.

In the following discussions, we will evaluate the effects of diffuse and specular multipath on the performance of PN systems. We have chosen to do this because the diffuse and specular reflection cases represent extremes and will allow us to bound the performance of the above systems under extreme multipath conditions.

The expected average time delay between the direct and indirect path for a satellite-to-aircraft link is now evaluated assuming that the satellite is in a synchronous orbit and that the aircraft is at an altitude of 100,000 feet or less.

From the geometry of the situation illustrated in Figure 7-1, we find that for grazing angles in excess of 20 degrees the difference in the path lengths between the direct and indirect path is accurately given by

$$\Delta \ell = 2h \sin \psi \tag{2}$$

where

$\quad$ h $\quad$ height of the aircraft
$\quad$ ψ $\quad$ grazing angle

Thus, the time delay becomes

$$\tau_d = \frac{2h}{c} \sin \psi \tag{3}$$

We expect that for grazing angles above 20° and for reasonable sea states or terrain roughness factors, the primary mode of reflection will be diffuse although for certain surfaces specular reflections will occur.

Given that the aircraft can be a high performance aircraft and operated at speeds up to roughly mach 3, the following equations adequately describe the fading bandwidth associated with reflected energy. This assumes that we can represent the terrain in terms of a rms fluctuation in its height and that its correlation in length along the surface of the earth can be adequately represented. It follows that the fading bandwidth is given by*

$$\left. \begin{array}{l} f_V = \sqrt{8} \ \frac{2\pi}{\lambda} \xi \sin (\psi - \pi/2) \ V_V \\[2mm] f_H = \sqrt{8} \ \frac{2\pi}{\lambda} \xi \cos (\psi - \pi/2) \ V_H \end{array} \right\} \text{Fading Bandwidth} \tag{4}$$

where

ξ = $\Delta h/L$

Δh = rms height variations

L = correlation distance along the reflecting surface

V_V = vertical velocity relative to the earth

V_H = horizontal velocity relative to the earth

For most situations, the differential Doppler and the fading bandwidth will be essentially overlapping; that is, the difference in Doppler between the direct path and the indirect path will be smaller than the total fading bandwidth for diffuse reflection and therefore the direct path and the indirect path will be overlapping in frequency spectrum for most circumstances.

.1.2 THE EFFECTS OF MULTIPATH ON ERROR PROBABILITY OF PN SYSTEMS

7.1.2.1 The Output from the PN Correlation Receiver in the Presence of Multipath

Since much of the analysis to follow, concerning the performance of PN systems, in the presence of multipath, depends upon an accurate knowledge of the output noise

---

*S. H. Durrani and H. Staras, "Multipath Problems in Communication Between Low-Altitude Spacecraft and Stationary Satellites," RCA Review, March 1963, pp. 77-105.

components of a correlation system, we will spend a few moments discussing the nature of these noise components so that the analysis will be relevant to the reader.

The input to a correlation receiver of the type used in a PN system can consist of a variety of interference sources. These include Gaussian background noise, intentional interference as well as self-noise or multipath generated from reflected signals off the earth's surface.

We will consider for the purpose of analysis that the output of a correlation receiver, having some processing gain (PG) or an equivalent time bandwidth product TW, in response to Gaussian noise and uncorrelated interference is essentially Gaussian. In other words, the input noise and interference is suppressed by the TW product of the receiver, and this resulting amount of noise represents the Gaussian noise that contributes to the degradation of the system.

In addition to the Gaussian noise, multipath can produce non-Gaussian noise at the correlator output. For example, if the multipath signal is essentially specular and the differential time delay between the direct and the indirect signal path is less than the duration of PN chip, the output of the correlation receiver will consist of two components, one of which is Gaussian and the other is non-Gaussian. The portion of the reflected signal within the correlation aperture will produce a randomly phased component that can be represented as a CW term whose power is proportional to the square of the correlation coefficient between paths times the power in the reflected path. That portion of the reflected signal that remains outside the correlation aperture produces essentially Gaussian noise suppressed by the TW receiver product, and this noise can be added directly to the Gaussian noise resulting from ambient noise and interference.

When the reflection is specular, a differential Doppler will exist between the direct and indirect path enforcing the postulation that the non-Gaussian component at the output of the correlation receiver will be a randomly phased CW component.

When the reflection from the earth's surface is completely diffuse and the differential time delay between the direct and indirect path is less than the correlation aperture, the output components of a correlation receiver will be all Gaussian. The ambient noise and interference will be reduced by the TW product of the receiver as

will the Gaussian noise produced by the reflected signal that lies outside the correlation aperture. That portion of the reflected signal whicn lies inside the correlation apertures will produce a Gaussian noise component whose power is proportional to the square of the correlation coefficient between the direct and indirect paths times the amount of power in the indirect path, and this term will not be diminished by the TW product of the receiver.

In the analysis which is to follow, the above model of the output of a correlation receiver will be utilized to obtain expressions and curves for the performance of a PN system in both specular and diffuse multipath. This performance will be measured in terms of the expected binary error probability and later in paragraph 7.6.2   , the rms time jitter for an optimum code tracking system for navigation purposes. The results will indicate the tolerable level of multipath for a typical CNI waveform.

7.1.2.2 Specular Multipath

When we consider the indirect path to be a perfect reflection, we are able to approach a reasonably accurate solution to the degradations imposed on PN systems by multipath. This is illustrated in Figure 7-3.

For the purpose of analysis let us assume that the data is PSK and that the system is a PN coded system. The amount of noise power found in the post-correlation filter is given by the following terms.

$$\text{Noise in post-correlation filter} = \underbrace{\frac{N_{in}}{TW} + \frac{(1-\rho^2)S_{ind}}{TW}}_{\substack{\text{Gaussian noise} \\ (\text{Power}=\sigma^2)}} + \underbrace{\rho^2 S_{ind}}_{CW} \qquad (5)$$

Here, S_{ind} is the power in the indirect path.

The noise power consists of the ambient Gaussian noise reduced by the processing gain plus a Gaussian noise resulting from partial decorrelation with the reflected path diminished by the processing gain (TW) and finally a CW term that represents the partial correlation ρ of the direct and indirect path. The factor ρ is
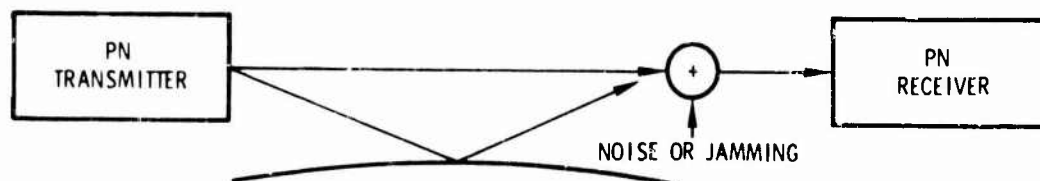
Figure 7-3.   Simplified Multipath PN System Geometry

a number that lies between 0 and 1, and the amount of energy in the indirect path
is a function of polarization, ground conductivity, grazing angle, etc.

After a few algebraic manipulations, a conditional binary error probability is
obtained with the following form.

$$P_\epsilon (\theta) = \frac{1}{2} \text{erfc} \left[\frac{A}{\sqrt{2}\,\sigma} \left(1 + \frac{\rho \sqrt{2S_{ind}}}{A} \left| \frac{\sin \Delta\omega \frac{T}{2}}{\Delta\omega \frac{T}{2}} \right| \cos \phi \right) \right] \tag{6}$$

where

$\phi = \theta - \Delta\omega T/2$, θ is a random phase angle

A = signal strength of the direct path

$\sqrt{2S_{ind}}$ = signal strength of the indirect path

T = duration of the binary symbol

$\Delta\omega$ = differential doppler radian frequency

Under the assumption that the phase angle θ associated with the specular
multipath interference is a random variable, we determine the average binary error
probability by averaging the conditional density over a uniform density in phase. This
results in

$$P_\epsilon = \frac{1}{2\pi} \int_{-\pi}^{\pi} (1/2) \text{erfc} \left[\frac{A}{\sqrt{2}\,\sigma} (1 + K \cos \phi) \right] d\phi \tag{7}$$

The above equation has been programmed on a digital computer and the results are
shown in Figure 7-4 for various values of K in terms of direct path energy per bit
E/N_o. K is the ratio of the signal strength of the reflected path to that of the direct
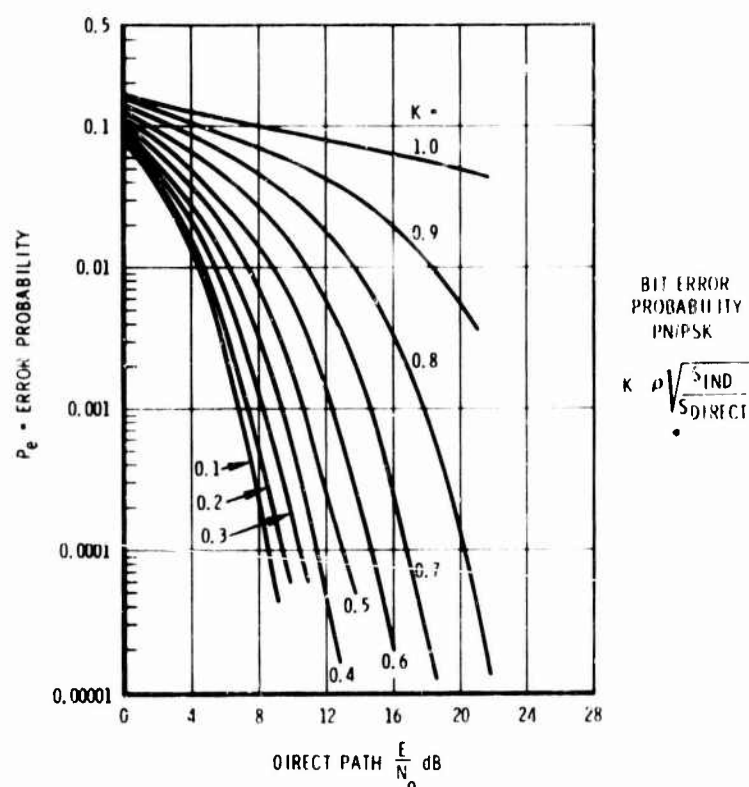
-207-

Figure 7-4. Average Binary Error Probability for PN/PSK in the
Presence of Specular Multipath and Gaussian Noise

path weighted by the correlation coefficient ρ.* Using the results shown in Figure 7-4,
it is now possible to determine the resultant average bit error probability as a function
of the correlation coefficient ρ given that the ratio of the direct to the indirect path
is fixed. For example, the average bit error probability versus ρ is illustrated in
Figure 7-5 under the assumption that the direct and indirect signal path ratio is
unity, the input signal to Gaussian noise is unity, and the TW product (or processing
gain) is 12 db. Note, that the noise power from the interfering path changes as a
function of ρ; that is, the Gaussian noise contribution resulting from partial correla-
tion approaches zero as a correlation between direct and indirect path increases. If
a conservative upper bound on the system performance is desired, this bound can
be obtained, in most cases, by simple drawing a straight line on Figure 7-4 between
the average bit error probability curve for zero correlation and the K value associated
with maximum correlation. Keep in mind that K is the product of the ratio of direct
and indirect signal strength times the correlation coefficient ρ. Such a line repre-
sents an upper bound on the system performance in that it does not consider the change
in noise power resulting from partial correlation.

---

* This is true when $\Delta\omega T/2$ is small.

-208-

Figure 7-5.   Average Error Probability Versus Correlation
Between Direct and Indirect Path

7.1.2.3 Diffuse Multipath

In the previous discussion, the effects of specular multipath on a direct PN system were evaluated. It is also of interest to evaluate the effects of diffuse scattering on PN systems since diffuse scattering will probably predominate for many of the L-band and X-band transmissions postulated for a CNI channel.

To carry out this evaluation, we assume that the diffuse reflected energy can be broken down into essentially discrete paths. Each path will assume to be fading according to a Rayleigh amplitude statistic, and each path will be essentially uncorrelated.

As two extreme cases, either the total time spread in the indirect path is assumed to be equal to the duration of one PN chip or the time spread is assumed to be much greater than the duration of a chip. Furthermore, it is assumed that each of the paths associated with the indirect path contains equal power and that the sum

-209-

total of powers associated with each of the subpaths equal to the total power contained in the reflected path. With these assumptions, it is possible to determine the performance of a PN system in diffuse multipath interference.

Case I - The time spread in the indirect path is assumed to be confined to the original correlation function of the PN sequence, and the indirect signal is diffuse. Under these circumstances the amount of noise power produced at the correlator output and seen by a detector (PSK) is given by Equation (8).

$$\text{Noise Total} \approx \frac{N_{in}}{TW} + \underbrace{\frac{(1-\rho^2)S_{ind}}{TW} + \rho^2 S_{ind}}_{\text{All Gaussian noise terms}} \tag{8}$$

where

ρ = degree of correlation or signal overlap, $0 \le \rho \le 1$

S_{ind} = amount of power in the indirect path

We see that as the indirect and the direct paths become more and more correlated, the amount of noise power that confronts a binary decision increases as the square of the correlation coefficient, and the noise will be essentially Gaussian since the diffuse path is fading according to a Rayleigh statistic. The amount of interference due to the reflected energy associated with the uncorrelated indirect path is suppressed by the system TW product as is the input noise that is always associated with the system. The post-correlation or predetection signal-to-noise ratio, therefore, will in effect approach 0 db when the correlation coefficient is 1 and the direct and indirect paths are essentially equal.

The resulting binary error probability (PSK) is given by

$$P_\epsilon \text{ (1/2)erfc} \sqrt{\frac{S_{direct}}{\frac{N_{in}}{TW} + \frac{(1-\rho^2)S_{ind}}{TW} + \rho^2 S_{ind}}} \tag{9}$$

diffuse (no time spreading)

where S_{direct} is the signal power in the direct path. Equation (9) has been plotted in Figure 7-6 for various values of $\sqrt{S_{ind}/S_{direct}}$ and shows that an irreducible error probability exists due to the diffuse multipath.

BIT ERROR PROBABILITY PN/PSK

$$K = \sqrt{\frac{S_{INDIRECT}}{S_{DIRECT}}}$$

ρ = SIGNAL PATH CORRELATION
= 1 FOR THESE GRAPHS

569-1182
UNCLASSIFIED
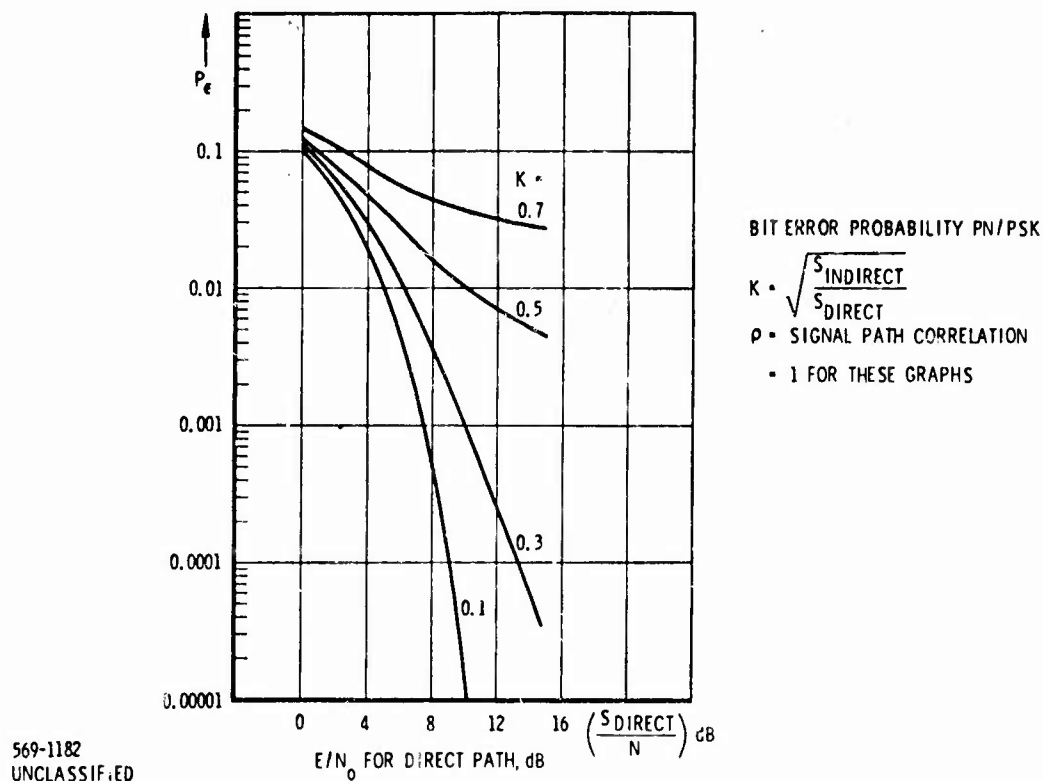
Figure 7-6. Average Error Probability, Diffuse Multipath
No Time Spreading

Case II - Now, let us assume that the multipath signal is time spread such that
the total reflected signal is distributed over a time that is large compared with the
correlation window of the binary sequence. We can expect that only a fraction of the
reflected power will contribute directly as additional Gaussian noise in the receiver,
the rest will remain uncorrelated and suppressed by the TW product. Thus, as a
function of the correlation coefficient we have noise terms which have the following
form.

$$N_{total} = \frac{N_{in}}{TW} + \frac{\left(1 - \rho^2 \frac{\Delta}{T_{spread}}\right) S_{ind}}{TW} + \rho^2 S_{ind}\left(\frac{\Delta}{T_{spread}}\right) \qquad (10)$$

-211-

where

Δ = the duration of a PN chip

T_{spread} = the multipath time spread

ρ = the overlap or correlation between direct and indirect paths

S_{ind} = the total power in the indirect signal.

Time smear in the indirect path will be advantageous since time smearing in the indirect path forces more of the reflected energy to be decorrelated in the receiver, thus subject to the suppression by the processing gain of the receiver.

7.1.3 DEGRADATION IN PROCESSING GAIN FOR A PN SYSTEM TRANSMITTED THROUGH THE IONOSPHERE

The ionosphere is a dispersive transmission channel and therefore acts to degrade the performance of wideband signals that pass through the ionosphere. The ionosphere amplitude response may be considered as constant with frequency for the frequencies of interest, whereas, the ionosphere phase response is nonlinear with frequency.

The dispersive nature of the ionosphere can be evaluated by expanding the ionosphere phase response in a Taylor series about the carrier frequency. The first distortion term in the phase response is associated with the third term of the Taylor series expansion.

$$B(\omega) = B_0 + K_1 \omega_0 (\omega - \omega_0) - K_2 \omega_0^2 (\omega - \omega_0)^2$$

To determine the degradation in processing gain for a PN system, it is necessary to first determine the approximate impulse response of the dispersive channel. Elliott* has determined the impulse response for a dispersive channel having essentially the same nonlinear phase characteristics as the ionosphere. The impulse response is complex and given in Equation (11).

---

*R.S. Elliott, "Pulse Waveform Degradation Due to Dispersion in Waveguide," MTT-5, No. 4, October 1957, IRE Trans on Microwave Theory and Techniques, pp. 254-257.

$$h(t) = h_I \cos\omega_0 t + h_q \sin\omega_0 t$$

$$h(t) = \frac{2 e^{-t^2/4K_2 L}}{\sqrt{4\pi K_2 L}} \cos\omega_0 t + \frac{d}{dt}\left[C\left(\frac{t}{\sqrt{4K_2 L}}\right)^2 - S\left(\frac{t}{\sqrt{4K_2 L}}\right)^2\right]\sin\omega_0 t \qquad (11)$$

where

L = width of the ionosphere

$$C(z) = \sqrt{\frac{2}{\pi}} \int_0^{\sqrt{z}} \cos u^2 du$$

$$S(z) = \sqrt{\frac{2}{\pi}} \int_0^{\sqrt{z}} \sin u^2 du$$

The impulse response consists of an inphase and quadrature component.

When a PN system is transmitted through the ionosphere, both inphase and quadrature components will serve to degrade the system, however, since the quadrature component of the impulse response gives rise to an odd function of frequency, the quadrature component will not degrade the correlation peak or maximum processing gain of the system; rather, the inphase component of the impulse response, which gives rise to an even function in frequency, will be the major contributor to the reduction in processing gain for a PN system. In Figure 7-7, we illustrate a low pass equivalent model for the PN correlation system that reflects the frequency transfer function resulting from inphase and quadrature components of the impulse response of the ionosphere. Since the inphase component of this impulse response is Gaussian in shape, its frequency weighting is also Gaussian. The reduction in processing gain for a PN system can be calculated from the following Equation (12).

$$R = \frac{2\alpha}{\pi} \int_0^\infty \frac{\sin^2\alpha x}{(\alpha x)^2} e^{-x^2} dx \qquad (12)$$

where

$H_i(\omega)$

S(t) ───

LOW PASS EQUIVALENT
OF IONOSPHERE

$H_q(\omega)$

S(t) cos $\omega_0 t$ ───► h(t) ───► $g_i(t)$ cos $\omega_0 t + g_q(t)$ sin $\omega_0 t$

669-1534
UNCLASSIFIED

BAND PASS REPRESENTATION
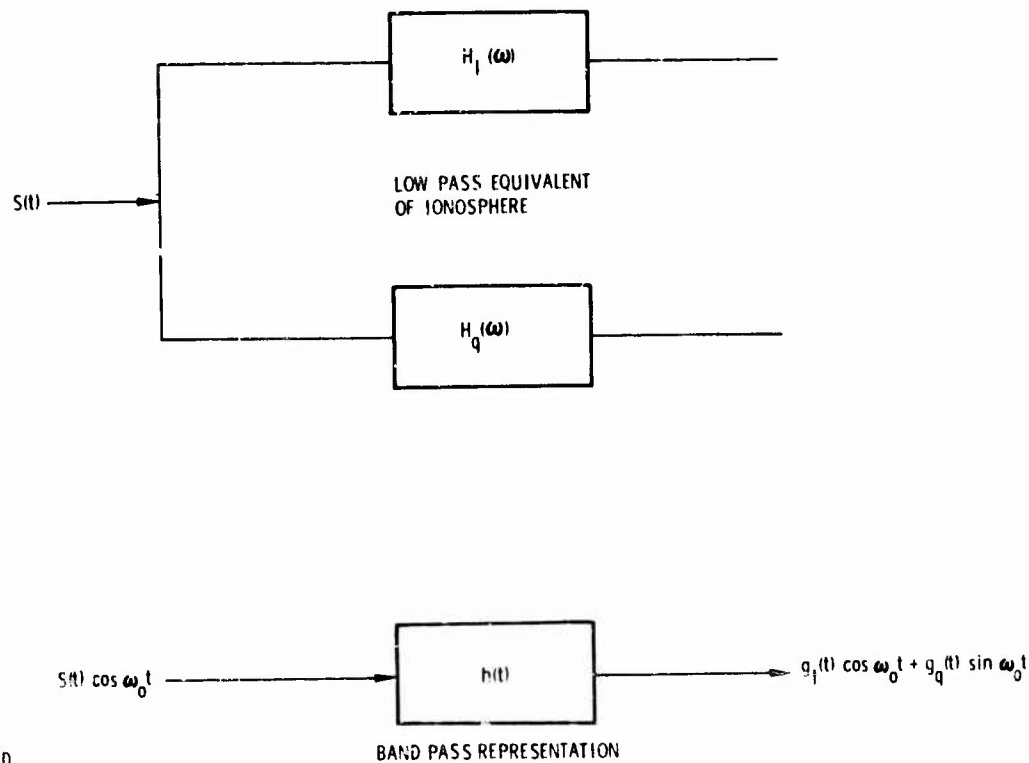
Figure 7-7.   Ionospheric Channel Transfer Function

$$\alpha = \frac{\Delta}{2\sqrt{K_2 L}}$$

Δ = Chip Duration

The reduction in processing gain is plotted as a function of the phase constant in Figure 7-8. In Figure 7-8, the pulse shape distortion factor $a = 2/\alpha$ related to the phase constant is also plotted for an electron density of 50×10^{12} electrons per cubic centimeter.* From the above analysis and Figures 7-8 and 7-9, we see that it is advisable not to use PN chip rates in excess of 100 MHz when operating at a carrier frequency of 2000 MHz. Wider bandwidth signals can be used if higher frequencies are available.

---

* Counter & Reidel, Calculations of Ground Space Propagation Effects, Lockheed Report LMSD-2461, 22 May 1958.

-214-

$$R \cdot \frac{2\alpha}{\pi} \int \frac{\sin^2(\alpha x)}{(\alpha x)^2} e^{-x^2} dx$$
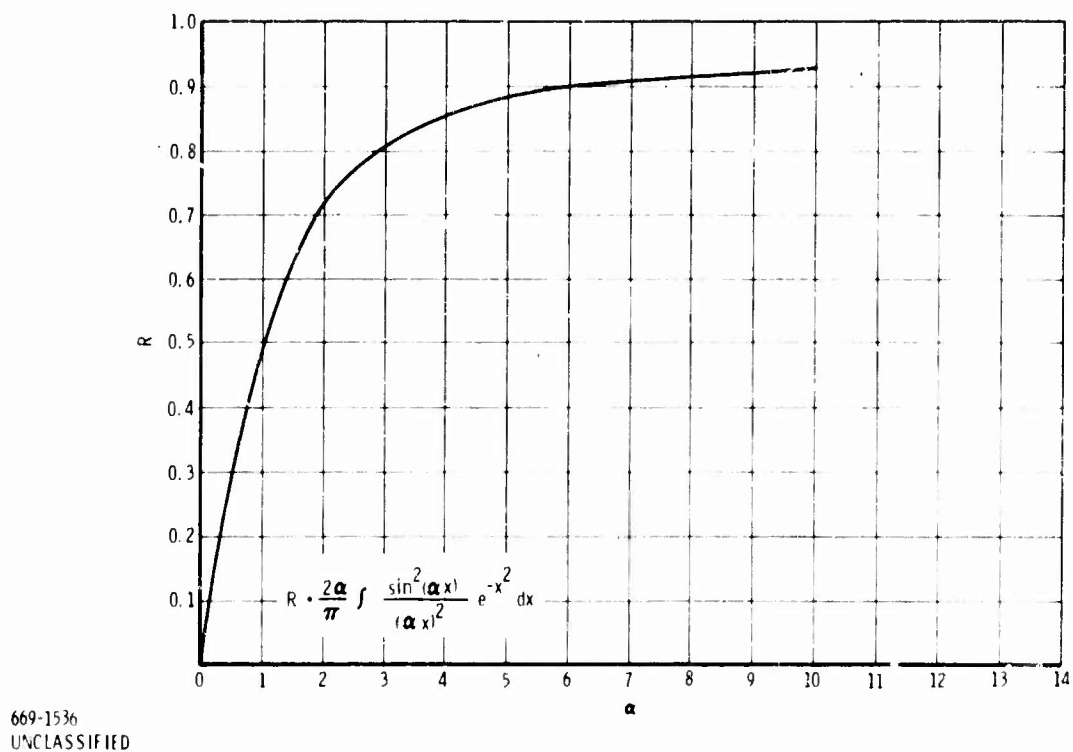
Figure 7-8. Processing Gain Reduction
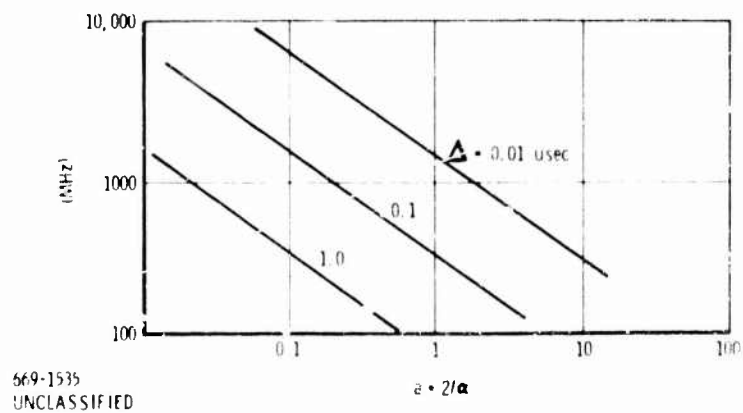
Figure 7-9. Distortion Factor Versus Frequency for
Various Chip Durations Δ

-215-

7.2 MULTIPLE ACCESS CONSIDERATIONS

This study task goal provides a quantitative comparison of the multiple access capability of waveforms applicable to the specific problems of the CNI environment. This discussion of the problem outlines what are considered to be the specific CNI problems, forwards several criteria for evaluating the performance of a specific waveform and provides preliminary comparisons based on theoretical best and worst cases. Following these discussions - during which it is concluded that some form of TDMA is required - a simulation is performed using random selected terminal positions within a communication range circle. The simulation shows good performance for a system employing TDMA with parallel channels.

Because of the desire to integrate the navigation functions with the communication and IFF functions, only those waveforms that are inherently wideband are considered. This restriction eliminates FDMA or self-organizing narrowband systems and confines the waveforms to the categories listed in Table 7-1. There, the available multiple access techniques are classified according to their continuous or intermittent use of time, and by their total or partial occupancy of the total bandwidth at any instant in time. A further distinction is made when intermittent use of time is employed, between synchronous and asynchronous systems. The examples given in Table 7-1 are examined for their specific applicability to the CNI net configurations evaluated in the following sections.

Table 7-1. Available Multiple Access Techniques

Classification	Example
Continuous Use of Time	
Total Bandwidth	Pseudonoise
Partial Bandwidth	Frequency Hopping
Intermittent Use of Time	
Synchronous	
Total Bandwidth	Time Division Multiple Access
Partial Bandwidth	Frequency Hop-Time Division Multiple Access
Asynchronous	
Total Bandwidth	Time Hopping
Partial Bandwidth	RADA (Time Frequency Matrix)

A significant difficulty in this study, over and above a definition of the actual problem, is the establishment of the criteria upon which a quantitative comparison is to be made. Since real CNI operational requirements are presently nonexistent, other criteria must be developed. Following a description of the criteria to be employ, the parameters of the CNI environment used to derive performance compari are discussed.

7.2.1 COMPARISON CRITERIA

Since no specific criteria exist, and different waveforms show varying susceptibilities to specific environments, several arbitrary comparison criteria for multiple access performance are used. First, the basic theoretical best performance will be given for the various waveforms. This criterion will give the theoretically attainable multiple access capability in terms of a bandwidth efficiency parameter-multiple access rate - which expresses the multiple access capability in terms of bits per second per Hertz.

The multiple access rate criterion is useful in demonstrating what is theoretically possible; it does little to predict the capability in a realistic environment, however. Another comparison criteria set would then be a worst case evaluation. The worst case condition for each seriously considered waveform is established. These evaluations provide a set of performance levels for each waveform showing its worst case performance and the performance of all waveforms in the same environment. Four fundamental worst case parameters consistently appear in waveform evaluations: signal strength variation, differences in time of arrival, and signal time dispersion and spectral occupancy. These parameters, described in more detail subsequently, are mentioned here to provide examples of the comparisons to be made.

Both the theoretical best and worst case performance evaluations are useful in that they provide bounds on the capability of a particular waveform. Their shortcoming is that these extreme cases usually do not reflect realistic representations of the environment to be encountered. A procedure that gives more realistic results is to form a probabilistic model of the net and simulate total net performance, given the assumed geographical distribution of the terminals, any power control constraints imposed, random selection of subscribers in time given duty factor, and varying numbers of subscribers.

-217-

The results of such a comparison provide probability curves of successful message completion as a function of the number of subscriber in the net. Parameters that could be varied would be duty factor for subscribers, geographical distribution, modulation technique, data format, and coding assumptions. Simulations still do not give precise answers about the performance in a CNI environment. They do, however, give realistic quantitative comparisons of the modulation formats of interest and show trends that will indicate parameters to which each waveform is particularly susceptible.

Three different means of comparing the selected waveforms have then been chosen to provide complementary means of comparison. The theoretical best case shows what can be attained under perfect conditions. Worst case evaluation shows limitations that set performance (and applicability) bounds. The probabilistic models provide more realistic, quantitative performance data and will be applied to waveforms surviving the preliminary comparisons. To evaluate performance under these criteria, some typical parameters of a CNI net must be assumed. The following section discusses these assumptions.

7.2.2 PARAMETER MODELING

The fundamental requirement for CNI multiple access is the support of a number of information sources having different duty factors, data rates, user requirements, and relative importance. The CNI system must provide these different information transfers in an environment causing large variations in signal strength received from users and interferers, differences in time of arrival due to propagation time delays, and signal dispersion caused by multipath and other phenomena behaving as channel memory. Since the goal of this study is to provide a quantitative comparison of applicable waveforms, the requirements and the environment are modeled in a definitive manner. The modeling presented is considered to be representative and will, therefore, provide a more realistic evaluation than simple worst or best case evaluations.

7.2.2.1 Requirements Parameters

The information transfer modes can logically be divided into five categories: direct communication, remote communication, enroute navigation, landing navigation, and IFF. Within each of these categories subcategories exist that affect the multiple access performance and criteria.

-218-

In the direct communication mode, several types of information must be considered. At present, the great majority of communication nets are voice. For the CMI system only digital formats will be considered for voice; two digital voice formats seem reasonable to consider. The first is 19.2 Kb/sec delta modulation. This modulation format has been shown to product tactical quality voice even with a random bit error rate of ten percent (see paragraph 7.3.3). The second type of digital voice to be considered is 2400 bit-per-second vocoded voice. Present vocoders perform adequately at bit error rates of two percent and even higher. These two digital voice formats are the only modulations considered for voice, and the ten and two percent random error rates are considered as the threshold criteria for each technique.

In addition to voice, the direct communication model must support at least two distinct forms of data links. The first will be essentially continuous in nature. Long messages will be transmitted allowing decoding processes to be performed over a large number of data bits. The second type of message would be typical of tactical data control nets that use burst transmissions of 50 to 200 bits duration. Thus, only limited duration decoding intervals can be employed. This distinction becomes important when modulation techniques yielding burst interference are considered. The message duration is the only distinction that will be made between the above data links. Both will be considered to be 2400 bits-per-second channels and both require a 10^{-5} output error rate. The data transfer in the direct mode, thus, has more demanding requirements than either of the voice formats. In the discussions that follow, then, modulation comparisons are based on the 2400 bps and a 10^{-5} error rate.

Typical subscriber needs are hypothesized to provide a needed comparison. An airborne subscriber must be able to continuously guard and transmit on at least two separate addresses or channels. He must further be able to simultaneously participate actively in a tactical control net. This requirement to simultaneously transmit and receive (overlapping message intervals is implied here) from a single platform, will be shown later to eliminate all strictly continuous wavefor, s from consideration.

A typical ground station will be considered to control up to 100 aircraft, participate in up to 25 voice nets, and operate two data nets, one for tactical control

and one for landing. Further, continuous data links are maintained with other control terminals in the area. There may be as many as three such terminals in a single operational area. These parameters for the control station participation in the direct nets are mentioned because use can be made of transmission multiplicity from a single point. Subsequent netting requirement discussions show the specific applicability.

The remote communication nets comprise voice and continuous (i.e., long duration) data transmissions. With the exception of short data message requirement elimination, the subscriber requirements are the same as the direct mode. It is assumed that tactical airborne platforms do not have to transmit and receive simultaneously in the remote mode, but that ground terminals must. Large airborne platforms (command posts, AWACS, etc.) have the same requirements as a ground control terminal.

The enroute navigation signals considered involve updating at least once per second, of information received from each of four or possibly five navigation satellites. A 100 bit-per-second data rate is assumed to be associated with each of the satellite signals and the previous assumption of a 10^{-5} error rate remains.

The IFF is considered as a unique requirement only in the direct mode. Each airborne terminal must be capable of simultaneously detecting at least three interrogations in an environment typically including at least 100 interrogations. Subsequent response to all three interrogations is required. IFF again requires simultaneous reception and transmission from a single aircraft.

The landing navigation mode is not addressed directly here since it is not expected to greatly influence multiple access usage. Localized use, directive antennas, and limited aircraft all reduce the landing mode load significantly below that of the other nets.

It is useful in subsequent discussions to typify the nets described above into four general netting configurations; each warrants individual consideration when considering multiple access for CNI. The characteristic that distinguishes the individual configurations is the degree to which differences in signal arrival time and power variations can be controlled. These factors have significant effect upon the CNI waveform selection and, therefore, each netting configuration is considered separately.

The four classes of nets are shown diagrammatically in Figure 7-10. In Case I, there are no fixed geographical relationships between individual subscribers in the net. This configuration models the general air-to-air communication and IFF. Case I is the most difficult of the cases shown in Figure 7-10 from the multiple access point of view in that there is no mechanism available for controlling differences in time of arrival or signal strength variation. It is in Case I that the full range of the time of arrival and signal strength differences from remote terminals is realized.

Case II in Figure 7-10 represents the situation in which a large number of aircraft are controlled from a single terminal. This case is important because of the large amount of such traffic and because the case allows control not available in Case I. Several nets from such a ground station are continuous in nature and, in general, the traffic will be quite high. The terminal can easily control both timing and power balance between the links; therefore, the aircraft will be receiving well coordinated signals from the terminal. In a similar manner, each aircraft can time its transmission and, in principle, control power to provide a well structured signal sum at the ground station.

In Case II, there is again no way to control signals transmitted from one aircraft and arriving at another. Further, it is not obvious how the control available in Case II would actually be employed in an overall net. The case is singled out because the availability of control can make these particular, high traffic density nets more efficient from a multiple access standpoint if the coordination is properly used.

Case III represents the communication relay case. The most common relay mode will be via satellite, but an airborne relay mode may be used for range extension in a tactical environment. In the satellite mode the ranges cause round trip delays on the order of tenths of seconds. Because each terminal can easily monitor its own signal, however, it is a relatively easy matter to achieve very
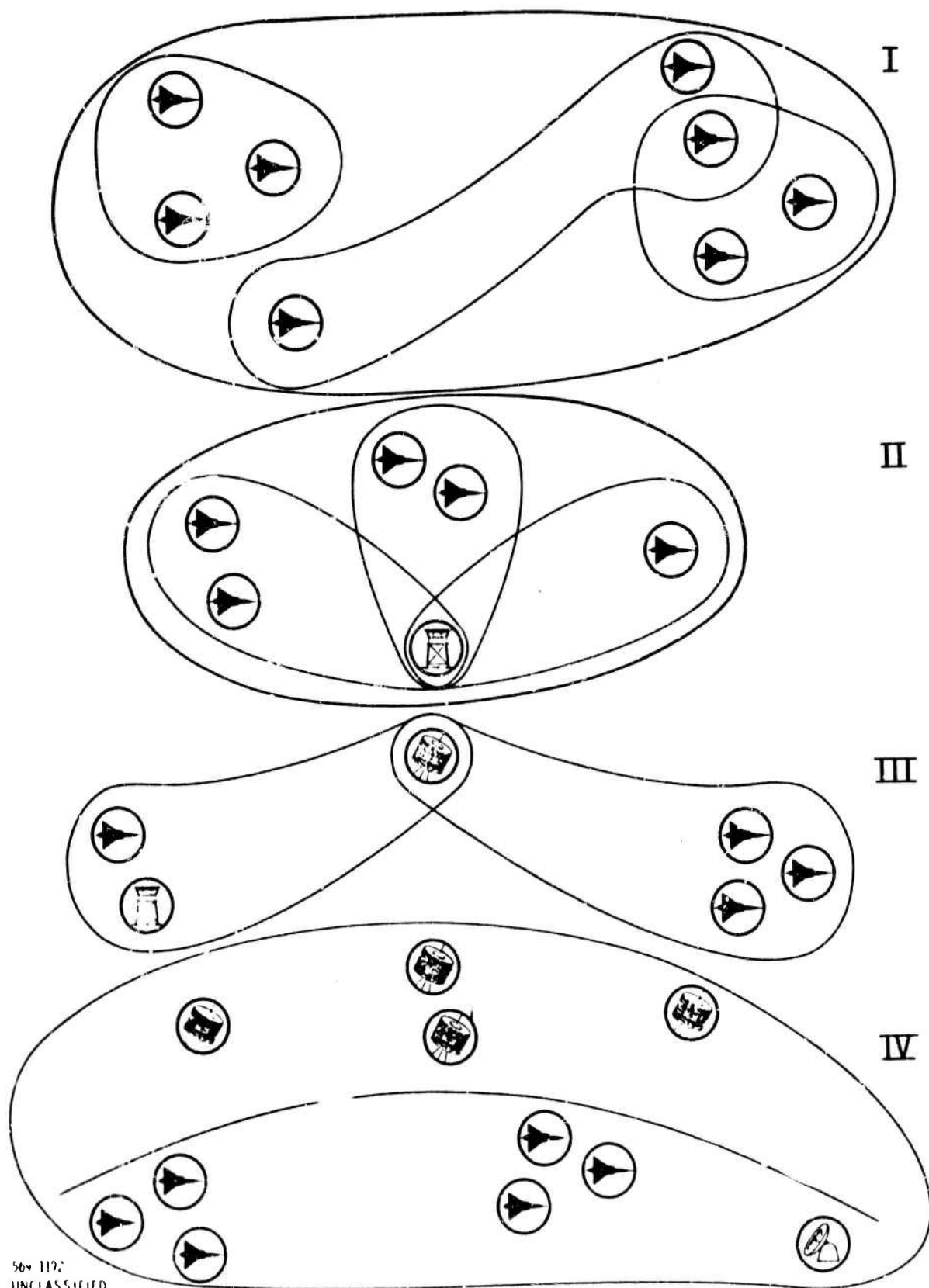
Figure 7-10. Classes of Net Organization.

-222-

accurate relative timing at the satellite. Experiments run to date have shown that timing accuracies better than 100 nanoseconds can be achieved relatively easily.

Power control at the satellite will remain a problem, however. Even if steerable antennas are employed on the aircraft significant power variations are inevitable. With omni directional antennas the variation will be extensive.

A difference between the remote mode and the direct mode will be that, even with advanced satellites, the received signal from the satellite will be extremely weak. This will complicate any attempt to have the direct and remote modes occupy the same spectrum.

Case IV is included to demonstrate the problems associated with making the planned navigational technique multiple access with the direct and remote communication nets. In a subsequent discussion on net timing, the time differences realized are described. The satellite used for navigation could also be used for communication, but again the ellipticity of the orbits will be a problem.

7.2.2.2 Environmental Parameters

Four environmental characteristics that drastically affect the multiple access capability are: variations in signal strength, differences in arrival time, signal dispersion, and spectral occupancy. These topics are discussed and parameters established that are typical of the CNI environment.

1.   **Signal Strength Variations:** Fundamental to both the signal strength variation problem and that of differences in arrival time is the question of range differences between communicating terminals and interfering terminals. In the direct mode, it is assumed that the minimum range will be 100 feet between a receiving terminal and an interfering terminal while maximum range is 300 nautical miles. This range difference causes a difference in received signal strength for equal ERP transmitters of 85 db considering free space loss only.

In the remote mode, the range from the satellite is greater than 19.6 Knm. This great range causes a significant problem when remote and direct modes are operated in the same bands. For satellite transmissions having ERP equal to the direct mode transmissions, the received signal is 36 decibels below the weakest signal and 120 decibels below the strongest. If a 1-KW transmitter is used in the direct mode, then, a 66 dbw ERP would be required at the satellite to make the remote mode equivalent to the weakest direct mode signal.

Here, it is considered that the dynamic range of the received signal strengths because of range differences, is limited to that realized in the direct mode. Thus, it is assumed that the remote mode either has sufficient power or is placed in another band. The signal strength variations because of range differences are not the only ones that must be contended with, however. Atmospheric and propagation effects will significantly increase the signal strength variation.

Several factors cause power variations in the direct mode that significantly exceed those predicted solely by range differences. Antenna patterns, multipath, and radio holes are examples of these phenomena. These variations are statistical in nature and depend on the specific aircraft, its maneuvers, and its environment. The following presents data showing the typical extent of some of these variations. While these data are not considered to give accurate quantitative results, they demonstrate the variations that affect the multiple access capability of the CNI network.

Signal variations arising from propagation anomalities can be appreciated by a direct quotation of the abstract of a paper by M. S. Wong. *

---

* Ming S. Wong, "Refraction Anomalies in Airborne Propagation," Proceedings of the IRE, September 1958, pp. 1628-1638.

"Propagation at 250-10,000 mc often encounters: (1) dense fading where the radio signal fluctuates spatially with large amplitudes and small spacings from maxima to minima, e.g., amplitudes of up to 40 db and spacings at 3000 mc of 1 mile; (2) radio holes, where the signal falls spatially to a level often 15 db below the levels outside; (3) anti-holes where the signal fluctuates spatially with large amplitudes and irregular spacings; (4) radio ducting, including cases where the transmitter or receiver is often far above a ducting layer in the air."

Figure 7-11 is a reproduction of data obtained during actual flight tests.* The figure represents measured signal versus range levels on different days on a ground to air path over Chesapeake Bay. The aircraft altitude was 10,000 feet, and the frequency was 2.3 GHz. Wong considers the top curve "nearly standard" while the bottom curve reflects "mild case of dense fadings."

Another example from the same paper is illustrated by Figure 7-12, that shows measured holes and anti-holes realized in flight tests over Ohio. The path here is air-to-air with both terminals at 10,000 feet and the frequency is 3 GHz. The extended hole shown in the vicinity of 175 miles indicates received signal strength at least 25 db down from the theoretical.

These examples illustrate occurrences of deep fades but do not supply any information about their relative probability of occurrence. No direct applicable presentation of statistical results was found, but a study performed for television and reported by Egli** gives data that is indicative of performance that might be realized in reasonably rough terrain. The study included transmissions to 980 MHz. The data were taken over ground-ground paths principally of 30-40 miles in length.

Figure 7-13 was taken from Egli's presentation, and shows the signal strength variation at a frequency of 1 GHz. The abscissa is referenced to the free space level. The figure shows that within the limits shown, the data are well represented by a normal distribution of mean -28 db and a standard deviation of 13 db. These data demonstrate the probability of occurrence of signal strength variations of considerable

---

* C.H. Duerfeldt, "Propagation in the 328-2300 MC Frequency Band," Naval Air Test Center, Patuxent River, Md., Report No. EL 44012.3, pp. 10-17, Oct. 1954.

** Egli, J.J., "Radio Propagation Above 40 MC Over Irregular Terrain," Proceedings of the IRE, October 1957, pp. 1383-1391.
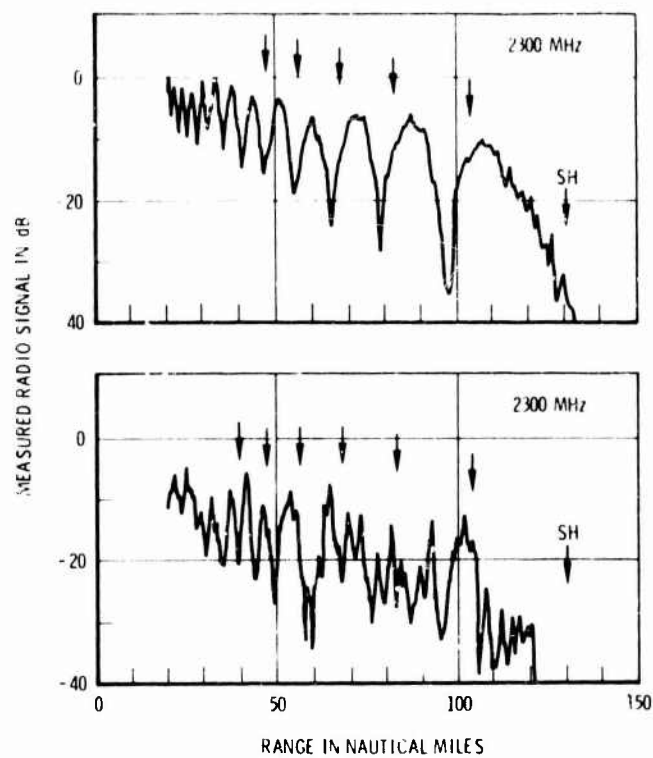
Figure 7-11. Signal Versus Range Curves on Different Days at 10,000 Foot
Altitude in Ground-to-Air Propagation Over Chesapeake Bay
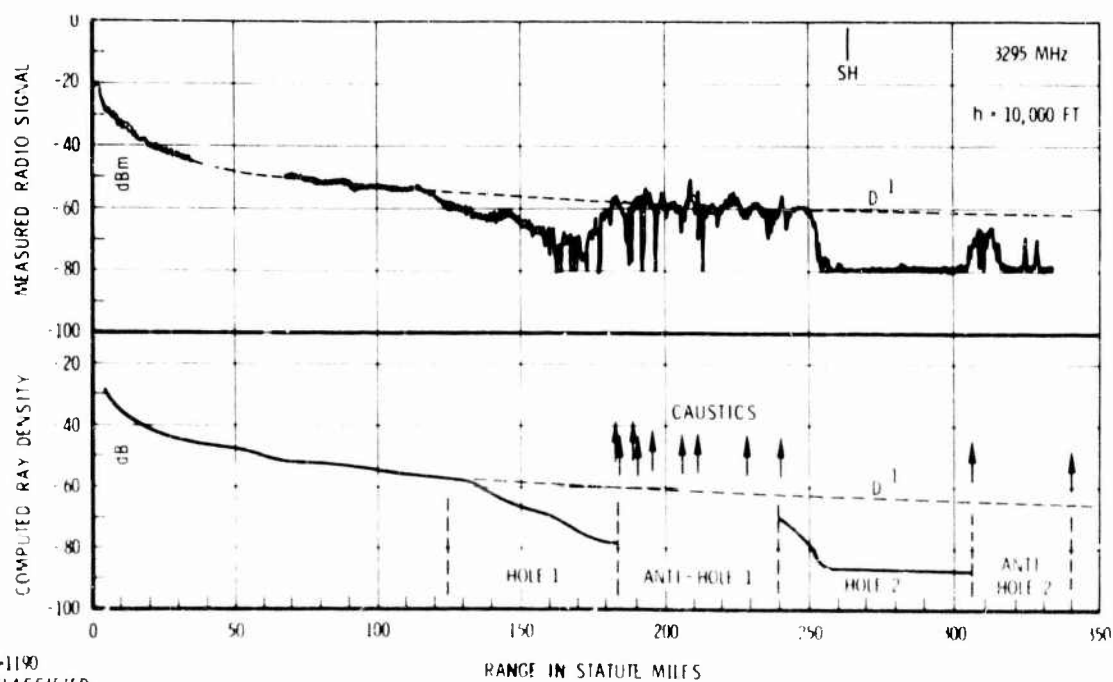
Figure 7-12. Signal Versus Range Curve at 10,000 Foot Altitude in Air-to-
Air Propagation, and Ray-Density Curve Computer from N-Profile Data

-226-
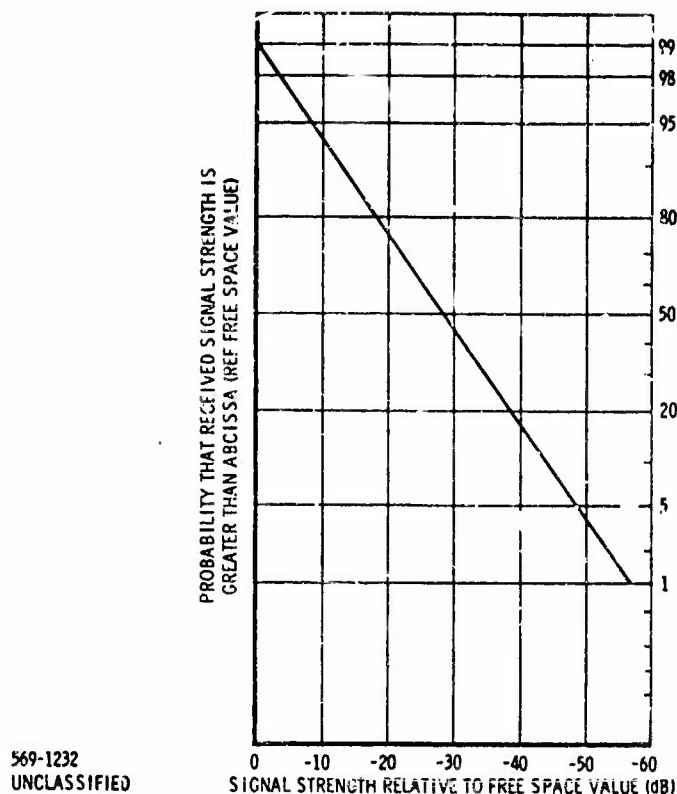
Figure 7-13. Variation in Signal Strength at 1 GHz

magnitude. The data are not, as mentioned, strictly applicable and are probably somewhat pessimistic. However, it is likely that the pessimism lies primarily in the mean value and that the variations in signal strength are realistic.

The variations in signal strength discussed so far have been concerned with propagation effects. Antenna pattern variations have not been included. It is assumed that all terminals in the multiple access net employ omnidirectional antennas. The lack of the spatial selectivity attainable even by moderate directivity severely degrades systems that must tolerate interference from other members of the net. The assumption of omnidirectional antennas, then, will give pessimistic results for overall net performance.* For the present, however, omnidirectional antennas are assumed.

_____

*While it is questionable that antennas having substantial directivity will be employed on tactical airborne platforms, this is not true of the net control stations. Control stations will know where the aircraft are and have no physical constraints barring directive antennas; control stations will handle a great deal of the total net traffic; therefore, directivity at such stations could greatly increase the total net capacity.

Since aircraft antenna patterns are notoriously variable, exact data is difficult to use. A model of a representative communication antenna gain distribution is shown in the insert in the upper left hand portion of Figure 7-14. The model is a Rayleigh distribution having a maximum gain of plus six decibels and having ten percent of the gain below minus six decibels. With this model, Figure 7-14 shows the cumulative probability distribution for the gain of a pair of such antennas. This gain distribution can be roughly modeled as Gaussian with mean minus one decibel and standard deviation of five decibels.

Figure 7-14 demonstrates the large variation in signal strength due to antenna patterns - differences of twenty decibels are common. Figures 7-11 through 7-13 show propagation effects, where 25 decibel fades are common with even greater variations realized. This modeling predicts that the combined effects of antenna gains, propagation effects, and range differences will lead to signal strength differences greater than 130 decibels in the direct mode. Reasonable minimum variations are then 85 db with the maximums of 130 db.
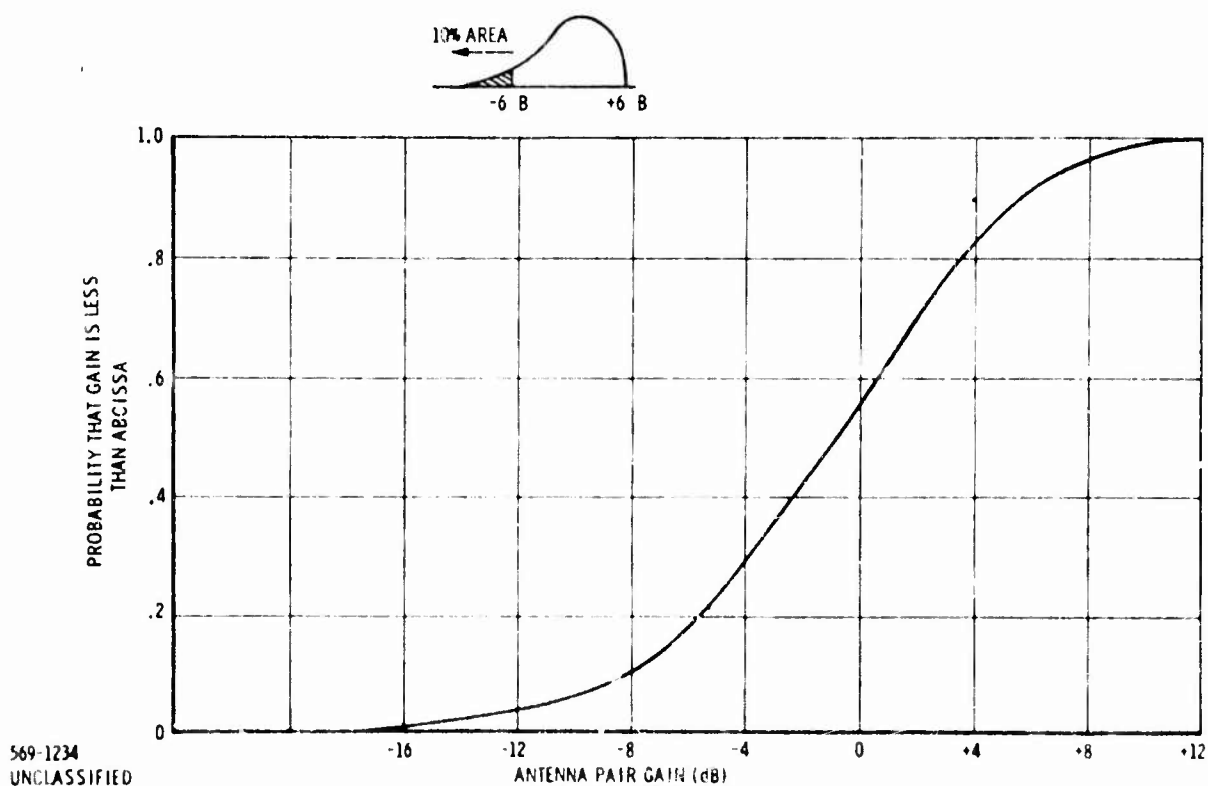
Figure 7-14. Cumulative Probability of Antenna Pair Gain

-228-

2.　　Timing: Multiple access efficiency can often be increased if the waveform is chosen so that the users occupy orthogonal time slots. To do this, the entire net must be operated in synchronism. Modern oscillator and clock setting techniques make it relatively easy to deploy time sources accurate to within less than 1 microsecond of some absolute time reference even in tactical aircraft. The timing uncertainties, therefore, result primarily from propagation delays.

The propagation times of concern in the CNI problem are shown in Table 7-2. In the direct mode, the 1.8 millisecond time differences associated with the 300 nautical mile maximum range often cannot be reduced. Even if a communicator has position knowledge of everyone in the net there is no way of reducing the 1.8 millisecond difference in time of arrival between near and far terminals. These differences would apply in both the direct communication and IFF modes.

The time delays shown in the remote modes in Table 7-2 would be a considerable problem if they were treated as uncertainties. Because relays are involved, however, differences in time of arrival from these relays can be essentially eliminated by making the relay a virtual time reference. When each terminal can hear its own return from the satellite, the transmitting time reference can be shifted ahead to make the time of arrival at the satellite coincide with the net time reference. This technique makes the remote mode relatively easy to synchronize.

Table 7-2. Approximate Propagation Times

Direct Mode	
300 nm maximum range	1.8 ms
Remote Mode	
Satellite – maximum to synchronous equitorial satellite	144 ms
Round Trip	288 ms
Earth Relay – Airborne 600 nm maximum range	3.6 ms
Navigation	
Maximum Range – 49×10^6 m	163 ms
Minimum Range – 23×10^6 m	76 ms
Difference (not fully realizable at one user)	87 ms

While an airborne relay is being considered in this study solely as a means of providing range extension in tactical areas, the ease of time synchronism makes an earth relay mode a possible means of providing the normal direct mode communication. Signal level control also becomes a much simpler problem in the relay mode.

The navigation time differences shown in Table 7-2 reflect the maximum and minimum slant ranges that would be realized in a typical synchronous satellite navigation constellation. The high ellipticity of the inclined orbits creates the differences. While the full differences shown in Table 7-2 cannot be realized by a single user, these propagation differences can pose a formidable problem in trying to synchronize the arrival times of the navigation signals over extended portions of their coverage.

In considering the susceptibilities of various waveforms to differences of arrival time, then, the 1.8 ms difference associated with the direct mode will be used. This is done because the single satellite remote mode can be easily compensated while the navigation satellite constellation probably precludes synchronization.

3. Signal Dispersion: In connection with time division modulations, it is of interest to determine the pulse time persistence. Two significant contributions to the persistence are realized: scatter from the terrain and returns from specular reflections. The terrain reflections are most significant at a receiver co-located with an active transmitter. This geometry is illustrated in Figure 7-15 and illustrates how multipath due to backscatter causes a time spread.

To evaluate the persistency of multipath - the amplitude of the residual multipath - and response to a pulse at a potential receiver resulting from a transmission from a nearby or co-located transmitter, we have utilized a model based upon a radar clutter analysis of the return from the earth which consists of the variable terrain. As shown in Figure 7-15, this model evaluates the back scatter from a pulse emitted at transmitter T_1 and viewed by a potential receiver located nearby. To determine the amount of power received by the potential receiver R_1 in response to a transmitted pulse from transmitter T_1, consider that the transmitter is a radar signal with omnidirectional antenna and that reflections will occur off a flat earth at various distances from the potential receiver R_1. The received signal in response to a specified duration pulse by the transmitter T_1 can be given by the following equation.

-230-
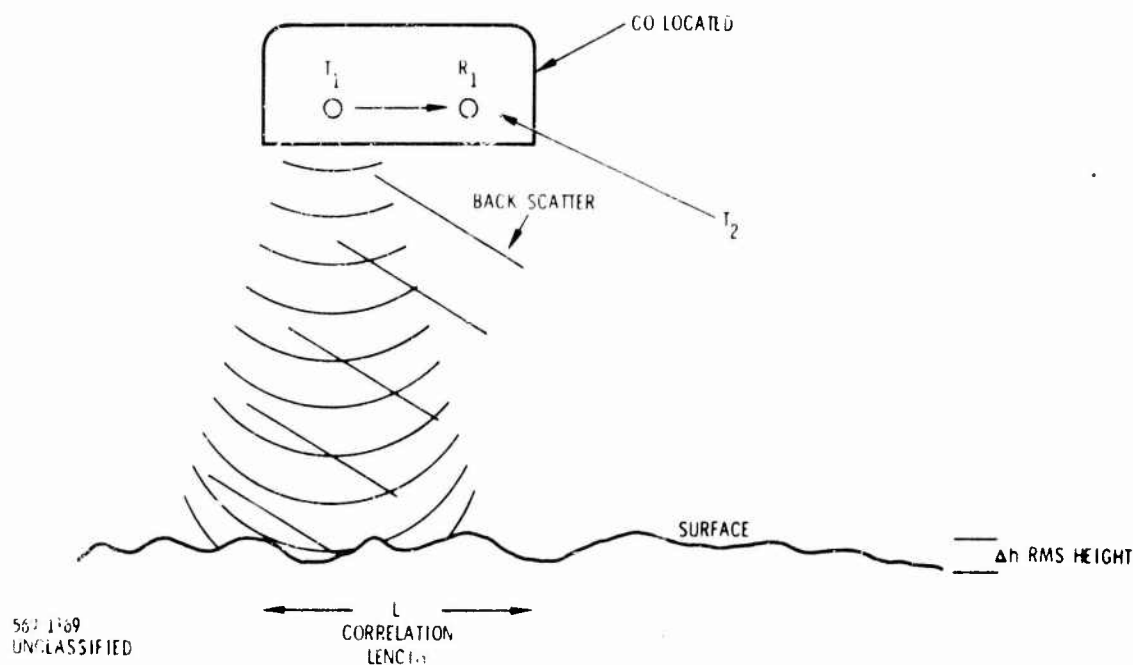
Figure 7-15. Multipath Backscatter Model to Determine Persistency

$$\frac{P_{R_1}}{\delta^2 P_T} = \frac{\lambda^2 2\pi \Delta r\, h \tan \theta\, G(\theta,\, B_o)}{(4\pi)^3 h^4 \left[1 + \tan^2 \theta\right]^2} \qquad (13)$$

where

λ = wavelength

$\Delta r/c$ = pulse duration

h = height of receiver R_1

δ = reflection coefficient at vertical incidence

$G(\theta, B_o)$ = backscatter law = $\cot^2(B_o) \exp\left(-\dfrac{\tan^2 \theta}{\tan^2 B_o}\right)$

$\tan B_o = \dfrac{2\Delta h}{L}$

The above equation depends upon the wavelength λ of the transmitted signal, the roughness Δh of the earth, the correlation distance L along the earth surface, the angle of incidence θ measured from the vertical, and a composite backscatter law. Other important factors such as polarization, reflection coefficient, etc., are imbedded

-231-

In the reflection coefficient. We have selected a theoretical backscatter law* for uniform surfaces with rms height variations far in excess of the wavelength, (i.e., $\Delta h >> \lambda$) but, nevertheless, uniform in the X and Y directions. There are other back scatter laws which have been used to fit experimental data; however, by in large, these laws do not differ appreciably from that used by Beckman and Spizzichino.

By varying the absolute value of the reflection coefficient, the roughness factor, and the correlation length, we can utilize the above back scatter model for a smooth sea, a rough sea, or a variety of terrain conditions. Equation (13) is plotted in Figure 7-16 for various altitudes (curves are simply displaced by h^3) above the earth and normalized with respect to reflection coefficient and transmitted power. The data is plotted for 1000 MHz frequency. It assumes that a pulse of 1 microsecond duration has been utilized as a basic chip duration and therefore the amount of power plotted for various values of angle in Figure 7-16 result from annular rings of 1000 feet
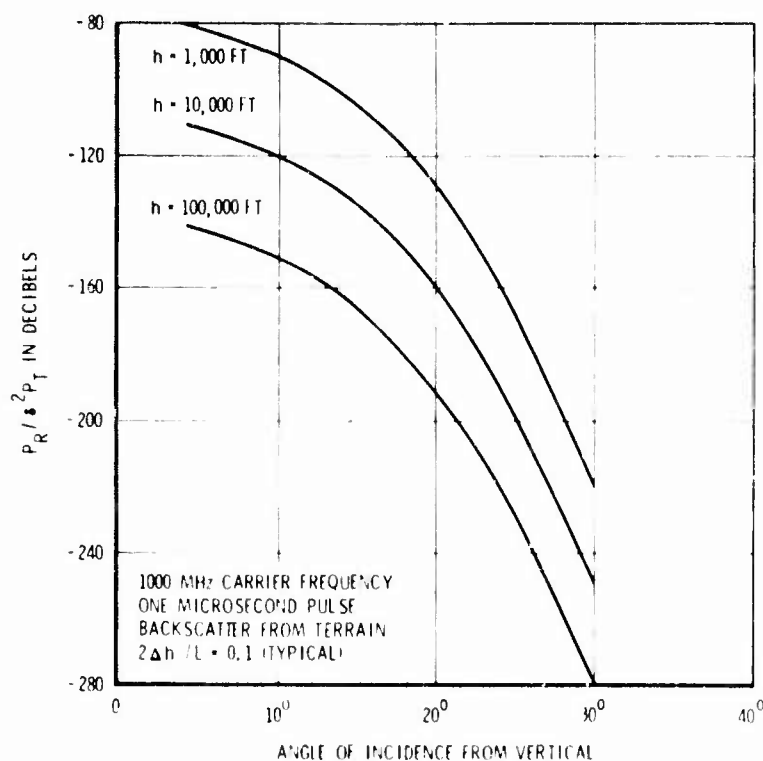
569-1170
UNCLASSIFIED

Figure 7-16. Example of Multipath Persistence

---

*Beckman and Spizzichino, "Scattering of Electromagnetic Waves from Rough Surfaces," Pergamon Press, 1963.

-232-

approximate width. The data for the theoretical back scatter or multipath persistency can be converted into units of time in accordance with the angle of incidence, as follows:

$$\text{Multipath Delay} = 2(h/c) \sqrt{1 + \tan^2\theta} \tag{14}$$

Since the transmitted pulse must be down 150 to 200 db to receive a signal at maximum range (free space loss at 300 miles is 147 db at 1 GHz), Figure 7-16 shows that returns out to an angle of incidence of as much as 25 degrees are significant at 10,000 feet altitude. This corresponds to a multipath delay of approximately 22 microseconds. The situation becomes almost proportionately worse at an altitude of 100,000 feet. Now, the angle of incidence goes out to roughly 20 degrees, and significant returns exist for as long as 200 microseconds. At high altitudes, the maximum delay for which significant returns are received is approximately 2h/c.

4.   Spectral Occupancy: In connection with frequency division schemes, it is important to evaluate the amount of adjacent channel interference produced by pulse transmissions of the type considered for CNI applications. Usually these signaling schemes involve time limited pulse shapes to convey intelligence for ranging information; because of the time limited nature of the pulses, spectrum splatter is created. The effects of spectrum splatter can be reduced by judicious filtering in the transmitter final power amplifier but this technique may require rapid tuning to accomplish the needed filtering. Furthermore, ringing will be produced by restrictive filtering in the transmitter and will create a source of time persistent signals. If we assume for the time being that pulses are emanated from a wideband transmitter with little or no filtering, as in the case of a frequency hopping system, pulses or signaling elements will cause spectrum splatter and be observed in adjacent channels that can be occupied by low-level signals.

The amount of spectrum energy that can appear in an adjacent channel can be determined through a Fourier transform.

$$F(\omega) = \int_{-\infty}^{\infty} f(t)\, e^{-j\omega t}\, dt \tag{15}$$

The results* of the transform are shown in Figure 7-17 and indicate the relative spectrum splatter for a variety of pulse shapes illustrated in Figure 7-17. For convenience, we have taken a 1 microsecond pulse and plotted the frequency spectrum. Figure 7-17 shows that the Gaussian shaped pulse produces the minimum spectrum splatter and that the next best pulse shape is the raised cosine or cosine squared pulse. The square or rectangular pulse produces the greatest spectrum splatter of the pulse shapes considered.

It is theoretically impossible to generate a perfect Gaussian shaped pulse, although approximations have been utilized for radar applications. The generation of raised cosine pulses on the other hand may be more feasible and probably represents the best selection of pulse shape for pulse type CNI waveforms. This conclusion is valid from the standpoint of minimum spectrum splatter; however, from a power economy point of view, that is, from the design of the final amplifier in the transmitter, one would like to have a constant envelope signal for transmission, which would indicate the desirability of a rectangular pulse. Rectangular pulses, as illustrated
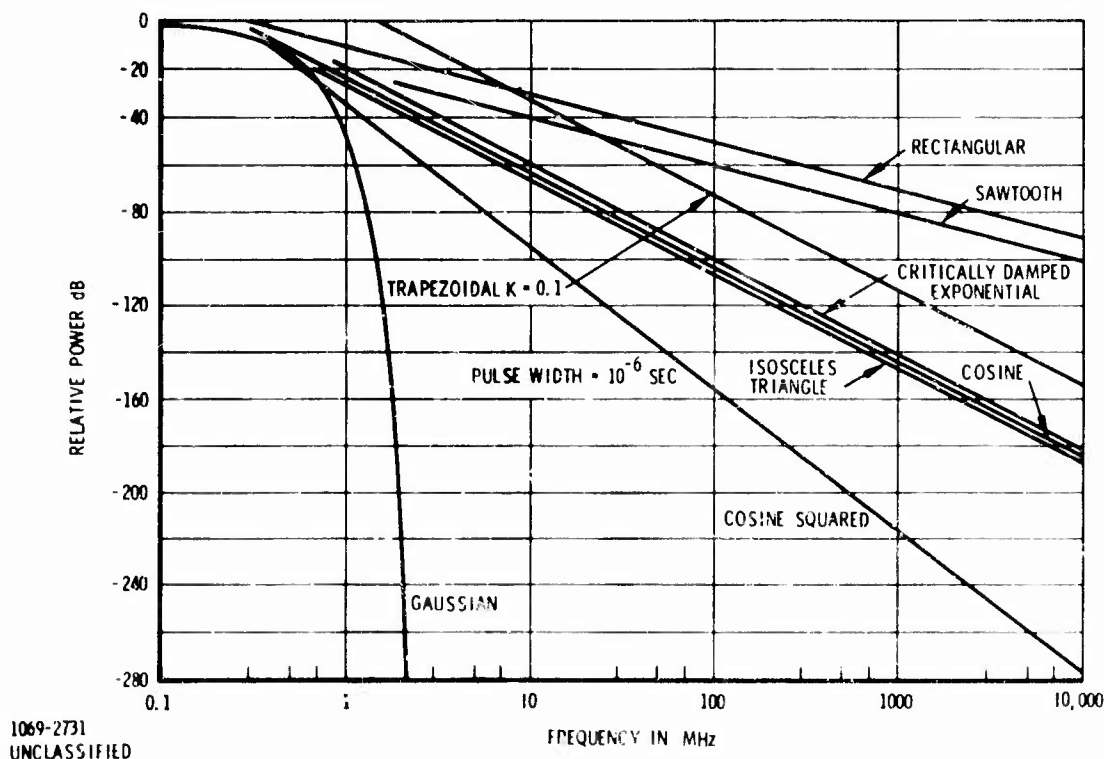
Figure 7-17. Envelope of Spectra of Various Pulse Waveforms

*O.M. Salati, RADC-TDR-63-359, 16 September 1963.

-234-

in Figure 7-17 produce wide spectrum splatter. Thus, we are presented with a trade-off between reducing adjacent channel interference through appropriate waveform design and a power tradeoff in efficiency.

7.2.3 SUMMARY MODEL MULTIPLE ACCESS PERFORMANCE BOUNDS

The generic forms of multiple access waveforms to be discussed are listed in Table 7-1. This table lists the waveforms on the basis of their use of channel time and bandwidth. This categorization describes CNI waveforms in terms of their theoretical best performance and their - usually practical - worst case performance. The best case performance will be given in terms of net capacity; worst case in terms of the situation in which a particular receiver is denied access. Both viewpoints are pertinent. Where possible, quantitative evaluation is made and when hardware implementations are the basic limitations, the critical parameters are discussed and typical attainable values stated.

7.2.3.1 Pseudonoise Modulation

For pseudonoise modulation, the best case multiple access performance occurs when all signals arrive at all receivers in the net with equal power. This situation would be realized in a satellite communication link having perfect power control. Assuming that all accesses have the same data rate, that power control is perfect, and that bandwidth limited operation has been reached, the resulting energy per bit to noise power spectral density ratio (E_b/N_o) for each access is

$$E_b/N_o = B[R(M-1)]^{-1} \tag{16}$$

where

B = the channel bandwidth in Hertz

R = the information rate per channel in bits per second

M = the total number of users in the net

For systems having a large number of users

$$M \approx B[R(E_b/N_o)]^{-1} \tag{17}$$

and the multiple access efficiency, R_{PN} is

$$R_{PN} = MRB^{-1} = (E_b/N_o)^{-1} \text{ bits per sec/Hz} \qquad (18)$$

A representative coding technique that would be employed with a CNI system is rate one-half convolutional encoding with hard-decision sequential decoding. This technique gives a 10^{-5} error rate at an E_b/N_o of 4.5 db for coherent detection. The multiple access efficiency, then, becomes

$$R_{PN} \approx 0.35 \text{ bits per second/Hz} \qquad (19)$$

This multiple access efficiency would provide for 14×10^3 accesses of 2.4×10^3 bits per second each in a 100 MHz bandwidth. The assumption of power control is very restrictive, however.

When significant power variations are encountered, continuous pseudonoise modulation becomes unusable. The allowable power ratio (P_i/P_d) between interfering and desired signals is

$$P_i/P_d = B[R(E_b/N_o)]^{-1} \qquad (20)$$

For the above bandwidth, rate, and E_b/N_o this gives a received power ratio of 42 db. Without consideration of any propagation losses other than range difference, this allows a 100:1 range ratio; the anticipated ratios are at least as great as 2000:1.

It can be concluded, then, that: (1) continuous pseudonoise modulation is not applicable to the direct mode; (2) if it is used in the satellite mode, strict power control would be required to approach the multiple access efficiency stated in Equation (19); (3) since the allowable power ratios are a function of the data rate, very low rates could be supported in the background of other modulations (a command link or the low rate navigation signals are typical).

7.2.3.2 Frequency Hopping

If the system is operated in an uncoordinated manner, the best case operation of frequency hopping the situation is identical to that of pseudonoise modulation. Again

the satellite link is the only practical application. While the model is less obvious,
the performance is again

$$M \approx B[R(E_b/N_o)]^{-1}$$

If noncoherent detection and an efficient coding scheme are employed, the required
E_b/N_o is about 8 db. The resulting multiple access efficiency is

$$R_{FH} = 0.16 \text{ bits per second/Hertz} \tag{21}$$

If it is assumed that the frequency hopping system operates in a coordinated
manner, significantly better multiple access can be obtained. With both time and
power coordination, the frequency hopping system can achieve the multiple access of
standard frequency division multiplex. Because orthogonal waveforms are now
employed, the lack of self-interference makes the multiple access efficiency a
function of the power available, if complete orthogonality and coherent M-ary signal-
ling are assumed. When the intersymbol interference effects of narrowbanding are
ignored the multiple access capability becomes

$$R_{FHC} = \log_2 m \tag{22}$$

where
    m = the number of phases used in the signaling alphabet.

A representative system would employ quadriphase modulation and thus obtain a
R_{FHC} of 2 bits per second per Hertz.

The worst case performance of a frequency hopping is again set by the variation
in received signal power. For frequency hopping systems, however, the tolerable
variation is a function of hardware parameters. Some limitations on such a system
are considered here.

One requirement for operation in the CNI environment is to receive navigation
and data messages while transmitting. If this is done in a common band, the hardware
problems associated with continuous frequency hopping become very significant. In
Volume I, RF preamplifiers are discussed. Transistor amplifiers are shown

to have good linearity and strong signal characteristics. Such amplifiers have typical 1 db compression input levels of -20 dbm and a maximum tolerable input of 20 dbm. Thus, for a 1 kilowatt transmitter, 80 db of isolation would be required for linear operation and 40 db would be required for protection from destruction. Because of the coverage patterns required such isolation is difficult to obtain on an aircraft.

Frequency hopping systems are particularly susceptible to the proliferation of signals caused by nonlinearities in the receiving systems. A multiplicity of strong signals producing numerous third and fifth order intermodulation products can effectively saturate the access to a particular receiver. Quantitative evaluation cannot be generalized since the effects are set by RF preamplifier, down converter, and IF linearities, which are drastically affected by the type of AGC employed. Table 7-3 shows the intermodulation products that result if the third and fifth order products have levels significant enough to provide interference. From the expressions shown in the table for the total number of each order, the number of interfering frequencies can be computed. Assuming that all the fifth order intermodulation products are significant, three strong input signals provide 27 interfering signals; five strong inputs produce 255 interfering signals.

Table 7-3. Intermodulation Products in Fundamental Zone

Order	Form	Total Number
1	A	N
3	A + B - C	$N(N-1)(N-2)/2$
	2A - B	$N(N-1)$
5	A + B + C - D - E	$N! \, (12(N-5)!)^{-1}$
	A + 2B - C - D	$N! \, (2(N-4)!)^{-1}$
	A + B + C - 2D	$N! \, (6(N-4)!)^{-1}$
	A + 2B - 2C	$N(N-1)(N-2)$
	3A - B - C	$N(N-1)(N-2)/2$
	3A - 2B	$N(N-1)$
Sum	First	N
	Thirds	$\dfrac{N^3 - N^2}{2}$
	Fifths	$N^2(N^3 - 2N^2 + 5N - 4)/12$

Good receiver linearity under wideband conditions with an input including a sum of moderately strong signals will produce intermodulation products that are 70 to 100 db down from the individual inputs. Thus, the power in the intermodulation is significant in the environment considered where a weak signal from a distant transmitter must be received with the strong signals present.

The problem of strong signals causing significant bandwidth occupancy can also be considered in terms of the actual bandwidth of the frequency hopping pulse. In the previous section it was shown that the worst pulse shape from a spectral occupancy viewpoint is the rectangular pulse, which is the most efficient from a peak power viewpoint. The $\sin^2 x/x^2$ power spectrum is only 50 decibels below the transmitted power in the intended channel at a distance of 100 channels. The cosine shaped pulse is 100 decibels down at this point, but even that is not sufficient to prevent a nearby transmitter from blocking 200 channels from access by a weak signal.

For best case operation, uncoordinated frequency hopping provides performance only slightly degraded from that of pseudonoise. The degradation is largely due to the assumption of noncoherent detection which raises the E_b/N_o needed. When operated in a coordinated manner using coherent demodulation, the multiple access capability is essentially that of FDMA. A representative rate based on quadriphase PSK is 2 bits-per-second per Hertz. The worst case situation for frequency hopping involves variation in signal strength as did pseudonoise modulation. The quantitative evaluation is not straightforward, however. Antenna isolation, receiver linearity, and transmitter noise power all could set the performance limits. In any case, it is concluded that continuous use of frequency hopping is not applicable to the direct mode of operation for CNI.

7.2.3.3 TDMA

Like idealized coordinated frequency hopping, the TDMA system operates with truly orthogonal signals in the best case. No power control is required, but for best case operation, the net timing must be maintained to eliminate the requirement for significant guard times. In practice, this is most easily achieved in the satellite mode again. However, if sufficiently long pulse durations are employed, the effects of any required guard times can be made negligible. Best case performance is a function of

the signal power available, but again the representative case of quadriphase coherent signaling leads to a multiple access rate R_{TDMA} = 2 bits/second per Hertz.

Worst case performance of the TDMA multiple access characteristics is determined by the uncertainty in arrival time of significant power amounts. Two factors are involved. First is the uncertainty in the arrival time for the direct transmission. Secondly, the memory of the channel must be considered. In the direct mode of operation the uncertainty in time both of arrival and the channel memory are 1.8 milliseconds. A guard time that would ensure orthogonal signaling in the direct mode, would then be 1.8 milliseconds.

The efficiency of a TDMA system is a function of the ratio between the transmitted pulse duration and the guard time. The efficiency, ρ, becomes

$$\rho = \left(1 + \frac{t_G}{\tau}\right)^{-1} \tag{23}$$

where

τ = the transmitted pulse duration

t_G = the guard time

Equation (23) is plotted in Figure 7-18 to show the effects of the variation in the ratio, t_G/τ. Figure 7-18 shows that a pulse on time of around 20 milliseconds would be required to obtain a .9 efficiency if a 1.8 millisecond guard time for the direct mode was employed. Further, pulse times below 10 milliseconds would cause significant degradation in efficiency. The cost of such long burst times is long frame times and the associated storage and turn-around lags.

A generalization of the TDMA concept employs frequency channelization and pulse-by-pulse frequency hopping. This waveform structure is identical to the coordinated frequency hopping and the TDMA multiple access under best conditions. These conditions now require simultaneous timing and power constraints. As before, timing can usually be solved by long pulse durations. The power problem becomes even more severe, however. Since the number of channels is reduced in direct proportion to the duty factor of the TDMA, intermodulation products and spectral splatter become a severe problem. If the total number of channels is 100, even the cosine squared

-240-
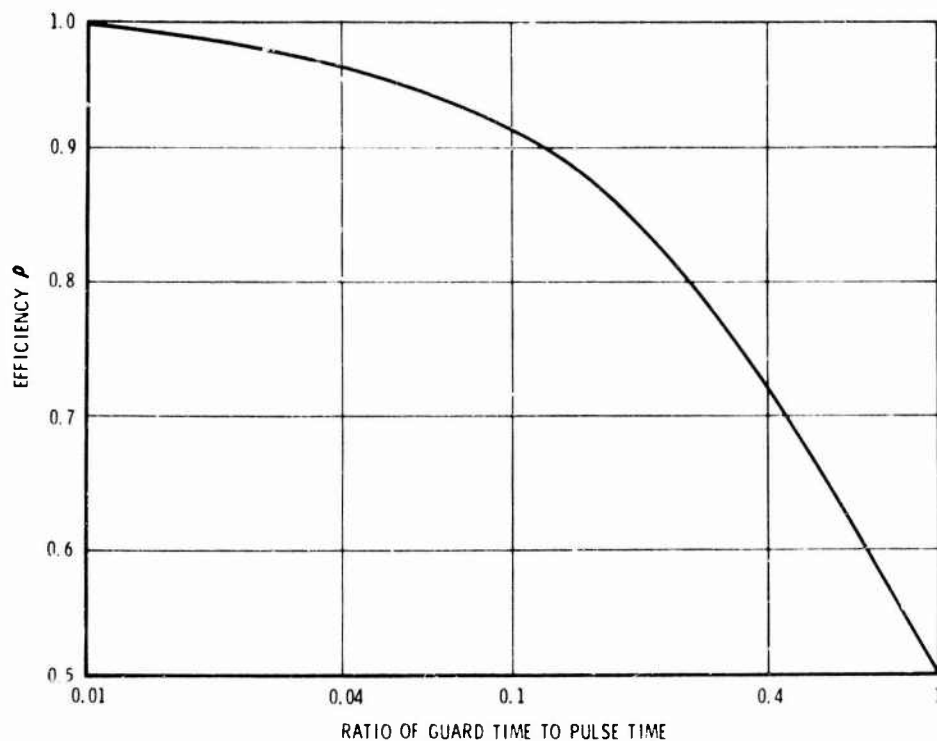
Figure 7-18. Effects of Guard Time of TDMA Efficiency

waveshape, which is down 100 db at 10 bandwidths, will give intolerable interference in the direct mode. If the cosine pulse is used - and the spectral characteristics of the cosine pulse will be very difficult to better - a single near transmitter will blank all frequencies received from a distance.

For best case operation of TDMA, then, the full multiple access of truly orthogonal waveforms is easily obtained. No restrictions are imposed by power variations, but timing control is required. The worst case performance results from timing uncertainties. With sufficiently long burst times, however, the TDMA waveform can operate arbitrarily close to the maximum performance. The hybrid TDMA-FH waveform suffers in the worst case from spectrum splatter. As discussed above, however, in the worst case, the TDMA performance is still attained for this waveform.

7.2.3.4 Time Hopping

Best case for asynchronous multiple access techniques using low duty factor waveforms is a memoryless channel and a geometric distribution such that interfering signals are equally likely to be greater or less than the desired signal. Power levels are considered sufficient to ignore background noise interference. To compute the number of active users that the system can handle under these assumed best case conditions, it is convenient to consider as an approximation that a desired pulse either is received completely overlapped by interfering pulses or it is received in the clear. This amounts to the assumption of quantization in time to increments of the duty factor. As described above, if the pulse is contaminated, the resulting error rate is 0.5 half the time and 0 half the time.

Using the above representation of the best case, the probability of error for the time hopping system is approximately

$$p_e \approx 0.25\, p_h \tag{24}$$

where

p_h = the probability that the desired pulse is hit by other pulses

The quantity p_h can be evaluated as

$$p_h = \sum_{i=1}^{M-1} \binom{M-1}{i}\left(1-d\right)^{M-1-i} d^i \tag{25}$$

where

M = the total number of users in the net

d = the waveform duty factor

For reasonably small duty factors, Equation (25) gives an approximate expression for the number of users as a function of the tolerable probability that a pulse is hit

$$M \approx p_h d^{-1} \tag{26}$$

This approximation is equivalent to saying that events consisting of more than one interfering pulse can be neglected. This situation reinforces the previous assumption that desired and interfering signals are equally likely to be the greater.

Equations (24) and (26) then show that

$$M \approx 4 p_c d^{-1} \tag{27}$$

for the range in which the approximation leading to Equation (25) is valid. For a required error rate of 0.05, typical of the threshold for rate one-half error correcting coding for 10^{-5} error rate, the number of users becomes $.2d^{-1}$. Since the minimum duty factor can be considered to be 2R/B because of the rate one-half coding, the multiple access efficiency becomes

$$R_{TH} = MRB^{-1} = 0.1 \text{ bits per second/Hertz} \tag{28}$$

A 100 MHz channel and a 2.4 K bits per second rate can operate at a duty factor of $d = 5 \times 10^{-5}$. The number of users in this case is 4000.

The worst case for the time hopping system in the direct mode is, as with TDMA, severe pulse stretch and multiple pulse reception due to channel memory. Equation (26) shows that the tolerable number of users is inversely proportional to the pulse duty factor. The channel memory creates an effective increase in duty factor. Typical implementations of the time hopping concept employ pulse durations of between 1 and 10 microseconds. The 200 microsecond pulse stretch mentioned earlier would, then, greatly reduce the multiple access efficiency of such a system. For a .05 duty factor using 10 microsecond pulses, the user capacity drops from 2000 for the best case to 100 for the 200 microsecond pulse stretch case. If a 50 microsecond pulse is used, however, the decrease is only to 400. Thus, as in the case of TDMA, the pulse stretch problem is ameliorated by the use of longer pulses.

Performance of the TH system in the remote mode is developed in Section 7.3.5.1. The power limited case was presented and it was shown as a result of the necessary compromise between reduced duty factor and increased energy the multiple access efficiency is reduced. The results show a 14 decibel reduction in performance relative to that attainable using coordinated access to the satellite.

The generalization to the TH-FH system similar to that described for the TDMA has shortcomings revolving around the large signal power differentials and the wide spectrum occupancy.

The time hopping system shows a multiple access efficiency comparable to that of the other noncoordinated waveforms. Pulse stretch forms the worst case and long pulses are required to reduce this problem. Performance in the remote mode is reduced and thus TH/PN is not recommended for this application. A waveform based on time hopping is the only noncoordinated one considered applicable to the direct mode of CNI.

7.2.3.5 Conclusions

The examination of worst case generic modulations has led inexorably to the conclusion that the CNI environment can be accommodated In the direct mode only with a waveform that uses time intermittently. The continuous modulations simply cannot handle the near/far dynamic range. In the remote mode, continuous modulations introduce power control requirements, and these are considered undesirable operational constraints or hardware complexity (e.g., a highly channelized satellite repeater).

In performance aspects, some form of TDMA clearly is the best choice if the practical matters of coordination and buffer storage for long frame times can be accepted. Otherwise, noncoordinated time hopping may be retained as a candidate for the direct mode. The performance loss in the remote mode is so severe, however, that TDMA (i.e., coordinated orthogonal modulation structures) is indicated for this mode.

7.2.4 MULTIPLE ACCESS SIMULATION

A means for providing another evaluation of multiple access capacity is through simulation. The simulation described here is limited to the TDMA waveform described earlier that uses parallel channels to extend bandwidth occupancy rather than providing completely orthogonal slots on a time basis. The simulation is used to evaluate the influence of the fact that because of the pulse spectral occupancy, the parallel channel system no longer has truly orthogonal assignments.

The Monte Carlo simulation creates a geometric distribution of terminals within a circle of arbitrary radius. The number of active terminals is selected, as is the minimum distance. The terminal positions are selected from a uniform distribution over the circle area. To provide this distribution, independent uniformly distributed random numbers are selected for x and y coordinates of a terminal position.

-244-

If the selected position is within the circle, and is not within the minimum distance of another terminal previously positioned, tne x and y coordinates are accepted and another pair is developed. Otherwise new coordinates are developed for the terminal until the tests are passed. This continues until all terminals are positioned.

Once the terminal positions have been determined, half of them are assigned the roles of transmitters, half as receivers. The simulation of system operation is then undertaken. For each of the transmitters, a time-frequency cell is randomly selected. Independent, uniformly distributed random numbers are used to provide both the time and the frequency dimension of each time-frequency cell. A test is made to assure that exclusive time frequency cells are assigned to each transmitter. If the test fails, new random numbers are selected, cell generated, and test made. This process is continued until each transmitter has been assigned an exclusive time frequency cell within the total time frequency matrix.

The energy to noise power spectral densities are developed in the following way. First, the transmitted energy per bit is assumed to be independent of the number of time slots employed. Pulse transmitters are, therefore, assumed that maintain constant average power by increasing the peak power as the duty factor is decreased. The transmitted energy is then the product of the average power divided by the average bit rate. The received energy is just the transmitted energy attenuated by the path loss.

It is assumed that the interference can adequately be modeled as Gaussian noise. The power spectral density contributed by each interferer is a function of the duty factor, the channel separation, the spread factor, and the distance between terminals. The interfering power spectral densities are treated as if the interference is white Gaussian noise. The level of interference is taken to be the average value of the spectral density over that portion of the interfering spectra that coincides with the primary band of the desired signal. Thus,

$$N_i = \frac{P}{DC^2} \int_{C(N-1)}^{C(N+1)} df \, \frac{\sin^2(2\pi fT)}{(2\pi fT)^2}$$

-245-

where

N = number of channels between desired and interfering channel

C = the channel separation in Hertz

f = the frequency in Hertz

T = the signaling bit duration in seconds

D = the duty factor

P = the average power in watts

The quantity D affects the interference intensity since it is assumed that the peak power employed is inversely proportional to the duty factor.

The received interference is computed for each transmitter-receiver pair by summing the interference produced by all other transmitters that are on in the time slot with the transmitter being considered. Channel separations are computed, the transmitted density looked up, and the attenuation associated with the interferer to receiver path used. The interference from each interferer is summed with an assumed background noise of -204 dbw per Hertz to obtain the resulting noise power spectral density.

The simulation then determines the received energy to noise power spectral densities (E_b/N_o) for all possible transmitter-receiver combinations given the selected time frequency assignments. The bit error probabilities are computed and stored in a two dimensional array that contains the error probability for all possible transmitter-receiver pairs. The error probability is computed assuming completely coherent detection in the present simulation program.

Once the above error probabilities have been computed and stored, a new time frequency assignment is made. The terminal positions remain fixed, but new assignments are made just as they would be in a subsequent time period in an actual system. With this new set of assignments, the error probabilities are again computed and the new values are added to the previous values in the array accumulating error probabilities. New time-frequency assignments are repetitively made and the results stored until representative data has been collected. The results in the accumulator array are then normalized by the number of iterations and the array then contains the average probability of error for each transmitter talking to each receiver. When the error rates for a given geometry are established, a new geometry is selected and

the error rates determined again. The final data, then, represent the results averaging over a selected number of geometries and time frequency. Figure 7-19 shows typical results of this simulation when the average error rate is plotted as a function of the communication range. The waveforms shown in Figure 7-19 all employ 21 MHz; fifty time slots are employed with 10 allowed frequencies. At a bit rate of 4.8 kbps the bandwidth occupancy results from a pseudonoise spread factor of eight. The upper curve in Figure 7-19 represents results when 40 users are active. The lower curve represents use by 20 users. The curves represent, then, a multiple access efficiency of 2 and 1 user per megahertz.
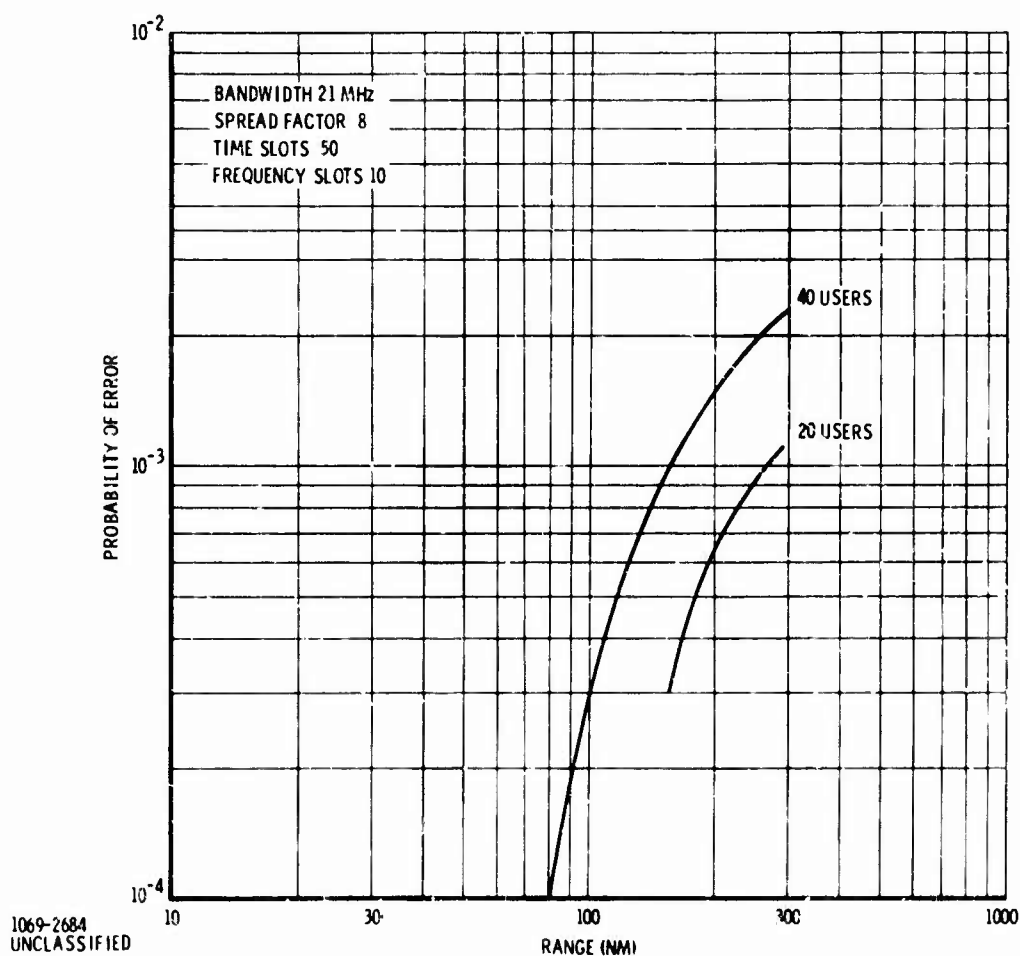
Figure 7-19. Average Probability of Error as a Function of Range

-247-

In Figure 7-19, the upper curve also represents the performance for a system
that is identical to the one described above except that the time bandwidth product is
divided into 10 time slots and 50 frequency slots. For the simulation in Figure 7-19
allowing a maximum 300 nautical mile range, no difference was discernable between
these two systems. In another simulation with range constrained to a 150 nmi maxi-
mum range, a slight bias in favor of the 50-10 system was developed. These results
are plotted in Figure 7-20. The simulation is identical to the previously described
system except that the range is constrained to 150 nmi. The maximum average bit
error rate is only slightly higher than for the 300 nmi system. At shorter ranges,
however, the error rate in the more constrained system is about three times that of
the larger system. The increased density is the cause.
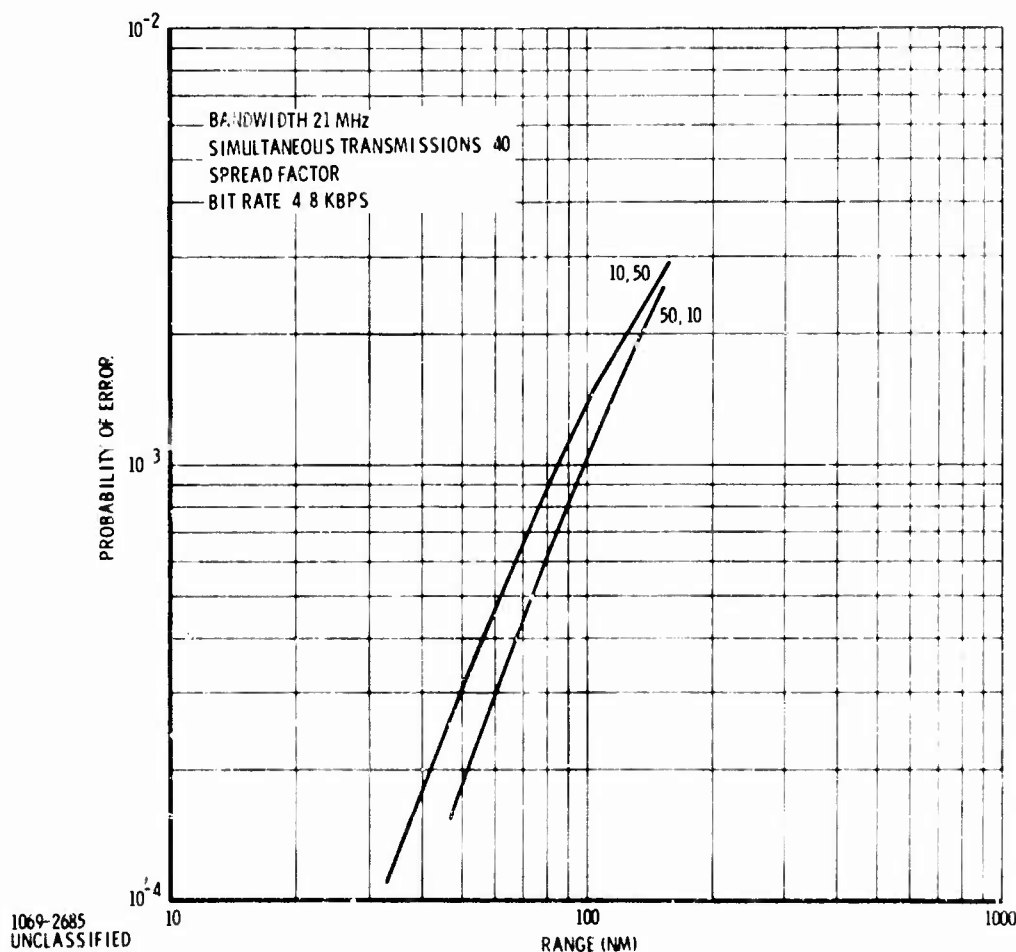
Figure 7-20. Average Error Rate Performance for Different
Time, Frequency Matrices

Figure 7-21 shows net performance when the spread factor is reduced from the factor of 8 previously employed. The higher error rate 150 nmi range limit was employed as were the original 40 users. The total bandwidth is reduced with the spread factor.

The maximum average error rate for a spread factor of 1 was 0.013 and the bandwidth occupancy was 2.5 MHz. This error rate performance is not completely realistic because the simulation models the interference as noise. Without the spreading pseudonoise the noise-like interference model is not adequate. With this reservation, Figure 7-21 shows good average error rates all the way up to 16 users per megahertz.
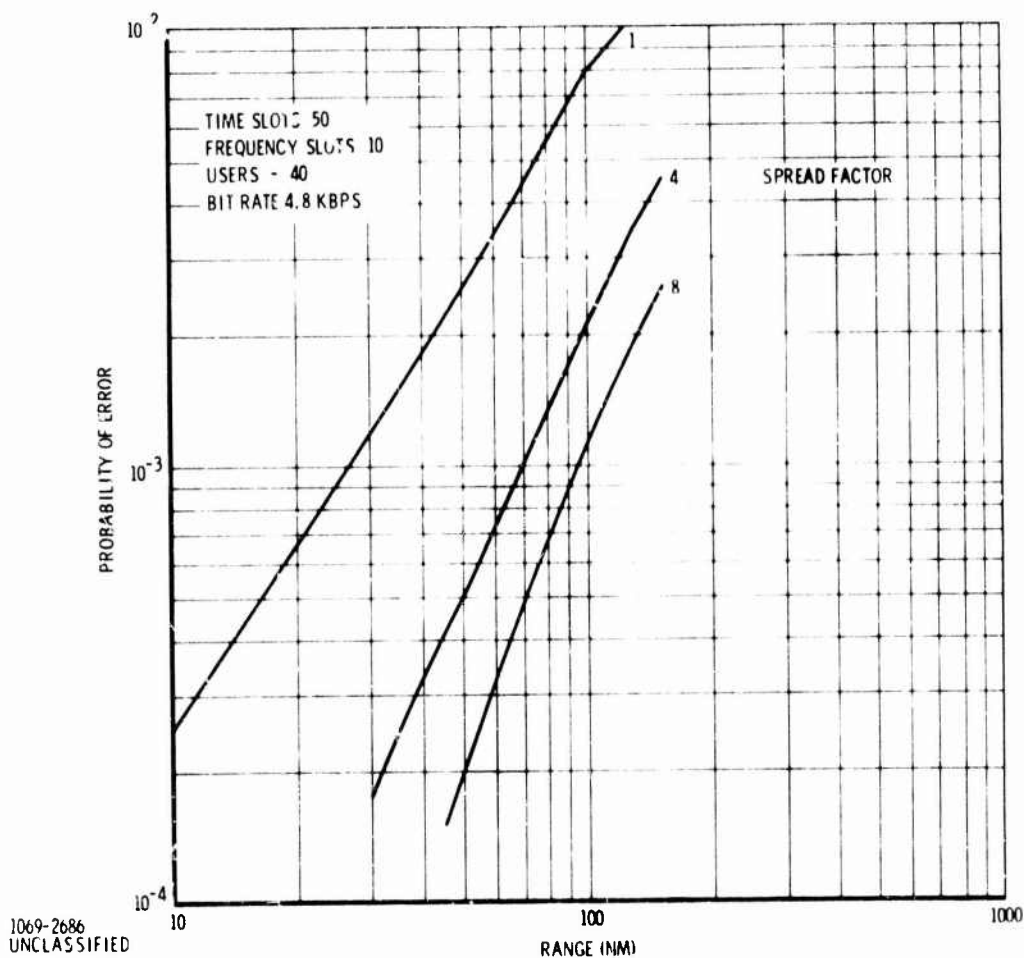
Figure 7-21. Average Error Rate Performance
Different Spread Factors

-249-

All of the previous result discussion has been oriented towards performance description in terms of average error rate for all aircraft at a given range. Ai other useful parameter is the probability that the same threshold probability of error is exceeded. Figure 7-22 shows this parameter as a function of range. The threshold is taken as 0.045. The results in Figure 7-22 are based on somewhat limited statistics, but the trends are well established in the figure. For the systems employing a spread factor of 8, a 0.99 reliability of communications is realized. The probability of outage goes up quickly if the spread factor is reduced.
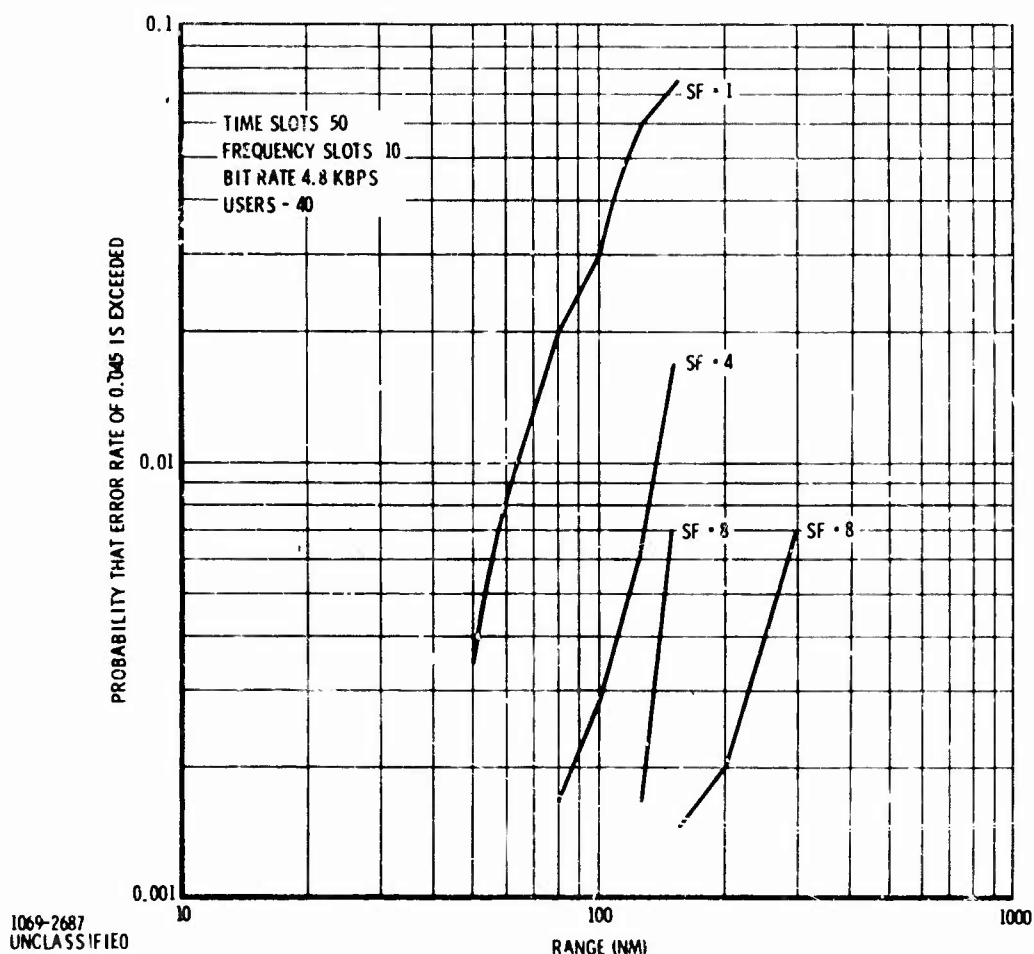
Figure 7-22. Probability that Error Rate Exceeds 0.045

-250-

This simulation, while dealing with a significantly scaled down version of the net to facilitate computation, has shown that a coordinated system employing a basic TDMA system with contiguous parallel channels can be expected to give good performance for the randomly located terminal model. The 100 MHz system, linearly extrapolated from the 21 MHz system, shows that a minimum of 200 users could be accommodated with outage probability less than 0.01. This performance is achieved using the spectral occupancy of the $\sin^2 x / x^2$ spectrum. Filtering would improve performance; only range difference power variations were considered, however. Finally, the required 10^{-5} error rate was achieved using an encoding process that requires 0.045 error rates at rate one-half to achieve the desired performance.

7.3 MODULATION AND CODING FOR MULTIPLE ACCESS AND ANTIJAM

This section presents performance comparison of various coded waveforms with respect to their theoretical multiple access and antijam characteristics. By theoretical it is meant that with frequency slotting, as a typical example, there is ideal orthogonality; i.e., the limitations of near/far dynamic range are not brought in here. Similarly, with time slotting, the transmitter is assumed to have the capability to increase peak power inversely with duty factor, and no time overlap occurs.

7.3.1 THEORETICAL SEQUENTIAL DECODER PERFORMANCE

The simplest demodulation-decoding combination for CNI implementation utilizes hard binary decisions on the received coded digits, which are the input to the decoder. It is desirable to know what performance is theoretically feasible by utilizing quantized amplitude information from a binary PSK demodulator over a nonfading channel with jamming. The value of R_{comp} for each of the respective channels and E/N_0 operating point is the basis of performance comparison; this implies use of sequential decoding implementation schemes[*].

Although continuous interference or jamming (i.e., white Gaussian noise) is of primary interest, the analysis has also considered intermittent strategies (corresponding to pulse jamming of a PN waveform or partial band jamming of a FH/PN waveform). The point of view is adopted here that the worst (minimax design) case is presumed, considering choice of communicator's and jammer's strategies.

7.3.1.1 Measure of Performance

For the present analysis, the jammer's choice of strategies is presumed to be confined to use of Gaussian noise with pulse and partial band coverage, maintaining a fixed average power independent of duty factor or fraction of total channel bandwidth occupied. It is evident that this represents an idealization appropriate for a first-look comparison, and a sophisticated analysis should characterize the jammer in a more realistic manner. Furthermore, the basic postulate is made that the channel is effectively made memoryless by the use of random interleaving over a long duration in which the jammer is statistically stationary. As a result, each digit of the signal can be assumed to be independently perturbed by the jamming.

---

[*] K. Jordan, "The Performance of Sequential Decoding in Conjunction with Efficient Modulation", IEEE Trans on Comm. Tech., June 1966, pp 283-297.

The ratio of average jamming power to signal power can be characterized by the parameter E/N_0, where

$$E = \text{signal energy per digit}$$

$$N_0 = \text{average jamming power per Hz}$$

For digital transmission at the rate R, expressed as bits per digit, the normalized parameter

$$E_b/N_0 = (1/R) \cdot E/N_0 \tag{29}$$

is defined to facilitate comparing performance of different combinations of modulation and coding. For a fixed E/N_0, the jammer can arbitrarily choose duty factor = k. This represents his choice of strategies and can be extended in a direct manner to include partial time and bandwidth occupancy, more generally for FH/PN waveforms.

Equation (29) may be applied as a first-look approximation to estimate performance for sequential decoding by setting $R = R_{comp}$. It is also of significance with block codes if R is equal to the transmission rate for the block code (expressed as bits per digit).

7.3.1.2 Amplitude Quantized PN/PSK Channel

For purposes of analysis, the coherent pseudonoise channel with PSK modulation is presumed to yield, for each transmitted digit, a demodulated output amplitude referenced to the jamming power occurring over the duration of that digit. The jammer's strategy of interest is duty factor k.

It is assumed here for simplicity that a perfect carrier reference is available for coherent demodulation. Consequently, the output amplitude v for ideal integrate-and-dump demodulation has the probability density, conditional on a positive or negative digit being transmitted,

$$p(v/\pm 1) = (1 - k) \delta (v \mp \infty) + \frac{k}{\sqrt{2\pi}} \exp \left[- (v \mp \sqrt{2kE/N_0})^2 /2 \right] \tag{30}$$

the delta function arises from the normalization by jammer power, which instantaneously is zero during the jammer's off interval.

A practical system will necessarily quantize the output amplitude to enable storage prior to de-interleaving, examples being

- Binary Quantization (Hard Decision)
- Tertiary Quantization (Null Zone)
- Four-Level Quantization (Double Null Zone)

These are representative of increasing conceptual difficulty, since tertiary quantization involves optimization of null-zone threshold, and four-level quantization in addition involves optimization of the decoding metric.

The applicable formulas can be derived from Equation (30) to be

Binary
$$R_{comp} = 1 - \log_2 \left(1 + 2 \sqrt{p(1 - p)}\right) \tag{31a}$$

p = probability of error

Tertiary
$$R_{comp} = 1 - \log_2 \left(1 + 2 \sqrt{p(1 - p - w)} + w\right) \tag{31b}$$

p = probability of error

w = probability of null

Four Level
$$R_{comp} = 1 - \log_2 \left(1 + 2 \sqrt{p(1 - p - w - v)} + 2 \sqrt{wv}\right) \tag{31c}$$

p = probability of error

w = probability of incorrect null

v = probability of correct null

The various transition probabilities depend on the value of duty factor k and null threshold setting, and are obtained from the probability density of Equation (30).

The minimax concept may now be applied to maximize R_{comp} by choice of null threshold while the jammer attempts to minimize R_{comp} by choice of duty factor. Actually the binary case does not involve a minimax calculation, since the only variable is duty factor, and the problem reduces simply to maximization of p by choice of duty factor. If this is done, the result is

$$p = \frac{0.083}{E/N_0} \quad E/N_0 > -1.6 \text{ db} \tag{32}$$

for the worst case duty factor. Below the region of Equation (32), the jammer's duty factor is unity for computing p.

The performance results are presented in Figure 7-23, along with the theoretical curve for an unquantized output. The latter can be shown to be given by

$$R_{comp} = 1 - \log_2 \left(1 + k e^{-kE/N_0}\right) \tag{33}$$

where k, again, is to be selected to minimize R_{comp}. Also shown in Figure 7-23 is the result for binary demodulation with continuous jamming, rather than the worst-case pulsed which yields Equation (32).

For a hard decision, rate- 1/2 sequential decoder, the channel error probability at $R_{comp} = 0.5$ is the significant performance parameter. From equation (31a), or alternatively through Figure 7-23, the channel error probability is p = 0.045. Hence, in terms of channel errors, this indicates the design objective for specialization to these decoder basic parameters. The performance actually attained with simulations is given in Section 7.3.2 for this decoder.

The minimax optimization of the four-level case is presented in more detail in Tables 7-4 and 7-5. The decoding metric is determined from the maximum likelihood demodulator for each digit. The logarithm of the likelihood function is convenient because the decision for a code word is then based on the sum of the log likelihood over the digits of the word. This decoding metric is shown in Table 7-4, where p, w, and v are determined for the minimax values of duty factor and threshold at each E/N_0. Of course, only the relative magnitudes of the differences are actually significant.

The meaningfulness of this choice of threshold and decoding metric should be noted[*]. The jammer strategy, within the allowed constraints of pulse jamming and average power denoted by E/N_0, cannot prevent satisfactory decoding for the R_{comp} of Table 7-4, if the threshold settings of that table and the decoding metric of Table 7-5 are utilized.

---

[*] I. G. Stiglitz, "Coding for a Class of Unknown Channels, "IEEE Trans. on Info. Theory, April, 1966, pp. 189-195.
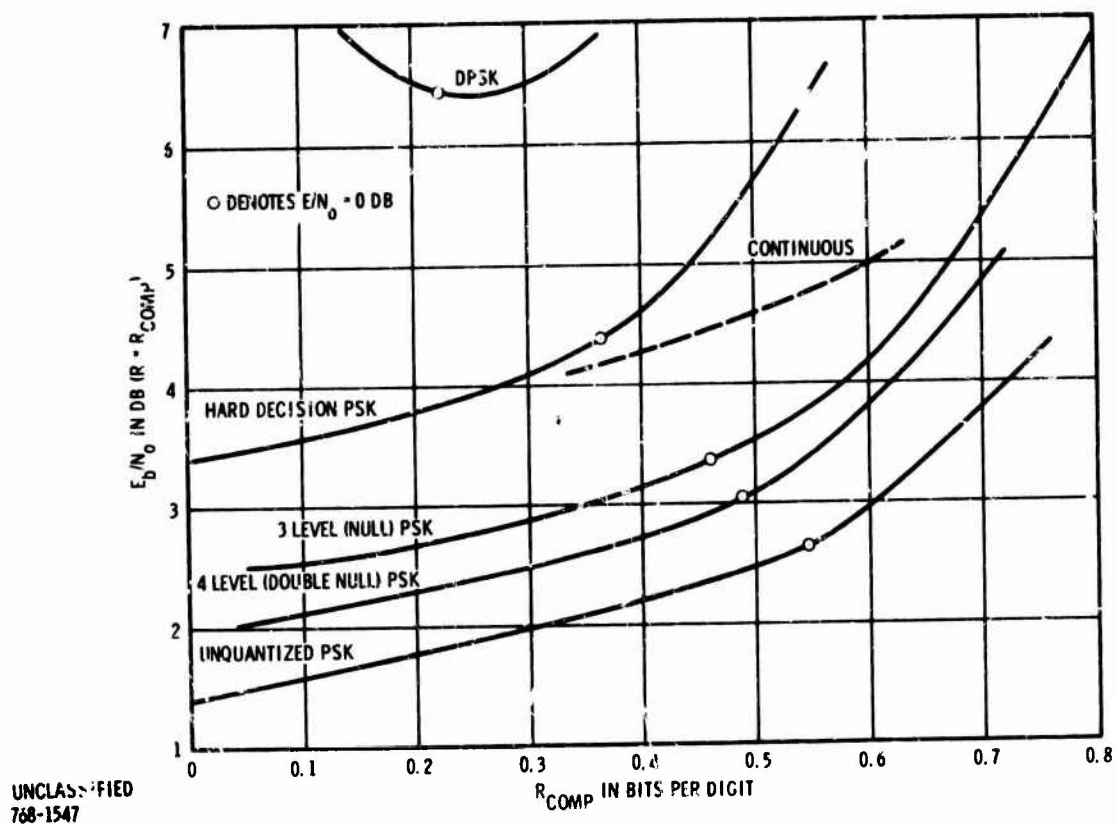
Figure 7-23. Comparison of Performance for Minimax
Design Pulse Jam

Table 7-4. Minimax Strategies, Four-Level Quantization

E/N_o (db)	R_{comp} (Bits/Digit)	Duty Factor	Normalized Threshold
6	0.824	0.27	1.28
3	0.691	0.48	1.12
0	0.494	0.86	0.87
-3	0.283	1.00	1.01
-6	0.1508	1.00	1.40
-9	0.0779	1.00	1.97

Table 7-5. Decoding Metric, Four-Level Quantization

Received Digit	Decoding Metric
Correct	$\log(1-p-w-v)$
Correct Null	$\log v$
Incorrect Null	$\log w$
Incorrect	$\log p$

The performance of coherent PSK systems will now be compared with that of a differentially encoded system (DPSK). Equation (31a) applies provided that the probability of error for DPSK, given by

$$\text{DPSK probability of error} = 2p(1-p) \tag{34}$$

replaces p in the equation. Again the minimax concept leads to finding the worst case jammer duty factor k which maximizes probability of error in Equation (34) It is found to be given by

$$\text{Probability of error} = \frac{0.147}{E/N_0} \quad \text{for } E/N_0 > -0.7 \text{ db} \tag{35}$$

with k = 1 for lower values of E/N_0.

The result of DPSK is also plotted in Figure 7-23 and it is observed that a minimum of E_b/N_0 occurs as a function of R_{comp}, roughly at $E/N_0 = 0$ db This minimum is degraded approximately 2.5 db from the hard-decision coherent PSK system operating at the same R_{comp}.

It is concluded that the DPSK system is considerably inferior to the coherent PSK system using hard decisions (as measured by E_b/N_0); however, some of the differential is used up by the need for a transmitted reference with the latter to resolve the 180° phase ambiguity. The further conclusion is reached that a significant performance gain (approximately 1.5 db) is available with PSK by the expedient of going to four-level quantization from binary hard decision. However, this involves the additional complexity of threshold adjustment. The improvement beyond four-level is seen to be marginal, and can be obtained only by providing additional storage and complexity.

Further note that there is also only a marginal improvement in performance (E_b/N_o) associated with operation at E/N_o less than 0 db. Hence, it appears that a rate in the range $0.25 \leq R \leq 0.5$ represents a practical design. Lower rates actually will lead to degradation due to difficulty of maintaining coherent demodulation.

7.3.1.3 Noncoherent DPSK Channel

For CNI, there is interest also in noncoherent DPSK (to be contrasted with differentially encoded PSK described above), since an allowance for Costas loop reacquisition is then unnecessary after hopping to a new frequency slot. The hard decision probability of error for continuous jamming is well known to be

$$p = 0.5 e^{-E/N_o} \tag{36}$$

and for intermittent jamming, the worst case is found to be

$$p = \frac{0.184}{E/N_o} \tag{37}$$

for $E/N_o > 0$ db. Equation (36) applies for $E/N_o < 0$ db. At $E/N_o = 1.4$ db, it is found that $R_{comp} = 0.25$, and therefore $E_b/N_o = 7.4$ db, and this is the minimum. This result shows one db degradation compared with performance of differentially encoded PSK, displayed in Figure 7-23.

Amplitude quantizing is possible with noncoherent DPSK directly on the non-limited product demodulator output, given by

$$v = \text{Product Demodulator Output} = V_1 V_2 \cos(\theta_1 - \theta_2) \tag{38}$$

where V is the envelope and θ is the phase of each digit as received with noise present. From the results on the coherent channel, four-level quantization appears the most practical candidate to study. The decision regions are defined by decision thresholds at $\pm v_{threshold}$, in addition to the usual polarity decision.

A direct computation of the transition probabilities for a given $v_{threshold}$ does not seem feasible in tabulated form. An empirical computation may be obtained by Monte Carlo simulation of the product demodulation process, following which an approximate value of the performance improvement with quantized demodulation is obtained.

-258-

The evaluation was restricted to continuous jamming. The roughly optimum threshold setting to maximize R_{comp} is found to be 0.5 of signal amplitude, obtained by testing different values and empirically measuring the transition probabilities to compute R_{comp}. As a typical result, at $E/N_0 = 3$ db, R_{comp} was determined to be in the range 0.5 to 0.53, the scatter being due to statistical fluctuations of finite-time averaging. Since R_{comp} with hard decisions is 0.41 for this E/N_0 (continuous jamming), the improvement by going to 4-level demodulation is seen to be approximately one decibel. Thus, the improvement is roughly comparable with that previously computed for coherent PSK. Note, however, that even with the improvement realized by going to the complexity of 4-level demodulation, noncoherent DPSK still does not outperform differentially-encoded PSK.

7.3.2 SEQUENTIAL DECODER SIMULATION

As shown in Section 7.3.1, the performance of sequential decoding has great potential value when applied to a CNI system. Therefore, sequential decoding algorithms were investigated and corresponding sequential decoders simulated. The emphasis in the investigations was to determine how effective a sequential decoder could be when designed to minimize cost at the expense of memory and performance criteria. The interest in this sequential decoder design was caused by its prospective applicability to applications wherein low data rates will be communicated over the channel.

A significant parameter of a sequential decoder is the desired bit error rate out of the decoder. Because of the desire to use these decoders for a variety of input data requiring somewhat different output error rates, the proper design criteria in this area is not obvious. Voice and data will both be processed by the machine but these require significantly different resultant error rates. As a compromise, the error rates of 10^{-3} and 10^{-5} were selected. It is considered that these error rates are both representative of actual requirements and would display the difference in machine design that would be occasioned by more specific error rate specifications.

An inportant decision in the design of the sequential decoder is the memory to be used. In the discussions, three general types of memory were forwarded as being applicable to the problem: cores, small transistor matrix memories providing 16-bits per package, and MOS shift register techniques. Sequential decoders to date

have almost universally employed core memories.[*] However, investigations show that the other types of memories presented may be nearly compatible in price with core memories today (when military environments are considered) and will probably be significantly cheaper and more convenient in the future. The memory size of interest appears to be in the region between 512 to 2048 words of 2 bits each. Thus, the memory is not large enough to gain the potential low cost of cores associated with large memory sizes. In addition with such a small memory, small transistor matrix memories and MOS shift register techniques will give increased performance due to the speed of memor access, the degree of accessibility, and the ease of manipulation and interfacing with the remainder of the logic elements.

From the above requirements, it was decided to develop in further detail a sequential decoder employing a rate one-half, systematic code, and hard decision detection techniques. This decision was made to simplify the decoder and make resulting error rates and E_b/N_0 operating points consistent with known operational constraints. Having decided on these parameters for the sequential decoder, the design of a mechanization with the algorithm making use of these specific features was undertaken.

The decoder being designed is new both in processing to reduce the accessible memory requirements and in the algorithm used for decoding. The processing is described first, with the actual decoder treated as a general block.

The proposed decoder makes use of three characteristics of the code and channel to permit a significant reduction in the accessible memory requirements. The characteristics - hard decision, systematic code, and rate one-half - allow a simple implementation that essentially reduces the requirements for addressable memory by half. The mechanization is shown in block diagram form in Figure 7-24. The received bit stream is shown separated into information and check bit sequences; this operation can be performed directly because of the systematic nature of the code. The received information bits are shifted into both an encoder identical to the original encoder and into an L bit delay line memory. (Actually, the encoder can be part of the L bit memory.) The output of the local encoder is combined modulo-2 with the received check bits and the resulting sequence (the "syndrome") is processed in the decode The

[*] Codex Corp., High Speed Sequential Decoder Study, Contract DAAB07-68-C-0093, 15 April 1968.

decoder output, as is shown subsequently, is the received error sequence delayed L bits. When this sequence is summed modulo-2 with the received information bits (also delayed) an information bit sequence with low probability of error results. The basic idea is that of calculating the syndrome and processing to obtain the error sequence rather than the information sequence. Because the code is linear (i.e., modulo-2) only check bits are needed in the decoder memory, and the configuration shown in Figure 7-24 actually does decode the error sequence. The information digits are hypothesized to be zero in the decoder portion.

It is this ability to hypothesize all zeros for the information bits in the decoder that permits the reduction of the accessible decoder memory. For a rate one-half code the reduction is by a factor of two. There is no overall memory reduction, however, since the additional delay line memory shown in Figure 7-24 equals the gains in the decoder memory. The advantage lies in the fact that the additional memory can be a simple, moderate rate shift register since access is only required at the ends. The configuration shown in Figure 7-24 then, offers a less expensive implementation than the standard mechanization.

With the decoder implementation structure defined, it is necessary to derive the required algorithms and determine the experimental program to specify design parameters. Two algorithms were developed to take advantage of the systematic rate one-half code and the hard decision bit detection. These are the Fano threshold[*] and the modified threshold algorithms described in Appendix I. Some of the design factors
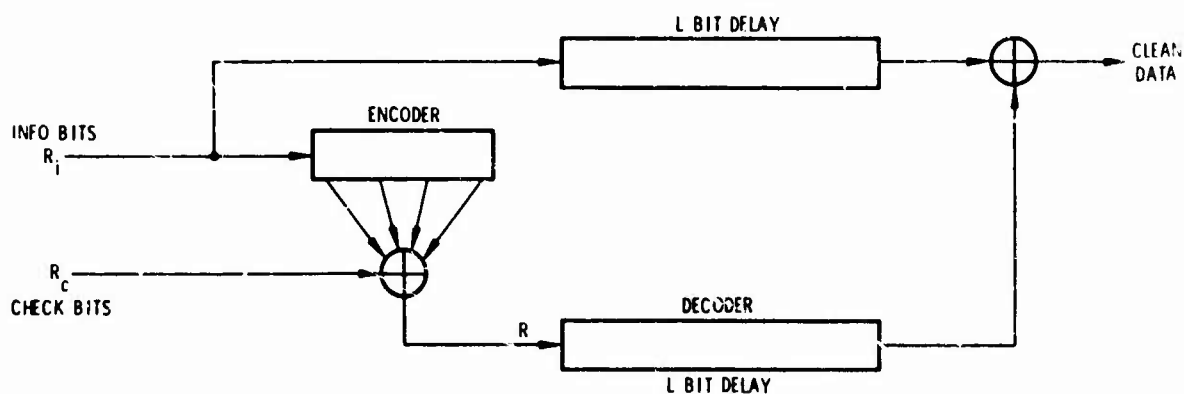
Figure 7-24. Sequential Decoder Configuration

UNCLASSIFIED
469-972

_____
[*] J. Wozencraft and I. Jacobs, Principles of Communication Engineering, John Wiley, 1965, pp 431-439.

-261-

to be established were, the backup buffer size, the overall buffer size, the required speed advantage, and the error rate performance. To determine these factors, the following experimental program was set up. Given a specific code and a channel error rate, select the algorithm parameters (these parameters will be discussed with the development of the algorithm) to minimize the computation distribution. Using the algorithm parameters, determine the undetected error probability at the given channel error rate. This procedure is then to be iterated to determine the performance of that same code at different channel error rates. The channel error rate interval of interest is from 5×10^{-2}. The constraint lengths investigated were 10, 21, 32, and 44.

A second set of experiments was made to determine the probability of overflow for various buffer sizes and speed advantages. The probability of overflow was found by measuring the computation distribution. The required backup buffer was found from a distribution of the deepest backup the decoder incurred in any search.

A final set of experiments were set up to determine the performance of statistical resynchronization of the decoder after buffer overflow. Statistical resynchronization involves repeated guessing of a constraint length of information bits in an attempt to restart the convolutional encoder used in the decoder to generate check bits to be compared with the received check bits. The alternate method of resynchronization is the familiar block resynchronization. In this case, periodically a constraint length of predetermined information bits forming the tail of each block is transmitted. Thus, resynchronization is possible because the information bits at the end of each block are known. However, the insertion of the tail sequence makes the code rate not exactly one half. This is a disadvantage because it is often not compatible for existing systems. In addition, there is a small rate loss due to the required tail, typically about .2 db.

7.3.2.1 Simulation Results

Simulations of the syndrome sequential decoder were run using both the modified and the Fano threshold algorithms. These simulations showed that in the cases of interest, where a significant part of the probability of error is due to overflows, the Fano threshold algorithm gives superior performance over the modified threshold algorithm.

To establish the performance of the algorithms, statistics on the number of computations (moves) to advance a node in the code tree, the maximum backsearch

-262-

to advance a node and the undetected errors were measured. The binary symmetric channel was simulated by assuming that the all zeros vector was transmitted and ones were produced for errors in the data stream by a random number generator. Thus, the stored information bits should be corrected by the decoder to give the all zeros vector and any ones appearing in the information bit stream after correction indicate undetected errors.

Statistics on the computations to advance a node in the code tree are obtained by counting the number of moves backward and forward before the decoder advances to a new node deeper in the code tree. From these statistics on the computations, a distribution of these computations to advance a node can be found. This computation distribution is approximately of the Pareto type. For a given probability of overflow, the number of incoming nodes to be stored is specified from the computation distribution, the time to make a forward or backward move, and the data rate. For example, let N be a number such that the probability that the number of moves to advance a node C is greater than or equal to N is equal to p, where p is the probability of overflow. Let T be the time in seconds to make a forward or backward move and let R equal the data rate (bits/second). Then the number B of incoming nodes to be stored is given by

$$B = NRT \tag{59}$$

The parameter $1/RT$ is usually referred to as the speed advantage S, since it denotes the number of moves in a data bit time.

While the number of incoming nodes to be stored for a given probability of overflow is dependent on the speed advantage, the probability of a backup overflow is mainly dependent on the number of nodes stored and only slightly dependent on the constraint length of the code. To obtain statistics on the backup, the number of nodes between the most advanced node reached by the decoder and the node reached during the deepest backsearch is recorded for each node as a more advanced node is reached. From these statistics, a backup distribution is obtained.

Table 7-6 illustrates the observed probability of undetected errors versus constraint length for bias equal to 1/9 and 1/11. The bias refers to the weight given to a double agreement (information and check bit) of the hypothesized node and the received node relative to the weight given to a double disagreement of these nodes. For example, a bias of 1/9 indicates that a double agreement is weighted + 1

relative to a double disagreement weighted -9. In theory,[*] the probability of undetected error for a systematic convolutional code with the rate $R = 1/2$ and $R_{comp} = 1/2$ (binary symmetric channel error probability about 0.045) is asymptotically equal to

$$P_{ue} \simeq C\, 2^{-k/2} \qquad (40)$$

where C is a constant independent of the constraint length k and the bias. However, Table 7-6 indicates that while the probability of undetected error decreases exponentially with constraint length as predicted by Equation (40) for a bias of 1/11, it does not decrease as rapidly for a bias of 1/9. This result provides an advantage of using a bias of 1/11 for a lower total error probability.

Comparing the performance of the two algorithms, the probability of undetected errors is somewhat smaller with the modified threshold algorithm for short constraint lengths than with the Fano threshold algorithm as seen in Table 7-6. However, in Figure 7-25 the computations distribution indicates that even for constraint length 10, the probability that the computations C, is greater than or equal to some number N, $P(C \geq N)$, is considerably less with the Fano threshold algorithm than under the same conditions with the modified threshold algorithm. The backup distribution for constraint length 10 in Figure 7-26 shows only slight improvement of the modified threshold algorithm over the Fano threshold algorithm.

Table 7-6. Sequential Decoder Undetected Error Probability

Constraint	Bias[*]	Channel Error Probability	Undetected Error Probability	
			Modified	Fano
10	1/9	0.04	4.3×10^{-3}	5.3×10^{-3}
10	1/11	0.04	2.9×10^{-3}	4.0×10^{-3}
21	1/9	0.04	7.0×10^{-4}	7.9×10^{-4}
21	1/11	0.04	2.3×10^{-4}	2.8×10^{-4}
32	1/9	0.04	2.0×10^{-4}	2.0×10^{-4}
32	1/11	0.04	$< 5 \times 10^{-6}$	$< 5 \times 10^{-6}$

[*] E.A. Bucher, "Error Probability for Systematic Convolutional Codes," S. M. Thesis, MIT, February 1967.

Figure 7-26. Backup Distribution for Sequential Decoder with Constraint Length 10

Figure 7-25. Computations Distribution for Sequential Decoding with Constraint Length 10

When the constraint length is increased to 21, the change of bias has a smaller effect on the computations distribution as shown in Figure 7-27. In comparing the backup distribution for constraint length 21 of Figure 7-28, the Fano threshold algorithm now shows an improvement over the modified threshold algorithm. An increase in constraint length to 32 shows a further decrease in the effect of bias. In Figure 29, the Fano threshold algorithm shows no effect at all of a change in bias for the computations distribution. Also, in Figure 7-30, the Fano threshold algorithm shows only a slight effect in the backup distribution over part of the range for a change in bias.

While the backup distribution shows only slight variation with constraint length, the computation distributions continually show an increase of computations with an increase in constraint length. When the constraint length is short, a pattern of errors may look like a correct pattern and the decoder moves directly through the pattern. Thus, for short constraint lengths, undetected errors are made instead of a large number of computations and anything (such as bias) that decreases the number of undetected errors will increase the computations. As the constraint length gets longer, the number of undetected errors decrease to very small numbers, an increase in constraint length has little effect on the number of computations. This effect can be seen by comparing Figure 7-27 for constraint length 21 with Figure 7-29 for constraint length 32.

From the performance comparisons between the two algorithms, the Fano threshold algorithm was chosen with a constraint length of 32, a bias of 1/11, and a Δ (threshold spacing) of 9. In Figure 7-31, the effect of Δ is illustrated for a channel error probability of 0.04. While the effect is small, simulations indicate that Δ of 9 gives the best performance. However, upon careful examination of the computation distributions in Figure 7-31, it is found that the performance does not reach theoretical expectations. Since hard decision rate one-half systematic sequential decoders are known to degrade in an environment having correlated errors, the random number generator used in the simulation of the channel was investigated for the possibility of dependency between generated numbers.

It was found that the random number generator used in the simulations did indeed have dependency between generated numbers. In Appendix II, the program for testing the dependency in the random number generator is presented along with the dependency that was found. Using this test program, a random number generator with satisfactory statistics was found for a computer with a 24-bit word size.

Figure 7-28. Backup Distribution for
Sequential Decoding with
Constraint Length 21

Figure 7-27. Computations Distribution
for Sequential Decoding with
Constraint Length 21

Figure 7-30. Backup Distribution for
Sequential Decoding with
Constraint Length 32

669-1505
UNCLASSIFIED

Figure 7-29. Computations Distribution
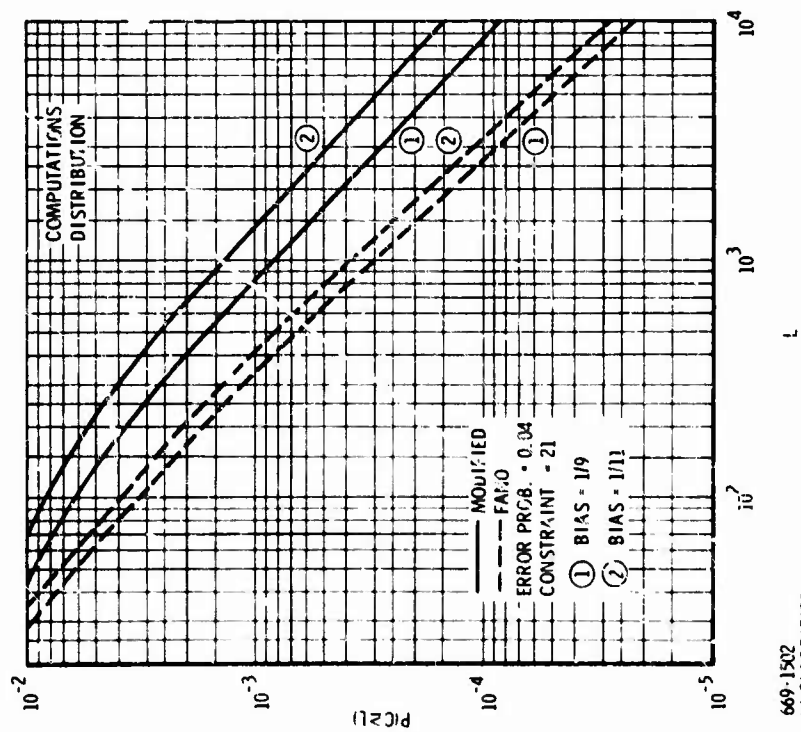for Sequential Decoding with
Constraint Length 32
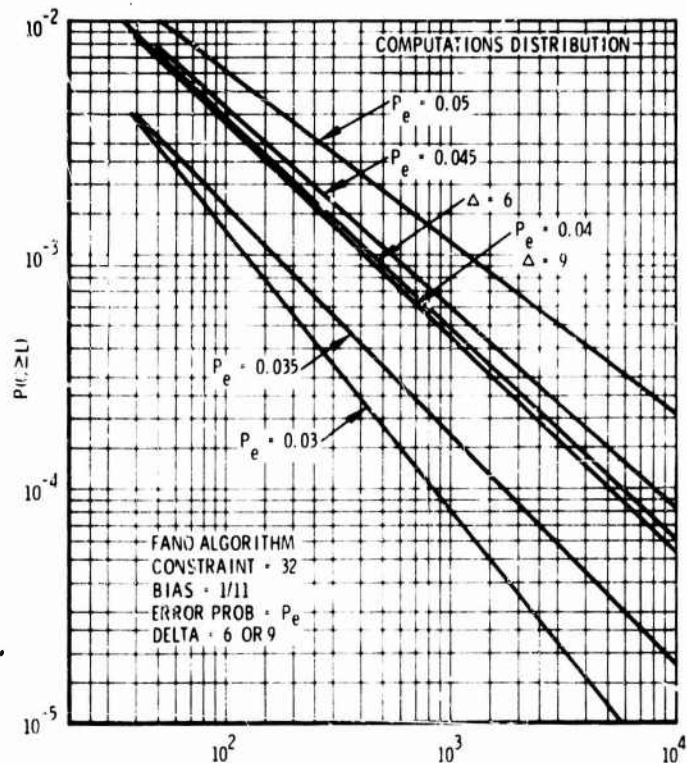
669-1504
UNCLASSIFIED

Figure 7-31. Computations Distribution for Sequential Decoding
with Constraint Length 32

Using the random number generator, which was found to have satisfactory
statistics, the simulations for the sequential decoder with the Fano threshold algo-
rithm were redone. The computations distributions are shown in Figure 7-32 for
various probabilities of error in the channel. For comparison of the improvement
obtained by using the new random number generator over the results obtained by
using the original random number generator, the computation distribution for prob-
ability of error in the channel equal to 0.04 obtained previously is presented. Figure
7-33 illustrates the improvement in the backup distribution and presents the backup
distributions for various probabilities of channel errors.

An interesting comparison can be made between the computations distribution
obtained for the Fano threshold algorithm with its stored moves and the computations

-269-

COMPUTATIONS DISTRIBUTION

FANO THRESHOLD DISTRIBUTION
CONSTRAINT · 32
BIAS · 1/11
ERROR PROB. · Pe
THRESHOLD DELTA · 9
—— NEW RANDOM NUMBER GENERATOR
— — ORIGINAL RANDOM NUMBER
GENERATOR

769-1781
UNCLASSIFIED
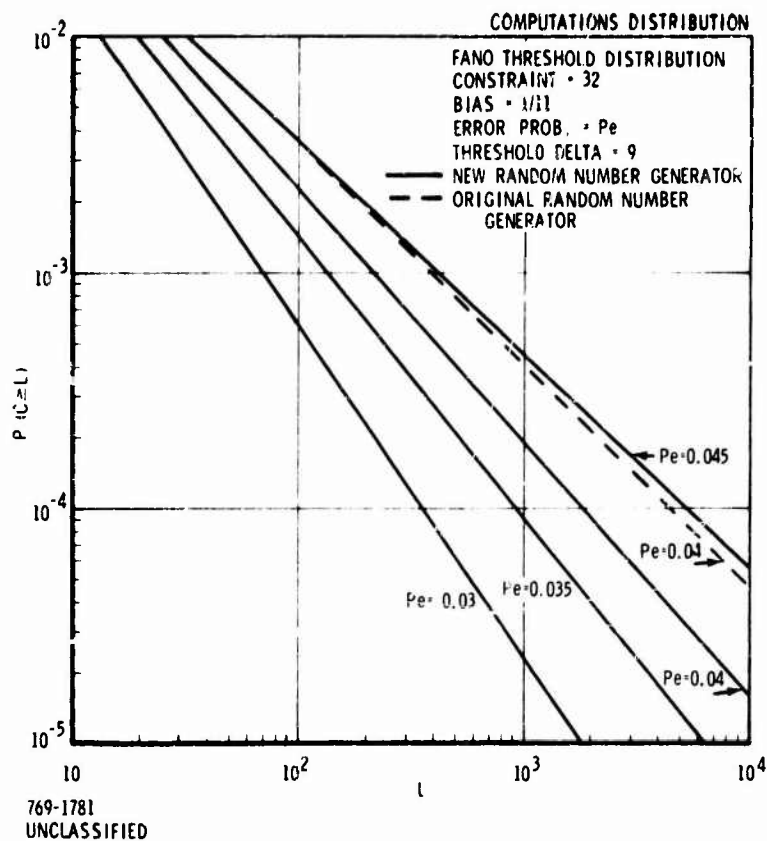
Figure 7-32.   Computations Distribution for Sequential Decoding
With Chosen Random Number Generator

distribution of algorithms that have been simulated in the past.[*]   It is found that the
Fano threshold algorithm shows a four-fold improvement in the computations distri-
bution over the distributions presented by Codex Corporation.   This improvement can
be thought of as a four-fold increase in the speed advantage, and leads to a reduced
memory size requirement and a proportionally greater maximum allowed data rate.

To arrive at a bound on the probability of error out of the decoder for various
channel error probabilities, 160 modes were assumed to be available for backup.   Thus,
the probability of backup overflow was negligible in the range of interest, probability
of error out of the decoder from 10^{-3} to 10^{-5}.   The remaining portion of the buffer was
considered to be used to store incoming nodes as the decoder made computations to
advance a node.   The speed advantage chosen for the example was 16.6.   With the

_____
[*] Codex Corp., op. cit.

-270-

BACKUP DISTRIBUTION
FANO THRESHOLD DISTRIBUTION
CONSTRAINT · 32
BIAS · 1/11
ERROR PROB. · Pe
THRESHOLD DELTA · 9
—— NEW RANDOM NUMBER
GENERATOR
— — ORIGINAL RANDOM NUMBER
GENERATOR

$P(B \geq L)$

Pe · 0.035
Pe · 0.03
Pe · 0.04
Pe · 0.045

L

769-1782
UNCLASSIFIED
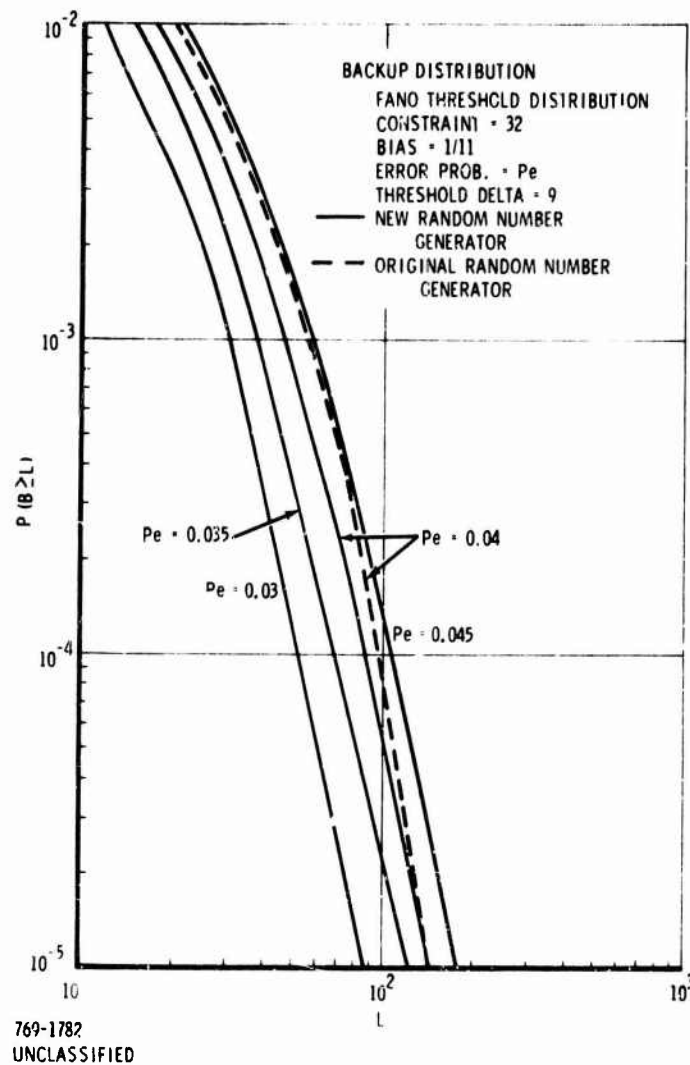
Figure 7-33. Backup Distribution for Sequential Decoding with
Chosen Random Number Generator

speed advantage and the number of incoming nodes stored known, the probability of
overflow was computed from the computation distributions in Figure 7-32. Combining
the probability of overflow with the probability of undetected errors, the total proba-
bility of error[*] out of the decoder is obtained and plotted versus energy per bit/noise
energy in Figure 7-34, presuming an ideal binary PSK channel. Figure 7-34 illustrates

---

[*] After an overflow, the received information digits have the channel error rate; hence,
this calculation gives a pessimistic result.

-271-
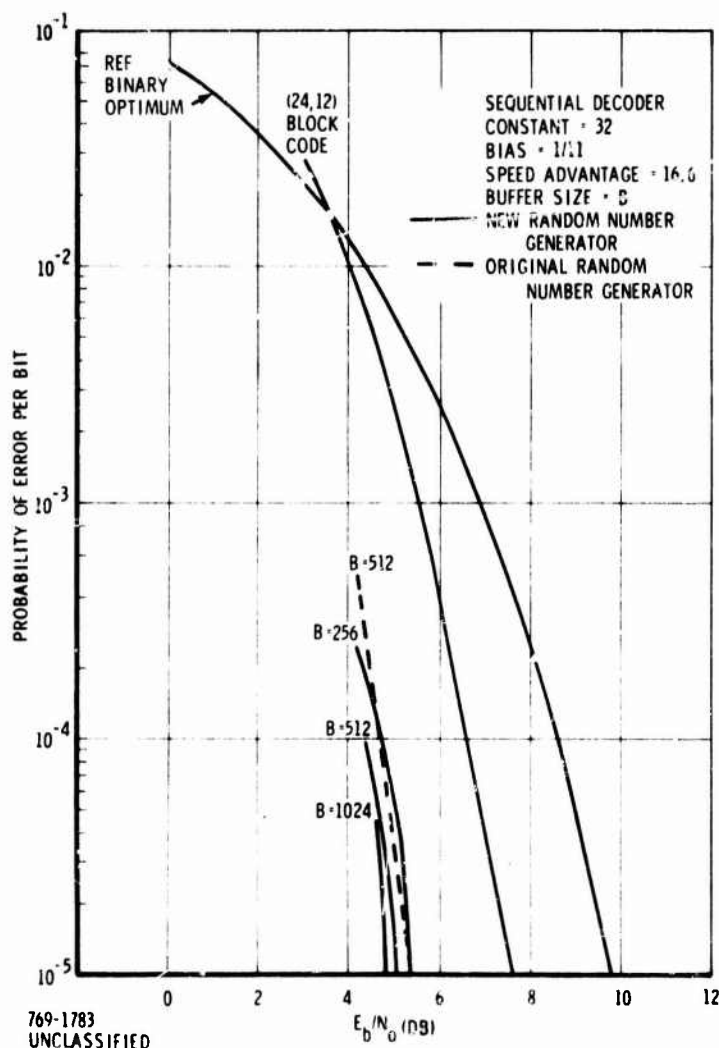
Figure 7-34. Sequential Decoder Performance with Chosen
Random Number Generator

the performance of the sequential decoder for three buffer sizes: 256, 512, and 1024
nodes. The performance using the original random number generator with a buffer
size of 512 is presented for comparison. Finally, Figure 7-34 compares the perform-
ance of the sequential decoder against the (24, 12) Golay block code and the uncoded
channel (reference optimum binary curve).

7.3.2.2 Synchronization

The occurrence of buffer overflow is a problem in sequential decoder design
because the sequential decoding process requires the ability to back up and change

-272-

previously hypothesized bits. Buffer overflow occurs if in order to decode a given bit such a long search is required that the input data stream fills all the available backup buffer. To gain buffering between the input data stream and the current bit to be decoded after buffer overflow, the decoder has to be advanced a distance beyond the input stream. However, before the decoder may be advanced, a number of information bits must be placed in the output data stream with the channel errors uncorrected. After the decoder has been advanced, resynchronization is required before decoding may continue.

The simplest and most familiar resynchronization scheme is block resynchronization. In this case, periodically a constraint of predetermined information bits forming the tail of each block is transmitted. The required tail algorithms for this resynchronization scheme are discussed in Appendix I under normal conditions, when buffer overflow has not occurred. When a buffer overflow does occur, the remaining information bits in the block are placed in the output data stream with channel errors uncorrected. The decoder can now be moved to the beginning of the next block. Since a constraint length of predetermined information digits was transmitted, the decoder can correctly choose the hypothesis digits to begin decoding again. Hence, the decoder is resynchronized. However, a tail sequence must be inserted for resynchronization, making the code rate not exactly one half. This is a disadvantage because it is often not suitable for existing systems. In addition, there is a small rate loss due to the required tail, typically about .2 db.

Another possible resynchronization scheme is referred to as statistical resynchronization. In this case, when a buffer overflow occurs, the decoder is jumped a specified distance forward and a constraint length minus one of information bits is guessed for the hypothesis digits to begin decoding again. The distance the decoder is jumped forward is dependent on the computations distribution for resynchronization attempts.

The present decoder structure calculates a syndrome from the incoming data stream. Thus, if no errors occur in the information digits, the correct hypothesis digits are all zeros. A resynchronization strategy is to have the decoder jump ahead a specified distance making this point the "origin" such that the decoder cannot back up past it. The hypothesis digits are set to zero, and decoding is attempted. Resynchronization is declared if the decoder advances three constraint lengths because

simulations of the limited back search concept discussed in Appendix I have shown that a reasonable backup buffer contains only three constraint lengths of nodes. Hence, when the decoder has advanced three constraint lengths, the backup buffer is again filled and as the decoder advances, the hypothesis behind the backup buffer may be output to correct the information bits. As in the block resynchronization scheme, channel errors in the information digits are not corrected between buffer overflow and resynchronization. The probability of error over this period is just equal to the channel probability of error.

During resynchronization, the decoder occasionally must return to the "origin" several times. When the decoder returns to the "origin" a specified number of times, the resynchronization attempt is rejected. A new resynchronization attempt is begun by advancing the decoder the specified distance. With a correct choice of the hypothesis digits, the decoder usually will not return to the "origin" three times. Hence, if the decoder returns to the "origin" more than three times, the initial hypothesis digits are probably incorrect and the decoder probably cannot resynchronize. Thus, the resynchronization attempt should be rejected.

Simulations performed indicate the statistical resynchronization scheme is feasible for constraint lengths as large as 44. Indeed, the theoretical probability of resynchronization, P_{rt}, is

$$P_{rt} = (1 - P_e)^{k - 1} \tag{41}$$

where

P_e = channel probability of error

k = constraint length.

For $P_e = 0.045$ and $k = 44$,

$$P_{rt} = (1 - 0.045)^{43} = 0.138 \tag{42}$$

and repeated guessing would give a correct constraint length in approximately 7 trials on the average. Table 7-7 presents the results of the simulations to measure the probability of resynchronization. In the table and the figures to follow:

N = number of allowed returns to the "origin"

P_{rch} = the probability of a resynchronization attempt with correct hypothesis being rejected.

Table 7-7. Measured Probability of Resynchronization

P_e	k	Prob. of Resynchronization		N	P_{rch}
		Theoretical	Measured		
0.045	44	0.138	0.256	3	7.25×10^{-3}
			0.215	2	1.45×10^{-2}
			0.164	1	7.25×10^{-2}
			0.075	0	0.508
	32	0.24	0.345	3	4.16×10^{-3}
			0.281	2	1.66×10^{-2}
			0.234	1	0.1
			0.134	0	0.462
0.035	44	0.216	0.338	3	0
			0.293	2	9.36×10^{-3}
			0.252	1	1.85×10^{-2}
			0.142	0	0.381
	32	0.331	0.454	3	0
			0.382	2	3.02×10^{-3}
			0.338	1	3.92×10^{-2}
			0.222	0	0.365

It should be noted that the measured probability of resynchronization is considerably larger for N > 1 than the theoretical. The larger measured probabilities result from the ability of the decoder to resynchronize even when errors have occurred in the initial hypotheses. The density of the possible errors in the initial hypotheses that can occur in a successful resynchronization attempt is illustrated in Figure 7-35.

To produce the curves in Figure 7-35, each successful resynchronization was tested for one or more errors in a group of five hypothesis bits. For example, if a successful resynchronization had an error in the third and the seventh hypothesis bits, then the group of the 1-5 hypothesis bits and the group of 6-10 hypothesis bits would each be credited with containing errors. The fraction of successful resynchronization attempts having errors in a group of five is illustrated by the horizontal lines in Figure 7-35. The curves connecting the horizontal lines are drawn to illustrate the shape of the density. As N decreases, only errors in the beginning of the initial hypotheses will allow resynchronization. Indeed, when N = 0, the successful resynchronization attempts containing errors in the initial hypotheses had errors only in the first five hypothesis bits. This decrease in the allowed positions of errors in the initial hypotheses partly accounts for the decrease in the probability of resynchronization

F = FRACTION OF SUCCESSFUL RESYNCHRONIZATION
ATTEMPTS CONTAINING ERRORS IN A BLOCK OF
FIVE HYPOTHESIS BITS

N = NUMBER OF ALLOWED RETURNS TO "ORIGIN"

PROBABILITY OF CHANNEL ERROR = 0.045

CONSTRAINT LENGTH = 44

BIAS = 1/11

THRESHOLD = 9

N = 3

N = 2

N = 1

N = 0

0.2

0.1

F

0

10   20   30   40

HYPOTHESIS BIT

1069-2542
UNCLASSIFIED
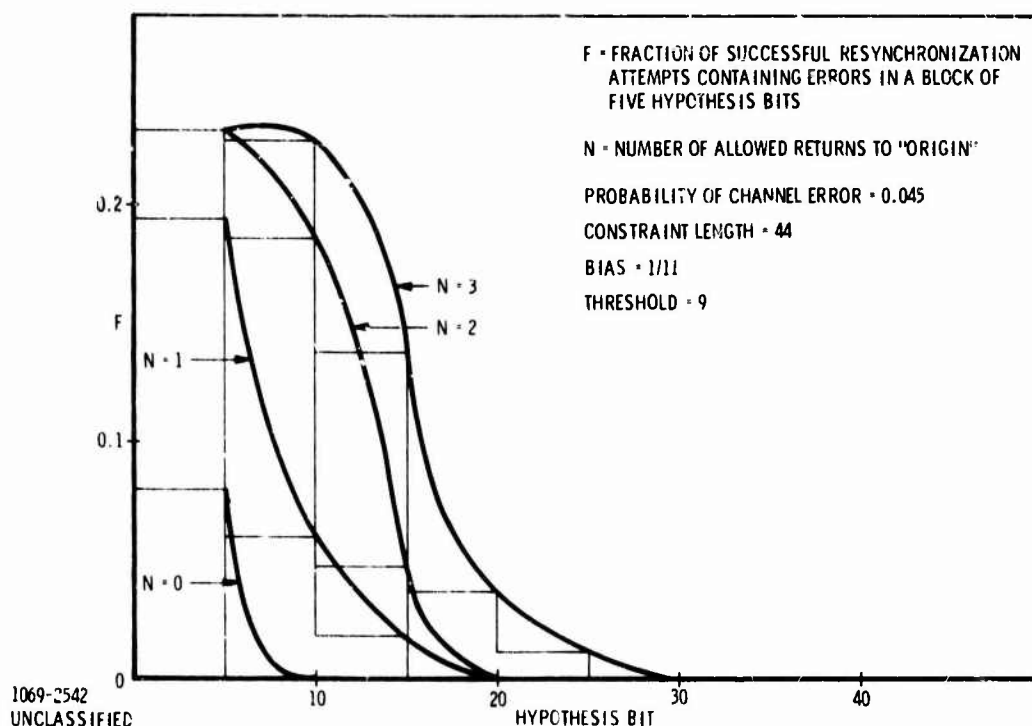
Figure 7-35.   Density of Frrors in initial Hypothesis for a Given
Successful Resynchronization

as N decreases.   The additional decrease in probability of resynchronization as N
decreases results from the increase in P_{rch}.

Figure 7-36 illustrates the computations distribution for statistical resynch-
ronization with a constraint length 44.   This distribution is for the computations to
advance three constraint lengths beyond the "origin" which specifies a successful
resynchronization.   For comparison, the computations distribution under normal
decoding conditions to advance three constraint lengths is included.   By specifying a
number of allowed returns to the "origin" , blocks of data containing a large number
of errors are rejected after too many returns to the "origin".   Thus, the curves where
N is specified illustrate smaller number of computations than the curve for normal
decoding conditions.

The computations distribution for rejection of a resynchronization attempt with
constraint length 44 is presented in Figure 7-37.   As N decreases, it is shown that the
number of computations to reject an attempt decreases rapidly.   It also should be noted
that the distributions do not vary greatly with the channel probability of error.

Figure 7-37. Computations Distribution for Rejection of a Resynchronization Attempt with a Constraint Length 44.

Figure 7-36. Computations Distribution for Statistical Resynchronization with a Constraint Length 44.

The computations distribution for resynchronization with a constraint length 32 is shown in Figure 7-38. The distributions are similar to those for constraint length 44 except the curves do not decrease as rapidly in computations for a decrease in N as for constraint length 44. In fact, the distribution for N = 1 is identical with that for N = 0. Figure 7-39 illustrates the computations distribution for rejection of a resynchronization attempt with constraint length 32. In this case, it is also apparent that the computations do not decrease as rapidly with a decrease in N as for a constraint length 44. In addition, the channel probability of error has a greater effect, expecially for N = 1 or 0.

To apply the computations distribution to accept or reject a resynchronization attempt, it is necessary to establish a resynchronization strategy and performance criteria. First, buffer overflow occurs when all available buffer is filled with undecoded data and the next piece of data will have to be placed in the portion of the buffer reserved for backup by the decoder. To gain buffer space, some information bits must be placed in the output data stream with channel errors uncorrected. It is,
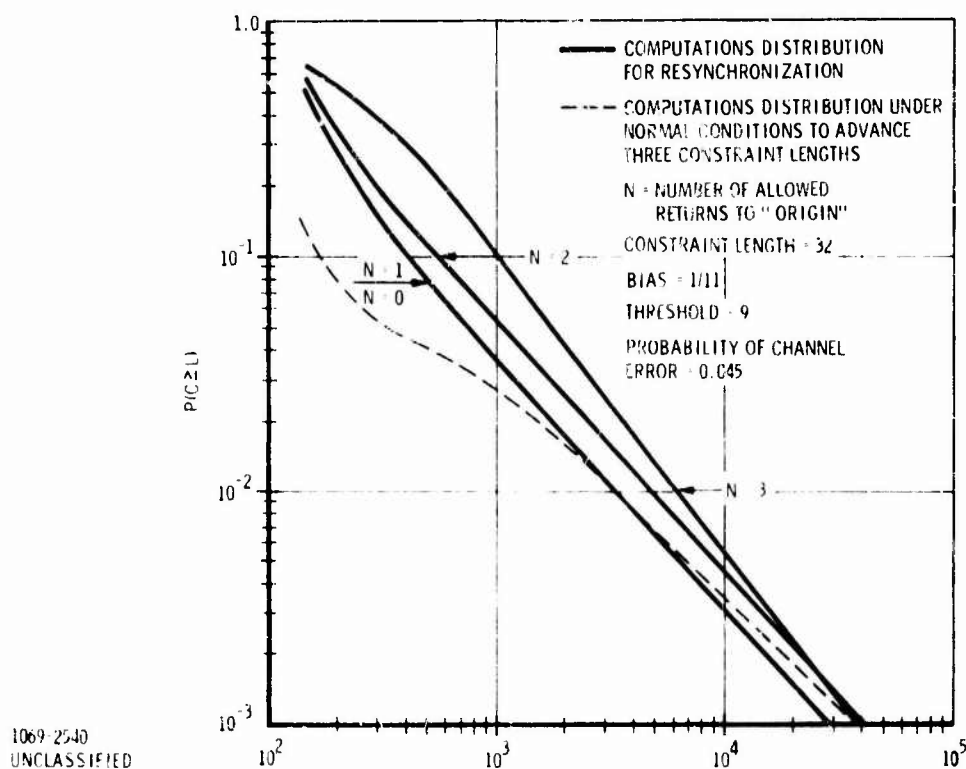
Figure 7-38. Computations Distribution for Statistical Resynchronization with a Constraint Length 32

-278-
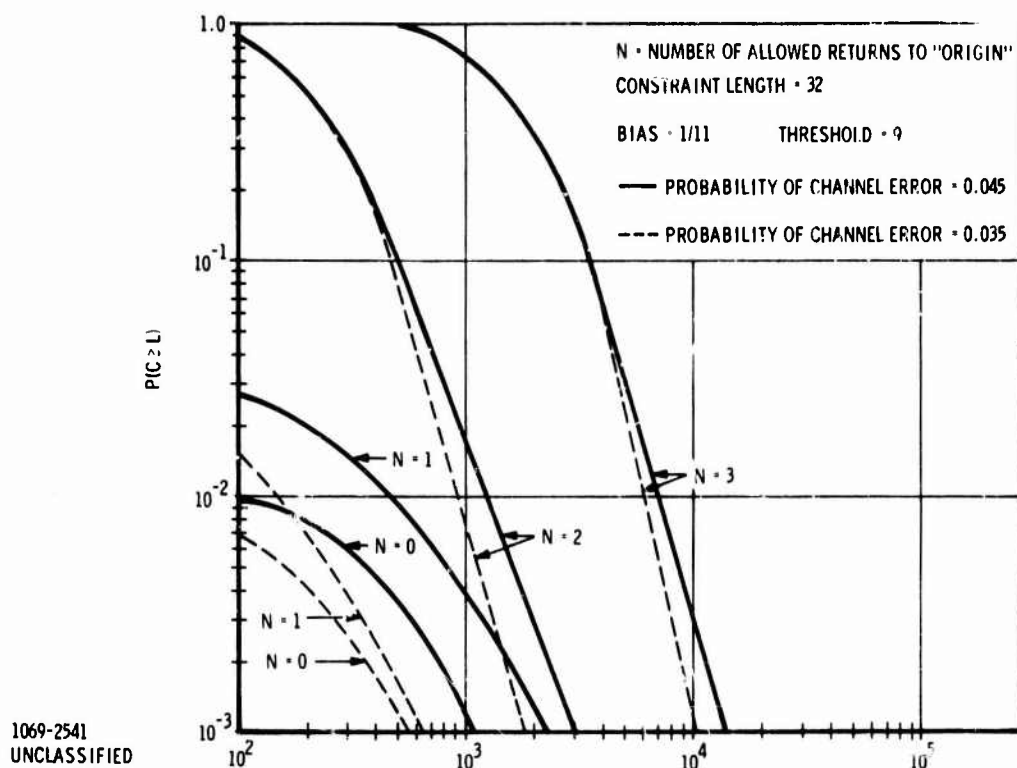
Figure 7-39. Computations Distribution for Rejection of a
Resynchronization Attempt with Constraint Length 32

therefore, possible by advancing the decoder a full buffer distance that all the stored
information bits will have been placed in the output data stream, and the decoder must
wait for more incoming data before resynchronization can occur. This situation is
somewhat undesirable because resynchronization may take considerable time under
this condition. However, with the buffer completely empty, the probability of another
overflow immediately after resynchronization is extremely small, and it is desirable
to minimize the probability of additional overflows immediately after synchronization.
Thus, an arbitrary but reasonable resynchronization strategy is to divide the buffer
into parts such that, on the average, resynchronization will occur without the delay
of waiting for new data bits. For example, if the buffer B is 512 nodes and the con-
straint length k is 44, then, the backup buffer is 132 (three constraint lengths) and the
forward buffer B_F is 380. The probability of resynchronization is 0.256 for $N = 3$ and
$P_e = 0.045$. Therefore, the decoder should jump forward

$$N_a = \frac{B_F}{P_r} = \frac{380}{0.256} = 97 \text{ nodes} \tag{43}$$

-279-

For a speed advantage S (moves or computations per data bit) equal to 16.6, the probability of overflow during a normally successful resynchronization attempt, P_{so}, can be found to be 2.3×10^{-2} in Figure 7-36. The fraction F of resynchronization attempts rejected by overflow that would normally be rejected by too many returns to the "origin" can be found to be 0.51 in Figure 7-37.

Using Figures 7-36 through 7-39 with S = 16.6 and P_e = 0.045, Table 7-8 is produced to illustrate resynchronization performance. For various values of N, constraint length k, and buffer B, the parameters, P_{so}, F, and number of nodes to advance N_a are presented. The probability of overflow under normal conditions is P_o and is presented here to compare probability of overflow during resynchronization with normal conditions.

When F is very small, then the resynchronization attempts tend to be rejected by returns to the "origin" rather than for too many computations. Hence, the buffer begins to empty because more information bits are being put into the output data stream than arc being placed in the buffer by the input data stream. Therefore, with F small

Table 7-8. Statistical Resynchronization Performance

	B	B_F	P_o	N_a	P_{so}	F	N
44	512	380	8.5×10^{-5}	97	2.3×10^{-2}	0.51	3
				81	1.04×10^{-2}	1.7×10^{-3}	2
				62	1.20×10^{-2}	2.8×10^{-4}	1
				28	1.60×10^{-2}	4.2×10^{-4}	0
	1024	892	4.0×10^{-5}	228	8.20×10^{-3}	8.2×10^{-2}	3
				191	3.40×10^{-3}	3.5×10^{-5}	2
				146	3.65×10^{-3}	4.9×10^{-5}	1
				67	4.80×10^{-3}	9.8×10^{-5}	0
32	512	416	7.8×10^{-5}	143	3.30×10^{-2}	0.255	3
				117	2.60×10^{-2}	3.1×10^{-3}	2
				97	2.10×10^{-2}	1.8×10^{-3}	1
				55	3.90×10^{-2}	1.3×10^{-3}	0
	1024	928	5.85×10^{-5}	320	1.20×10^{-2}	2.5×10^{-2}	3
				261	1.10×10^{-2}	4.45×10^{-4}	2
				217	9.00×10^{-3}	4.9×10^{-4}	1
				124	1.65×10^{-2}	3.3×10^{-4}	0

the probability of an overflow occurring immediately after synchronization is much smaller than P_{so}. The best value for N is then the value that gives small P_{so} and F. For k = 44, the best value of N is 2, but for k = 32 the best value of N is 1 since in both cases P_{so} is minimized and F is near minimum.

7.3.2.3 Conclusions

Many modifications have been developed that improve on the basic sequential decoder. A unique decoder configuration using the error syndrome was found to reduce the accessible memory requirements. A Fano threshold algorithm was developed that had several stored moves that reduced a considerable amount of the short sequence of moves necessary to change hypotheses. In addition, a parameter KBACK was used in the algorithm to limit backup to three constraint lengths. This was a reflective type limit that turned the decoder around similar to what happens when the decoder backs up to the origin.

Simulations were performed that indicated the best distance values for the Fano threshold algorithm was 1 for a double agreement between the hypothesis and the received bits, α = 5 for a single agreement and β = 11 for a double disagreement (bias of 1/11). The best value of threshold spacing was 9. Finally, simulations indicate that statistical resynchronization is feasible and the best value for N, the allowed returns to the "origin" is 2 for constraint length 44 and 1 for constraint length 32.

Statistical resynchronization is desirable because it avoids the small rate loss associated with block resynchronization, typically about 0.2 db, and permits the code rate to be exactly one half. The one-half code rate is more suitable for insertion in existing systems and avoids the hardware needed to insert the tail sequence and to buffer the input during insertion.

7.3.3 DELTA MODULATION FOR VOICE

Although emphasis has been placed on using a 2400 bps data channel for vocoded voice, a much more economical voice digitization can be achieved by delta modulation. Typical delta mod schemes transmit at 19.2 kbps, which leads to an eight-fold increase in the requisite data rate for a CNI voice channel. However, now the receiver can tolerate a much higher error rate, so that error correction coding becomes unnecessary.

Although the tolerable error probability for delta mod can only be ascertained subjectively, an accepted quantitative approximation is available through articulation measurements with standard word lists. A variable-slope delta mod (VSD) unit was tested by Magnavox in conjunction with a digital PSK modem with interference introduced to cause random errors.[*] The results are shown in Figure 7-40. It is noted that articulation scores approaching 100 percent are obtained at low error probabilities, and the score stays high, well over 90 percent, for an error probability of 0.1. The 38.4 kbps version of variable slope delta mod is found to be more susceptible to errors, and at 9.6 kbps, articulation was reduced undesirably below 100 percent even in the absence of channel errors.

It may be concluded that 19.2 kbps delta mod is a reasonable parameter choice which can be used effectively over a channel producing ten percent random error rate. It is likely that burst errors at the same average error rate are even less of a problem.

---

[*]F. J. Spayth, "Report on Voice and Data Testing Program at Fort Huachuca," 15 July 1969, Magnavox Memorandum.
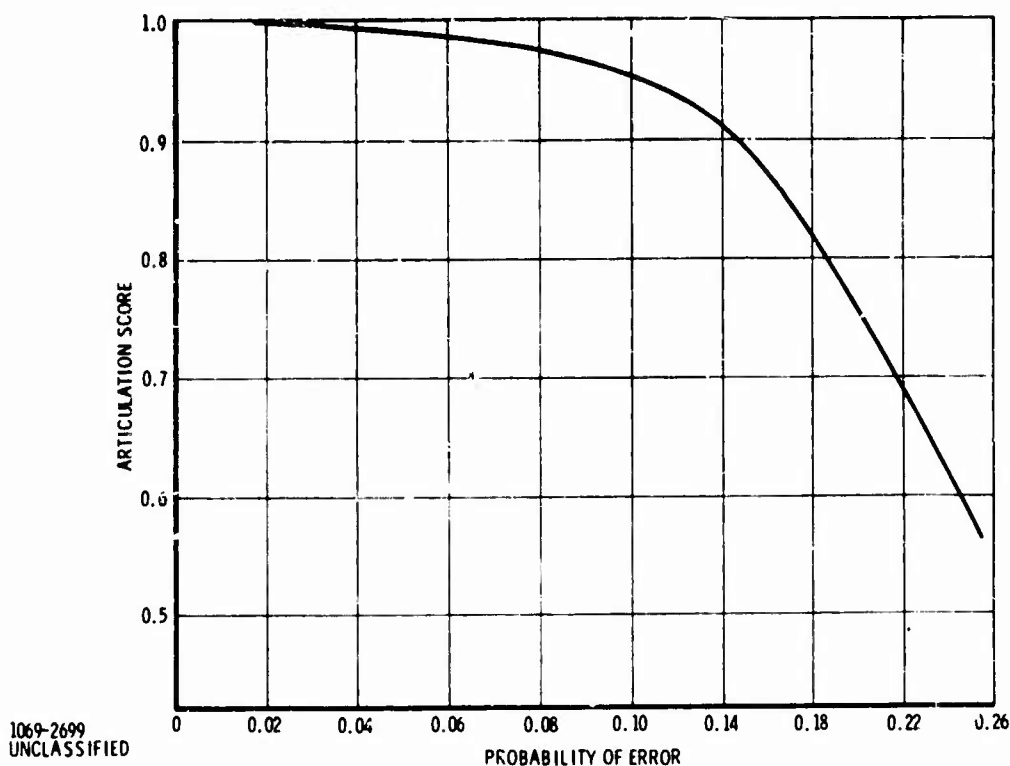
Figure 7-40. Articulation of Variable Slope
19.2 Kb/s Delta Mod with Channel Errors

7.3.4 ALTERNATE MODULATIONS FOR A NON-COORDINATED TH/FH WAVEFORM CONCEPT

The non-coordinated TH/FH/PN waveform approach described in Section 4.4.2 of Volume I was configured so as to avoid the coordination limitations (e. g. , speed of slot permutation and system reaction time) and problems (e. g. , complexity and need for either central control or else self-adaptive control), while achieving reasonably efficient system performance otherwise (though not as good ideally as for the coordinated waveforms). In the latter regard it is noted that the particular TH/FH/PN scheme with binary modulation, as described, gives protection against multipath ringing (by transmitting in a minimum burst length of 50 μsecs), multipath intersymbol interference (by 10 db of PN processing and error correction coding), spectrum splatter for severe dynamic range situations (by at least having some time-gating of the transmitted waveform; e. g. , 1/20 time duty factor, though one still frequency hops over 100 frequency channels), and moderate dynamic range interference (by using the 100 additional frequency slots so that interference must statistically fall into a channel to be effective). Moreover, the scheme has a reasonable sync acquisition time (the use of frequency hopping to make up the full system processing gain makes this possible;

-283-

i. e., by using multiple frequency channels the processing gain requirements in each channel for sync are eased). On the other hand, the scheme is limited in terms of the number of strong multiple accesses possible in the direct mode for a given 100 MHz bandwidth (that is, multiple access capacity, which was illustrated at 200 maximum, is significantly less than that readily achieved with coordinated waveforms, and also less than one intuitively would expect to achieve with non-coordinated waveforms if the modulation were optimized for this alone). The purpose of this discussion is to compare several alternate plausible modulations for the non-coordinated TH/FH wave- form approach so as to improve performance in regards to direct mode multiple access capacity, while still retaining nominally equivalent performance in all other regards (i. e., multipath, wide dynamic range. spectrum splatter. sync ease) including also anti-jamming. That is, one would not really want to trade any of these other perform- ances (to a first approximation) for an increase in multiple access efficiency.

The particular alternate modulation waveforms selected for discussion in this section are: 1) in a frequency-time slot one uses an M'ary time-shift-keyed waveform with PN modulation, receiver amplitude limiting of the received signal together with threshold detection; 2) in a given frequency-time slot one uses M'ary frequency shift keying together with threshold detection in a sequential receiver channel scan; 3) in a given frequency-time slot one uses M'ary frequency shift keying together with hard decisions on the channel with the maximum amplitude (list decoding with $\ell = 1$); 4) the same as in (3) but with "list of ℓ" decoding and $\ell = m$, the alphabet size. In each case above. the modulation is combined with sequential decoding with rate 1/2 The more specific waveform parameters used in each case together with an explanation of the equations used in the analysis, are now given as follows. starting first of all with a recapitulation of the baseline binary modulation.

7.3.4.1 Baseline-Binary DPSK/Sequential Decoding (10 db PN, 20 TH, 100 FH)

The signal structure comprises a 60 μsec burst (to minimize ringing) which is sent out in one of 20 possible time-gated slots (permuted each frame) in a frame (frame is actually 1250 μsecs) and on one of 100 possible frequencies (channel bandwidth is 1 MHz) in a 100 MHz bandwidth. The 60 μsec burst actually comprises a sequence of 6 binary digits that are each encoded by 10 chips of PN. The PN chip width then is 1 μsec (1 MHz channel bandwidth results from this). The PN chips are correlation

detected in the receiver to give 10 db of processing gain against intersymbol interference and other in-band interference. DPSK modulation is used for each digit. Sequential decoding at rate 1/2 is also used so that the 6 digits represent 3 information bits. For 2400 bps information rate the frame is, therefore, 800 per sec (frame time is 1250 μsecs).

For comparison with other modulations here only the direct mode case involving just very strong multiple access interferers and/or broadband noise jamming will be considered. The computation is done in terms of R_{comp} which by design will be set for rate 1/2. The resulting multiple access capacity and J/S performance is computed from the R_{comp} expression.

$$R_{comp} = -\log_2 \sum_j \left[\sum_i p(i) \sqrt{p(j/i)} \right]^2 \quad \text{bits/digit} \quad (44)$$

For a digit error probability p (due to either multiple access interference or jamming) the evaluation of the above expression becomes

$$R_{comp} = -\log_2 \ 2\left[\frac{1}{2}\sqrt{p} + \frac{1}{2}\sqrt{(1-p)} \right]^2$$

$$= 1 - \log_2 \left[1 + 2\sqrt{p(1-p)} \right] \quad (45)$$

For strong multiple access interference only (no jamming or thermal noise), the digit error probability is the probability of an interferer landing in the correct time and frequency slot, times a probability of 1/2 that DPSK demodulation gives the right phase. The effect of PN processing is neglected for strong multiple access interference.

$$p = \epsilon \frac{1}{2}$$

$$\epsilon = \left[1 - \left(1 - \frac{k}{N} \right)^{(M-1)} \right] \approx M \frac{k}{N} \text{ for M large and } \frac{Mk}{N} \text{ small} \quad (46)$$

M = number of multiple accesses

k = time slot duty factor

N = number of frequency channels

$$R_{comp} \text{ (multiple access)} = 1 - \log_2 \left[1 + 2\sqrt{\frac{\epsilon}{2}} \left(1 - \frac{\epsilon}{2} \right) \right] \qquad (47)$$

for $R_{comp} = 0.5$ bits/digit, $\epsilon = 1/10$, M = 200

For just broadband noise jamming alone

$$p = \frac{1}{2} \exp (-S/J_o) \qquad (48)$$

S/J_o = signal-to-jam ratio into DPSK demodulation

Substituting into the previous R_{comp} expression one gets for

$$R_{comp} = 0.5 \text{ bits/digit}, \quad p = 0.045, \quad S/J_o = 3.8 \text{ db}$$

The corresponding J/S_i required equals this value from 10 db for PN processing gain, plus 13 db for TH process gain, plus 20 db for FH process gain. The result is about

$$J/S_i \approx 39 \text{ db}$$

For strong multiple access interference and broad-band noise jamming simultaneously present, the DPSK digit error is taken approximately to be the sum of that when each effect is evaluated separately. Included in Figure 7-41 is the result for the two computed asymptotes above (just multiple access and just jamming, respectively) plus an interpolation curve for simultaneous jamming and multiple access, when a point is computed midway using the latter approximation.

7.3.4.2 Alternate - M-ary PN/TSK/Sequential Decoding, Threshold Detection, (10 db PN, 16 TH, 500 FH)

The signal structure comprises a 50 μsec PN-coded burst (approximately equivalent, though not exact, ringing performance to the binary system; also because of the PN, protection against multipath intersymbol interference results) which is deviated over 16 (M'ary of 16) possible time positions (consecutively spaced by a PN chip width) so as to convey 4 bits in the transmission of one burst in a frame. Since a rate 1/2 sequential decoding is also used, then for a 2400 bps information rate the

-286-

detected in the receiver to give 10 db of processing gain against intersymbol inter-
ference and other in-band interference. DPSK modulation is used for each digit.
Sequential decoding at rate 1/2 is also used so that the 6 digits represent 3 information
bits. For ?400 bps information rate the frame is, therefore, 800 per sec (frame time
is 1250 ⌐s).

For comparison with other modulations here only the direct mode case involving
just very strong multiple access interferers and/or broadband noise jamming will be
considered. The computation is done in terms of R_{comp} which by design will be set
for rate 1/2. The resulting multiple access capacity and J/S performance is computed
from the R_{comp} expression.

$$R_{comp} = -\log_2 \sum_j \left[\sum_i p(i) \sqrt{p(j/i)} \right]^2 \quad \text{bits/digit} \qquad (44)$$

For a digit error probability p (due to either multiple access interference or jamming)
the evaluation of the above expression becomes

$$R_{comp} = -\log_2 2 \left[\frac{1}{2}\sqrt{p} + \frac{1}{2}\sqrt{(1-p)} \right]^2$$

$$= 1 - \log_2 \left[1 + 2\sqrt{p(1-p)} \right] \qquad (45)$$

For strong multiple access interference only (no jamming or thermal noise), the digit
error probability is the probability of an interferer landing in the correct time and fre-
quency slot, times a probability of 1/2 that DPSK demodulation gives the right phase.
The effect of PN processing is neglected for strong multiple access interference.

$$p = \epsilon \frac{1}{2}$$

$$\epsilon = \left[1 - \left(1 - \frac{k}{N}\right)^{(M-1)} \right] \approx M \frac{k}{N} \text{ for M large and } \frac{Mk}{N} \text{ small} \qquad (46)$$

M = number of multiple accesses

k = time slot duty factor

N = number of frequency channels

$$R_{comp} \text{ (multiple access)} = 1-\log_2\left[1 + 2\sqrt{\frac{\epsilon}{2}\left(1 - \frac{\epsilon}{2}\right)}\right] \qquad (47)$$

for $R_{comp} = 0.5$ bits/digit, $\epsilon = 1/10$, $M = 200$

For just broadband noise jamming alone

$$p = \frac{1}{2} \exp{(-S/J_o)} \qquad (48)$$

S/J_o = signal-to-jam ratio into DPSK demodulation

Substituting into the previous R_{comp} expression one gets for

$$R_{comp} = 0.5 \text{ bits/digit}, \quad p = 0.045, \quad S/J_o = 3.8 \text{ db}$$

The corresponding J/S_i required equals this value from 10 db for PN process-ing gain, plus 13 db for TH process gain, plus 20 db for FH process gain. The result is about

$$J/S_i \approx 39 \text{ db}$$

For strong multiple access interference and broad-band noise jamming simultaneously present, the DPSK digit error is taken approximately to be the sum of that when each effect is evaluated separately. Included in Figure 7-41 is the result for the two computed asymptotes above (just multiple access and just jamming, respectively) plus an interpolation curve for simultaneous jamming and multiple access, when a point is computed midway using the latter approximation.

7.3.4.2 Alternate - M-ary PN/TSK/Sequential Decoding, Threshold Detection, (10 db PN, 16 TH, 500 FH)

The signal structure comprises a 50 μsec PN-coded burst (approximately equivalent, though not exact, ringing performance to the binary system; also because of the PN, protection against multipath intersymbol interference results) which is deviated over 16 (M'ary of 16) possible time positions (consecutively spaced by a PN chip width) so as to convey 4 bits in the transmission of one burst in a frame. Since a rate 1/2 sequential decoding is also used, then for a 2400 bps information rate the

Figure 7-41. Multiple Access-A/J Performance of Alternate
Non-Coordinated TH/FH Waveforms

frame time is 800 μsec ($\approx$ 1/1200 sec).. The net TH duty factor, considering burst
length and frame time, that results is 1/16. The scheme here uses 5 μsec wide
PN chips (so that a total of 10 chips are contained in the 50μsec sequence burst) for a
channel bandwidth of 200 KHz. The number of frequency channels then is 500 FH. As
indicated previously, the PN chips are deviated by at least a PN chip (rather than a
whole sequence burst length). This is so as to minimize the total time deviation and
thereby gain a time gating effect against frequency channel spectrum splatter. Actually,
for a total deviation interval of 130 μsec (= 5 x 16 + 50 μsec) out of a 800μsec frame interval,
the protection afforded against spectrum splatter is not as great as for the other
schemes (however, this is how the design parameters fall out). Now the total received
signal is limited, so that amplitude is normalized, and the 10 PN chips are correla-
tion detected. Each possible sequence position is tried until a threshold setting is

exceeded, and that position then is decided on as the correct position in which the sequence was sent. An error in detection will occur primarily when the desired sequence is suppressed in the limiting action by strong interference so that threshold is not exceeded. An error could also occur if the limited, interference signals are not discriminated against by 10 db of PN processing gain after the limiting action; the threshold can be set to make this type of error improbable (it is noted that the reason for the PN part of the waveform structure is primarily to provide the above error protection, as well as to discriminate against multipath intersymbol interference).

The performance analysis for this waveform structure, as well as the subsequent alternate waveforms, uses the same assumptions (i.e., R_{comp} analysis for strong multiple access interference and broadband noise jamming) as for the binary waveform already discussed, and uses the same symbol definitions where possible (only new symbols will be defined here and subsequently). The transitional probabilities in the R_{comp} expression are

$$p(j/i) = \left[\int_b^\infty p_{S+N}(x)dx\right]\left[\int_{-\infty}^b p_N(y)dy\right]^{j-1} + \left[\int_{-\infty}^b p_{S+N}(x)dx\right]\left[\int_{-\infty}^b p_N(y)dy\right]^{m-1}\left[\frac{1}{m}\right] \quad \text{for } i=j$$

$$p(j/i) = \left[\int_{-\infty}^b p_{S+N}(x)dx\right]\left[\int_{-\infty}^b p_N(y)dy\right]^{j-2}\left[\int_b^\infty p_N(y)dy\right] + \left[\int_{-\infty}^b p_{S+N}(x)dx\right]\left[\int_{-\infty}^b p_N(y)dy\right]^{m-1}\left[\frac{1}{m}\right]$$

$$\text{for } i \neq j \text{ and } i < j$$

$$p(j/i) = \left[\int_{-\infty}^b p_N(y)dy\right]^{j-1}\left[\int_b^\infty p_N(y)dy\right] + \left[\int_{-\infty}^b p_N(y)dy\right]^{m-1}\left[\int_{-\infty}^b p_{S+N}(x)dx\right]\left[\frac{1}{m}\right] \quad \text{for } i \neq j \text{ and } i > j$$

$$(49)$$

In Equation (49)

$$\left[\int_b^{\infty} p_{S+N}(x)dx\right] = \text{probability that total signal in the correct signal slot exceeds the threshold setting "b".}$$

$$\left[\int_{-\infty}^{b} p_N(y)dy\right] = \text{probability that signal in the incorrect slot does not exceed the threshold setting "b".}$$

The probabilities for each interfering slot are assumed the same and independent. The M'ary TSK probabilities are all equally likely and independent.

$$p(i) = \frac{1}{m}$$

$$m = \text{number of M'ary TSK positions}$$

Now for just strong multiple access interference the above expressions become considerably simplified.

$$\left[\int_b^{\infty} p_{S+N}(x)dx\right] \approx 1-\epsilon = \text{probability of no interferer landing in correct slot.}$$

$$\left[\int_{-\infty}^{b} p_N(y)dy\right] \approx 1.0 = \text{probability that threshold not exceeded in incorrect slot.}$$

$$\epsilon = \left[1-\left(1-\frac{k}{N}\right)^{M-1}\right] = \text{probability that any of (M-1) other access interferers lands in a given slot.}$$

(50)

The transitional probabilities then become

$$p(j/i) = \left(1-\epsilon\right) + \left(\epsilon\frac{1}{m}\right) \text{ for } i = j$$

$$p(j/i) = \left(\frac{\epsilon}{m}\right) \text{ for } i \neq j \tag{51}$$

-289-

Substituting in R_{comp}

$$R_{comp} \text{ (multiple access)} = -\log_2 \left\{ m \left[\frac{1}{m} \sqrt{(1-\epsilon) + \left(\epsilon \frac{1}{m} \right)} + \frac{m-1}{m} \sqrt{\epsilon \frac{1}{m}} \right]^2 \right\}$$

$$\approx -\log_2 \left[1 + m\epsilon + 2\sqrt{(1-\epsilon)\,\epsilon\, m} \right] \tag{52}$$

Evaluation of this expression for $m = 16$ and to get $R_{comp} = 2$ bits/digit, which represents rate 1/2 coding, yields

$$\underline{M = 400} \text{ for } N = 500 \text{ FH and } k = \frac{1}{16} \left(\text{resulting } \epsilon = \frac{1}{20} \right)$$

Now consider just broadband noise jamming. For incoherent detection of energy in a sequence burst interval (but after PN correlation detection) the integral expressions for the transitional probabilities are the familiar Rician and exponential ones, respectively.

$$\int_b^\infty P_{S+N}(x)dx = \int_b^\infty x \exp\left(\frac{x^2 + a^2}{2} \right) I_0(ax)\,dx, \quad x \geq 0$$

$$a = \sqrt{2\frac{E_{burst}}{N_0}}$$

$$\int_{-\infty}^b P_N(y)dy = \int_{-\infty}^b y \exp\left(-\frac{y^2}{2} \right)dy, \quad y \geq 0$$

$$= 1 - \exp\left(-b^2/2 \right) \tag{53}$$

Though there likely is an optimum threshold setting considering system performance for purposes of analysis the threshold setting was selected so that to a first approximation the commissive error terms can be neglected. Corresponding terms are therefore neglected in the transition probability expressions, as they were for evaluation of just multiple access interference. Instead of the probability in terms of ϵ, one now has, however, the Rician distribution to evaluate. Solving R_{comp} for rate 1/2

coding one gets an E_{digit}/N_o required of 10 db. For this computation a normalized threshold setting of 6 db was used. Taking into account the total processing gain of 49 db (=10 db PN + 12 db TH + 27 db FH) the allowed jam-to-signal ratio is 39 db. The asymptotic results computed for jamming and multiple access interference alone, are shown in Figure 7-41. To evaluate the intermediate cases of simultaneous types of interference, the assumption or approximation is made that one can add the jam slot error probability (given by the Rician distribution) to the multiple access slot error probability (given in terms of ϵ). Computing a sample intermediate point and interpolating one gets the shape of the curve in Figure 7-41.

7.3.4.3 Alternate - M'ary FSK/Sequential Decoding, Threshold Detection, (16 TH, 5000 FH

The signal structure comprises a single 50 μsec pulse (same ringing performance as before; also there is no multipath intersymbol interference in this case but only a fading effect which is easily handled by the error correction coding) which is sent on one of 16 (M'ary of 16) possible frequencies so as to convey 4 bits in the transmission of one pulse in a frame. Since a rate 1/2 sequential decoding is also used then the frame time is 800 μsecs once again. The time duty factor allowed for the MFSK modulation is also 1/16 (the time slot is permuted on a frame-to-frame

basis. This TH factor is also the time-gating factor for spectrum splatter due to wide dynamic range interferers. Now the channel bandwidth allowed for a 50 μsec pulse is nominally 20 KHz. In 100 MHz there is then a frequency slotting factor of 5000 FH. That is, frequency hopping of the MFSK waveform (in which the M'ary frequency channels are different 20 KHz ones also) occurs over this number of channels, with frequencies changed on a frame-to-frame basis (every 800 μsecs, or at 1250 bps). The transmitted pulse, being only of 50 μsecs duration, of course, gives better repeat jam protection than this Now receiver detection of the MFSK waveform in this scheme involves threshold detection of the first channel, in an arbitrary channel sampling sequence, with an output. This scheme then is insensitive to the absolute value of the channel signal provided only that it is above the threshold setting. Commissive type errors will occur then, if there is sufficiently strong interference in any channel that precedes the correct one in the scan sequence. Omissive type errors (which involve suppression of the correct signal) are however unlikely to occur, since when an interferer lands in the correct channel it will mainly

serve to reinforce the energy and, thus, actually aid detection of the correct signals. Now with regard to commissive errors one would expect that the large number of frequency and time slots (80,000 total) reduces the probability of an interferer landing in a given channel. Furthermore, since the first threshold exceedance in a scan sequence is accepted, and since M'ary channel transmission is equally likely over all channels then half the time, on the average, the interference-containing channels will be ignored. The sequential decoding then would handle the remaining commissive errors that would occur after threshold detection.

The transitional probabilities for use in the R_{comp} expression have the same general form as already given for the M'ary PN/TSK scheme and, therefore, need not be repeated here. On the other hand, whereas the M'ary PN scheme for strong multiple access interference allows simplification of the expression by neglect of the commissive error terms, the MSK scheme here allows simplification of the expression by neglect of the omissive error terms (assuming the threshold is set appropriately).

$$\left[\int_b^\infty p_{S+N}(x)dx \right] \approx 1.0$$

$$\left[\int_{-\infty}^b p_N(y)dy \right] \approx 1 - \epsilon \tag{54}$$

Therefore,

$$p(i/i) = (1 - \epsilon)^{j-1} \qquad \text{for } i = j$$

$$p(j/i) = (1 - \epsilon)^{j-1}\epsilon \qquad \text{for } j < i$$

$$= 0 \qquad\qquad j > i \tag{55}$$

Substituting the above into, and then evaluating, the R_{comp} expression for multiple access interference alone becomes

$$
\begin{aligned}
r_{comp} = -\log_2 \Bigg| &\left[\frac{1}{m}\left(1 + (m-1)\sqrt{\epsilon}\right)\right]^2 \\
&+\left[\frac{1}{m}\left(\sqrt{1-\epsilon} + (m-2)\sqrt{\epsilon(1-\epsilon)}\right)\right]^2 \\
&+\left[\frac{1}{m}\left(\sqrt{(1-\epsilon)^2} + (m-3)\sqrt{\epsilon(1-\epsilon)^2}\right)\right]^2 \\
&+\ \vdots \\
&+\left[\frac{1}{m}\left(\sqrt{(1-\epsilon)^{m-2}} + \sqrt{\epsilon(1-\epsilon)^{m-2}}\right)\right]^2 \\
&+\left[\frac{1}{m}\sqrt{(1-\epsilon)^{m-1}}\right]^2 \Bigg|
\end{aligned}
\tag{56}
$$

For R_{comp} equal to 2 bits/digit and m of 16, one gets

$$
\underline{M \doteq 1500} \text{ for } \epsilon = \frac{1}{50}, \quad N = 5000, \quad k = \frac{1}{16}
$$

For analysis of just broadband noise jamming it is desired for convenience of analysis (though not necessarily for optimum design) to make similar assumptions on commissive versus omissive errors. Under this assumption then one sets the jam slot commissive error probability (since incoherent detection is used here the same exponential expression, as indicated in the M'ary PN discussion, applies) equal to the value of 1/50 just solved for ϵ above. The normalized threshold setting required is then

error probability (since incoherent detection is used here the same exponential expression, as indicated in the M'ary PN discussion, applies) equal to the value of 1/50 just solved for ϵ above. The normalized threshold setting required is then solved to be 6 db. One evaluates the slot omissive error rate probability (given by a Rician distribution) now to determine the value of E_{digit}/N_0 needed for this normalized threshold setting, so that the effect on R_{comp} of omissive errors can indeed be neglected as already assumed above. As already stated, this may not give an optimum system design but it is convenient for analysis here. Solving this way one gets a required E_{digit}/N_c of 12 db. Factoring in the processing gain of 49 db results in a jam-to-signal ratio required of 37 db. The asymptotic jam and multiple access

results are superposed on Figure 7-41. The shape of the intermediate connecting curve is obtained by computing an intermediate sample point and interpolating. This sample point is obtained by assuming that the slot error rate due to simultaneous jamming and multiple access interference is the sum of the error rates computed for each alone. One then proceeds in a similar manner to the above to compute J/S and M.

7.3.4.4 Alternate - M'ary FSK/Sequential Decoding, m = 16, List of ℓ Decode, (1/16 TH, 5000 FH)

The signal structure for this scheme is identical with the scheme just described in Section 7.3.4.3. What is different is that instead of threshold receiver detection, one uses list of ℓ decoding instead. This detection scheme involves examining the actual amplitudes in each of the m received channels and ordering them in a list of ℓ, largest in amplitude. Sequential decoding is used in combination. By making the list large (ℓ = m) maximum use is made of available information in the received channel signals. One would expect in this case then that better performance can be obtained than with threshold detection that has just been described for the same waveform structure. On the other hand, one trades increased complexity for this. The "list of ℓ" decoding scheme has been implemented in the LET terminal. What we seek to do here is to evaluate for comparison purposes the performance of it for our waveform structure and for strong multiple access interference (results are not given in the published literature) and also to apply the published jam results (this saves on computations here) to our waveform structure. The analysis here will be for both ℓ = m = 16 and ℓ = 1 and m = 16. The latter, hard decision case is, of course, not as good and one would expect that it is also not as good as that for the threshold detection scheme of Section 7.3.4.3 in strong multiple access interference (reason is that since one picks the channel with the biggest amplitude, and since all interference channels will be strong, then the only useful aspect of the detection scheme is that when the correct channel is also hit its energy is reinforced and one has an improved probability of success). It is given here only to bound the results.

The expression for R_{comp} for list of ℓ has been derived in the published literature[*] to be

---

[*] K. Jordan, op.cit.

$$R_{comp} = -2 \log_2 \left[\frac{1}{\sqrt{m}} \sum_{j=1}^{\ell} \sqrt{r_j} + \sqrt{\left(1-\frac{\ell}{m}\right)} \sqrt{1- \sum_{j=1}^{\ell} r_j} \right] \qquad (57)$$

where

$$r_j = \binom{m-1}{j-1} \int_{-\infty}^{\infty} p_{S+N}(x)dx \left[\int_{-\infty}^{x} p_N(y)dy\right]^{m-j} \left[\int_{x}^{\infty} p_N(z)dz\right]^{j-1} \qquad (58)$$

r_j is the probability that the correct signal channel occupies position j in the list.

For just strong multiple access interference, the assumption is made here that when the correct signal channel is not hit, then its amplitude is greater with unity probability than any other channel that has not been hit. Whereas with unity probability, the correct channel (when not hit) is smaller than a channel that has been hit. On the other hand, if the correct signal channel is hit then it is assumed that with probability of 1/2 it is greater than any other channel that has been hit. Under these assumptions, the above expression for r_j is seen evaluated to be

$$r_j = \binom{m-1}{j-1} \left\{ (1-\epsilon)(1-\epsilon)^{m-j} \epsilon^{j-1} + \epsilon \left[(1-\epsilon) + \left(\epsilon \frac{1}{2}\right)\right]^{m-j} \left(\epsilon \frac{1}{2}\right)^{j-1} \right\} \qquad (59)$$

Substituting into R_{comp} and evaluating for m = 16 and R_{comp} = 2 bits/digit one gets the following:

For ℓ = 16, $\epsilon > \frac{1}{20}$ and <u>M $\approx$ 4000</u>, k = $\frac{1}{16}$, N = 5000 FH

For ℓ = 1, $\epsilon = \frac{1}{179}$ and <u>M = 450</u>, k = $\frac{1}{16}$, N = 5000 FH

For just broadband noise jamming alone the published results can be applied with our processing gain to give:

For ℓ = 16, $\frac{E_{digit}}{N_o}$ = 8 db, <u>J/S = 41 db</u>

For ℓ = 1, $\frac{E_{digit}}{N_o} \approx 9.5$ db, <u>J/S = 39.5 db</u>

-295-

These asymptotic results are superposed on Figure 7-41.

7.3.4.5 Effect of Partial Band and/or Pulsed Jamming

Although it is common to compute performance for white Gaussian noise interference, an AJ receiver actually should be considered with jamming optimized as a threat for the presumed waveform parameters. The jammer can gain effectiveness by a partial band and/or a pulsed strategy, rather than uniformly occupying all frequency-time slots. This behavior will be examined with respect to the hypothesis that the jammer maintains a fixed average power. The parameter describing jamming strategy is α, the fraction of total time-frequency slots occupied at random.

For data transmission after synchronization, the behavior of PSK waveforms has already been investigated as part of Section 7.3.1. If interleaving is presumed to render the channel effectively memoryless, the degradation was shown to be relatively small; as an example with a rate 1/2, hard decision channel, the degradation is about 1 db with coherent PSK data modulation (see Figure 7-23). Thus, the error correction capability of sequential decoding is able to combat partial occupancy jamming very effectively provided that the resultant errors are randomized.

Now refer to the M'ary FSK waveform using threshold detection to enhance multiple access described in paragraph 7.3.4.3. Although the AJ performance was estimated for broadband noise jamming, an optimized jamming threat was not considered there, and is now analyzed. For purposes of worst-case analysis here, the jamming will be composed of tones randomly occupying a specified fraction α of the total number of frequency slots (5000). They each have an amplitude slightly exceeding the threshold setting $A < 1$, where the desired signal has unit amplitude. In the previous analysis, the allowed false threshold triggering was designated to be ϵ, and a value $\epsilon \sim 0.02$ yielded R_{comp} 2 bits/digit. Thus, if the effect of the jamming falling on the frequency of the desired signal is ignored for the moment, the maximum occupancy is $\alpha = \epsilon = 0.02$.

It appears a reasonable choice that the threshold setting $A = 0.707$, which allows some margin for amplitude fluctuation of the desired signal. With this, the resulting J/S, considering the time hop factor of 16 slots, is

$$J/S = (.02)(.707)^2 (5000)(16) = 29 \text{ db} \tag{60}$$

This J/S is degraded from the value previously estimated for broadband jamming by 8 db and corresponds to an $E_b/N_o = 17$ db.

The effect of jamming falling on the desired signal is to cause a probability δ that the threshold will not be tripped in the correct frequency slot. These omissive errors were previously not considered. The transition probabilities for receiving j if i is transmitted can now be written.

$$p(j/i) = (1 - \epsilon)^{j-1}\epsilon + \frac{(1 - \epsilon)^{M-1}\delta}{M} \qquad j < i$$

$$p(j/i) = (1 - \epsilon)^{j-1}_i (1 - \delta) + \frac{(1 - \epsilon)^{M-1}\delta}{M} \qquad j = i \qquad (61)$$

$$p(u/i) = (1 - \epsilon)^{j-2}\delta\epsilon + \frac{(1 - \epsilon)^{M-1}\delta}{M} \qquad j > i$$

and R_{comp} computed for various choices of ϵ and δ.

For the previous choice of threshold A = .707, the envelope of a randomly phased jamming tone of amplitude A combined with the signal of unit amplitude is less than A with probability 1/4. This leads to the omissive probability of 0.25ϵ. It is found that the allowed occupancy α is reduced from 0.018 for $\delta = 0$ to 0.014 for $\delta = 0.25\epsilon$. Thus, the more accurate computation reduces J/S to about 28 db, and the previous approximation turns out to be reasonably accurate.

7.3.4.6 Conclusions

If one examines the asymptote results for the different modulations in Figure 7-41 (the intermediate points on the curve are not of as great significance, both because one expects the curve to be monotonic and because all points on the curve have not been determined precisely for reasons of ease of analysis here), it is seen that substantial improvements in multiple access capacity are possible whereas these systems main-tain comparable J/S performance; i.e., within a few db for noise jamming. Though the MFSK scheme with list $\ell = 16$ is best, it is also expected to be more complex than the MFSK scheme with threshold detection, which is second best. The latter still gives a reasonably high multiple access capacity at 1500. It therefore appears that this MFSK scheme be retained for further consideration. The AJ implications of the use of threshold detection to improve multiple access has been further examined. The observed AJ vulner-ability leads to rejection of threshold detection schemes. It is reasonable to consider

-297-

yet another TH/FH version using MFSK with M'ary block codes replacing M'ary sequential decoding to reduce implementation complexity (with consequent performance degradation). This waveform is retained as a candidate for further study in Section 4.2.3 of Volume I.

7.3.5 MULTIPLE ACCESS WITH NONCOORDINATED WAVEFORMS OVER A POWER-LIMITED SATELLITE CHANNEL

In the satellite (remote) mode for CNI, the question arises of relative system utilization with coordinated and uncoordinated waveforms. In view of the assumption of an omni aircraft antenna, a 100 MHz satellite channel typically is power starved for the comparison. (Received power in earth terminal less than noise in the channel bandwidth.) Because of this, the remote mode is a different problem than the direct mode.

The channel can be characterized by orthogonal slots that are non-interacting These are entirely time slots for the simplest example of a hard limiting repeater and are the product of time slots and frequency slots for a channelized repeater with separate limiting in each channel.[*] For a specified number of accesses, a coordinated system needs exactly that number of orthogonal slots, and the required satellite power can be computed directly therefrom by sharing among the accesses. An uncoordinated system needs a larger number of slots to accommodate statistical overlap, and the required satellite power is thereby increased.

7.3.5.1 Worst Case of Large Transmitter Power Differentials

The general analysis of uncoordinated systems without power control of transmitter outputs has previously been outlined.[**] Numerical results of coherent PSK modulation are extended here to provide a more detailed comparison with coordinated systems. The system model is worst case in that the probability of error is assumed to be 0.5 for the desired signal whenever overlap in its slot occurs. Otherwise, the probability of error is determined by downlink S/N. The average probability of error is to be computed.

---

[*] Second order considerations such as losses for 'tiple channels in a satellite are ignored in this discussion.

[**] Aein and Schwartz, eds., "Multiple Access to a Communication Satellite with a Hard-Limiting Repeater," IDA Report R-108, Vol. II, April 1965.

If the ratio of number of accesses to number of slots is denoted by ϵ, the average probability of error is, to a good approximation with a large number of slots,

$$P_e\bigg|_{uncoordinated} = \left[1 - \exp(-\epsilon)\right] 0.5 + \exp(-\epsilon)\left[1 - \Phi\left(\sqrt{\epsilon\, 2S/N}\right)\right] \qquad (62)$$

where S/N is the signal-to-noise ratio per access, assuming ideal sharing, as is the case for the coordinated system. That is,

$$P_e\bigg|_{coordinated} = 1 - \Phi(\sqrt{2S/N}) \qquad (63)$$

where $\Phi(x)$ denotes the Gaussian probability distribution applying to coherent PSK.

For any value of S/N in Equation (62), ϵ can be optimized to yield minimum probability of error. This corresponds to making the best choice of number of slots as a compromise between effects of overlap and downlink noise. The S/N for the same probability of error in the coordinated system then gives the multiple access degradation, to be interpreted as savings in satellite power for the identical number of access with coordination. Alternatively, the degradation may be interpreted as the additional accesses which can be handled in a coordinated system with the same satellite power, provided that the available bandwidth is not exceeded. Numerical results are presented in Figure 7-42.

The degradation is less at high digit error probabilities, which implies desirability of PN processing as an example of high redundancy coding in a slot in order to reduce the multiple access degradation. This is feasible until the available bandwidth is used up for the required number of accesses. Performance may be approximated by assuming transmission at R_{comp} for the binary channel given by

$$R_{comp} = 1 - \log_2\left(1 + 2\sqrt{P_e(1 - P_e)}\right) \text{ bits/digit} \qquad (64)$$

As an illustration, suppose $P_e = 0.31$ for which $R_{comp} = 0.05$, approximately corresponding to a system with 10 db of PN processing and rate 1/2 sequential decoding. Figure 7-42 shows the optimum occupancy to be 0.4 and the multiple access
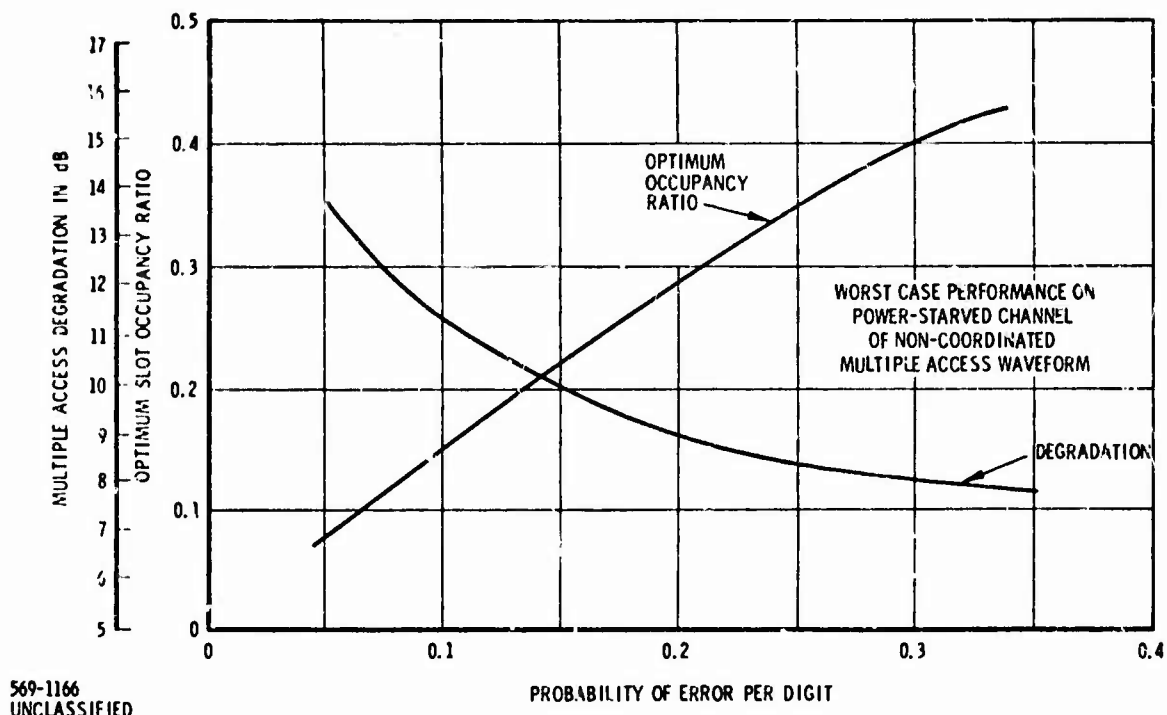
Figure 7-42. Multiple Access on Satellite Channel

degradation to be 8 db. For a channel bandwidth of 100 MHz and a data rate per access of 2400 bits/sec, this allows

$$\text{No. of accesses} = \frac{10^8}{2400} \ (.05) \ (.4) = 833 \tag{65}$$

provided that the available satellite power is 8 db higher than would suffice for orthogonal occupancy with this number of accesses. A coordinated system with identical PN processing and coding (yielding .05 bit/digit) would utilize 40 MHz for the same number of accesses. Thus, the 8 db cannot be directly interpreted as allowing 6.3 times as many accesses. Actually, the number can be increased only the the factor 2.5 unless the amount of PN processing is reduced below the 10 db presumed for the illustrative calculation.

To continue the comparison, now suppose that the PN processing is eliminated and rate 1/2 coding is employed. Then, $P_e = .045$, and Figure 1 shows the optimum occupancy to be 0.07 and the multiple access degradation to be about 14 db. The number of accesses for the channel is then

-309-

$$\text{No. of accesses} = \frac{10^8}{2400} \; (.5)\,(.07) = 1460 \tag{66}$$

Now, the coordinated system for the same number of accesses would occupy 7 MHz. The overall performance of the non-coordinated system for the last computation although showing more accesses (higher bandwidth efficiency) is actually poorer in terms of use of satellite power, since the multiple access degradation now is 6 db greater than previously computed.

If 10 db of PN processing is now included within a slot, the number of slots is reduced by the factor of 10. In that case, the number of accesses is reduced to 146. instead of the value in Equation (66), still leaving a multiple access degradation of 14 db. This result may be compared with the value of 833 computed in Equation (65) for the identical modulation structure. The difference is due to the independent use of each of the 10 PN chips assumed in the previous model, as opposed to use of the sum (correlation) for the present result.

7.3.5.2   Ideal Equalized Transmitter Powers

The impact of satellite power limitations for a hard-limiting repeater satellite on multiple access capacity for a non-coordinated TH/FH/PN waveform is now indicated. As an ideal goal, power control for all signals accessing the satellite is assumed (the waveforms are uncoordinated only in the sense that their time of accessing is random and independent of each other) so that they appear at the satellite with equal strength. Two cases of satellite power impact are considered here: (1) the case where the satellite mode and direct mode are in separate frequency bands - the satellite power impact occurs in that different signal accesses will randomly overlap so that total satellite power is divided up for these instants whereas when there is no overlap full satellite power is available to each signal; also for those cases of time overlap in the same frequency channel, there is in-band mutual interference which is discriminated against by PN processing in the ground receiver; (2) the case where the satellite downlink and the direct mode are in the same frequency band so that the satellite downlink receiver sees direct mode interference - an increase in satellite power is needed to reduce the satellite access effect on signal-to-thermal noise ratio so as to allow for the added direct mode interference. The non-coordinated TH/FH/

-301-

PN waveform considered is as described in Section 4.2.2 of Volume I, except that the situation is discussed where the system is more limited by satellite power than bandwidth (the reason is that omni aircraft antennas make the satellite power budgets marginal at L-band).

Let us now determine the results. Since the interference is statistical, the link performance is expressed in terms of digit error rate after DPSK demodulation in the satellite downlink receiver. This then is the error rate into the sequential decoder. A value of 0.05 for it is taken to give a 10^{-5} bit error rate out of the decoder for rate 1/2 coding. The bit error rate expression after DPSK demodulation, and for satellite signal in a separate band from the direct mode, is formulated to be the following.

$$P_{e_1} = \sum_{n=0}^{M_s} \sum_{m=0}^{n} k^n (1-k)^{M_s-n} (1/N)^m (1-1/N)^{n-m} 1/2$$

$$\exp - \left[\frac{\dfrac{P_s S \alpha_n}{(n+1) S + n_{os} W} \times TW_{PN}}{P_s \times \dfrac{S(n-m)(1-\alpha_n) + Sm + n_{os} W}{(n+1) S + n_{os} W} + n_{oG} W_{PN}} \right]$$

where

k = duty factor

N = number of frequency channels

M_s = number of other access signals at satellite

n = number of these that overlap at a given time

m = number of the latter that are also in the same frequency channel as well as overlapping in time.

S = power of each access signal arriving at satellite – the same for all accesses because of perfect power control.

$n_{os} W$ = satellite uplink receiver noise in a bandwidth of W (W = 100 MHz).

P_s = satellite peak power as reflected to the downlink ground receiver input.

α_n = signal suppression effect because of interaction of multiple signals into a hard-limiter

For $n_{os} W \ll S$ for equal strength signals $\alpha_n \approx -1$ db when there is overlap.

-302-

$n_{oG}W_{PN}$ -- downlink ground receiver thermal noise level in PN channel bandwidth of 1 MHz.

TW_{PN} -- PN processing gain in ground receiver = 10 db.

In the above digit error rate expression, the instantaneous error rate expression for DPSK demodulation is $\left[\frac{1}{2}\exp -\left(\frac{S}{N_0}\right)\right]$ where the instantaneous S/N_0 accounts for the fact that the signal share of satellite power is down by the number n of signal overlaps and by the signal suppression effect α_n and by the retransmitted satellite receiver noise share of satellite power, and the fact that the channel additive Gaussian interference includes the in-band multiple access interference due to m signals at that instant plus ground receiver thermal noise. The DPSK error expression is weighted by the probability of occurrence of n simultaneous overlaps in time and m simultaneous overlaps in the same frequency channel. One performs a double summation of these probabilities over m and n to get the resultant digit error rate P_{e1} into the sequential decoder in the satellite downlink ground receiver.

Figure 7-43 gives plots of what the increase in satellite power P_s must be, for $P_{e1} = 0.05$ so that the system bit error rate is 10^{-5}, versus the number of other signal accesses M_s. The increase in satellite power required is referenced to that value needed when there is no overlap of signals, such as in a corresponding coordinated TDMA system that is designed for full capacity. The increase in satellite power required then is the penalty paid for use of non-coordinated TH/FH/PN waveforms. Figure 7-43 plots the results for just one TH duty factor; i.e., 1/100. The preceding equation could be evaluated on a computer to get a comprehensive range of parametric results for different TH duty factors, numbers of FH frequency channels, and amount of PN processing gain. For the results in Figure 7-43, satellite receiver noise is assumed to have a negligible effect because narrow beam satellite antennas are assumed on the uplink. To reduce the degrading impact on satellite power requirements as given in Figure 7-43, one should go either to an all frequency hop-PN system with power control (so that for a given system capacity at least the satellite-power-splitting is constant since the overlap is constant), or preferably to an all coordinated TH design (with either FH or PN allowed in each TDMA slot). The latter is, of course, preferred since no mutual interference of any type results. It is noted that if power control of uplink signals were not assumed in the analysis, then the impact on satellite power would

be significantly greater than in Figure 7-43 (results would be worse), as previously computed.

Similarly, if in practice power control cannot be maintained, say to within 1 db, then the satellite power needed increases perceptibly. To place the results of Figure 7-43 in perspective, and to justify the assumption on satellite receiver noise, Table 7-9 gives a possible satellite power budget for frequencies in the 1 to 2 GHz range. It is seen from Table 7-9 that by assuming 2° uplink satellite receiver antenna beams, a peak-to-average power trade for a 1/20 duty cycle transmitter and 1 KW average, and a 1 GHz frequency that a positive S/N-received occurs on the satellite uplink for one access. Satellite receiver noise can, therefore, be neglected even for this case. For a smaller time duty factor yet; i. e., 1/200, the positive S/N at the satellite receiver will be even more pronounced. It is also seen from Table 7-9 for the satellite downlink that even with the assumption of a powerful satellite transmitter; i. e., 200 watts, and 2° satellite antenna downlink beams, a low L-band carrier
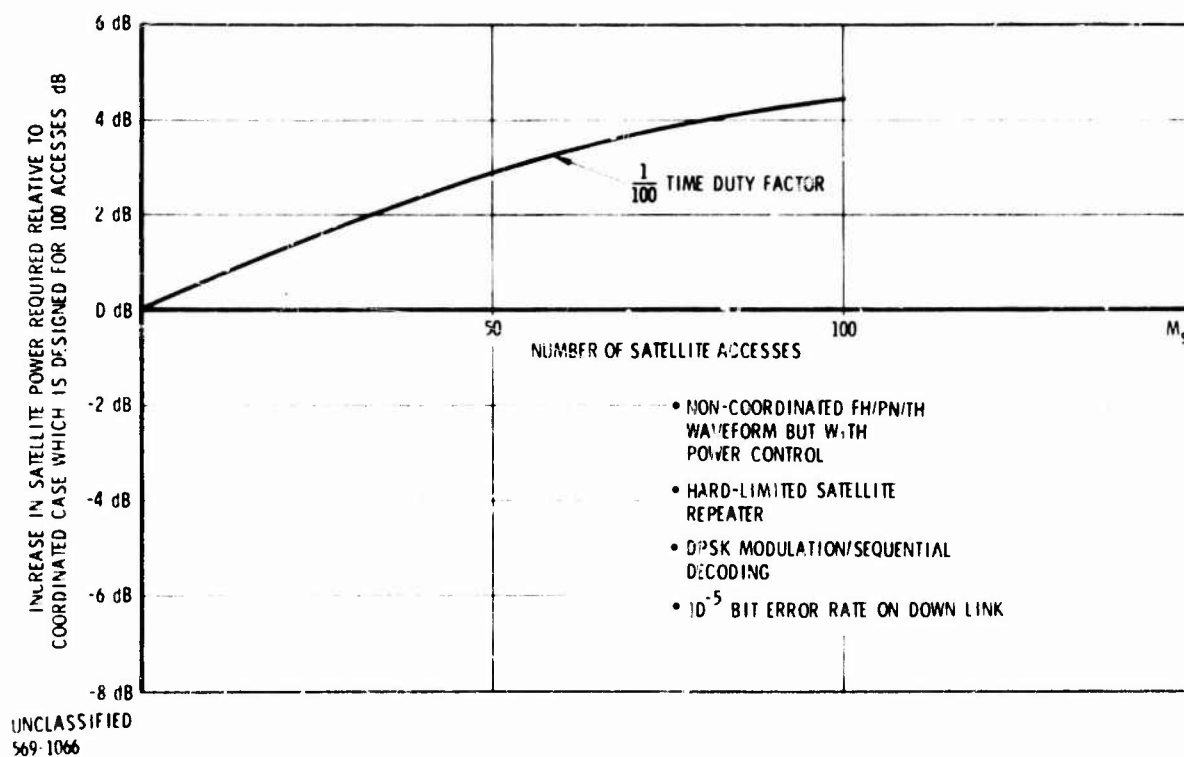
Figure 7-43. Impact on Satellite Power for Just Satellite Access with Power Control

-304-

frequency of 2 GHz, that the aircraft-received signal strength has only +2.9 db margin over the minimum needed for the system to have a 10^{-5} bit error rate. Now this condition is for a 1/200 time duty factor (allowing therefore 200 simultaneous accesses ideally) and no allowance made for signal overlap effects as in Figure 7-43. It is seen, therefore, that the satellite downlink is indeed power starved. Satellite power degradation of the type indicated in Figure 7-43, therefore, must be minimized, and this is a strong argument for insisting on a coordinated waveform design for the remote mode.

Table 7-9. Possible Satellite Power Budgets

	Downlink	Uplink
Frequency	2 GHz	1 GHz
Transmitter power peak	200 W (23 dbw) satellite	20 KW (37 db) ground for 1/20 duty factor and 1 KW average
Satellite antenna	2° beam (37 db)	2° beam (37 db)
Link loss (space & misc)	193 db	187 db
User antenna gain	0 db	0 db
Net received carrier power	-133.1 dbw	-107 dbw
Receiver noise spectral density (6 db NF)	-199.0 dbw/Hz	-199.0 dbw/Hz
Ratio of carrier power-to-noise density	65.9 db-Hz	92 db-Hz
Corresponding S/N	+5.9 db for 1/200 time duty factor and 4800 digit per sec. ch.	+12 db in 100 MHz bandwidth
Required S/N	+3 db per digit for DPSK/ Seq. Dec.	
Margin	+2.9 db	

7.4 CHANNEL DISTORTION ANALYSIS

This section contains a discussion of two problems associated with signalling through a bandpass limiting channel, such as a satellite communication repeater. The first discussion treats the effect of limiting that increases spectrum splatter of a pulse filtered to reduce out of band interference. The second discussion considers the degradation in downlinks E_b/N_o to support high-rate burst transmission (such as pure TDMA) through a hard limiting bandpass channel.

7.4.1 SPECTRUM SPLATTER OF A GAUSSIAN FILTERED PULSE AFTER SOFT LIMITING

In considering transmission of a pulse shaped to reduce spectrum splatter into adjacent frequency slots, linearity requirements imposed on the power amplifier become critical. For example, efficient operation of a TWT requires operation in the nonlinear region. The purpose of this discussion is to illustrate this by a computer analysis of a simplified model to display the power spectrum of a signal at the output of an overdriven soft limiter to determine channel interference for particular operation of the soft limiter (TWT). Figure 7-44 shows a pulse waveform modulated on a carrier, filtered, and transmitted through a soft limiting amplifier. For analysis, the pulse is assumed rectangular in shape, a Gaussian filter $H(j\omega)$ is introduced, and the amplifier includes a memoryless finite peak clipper. The channel, denoted by $G(j\omega)$, is presumed to be very wideband. Because the signal has symmetrical sidebands, the system can be analyzed at low pass by frequency translating the filters and spectrums
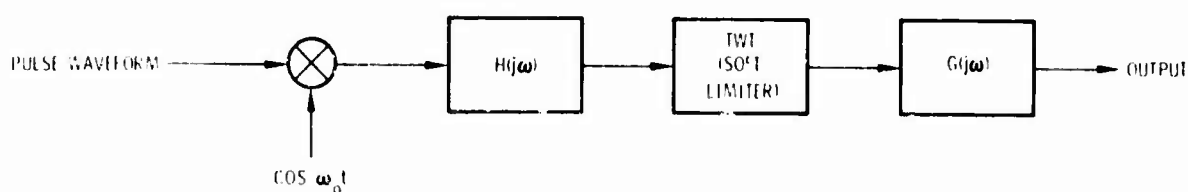
Figure 7-44. Block Diagram of the System Model

The Gaussian filter is assumed to have no phase distortion and therefore is specified by the transfer function

$$H(j\omega) = \exp\left[-.35\frac{\left(\omega-\omega_o\right)^2}{\omega_c^2}\right] \tag{67}$$

where

$\omega_o = 2\pi f_o$ = signal center frequency

$\omega_c = 2\pi f_o$ = 3 db frequency offset from center

The TWT (soft limiter) characteristic is described in terms of the input-output power relationship as

$$P_o = f(P_{in}) \tag{68}$$

where

P_{in} = input power

P_o = output power

For analysis, a memoryless voltage transfer function was presumed of the form

$$v_o = \begin{cases} v_{in} & , \; |v_{in}| < \alpha \\ \alpha v_{in}/|v_{in}| & , \; |v_{in}| > \alpha \end{cases} \tag{69}$$

The output spectrum was found by multiplying the pulse signal transform with the transfer function of the Gaussian filter. The resulting transform was inversely Fourier transformed yielding a time domain signal which was passed through the soft limiter. The output was then Fourier transformed and the power spectrum was determined.

The calculations and transforms were performed using a digital computer and a Fourier transform algorithm. The total number of samples in the transforms was chosen to be

$$N = W_s T_s = 512 \tag{70}$$

It was specified that the study examine 32 lobes from the center lobe and power density as low as -80 db. From these requirements the transform frequency region was chosen to be

$$W_s = 80./T \qquad (71)$$

where

T = bit duration

and the time-frequency region is

$$T_s = \frac{N}{W_s} = 6T \qquad (72)$$

The number of samples in a spectrum lobe is

$$2n_f = \frac{2T_s}{T} \qquad (73)$$
$$= 12$$

with T normalized to 1.

The number of samples in a bit duration of T is

$$n_t = \frac{NT}{T_s} \qquad (74)$$
$$= 80$$

Thus, fine sampling in the time domain is used to achieve the required frequency range.

Shown in Figure 7-45 is a typical output plot. The upper curve is a plot of sin x/x and the lower plot is the power spectrum with $\alpha = 1.5$. The 3 db filter bandwidth is taken to be 5/6 of the null-to-null pulse bandwidth, 2/T, for this plot. Also shown are the computed spectrum peaks for a linear amplifier, obtained by simply reducing the peaks of the spectrum of the rectangular pulse by the power transfer function of the Gaussian filter.

It is observed that even a modest degree of clipping will bring up the spectrum splatter considerably from the idealized Gaussian filter case.
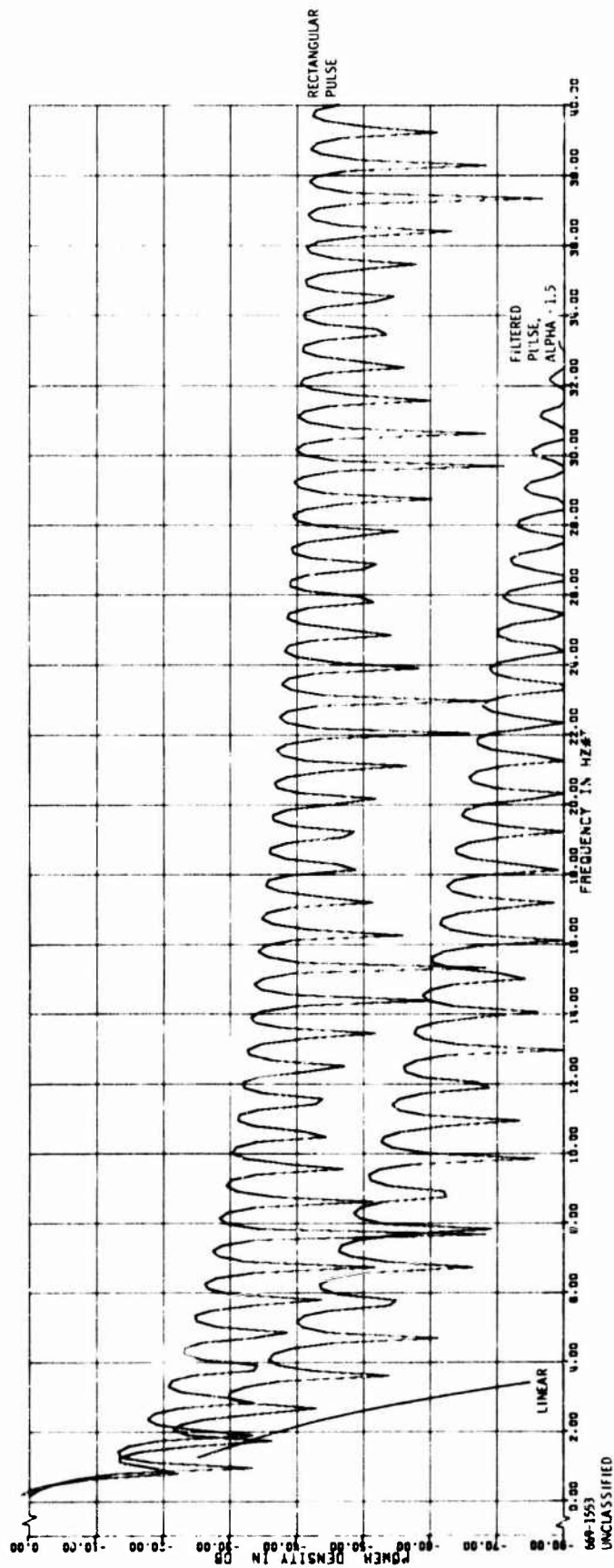
Figure 7-45. Plot of Output Spectrum Showing Effects of
Soft Limiting

7.4.2 EFFECT OF BANDLIMITING ON PSK SIGNAL IN TDMA BURST THROUGH HARD LIMITING CHANNEL

Transmission of a signal through a channel, such as a satellite communication channel, results in distortion of the signal due to bandlimiting in the individual channels, hardlimiting, and placement of the narrow individual channels in an unsymmetrical portion of the wideband channel particularly near its edge. The purpose of this discussion is to study the effects that channel distortion due to filtering and hardlimiting have on the performance of 2-phase PSK and 4-phase PSK. The results will be used to determine the maximum bit rate which can be transmitted through a channel having a particular bandwidth with a specified limit in degradation of performance. These results are preliminary and further extension and capabilities will be discussed.

Shown in Figure 7-46 is the block diagram of the system being studied. A 2-phase or 4-phase signal is transmitted through the channel as shown and is coherently detected at the detector. Transmission of a signal through a bandpass filter results in amplitude distortion, phase distortion, and group delay. Each pulse is smeared into the preceding and following pulse (or pulses for narrow bandwidths). The nonlinearity operates on the absolute value (i.e., the envelope amplitude) of the distorted signal producing a signal with an absolute value that is constant but whose duration at any one phase varies depending on the preceding and following pulses. Thus, the integration start time and integration time which will yield minimum degradation must be determined.
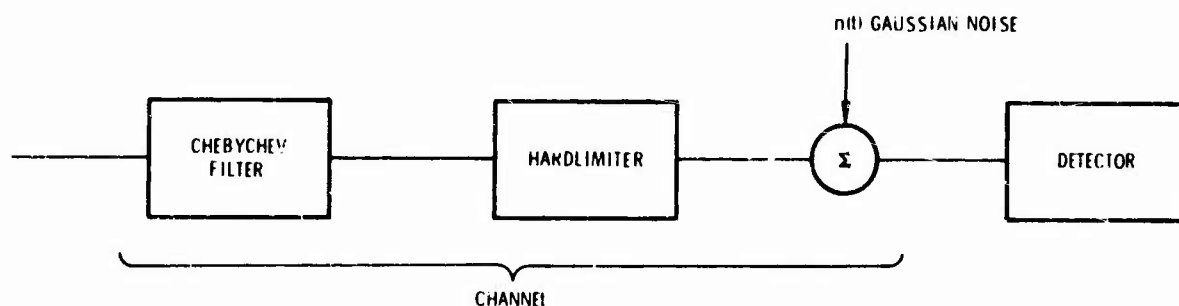
Figure 7-46. System Model

-310-

The study is performed using a FORTRAN program that performs the following operations:

1.   The amplitude spectrum of a single square pulse of duration T is generated and then transformed with a Chebychev filter having a particular number of poles, a specified ripple, and bandwidth W.

2.   The amplitude spectrum at the output of the filter is inversely Fourier transformed resulting in a single distorted pulse.

3.   The single pulse is advanced and delayed in time and given the appropriate phase resulting in a set of pulse sequences exhausting all possible cases for the chosen number of pulses in a sequence.

4.   Each sequence is passed through the nonlinearity and a vector representing the pulse to be detected is determined by integrating the real and imaginary components of the pulse using different starting points in time and different integration times.

5.   A reference is determined from the set of received signal vectors and the probability of a bit error is found for various signal-to-noise ratios, integration start time and integration time; i. e., delay and aperture.

6.   The probability of bit error is plotted versus signal-to-noise ratio for various delays and aperture in the region of the best values determined above.

Thus, in general, the study yields probability of error curves for a particular filter and nonlinearity given either 2-phase antipodal modulation or 4-phase biorthogonal modulation.

7.4.2.1 <u>Discussion of the Solution Techniques</u>

7.4.2.1.1 Distortion of the Signal Vectors

A signal having energy E, to be transmitted through a channel and detected at a receiver, can be represented as a vector in a signal space as shown in Figure 7-47. Both the 2-phase and 4-phase cases can be studied since the distortion to a single vector in either case is the same. The programs for each case are identical in

ψ₂

② d/2 d/2 ①
- √E̅ √E̅ ψ₁
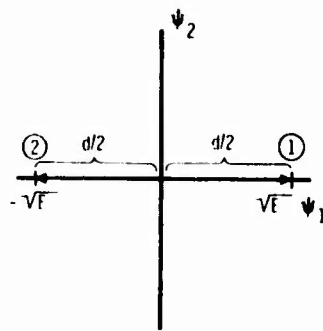
2 - PHASE ANTIPODAL

4 - PHASE BIORTHOGONAL

② ① √E̅
d/2
ψ₂
ψ₁
d/2
③ ④
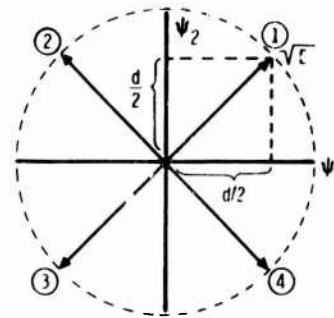
Figure 7-47. Signal Space for 2-Phase Antipodal and
4-Phase Biorthogonal Signals

procedure. They differ only in the configuration of decision regions and in the number of cases required when a fixed nimber of signals in a sequence is specified.

The number of signals in a sequence is chosen so that each signal around the signal being detected causes interference with it. For the filter bandwidths to be studied, the filtered pulse decreases sufficiently rapidly that only a sequence of three signals is studied. This results in cases as shown in Table 7-10. The vector being detected is represented by one of the vectors in the signal space and the signals leading and trailing it are varied until all possible sequences are exhausted. Note also that only detection of one of the possible vectors need be studied since the signal space is symmetrical and distortion to a vector transmitted through a filter is independent of its phase, thus studying the effect of distortion on a single vector in a sequence exhausts all cases.

One vector, represented by its time samples, is transformed through the filter. It is then delayed and advanced and given a corresponding phase shift depending on the case. For the 4-phase case considering the required method of detection of the binary digits, the pulse to be detected is first given a 45° shift and all other vectors are given an additional multiple of 90° shift. The signals are then summed producing a sequence of three signal vectors. Each component of the sequence is divided by its absolute value which corresponds to passing the signals through a hard limiter. The inphase and quadrature components of the signal to be detected are integrated for various delays and apertures. The procedure is performed for each case. Thus, for each aperture and delay a received vector is defined corresponding to a particular case.

-312-

Table 7-10. Signal Sequence Cases

Case	First Signal	Signal of Interest	Last Signal
I	1	1	1
II	1	1	2
III	2	1	1
IV	2	1	2
(2-Phase Signals)			
I	1	1	1
II	1	1	2
III	1	1	3
IV	1	1	4
V	2	1	1
VI	2	1	2
VII	2	1	3
VIII	2	1	4
IX	3	1	1
X	3	1	2
XI	3	1	3
XII	3	1	4
XIII	4	1	1
XIV	4	1	2
XV	4	1	3
XVI	4	1	4
(4-Phase Signals)			

Figure 7-48 illustrates the locations of the received vectors of each sequence case for 2-phase signals and a particular delay and aperture. These vectors represent all possible received vectors, thus summing these vectors will generate the reference angle equivalent to a reference generated by averaging over a large number of received signals in noise.[*]

---

[*] Strictly speaking, this computation assumes either correct reception of each signal in a decision-directed process or deriving the reference from signals of known phase (gated reference).
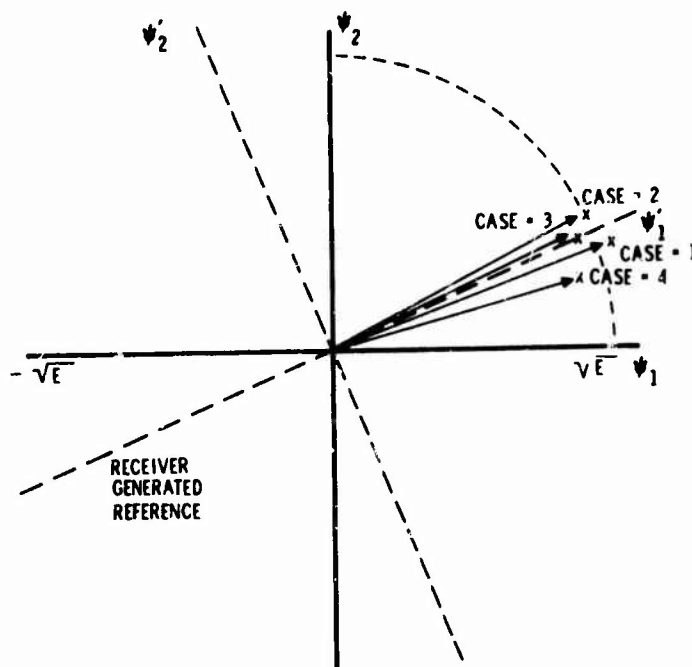
Figure 7-48. Received Vectors with Receiver Generated
Reference (2-Phase Case)

Using the generated reference the decision regions can be defined. For the
2-phase case the receiver reference is equal to the transmitted reference shifted by
the average phase shift of the received vectors. The 4-phase case shifts the trans-
mitted reference by the measured angle minus 45°. The probability of error for each
sequence can be found for a given noise variance. The average probability of error
is then the average of the probability of error for each sequence. The average pro-
bability is calculated as follows:

Let

$$Q(\alpha) \triangleq \frac{1}{\sqrt{2\pi}} \int_{\alpha}^{\infty} e^{-\gamma^2/2} \, d\gamma \qquad (75)$$

and also define

N_o = single sided density of Gaussian noise

d_i = the distance on the inphase reference axis to the
vertical decision line for the ith vector

$\hat{d}_i$ = the distance on the quadrature axis to the vertical
decision line for the ith vector.

-314-

Then, for the 2-phase case the average probability of error is

$$\overline{P}_E \quad \frac{1}{4} \sum_{i-1}^{4} p_i \tag{76}$$

where

$$p_i = Q\left(\frac{d_i}{\sqrt{2 N_o}}\right), \quad d_i \geq 0 \tag{77}$$

or

$$p_i = 1 - Q\left(\frac{|d_i|}{\sqrt{2 N_o}}\right), \quad d_i < 0 \tag{78}$$

The average probability of a character error for the 4-phase case is

$$\overline{P}_E = \frac{1}{16} \sum_{i=1}^{16} (p_i + \hat{p}_i - p_i \hat{p}_i) \tag{79}$$

and the average probability of a bit error is

$$\overline{P}_b = \frac{1}{16} \sum_{i=1}^{16} \frac{1}{2} (p_i + \hat{p}_i) \tag{80}$$

where

$$p_i = Q\left(\frac{d_i}{\sqrt{2 N_o}}\right), \quad d_i \geq 0 \tag{81}$$

or

$$p_i = 1 - Q\left(\frac{|d_i|}{\sqrt{2 N_o}}\right), \quad d_i < 0 \tag{82}$$

and similarly

$$\hat{p}_i = Q\left(\frac{\hat{d}_i}{\sqrt{2 N_o}}\right), \quad \hat{d}_i \geq 0 \tag{83}$$

-315-

or

$$\hat{p}_i = 1 - Q\left(\frac{|\hat{d}_i|}{\sqrt{2N_o}}\right), \quad \hat{d}_i < 0 \tag{84}$$

The negative distance can occur for poor choices of the integration start time and integration time for certain sequence cases.

Using these equations $\overline{P}_E$ can be determined for various delays and apertures. The delay and aperture which minimizes $\overline{P}_E$ are chosen as the best values and values of $\overline{P}_E$ versus signal-to-noise ratio can then be calculated.

7.4.2.1 2 Sampling of the Signal and Its Amplitude Spectrum

The signal which is transmitted through the channel and its amplitude spectrum are presented by complex discrete samples. Figure 7-49 shows the placement of samples on an axis equivalent to placement in an array. In the array there are N points,

$$N = W_s T_s \tag{85}$$

where

W_s = frequency axis range

T_s = time axis range

The number of samples in a pulse duration T is,

$$n_t = \frac{NT}{T_s} \tag{86}$$

and the number of samples between zero crossings of the amplitude spectrum is

$$2n_f = \frac{2T_s}{T} \tag{87}$$

There should be 40 samples between zero crossings of the signal spectrum. This is approximately the number of samples that would be required to study the effect of a four pole Chebychev filter with a bandwidth as narrow as $W = .25/T$ or an eight pole filter as wide as .5/T. The signal of duration T should contain approximately 20 samples. The particular FFT algorithm used required N to be a multiple of 2.
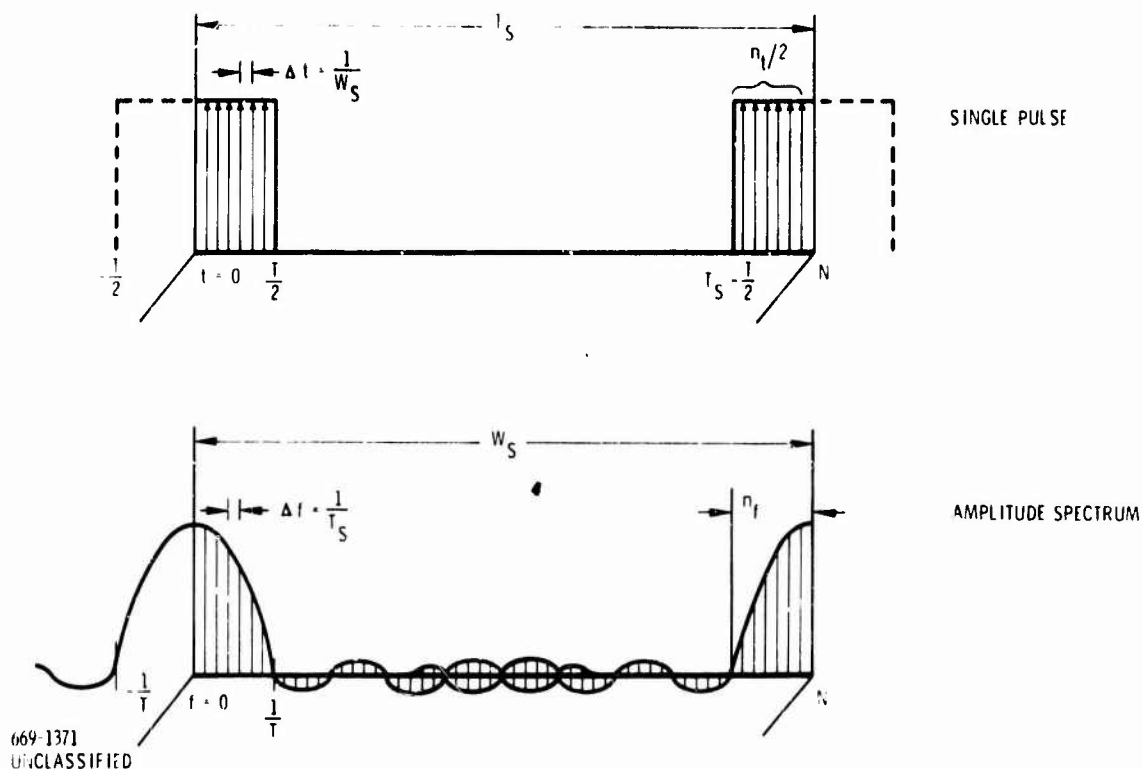
Figure 7-49. Placement of Signal Samples for Fourier
Transformations Using the FFT Algorithms

Thus, if the total number of samples, N, is chosen to be 512, then

$$2n_f = \frac{2T_s}{T} = 40$$

and

$$n_t = \frac{NT}{T_s} \approx 25$$

Thus, there are 512 time samples with 25 samples within the signal duration
T. Note also that the frequency axis range W_s is,

$$W_s = \frac{N}{20T} \approx \frac{25}{T}$$

The image spectrum of the periodic Fourier transform are separated by 25 lobes of
the amplitude spectrum, thus, virtually eliminating any aliasing effects for normal
spectrums.

-317-

7.4.2.1.3 Signal Transformations and Generation of the Signal Vectors from the Signal Samples

The single pulse is samples as shown in Figure 7-49 and has an amplitude spectrum which is also shown in Figure 7-49. The pulse is chosen to have only real components and is positioned on the time axis so that its amplitude spectrum is real. The time samples can be represented by a vector,

$$\underline{V} = \begin{bmatrix} v_1 \\ \cdot \\ \cdot \\ \cdot \\ \cdot \\ v_N \end{bmatrix} \tag{88}$$

where

$$v_i = 1, \text{ for } 1 \leq i \leq n_t/2 \text{ and } N - n_t/2 \leq i \leq N$$

$$= 0 \text{ elsewhere}$$

The samples of the amplitude spectrum of the pulse can be represented by a vector

$$\underline{S} = \begin{bmatrix} s_1 \\ \cdot \\ \cdot \\ \cdot \\ \cdot \\ s_N \end{bmatrix} \tag{89}$$

For the calculations performed, the vector was loaded as follows:

$$s_i = \frac{n_t \, \sin(i-1)\frac{\pi}{T_S} \, T}{(i-1)\frac{\pi}{T_S} \, T} \qquad \text{for } i = 1, 2, \ldots, \frac{N}{2} \tag{90}$$

and

$$s_i = \frac{n_t \, \sin(N-i)\frac{\pi}{T_S} \, T}{(N-i)\frac{\pi}{T_S} \, T} \qquad \text{for } i = \frac{N}{2}+1, \frac{N}{2}+2, \ldots, N \tag{91}$$

The transform of the Chebychev filter placed in vector form is,

$$\underline{H} = \begin{bmatrix} H_1 \\ \cdot \\ \cdot \\ \cdot \\ \cdot \\ H_N \end{bmatrix}$$ (92)

where

$$H_i = \prod_{v=1}^{4} \frac{\left| -\sigma_v + j\omega_v \right|}{-\sigma_v + j(\omega_v + X)}$$ (93)

and

$$X = (\frac{\omega}{2\pi} - (f_c + W) (f_c - W) \frac{2\pi}{\omega})/2W$$ (94)

with

W = single sided bandwidth of the Chebychov filter

    = α/Γ

α = the time bandwidth product

f_c = carrier frequency

ω = $i \dfrac{2\pi}{T_S}$

and the values,

σ_v, ω_v = describe the pole locations of a low pass Chebychev filter with a bandwidth of one

The equation for X transforms the low pass filter to a bandpass filter, at center frequency f_c, with bandwidth 2W.

The amplitude spectrum is then transformed with the filter transfer function and inversely Fourier transformed using a Fast Fourier Transform algorithm resulting in a time sample at the filter output

$$\underline{V}^{(1)} = F^{-1}\{\underline{H}^T \underline{S}\} = \begin{bmatrix} v_1^{(1)} \\ \cdot \\ \cdot \\ \cdot \\ v_N^{(1)} \end{bmatrix}$$ (95)

The vector is rearranged to facilitate computations by placing the pulse in the center of the vector

$$
\underline{V}^{(2)} = \begin{bmatrix} v^{(1)}_{N/2+1} \\ v^{(2)}_{N/2+2} \\ \cdot \\ \cdot \\ \cdot \\ v^{(1)}_1 \\ v^{(1)}_2 \\ \cdot \\ \cdot \\ \cdot \\ v^{(1)}_{N/2} \end{bmatrix} = \begin{bmatrix} v^{(2)}_1 \\ \cdot \\ \cdot \\ \cdot \\ v^{(2)}_N \end{bmatrix} \tag{96}
$$

The vector $\underline{V}^{(2)}$ contains the single distorted pulse from which the sequence cases are generated.

For the two phase case the sequences are found as follows for the four cases:

$$
\underline{V}^{(3)}_I = \begin{bmatrix} v^{(2)}_{1+n_t} \\ \cdot \\ \cdot \\ \cdot \\ v^{(2)}_N \\ 0 \\ 0 \\ \cdot \\ \cdot \\ 0 \end{bmatrix} e^{jn\pi} + \begin{bmatrix} v^{(2)}_1 \\ v^{(2)}_2 \\ \cdot \\ \cdot \\ \cdot \\ \cdot \\ \cdot \\ v^{(2)}_N \end{bmatrix} + \begin{bmatrix} 0 \\ 0 \\ \cdot \\ \cdot \\ v^{(2)}_1 \\ v^{(2)}_2 \\ \cdot \\ \cdot \\ v_{N-n_t} \end{bmatrix} e^{jm\pi} \quad \begin{array}{l} \text{for } n = 1, 2 \\ m = 1, 2 \end{array} \tag{97}
$$

$$
\underbrace{\qquad}_{\substack{\text{Leading} \\ \text{Pulse}}} \qquad \underbrace{\qquad}_{\substack{\text{Pulse} \\ \text{to be} \\ \text{Detected}}} \qquad \underbrace{\qquad}_{\substack{\text{Trailing} \\ \text{Pulse}}}
$$

$$
= \begin{bmatrix} v^{(3)}_1 \\ \cdot \\ \cdot \\ \cdot \\ v^{(3)}_N \end{bmatrix} \tag{98}
$$

where $I = m + 2(n - 1)$.

The sequence of pulses for the 4-phase case are formed as follows for the sixteen cases,

$$
\underline{V}_I^{(3)} = \begin{bmatrix} v_{1+n_t}^{(2)} \\ \cdot \\ \cdot \\ \cdot \\ v_N^{(2)} \\ 0 \\ 0 \\ \cdot \\ \cdot \\ \cdot \\ 0 \end{bmatrix} e^{j(n\frac{\pi}{2} + \pi/4)} + \begin{bmatrix} v_1^{(2)} \\ \cdot \\ \cdot \\ \cdot \\ v_2^{(3)} \\ \cdot \\ \cdot \\ \cdot \\ v_N^{(2)} \end{bmatrix} e^{j\pi/4} + \begin{bmatrix} 0 \\ 0 \\ \cdot \\ \cdot \\ v_1^{(2)} \\ v_2^{(2)} \\ \cdot \\ \cdot \\ \cdot \\ v_{N-n_t} \end{bmatrix} e^{j(m\frac{\pi}{2}+\frac{\pi}{4})} \quad \begin{matrix} \text{for } n = 1,2,3,4 \\ m = 1,2,3,4 \end{matrix}
$$

$$
(99)
$$

$$
= \begin{bmatrix} v_1^{(3)} \\ \cdot \\ \cdot \\ \cdot \\ v_N^{(3)} \end{bmatrix}
$$

where $I = m + 4 (n - 1)$

The vectors are then hard limited by normalizing the absolute value of each of the vector components resulting in the received signal

$$
V_I^{(R)} = \begin{bmatrix} v_1^{(R)} \\ \cdot \\ \cdot \\ \cdot \\ v_N^{(R)} \end{bmatrix}
$$

$$
(100)
$$

with $\quad v_i^{(R)} = \dfrac{v_i^{(3)}}{\left| v_i^{(3)} \right|} \quad$ for $i = 1, N$.

The projected components of the received vector from the decision region are

$$d_I^{(R)} = \frac{2}{n_t} \sum_{i = \frac{N-n_t}{2} + \Delta \frac{n_t}{T}}^{(\Delta + T_a)\frac{n_t}{T}} \text{Re} \left\{ v_i^{(R)} \right\} \tag{101}$$

and

$$\hat{d}_I^{(R)} = \frac{2}{n_t} \sum_{i = \frac{N-n_t}{2} + \Delta \frac{n_t}{T}}^{(\Delta + T_a)\frac{n_t}{T}} \text{Im} \left\{ v_i^{(R)} \right\} \tag{102}$$

where

Δ = the integration delay

T_a = the integration time.

The reference at the receiver is generated by averaging the received vectors for all the cases

$$\overline{d} = \frac{1}{L} \sum_{I=1}^{L} d_I^{(R)} \tag{103}$$

$$L = \begin{cases} 4 \text{ for the 2-phase case} \\ 16 \text{ for the 4-phase case} \end{cases}$$

$$\overline{\hat{d}} = \frac{1}{L} \sum_{I=1}^{L} d_I^{(R)} \tag{104}$$

then,

$$\theta = \tan^{-1}\left(\frac{\overline{\hat{d}}}{\overline{d}}\right) \tag{105}$$

For the 2-phase case the phase shift is

$$\phi_e = \theta \tag{106}$$

and for the 4-phase case it is

$$\phi_e = \theta - \pi/4 \tag{107}$$

Thus, the distances along the receiver reference axii are,

$$d_I = d_I^{(R)} \cos \phi_e + \hat{d}_I^{(R)} \sin \phi_e \qquad (108)$$

and

$$\hat{d}_I = - d_I^{(R)} \sin \phi_e + \hat{d}_I^{(R)} \cos \phi_e \qquad (109)$$

The received distance can be calculated for different values of delay Δ and integration time T_a until the values which yield the minimum probability of error are found. The values can then be used to calculate P_E versus E_s/N_o.

7.4.2.2 Preliminary Results and Extensions

7.4.2.2.1 Presentation of Results

The model discussed above was programmed to produce results in plotted form. The results to be presented in this section will demonstrate the procedure discussed above and the capabilities of the analysis. Some conclusions will be made from these preliminary results. Simple extensions and projected results will be discussed.

The single pulse of duration T is transformed through a 4 pole 1 db Chebychev filter with bandwidth W. For the preliminary results discussed below the amplitude spectrum of the pulse is located in the center of the filter with $T = 50$ nanoseconds and $f_c = 8000$ MHz. The pulse at the output of the filter is shown in Figure 7-50 for $WT = 1$ and .5. The single pulse illustrates the linear distortion effect. The dashed line represents the shape and position of the original pulse and is centered at time/T = 2.50. The power in the pulse produced by $WT = 1$ is delayed by about .6T and is distributed through 2T. Thus, the 3 pulse sequence for $WT = 1$ will produce very accurate results. The pulse produced by $WT = .5$ has a large part of its power delayed by 1.3T and is distributed over 3T but has less than 1% of its power distributed outside the 2T region. Thus, the three pulse sequence will yield accurate results. Note that for the case discussed above (the filter is symmetrical about the spectrum) that a quadrature component does not exist.

At this point we diverge toward the 2-phase case with a 4-phase case to be discussed below. The single pulse is advanced and retarded by T and given the appropriate amplitudes so that there are three pulses resulting in the four sequence cases. The advanced and retarded pulses interfere with the center pulse causing distortion. The three pulse sequence is then transmitted through a hard limiter which operates

-323-
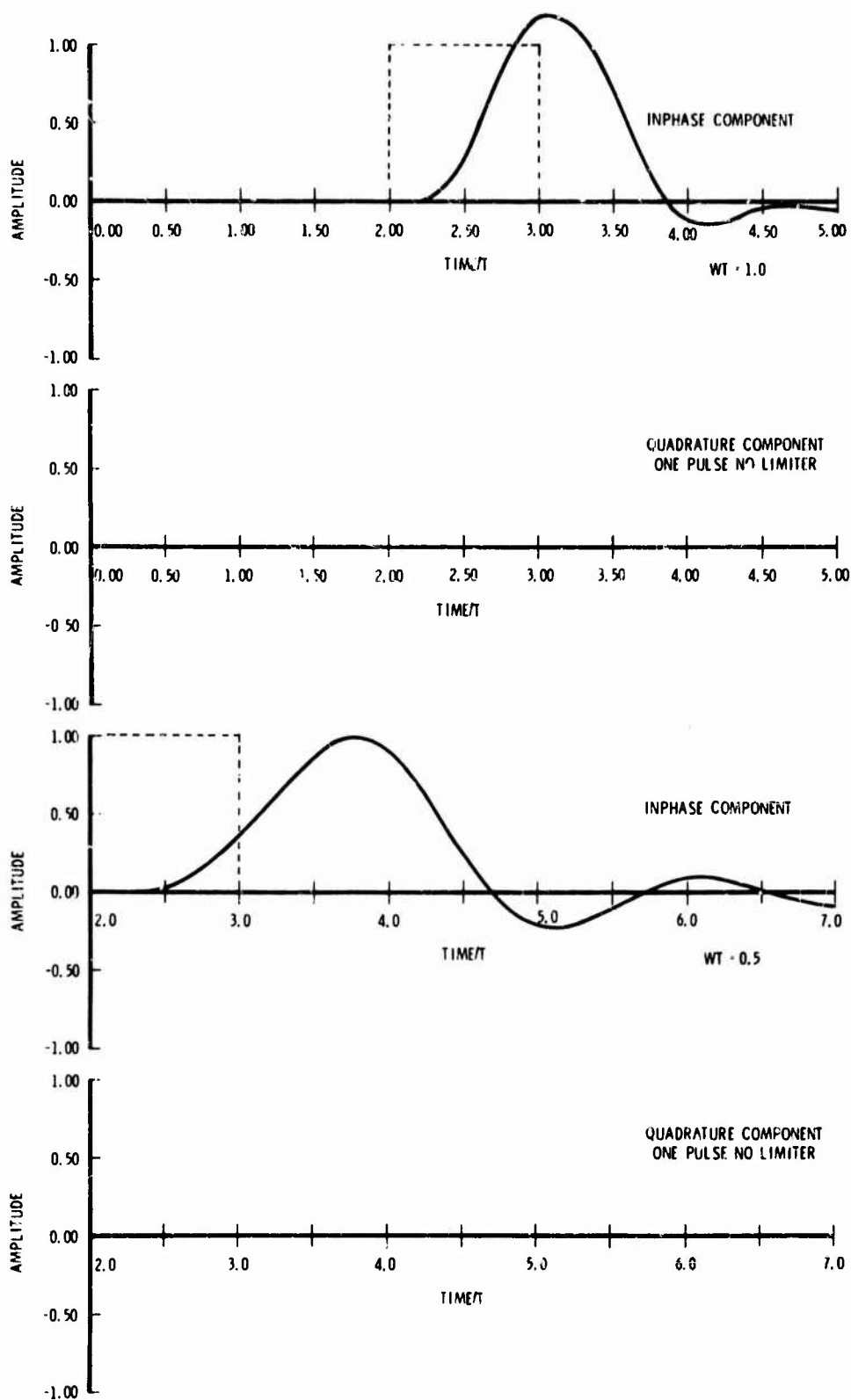
Figure 7-50.   Output Pulses of the Chebychev Filter for WT = 1. 0 and 0. 5

on the absolute value of the pulse so as to normalize it. Thus, only distortion to the zero crossings has significance at the limiter output. The four cases for both WT = 1 and .5 are presented in Figure 7-51. It can be seen in Figure 7-51 for WT = 1 that near ideal detection can be achieved if a delay of .6T and an integration time of T is used. The zero crossings for WT = .5 show greater distortion. The best delay and integration time for this case is not obvious. Observe that in Figure 7-51 quadrature signals occur at the hardlimiter output. This is due to inverse transform errors which result in quadrature components. If these values are somewhat larger than those of the inphase components the result of hardlimiting will be an enhancement of the quadrature component. The irregularity manifests itself along the time axis where the signal is not present or it crosses the time axis.

As the integration time is reduced the mean of the signal decreases as does the noise variance. Decrease in the signal mean is a function of the signal shape and the noise variance decrease is proportional to decrease in integration time. Thus the integration time is reduced until any further reduction results in less decrease of the noise variance than of the signal mean squared.

Figure 7-52 presents plots of probability of error versus delay for various apertures (integration times) with WT = 1 and WT = .5. These plots were used to select the best delay and aperture. For WT = 1 a delay of .6T and an aperture of T produced the best results. When WT was reduced to .5, the best results were achieved when the delay equaled 1.3T with an aperture equal to .9T.

Using these aperture values, probability of error was plotted versus signal-to-noise ratio for three delays. The results are shown in Figure 7-53. With WT = 1 and 10^{-5} probability of error there exists a .5 db degradation from the ideal coherent curve. When WT = .5, the degradation is 1.1 db at the same error rate. Thus, the loss in reducing the time bandwidth product results in a loss of .6 db.

A similar procedure was followed for the 4-phase modulation case. The sequence of signals was not plotted for the 4-phase case because of the large number of sequence cases (16). To demonstrate the phase shift of the vector for the 4-phase case a single pulse, before limiting, was plotted and is shown in Figure 7-54. The signal is the same signal as shown in Figure 7-50 for WT = 1 only phase shifted 45°. For the particular WT product being studied the signal was advanced and delayed with the appropriate phases respectively and added into the single pulse being studied to form the 16 sequence cases.

CASE = 1

CASE = 2
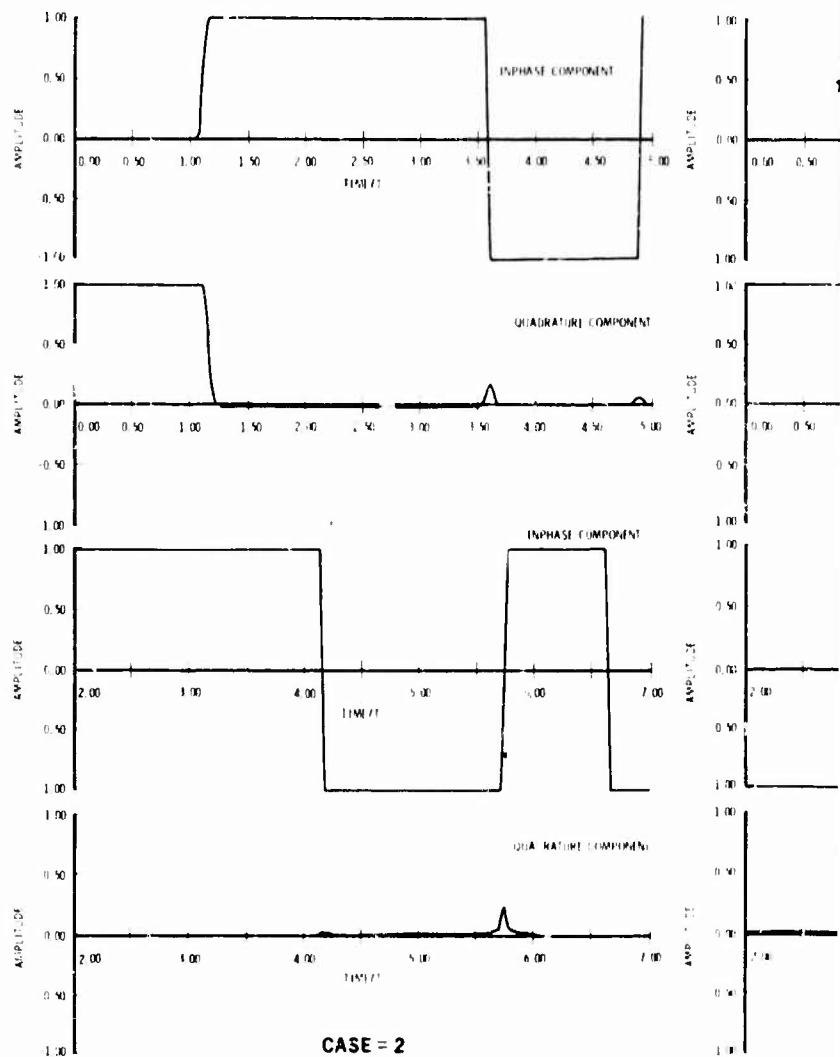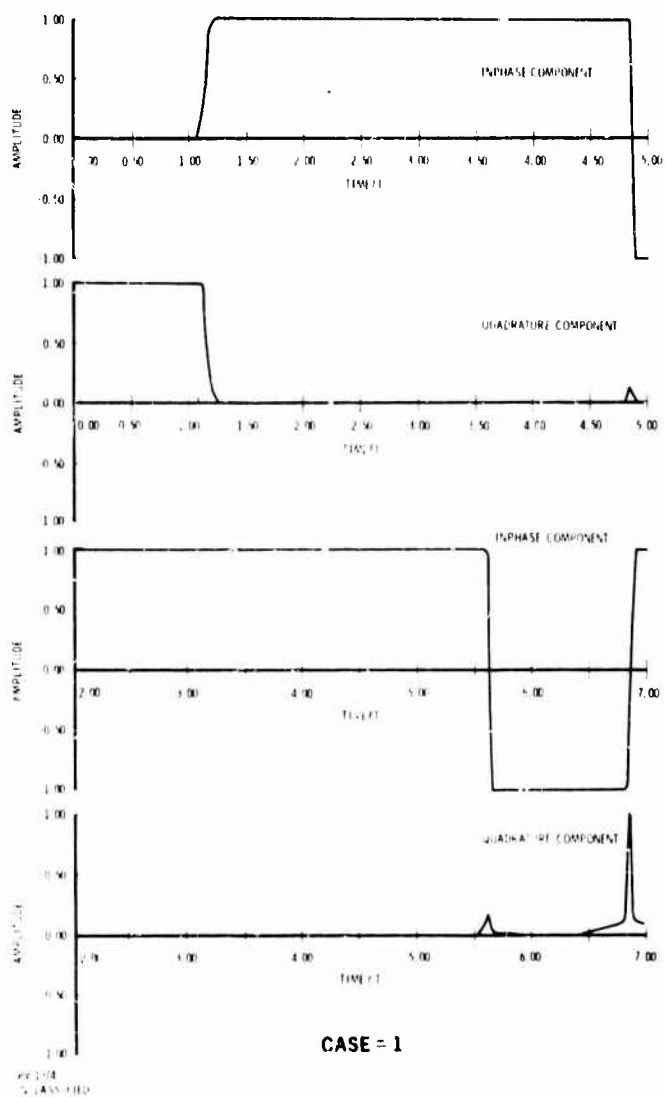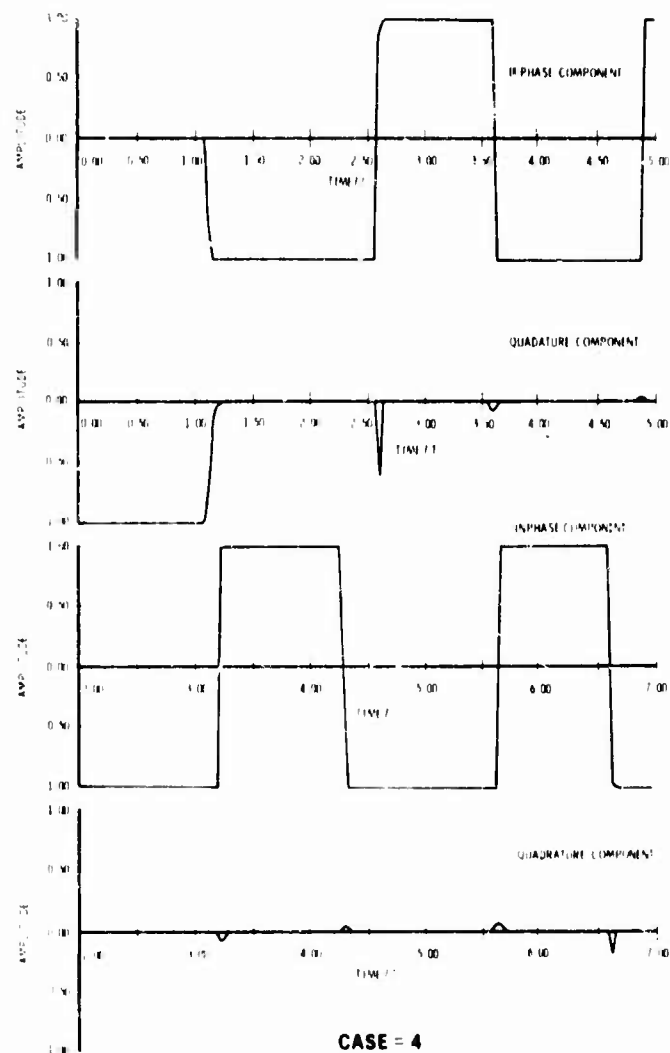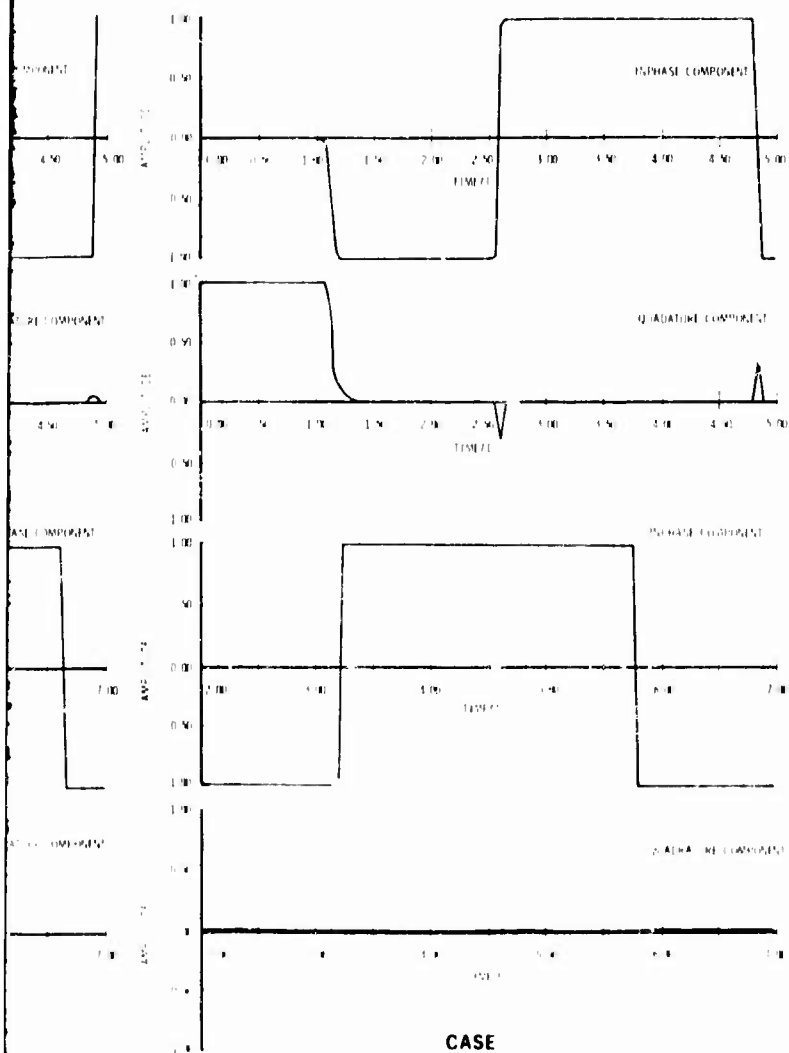
Figure 7-51. Illustration of the Four Cases
for the Three Pulse Sequences with ST = 1.0
for the Upper Plots and WT = 0.5 for the Lower Plots
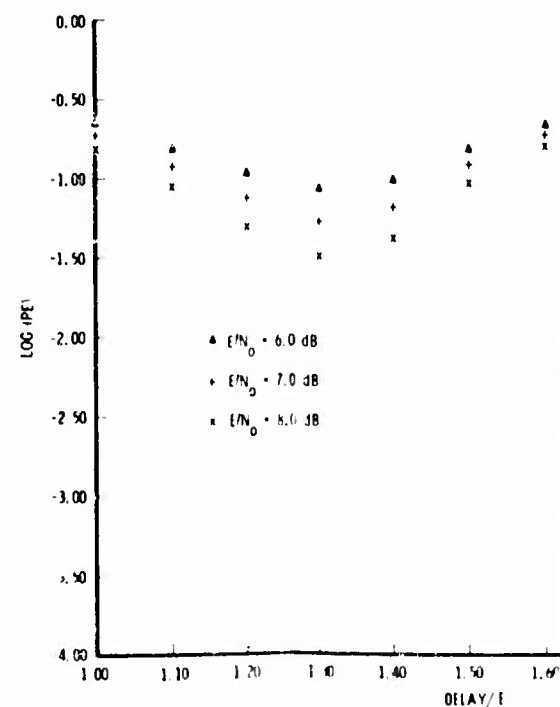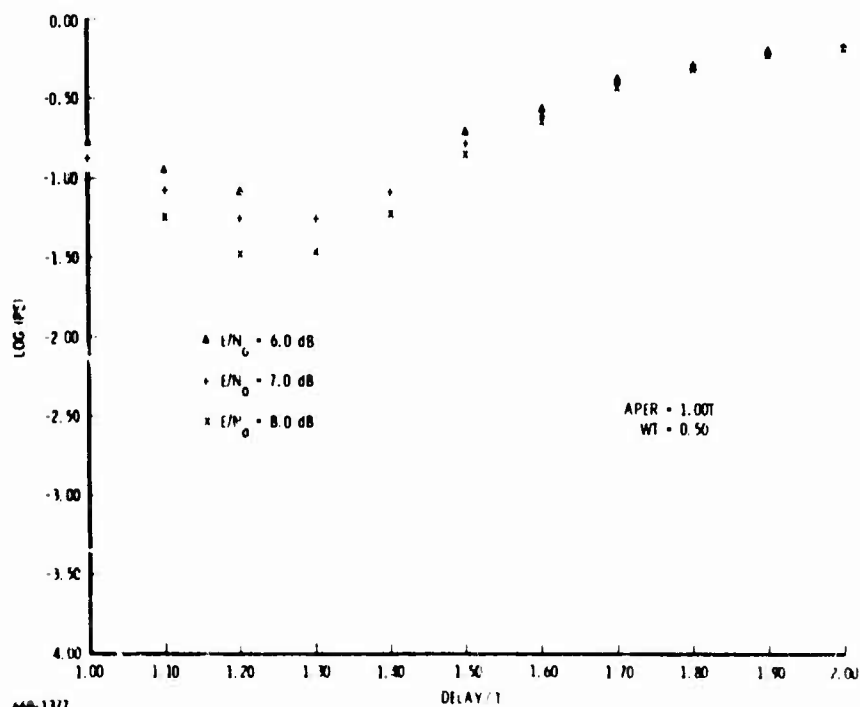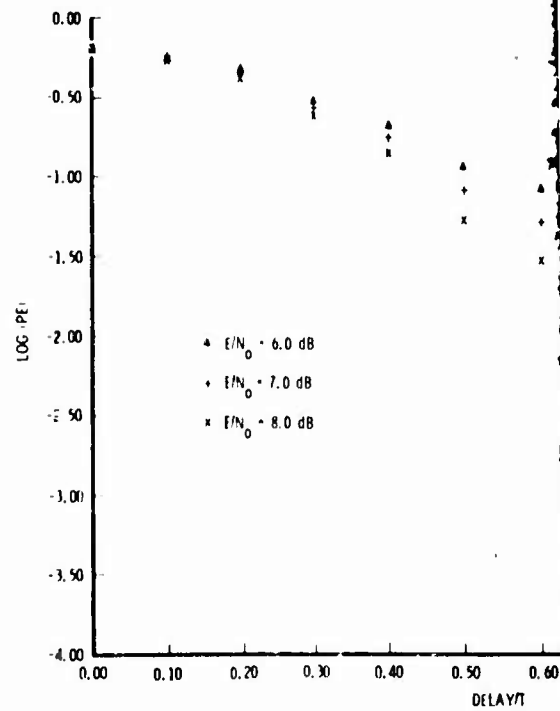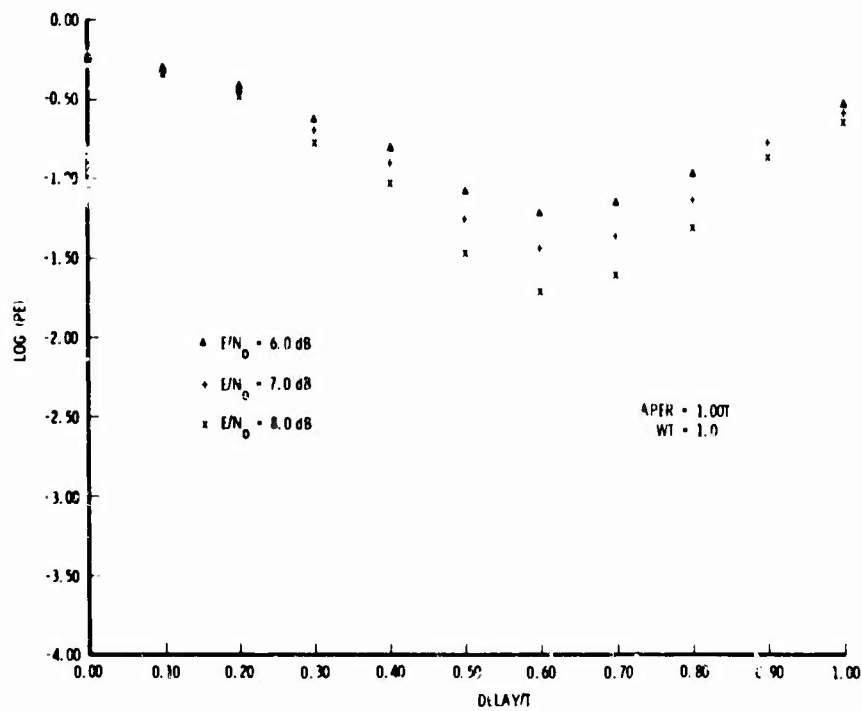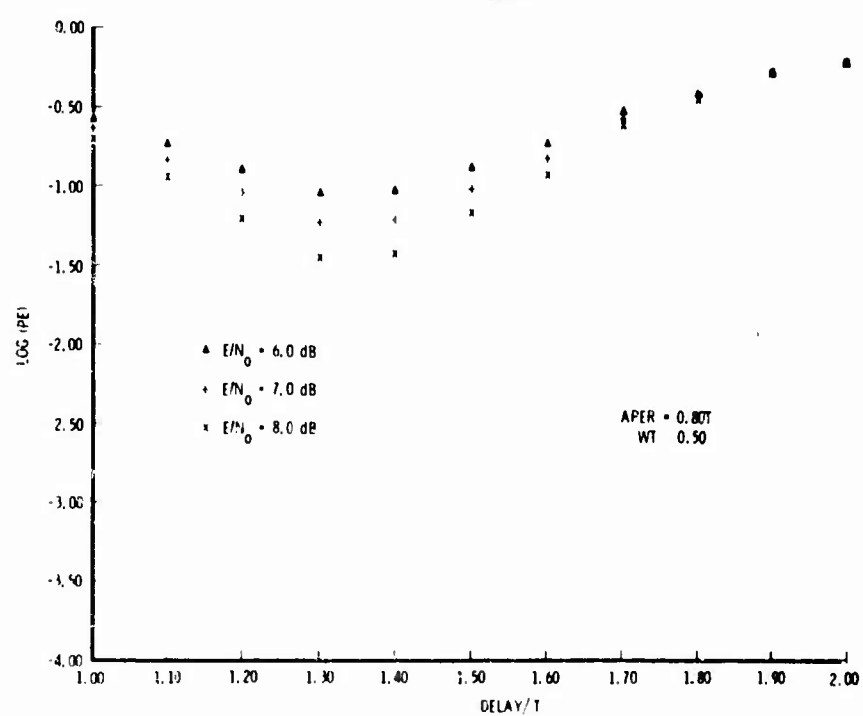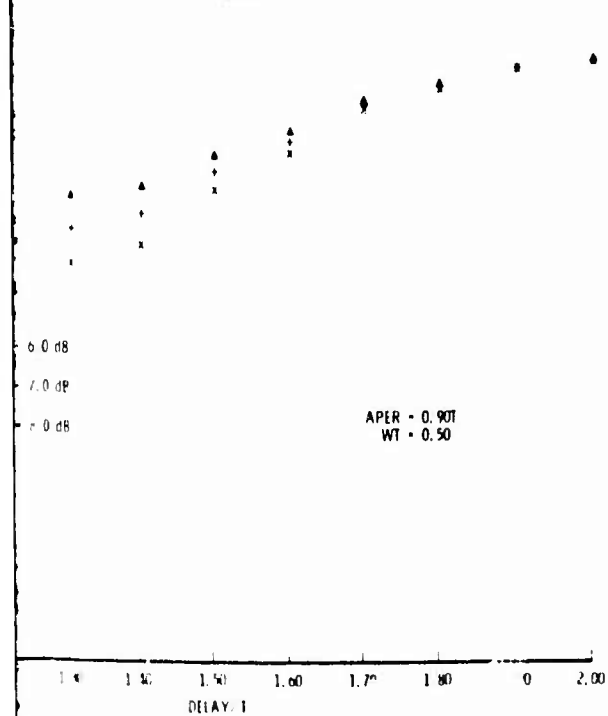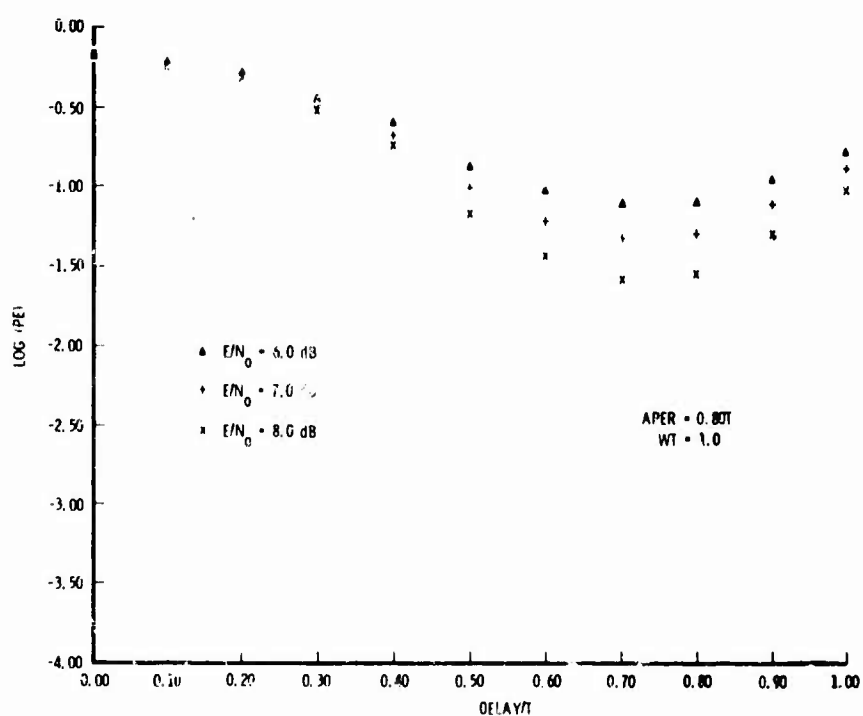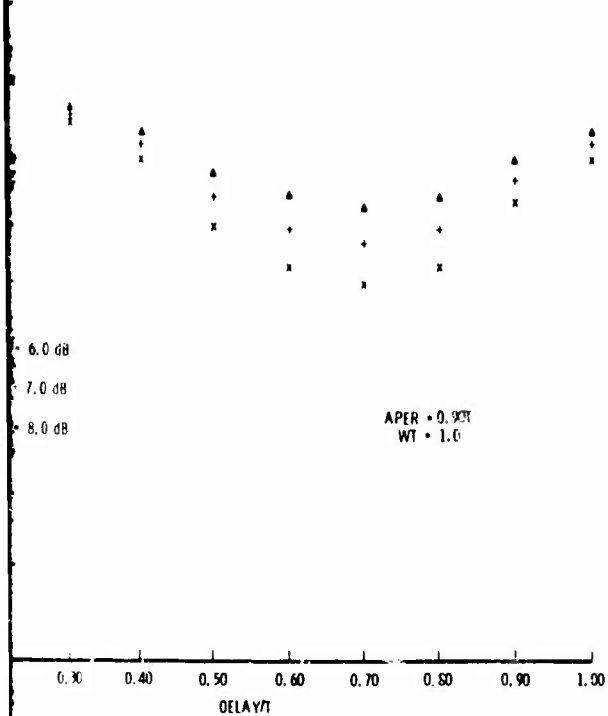
Figure 7-52. P_E Versus Delay for Various Apertures

Figure 7-53. P_E Versus E/N_o

-328-

INPHASE COMPONENT

QUADRATURE COMPONENT
ONE PULSE NO LIMITER
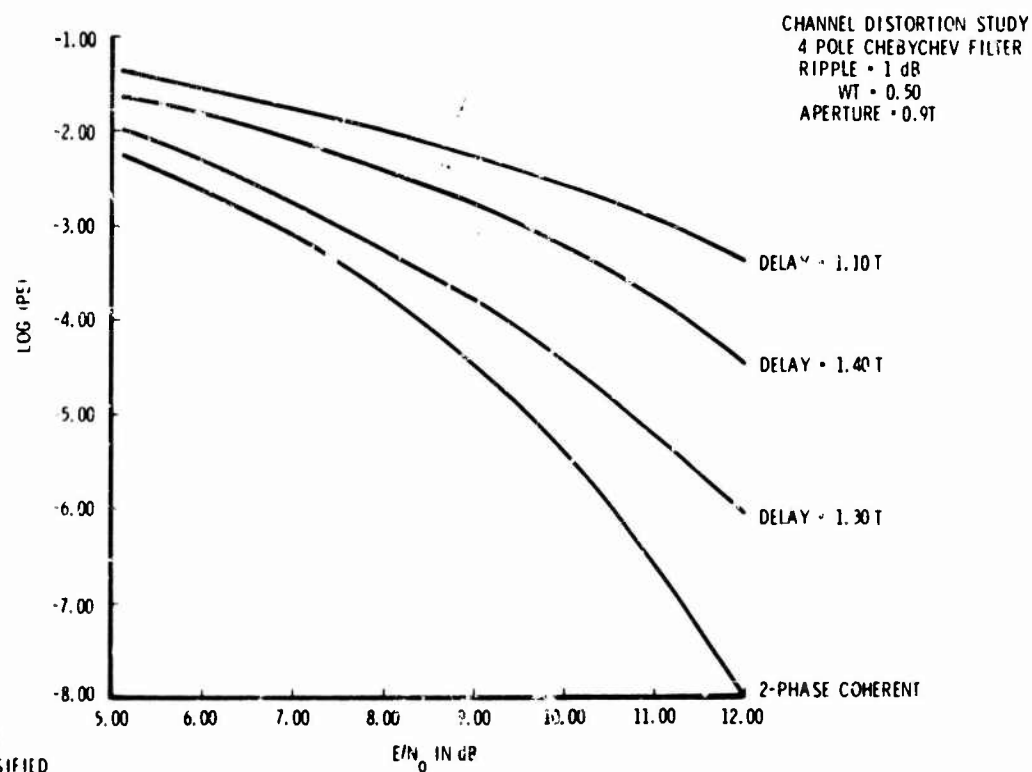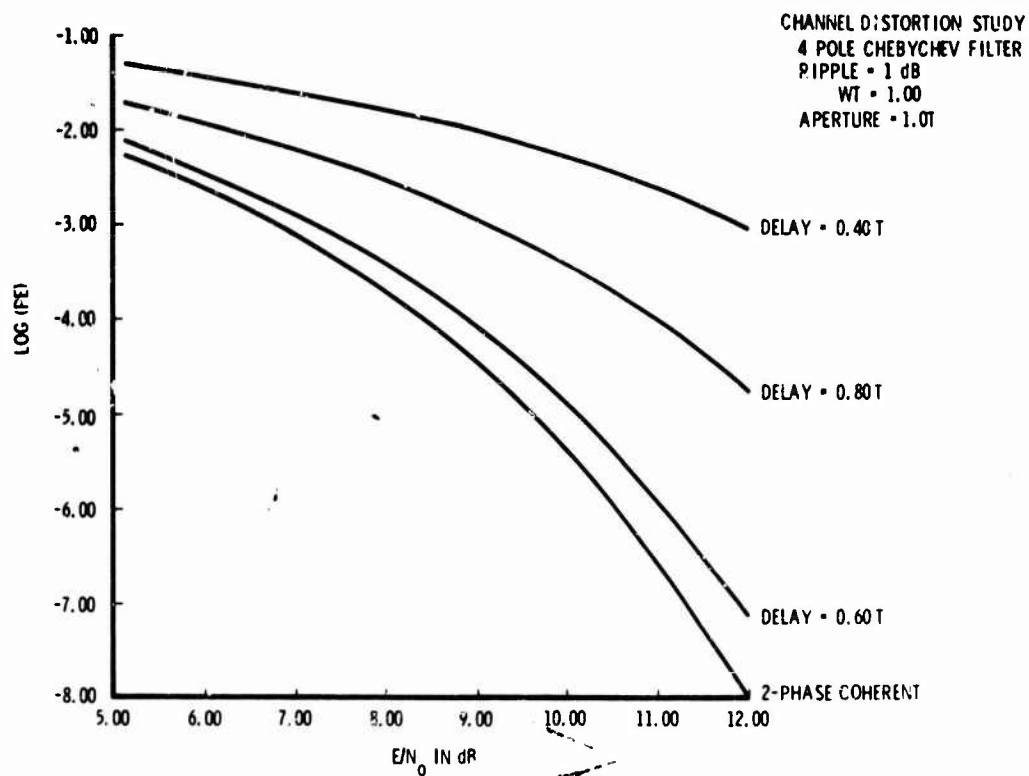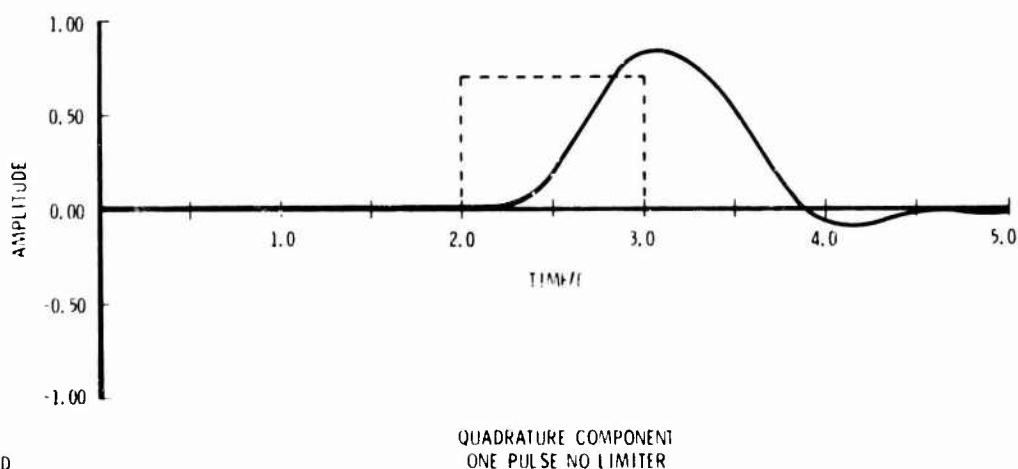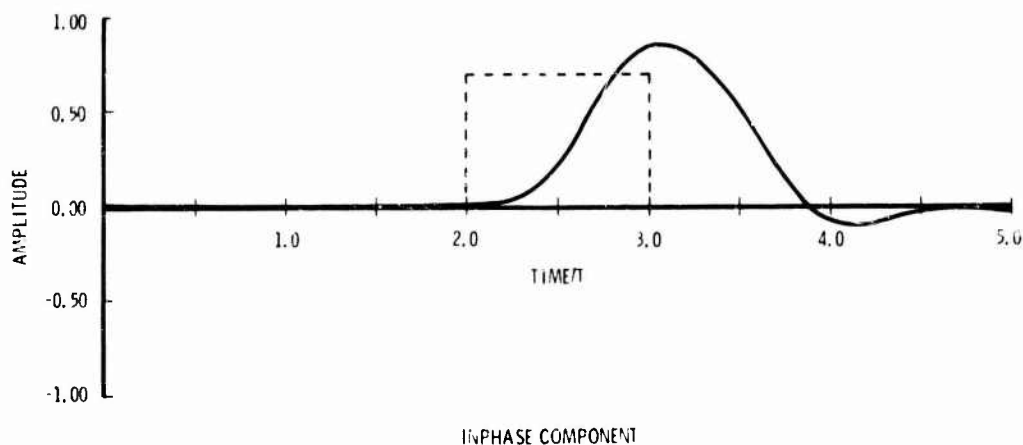
Figure 7-54.   Single Pulse for the 4-Phase Case with WT = 1

The sixteen cases were then passed through the hard limiter to form the received sequences.   The center signal was integrated for various delays and apertures. Figure 7-55 presents the resulting plots.   Examination of Figure 7-55 results in a best delay of . 6T and an aperture of T for WT = 1 and a best delay of 1. 3T and aperture of . 9T for WT = . 5.

Using these values P_E for the 4-phase case versus signal-to-noise ratio was plotted for both WT = 1 and . 5.   The plots are presented in Figure 7-56.   The solid lines represent the probability of a character error and were calculated with the method described above using Equation(79).   The dashed lines represent probability of bit error

-329-

330
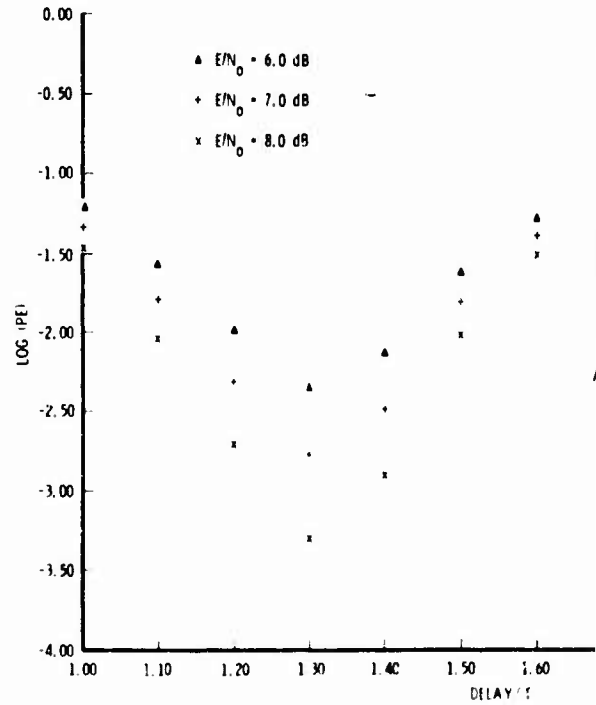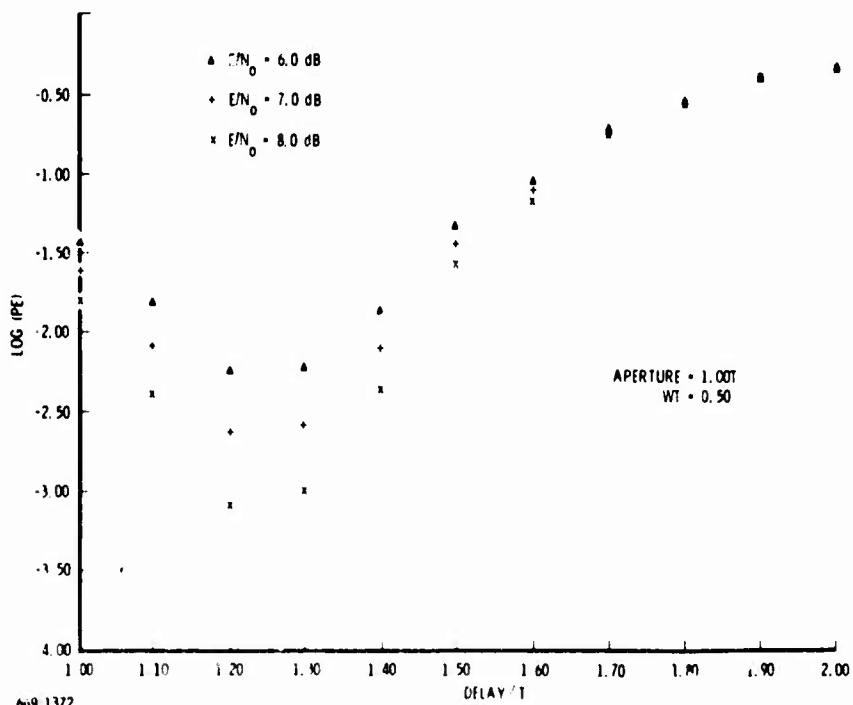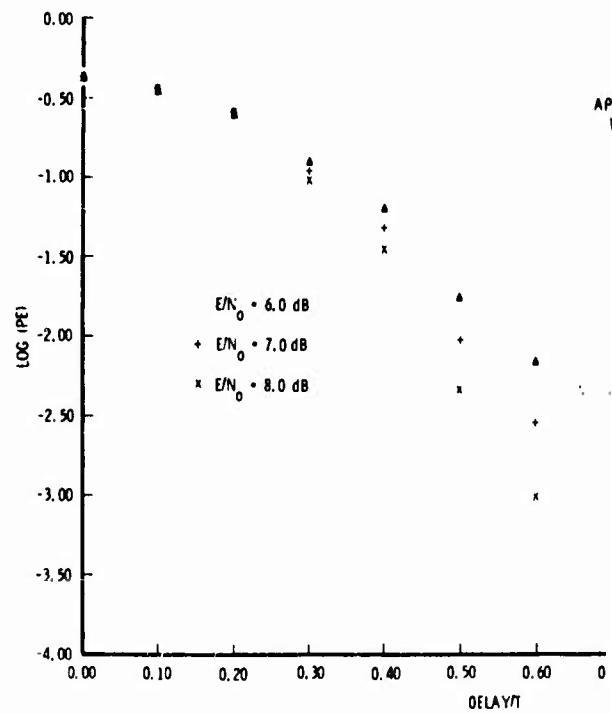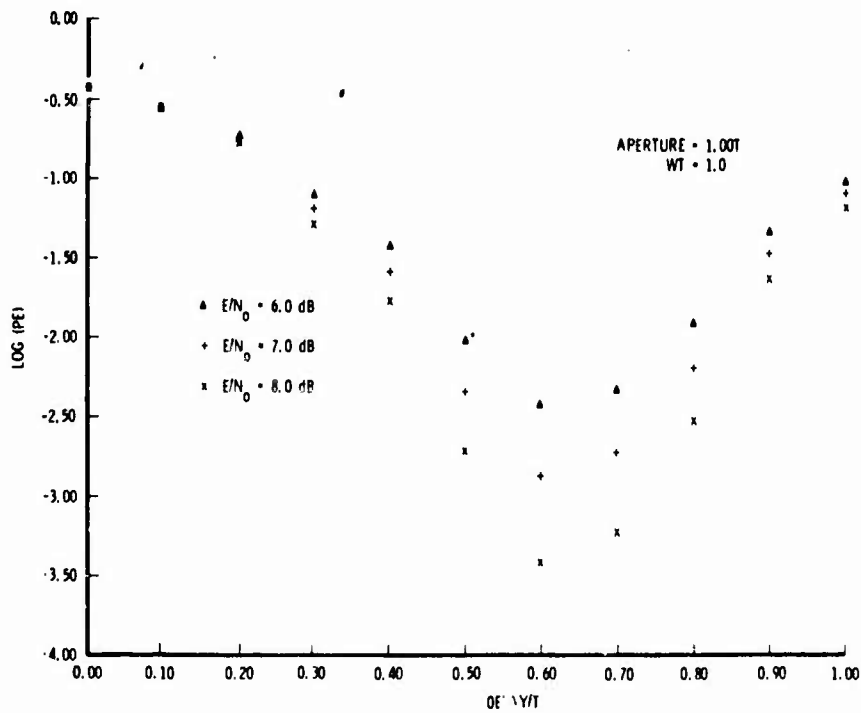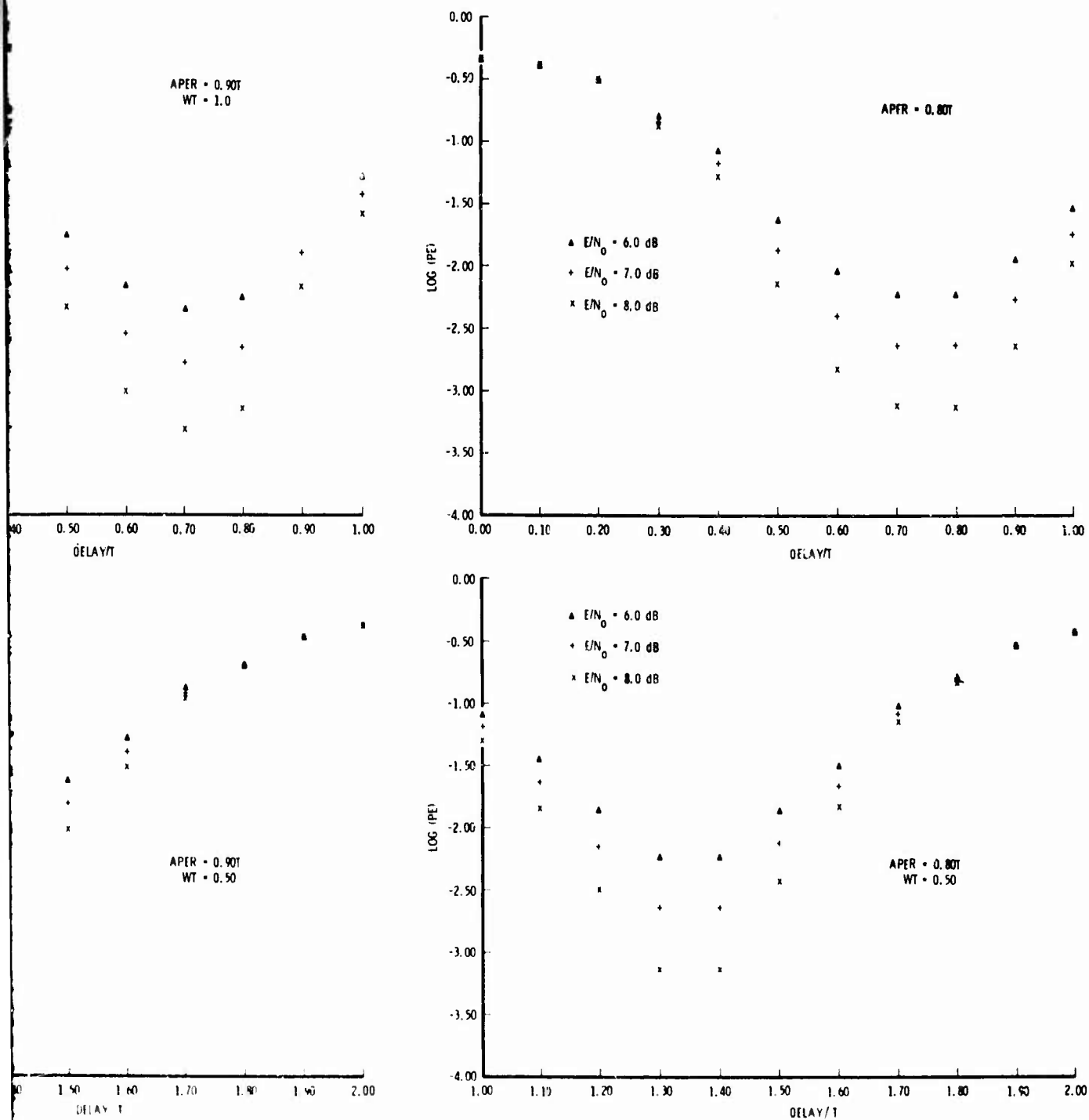
Figure 7-55. P_E Versus Delay for
Various Apertures (Four-Phase Modulation
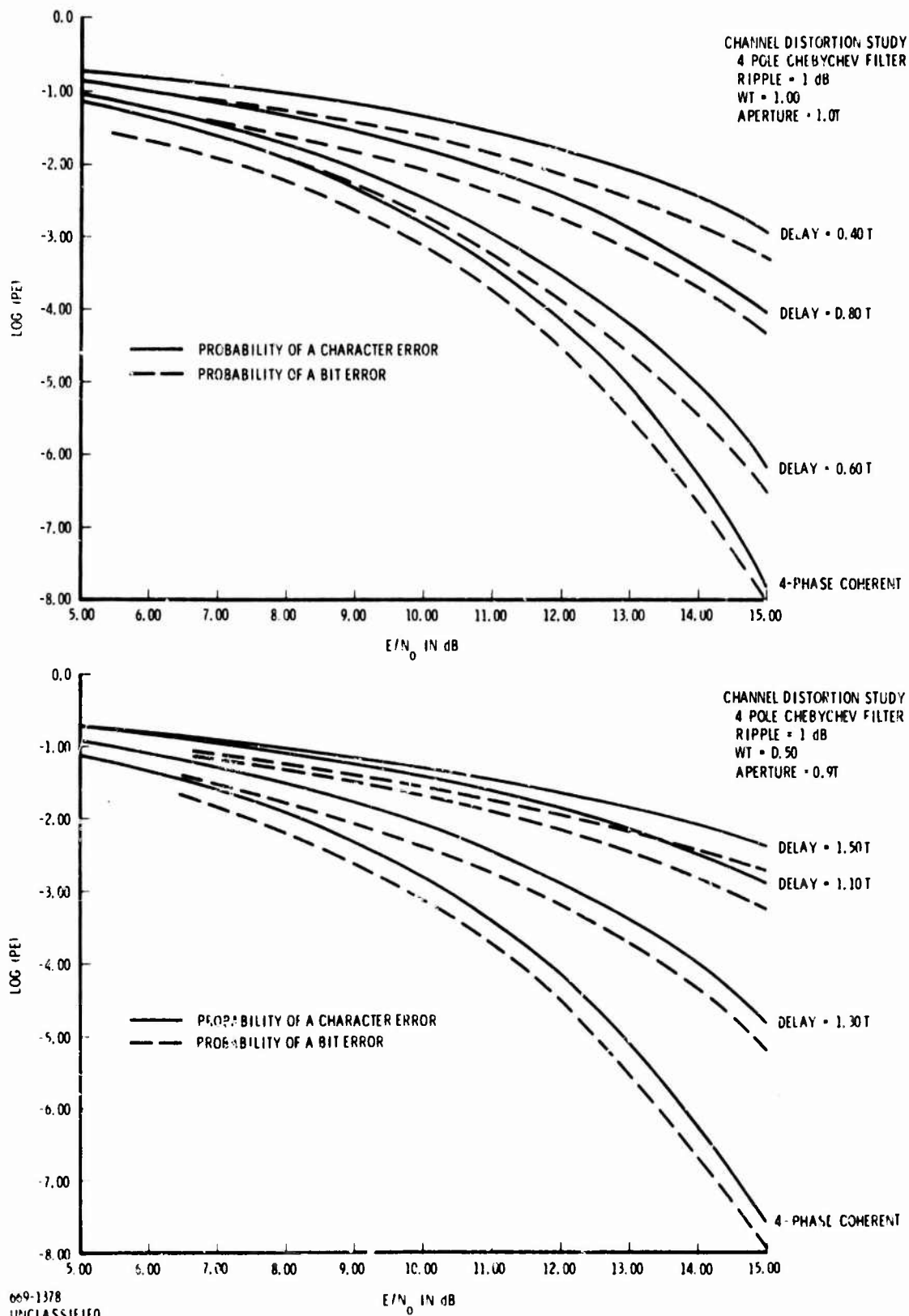
Figure 7-56. P_E Versus E/N_o (4-Phase Modulation)

-331-

and were placed on the plot by using Equations (79) and (80) with assumption that for small P_E the p_i and/or $\hat{p}_i$ would also be small. The term of Equation (79) $p_i\hat{p}_i$ is then negligible compared to $p_i + \hat{p}_i$. Thus, the probability of a bit error is half that of the probability of a character error. The assumption was verified by calculating the probability of a bit error for selected signal-to-noise ratios with WT ⋅ .5.

The plot shows that for WT = 1, there is a 1 db degradation from ideal at an error rate of 10^{-5} and with WT = .5 the degradation is approximately 2 db at the same error rate. Above it was seen that (Figure 7-53) for the 2-phase case degradations were .5 db and 1.1 db respectively. Thus, the 4-phase case is more sensitive to distortion of the signal vector than is the 2-phase. The greater sensitivity of the 4-phase case to distortion of the signal vectors is due to the smaller decision regions which must be used for detection.

By comparing the probability of bit error curves of Figures 7-53 and 7-56 after adjusting the signal-to-noise ratio to E_b/N_o (E_b = E for the 2-phase case and E_b = E/2 for the 4-phase case) it is seen that 2-phase modulation outperforms 4-phase modulation when E_b/N_o is fixed. With WT = 1 and an error rate of 10^{-5} the 2-phase case is superior by .6 db. Since, as discussed above, the 2-phase case is less sensitive to distortion than the 4-phase case it outperforms the 4-phase case even more when WT = .5. With an error rate of 10^{-5} the 2-phase case is now superior by 1 db. In a practical sense, a more meaningful comparison of E_b/N_o performance of 2-phase versus 4-phase modulation is to assume equal data rates and filter bandwidth. A representative comparison of this kind can be made by studying the 2-phase curves of Figure 7-53 with WT = .5 and the 4-phase curves of Figure 7-56 with WT = 1. For an error rate of 10^{-5} the performance of 4-phase and 2-phase modulation is essentially equal with E_b/N_o = 10.6 db for both. At error rates lower than 10^{-5} the 4-phase modulation begins to outperform the 2-phase. For higher error rates where error correction coding is applicable, 2-phase modulation is superior. As an example, at an error rate of 1% (10^{-2}) the E_b/N_o required for 2-phase is 5.1 db against 5.8 db required for 4-phase.

For narrower bandwidths, WT < 1, it may be expected that the inter-symbol interference, which increases rapidly, will cause 2-phase to degrade relative to 4-phase at the same total data rate. Further analysis requires inclusion of longer data sequences than considered here.

7.5 <u>INITIAL SYNCHRONIZATION ANALYSIS</u>

In view of the crucial issue of initial synchronization time for a spread-spectrum waveform, an extensive performance analysis effort was devoted to this topic study. Presented here are results on both serial search and matched filter schemes. The analysis for serial search schemes emphasizes sequential detection theory applied to the reception of a signal of known waveshape with the objective of computing search rates for a specified sync reliability. The analysis for matched filter detection examines the losses due to quantization in digital implementations (digital matched filter).

7.5.1 SEQUENTIAL DETECTION APPLIED TO A PSEUDONOISE SYNCHRONIZATION MODEL WITH QUANTIZED SEARCH

7.5.1.1 Introduction

The basic PN spread-spectrum system correlates the received signal plus interference with a local replica which is required to be in time synchronism with the received signal. This basic system is sketched in Figure 7-57. Since there is initially a time error, a search over the possible clock time positions for the bit stream generator must be performed to achieve synchronism. One way to perform the search is serially whereby all time positions are successively tested until the correct position is located, as indicated by an increase in the measured correlation output amplitude. The ability to decide which position is correct is, of course, reduced by the interference.

It is desired to investigate the use of sequential detection principles to gain a reduction in serial search time for acquiring synchronism in the presence of a given
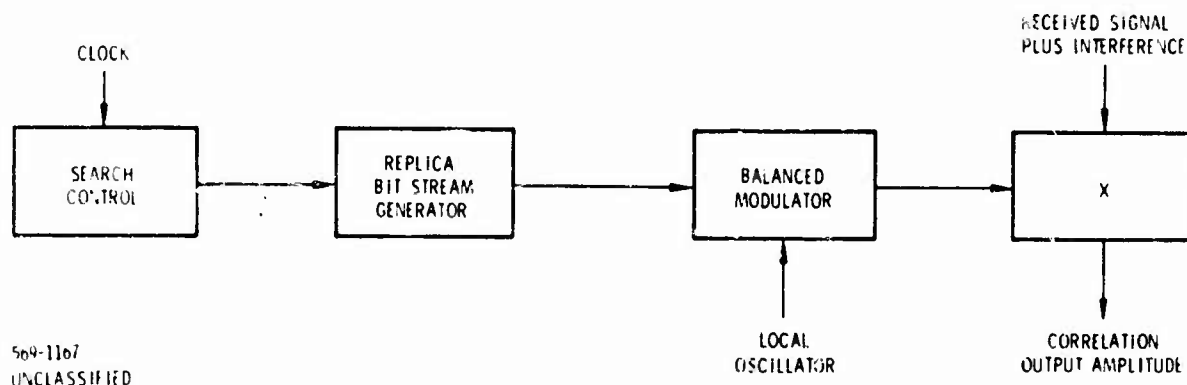
Figure 7-57. Basic PN Spread-Spectrum System

interference power. The communication system model considered for analysis utilizes ideal rectangular bits in the presence of Gaussian noise. Hence, if a search over time position is made and RF phase coherence of the local oscillator is presumed (for the moment), the correlation amplitude appears as shown in Figure 7-58. The correlation goes from its maximum to zero for a time error equal to the width of one pseudonoise bit of the signal. (If the received signal has been filtered, the triangular function is rounded off somewhat; however, the search philosophy remains the same.)

A serial search over the aperture allowed a priori for time error is to be performed. If the search is carried out in discrete steps, the problem reduces to a statistical decision between signal present and signal absent for each search position. Signal present is indicated by a non-zero correlation amplitude. Success will be defined here as a decision that signal is present for any time error within the extremes of the triangular correlation function; i.e., an error of at most one bit of the signal.

A sequential detection procedure continues the test of signal present/absent at any given search position for a variable duration until a dismissal threshold is reached indicating signal absent. The next search position is then tested. Signal present is indicated by dismissal not occurring in the given search position. The rate of search is determined from the product of the average duration to dismiss a position not containing signal and the number of positions tested per bit of time error. This computation ignores the duration associated with accepting signal present and concentrates on computing the total dismissal time for all incorrect time positions within the search aperture, on the assumption that the former is small compared with the latter total time.

7.5.1.2 Review of Sequential Detection Theory

Let us review results of sequential detection theory for detecting presence of a DC signal of amplitude A in the presence of Gaussian noise of density (one sided)

569-1168
UNCLASSIFIED
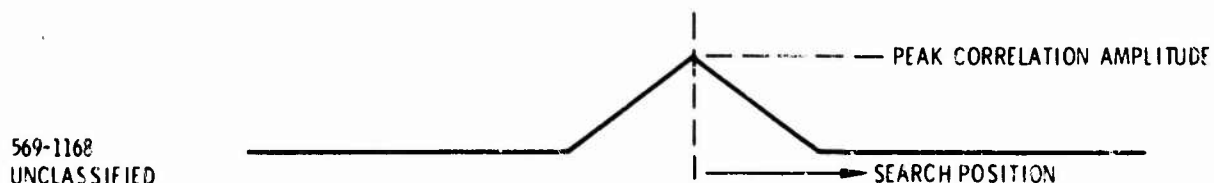
Figure 7-58. Ideal Triangular Correlation Function

-334-

N_0. Let the test proceed in multiples of an interval T_s, so that the Gaussian noise has variance $N_0/2T_s$ when smoothed over this interval. Let β = probability of false dismissal desired for the test. The sequential detection process will measure amplitude v of noise, or signal plus noise, smoothed over each T_s interval, and sum over the successive intervals of the test until the dismissal threshold log β is crossed. The quantity needed for the statistical test is given by the logarithm of the likelihood ratio of the two hypotheses (signal present or absent), and simplifies to the expression

$$z = \frac{2A_d T_s}{N_0} v - \frac{A_d^2 T_s}{N_0}. \tag{110}$$

where $2A_d^2 T_s/N_0$ denotes the design value, $2E_s/N_0$, for signal energy/noise for the interval T_s. Thus, the test depends on the design amplitude of signal, A_d, and β is defined for a signal with this amplitude.

The results (for the case of an arbitrarily high acceptance threshold as described above) may now be summarized. * First,

$$L(A) = \text{Probability of dismissal with signal present}$$

$$= 1 \qquad , \quad \frac{2A}{A_d} < 1$$

$$= \beta^{\frac{2A}{A_d} - 1} \quad , \quad \frac{2A}{A_d} > 1 \tag{111}$$

This function, the "operating-characteristic function," describes the probability of crossing the dismissal threshold (i.e., a false dismissal) for an arbitrary value of signal amplitude A. The average number of intervals tested in the absence of signal $(A = 0)$ is

$$\frac{\text{Average number of}}{\text{intervals per test}} = \frac{\log \beta}{E(z/0)} \tag{112}$$

where $E(z/0)$ denotes the average of the log-likelihood with signal absent. For the model under discussion, z is given by Equation (110). Then, the average duration of the test with signal absent is

---

*Di Franco and Rubin, Radar Detection, Prentice-Hall, 1968, pp. 556-559.

$$\text{Average duration} = T_A = T_s \left\{ \begin{array}{l} \text{average number of} \\ \text{intervals per test} \end{array} \right\}$$

$$= T_s \left\{ - \frac{N_o}{A_d^2 T_s} \log \beta \right\} = - \frac{N_o}{A_d^2} \log \beta \qquad (113)$$

which is independent of T_s and, therefore, suggests that a continuous integration process could be used for the test (for the ideal coherent model).

7.5.1.3 Analysis for Coherent Model

As a first approach to obtain quantitative results for the coherent model, assume a worst case situation for the quantized search where the maximum possible displacement from the correlation peak occurs for the "best" search position (that one yielding maximum correlation). If there are m steps per bit of the signal, this maximum error is $1/2m$, expressed as a fraction of one bit. As an example, the worst case situation is illustrated in Figure 7-59 for $m = 2$. Note that the peak correlation amplitude is denoted by A_p. Furthermore, a pessimistic result is obtained if the probability of dismissal is computed only for the best search position; this assumes sync can not be detected at the other search positions within one bit of the peak.

Following the above approximations, one has

$$\text{Amplitude at search position} = A = A_p \left(1 - \frac{1}{2m} \right) \qquad (114)$$

$$\text{Time to search one bit} = T = mT_A = -m \frac{N_o}{A_d^2} \log \beta \qquad (115)$$

where Equation (115) follows from Equation (113), noting the number of search positions per bit. If the required probability of false dismissal is P, Equation (114) substituted in Equation (111) yields

$$P = \beta^{2 \left(1 - \frac{1}{2m} \right) \left(\frac{A_p}{A_d} \right) - 1} \qquad (116)$$
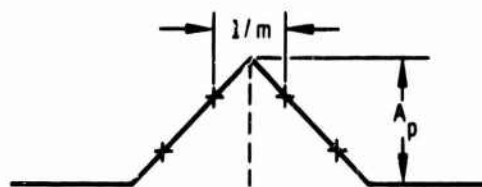
Figure 7-59. Worst Case Quantized Search

from which β can be solved. The, the result may be expressed in the normalized form

$$\frac{A_p^2 T}{N_o} = \frac{-m \log P \, (A_p/A_d)^2}{2\left(1 - \frac{1}{2m}\right)\frac{A_p}{A_d} - 1} \tag{117}$$

and this is to be minimized by choice of parameters.

Minimizing over the possible values of A_p/A_d yields

$$\frac{A_p}{A_d} = \frac{1}{1 - \frac{1}{2m}} \tag{118}$$

which shows that the worst-case amplitude should equal the design value A_d. Equation (117) becomes

$$\frac{A_p^2 T}{N_o} = \frac{-m \log P}{\left(1 - \frac{1}{2m}\right)^2} \tag{119}$$

Then, minimizing over m yields the optimum m = 1.5 (restriction to integer m was not previously implied), and finally

$$\left.\frac{A_p^2 T}{N_o}\right]_{min.} = -\frac{27}{8} \log P \tag{120}$$

As an example, if P = 0.3, corresponding to a detection probability of 0.7 on one pass through the correlation peak, $A_p^2 T/N_o = 4.1$ from Equation (120). For integer m, the optimum choice is m = 2, yielding $A_p^2 T/N_o = 4.3$.

-337-

The above pessimistic analysis will now be relaxed. In particular, the assumption of a worst search position as shown in Figure 7-59 will be replaced by averaging over the equally likely clock phases from worst case to best case. This is realistic since the clock phase defining the search position on any pass through the correlation peak is random and uniformly distributed in time. Also, the probability of dismissal when signal is present must be taken as the product over all search positions, since the signal is deemed present if dismissal does not take place at any search position. (It can only happen within the region of correlation, according to Equation (111).)

A computer program was written to perform the requisite averaging over the range of clock phase. The minimization is now performed by computational trial and error by adjusting A_p/A_d as a parameter for each m. The computer program sets β to give the desired average probability of dismissal, following which Equation (115) is applied. The results obtained are as follows, again taking $P = 0.3$.

$$\frac{A_p^2 T}{N_o} = 2.1 \qquad m = 1$$
$$= 2.1 \qquad m = 2$$
$$= 2.0 \qquad m = 3$$
$$= 2.0 \qquad m = 4$$

In all these cases $A_p/A_d = 1.5$ proved to be the optimizing parameter. It is seen that a saving of 3 db is realized, comparing the average peformance with the worst case performance previously obtained, and no clearly indicated optimum step size exists.

7.5.1.4 Comparison with Discrete Approximations to Uniform Search Rate

It presumably would be desirable to formulate a search strategy based on sequential detection which would take into account the known triangular correlation function. The basic theory used actually applied to a quantized search model with signal in one search position only. A proper model for the actual case of triangular correlation has not yet been found. Nevertheless, the computed results appear to be very good for the simple step search procedure applied to the coherent model. For comparison, performance can be compared with a system employing a filter matched to the triangular correlation function, which is the output signal when the

search is at a uniform rate of T seconds per bit of signal.[*] Since the energy in the triangle is $2A_p^2 T/3$, the peak output S/N from the matched filter is

$$\frac{S}{N}\Big]_{max} = \frac{2E}{N_o} = \frac{4}{3} \frac{A_p^2 T}{N_o} \tag{121}$$

to achieve a probability of dismissal of 0.3 at a false alarm probability[**] of 0.01, the requirement is then computed to be

$$\frac{A_p^2 T}{N_o} = 6$$

displaying in the order of a 5 db improvement for the sequential detection strategy.

Consider now what happens with a filter scheme if a discrete search is employed as illustrated previously in Figure 7-59. Suppose that the amplitudes from the present and the immediately preceding search positions are summed for the scheme. If the two search positions symmetrically straddle the correlation peak, the resulting S/N is

$$\frac{S}{N} = \frac{2(1 - \frac{1}{2m})^2 A_p^2}{m N_o/2T} \tag{122}$$

where the denominator gives the noise variance based on the duration T/m of integration per search position. Equation (122) is maximized for m = 1.5, yielding

$$\frac{S}{N} = \frac{32}{27} \frac{A_p^2 T}{N_o} \tag{123}$$

which shows a degradation from the ideal match given by Equation (121) of only 0.5 db.

A further interesting characteristic is that the S/N of Equation (122) or (123) is obtained regardless of the clock phase. This is true because the sum of the amplitudes at the two search positions straddling the correlation peak is a constant for the assumed triangular function.

---

[*] G. F. Sage, "Serial Synchronization of Pseudonoise System", IEEE Trans on Comm Tech, Dec. 1964, p. 123-127.

[**] It is assumed that false alarms are rejected by an unstated process which negligibly slows the average search rate, if the false alarm rate is not too high.

In view of the preceding result, the strategy for search based on sequential detection is suggested of alternately switching between the present and the previous search positions, rather than staying at one position for the test. This is similar to the excellent matched filter approximation of Equation (123) obtained by summing over two adjacent search positions. Clearly, dismissal behavior in the absence of signal is unchanged by this strategy, and Equation (113) continues to specify the average time to dismiss the present search position. Furthermore, Equation (111) continues to specify the probability of false dismissal of the present search position, provided that the amplitude A is interpreted[*] as the average for the present and the previous search positions. Note that for m large, this search strategy approaches the previous sequential detection strategy analyzed.

A computer program to average over all clock phases was devised similar to that described previously. The results for m = 1 and 2 showed this strategy of alternating between adjacent search positions actually is degraded from the simpler one of successively testing each position. The degradation was a factor of about 1.5 for m = 1 and close to unity for m = 2, confirming the trend anticipated for m large.

7.5.1.5 Noncoherent Analysis Model

The preceding analysis has presented performance calculations for a coherent model; a similar approach can be applied to the noncoherent model in which carrier phase is unknown. Now, the correlation amplitude of Figure 7-58 is to be viewed as the envelope of a carrier, and envelope detection is used to give the quantity for the statistical test at each search position. The theory is first reviewed, following the reference[**] with some modification.

Let r denote the normalized envelope output for a time duration T_s (integrate-and-dump followed by envelope computation). The logarithm of likelihood needed for the statistical test is now

$$z = -\frac{a_d^2}{2} + \log I_0 (a_d r) \tag{124}$$

---

[*] This requires both search positions to be included in the test an equal number of times, a minor consideration with the average number of intervals per test is large

[**] Di Franco and Rubin, Radar Detection, Prentice-Hall, 1968, pp. 556-559.

where a_d^2 is the design value of $2E_s/N_o$ for the interval T_s given by

$$\frac{2E_s}{N_o} = \frac{2E_d}{N_o} = a_d^2 = \frac{2A_d^2 T_s}{N_o} \qquad (125)$$

and A_d represents the design amplitude of the signal.

Again assuming an arbitrarily low false acceptance probability $(\alpha \longrightarrow 0)$, the average time to dismiss a search position not containing signal is given by

$$T_A = T_s \left\{ \text{average number of intervals} \right\} = T_s \frac{\log \beta}{E(z/0)} \qquad (126)$$

where $E(z/0)$ denotes the average of z in Equation (124) with signal absent. This average is

$$E(z/0) = \int_0^\infty \left[-\frac{a_d^2}{2} + \log I_o (a_d r) \right] r e^{-r^2/2} dr$$

and by some manipulation

$$= -\frac{a_d^2}{2} + a_d \int_0^\infty \frac{I_1(a_d r)}{I_o(a_d r)} e^{-r^2/2} dr \qquad (127)$$

The average can be computed in closed form if a_d is small by the series expansion

$$\frac{I_1(x)}{I_o(x)} = \frac{\frac{x}{2} + \frac{x^3}{16} \cdots}{1 + \frac{x^2}{4} + \cdots} = \frac{x}{2} - \frac{x^3}{16} + \cdots \qquad (128)$$

from which is evaluated $(a_d \longrightarrow 0)$

$$E(z/0) \cong -\frac{a_d^4}{8} \qquad (129)$$

Substituting into Equation (126) yields

$$T_A \cong \frac{-2 \log \beta}{A_d^4 T_s/N_o^2} \qquad (130)$$

for $2A_d^2 T_s/N_o \ll 1$.

When signal is present with amplitude A, the probability of dismissal is approximately given by

$$L(A) = 1 \qquad , \quad 2(\frac{A}{A_d})^2 < 1$$

$$= \beta^{2(\frac{A}{A_d})^2 - 1} \qquad , \quad 2(\frac{A}{A_d})^2 > 1 \tag{131}$$

where the approximation is valid, again, for $2A_d^2 T_s/N_o \ll 1$. Considering again a quantized search of m steps per bit of signal and a worst case straddling of the correlation peak of power A_p^2, one has

$$P = \beta^{2\left[(1 - \frac{1}{2m})\frac{A_p}{A_d}\right]^2 - 1} \tag{132}$$

and letting $T = mT_A$

$$\frac{A_p^2 T}{N_o} = \frac{-2 \log P}{(A_p^2 T_s/N_o)} \frac{m(A_p/A_d)^4}{2\left[(1 - \frac{1}{2m})\frac{A_p}{A_d}\right]^2 - 1} \tag{133}$$

which is similar to Equation (117) for the coherent case.

Equation (133) is minimized over the parameter A_p/A_d by Equation (118) again, from which

$$\frac{A_p^2 T}{N_o} = \frac{-2 \log P}{(A_p^2 T_s/N_o)} \frac{m}{(1 - \frac{1}{2m})^4} \tag{134}$$

Next, minimizing over m yields the optimum m = 2.5 (as compared with 1.5 for the coherent case), and

$$\frac{A_p^2 T}{N_o}\Bigg]_{min} = \frac{-12.2 \log P}{(A_p^2 T_s/N_o)} \tag{135}$$

-342-

The result in Equation (135) may be compared with Equation (120) previously obtained for the coherent case. The derivation required $A_p^2 T_s / N_0$ to be small compared with unity; hence, the noncoherent testing under this condition is quite inferior to coherent testing.

It would appear that the incoherent test should be designed with a smoothing interval T_s to yield $A_p^2 T_s / N_0$ somewhere in the vicinity of unity in order to avoid a significant performance degradation. However, the analysis computations must be further refined to allow quantitative comparison with the coherent model. Noting in the above analysis for $A_p^2 T_s / N_0$ small that the optimum A_p / A_d sets the worst-case power equal to the design value, this selection can be presumed to be a reasonable choice for larger values of $A_p^2 T_s / N_0$. As a result, β now equals the actual probability of false dismissal P at the search position for the worst case straddling of the correlation peak, and the approximation of Equation (131) need not be employed.

The average number of tests to dismiss in the absence of signal must now be more accurately computed by Equation (127). Figure 7-60 shows the numerical results for the noncoherent model, which may now be applied to obtain quantitative comparisons from Equation (126).

Again setting $T = mT_A$, one may write Equation (126) as

$$\frac{A_p^2 T}{N_0} = \frac{A_p^2 T_s}{N_0} \log P \frac{m}{E(z/0)} \tag{136}$$

where $E(z/0)$ is a function of

$$a_d^2 = \frac{2 A_p^2 T_s}{N_0} (1 - \frac{1}{2m})^2 \tag{137}$$

according to Figure 7-60. As an example, let $A_p^2 T_s / N_0 = 1$. Then, a numerical calculation shows m = 2 is roughly optimum, and

$$\frac{A_p^2 T}{N_0} \cong - 20 \log P \tag{138}$$

which shows a degradation of 7.7 db from the coherent system result given in Equation (120).

-343-
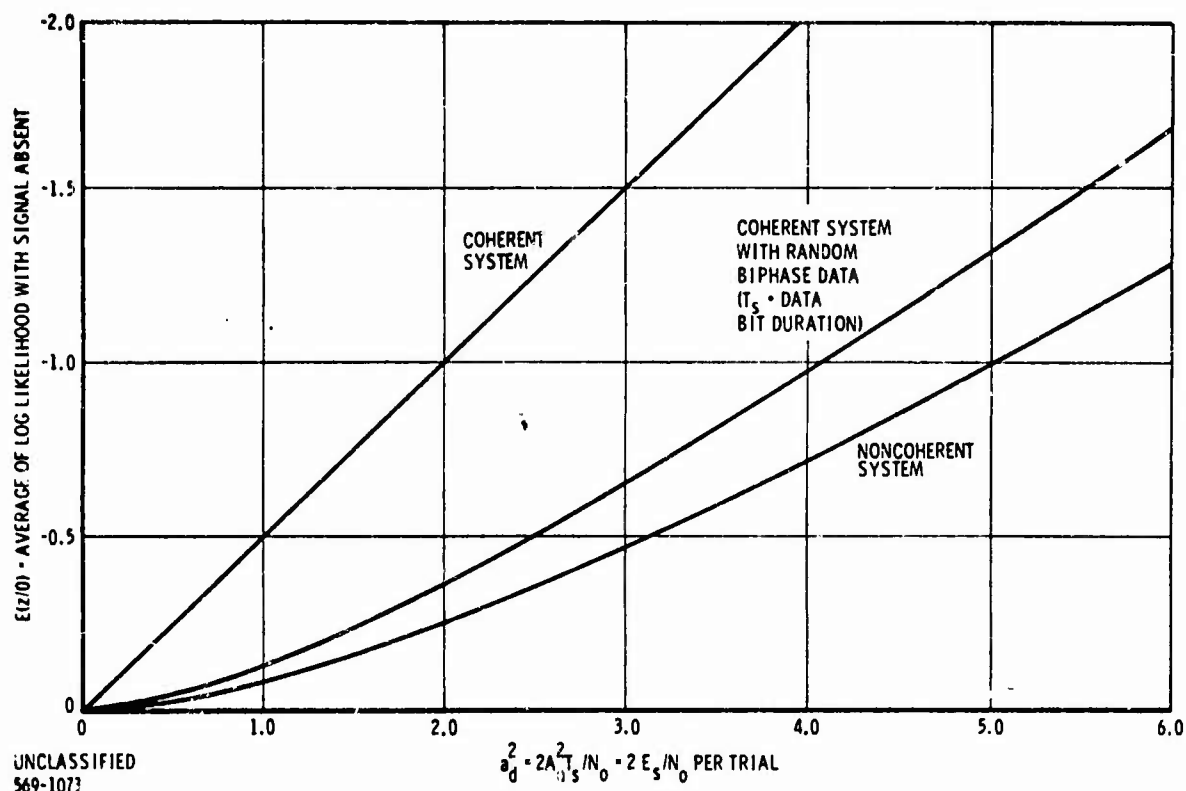
Figure 7-60. Evaluation of Expectation of Log-Likelihood

The degradation from coherent is considerably less if $A_p{}^2 T_s/N_o$ can be greater than unity; for example, if $A_p{}^2 T_s/N_o = 2$, the resultant for $A_p{}^2 T/N_o$ is reduced to $-13 \log P$. However, T_s actually cannot be arbitrarily increased when other considerations such as data modulation on the signal are taken into account.

In Figure 7-60, $E(z/0)$ for the coherent case is plotted for comparison, derived by taking the expectation of z in Equation (124).

7.5.1.6 Signal With PSK Data Modulation

The system may require the capability for synchronization with polarity reversal (PSK) data modulation on the signal. Thus, the ideal coherent model no longer applies. The noncoherent model in the preceding section can be retained if T_s = data bit duration*, since phase was not known anyway. For a comparison, a

---

*It is assumed that the data bit timing is locked to the PN bit sequence, hence is known when the search falls into the correct position.

-344-

direct analysis of the coherent system with PSK data modulation may be made. In other words, phase coherence is presumed but the random data polarity after correlation still must be allowed for.

The logarithm of the likelihood ratio is found by direct derivation, assuming random data, to be

$$z = \frac{-a_d^2}{2} + \log \cosh (a_d v) \tag{139}$$

where v is normalized to unit variance (in the absence of signal) and a_d is still given by Equation (125), with T_s denoting the data bit duration. The similarity with Equation (124) for the noncoherent case is evident. Furthermore, Equation (139) approaches Equation (110) for a_d large. As before, the quantity $E(z/0)$ is required, and this has been numerically evaluated in Figure 7-60.

It may be observed from Figure 7-60 that there is a surprisingly small differential between the coherent system with random data and the noncoherent system (which is invariant to the data). At low values of $2E_s/N_o$ the separation is by less than a factor of 2 in $E(z/0)$.

Thus, it may be concluded that a requirement to synchronize a coherent system with random data present severely degrades performance compared with an idealized coherent model, and the possible improvement from the noncoherent system is small (in the order of 1 to 2 db at practical design levels for $2E_s/N_o$).

7.5.1.7 Use of Phase Lock Loop

An example of a practical implementation towards obtaining coherence is to use a phase lock loop on the correlator output (see Figure 7-57) so as to correct local oscillator phase. Such a system is difficult to analyze because of the dynamics of the nonlinear phase lock loop. Two cases may be distinguished: (1) carrier unmodulated by data, and (2) random data. The second case is handled by a Costas loop (modification to phase lock loop). However, theoretical analysis has already shown that very little improvement over the noncoherent detector is inherently available for this case, although the Costas loop may have some practical implementation advantages.

For the first case without data modulation, the basic phase lock loop can be considered. Qualitatively, after phase lock acquisition of the correlator output takes place, the detection process becomes essentially coherent. Furthermore, in the absence of signal, the dismissal process is identical with a conerent detector. Thus, with the phase lock loop the sequential detection still uses the log-likelihood function, Equation (110), of the coherent system. This, of course, is not optimum, but appears a reasonable choice.

A Monte Carlo computer simulation was performed to obtain performance results for the phase lock loop system and, as a by-product, for a coherent system The latter will give a check on the basic sequential detection theory. Since operation in the vicinity of 0 db in a sampling interval is desired, the phase lock loop was set up with a second-order function with a noise bandwidth of 0.1 times the sampling rate; this was found in other prior simulations to represent a rough thresholding for the loop at this S/N level. The simulation applies the appropriate difference equation for the loop.

Presuming a second-order loop transfer function and integrate-and-dump smoothing over the sampling time, the difference equation for the loop may be shown to be

$$\emptyset(k) = 2\emptyset(k-1) - \emptyset(k-2) + W_1 \, e(k-1) - W_2 \, e(k-2) \tag{140}$$

where the argument k denotes the value at time $t_k = kT_s$, $\emptyset$ is the VCO phase, and e is the error feedback, given by

$$e = \text{quadrature} \tag{141}$$

for the error feedback, where the pair of product detector outputs is

$$\text{quadrature} = \left(\sqrt{2E_s/N_o} \sin(\theta - \emptyset) + y \right) / \sqrt{2E_d/N_o}$$

$$\text{in-phase} = \left(\sqrt{2E_s/N_o} \cos(\theta - \emptyset) + x \right) / \sqrt{2E_d/N_o} \tag{142}$$

In Equation (142) θ equals input signal phase, x, y are independent Gaussian variables of zero mean and unit variance, E_s/N_o equals actual energy/noise, and E_d/N_o equals design energy/noise of the carrier in the sampling interval T_s. In Equation (140) the constants W_1 and W_2 in terms of the one-sided loop noise bandwidth B_L are obtained from

-346-

$$W_1 = (2\zeta + \omega_n/2)\, \omega_n$$

$$W_2 = (2\zeta - \omega_n/2)\, \omega_n \tag{143}$$

$$B_L = (\zeta + 1/4\zeta)\, \omega_n \quad \text{(Hertz)}$$

where ζ equals loop damping factor and ω_n is the loop resonant frequency in rad/sec. The difference equation, Equation (140), is based on the open loop transfer function $G(s)$ for an ideal second order loop with infinite gain, or

$$G(s) = 2\zeta\omega_n + \omega_n^2/s \tag{144}$$

To collect statistics on the sequential detection, the test was truncated at a fairly large number. If a test persists until truncation occurs, acceptance of synchronization is declared; hence, a small false acceptance probability ($\alpha > 0$) is thereby introduced. The test was repeated as independent trials, starting the phase lock loop at zero frequency error and a random phase. The correlation amplitude was set at the design value for the loop.

In the actual simulation, truncation was done after 50 intervals. The results for the basic coherent system (loop not simulated) are shown in Table 7-11, based on averaging over 2000 intervals. The theoretical number to dismiss is obtained from Equation (112) using the observed dismissal probability rather than the setting of β. In no test did a false acceptance occur with the above truncation. The deviation from theory is presumably explained by the fact that the basic theory ignores "the excess over boundary"; hence, is accurate only for a large average number to dismiss. The correspondence of simulation results to theory appears to be relatively good.

Table 7-11. Simulation of Coherent System

$\dfrac{2A_d^2 T_s}{N_o}$	β Setting	Fraction Dismissed (Signal Present)	Average No. to Dismiss (Signal Absent)	Theoretical Average to Dismiss
3 db	.5	0.23	2.1	1.5
0 db	.5	0.25	3.3	2.3

Next, the phase lock loop system was simulated as described above with results shown in Table 7-12 with averaging over several thousand intervals. A comparison of Table 7-12 with Table 7-11 shows that the phase lock loop system is degraded relative to the coherent system by approximately 5 db at both values of $2A_d^2 T_s/N_o$; this degradation shows up as a greater average number to dismiss in absence of signal, for approximately the same fraction dismissed.

Thus, preliminary results for the phase lock loop system show only a small improvement can be expected compared with the noncoherent system, as analyzed in Section 7.5.1.5. Furthermore, the phase lock loop requires the data modulation to be suppressed at the transmitter until synchronization has taken place. Since the detection is non-optimum (although a better scheme is unknown), conceivably some improvement in performance is still feasible.

One possible approach is to leave some time for phase lock acquisition at the start of each test. This implies a better approximation to coherent performance but with a fixed number of extra trials added. The potential payoff for this approach appears small, considering the simulation results in Table 7-12; i.e., only 7 intervals are required on the average to dismiss with $2A_d^2 T_s/N_o = 3$ db, while 2 plus the fixed extra number is the number needed according to Table 7-11.

7.5.1.8 Costas Loop Detection

As previously described, random polarity reversals by data cannot be handled by a phase lock loop, and a Costas loop may be introduced. Equation (139) derived for the coherent system with random data, is the appropriate likelihood function for this system. In the absence of signal, the dismissal process is identical with the coherent case.

Table 7-12. Simulation of Phase Lock Loop System

$\dfrac{2A_d^2 T_s}{N_o}$	β Setting	Fraction Dismissed (Signal Present)	Average No. to Dismiss (Signal Absent)
3 db	0.005	0.32	7.0
0 db	0.02	0.3	11.0

-348-

A simulation was obtained by modifying the program for phase lock detection into a Costas loop program with the appropriate likelihood function from Equation (139). The modification consists of switching the quadrature by the polarity of the in-phase quantities in Equation (142), or

$$e = \text{quadrature} \cdot \text{sign in-phase} \tag{145}$$

to simulate the Costas loop.

Again truncation was utilized, and persistence beyond this point was deemed acceptance. The one sided noise bandwidth of the loop was set at 0.1 times the sampling rate, as for the phase lock simulation.

Performance observed for a limited set of tests was surprisingly good. A typical result for $E_s/N_o \approx 0$ db is shown in Table 7-13, for averaging over several thousand intervals. Comparison of Table 7-11 and Table 7-12 shows the unanticipated result that the Costas loop actually outperforms the phase lock loop slightly at the higher E_s/N_o. (It should be remembered that the data timing is presumed known for the Costas loop operation.) At lower E_s/N_o, the degradation inherent in the nonlinear operation causes the Costas loop to become inferior to the phase lock loop, the cross-over occuring between $2E_s/N_o = 3$ db and 0 db.

The concept of utilizing a Costas loop followed by a sequential detector is developed in more detail in the following paragraphs.

The advantage of a Costas loop over a phase lock loop appears to derive from the fact that the stable equilibrium points are separated by π radians rather than 2π. Two approaches may be examined for resolving the effect of the Costas loop phase ambiguity on the demodulated amplitude. The first assumes random polarity modulation, and the likelihood ratio is defined on this basis. The second assumes an unmodulated carrier and performs a parallel test for both of the possible lock-in conditions.

A further question is whether the shape of the triangular correlation function can be taken advantage of to improve synchronization reliability.

Table 7-13. Simulation of Costas Loop

$\dfrac{2A_d^2 T_s}{N_o}$	η Setting	Fraction Dismissed (Signal Present)	Average No. to Dismiss (Signal Absent)	Truncation
3 db	0.3	0.37	4.5	50
3 db	0.25	0.3	5.0	50
0 db	0.15	0.42	16.0	100

7.5.1.8.1 Basic Strategy

The basic sequential detection strategy performs a search with a specified number of discrete positions per bit of the PN waveform. At each new position, the past is wiped out, and the Costas loop is started with the initial conditions of a random phase and specified frequency offset determined from the assumed frequency error. For the first approach given above, the log-likelihood function to be summed over the successive intervals and compared with the dismissal threshold is

$$z = -E_d/N_o + \log \cosh \left[(2E_d/N_o) \text{ in-phase} \right] \tag{146}$$

where in-phase is normalized as in Equation (142). This function is invariant to polarity reversal modulation.

The second approach depends on the loop maintaining its lock-in condition for the duration of the test for the given search position. Since either polarity can exist, a parallel test is run for both using log-likelihood for the coherent detector, as follows:

$$z_1 = -E_d/N_o + (2E_d/N_o) \text{ in-phase}$$

$$z_2 = -E_d/N_o - (2E_d/N_o) \text{ in-phase} \tag{147}$$

Only the larger of the z_1 and z_2 sums is compared with the dismissal threshold. In other words, dismissal is required to occur on both parallel tests before moving to the next search position.

A computer simulation was written for each of the above approaches to obtain quantitative data on the synchronization performance. The results are presented in Figures 7-61 and 7-62. These show the behavior as a function of received energy/ noise per interval and are both for a design value, E_d/N_o of 0 db. The probability of synchronization at $E_s/N_o = E_d/N_o$ depends on the dismissal threshold, defined by

$$\text{Dismissal threshold} = \log (\beta) \qquad (148)$$

where β is the theoretical probability of false dismissal for a coherent system. The probability of synchronization at $E_s/N_o = E_d/N_o$ was to be roughly 0.7 in the simulation; the actual values obtained are seen from Figures 7-61 and 7-62

The two approaches may now be compared, with the qualification that the loop parameters are not optimized but have been selected heuristically on the basis of behaviors observed in prior phase lock simulations. The normalized parameter E/N_o, defined as the energy/noise in the average time to search through one bit of the PN signal, is the appropriate comparison. It is observed that the second approach, Figure 7-62, although 1.1 db degraded in E_s/N_o, can search faster by the ratio 7.8/4.1 or 2.8 db. Thus, the second approach demonstrates a net advantage of 1.7 db in E/N_o for a synchronization probability of 0.7 at a given search position, maintaining $B_L = 0.1$.

7.5.1.8.2 Effect of Triangular Correlation

The results of the basic sequential detection strategy still do not give actual probabilities of synchronization, considering the triangular correlation function. If the search is quantized to m positions per bit, there is more than one chance to synchronize on a given pass through correlation, and the probability of synchronization for one pass must be appropriately computed. Furthermore, on any one pass through correlation, the quantized search positions are randomly related to the position of the correlation peak.
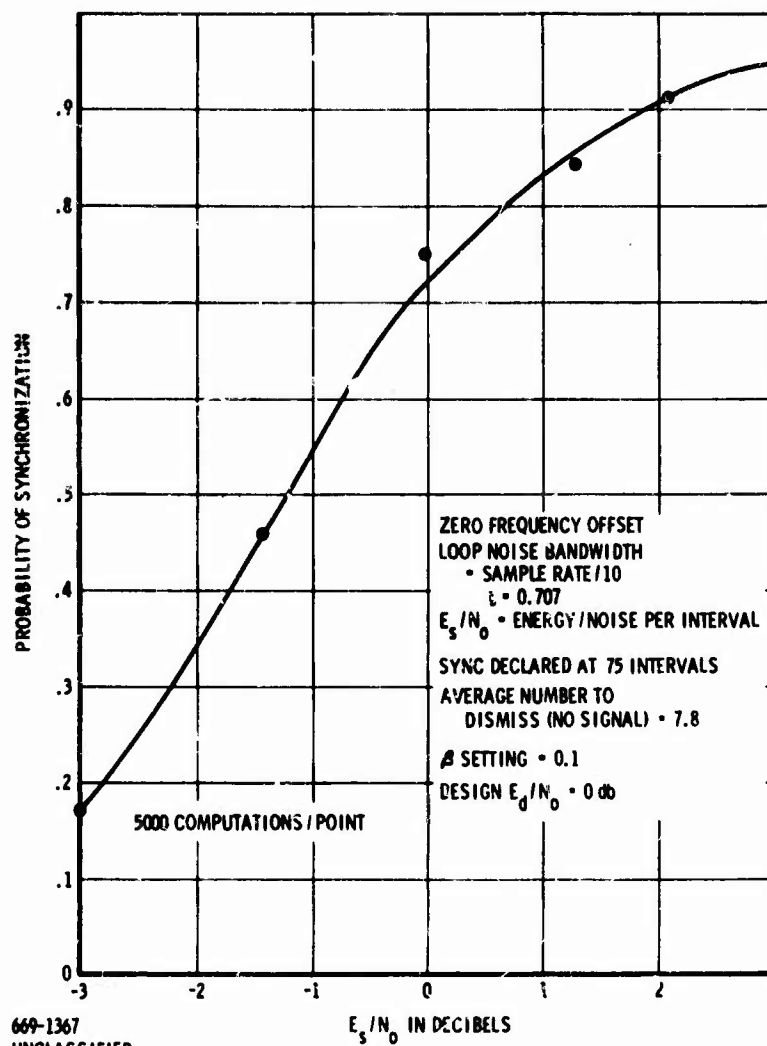
Figure 7-61. Sequential Detection by Costas Loop with Random Data
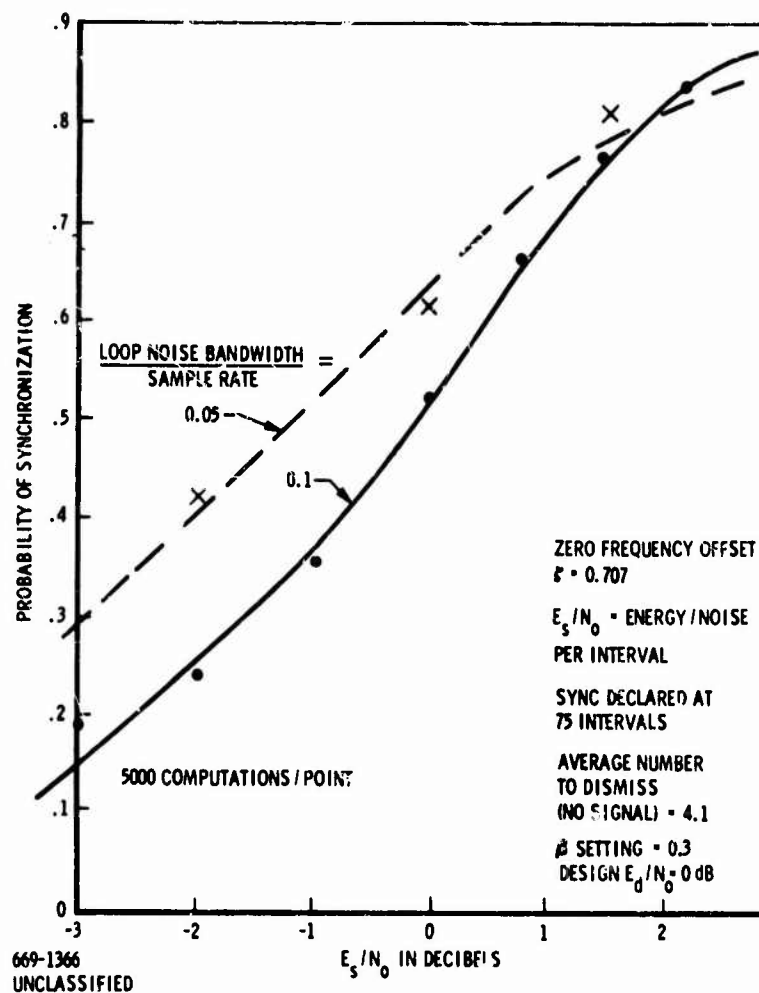
Figure 7-62. Sequential Detection by Costas Loop with No Data Modulation

To study the situation further, consider the choice $m = 2$. The extremes of "best" and "worst" cases on any given pass through correlation are shown in Figure 7-63. For either of these extremes or any case in between, the overall probability of synchronization can be computed from the curve* for a single position by noting that the probabilities of dismissal at the successive positions are statistically independent.

Results for the two extremes are shown in Figure 7-64, expressed in terms of E_p/N_o defined as the energy/noise at the correlation peak.

---

*The probability in Figure 7-61 or 7-62 may be taken as 0 or unity outside the plotted range of E_s/N_o.
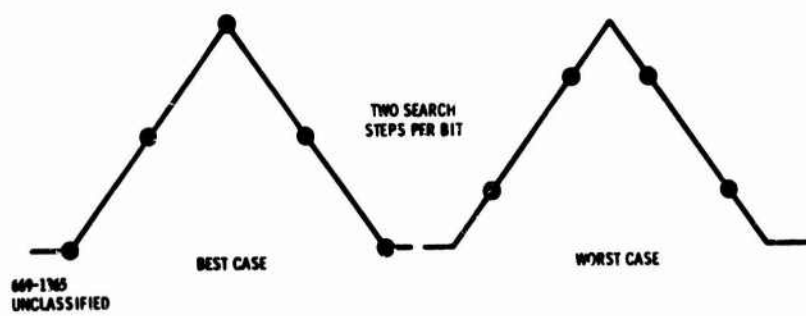
Figure 7-63. Cases of Quantized Search
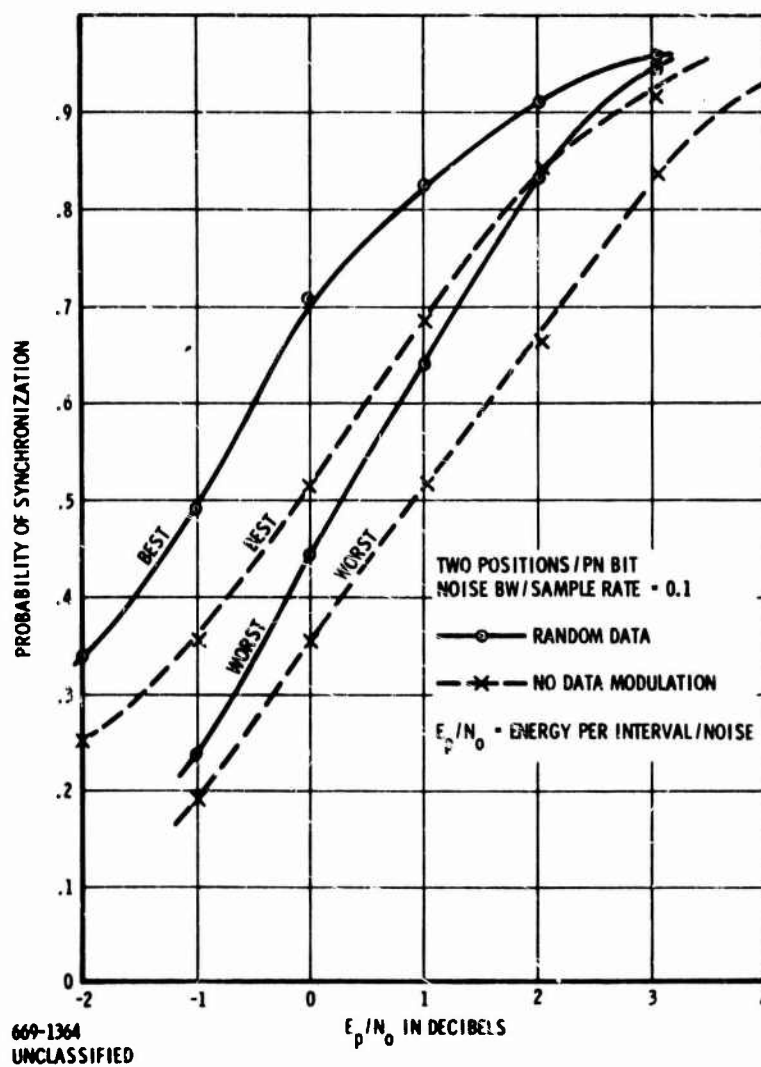
Figure 7-64. Costas Loop Simulation

-354-

7.5.1.8.3 Continuous Operating Loop

In the previous section, the Costas loop is assumed reset to zero frequency offset when shifting to a new search position. One may, instead, cause the Costas loop to operate on a continuous basis as the search proceeds. Conceivably, this could give improved performance in the worst case of Figure 7-63 since the loop now has twice as long to acquire at the maximum worst case correlation. However, the problem now is that the loop VCO frequency can be driven arbitrarily far away from zero in a "random walk" due to noise.

To see this directly, Equation (140) is rewritten for the average frequency in an interval, i.e., the VCO phase increment $\Delta \phi(k) = \phi(k+1) - \phi(k)$:

$$\Delta \phi(k) = \Delta \phi(k-1) + W_1 e(k) - W_2(k-1) \tag{149}$$

If $\Delta \phi(0) = 0$, one can sum over k to obtain

$$\Delta \phi(k) = \sum_{i-1}^{k-1} (W_1 - W_2) e(i) + W_1 e(k) - W_2 e(0) \tag{150}$$

where the $e(i)$ are statistically independent Gaussian variables in the absence of a correlated signal amplitude. The mean $E\{\Delta \phi(k)\}$ is zero, and the variance is

$$E\left\{[\Delta \phi(k)]^2\right\} = [(k-2)(W_1 - W_2)^2 + W_1^2 + W_2^2] E\left\{e^2\right\} \tag{151}$$

which shows how the frequency fluctuation grows with time. The two components in Equation (151) are approximately equal for

$$k \simeq 8 \zeta^2/\omega_n^2 \tag{152}$$

or $k = 110$ for $\zeta = 0.707$ and $B_L = 0.1$ (see Equations (143). For larger k, the variance effectively starts growing.

One way out of the problem is to apply a loop with finite open loop gain so that a finite equilibrium condition can be reached. The open loop gain $G(s)$ is now

$$G(s) = \frac{K(1 + \tau_1 s)}{1 + \tau s} \tag{153}$$

and

$$\omega_n = \sqrt{K/\tau}$$

$$B_L = \frac{1.11}{2\pi} \omega_n \left[1 + (\sqrt{2} - 1/\omega_n \tau)^2 \right] \tag{154}$$

where $\zeta = 0.707$ has been assumed in the expression for B_L.

The difference equation for the finite gain loop is found to be

$$\phi(k) = (1 + \alpha) \phi(k - 1) - \alpha \phi(k - 2) + W_1 e(k - 1) - W_2 e(k - 2) \tag{155}$$

where

$$\alpha = \exp(- T_s/\tau)$$

$$W_1 = \omega_n^2 T_s \tau - (1 - \alpha)(\omega_n^2 \tau^2 - \sqrt{2} \omega_n \tau + 1) \tag{156}$$

$$W_2 = \omega_n^2 T_s \tau \, \alpha - (1 - \alpha)(\omega_n^2 \tau^2 - \sqrt{2} \omega_n \tau + 1)$$

Again, Equation (155) can be rewritten in terms of $\Delta \phi(k)$ The mean of $\Delta \phi(k)$ is again zero in the absence of a correlated signal amplitude, and the variance approaches a steady state value for large k. This steady state value is found by direct computation from Equation (155), rewritten, to be

$$E\{\Delta\phi^2\} = \frac{(W_1 - W_2)^2 + 2(1 - \alpha) W_1 W_2}{1 - \alpha^2} E\{e^2\} \tag{157}$$

Since the e(k) are Gaussian variables in the absence of signal, $\Delta \phi$ has a Gaussian distribution.

The method for Monte Carlo simulation of the continuously operating loop is now clear. The initial condition for VCO frequency is chosen from a Gaussian distribution with the requisite variance. The probability of synchronization is empirically determined by repetitively searching through the triangular correlation function peak for each successive pass. Synchronization is declared if dismissal does not take place at any search position (necessarily within the triangle function).

The results for m = 2 steps/bit are presented in Figure 7-65, with the numerical choice

$$\frac{1}{\omega_n \tau} = \frac{\omega_n}{K} = 0.2$$

for the Costas loop with random data. This curve may be compared with the curves for the corresponding case (solid lines) in Figure 7-64, since the average number to dismiss in the absence of signal is the same for both the finite-gain and the infinite-gain loops. (Simulation results for a finite average were 7.8 versus 7.4.) It is seen that Figure 7-65 is between the best and worst cases in Figure 7-64. Hence, it is concluded that the possible advantage of a continuously operating loop is offset by the noise-induced frequency fluctuation, and there is no significant performance difference from the reset in-frequency loop previously studied.

FINITE GAIN LOOP $(\omega_n / K = 0.2)$
LOOP NOISE BANDWIDTH / SAMPLE RATE = 0.1
NOISE DRIVEN INITIAL FREQUENCY ERROR
SYNC DECLARED AT 75 INTERVALS
AVERAGE NUMBER TO DISMISS (NO SIGNAL) = 7.4
β SETTING = 0.1

6000 COMPUTATIONS/POINT

PROBABILITY OF SYNC

E_p / N_o IN DECIBELS
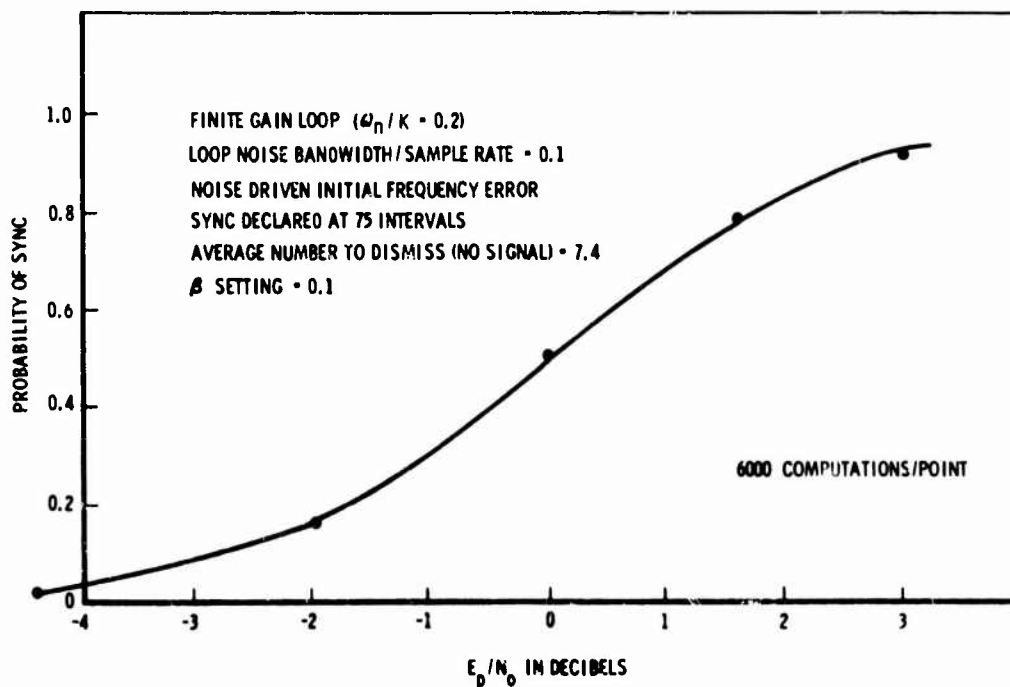
Figure 7-65. Sequential Detection by Costas Loop, Search
Through Triangle in Two Positions per Bit

-357-

7.5.1.8.4 Synchronization with Four-Phase Tracking Loop

The Costas loop for biphase modulation has displayed an advantage over a standard phase lock loop for acquisition, presumably because of the reduced maximum phase error ($\pi/2$ instead of π) in the former. This hypothesis can be extended to a phase tracking loop for multi-phase modulation; specifically, to a four-phase loop.

The form of the four-phase loop is made evident from the trigonometric relation

$$\cos x \sin x (\cos x + \sin x)(\cos x - \sin x) = \frac{\sin 4x}{4} \tag{158}$$

which shows how the components in Equation (142) can be applied to develop an error signal repetitive in $\pi/2$, as compared with π for the Costas loop and 2π for the standard loop. In similarity with Equation (145), introduction of hard limiting of some quantities improves performance, and therefore the error feedback is

$$e = \text{in-phase} \cdot \text{quadrature} \cdot \text{Sign} \{\text{in-phase} + \text{quadrature}\} \cdot$$
$$\text{Sign} \{\text{in-phase} - \text{quadrature}\} \tag{159}$$

When the loop is tracking, either the in-phase or the quadrature, but not both, is driven to zero.

The dismissal test for the sequential detection is an extension of Equation (147) taking into account the four possible lock-in conditions. Thus, we add to Equation (147)

$$z_3 = -E_d/N_o + (2E_d/N_o) \text{ quadrature}$$
$$z_4 = -E_d/N_o - (2E_d/N_o) \text{ quadrature} \tag{160}$$

and compare the largest of z_1, z_2, z_3, and z_4 with the dismissal threshold.

Simulations were performed at $E_d/N_o = 0$ db. The observed probability of synchronization with $E_s/N_o = E_d/N_o$ was degraded from the Costas loop performance shown in Figure 7-62 for the same β setting. Furthermore, the four parallel tests, rather than two, increased the average number of intervals to dismiss. Presumably, the degradation inherent in Equation (159) at $E_s/N_o = 0$ db more than offsets the reduction in initial phase error. The four-phase loop is, therefore, not considered further, since it is inferior to the Costas loop for synchronization at the desired low E_s/N_o of 0 db.

7.5.1.8.5 Summary of Costas Loop Results

The results of the preceding detailed analysis of Costas loop sequential detection may be summarized in terms of the parameter E/N_o, where E is the received signal energy over the time to search one bit of the PN signal. Note that

$$E/N_o = m \, E_p/N_o \text{ (average number to dismiss)} \tag{161}$$

For simplicity, the best case and worst case curves in Figure 7-64 have been averaged and presented in Figure 7-66; this presumes a simple linear relation between probability of synchronization and time displacement, and is not too unreasonable for an approximation.

A limited attempt at loop parameter optimization was made for the approach of no data modulation. At a fixed $E_s/N_o = 0$ db, the loop noise bandwidth was varied about the value 0.1 times the sample rate, with the results in Table 7-14. (Naturally, loop bandwidth has no effect on average number of intervals to dismiss in the absence of signal.) From Table 7-14 it appears that a loop noise bandwidth of 0.05 is roughly the optimum at the E_s/N_o of 0 db.
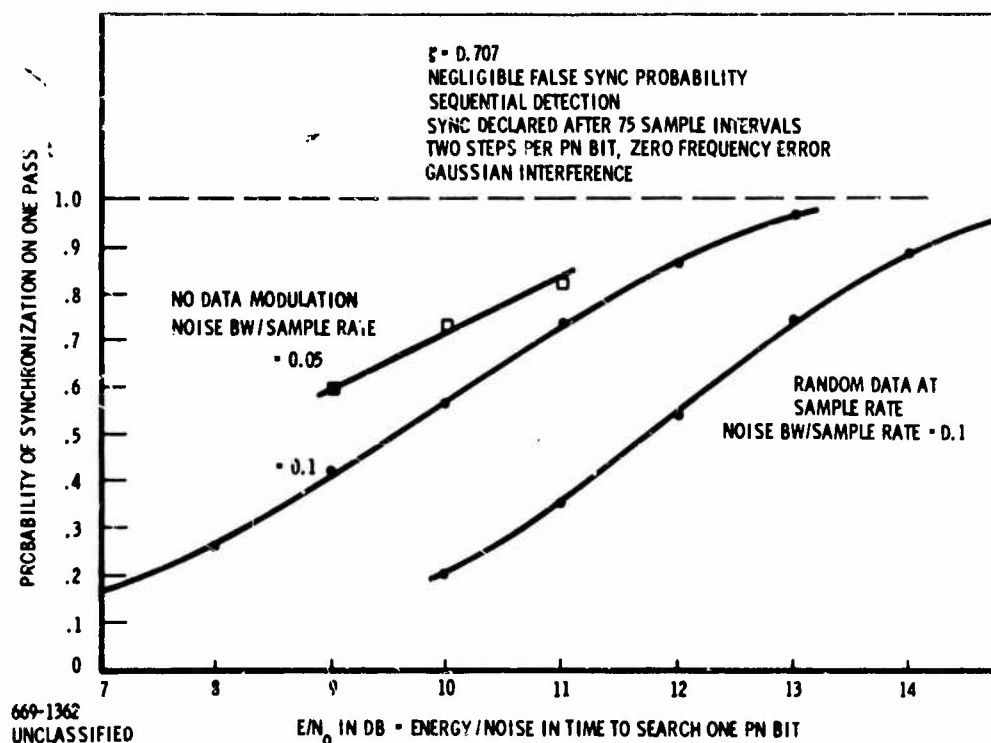
Figure 7-66. Costas Loop Simulation

Table 7-14. Effect of Loop Bandwidth

E_s/N_o	Loop Noise BW	Probability of Sync	Number of Computations
0 db	.02	0.54	1000
0 db	.03	0.58	3000
0 db	.05	0.60	16000
0 db	.07	0.59	3000
0 db	.10	0.51	10000
0 db	.20	0.12	1000

A simulation over a range of E_s/N_o has been plotted in Figure 7-62 for comparison of the two bandwidth cases, .05 and .1. This figure shows the narrower bandwidth to be an advantage only at low E_s/N_o. Intuitively, this makes sense, since the loop dynamics limit the response time at high E_s/N_o. Following the procedure previously described, representative synchronization probabilities are plotted in Figure 7-66 for the narrower loop bandwidth and display approximately a 1 db improvement compared to values for the wider bandwidth.

7.5.1.9 Pseudonoise Synchronization By Serial Search With Noncoherent Detection

In the preceding sections describing application of sequential detection to the serial search process for a PN system, it was concluded that use of (Costas) phase lock loop techniques offered somewhat better performance than noncoherent detection techniques. The discussion which follows indicates possible improvement for noncoherent schemes and presents simulation results for a particular scheme which somewhat outperforms the Costas loop scheme.

The discussion is initiated with the observation that noncoherent detection of the successive sample intervals clearly is non-optimum, since it ignores the continuity of signal phase from one interval to the next. Since absolute phase is unknown, some version of noncoherent detection is still required; however, relative coherence should be maintained over as long an integration as possible. In a practical sense, the interval of coherence is limited by phase perturbations on the signal, such as caused by Doppler and Doppler rate.

Rather than postulate a theoretical detection process extending coherence requirements indefinitely, one may arbitrarily require the coherence to carry over only from one sample interval to the next, in similarity with DPSK modulation schemes. The simplest way to accomplish this, of course, is merely to extend the sample interval by a factor of two, retaining the basic noncoherent strategy except with coarser time quantization. Note, however, this is not possible when the signal is biphase modulated with random data at the original sample rate.

The scheme to be tested here retains the original sample interval but assumes phase coherence from one interval to the next; hence, it is termed here, "semi-coherent" detection. The situation is illustrated in Figure 7-67. The integration extends over two of the original intervals, but successive samples for the sequential detection trial are obtained by integrations displaced only by one interval, as shown. Because of the statistical effects of the overlap, the basic sequential detection theory is not as easily applied as in prior analyses.

One reasonable heuristic approach is simply to treat successive samples as independent when defining the likelihood ratio function. Thus, if x_{i-1}, y_{i-1}, x_i, y_i represent, respectively, the quadrature components of the first and second intervals of the ith sample, and no data modulation is present, the normalized envelope r_i is given by

$$r_i = \sqrt{\frac{(x_{i-1} + x_i)^2 + (y_{i-1} + y_i)^2}{2}} \qquad (162)$$
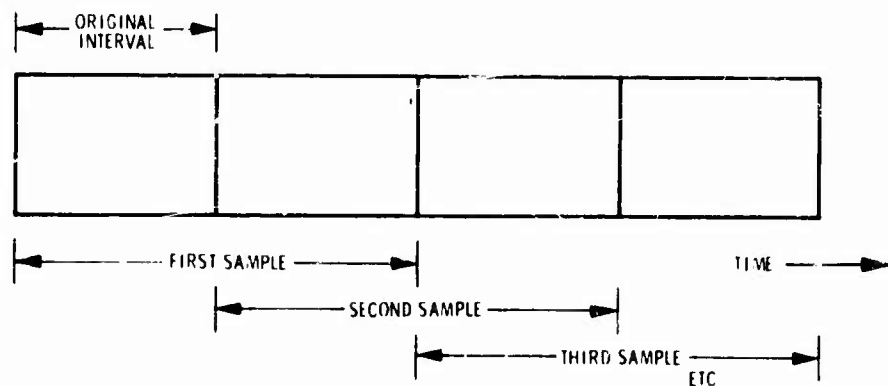
Figure 7-67. Modified Noncoherent Detection Strategy

-361-

If the design $2E_d/N_o = a_d^2$ per interval is specified, the log-likelihood, presuming random absolute phase, becomes

$$z_i = -a_d^2 + \log I_o(\sqrt{2}\, a_d\, r_i) \qquad (163)$$

As noted, successive z_i are actually not independent.

If biphase data modulation exists in each interval, Equation (162) is no longer valid, since a phase transition due to data may have occurred. Considering both events as equally probable, the log likelihood becomes

$$z_i = -a_d^2 + \log\left\{\frac{I_o(\sqrt{2}\, a_d r_i^+) + I_o(\sqrt{2}\, a_d r_i^-)}{2}\right\} \qquad (164)$$

where

$$r_i = \pm\sqrt{\frac{(x_{i-1} \pm x_i)^2 + (y_{i-1} \pm y_i)^2}{2}} \qquad (165)$$

represent the envelopes for the two events (phase transition due to data or no transition).

The above detection strategies have been simulated on a computer. In the simulation, the values of x_{-1} and y_{-1} are simply taken to be zero at the outset of each sequential detection test. The quadrature components are generated as independent Gaussian variables, with

$$E(x_i) = \sqrt{2E_s/N_o}$$
$$E(y_i) = 0 \qquad (166)$$
$$\mathrm{Var}(x_i) = \mathrm{Var}(y_i) = 1$$

In Equations (166), E_s/N_o is the actual energy/noise density for each interval. The design value is designated as E_d/N_o, and is needed for Equation (163) or (164). The results are given in Figure 7-68.

A comparison of the results is also made with the basic noncoherent strategy which also would integrate over two of the original intervals and requires no data modulation. On the basis of simulation results at $2E_s/N_o = 2E_d/N_o$, with a β setting to give 0.7 probability of synchronization, shown in Figure 7-68, the performance is

observed (note the average number to dismiss) to be close to that obtained with the postulated scheme for random data but inferior to that obtainable when data modulation is not present.

If the results in Figure 7-68 are compared with Figure 7-62 in which performance for the case of no data modulation with Costas loop acquisition is presented, it will be observed that performance shown is nearly 3 db better than previously obtained even with an optimized loop bandwidth ($B_L = 0.05$). We may show this explicitly by computing E/N_o, where E equals the signal energy in the time to search one PN bit assuming two search positions per bit. Averaging the best and worst cases yields Figure 7-69, which may be compared with Figure 7-66. With data modulation present in the noncoherent detection scheme, Figure 7-68 shows the resulting degradation to be approximately 1.4 db.
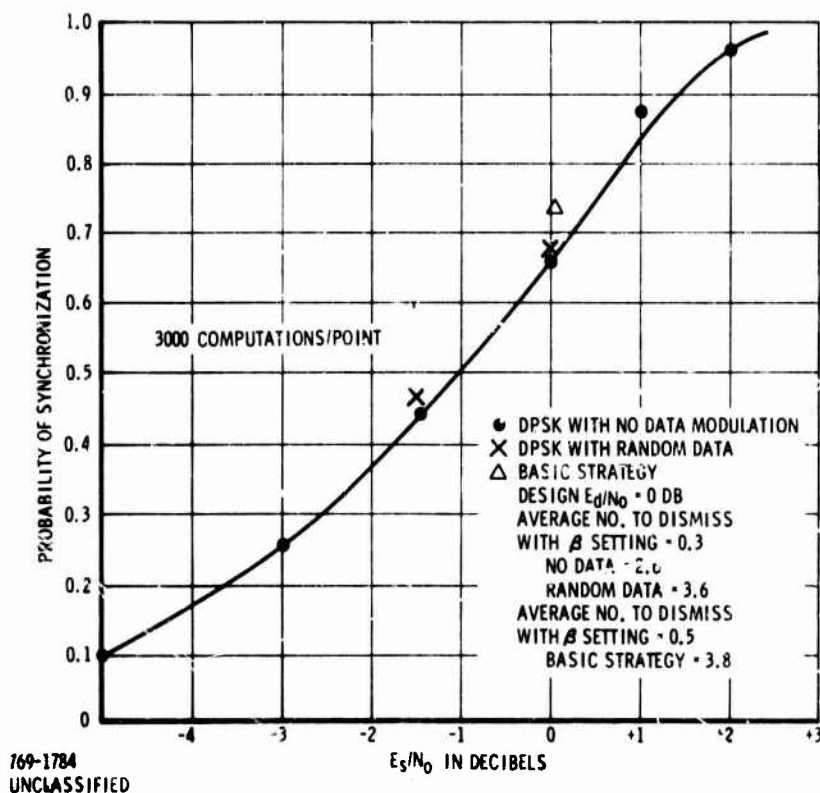
Figure 7-68. Semi-coherent Detection Over Two Intervals

-363-
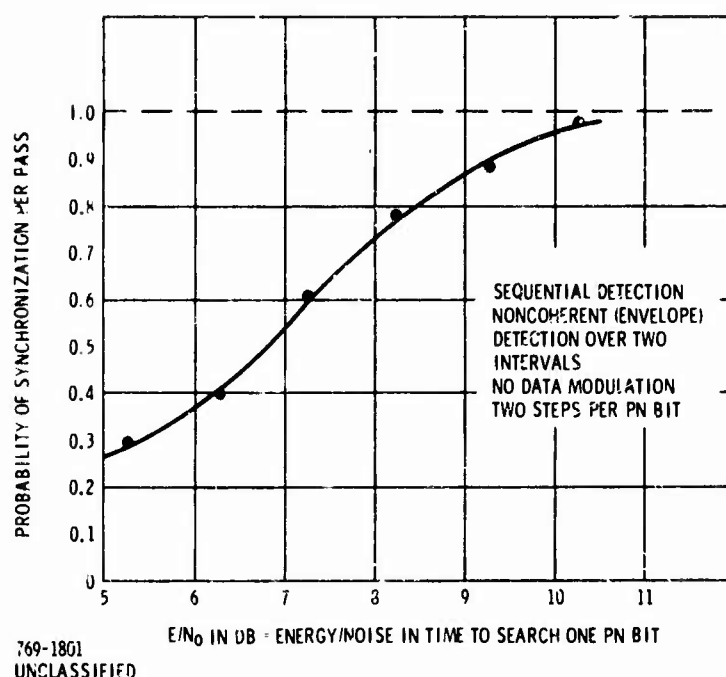
Figure 7-69. Sequential Detection

7.5.1.10 Conclusions

Theoretical analysis and simulations of sequential detection applied to the problem of serial search for synchronization have been carried out. The results show a significant advantage of sequential detection over simpler strategies for a coherent system; however, this does not represent a realistic system. Phase lock acquisition as well as noncoherent detection schemes are considered in an attempt to bridge the gap to a practical concept involving synchronization when absolute phase is initially unknown.

Little or no improvement over a noncoherent system is obtained by using a phase locked loop or a Costas loop. A semi-coherent system, in which coherence carries over only from one sample interval to the next was also investigated. This scheme was found to be two to three db. better than even the optimized bandwidth Costas loop. The results of the analyses and simulations on which the above conclusions are based are summarized in Table 7-15 which gives the average necessary E/N_o to obtain a probability of detection of .7, where E is the signal energy in the average time to search one PN bit.

-364-

Table 7-15. Summary of Analyses and Simulations
of Synchronization Performance

Probability of Detection = 0.7

	Uniform Search Rate Coherent No Data	Sequential Coherent No Data	Sequential Noncoherent No Data	Sequential Optimized Costas Loop		Sequential Differentially Coherent	
				No Data	Data	No Data	Data
$E/N_o =$	8 db	3 db	10 db	10 db	12 db	7.8 db	9.2 db

7.5.2 INTEGRATION LOSS WITH DIGITAL MATCHED FILTER SYNCHRONIZATION FOR PSEUDONOISE

7.5.2.1 Introduction

To avoid the long synchronization time for a serial search, an alternate technique for synchronization to a PN waveform can be considered, based on use of a matched filter, whose impulse response is a replica of a portion of the PN code. In effect, the matched filter acts as a correlator and detects the instant in time when the received signal "lines up" with the stored replica. In the past, analog implementations based on tapped delay lines have been the typical design concept; however, for the future digital implementations appear to have significant packaging (i. e., LSI) and cost advantages.

Since a digital matched filter is recommended as implementation for the preferred CNI waveform, an analysis of the effects of digitizing a received signal for processing by a digital matched filter has been carried out.

The basic configuration discussed is shown in Figure 7-70 for a biphase modulated signal. The extension to quadriphase and Doppler shifted signals is described in Appendix IV. The received signal plus interference is detected to quadrature baseband components, which are individual inputs to tapped delay lines in an analog system. In a digitized system, shift registers replace the tapped delay lines.

To obtain a digital representation of a received signal, it is necessary to time sample the signal and quantize each sample in accordance with an allotted number of levels. To evaluate performance for correlation in a matched filter, digitally implemented, an optimization for the number of quantum levels is desired, considering the effect of interference. Also, the sampling rate is to be specified.

To obtain a tractable problem for analysis, the question of sampling rate is initially deferred, and attention is directed at one sample of a baseband signal plus interference. Then, the sample amplitude v can be written

$$v = \pm 1 + y \tag{167}$$

where the desired signal has unit amplitude and a random polarity, and y denotes the instantaneous value of interference. The amplitude is quantized and then correlated with the known signal polarity.

-366-

The basic problem associated with quantizing is the possibility of suppression of the desired information. For example, if the spacing of the quantum level exceeds 2, the amplitude v for some values of interference will be quantized to the same quantum level for both polarities of the desired signal; correlation has been completely suppressed for those interference values. As the simplest example, consider binary quantization which retains polarity only of v. Correlation is fully suppressed for all $\left|y\right| > 1$; hence, operation at an input $S/J < 0$ db is not allowable with this basic binary quantization concept.

The suppression effect can be reduced or eliminated by a revised strategy of quantization which does not employ fixed thresholds but, instead, "dithers" them by adding additional "noise" prior to quantizing. This strategy prevents v from being stuck in any one quantum level. The analytical problem is posed of selecting the dither function to optimize performance, appropriately defined.
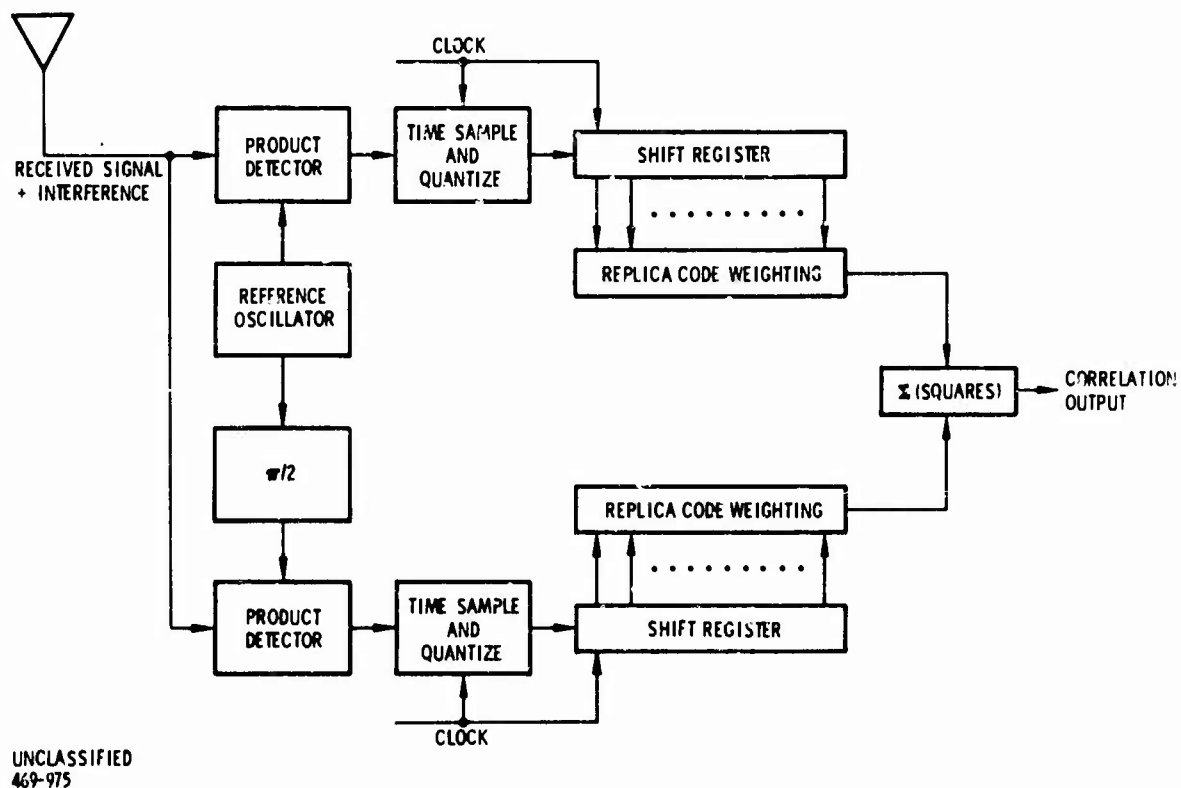
Figure 7-70. Concept of Digital Matched Filter

Since correlation implies integration over a large number of samples, the measure of performance may be taken as the "output S/N", defined for one sample as

$$\text{Output S/N} = \frac{(\text{Mean Correlation})^2}{\text{Variance of Correlation}} \tag{168}$$

where the variance is to be taken in the absence of signal. This may be compared with the "input S/N," defined as

$$\text{Input S/N} = \frac{\text{Average Signal Power}}{\text{Average Interference Power}}$$
$$= 1/\sigma^2 \tag{169}$$

where σ^2 is the average interference power. The correlation is defined as

$$\text{Correlation} = \pm \text{Quantize} \left[\pm 1 + y \right] \tag{170}$$

where $\pm$ denotes the two allowed polarities of the desired signal.

Optimization is attempted here on the basis that the interference y is a random variable with an unknown probability density subject only to the constraint that its second moment does not exceed $\sigma^2 >> 1$ (the case of low inputs S/N). It is desired to maximize output S/N for the worst case probability density on y. A useful measure of performance is degradation, defined as

$$\text{Degradation (in db)} = 10 \log_{10} \frac{\text{Input S/N}}{\text{Output S/N}} \tag{171}$$

and this quantity is to be minimized.

7.5.2.2 Binary Quantization

A complete solution can be given for the simplest case of binary quantization. Here a dither voltage β of probability density $g(\beta)$ is added to the sample amplitude v prior to polarity quantizing. It is required to select $g(\beta)$ to maximize the probability of quantizing to the correct polarity (same as that of the desired signal) while the probability density p(y) of interference is selected to minimize probability of correct polarity. This minimax (game theory) problem is treated in detail in Appendix III.

-368-

The results of the analysis give the minimax solution

$$g(\beta) = \frac{\sqrt{3}}{4\sigma} \left(1 - \frac{\beta^2}{3\sigma^2}\right) \qquad |\beta| < \sqrt{3}\sigma$$

$$= 0 \qquad\qquad\qquad |\beta| > \sqrt{3}\sigma \tag{172}$$

and the performance

$$\text{Output S/N} \geq \frac{1}{3\sigma^2} \tag{173}$$

irrespective of the interference probability density. The degradation, defined in Equation (171), is seen to be equal to or less than 4.8 db for this case of optimized binary quantization.

To illustrate the minimax nature of the solution of Equation (172), consider interference at any value y, with $|y| < \sqrt{3}\sigma$. Correlation is obtained for the range of β satisfying $-1 < y + \beta < 1$, since the two signal polarities then cause different quantized outputs. The correlation for this value of y is

$$\int_{-1-y}^{1-y} g(\beta) d\beta = 2g(y) \tag{174}$$

and the average correlation is

$$\text{Average Correlation} = 2 \int_{-\sqrt{3}\sigma}^{\sqrt{3}\sigma} g(y)\, p(y)\, dy$$

$$= \frac{\sqrt{3}}{2\sigma} \int_{-\sqrt{3}\sigma}^{\sqrt{3}\sigma} p(y)\, dy - \frac{1}{2\sqrt{3}\,\sigma^3} \int_{-\sqrt{3}\sigma}^{\sqrt{3}\sigma} y^2 p(y) dy \tag{175}$$

$$= \frac{1}{\sqrt{3}\,\sigma}$$

independent of p(y) if y is entirely confined within the range $|y| < \sqrt{3}\,\sigma$.

7.5.2.3 Multilevel Quantization

For the case of multilevel quantization, a complete solution has not been obtained. As a first approach, a specific dither function will be postulated and the worst case probability density of interference ascertained with respect to that dither. Also, an even number of uniformly spaced quantum levels is assumed. The received signal amplitude remains as defined in Equation (167).

The probability density of dither will be selected as uniformly distributed with a peak-to-peak amplitude D equal to one quantum. It appears reasonable that this choice will be roughly optimum for a large number of levels. It is sub-optimum for the case of two levels which has already been analyzed. The quantizing concept for a received amplitude v is to generate a random value β of dither and quantize $v + \beta$ to the closest value of the form $(k + .5)D$, where k is an integer specifying the level (both positive and negative polarity).

In similarity with Equation (174), correlation is obtained for a β satisfying $kD - 1 < y + \beta < kD + 1$, with any one of the allowed integers k. Since the quantizer levels are spaced by D, the correlation for this value of y is

$$\frac{1}{2} D \int_{kD-1}^{kD+1} \frac{1}{D} \, d\beta = 1 \tag{176}$$

and the average correlation is Equation (176) multiplied by the probability that y does not lie outside the finite quantizing range. If the number of levels is L, correlation is suppressed whenever

$$|y| > (\frac{L}{2} - .5) D \tag{177}$$

since the dither then will not cause any quantizing threshold to be crossed.

Now consider the interference strategy which will be worst case. This p(y) will have a portion of its distribution within the bound of Equation (177) and the remainder should be concentrated just outside in order to minimize the resulting

average power. At least for a reasonably large number of levels, the average inter-ference is essentially unchanged by the quantizing. Thus, the worst case strategy is to maximize the probability that y lies outside the range of Equation 177 and this is accomplished by letting y assume only the values 0 and $\pm (\frac{L}{2} - .5) D$. For the value 0, the output is $\pm .5D$.

Against the above strategy, the output S/N can be obtained in terms of the probability K that y is not zero. From the average power constraint

$$K (\frac{L}{2} - .5)^2 D^2 = \sigma^2 \tag{178}$$

and

$$\text{Output S/N} = \frac{(1-K)^2}{(1-K)(.5D)^2 + \sigma^2} \tag{179}$$

The degradation is

$$10 \log_{10} \frac{\text{Input S/N}}{\text{Output S/N}} = 10\log_{10} \left\{ \frac{\frac{1-K}{(L-1)^2 K} + 1}{(1-K)^2} \right\} \tag{180}$$

and this can be minimized by choice of the quantum spacing, which sets K according to Equation 178. It is found that the value of K yielding the minimum is

$$K = \frac{-3 + \sqrt{1 + 8 (L-1)^2}}{4L(L-2)} \tag{181}$$

and the degradation for several values of L is given in Table 7-16. (The value for L = 2 cannot be obtained directly from Equation (181), and this case must be separately treated.) Note that the suboptimum strategy for L = 2 causes an additional 3.5 db degradation over that previously given based on the true minimax strategy.

7.5.2.4 Time Sampling Rate

An estimate of the requisite sampling rate can be made by optimizing this parameter in accordance with an appropriate criterion. For this, the signal is assumed to be composed of bipolar rectangular pulses of specified bit duration except that a finite bandwidth in practice leads to a non-zero transition time between the two polarities. Figure 7-71 shows the general nature of the assumed waveform.

Table 7-16. Degradation With Multiple Levels

Number of Quantizing Bits	Number of Levels	Degradation	Peak-to-Peak Dither
1	2	8.3 db	1.602 σ
2	4	3.5 db	0.965 σ
3	8	1.6 db	0.636 σ
4	16	0.8 db	0.434 σ
5	32	0.4 db	0.302 σ
6	64	0.2 db	0.212 σ

If this waveform is sampled an integral number of times per bit, most samples will lie upon the peak value of the waveform; however, a sample within a transition region will not contain useful polarity information.

The time phase of sampling cannot be locked in any specific relation to the received signal, and a minimax design philosophy may be introduced. Thus, performance under the worst-case sampling phase is to be computed, where the phase is considered variable over a full sampling interval. The worst case is seen to be that of one sample lying on the transition region. The remaining samples fall on the full signal amplitude.

BIT
DURATION
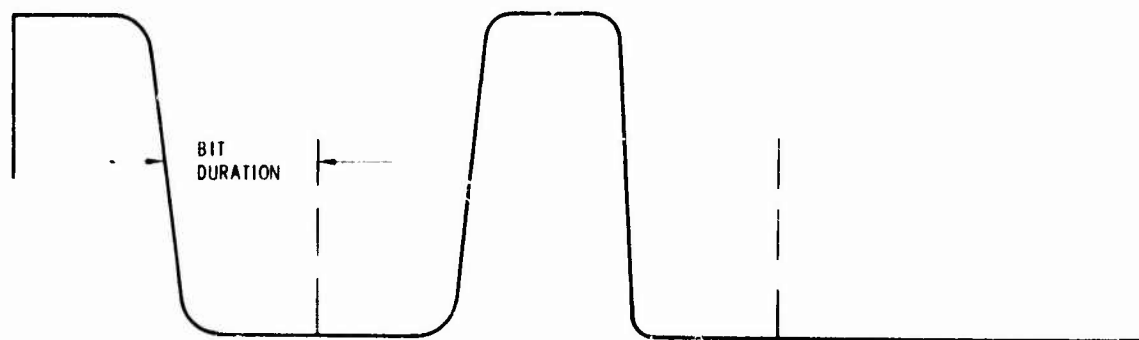
Figure 7-71. Filtered Bipolar Signal

The individual samples are presumed to be binary quantized with a dither function as already discussed. Consider first the situation in the absence of the desired signal. Let the number of samples per bit duration be m. If the interference is constant at the value σ, the probability that the polarity of a sample v is the same as that of the interference is given by

$$P_+ = \int_{-\sqrt{3}\,\sigma}^{-\sigma} g(x)\, dx = 0.1155 \tag{182}$$

where $g(x)$ given in Equation (172) has been substituted to yield the numerical value. Let v_i denote the m binary quantized samples per bit, so that the correlation summed over any bit is

$$v = \text{Sign (bit)}\ \frac{1}{m} \sum_{i=1}^{m} v_i \tag{183}$$

where the sign of the bit is, at random ± 1. Thus, the average of v is zero because of the random bit polarity, and the variance of v is

$$E\left(v^2\right) = \frac{1}{m}\, E\left(v_i^2\right) + \left(1 - \frac{1}{m}\right) \left[E\left(v_i\right)\right]^2$$

$$= \frac{1}{m} + \left(1 - \frac{1}{m}\right)\left(1 - 2P_+\right)^2 \tag{184}$$

$$= 0.591 + \frac{0.409}{m}$$

showing the behavior with m.

The mean correlation in the presence of the desired signal is obtained by applying Equation (175) generalized to include an arbitrary signal amplitude instead of simply unity. If a_i denotes the desired signal amplitude at the ith sample, the result is

$$\text{Output S/N} = \frac{(\text{Mean Correlation})^2}{\text{Variance}}$$

$$= \frac{\dfrac{1}{3\sigma^2}\left(\dfrac{1}{m}\displaystyle\sum_{i=1}^{m}\text{Sign (bit}_i)\ a_i\right)^2}{0.591 + \dfrac{0.409}{m}} \tag{185}$$

where Sign (bit$_i$) denotes the polarity of the reference bit applying to the ith sample.

When the signal is correctly aligned with the reference, except for the worst case sampling phase error, all a_i are unity in magnitude and have the same polarity as the reference except the one lying on the bit transition. That one may be taken as zero if the transition actually occurred, but as unity if a transition does not take place; hence, the average a_m is 0.5. The result is

$$\text{Output S/N} = \frac{1}{3\sigma^2}\ \frac{\left(1 - \dfrac{.5}{m}\right)^2}{.591 + \dfrac{.409}{m}} \tag{186}$$

values of which are given in Table 7-17.

These results indicate the most significant gain is achieved by going from one to two time samples per bit.

Table 7-17. Output S/N Per Bit With Multiple Time Samples

m	Output S/N	Degradation
1	$.0833/\sigma^2$	10.8 db
2	$.235/\sigma^2$	6.3 db
3	$.318/\sigma^2$	5.0 db
4	$.368/\sigma^2$	4.3 db
.		
.		
∞	$.564/\sigma^2$	2.5 db

A criterion for selecting the optimum m is on the basis of output S/N after integrating over a fixed number of samples, which is m times the number of bits. Since Table 7-17 lists the output S/N for one bit, the maximum S/N improvement for a fixed number of samples is achieved for $m = 2$. The result may be expressed as a type of degradation

$$\text{Degradation from } 10 \log_{10} \text{ (No. of samples)} = 9.3 \text{ db} \qquad (187)$$

In other words, compared with an ideal system which samples once per bit and avoids quantization loss, the worst case corresponds to a loss of 9.3 db in S/N improvement, using as the criterion the number of binary values summed in the digital matched filter. For $m = 2$, the loss is 6.3 db with respect to the duration of integration.

7.5.2.5 Conclusions

If complete suppression of correlation can be avoided by the introduction of dither in the quantizing, the only reason to increase the number of quantization levels is to reduce the degradation in S/N. It is seen from Table 7-16 that 4-bit quantization (16 levels) is required to reduce the degradation below one decibel.

In application to a digitally implemented matched filter, the above results tend to support the conclusion that binary quantization yields minimum overall complexity when the processing gain is specified as in the case of a synchronization process. The reason is that the digital matched filter complexity is roughly proportional to the required digital storage, which is the product of number of samples times the number of quantizing bits. Then, going from binary to 2-bit quantization would produce a standoff in complexity if the degradation were reduced by 3 db, thereby enabling the number of samples to be cut in half. However, comparison of the optimum binary quantization solution with 2-bit quantization shows that a 3 db gain is not attained.

Another criterion is the time function duration required to achieve a specified processing gain. The results show that going to multilevel quantization can save up to a factor of 3, compared with use of binary. This situation arises when a matched filter is to be employed as a data demodulator. The degradation associated with quantizing to a small number of levels must be interpreted as a loss in system performance for this case.

With respect to selection of the time sampling rate, consideration of a binary polarity-reversal waveform indicates an optimum of two samples per bit, where digital matched filter complexity is again the criterion. For binary amplitude quantization, the worst case degradation is 9.3 db with respect to the processing gain of the digital matched filter (number of binary samples integrated). As an alternative viewpoint, the loss is 6.3 db with respect to integration interval for the case of two samples per bit.

7.5.3 SYNCHRONIZATION VULNERABILITY TO OPTIMIZED JAMMING STRATEGY

The results in the previous sections have not considered the effects of an optimized jamming strategy which can lead to a significant vulnerability. As in Section 7.3.1, the jammer is presumed to maintain a fixed average power, and the jamming strategy is denoted by α, the fraction of slots occupied at random. The jamming power in a slot is denoted by J_{slot}, and $J_{av\ slot}$ is the average over time for each.

In a pure PN waveform, the slots are over time; hence, the jammer must be capable of trading peak power inversely with duty factor (i.e., with α). In a slow hopping FH/PN waveform to which the same basic synchronization analysis applies, α includes possibility of partial band jamming also. A partial occupancy enables the jammer to produce a relatively low probability of synchronization; that is, considerably lower than would result from continuous broadband Gaussian jamming of equal average power. The overall probability of synchronization is increased by allowing several chances, but at the expense of increased synchronization time.

To consider an extreme example, suppose that the synchronization process is such that

$$\text{Probability of missing sync on any trial} = P_M = 1; \quad \frac{J_{slot}}{S} > (J/S)_0 \tag{188}$$

$$= 0; \quad \frac{J_{slot}}{S} \le (J/S)_0$$

which idealizes the model to have a sudden threshold for sync acquisition. With uniform occupancy of all slots at $(J/S)_0$, synchronization is certain. If, however, a fraction α of the slots is jammed at slightly greater than $(J/S)_0$, the resultant miss probably is increased to α, while the average J/S is decreased by the factor α. Taking a numerical case, let the operational system requirement be a probability of synchronization of 0.9. Then, one computes

$$\alpha = 0.1 \text{ for one frame sync} \longrightarrow 10 \text{ db degradation}$$
$$\alpha = 0.32 \text{ for two frame sync} \longrightarrow 5 \text{ db degradation}$$
$$\alpha = 0.46 \text{ for three frame sync} \longrightarrow 3.3 \text{ db degradation}$$

where the degradation is related to the uniform occupancy yielding the same probability. This shows how the jammer is forced toward uniform occupancy by introducing a synchronization strategy based on independent chances in several frames, when overall synchronization probability is held fixed as a parameter. The effect on synchronization time is evident.

As a more realistic model of a smoother threshold, let

$$P_M(S/J_{slot}) = \frac{1.01}{\sqrt{2\pi}} \int_{-\infty}^{(2.33 - \sqrt{S/J_{slot}})} \exp(-x^2/2) \; dx \qquad (189)$$

which goes from zero to unity as J_{slot} increases from 0 to ∞. Equation (189) is roughly predicated on Gaussian detection statistics for the analysis model. The probability of missing synchronization in any one frame is αP_M for a partial occupancy strategy, since a miss can only occur in a jammed slot. The optimum jammer strategy is not as evident as in the previous example, but requires a maximization as follows

$$P_M\Big]_{worst\ case} = \frac{Max}{\alpha} \left\{ \alpha P_M(\alpha S/J_{av\ slot}) \right\} \qquad (190)$$

In Equation (190), $J_{av\ slot}$ is the average power per slot (i.e., for uniform occupancy). This maximum occurs at $\alpha S/J_{av\ slot} = 5.7$, so that

$$P_M\Big]_{worst\ case} = \frac{2.75}{S/J_{av\ slot}} \qquad (191)$$

The worst case occupancy and resulting degradation can now be computed, similarly to the previous example.

Again, taking the required probability of synchronization to be 0.9, the results are

$$\alpha = 0.21 \text{ for one frame sync} \longrightarrow 3.1 \text{ db degradation}$$
$$\alpha = 0.66 \text{ for two frame sync} \longrightarrow 0.4 \text{ db degradation}$$
$$\alpha = 0.96 \text{ for three frame sync} \longrightarrow 0 \text{ db degradation}$$

where the degradation is again related to the uniform occupancy which yields the same probability of synchronization in the same number of frames.

It can be concluded that the quantitative extent of the vulnerability during sync to partial occupancy jamming strategies depends both on the sharpness of the threshold characteristic and on the sync reliability objective. A sharp threshold and a high reliability objective imply a serious degradation in average J/S for optimized partial occupancy compared with uniform occupancy, if synchronization is attempted in a single frame. However, the example presented as a more realistic illustration of threshold behavior shows only a modest degradation at an objective of 0.9 reliability in a single frame. This example would be representative of the CNI requirement at least for a voice channel. For data, a synchronization reliability of 0.9 is probably inadequate, and one design concept is to obtain increased reliability by extending the sync preamble over several frames. With 0.9 per frame, the reliability is 0.999 when sync is simply attempted independently in three successive frames, for example. However, note the benefit of error correction coding for data transmission. With interleaving to randomize error locations, the rate 1/2 sequential decoder accepts up to about 0.05 probability of error. This implies a tolerance for a synchronization reliability of 0.9 even if the receiver operates by resynchronizing at the start of each slot (assuming no other errors). This should be contrasted with an uncoded system in which the resultant error probability is 0.5 times the fraction of slots missed. In that case, an error probability objective of 10^{-3} would require a synchronization reliability of 0.998 if resynchronization where specified at the beginning of each time slot.

7.5.4 A DIGITAL SYNCHRONIZATION TECHNIQUE FOR FREQUENCY HOPPING

A digital synchronization technique for a FH waveform is discussed here. The technique is basically a digital integration scheme whereby the received signal and

interference are first quantized in amplitude and time. The quantized signal pulses are then counted and when the count exceeds a threshold count, synchronization is declared and search is stopped.* A block diagram of this system is shown in Figure 7-72A. The system is **attractive** since, being a digital technique, it is very compatible with the concept of digital matched filter receivers. Furthermore, it may be adapted to a sequential detection procedure.
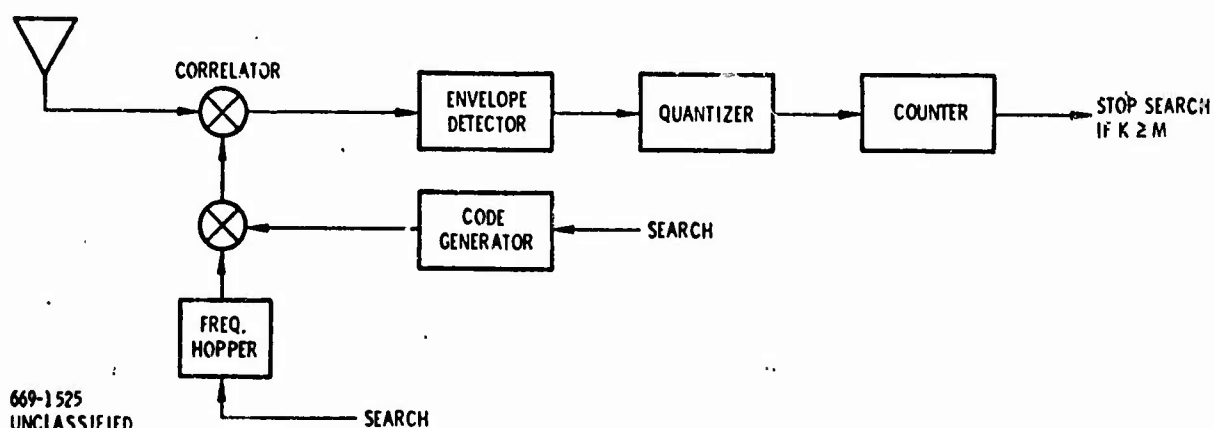
(A)
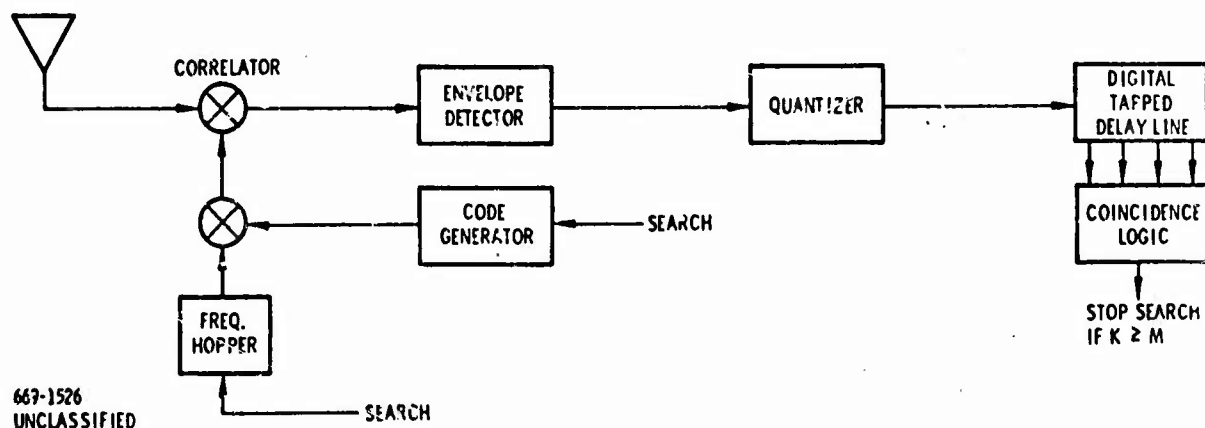
(B)

Figure 7-72. Digital Synchronizer Implementations

---

*Harrington, J.V., "An Analysis of the Detection of Repeated Signals in Noise by Binary Integration," IRE Trans. on Information Theory, IT-1; 3 March 1955, 1-9.

-379-

The sync detection problem is to detect and determine the time of arrival of pulses appearing at the output of the correlator. Since the receiver is not in sync and phase coherence has not been established, the individual pulses must be detected by envelope detection. It is obvious from radar detection theory that sync detection probability would be increased by integrating the sync pulse train, i.e., adding the pulses together. Since we are pursuing a digital system, the individual pulses will first be quantized, as shown in Figure 7-72A. The integration is then simply a digital counter. An alternate implementation is shown in Figure 7-72B. This scheme utilizes a digital "tapped delay line" with the tap spacing matched to the spacing of the synchronization pulses. The advantages of this scheme are that the pulse intervals may be chosen so that the matched delay line is sensitive to only that unique sequence of pulse intervals.

Sequential detection may be applied to frequency hop (FH) systems which integrate on a post-detection basis. The analysis could be restricted to noncoherent envelope detection in a Gaussian noise environment. The synchronization performance then is computed for the FH waveform by using the correlation function for the FH pulse shape. However, broadband noise is not an optimum jamming strategy, and a more refined analysis should consider more effective means for jamming a FH system.

The jamming strategy to be studied will consist of tones in a fraction α of the frequency slots. The integration will be binary quantized (0 or 1) and the dismissal will be on the basis of the count of 1 s over the number of pulse intervals in the test.

In the absence of the desired signal, the jammer will utilize tones of amplitude slightly exceeding the threshold A which performs the binary quantization. Clearly, this strategy maximizes the probability of 1 for any pulse interval, and this comissive probability is $\epsilon = \alpha$. The typical data demodulator for a FH coded system can work up to $\alpha = 0.1$ for tones equal in amplitude to the desired signal, and the threshold may typically be set at 0.707 times the amplitude of the desired signal. Thus, maintaining the same average jammer power of 0.1 per frequency slot, the worst-case strategy set $\alpha = 0.2$, yielding a commissive probability $\epsilon = 0.2$.

In the presence of the desired signal with amplitude $A_s > A$, there is an omissive probability δ that the threshold is not exceeded. Let the amplitude of the jamming tones be A_j. For a random phase relation, θ, the omissive probability is obtained from Figure 7-73 to be

$$\delta = \frac{\alpha}{\pi} \cos^{-1}\left[\frac{A_s^2 + A_j^2 - A^2}{2A_s A_j}\right] \tag{192}$$

where α is the probability of a jammer tone falling on the signal. For a fixed average jammer power, retaining an average of 0.1 per frequency slot,

$$A_j = \sqrt{0.1/\alpha} \tag{193}$$

an Equation (192) can be maximized* with respect to α to obtain the worst case.
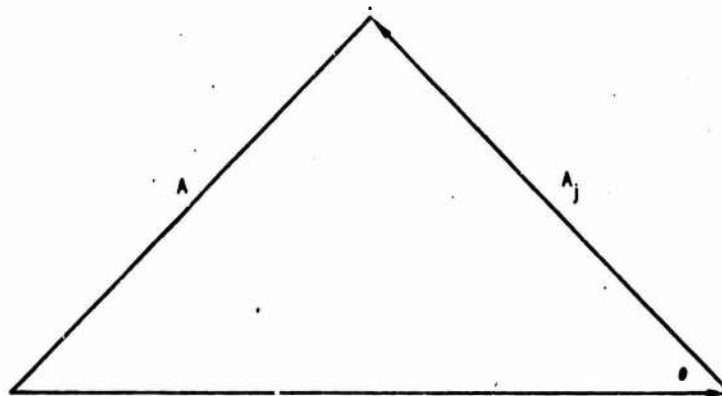
Figure 7-73. Vector Sum of Signal and Jammer.

---

*It is unrealistic to assume that the jammer can maximize both ϵ and δ, since these require different values of α; however, it is worst case.

The sequential detection sums the log-likelihood ratio according to

$$z = \log\left[(1 - \delta_d)/\epsilon_d\right] \text{ if 1 occurs}$$

$$= \log\left[\delta_d/(1 - \epsilon_d)\right] \text{ if 0 occurs} \tag{194}$$

where ϵ_d and δ_d are the design values. The resulting sum is to be compared with the dismissal threshold $\log \beta$. The average number of pulse intervals to dismiss in the absence of signal is given by

$$\text{Average Number to Dismiss} = \frac{\log \beta}{E(z/0)} \tag{195}$$

and

$$E(z/0) = \epsilon \log\left(\frac{1 - \delta_d}{\epsilon_d}\right) + \left(1 - \epsilon\right) \log\left(\frac{\delta_d}{1 - \epsilon_d}\right) \tag{196}$$

where ϵ is the actual probability of 1 in the absence of signal.

Continuing the typical numerical illustration, with $A_s = 1$ and $A = 0.707$, the maximum for δ is computed to be approximately 0.12. Taking $\epsilon_d = 0.2$ and $\delta_d = 0.12$, Equations (195) and (196) yield

$$\text{Average Number to Dismiss} = \frac{\log \beta}{-1.22} \tag{197}$$

For a probability of dismissal $\beta = 0.3$, Equation (197) yields an average number to dismiss of 0.99.

A Monte Carlo simulation was set up and performed to verify the analysis. Figure 7-74 shows the results for β set at 0.3. The average number to dismiss in the absence of signal, or $\delta = 1 - \epsilon_d$, is 1.65, relatively close to the theoretical expectation. The results in Figure 7-74 can now be applied to obtain synchronization probability as a function of received signal level.

From Equations (192) and (193), the maximum value of δ can be computed for the worst-case, as previously described. Figure 7-75 shows the results for the typical numerical illustration with average jammer power per slot of 0.2 and $A = .707$. The worst-case fractional occupancy is also indicated. This figure shows how the omissive probability approaches zero as the desired signal amplitude becomes large compared with the threshold.

The synchronization probability can now be computed from Figures 7-74 and 7-75 and presented as a function of E/N_0, where E is the signal energy in the time to
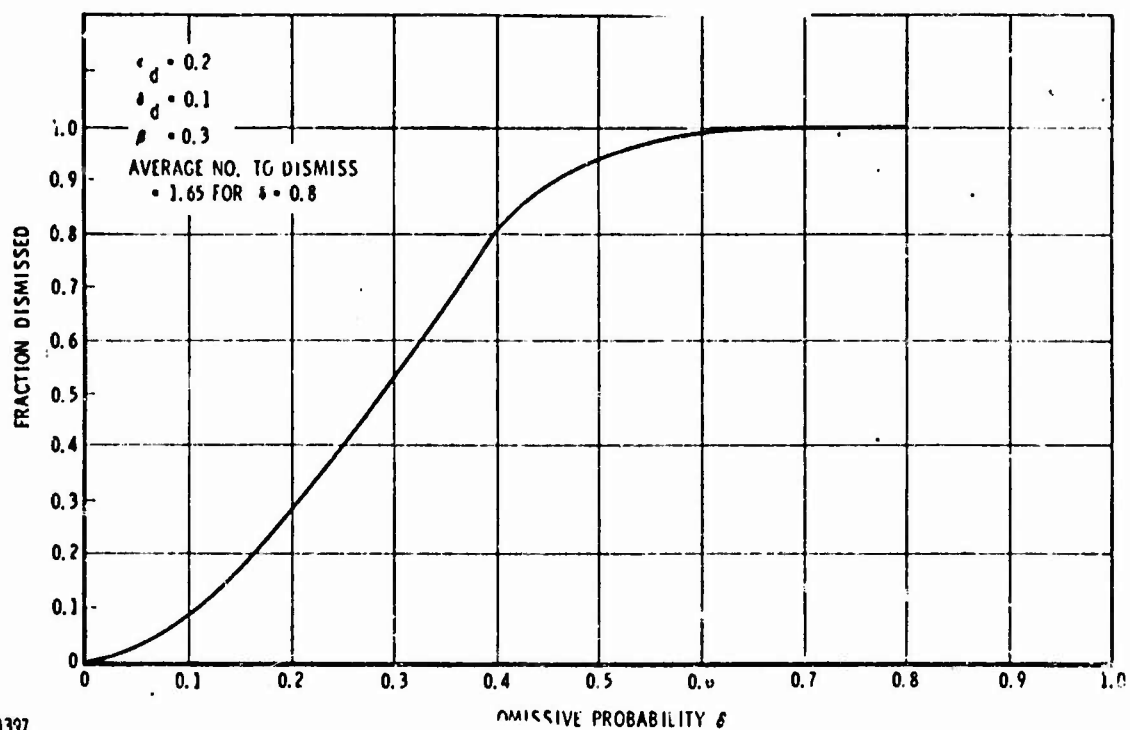
Figure 7-74. Sequential Detection by Binary Integration.
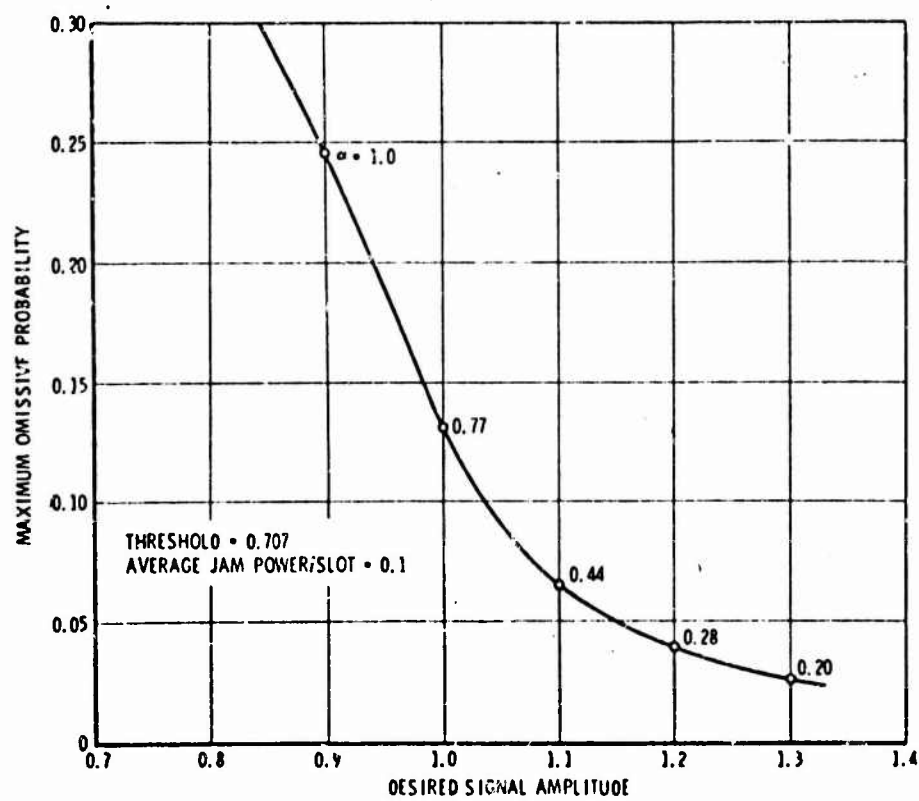
Figure 7-75. Worst-Case Omissive Probability.

search one frequency hop pulse width and N_o is the average interference power per Hz. The slot spacing is presumed equal to the reciprocal of pulse width. The serial search is presumed taken in two steps per pulse width. The results are shown in Figure 7-76 for the test and worst cases of alignment between received pulse and search position, as defined in Figure 7-63.

To understand the significance of E/N_o, note that

$$E/N_o = (BW)(S/J) \quad \begin{array}{l}\text{(Time to search one pulse} \\ \text{width of uncertainty)}\end{array} \qquad (198)$$

where BW = total bandwidth. Let BW = 100 MHz, E/N_o = 16 db, J/S = 35 db, and the number of pulse widths of time uncertainty = 2 msec/50μsec = 40. Then, the search time is

$$\text{Search Time} = \frac{40 \times 3000}{10^8} \, 40 = 48 \text{ milliseconds}$$

for an average synchronization probability of roughly 0.8, according to Figure 7-76.

It should be noted that the design parameters ϵ_d, δ_d, and β used in the simulation are not optimized, and a small improvement in performance from Figure 7-76 may still be realized.
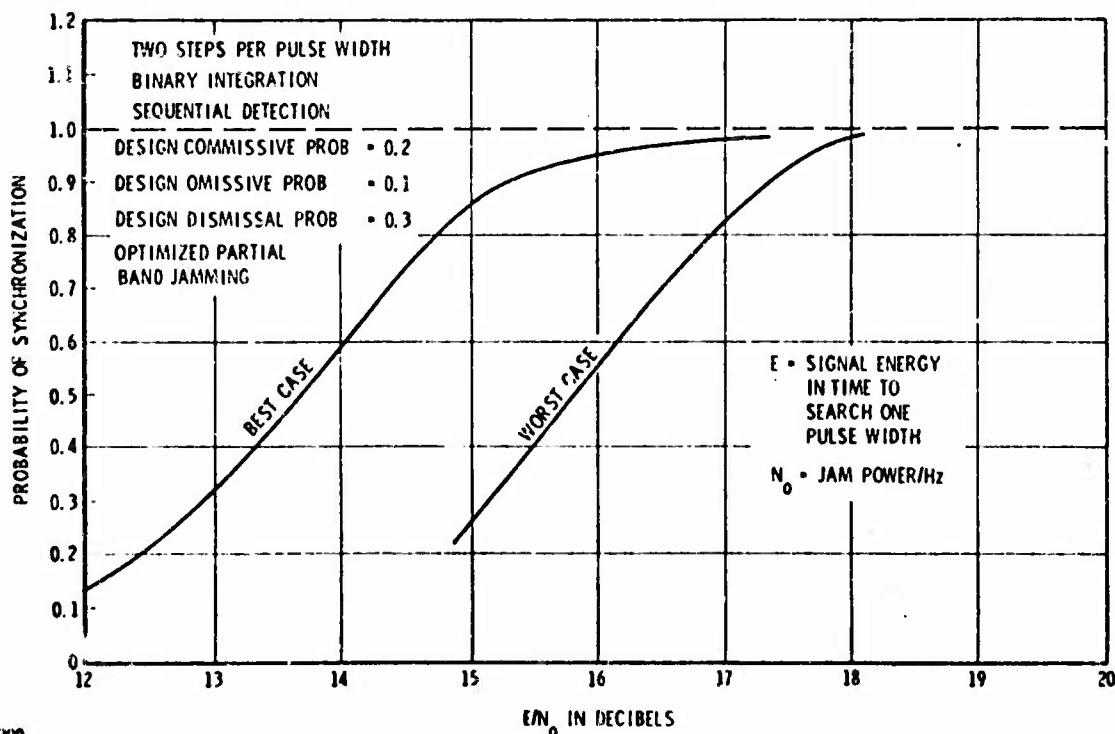
Figure 7-76. Frequency Hop Synchronization by Serial Search.

-384-

7.6 RANGE AND RANGE RATE MEASUREMENT ACCURACY

A primary consideration for the CNI waveform is the ability to extract precise range and range rate measurements from it. First, we shall present a discussion of the fundamental limitations to precision ranging; i.e., noise in the range (clock) tracking loops. We shall also discuss the range rate measurement accuracy. In addition, the range accuracy of a sidetone ranging system will be discussed and compared with the PN system. This will be followed by a discussion of the practical implications of extracting precision range from a FH/PN/TH waveform. Finally, the results of a computer simulation of range and range rate extraction from the coherent FH/PN/TH waveform is presented.

7.6.1 PN OR FH/PN THEORETICAL RANGE AND RANGE RATE MEASUREMENT ACCURACY

7.6.1.1 Introduction

In a PN or typical FH/PN system, the range difference measurement is made by comparing the phase between clocks which are synchronized to the respective received PN codes. Thus, the range measurement accuracy is limited by the time jitter error of the clock tracking loops. For purposes of analysis, in both the PN and FH/PN systems, it will be assumed that a separate implementation performs a coherent demodulation to extract the pseudorandom code, and the clock tracking loop operates on the low-pass demodulated signal. It will be further assumed that the hopping rate of the FH/PN system is slow enough so that any transient effects which may occur in the carrier track loop at the hop have negligible effect on the clock loop. Thus, the ranging performance of the FH/PN system is the same as the PN system with equal PN clock rate.

7.6.1.2 Theoretical Basis

The phase comparison measurement between receiver clocks is actually a relative time of arrival measurement of the signal. Measurement signal arrival time in the presence of background interference may be interpreted as a problem in the estimation of an unknown signal parameter. To examine the basic case, assume reception of a pulse waveform $s(t-\tau)$, where τ is the unknown time of arrival, in the presence of white noise of spectral density (one sided) N_o. The received signal is observed over some interval $-T/2$ to $T/2$ such that edge effects are eliminated; i.e., we write

$$r(t) = s(t - \tau) + n(t) \qquad -T/2 < t < T/2 \tag{199}$$

The estimation of the parameter τ is obtained through the log likelihood function, given by*

$$\log \Lambda \left[r(t), \tau \right] = \frac{2}{N_o} \int_{-T/2}^{T/2} r(t)\, s(t - \tau)\, dt - \frac{1}{N_o} \int_{-T/2}^{T/2} s^2 (t - \tau)\, dt \tag{200}$$

The maximum likelihood estimation is the value of τ which maximizes Equation (200). If the maximum is interior, it may be found by differentiation

$$\frac{\partial \log \Lambda}{\partial \tau} = \frac{2}{N_o} \int_{-T/2}^{T/2} \left[r(t) - s(t - \tau) \right] \frac{\partial s(t - \tau)}{\partial \tau}\, dt$$

$$\tag{201}$$

$$= -\frac{2}{N_o} \int_{-T/2}^{T/2} r(t)\, s'(t - \tau)\, dt$$

where it is noted that the last term in Equation (200) is independent of the parameter τ. The value of τ which sets Equation (201) equal to zero is the maximum likelihood estimator $\tau_{m\ell}$. That is,

$$\int_{-T/2}^{T/2} r(t)\, s'(t - \hat{\tau}_{m\ell})\, dt = 0 \tag{202}$$

Equation (202) is the theoretical basis for the time of arrival measurement. It leads to the concept of a tracking loop which correlates the received signal, with noise, against the derivative of the known waveform, driving the correlation to a null.

---

*H. L. Van Trees, "Detection, Estimation, and Modulation Theory, Part 1," John Wiley, 1968, pp. 274

A lower bound on the variance of the maximum likelihood estimator (or on any unbiased estimator) can be stated.* Ignoring edge effects and letting the true value be zero for convenience

$$E\left[\hat{\tau}^2\right] \geq \frac{N_o}{2 \displaystyle\int_{-T/2}^{T/2} \left[\varepsilon'(t)\right]^2 dt} \tag{203}$$

A case of importance here uses a signal of average power S, biphase modulated by a pseudorandom code with clock period T_c. After coherent demodulation, not of concern here, the desired signal may be written

$$r(t) = \sqrt{S}\, a(t) + n(t) \tag{204}$$

where a(t) is a repetitive pulse shape of energy T_c (for normalization to unit power) and whose polarity changes pseudorandomly at each clock period. The in-phase component of interference is denoted as n(t). The normalization is such at n(t) has density N_o if the received interference has density N_o. Then Equation (203) simplifies to

$$E\left[\hat{\tau}^2\right] \geq \frac{N_o/S}{(2T/T_c) \displaystyle\int_{-\infty}^{\infty} \left[a'(t)\right]^2 dt} \tag{205}$$

Letting $\alpha(\omega)$ be the Fourier transform of a(t), Equation (205) can be written as

$$E\left[\hat{\tau}^2\right] \geq \frac{N_o/S}{(2T/T_c)\frac{1}{2\pi} \displaystyle\int_{-\infty}^{\infty} |\alpha(\omega)|^2\, \omega^2\, d\omega} = \frac{N_o}{2TS(2\pi\beta)^2} \tag{206}$$

In Equation (206), β is defined as an rms bandwidth, in Hz, as follows:**

---

* Van Trees, op cit, p. 275.

** P.M. Woodward, "Probability and Information Theory with Applications to Radar," 2nd Edition, Pergamm Press, 1964, p. 102.

$$(2\pi\beta)^2 = \frac{\frac{1}{2\pi}\int\limits_{-\infty}^{\infty}|Q(\omega)|^2\,\omega^2\,d\omega}{\frac{1}{2\pi}\int\limits_{-\infty}^{\infty}|Q(\omega)|^2\,d\omega} = \frac{\int\limits_{-\infty}^{\infty}[a'(t)]^2\,dt}{\int\limits_{-\infty}^{\infty}[a(t)]^2\,dt} \tag{207}$$

It may be observed that assumption of a rectangular pulse shape yields an infinite bandwidth, according to Equation (207).

7.6.1.3 Loop Analysis

The clock tracking loop is usually implemented either as a delay lock loop or a τ jitter loop which time shares an early-late gate. A step-by-step analysis of the performance of both the delay lock loop and the τ jitter loop follows. The analysis considers the received signal and noise to be bandlimited by an IF filter. The noise itself is assumed to be white, Gaussian noise. The rms tracking errors for the delay lock and τ jitter loops are derived and presented by Equations (232) and (246), respectively. The tracking performance described by these equations is plotted in Figures 7-80 and 7-84, respectively. In addition, the effect of varying the jitter time displacement on tracking performance is shown in Figures 7-81 and 7-85.

The most significant result of this analysis is that the delay lock loop has better tracking performance than the τ jitter loop, as shown in Figure 7-86. In addition, as the time jitter displacement is made smaller, the delay lock loop tracking performance improves whereas the τ jitter loop tracking performance degrades.

Finally, in light of the superior performance of the delay lock loop, some consideration is given to channel gains and time delay differentials. It is shown that for reasonably well designed channels the tracking error does not increase very much with reasonable channel unbalances.

7.6.1.4 Analysis of the Delay Lock Loop

A block diagram of the delay lock tracking loop is shown in Figure 7-77. Coherent demodulation to baseband will be assumed as it is more convenient to analyze

a baseband loop and the results apply directly to an IF loop. The receiver filter will be assumed to be an ideal bandpass filter which represents the bandlimiting accomplished by the IF filtering. The loop can be modeled mathematically as shown in Figure 7-78, if the tracking error is $< 1/2$ radian. In the analysis which follows, the variance of the tracking error $\Delta \tau$ and thus the rms tracking error will be found.

From Figure 7-78 it can be seen that by superposition

$$\tau_2 = \left[AKF(p) \frac{1}{p} \right] \Delta \tau + \left[KF(p) \frac{1}{p} \right] n'(t) \tag{208}$$

where p is operator notation for d/dt. Furthermore, in response to noise alone,

$$\Delta \tau = -\tau_2 \tag{209}$$

so that by combining Equations (208) and (209) we obtain

$$\Delta \tau = - \frac{KF(p)/p}{1 + AKF(p)/p} \quad n'(t) \tag{210}$$

Since it is more convenient to work with power spectral densities, Equation (210) is written as

$$S_{\Delta \tau}(\omega) = \left| \frac{KF(j\omega)/j\omega}{1 + AKF(j\omega)/j\omega} \right|^2 S_{n'}(\omega) \tag{211}$$
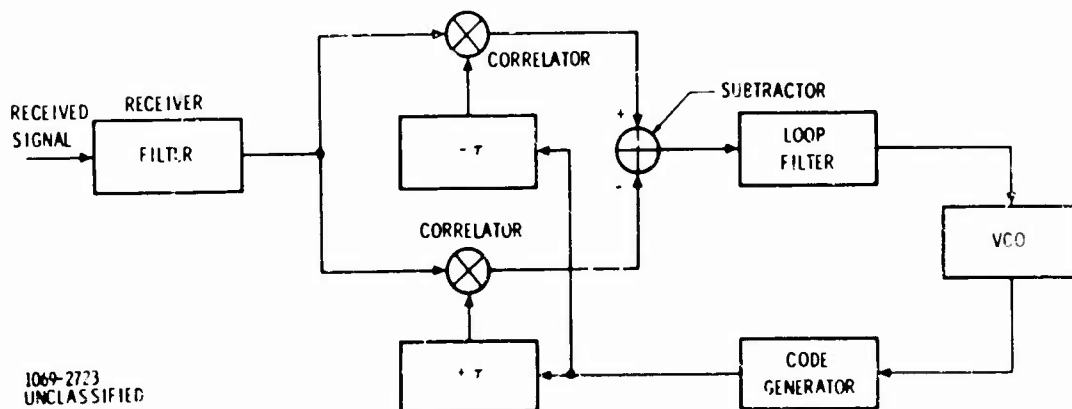
Figure 7-77. Block Diagram of Delay Lock Tracking Loop

-389-
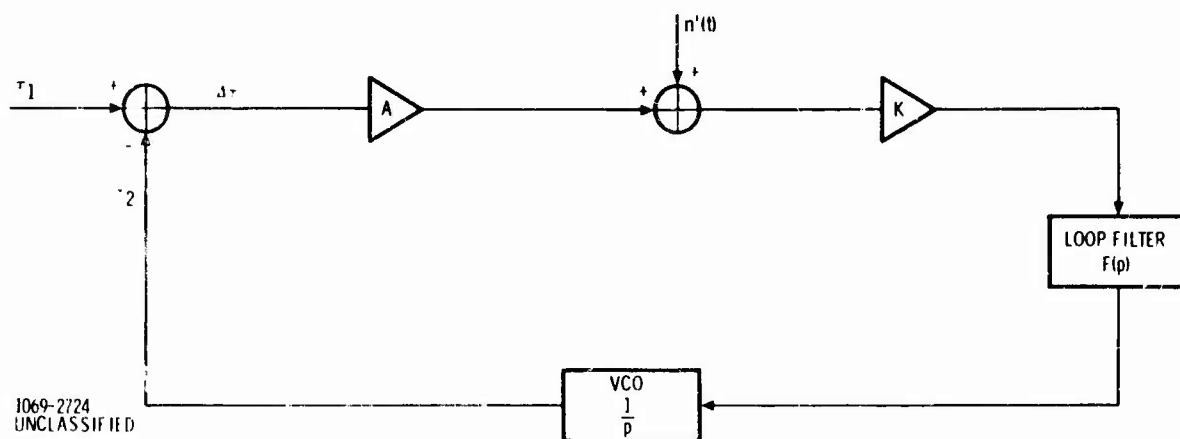
Figure 7-78. Mathematical Model of Delay Lock Tracking Loop

where

$S_{n'}(\omega)$ is the power spectral density of the noise

and

$S_{\Delta\tau}(\omega)$ is the power spectral density of the loop tracking error.

The noise density can be found from consideration of the process taking place in the loop "discriminator" shown in Figure 7-79. From examination of Figure 7-79, it is seen that the equivalent noise, $n'(t)$, for the math model is related to the actual input noise by

$$n'(t) = n(t) a (t - \tau_d) - n(t)a(t - \tau_d)$$

$$= n(t)\left[a (t - \tau_d) - a (t + \tau_d)\right]$$

(212)

where

$n(t)$ = the actual input noise $N(t)$ filtered by the receiver filter

$a(t - \tau_d)$ = reference PN code advanced by τ_d bits

$a(t + \tau_d)$ = reference PN code delayed by τ_d bits

Since multiplication in the time domain is equivalent to convolution in the frequency domain, the power spectral density of the noise $n'(t)$ is given by

$$S_{n'}(\omega) = S_n(\omega) \otimes A (\omega)$$

(213)

-390-
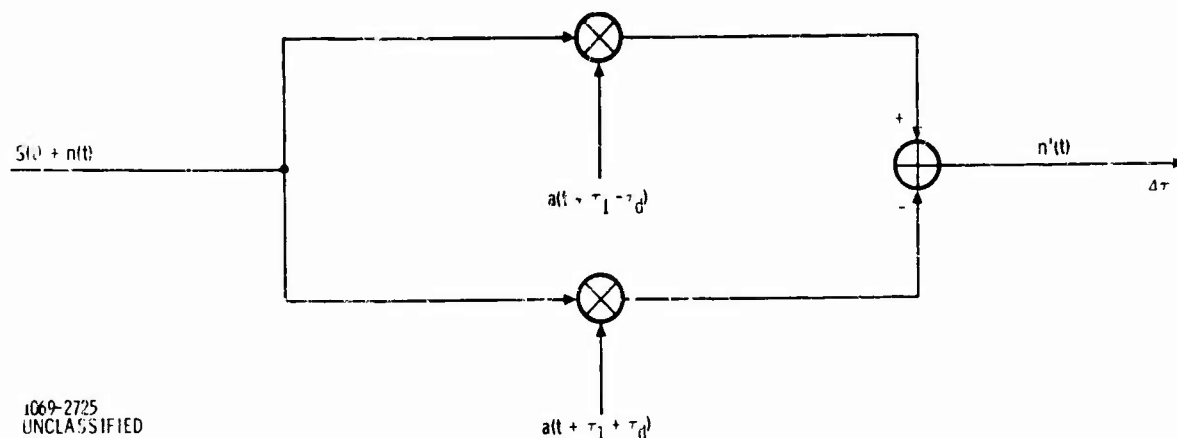
Figure 7-79. Delay Lock Loop Error Discriminator

where

$$A(\omega) = \text{power spectral density of } a(t - \tau_d) - a(t + \tau_d)$$

and $\bigotimes$ indicates convolution.

The power spectrum of $A(\omega)$ is given by

$$A(\omega) = a(\omega)\, a(\omega)^* \tag{214}$$

where

$$a(\omega) = \text{voltage spectrum for } a(t - \tau_d) - a(t + \tau_d)$$

$$a(\omega) = a_o(\omega) \left[e^{-j\omega\tau_d} - e^{+j\omega\tau_d} \right] \tag{215}$$

so that

$$A(\omega) = -A_o(\omega) \left[e^{-j2\omega\tau_d} + e^{j2\omega\tau_d} - 2 \right] \tag{216}$$

where $A_o(\omega)$ = power spectrum of reference PN code with zero delay and the exponential terms account for the advance of the reference code by τ_d. The noise spectral density $S_n(\omega)$ will be assumed to be white of value N_o watts/Hz and limited to f_R, the bandwidth of the receiver filter.* Thus, from Equations (216) and (213), the power spectral density of the equivalent noise is given by

---

* f_R = low pass equivalent bandwidth

-391-

$$S_{n'}(\omega) = S_n(\omega) \otimes A(\omega)$$

$$= \frac{N_o}{2\pi} \int_0^{2\pi f_R} A_o(\omega) \left[2 - e^{-j2\omega\tau_d} - e^{j2\omega\tau_d} \right] d\omega$$

$$= \frac{N_o}{2\pi} \left[2\int_0^{2\pi f_R} A_o(\omega) \, d\omega - \int^{2\pi f_R} A_o(\omega) e^{-j2\omega\tau_d} d\omega - \int_0^{2\pi f_R} A_o(\omega) e^{+j2\omega\tau_d} d\omega \right]$$

$$= N_o \left[2R(0)_{BL} - R(+2\tau_d)_{BL} - R(-2\tau_d)_{BL} \right]$$

$$= 2N_o \left[R(0)_{BL} - R(2\tau_d)_{BL} \right] \tag{217}$$

where $R(X)_{BL} \equiv$ the bandlimited autocorrelation function for the PN code evaluated at X. The equivalent noise spectral density given by Equation (217) may now be substituted into Equation (210) to obtain the tracking error power spectral density, $S_{\Delta\tau}(\omega)$. Thus,

$$S_{\Delta\tau}(\omega) = \left| \frac{KF(j\omega)/j\omega}{1 + AKF(j\omega)/j\omega} \right|^2 2N_o \left[R(0)_{BL} - R(2\tau_d)_{BL} \right] \tag{218}$$

Before proceeding further, it will be helpful to consider the term in the absolute value signs in hopes of simplifying Equation (218). First, examining the mathematical model block diagram, Figure 7-78, it is seen that the voltage transfer function may be written as

$$\frac{\tau_2}{\tau_1} = \frac{AKF(s)\frac{1}{s}}{1 + AKF(s)\frac{1}{s}} \tag{219}$$

and the power transfer function is given by

$$\left| H(j\omega) \right|^2 = \left| \frac{AKF(j\omega)\frac{1}{j\omega}}{1 + AKF(j\omega)\frac{1}{j\omega}} \right|^2 \qquad (220)$$

Since the error signal gain A is independent of ω, Equation (220) may be written as

$$\frac{\left| H(j\omega) \right|^2}{A^2} = \left| \frac{KF(j\omega)\frac{1}{j\omega}}{1 + AKF(j\omega)\frac{1}{j\omega}} \right|^2 \qquad (221)$$

The quantity in the absolute value sign on the right side of the equation is recognized as being the same quantity in the absolute value signs in Equation (218). Thus, substituting Equation (221) into Equation (218), we obtain

$$S_{\Delta\tau}(\omega) = \frac{\left| H(j\omega) \right|^2}{A^2} \quad 2N_o \left[R(0)_{BL} - R(2\tau_d)_{BL} \right] \qquad (222)$$

Each term in Equation (222) has been well defined with the exception of A. So far, A has been called the error signal gain. Referring again to the mathematical model block diagram, Figure 7-78, and to the loop "discriminator," Figure 7-79, it is seen that A:

1.   Must convert a time displacement, $\Delta\tau$, between the incoming code and the reference code to an error voltage.

2.   Is solely a function of signal and not noise; i.e., is really the loop "discriminator" function for signal.

3.   Has an output which is also proportional to the signal level $\sqrt{S}$.

4.   Being a discriminator, has a transfer function given by the slope of the discriminator characteristic.

Thus, based on the above considerations,

$$A = \sqrt{S} \frac{d}{d\tau} \left\langle a(t + \tau_1)\,\varepsilon(t - \tau_2 - \tau_d) - a(t + \tau_1)\,a(t + \tau_2 + \tau_d) \right\rangle_{\Delta\tau = 0} \qquad (223)$$

where

$\langle X \rangle \equiv$ average value of X

$S =$ signal power

By making a simple change of variables, Equation (223) may be written as

$$A = \sqrt{S} \frac{d}{d\tau} \left\langle a(t) \, a(t + \Delta\tau - \tau_d) - a(t) \, a(t + \Delta\tau + \tau_d) \right\rangle_{\Delta\tau = 0} \qquad (224)$$

$$= \sqrt{S} \frac{d}{d\tau} \left[R(\Delta\tau - \tau_d)_{BL} - R(\Delta\tau + \tau_d)_{BL} \right]_{\Delta\tau = 0} \qquad (225)$$

where the quantity $R(\Delta\tau - \tau_d) - R(\Delta\tau + \tau_d)$ is the discriminator characteristic for the delay lock tracking loop. Thus

$$A = \sqrt{S} \left[R'(\Delta\tau - \tau_d)_{BL} - R'(\Delta\tau + \tau_d)_{BL} \right]_{\Delta\tau = 0}$$

$$= \sqrt{S} \, 2R'(\tau_d)_{BL} \qquad (226)$$

where the bandlimited autocorrelation function is used since the signal is first filtered by the receiver filter. By substituting Equation (226) into (225), we obtain

$$S_{\Delta\tau}(\omega) = \left| H(j\omega) \right|^2 \frac{2N_o \left[R(0)_{BL} - R(2\tau_d)_{BL} \right]}{S \left[2R'(\tau_d)_{BL} \right]^2} \qquad (227)$$

From the noise theory,

$$\sigma_n^2 = \int_0^\infty S_n(\omega) \frac{d\omega}{2\pi} \qquad (228)$$

so that by substituting Equation (227) into (228) we obtain

$$\sigma_{\Delta\tau}^2 = \int_0^\infty \left| H(j\omega) \right|^2 \frac{2N_o \left[R(0)_{BL} - R(2\tau_d)_{BL} \right]}{S \left[2R'(\tau_d)_{BL} \right]^2} \frac{d\omega}{2\pi}$$

$$= \frac{2N_o}{S} \frac{R(0)_{BL} - R(2\tau_d)_{BL}}{\left[2R'(\tau_d)_{BL} \right]^2} \int_0^\infty \left| H(j\omega) \right|^2 \frac{d\omega}{2\pi} \qquad (229)$$

The noise bandwidth of a transfer function is defined as

$$B_L \equiv \int_0^\infty \left| H(j\omega) \right|^2 \frac{d\omega}{2\pi} \tag{230}$$

so that Equation (229) reduces to

$$\sigma_{\Delta\tau}^2 = \frac{2N_o B_L}{S} \cdot \frac{R(0)_{BL} - R(2\tau_d)_{BL}}{\left[2R'(\tau_d)_{BL} \right]^2} \tag{231}$$

Thus, the delay lock loop rms tracking error may be written as

$$\Delta\tau_{rms} = \frac{1}{\sqrt{\dfrac{S}{2N_o B_L}}} \cdot \frac{\sqrt{R(0)_{BL} - R(2\tau_d)_{BL}}}{2R'(\tau_d)_{BL}} \tag{232}$$

where

B_L = one sided loop noise bandwidth

N_o = one sided noise power density

S = average signal power

7.6.1.5 Delay Lock Loop Tracking Performance

It is desirable to plot the rms tracking error, $\Delta\tau_{rms}$, as a function of $S/N_o B_L$, the loop signal-to-noise ratio, and several values of bandlimiting and displacement τ_d. The bandlimited autocorrelation functions used in Equation (232) can be shown to be given by

$$R(X) = \frac{1}{\pi} \left[\frac{2}{B} \cos[BX](\cos[B]-1) - 2X \, si[BX] \right.$$

$$\left. + (1+X) \, si[B(1+X)] + (1-X) \, si[B(1-X)] \right] \tag{233}$$

where

B = $2\pi f_R \Delta$

f_R = one sided bandwidth of receiver filter

Δ = PN code bit width

X = time displacement in bits

and

$$\text{si} [X] = \int_0^X \frac{\sin y}{y} \, dy \tag{234}$$

The rms tracking error (Equation (232)) is plotted in Figure 7-80 as a function of S/N_oB_L and several values of B and τ_d. It is obvious that the larger B is, the smaller $\Delta\tau_{rms}$, and the smaller τ_d, the smaller $\Delta\tau_{rms}$. However, because of data transmission requirements and limited available spectrum, B is typically limited to 1.5π in a spread spectrum system. Thus, a plot of $\Delta\tau_{rms}$ versus τ_d 'or B = 1.5π, 3π, and ∞, as shown in Figure 7-81, shows that for no bandlimiting the tracking error may be made infinitesimally small by making τ_d infinitesimally small. However, for practical values of bandlimiting; i.e., B = 1.5π, $\Delta\tau_{rms}$ changes very little as a function of τ_d.

The theoretical conclusion that an improvement is achieved by letting $\tau_d \rightarrow 0$ ignores the threshold behavior of the tracking loop, and actually an optimum τ_d exists for delay lock. Appendix V discusses this effect further; however, with practical bandlimiting, the choice of τ_d actually has little impact.

7.6.1.6 Analysis of the τ Jitter Loop

A block diagram of a τ jitter tracking loop is shown in Figure 7-82. For analysis purposes, the equivalent math model for the τ jitter tracking loop is the same as that for the delay lock loop, with the exception of the error discriminator. Essentially, the error voltage is generated by correlating the received code with a reference code which is alternately advanced and delayed (jittered) by τ_d bits and phase detection the resultant signal with the square wave voltage which jittered the reference code. This error discriminator is modeled as shown in Figure 7-83. By calculating the error signal gain, A, and the output noise power for this discriminator, some of the results of the delay lock loop analysis based on Figure 7-78 may be used.

For the purpose of analysis, the jittering of the reference code is accomplished by means of a switching function U(t), which has the following properties:

1.   U(t) =
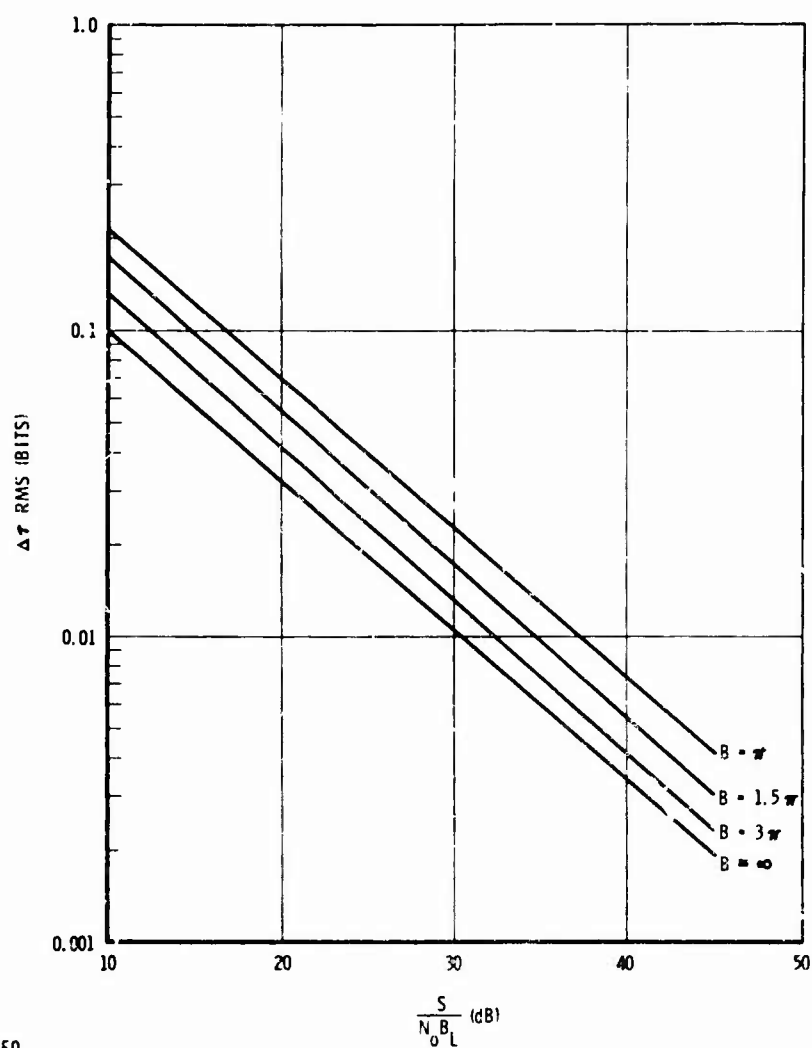
Figure 7-80. Delay Lock Loop rms Tracking Error Versus
Loop Signal-to-Noise Ratio; ($\tau_d = .1$)

2. $\widehat{U(t)}$ $\equiv$ $1 - U(t)$

3. $\langle U(t) \rangle$ $=$ $\langle \widehat{U(t)} \rangle$ $=$ $\frac{1}{2}$

4. $U(t)^N$ $= U(t)$, $\widehat{U(t)}^N = \widehat{U(t)}$, $N = 0, 1, 2, \ldots$

5. $U(t) \widehat{U(t)} = 0$

-397-
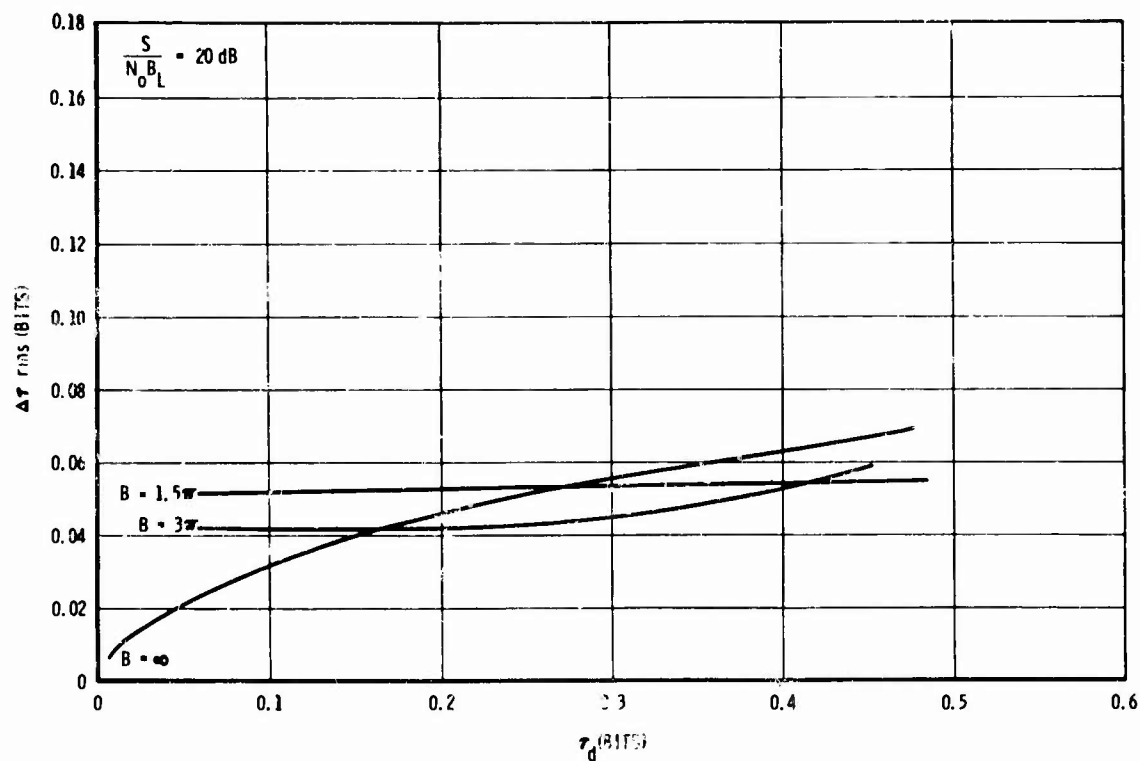
Figure 7-81.   Delay Lock Loop rms Tracking Error as a Function of Displacement τ_d

Figure 7-82. τ Jitter Tracking Loop

-398-

Figure 7-83. τ Jitter Error Discriminator Model
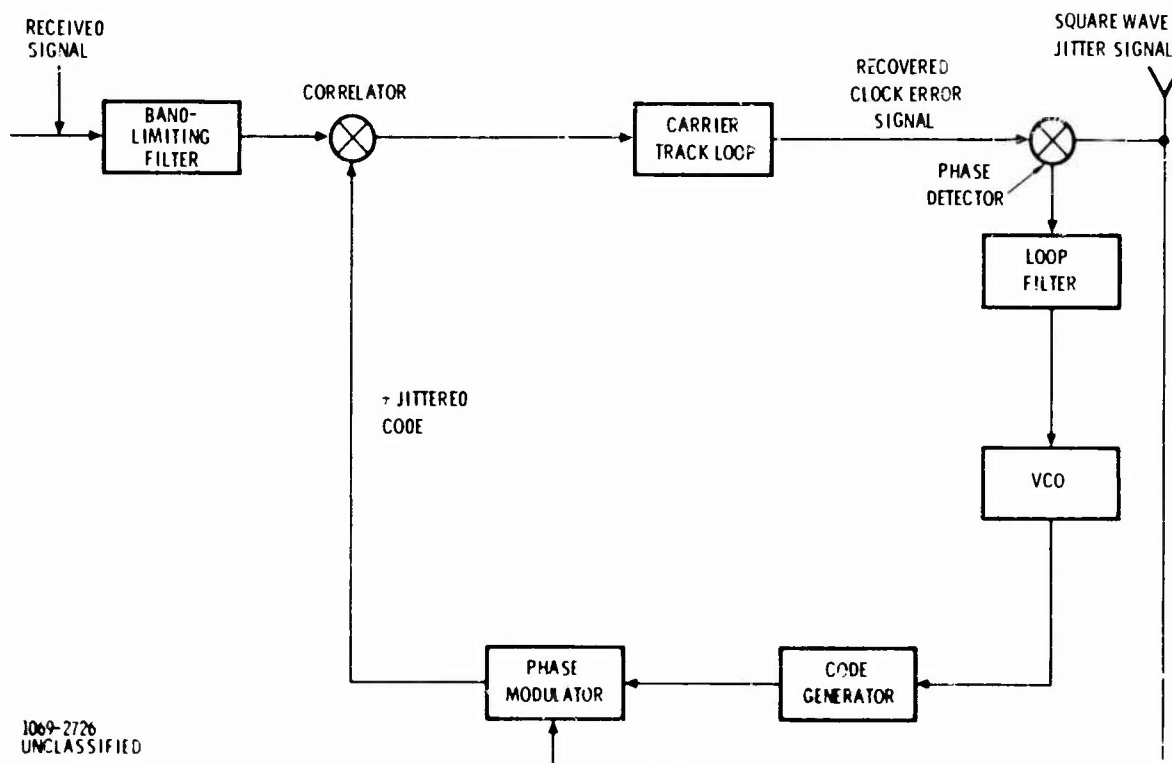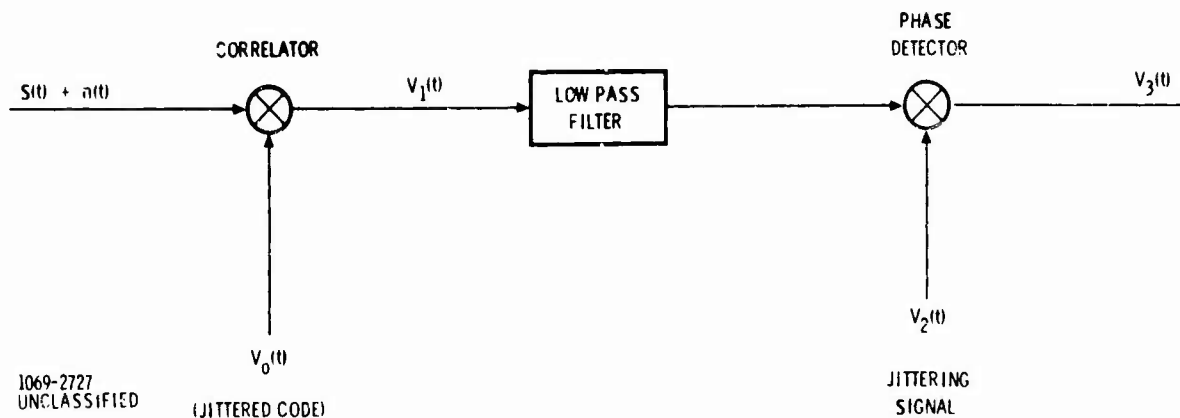
The jittered reference PN code is denoted by

$$V_0(t) = a(t + \tau_2 - \tau_d) U(t) - a(t + \tau_2 + \tau_d) \widehat{U(t)}$$

so that the correlator output is given by

$$V_1(t) = \left[\sqrt{S} \, a(t + \tau_1) + n(t) \right] \left[a(t + \tau_2 - \tau_d) U(t) - a(t + \tau_2 + \tau_d) \widehat{U(t)} \right]$$

The reference for the phase detector is the jittering signal and is denoted by

$$V_2(t) = U(t) - \widehat{U(t)}$$

The output of the phase detector is given by

$$V_3(t) = V_1(t) \, V_2(t)$$

$$= \left[\sqrt{S} \, a(t + \tau_1) + n(t) \right] \left[a(t + \tau_2 - \tau_d) U(t) - a(t + \tau_2 + \tau_d) \widehat{U(t)} \right] \cdot$$

$$\left[U(t) - \widehat{U(t)} \right]$$

$$= \sqrt{S} \, a(t + \tau_1) \left[a(t + \tau_2 - \tau_d) U(t)^2 - a(t + \tau_2 + \tau_d) \widehat{U(t)}^2 \right]$$

$$+ n(t) \left[a(t + \tau_2 - \tau_d) U(t)^2 - a(t + \tau_2 + \tau_d) \widehat{U(t)}^2 \right] \qquad (235)$$

-399-

The average value of the phase detector output, $V_3(t)$, is the discriminator error voltage,

$$V_3(t) = \left\langle \sqrt{S} \, a(t + \tau_1) \left[a(t + \tau_2 - \tau_d) \, U(t)^2 - a(t + \tau_2 + \tau_d) \, \widehat{U(t)}^2 \right] \right\rangle$$

$$= \frac{\sqrt{S}}{2} \left[R(\Delta\tau - \tau_d)_{BL} - R(\Delta\tau + \tau_d)_{BL} \right] \tag{236}$$

The quantity inside the square brackets is recognized as being the same discriminator characteristic as the delay lock loop. Thus, as before, the error signal gain, A, for the math equivalent model is given by

$$A = \frac{d}{d\tau} \left. \frac{\sqrt{S}}{2} \left[R(\Delta\tau - \tau_d)_{B_L} - R(\Delta\tau + \tau_d)_{BL} \right] \right|_{\Delta\tau \, = \, 0}$$

$$= \sqrt{S} \, R'(\tau_d)_{BL} \tag{237}$$

Since the discriminator shown in Figure 7-83 is a linear system, it is possible to find the relationship between the noise density at its input and at its output by finding the relationship between the input and output noise power. The noise power in the output is found by squaring $V_3(t)$ and averaging. Thus,

$$P_{N_{out}} = \left\langle V_3(t)_n^2 \right\rangle \qquad \text{(subscript n indicates noise component of } V_3(t))$$

$$= \left\langle n(t)^2 \left[a(t + \tau_2 - \tau_d)^2 \, U(t)^2 + a(t + \tau_2 + \tau_d)^2 \, \widehat{U(t)}^2 \right. \right.$$

$$\left. \left. + 2 \, a(t + \tau_2 - \tau_d) \, a(t + \tau_2 + \tau_d) \, U(t) \, U(t) \right] \right\rangle$$

$$= \left\langle n(t)^2 \left[a(t + \tau_2 - \tau_d)^2 \, U(t) + a(t + \tau_2 + \tau_d)^2 \, \widehat{U(t)}^2 \right] \right\rangle$$

$$= \left\langle n(t)^2 \right\rangle \left[\left\langle a(t + \tau_2 - \tau_d)^2 \right\rangle \left\langle U(t) \right\rangle + \left\langle a(t + \tau_2 + \tau_d)^2 \right\rangle \left\langle U(t) \right\rangle \right] \tag{238}$$

Since the noise is bandlimited by the receiver filter,

$$\left\langle a(t + \tau_2 - \tau_d)^2 \right\rangle = \left\langle a(t + \tau_2 + \tau_d)^2 \right\rangle = R(0)_{BL}$$

and Equation (238) reduces to

$$P_{N_{out}} = \left\langle n(t)^2 \right\rangle \, R(0)_{BL} \tag{239}$$

Since,

$$P_{N_{in}} = \left\langle n(t)^2 \right\rangle$$

We find that the noise power out of the τ jitter discriminator is related to the noise power in by

$$P_{N_{out}} = P_{N_{in}} \, R(0)_{BL}$$

so that by considering the noise in the same bandwidth

$$S_{n'}(\omega) = N_o R(0)_{BL} \tag{240}$$

where N_o is the input noise power spectral density. Thus, from Equation (211),

$$S_{\Delta\tau}(\omega) = \left| \frac{KF(j\omega)/j\omega}{1 + AKF(j\omega)/j\omega} \right|^2 S_{n'}(\omega), \tag{241}$$

the spectral density for the tracking error for the τ jitter tracking loop is given by

$$S_{\Delta\tau}(\omega) = \left| \frac{KF(j\omega)/j\omega}{1 + AKF(j\omega)/j\omega} \right|^2 N_o R(0)_{BL} \tag{242}$$

Upon substituting Equation (221) into Equation (242), the tracking error spectral density is found to be

$$S_{\Delta\tau}(\omega) = \frac{|H(j\omega)|^2}{A^2} \, N_o R(0)_{BL} \tag{243}$$

and since A for the τ jitter loop is given by Equation (237), Equation (243) reduces to

$$S_{\Delta\tau}(\omega) = \frac{N_o R(0)_{BL}}{SR'(\tau_d)_{BL}} \, |H(j\omega)|^2 \tag{244}$$

Thus, the variance of the tracking error is found to be

$$
\begin{aligned}
\sigma_{\Delta\tau}^2 &= \int_0^\infty S_{\Delta\tau}(\omega) \, \frac{d\omega}{2\pi} \\
&= \frac{N_o}{SR'(\tau_d)_{BL}} \int_0^\infty |H(j\omega)|^2 \, \frac{d\omega}{2\pi} \\
&= \frac{N_o B_L R(0)_{BL}}{SR'(\tau_d)_{BL}}
\end{aligned}
\tag{245}
$$

so that the rms tracking error for the τ jitter loop is given by

$$\Delta\tau_{rms} = \frac{1}{\sqrt{\dfrac{S}{N_o B_L}}} \, \frac{\sqrt{R(0)_{BL}}}{R'(\tau_d)_{BL}} \tag{246}$$

7.6.1.7 τ Jitter Tracking Loop Performance and Comparison with Delay Lock Loop Performance

The rms tracking error for the τ jitter tracking loop, Equation (246), is shown plotted in Figure 7-84. A bandlimiting factor of $B = 1.5\pi$ was used since that value is typically used in PN systems. As can be seen, the error increases as τ_d, the jitter displacement, decreases. The dependence of $\Delta\tau_{rms}$ on τ_d is better illustrated by the plot of $\Delta\tau_{rms}$ versus τ_d shown in Figure 7-85. This inverse relationship between τ_d and $\Delta\tau_{rms}$ is opposite of the relationship for the delay lock loop, where
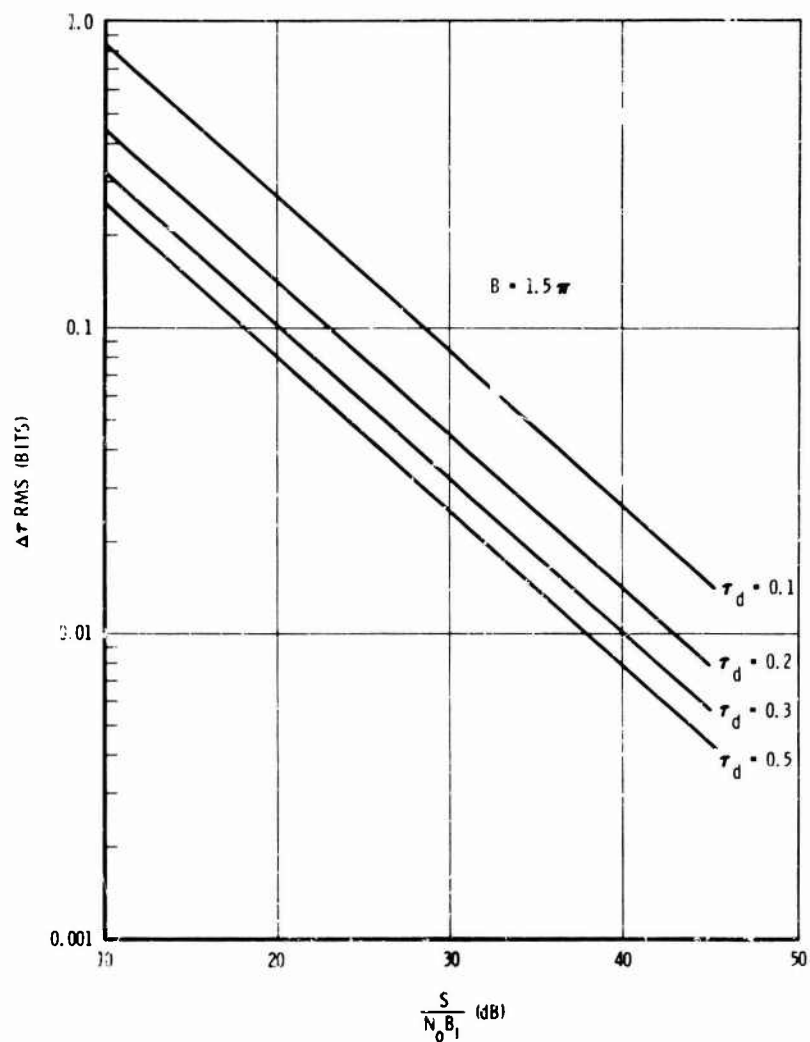
Figure 7-84. τ Jitter Tracking Loop Error as a
Function of Loop Signal-to-Noise Ratio

$\Delta\tau_{rms}$ decreases for decreasing τ_d. This performance difference is obvious from comparing Equations (232) and (246). However, a better understanding of the performance difference between the two loops is obtained from comparing what happens to the input noise in each of the "discriminators". In the delay lock loop, as τ_d becomes smaller, the noise at the output of each correlator becomes more correlated with the other channel's noise. Thus, as $\tau_d \rightarrow 0$ the noise in each channel becomes the same so that the subtractor is subtracting the noise from itself and the noise output becomes zero. If the noise approaches zero, it is obvious that the tracking error also
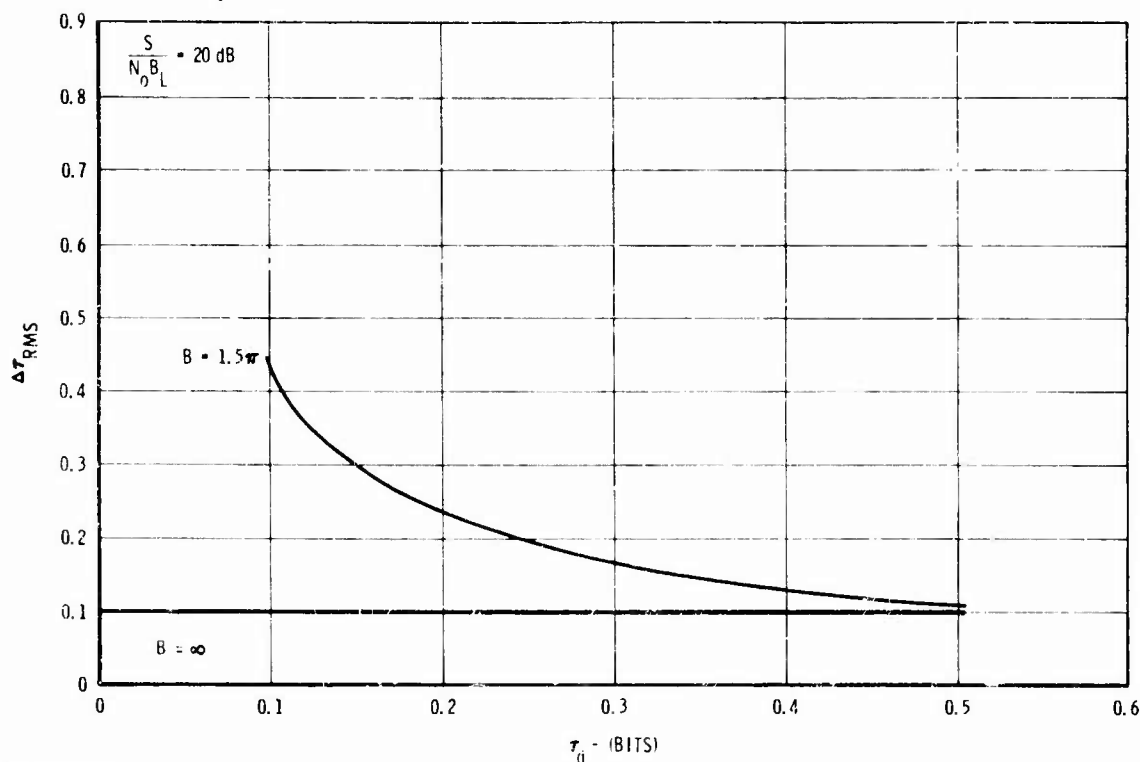
Figure 7-85. τ Jitter Tracking Loop Error as a Function
of Jitter Displacement τ_d

approaches zero. (However, due to bandlimiting and practical considerations, this does not actually happen in hardware loops.) The τ jitter loop, on the other hand, does not subtract noise from itself since it time shares (time multiplexes) a common channel between the advanced and delayed signals. Furthermore, as τ_d becomes smaller, the slope of the bandlimited autocorrelation curve decreases and since the error signal gain is given by this slope, the performance of the loop decreases. The error signal gain for the delay lock loop also decreases as τ_d gets smaller, however, this is offset by the decrease in effective loop noise.

The degradation of tracking performance for a τ jitter loop relative to a delay lock loop and a conventional phase locked loop is shown plotted in Figure 7-86. The plot is a function of τ_d , with $B = 1.5\pi$. Since it is sometimes the practice to make τ_d small (around .1 bit) so that the correlator output may also be used for data demodulation, it is obvious that much better tracking performance may be obtained from the delay lock loop. This is especially important for navigation and position location systems where range measurement from PN code delay determination is the primary concern.

-404-
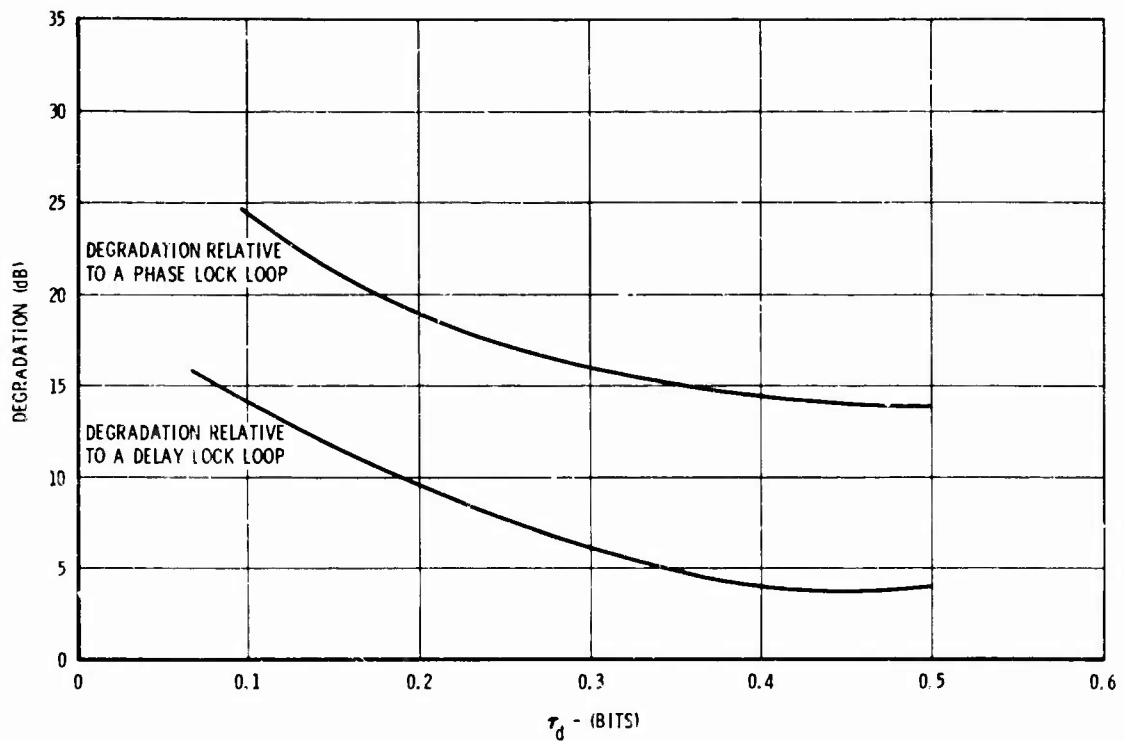
Figure 7-86. τ Jitter Tracking Degradation as a Function of τ_d

7.6.1.8 Effects of Channel Unbalance on Delay Lock Loop Performance

In view of the superior tracking performance of the delay lock loop, it is worthwhile considering the effects of channel gain and time delay differentials on tracking error. Figure 7-87 shows a delay lock discriminator model having a differential time delay of τ in one channel and a differential amplitude gain of K in the other channel.

This is merely the general case of the delay lock loop analysis given in paragraph 7.6.1.2, where $\tau = 0$ and K = 1. Thus, it is easy to show that the rms tracking error for the loop having the discriminator shown in Figure 7-87 is given by

$$\Delta \tau_{rms} = \frac{1}{\sqrt{\dfrac{S}{N_c B_L}}} \; \frac{\sqrt{(1 + k^2)R(0)_{BL} - 2kR(2\tau + \Delta)_{BL}}}{k R'(\tau)_{BL} - R(-\tau + \Delta)_{BL}} \tag{247}$$

-405-
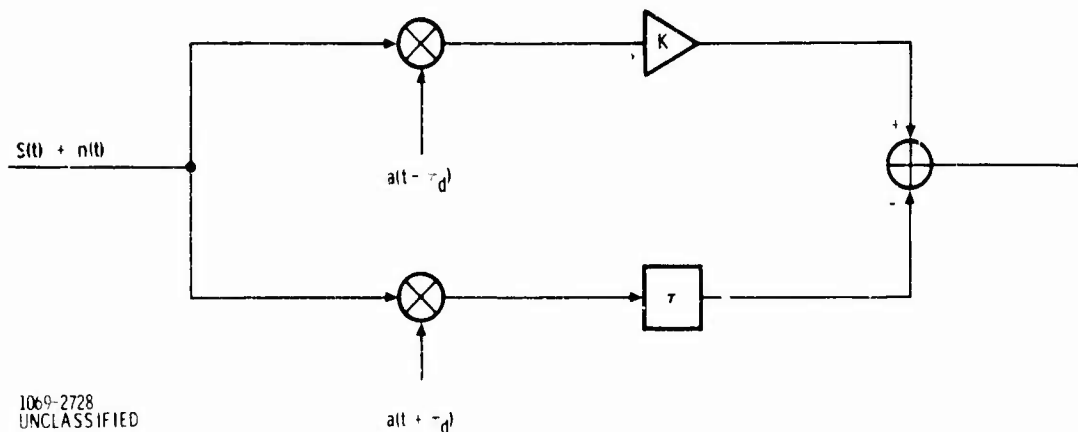
Figure 7-87. Delay Lock Loop Discriminator With Gain
and Time Delay Unbalances

By comparing the performance specified by Equation (246) with that specified by
Equation (247), the effects of Δ and k may be evaluated. These effects are shown
tabulated in Table 7-18. It seems reasonable that through good engineering design
the gain differenetial should be no greater than 1 db and the time delay differential
should be no greater than 10% of the time displacement of the reference code, τ_d.
From Table 7-18 it can be seen that this results in a 15% increase in the rms tracking
error or approximately 1 db performance degradation.

Table 7-18. Effect of Gain and Delay Differentials on
Delay Lock Loop Tracking Error

K(db)	τ (bits)	τ/τ_d (%)	Percent Change of $\Delta\tau_{rms}$
.1	.01	10	12
.1	.05	50	65
1.0	.01	10	15
1.0	.05	50	71

7.6.2 DETERMINATION OF THE EFFECTS OF MULTIPATH ON THE TRACKING
      PERFORMANCE OF THE DELAY LOCK LOOP

The coherent delay lock loop utilized to track PN codes in a correlation receiver
has been described in Section 7.6.1 as the basis for measuring a signal's time of
arrival for navigation purposes. A simplified coherent delay lock loop for discussion
of multipath effects is illustrated in Figure 7-88. For the purpose of analysis, we

-406-
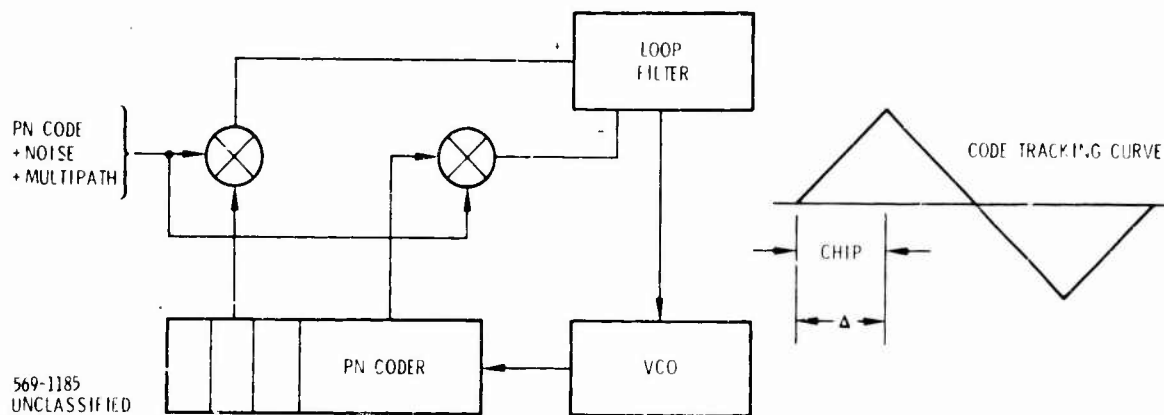
Figure 7-88. Low Pass Coherent Delay Lock Loop

will assume that the code tracking device is coherent and is operating at baseband and that a ± half chip delay is utilized in the shift register to realize the error tracking voltage curve, or discriminator characteristics.

We will assume that the phase lock loop associated with the tracking device has an averaging time of T and that the PN sequence has a chip duration of Δ. It follows from Equation (232) of Section 7.6.1 for an unrestricted predetection bandwidth that the mean squared time tracking error for coherent binary delay lock is given by Equation (248)

$$\sigma_\tau = \Delta / \sqrt{ST/N_o} \tag{248}$$

where

  T = averaging time of loop

  Δ = chip duration

  S = average signal power density

  N_o = noise power density

7.6.2.1 Diffuse Correlated Multipath

We desire to know the performance of a delay lock PN tracking system in the presence of diffuse correlated multipath. This can exist when the reflected energy from the earth's surface in a satellite-to-aircraft link is within the correlation aperture of the correlation receiver and is resulting from diffuse scattering. The rms error of the tracking loop takes the following form in the presence of correlated diffuse multipath.

-407-

$$\sigma_\tau = \frac{\Delta\sigma_{noise}}{\sqrt{S}}$$

$$= \Delta \sqrt{\frac{\dfrac{N_{in}}{TW} + \dfrac{(1-\rho^2)S_{ind}}{TW} + \rho^2 S_{ind}}{S}} \tag{249}$$

(Diffuse Multipath)

where

TW = processing gain = averaging time x bandwidth

ρ = correlation between the direct and indirect paths

S = desired or direct signal power

S_{ind} = power in the indirect path.

The channel model leading to Equation (249) is described in Section 7.1. We see that the input noise level is suppressed by the TW product (processing gain), there is a Gaussian term showing partial correlation suppressed by the TW product and a Gaussian term showing partial correlation which is unaffected by the TW product. The sum of these three terms represent the noise which is present in a correlation delay lock loop implementation.

When the TW product is large it is evident from Equation (249) that there exists a lower bound on the tracking error given by

$$\sigma_\tau \sim \Delta\rho / \sqrt{S/S_{ind}}$$

Rearranging terms and taking the ratio of the rms time jitter without multipath to the rms time jitter of the loop in the presence of diffuse multipath, we obtain an equation which indicates the relative performance of the delay lock discriminator in the presence of diffuse multipath.

$$\frac{\sigma_{\tau(no\ multipath)}}{\sigma_\tau} = \frac{\sqrt{N_{in}/TW}}{\sqrt{\dfrac{N_{in}}{TW} + \dfrac{(1-\rho^2)S_{ind}}{TW} + \rho^2 S_{ind}}} \tag{250}$$

(Diffuse Multipath)

In conclusion, we see that the multipath can dramatically affect the rms performance of a delay lock loop relative to its performance without multipath. In fact,

there is an asymptotic tracking error that is determined by the degree of correlation between the direct and indirect paths and the ratio of the powers contained in the paths.

7.6.2.2 Specular Multipath

The effects of specular fading on the tracking error in a conventional coherent binary delay lock loop is now of interest. To determine the tracking loop error resulting from specular fading, we assume that a portion of the received signal is correlated with the direct path and that this term will show up as a randomly phased CW component at the output of the delay lock loop and will remain within the loop bandwidth of the VCO.

In lieu of a sophisticated analysis we utilize the experimental results[*] obtained by Britt and Palmer and find that the phase error in a conventional second order phase lock loop resulting from CW interference is given by the following equation.

$$\sigma^2_{\emptyset \, error} \sim \frac{N/S}{1 + I/S} + \frac{I}{2S} \tag{251}$$

where S is the desired signal power, I is the CW interference power, and N is the noise power in the loop.

We can expect that the mean squared timing error for the coherent delay loop can be written as

$$\sigma^2_T \sim \Delta^2 \sigma^2_{\emptyset \, error} \tag{252}$$

where

Δ = duration of a PN chip.

In terms of Equation (4) and the parameters governing multipath

$I = \rho^2 S_{ind}$

S_{ind} = power in the indirect path

$S = S_{direct}$

[*] C. L. Britt and D. F. Palmer, "Effects of CW Interference on Narrow-Band Second-Order Phase-Lock Loops," IEEE Trans. on AES, Jan. 1967, pp. 128-135.

$$N = \frac{\left[N_{in} + (1 - \rho^2)S_{ind}\right]}{TW}$$

ρ = correlation between the direct and indirect signal paths

TW = the processing gain of the tracking loop

$$\sigma_\tau^2 = \Delta^2 \left[\frac{\left[N_{in} + (1 - \rho^2)\, S_{ind}\right]\frac{1}{TW}}{S + \rho^2 S_{ind}} + \frac{\rho^2 S_{ind}}{2S}\right] \tag{253}$$

(Specular Multipath)

which for large TW products reduces to Equation (254), the rms bound on the tracking time error

$$\sigma_\tau \simeq \frac{\Delta\rho}{\sqrt{2S/S_{ind}}} \tag{254}$$

The result is not surprising in that a similar equation was derived for the rms time jitter bound for a coherent delay lock loop in the presence of correlated diffuse multipath.

7.6.3 THEORETICAL ACCURACY OF TONE RANGING, COMPARED WITH PN

7.6.3.1 Introduction

A method of measuring range is to determine the time of arrival of a PN sequence modulated on a high frequency carrier. The rms range measurement error for this technique has been derived in Section 7.6.1. An alternate technique for measuring range is the so-called sidetone ranging system. This section presents an analysis that derives the rms range measurement error for a sidetone ranging system.

The sidetone ranging signal consists of a number of CW tones modulated on a high frequency carrier. Range is determined accurately by measuring the phase of the received highest frequency tone relative to some reference, which is the transmitted tone or a stable oscillator. The lower frequency tones are used to resolve the ambiguity in the range measurement obtained from the highest frequency tone. This is necessary since the range to be measured will typically be many times longer than the period of the highest tone.

The tone ranging system analyzed in this section possesses a discrete line spectra so that the receiver tracks each tone independently of the others. A block diagram of the system is shown in Figure 7-89. The tone filters shown in Figure 7-89 are typically phase locked loops whose VCO rest frequencies are the same as the frequency of the respective tones. The loop bandwidths should be as small as possible but should be consistent with acquisition time and Doppler rate requirements. Since this analysis, like the analysis of the PN system, is a theoretical performance analysis, it does not treat the effects of implementation limitations on performance.

It will be assumed that the probability of making a measurement error is the same for each tone. In addition, the following assumptions will hold:

1.   Narrow band FM (NBFM) or amplitude modulation (AM) is used.

2.   Equal power is allotted to each tone channel.

3.   The received signal-to-noise ratio is the same in each tone channel.

4.   The interference is white, Gaussian noise.

The following parameters are of interest:

1.   Lowest frequency tone.

2.   Highest frequency tone.

3.   Optimum number of tones.

4.   Optimum bandwidth.

5.   Minimum rms ranging error.

7.6.3.2 Analysis

If the initial range ambiguity is R_o, the first tone must have a wavelength

$$\lambda_1 \geq R_o \tag{255}$$
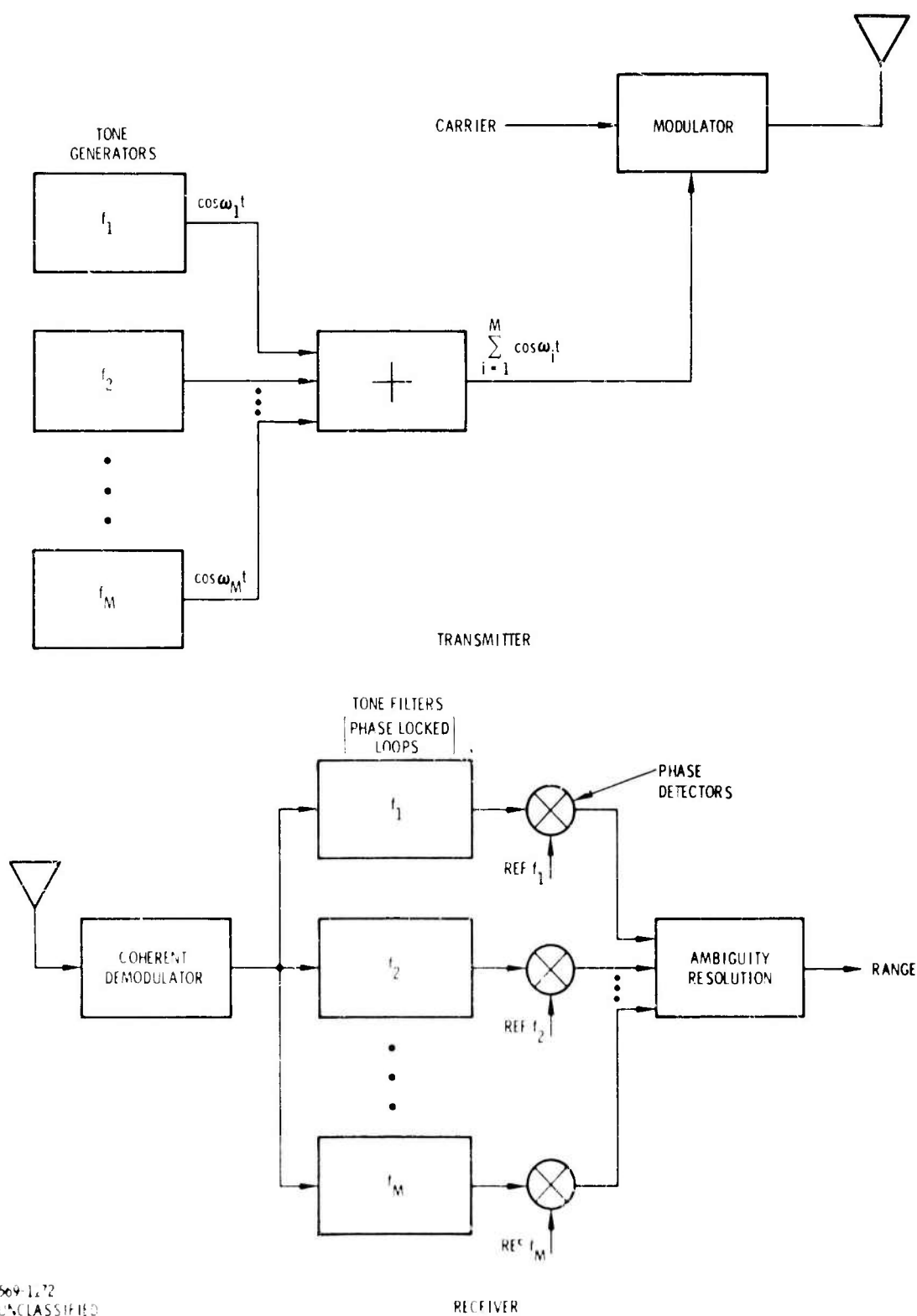
Figure 7-89. Tone Ranging System

If we use the equality, the frequency of the first tone is given by

$$f_1 = \frac{C}{R_o} \tag{256}$$

The next tone, f_2, must have a wavelength, λ_2, equal to or greater than the uncertainty in the measurement of range R_o obtained by making a phase measurement of the received tone f_1. The measurement of R_o from f_1 will be a Gaussian distributed random variable, R_1, with mean R_o and variance given by

$$\sigma_1 = \frac{C}{2\pi f_1} \frac{1}{\sqrt{S/N}} \tag{257}$$

where

S/N = signal-to-noise ratio in loop bandwidth of f_1 tone channel.

The distribution for random variable R_o and the measurement uncertainty region is shown in Figure 7-90.

It is reasonable to desire R_1 to be in the uncertainty region defined by

$$R_o - \frac{\Delta R}{2} < R_1 < R_o + \frac{\Delta R}{2}$$
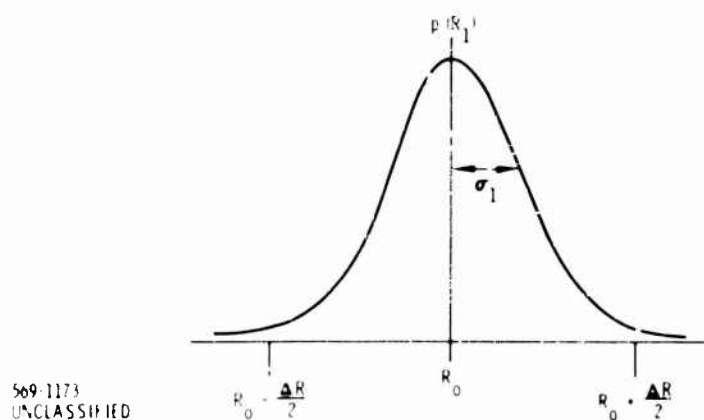
Figure 7-90. Probability Density Function for Range Measurement

with high probability, say .998. Thus, we have,

$$.938 = \int_{R_o - \frac{\Delta R}{2}}^{R_o + \frac{\Delta R}{2}} p(R_1) dR_1 \tag{258}$$

where

$$p(R_1) = \frac{1}{\sqrt{2\pi\sigma_1^2}} e^{-\frac{(R_1 - R_o)^2}{2\sigma_1^2}} \tag{259}$$

so that by solving for $\frac{\Delta R}{2}$, the uncertainty region ΔR is found to be $6\sigma_1$ wide, $\left(\left| R_o - \frac{\Delta R}{2} \right| = 3\sigma \right)$. Thus, tone f_2 is defined by

$$\lambda_2 \geq 6\sigma_1 \tag{260}$$

or by using the equality

$$\lambda_2 = \frac{6C}{2\pi f_1} \quad \frac{1}{\sqrt{S/N}} \tag{261}$$

and since $\lambda_2 = \frac{C}{f_2}$, we obtain

$$f_2 = \frac{2\pi f_1 \sqrt{S/N}}{6} \tag{262}$$

The general case is easily seen to be

$$f_M = \frac{2\pi f_{M-1} \sqrt{S/N}}{6} \tag{263}$$

or in terms of frequency f_1,

$$f_M = \left(\frac{2\pi \sqrt{S/N}}{6} \right)^{M-1} f_1 \tag{264}$$

-414-

where for the time being it will be assumed that the S/N for each tone channel is the same. The frequency of the highest tone, f_H, and consequently the number of tones required, is determined by the desired range measurement accuracy and the available S/N. Assume that the allowable rms range error is σ_H, and that the available signal-to-noise ratio for that channel is S/N. Thus, σ_H is given by

$$\sigma_H = \frac{C}{2\pi f_H} \frac{1}{\sqrt{S/N}} \tag{265}$$

so that the highest tone frequency is given by

$$f_H = \frac{C}{2\pi\sigma_H} \frac{1}{\sqrt{S/N}} \tag{266}$$

and the bandwidth required for a given accuracy requirement is just $2f_H$ (assuming double sideband modulation).

The system rms ranging error, given by Equation (265), may be written in terms of frequency f_1 by utilizing Equation (264). Thus,

$$\sigma_H = \frac{C}{2\pi \left(\dfrac{2\pi \sqrt{S/N}}{6}\right)^{M-1} f_1} \frac{1}{(S/N)^{1/2}}$$

$$\tag{267}$$

$$= \frac{1}{6\left[\left(\dfrac{2\pi}{6}\right)^2 \left(\dfrac{S'}{N}\right)\dfrac{1}{M}\right]^{\frac{M}{2}}} \frac{C}{f_1}$$

where

$$\frac{S'}{N} \frac{1}{M} = \frac{S}{N}$$

and

$\dfrac{S'}{N}$ — received signal-to-noise ratio if only one tone was transmitted

M — number of transmitted tones

The optimum number of tones for a given signal-to-noise ratio may be found by differentiating Equation (267) with respect to M, setting the result equal to zero, and solving for M. In doing this we obtain

$$M_{opt} = \exp \left| \log \left[\left(\frac{2\pi}{6} \right)^2 \frac{S'}{N} \right] - 1 \right| \tag{268}$$

Since the system bandwidth is twice the highest frequency tone, the optimum bandwidth is found from Equations (264) and (268) to be given by

$$BW_{opt} = 2f_1 \left[\frac{2\pi}{6} \frac{S'}{N} \exp \left(\frac{1 - \log \left(\frac{2\pi}{6} \right)^2 \frac{S'}{N}}{2} \right) \right] \exp \left(\log \left[\left(\frac{2\pi}{6} \right)^2 \frac{S'}{N} \right] - 1 \right) - 1 \tag{269}$$

Examination of Equation (268) reveals that for large S'/N

$$M_{opt} \approx \left(\frac{2\pi}{6} \right)^2 \frac{S'}{N}$$

which means that the optimum number of tones is directly proportional to the signal-to-noise ratio. This result is intuitively satisfying since the transmitted power is equally divided among all tones and a minimum S/N is required in each tone channel. Thus, if the S'/N is low we would want the number of tones to be low so as not to dilute the S/N in each channel below the minimum required S/N. If M_{opt} (Equation (268)) is substituted into Equation (267), the minimum error σ_{min} for the given S'/N is obtained. However, due to bandlimiting restrictions it may not be possible to use M_{opt} and BW_{opt} and consequently the error will be greater than σ_{min}. A plot of BW_{opt} and M_{opt} as shown in Figure 7-91, reveals that for a typical 621B range uncertainty, ($R_o = 3 \times 10^4$ bits), BW_{opt} exceeds the bandwidth allowed for a 10 MHz clock PN system (BW = 15 MHz; i.e., BW/fc = 1.5) for $M_{opt} > 21$. This point corresponds to a signal-to-noise ratio of 17.1 db. Consequently, a tone ranging system subject to this bandwidth constraint should be designed with the number of tones M = 21 for a design S'/N of 17.1 db or greater and $M = M_{opt}$ for S'/N less than 17.1 db. If no bandwidth restrictions are imposed (usually not the case) it is advantageous to use BW_{opt} and M_{opt} as given in Figure 7-91 for the entire S'/N range. Under these conditions the ranging error is given by
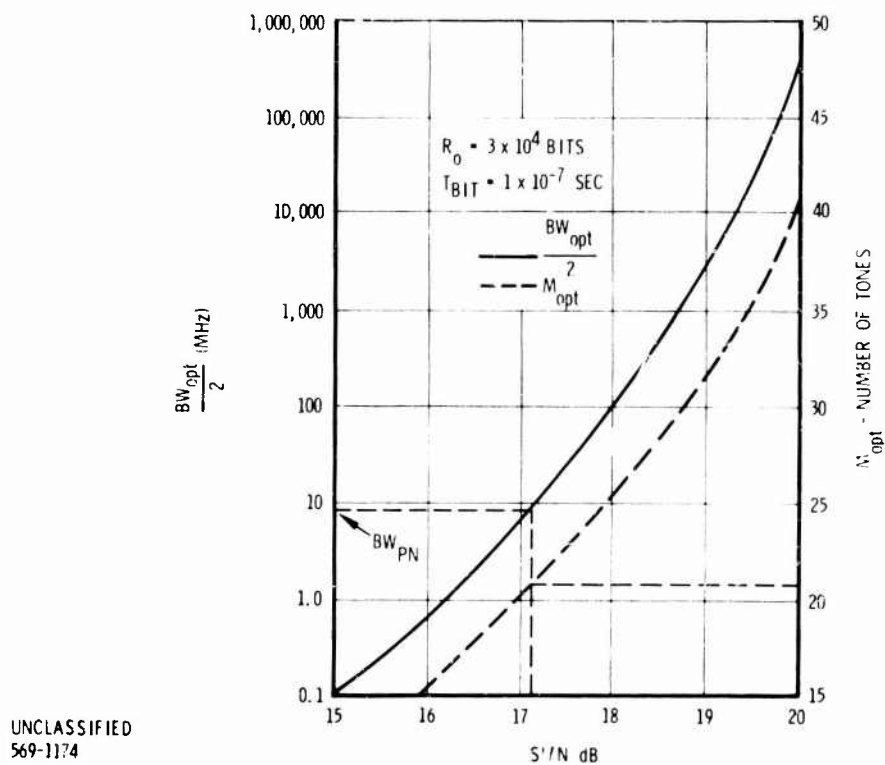
Figure 7-91. Optimum Bandwidth and Number of Tones
for Tone Ranging System

$$\sigma_{min} = \frac{c}{\pi BW_{opt} \sqrt{\frac{1}{M_{opt}} \frac{S'}{N}}} \tag{270}$$

and is shown plotted in Figure 7-92.

The success of the measurement using f_M, where $M = h$ (i.e., the highest tone) is dependent on each of the lower tones having an error within the allowed uncertainty area. Therefore, since it is assumed that each tone measurement is equally likely to be in error, the rms error σ_{min} is obtained with probability given by

$$P_{\sigma_{min}} = (.998)^{M-1} \tag{271}$$

-417-
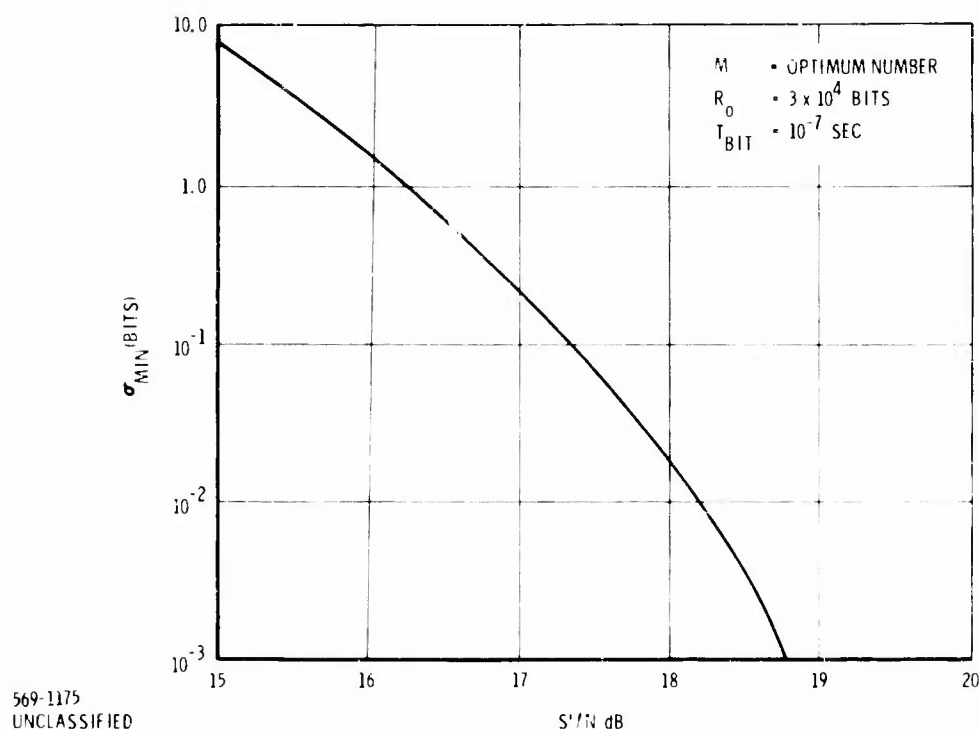
Figure 7-92. Minimum rms Range Error for a Tone Ranging System

7.6.3.3 Comparison with PN System

It is of interest to compare the performance of a tone ranging system with a PN system. The rms ranging error for a PN system has been previously derived and is shown plotted in Figure 7-93 as a function of S'/N for $BW_{PN}/fc = 1.5$ where BW_{PN} = PN system bandwidth and fc = PN clock frequency. Also shown in Figure 7-93 is the rms error for a tone ranging system having the same bandwidth constraint (BW = 15 MHz). The number of tones used is equal to M_{opt} below 17.1 db. Above 17.1 db BW_{opt} is greater than 15 MHz so that M is held constant at 21. It is apparent that the tone system has a fairly sharp threshold at 17.1 db since below this point tne error increases rapidly. Above 17.1 db the tone system performance is a constant 5 db poorer than the PN system performance.

7.6.4 SIMULATION OF COHERENT FH/PN PRECISE RANGING TRACKING LOOP

A computer simulation of the ranging loop in the coherent FH/PN receiver described in Volume I has been developed to permit evaluation of the performance of this technique in an environment subject to noise and aircraft dynamics.
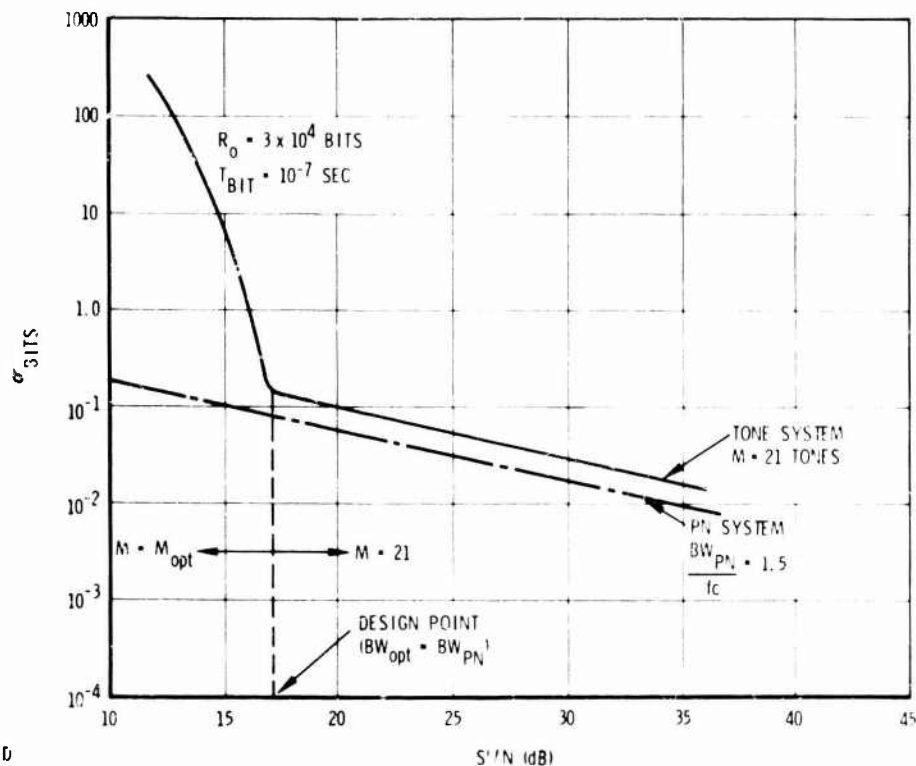
Figure 7-93. Comparison of Tone Ranging System
with PN Ranging System

The simulation model is composed of two parts. The first part is concerned with modeling the flight dynamics so that the appropriate signal parameters, as seen at the receiver terminal, reflect the hypothetical operational conditions. The second part is devoted to the signal processing aspects of the simulation.

7.6.4.1 Summary Description of the Coherent FH/PN System

A brief review of the system concept is provided now to facilitate subsequent discussion of the computer simulation model. The transmitter terminal in a coherent FH/PN system is essentially the same as that required in the traditional FH/PN hybrid, the only notable difference being the phase coherency requirement imposed on the frequency hopping synthesizer in the coherent scheme. Conceptually, we can think of the coherent frequency hopping synthesizer as a generator of phase coherent, harmonically related, frequency tones. At the transmitter one of these frequency tones is selected at random every T sec where T is some arbitrary multiple of the period of the lowest frequency tone. The selected tone is then used for

-419-

frequency translation of the pseudonoise carrier which is modulated with data. An additional fixed frequency up conversion stage conditions the signal for transmission in the appropriate RF band.

At the receiver terminal the signal is initially acquired in the conventional manner by synchronizing the receiver's PN code. During this initial phase of signal acquisition the properties of the coherent frequency hopping are ignored until PN synchronization has been fully achieved. Once this event has occurred the receiver's time uncertainty has been reduced to a fraction of a PN bit. At this point the receiver begins to coherently track the frequency hopping signal in order to reduce the remaining time uncertainty towards zero.

In this report all subsequent discussion will be primarily focused on those elements of the receiver related to the coherent tracking of the frequency hopping signal. Specifically, we will assume that PN acquisition has been achieved at the receiver and that the data modulation has been removed by the coherent reference PSK detector without loss of C/N_o.

7.6.4.2 Flight Dynamics Simulation

In order to realistically model the received signal parameters it was necessary to assume a specific flight profile. For the purpose of this simulation the transmitter was considered stationary while the receiver, onboard a high performance aircraft, was in motion. The hypothetical trajectory of the aircraft consisted of straight line supersonic flight for a time period lasting 4.8 secs during which signal acquisition must be accomplished. The initial range was 500,000 ft with a velocity of 300 fps directed radially outward. After 4.8 seconds the aircraft begins to gradually enter a turn. The radial acceleration is linearly increased from 0 to 100 fps^2 over a time period of 5 seconds to approximate the limited roll rate of an aircraft. Finally, once the radial acceleration has reached 100 fps^2 the trajectory becomes circular. Through these dynamics the range and range rate are computed on 1 millisecond intervals. A schematic illustrating this particular flight profile is shown in Figure 7-94. It can be readily shown that the range to the receiver is given by
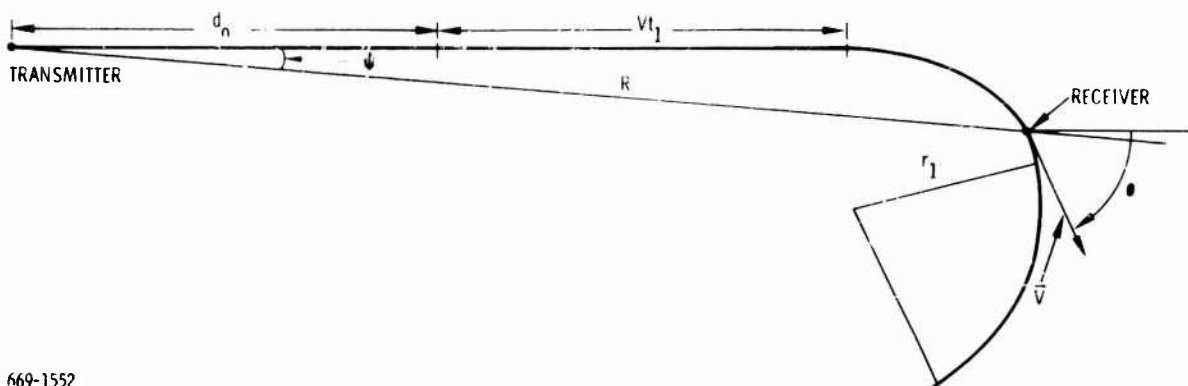
669-1552
UNCLASSIFIED

Figure 7-94. Flight Profile

$$R(t) = d_o + |V| \int_o^t \text{Cos} \, (\theta - \psi) \, dt \tag{272}$$

where

d_o denotes the initial range and

$$\theta(t) = \int_{t_1}^t \frac{a(t)}{|V|} \, dt, \quad a(t) \triangleq \frac{dV}{dt} \tag{273}$$

$$\psi(t) + |V| \int_{t_1}^t \frac{\text{Sin} \, (\theta - \psi)}{R(t)} \, dt \tag{274}$$

Note that t_1 is the instant of time at which the aircraft begins its roll maneuver. For five seconds after that the acceleration $a(t)$ increases linearly to a preset maximum and then remains constant at this maximum.

7.6.4.3 Signal Processor Simulation Model

A simplified block diagram of the coherent frequency hopping signal processor is shown in Figure 7-95. The mathematical description of the signal at the transmitter is of the form

-421-

669-1551
UNCLASSIFIED
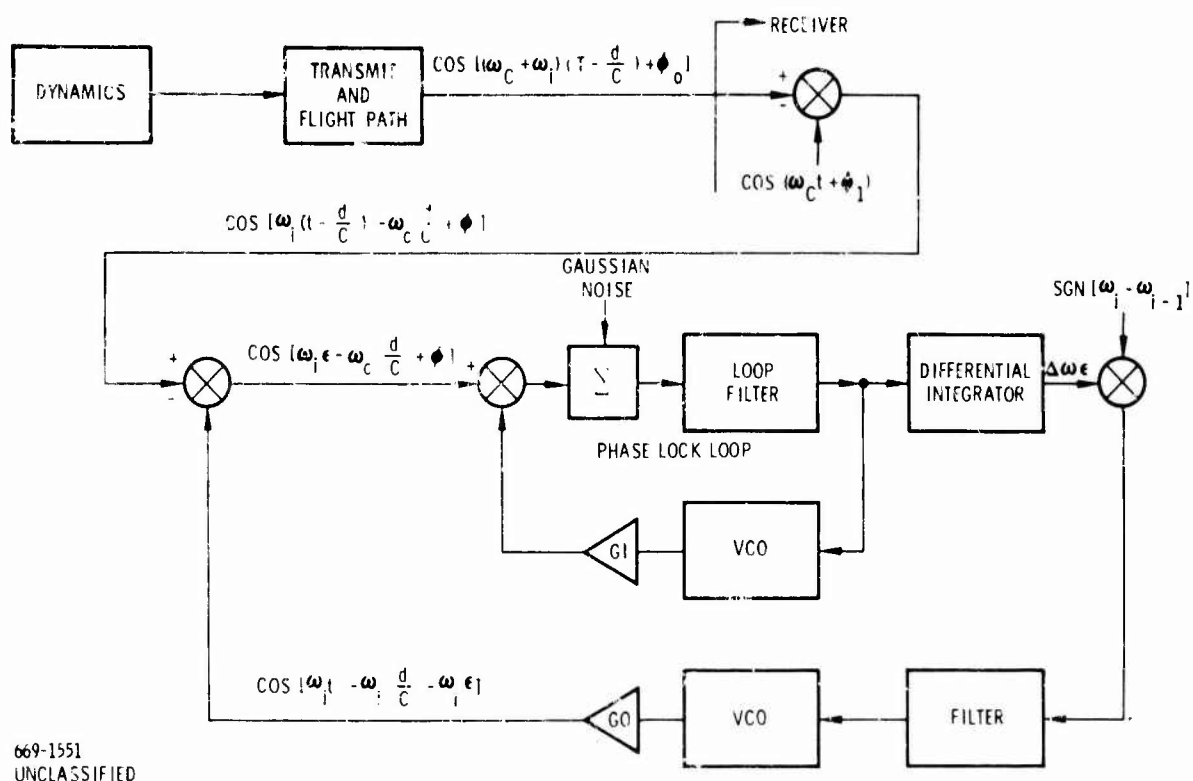
Figure 7-95. Coherent FH Signal Processor

$$\cos (\omega_c t + \omega_i t + \phi_0) \tag{275}$$

where

ω_c = the carrier frequency

ω_i = the hopping offset frequency

ϕ_0 = some arbitrary phase angle

If the distance to the receiver is d and the speed of light is c the received signal is of the form

$$\cos \left[(\omega_c + \omega_i) (t - d/c) + \phi_0 \right] \tag{276}$$

Upon down converting with a local oscillator

$$\cos \left[\omega_c t + \phi_1 \right] \tag{277}$$

we obtain

$$Cos\left[\omega_i(t-d/c) - \omega_c d/c + \phi\right] \tag{278}$$

where

$$\phi = \phi_0 - \phi_1$$

The possibility that the receiver local oscillator is not at the correct frequency does not have any effect on range tracking. It can affect the Doppler estimate with a bias, but this can be accounted for separately.

The signal is next converted by the receiver's estimate of the offset component; however, this estimate of time of arrival may be in error by a very small amount. (We have assumed that the conventional pseudonoise tracking loops have accomplished this.) This second injection is thus

$$Cos\left[\omega_i(t-d/c-\epsilon)\right] \tag{279}$$

and the result of this second conversion is

$$Cos\left[\omega_i\epsilon - \omega_c d/c + \phi\right] \tag{280}$$

This signal is applied to a conventional second order phase lock loop. Assuming an L band frequency allocation $\left(\frac{\omega_c}{2\pi} = 1500 \text{ MHz}\right)$ the loop parameters used were: loop natural frequency $\frac{\omega_0}{2\pi} = 500$ Hz and loop damping coefficient $\zeta = 0.75$. The noise is inserted into the loop and in this simulation corresponds to a C/N_0 of 44 db. The loop filter output is then integrated for T milliseconds before and T milliseconds after each frequency hop and the difference is set into a zero order hold which preserves this value until the next one replaces it. This operation performed on the loop filter output by the differential integrator is conceptually equivalent to sampling the phase of the loop VCO just prior to a frequency hop and T milliseconds after hop and taking the sample value difference. Figure 7-96 illustrates the concept where we have assumed that the phase lock loop tracks perfectly the phase at its input. In addition, ϕ is assumed constant at least over a hop period, the distance d is a linear function of time and the timing error ϵ is constant. From this simple schematic we

LOOP VCO PHASE

SAMPLE
DIFFERENCE

SAMPLE NO. 1

SAMPLE NO. 2

t_1

$t_1 + T$

$t_1 + 2T$

669-1550
UNCLASSIFIED

τ MILLISECONDS
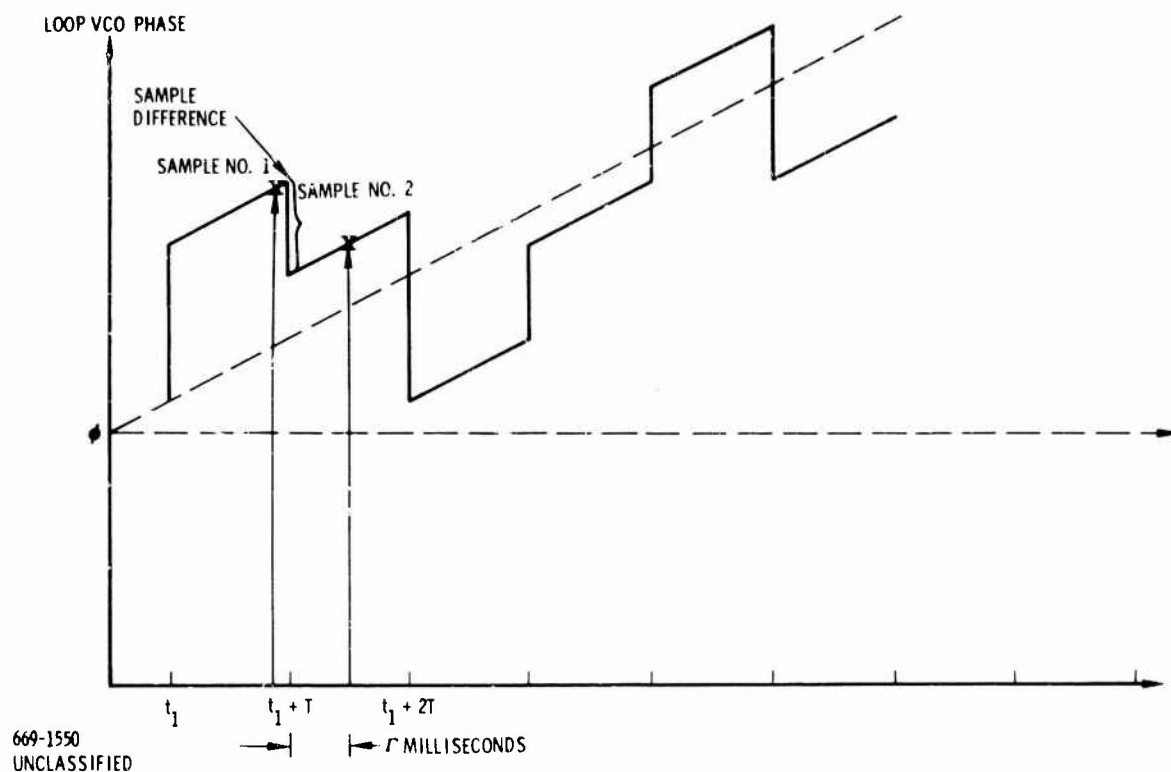
Figure 7-96. Simplified Conceptual Representation of Differential
Integrator

see that the differential integrator generates an output every T seconds which is
proportional to the difference in adjacent frequency tones $\Delta\omega$ times the timing error.
This signal is next applied, after multiplication by the sign of the ω_i jump, to the
outer loop filter which is a proportional plus integral control type. The output is
then applied to an integrator (VCO) whose phase is $(t - d/c - \epsilon)$. Finally, multiplication
by ω_i (the coherent synthesizer) yields the quantity necessary for closing the loop.
The ω_i are chosen randomly each 32 milliseconds from among 64 possible values spaced
over approximately 10 MHz for this particular waveform postulate.

The actual mathematical model of the receiver precision range tracking loop
which the simulation is based on is shown in Figure 7-97. A significant increase in
both the ease and accuracy of the computation is obtained by the simple expediency
of replacing phase angles by their time derivatives and performing a single integra-
tion at the appropriate point. For example, observe from Figure 7-95 that the
input to the phase locked loop can be expressed by

-424-
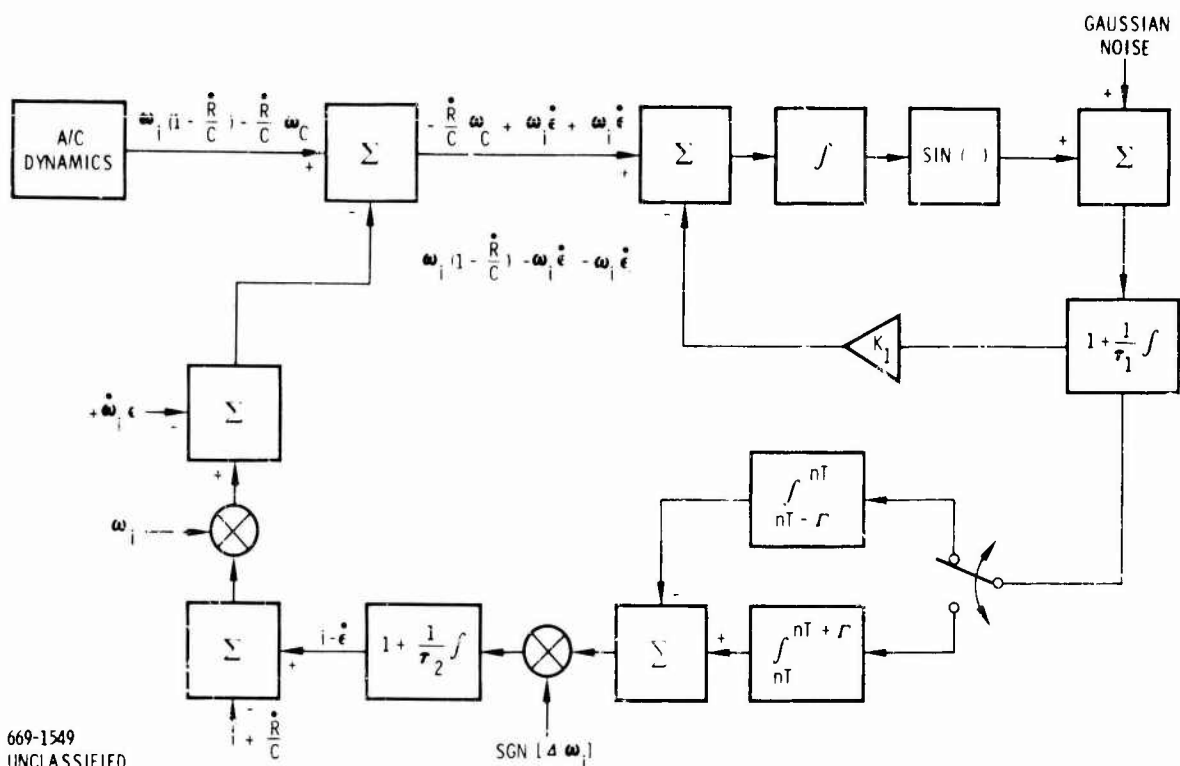
Figure 7-97. Signal Processor Simulation Model

$$-\omega_c \left(\frac{\dot{R}}{C}\right) + \omega_i \dot{\epsilon} + \dot{\omega}_i \epsilon \tag{281}$$

provided an integration is performed inside the loop as shown in Figure 7-97. Of course this same integration simultaneously satisfies the VCO phase transfer function so that the familiar 1/s block does not appear in the feedback path of the phase locked loop.

7.6.4.4 Computation Model

The model consists of four routines. The first of these is a generalized input routine in which the analyst is queried as to the initialization parameters, (loop constants, velocity, and range uncertainty and carrier-to-noise ratio). Upon input of these values an initialization routine is called which defines all other operational initial conditions. The third routine (distance) has two functions. The first of these is to compute the interceptor's range to the transmitter while accelerating through

-425-

high g maneuvers. The second function is to compute the random frequency hopping pattern. This routine is called every 32 milliseconds, which is consistent with the hopping rate.

The fourth routine (loop) performs the bulk of the simulation. The sampling rate was chosen as 1 sample/millisecond. Thus, every millisecond a normal deviate of noise and a new ϵ (range error) is computed. Being that the aircraft has a velocity of 3000 feet/second the maximum range differential between aircraft and observer in one millisecond is three feet. Flow diagrams of the distance routine and the loop routine are shown in Figures 7-98 and 7-99, respectively.

7.6.4.5 Simulation Results

A typical simulation printout is shown in Figure 7-100. Note that the clock rate is in milliseconds and that the various parameters have been scaled by a factor of 10^{-3}. For the first 320 milliseconds the results are printed every 32 milliseconds. Thereafter they are presented every 320 milliseconds. The second and third columns give the mean and standard deviation of the range error in feet. The fourth and fifth columns give the mean and standard deviation of phase error in the carrier tracking loop expressed in cycles at the carrier frequency.

For the particular run shown in Figure 7-100 with the parameters as listed we observe that the precision range tracking loop has fully acquired in approximately 2.5 seconds after which the range estimate exhibits a standard deviation of about 2-1/2 feet. After about 1-1/2 seconds the carrier tracking loop becomes extremely stable and exhibits a standard deviation of about .01 cycles due to noise. Thus, by cycle counting for 1/2 second the frequency of the incoming signal may be determined to -.14 cycles out of 1500 MHz which corresponds to the Doppler shift due to a velocity of approximately .01 fps.

In Figure 7-101 is shown the upper limits on the initial values of range and range rate errors for which the range tracking loop will acquire. The acquisition profile for the worst case initial conditions is illustrated in Figure 7-102.

Figure 7-103 represents the average error characteristic of the precision range tracking loop. The curve was generated by computing the statistical quantity
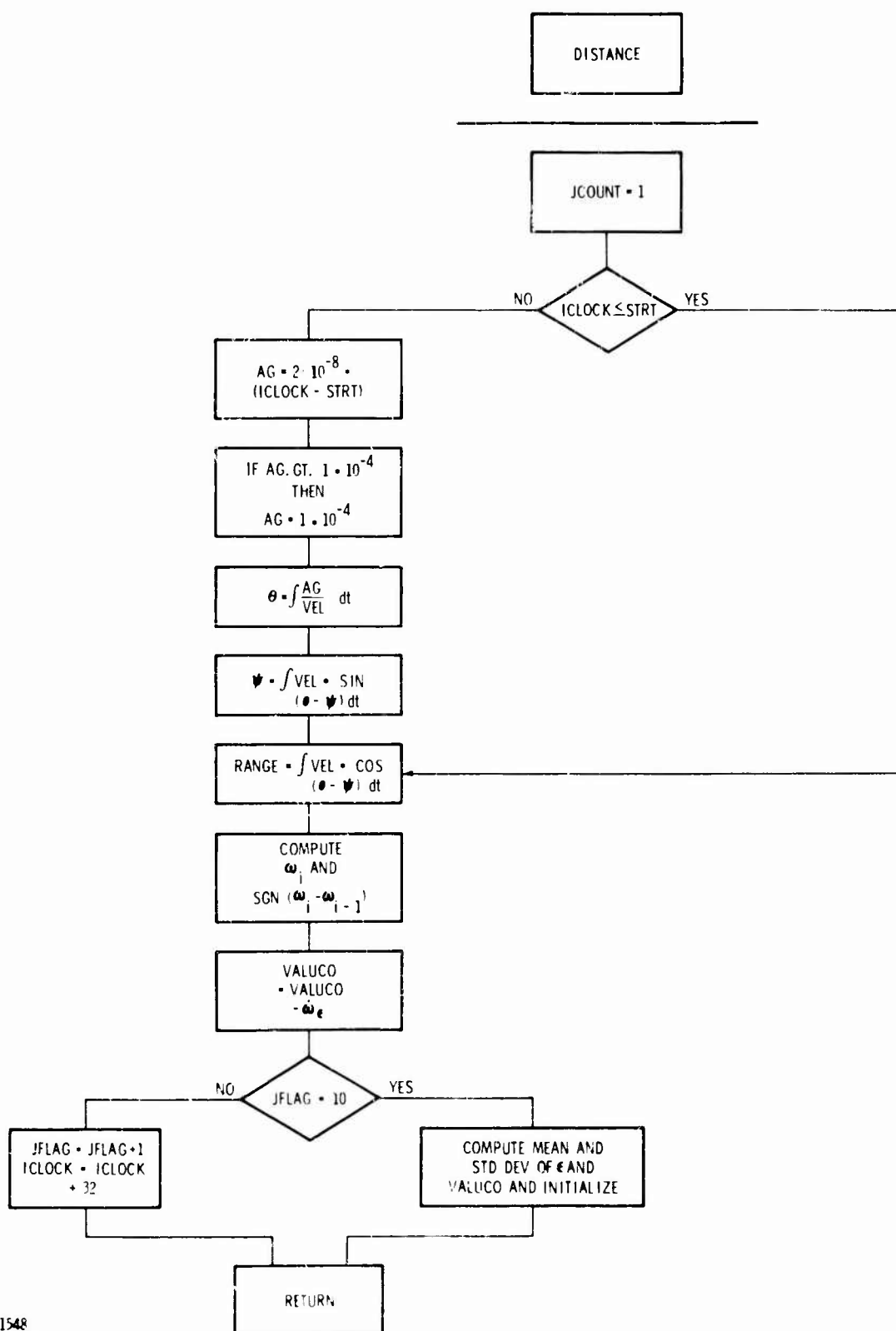
Figure 7-98. Distance Routine

Figure 7-99. Loop Routine

```
PRESENT VALUES OF TAU1 AND TAU3 ARE      .2100 .0075
NEW VALUES OF TAU1 AND TAU3              .2100,.0075,
PRESENT VALUES OF GAIN1 AND GAIN3 ARE    .470  .005-
NEW VALUES OF GAIN1 AND GAIN3            .470, .005-05,
PRESENT VALUE  OF EPSIL   AND PROP T ARE .0001 -.     ,
NEW VALUES OF EPSILON AND PROPT          .00000,-.1   -  ,
PRESENT SAMPLE TO NOISE RATIO  IS  5.000.0
NEW SAMPLE TO NOISE RATIO          5.000.0,
```

	0		.00000	
7	-00		.00400	
3	-05			
00	-107			
100	-137			
1 0	-1 3		.0017 0	
1 0	-250			
00	-001		-. 0 0	
00	-0 0		.00 0 0	
	-000		. 7 0	
5	-304		1.0 0 0	
5 0	-197	24	.5250 0	
40	-242	22	.5045	. 1.
0 0	-1 3	1	-.02107	. 7
1 00	-001	24	-3.5 0017	1.1
1600	-73	5	-4.7	.
1 0	20	3	-5.001	.
00 0	-9	5	-5.0	. 11 .
0 0	1	5	-5.000745	.
0 0	0	2	-4. 71	.
0 0	0	2	-4. 017	.
7 0	0	1	-5.501	.
0 0	0	0	-4.	. 7
41	-1	1	-4.0	. 1 7
	0	1	-4.	. 1
	1	0	-5. 11	. 7

```
I  0  TIME TYPE1,T  INITIALIZE PARAMET R  TY   2
NE  PA       TYPE 3, AND T  ST P TYPE 4
```

NOT REPRODUCIBLE

Figure 7-100. Simulation Output

$|\Delta\omega|_\epsilon$ as a function of the timing error ϵ. The characteristic is an odd function of ϵ and for convenience only values for positive ϵ were plotted.

This curve provides an intuitive basis for a superficial understanding of the loop dynamics. For example, the parameters chosen for the simulation model, the

-429-
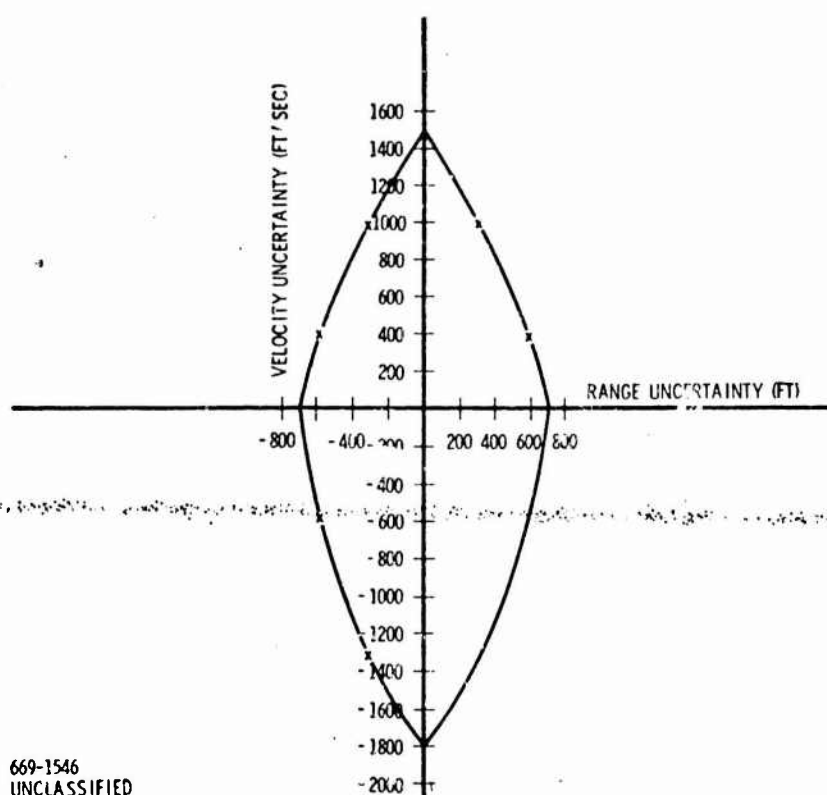
669-1546
UNCLASSIFIED

Figure 7-101. Acquisition Boundary
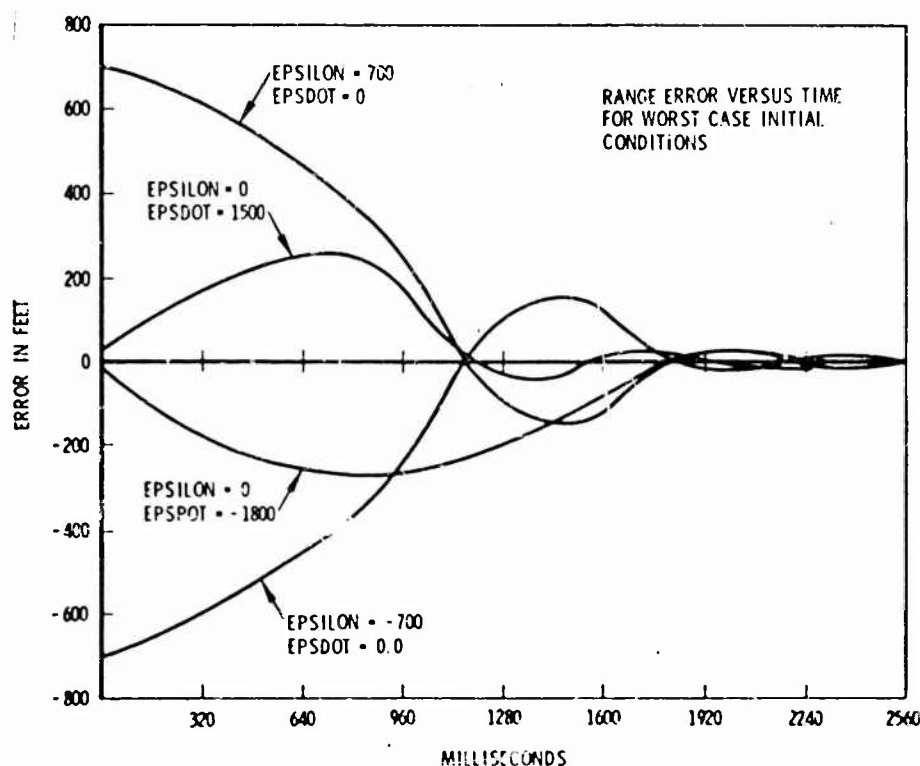
669-1545
UNCLASSIFIED

Figure 7-102. Acquisition Time Versus Range Error

-430-
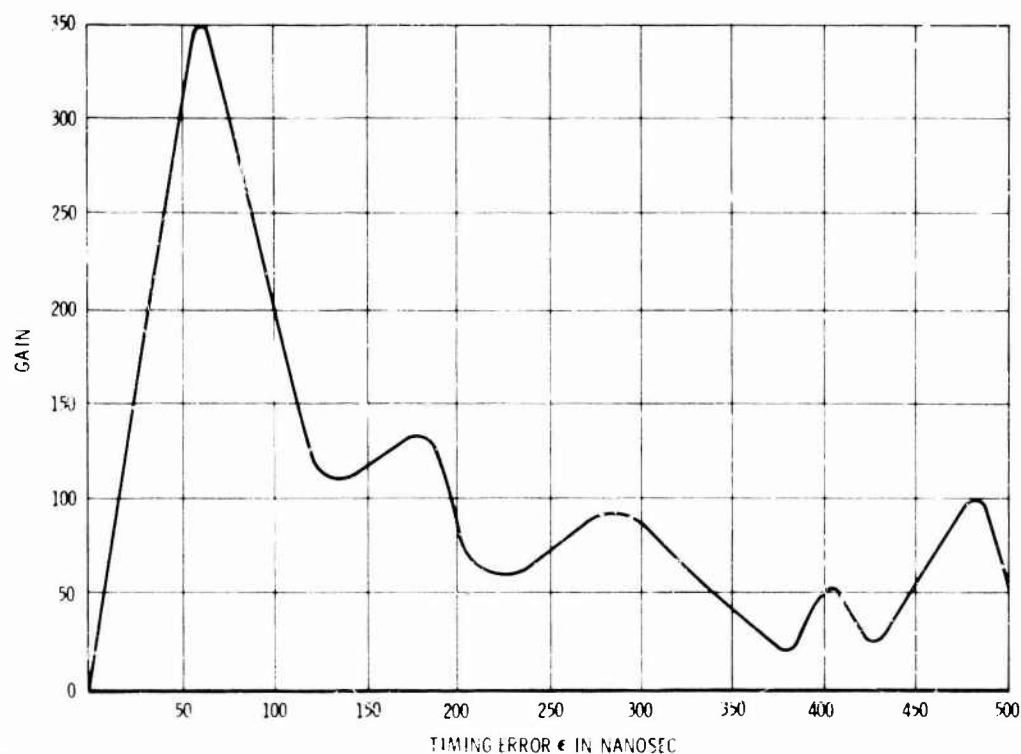
Figure 7-103. Error Characteristic of Precision Ranging Loop

basic tracking aperture is of the order of ± 60 nanoseconds. In addition, if the timing error is in excess of 150 nanoseconds the low value of gain will make acquisition unlikely without an external assist. It is for this reason that we insist on PN acquisition as an a priori condition for the large tracking loop to acquire.

Of course, the error characteristic is periodic with period equal to that of the lowest frequency tone in use. The ripple appearing on the curve for $\epsilon > 100$ nanoseconds is a consequence of the multiple frequency tones.

7.6.5 RANGE RATE MEASUREMENT

The two basic techniques by which range rate may be measured are differentiation of range and counting doppler frequency cycles of the received carrier. The differentiation technique, whereby range rate is given by

$$\dot{R} = \frac{\Delta R}{\Delta t} = \frac{R(t_2) - R(t_1)}{t_2 - t_1} \tag{2-2}$$

-431-

is limited in accuracy by the range measurement accuracy, as discussed previously. Thus, if the range measurement accuracy is σ_R (rms error), the range rate accuracy is

$$\sigma_R^{\cdot} = \sqrt{2} \ \frac{\sigma_R}{\Delta T} \tag{283}$$

For the case of range rate difference measurements, the rms error is $\sqrt{2}$ times larger. This technique is suitable when relatively low range rate measurement accuracy is required. For accuracies on the order of tenths of a foot per second rms, the doppler cycle count technique is more suitable. This technique allows range rate to be measured independently of the range measurement, and the range measurement interval, Δt.

The first fundamental accuracy limitation which must be considered for this technique is the carrier track loop frequency tracking error or phase jitter. If a 621B nominal power budget is considered to apply, i.e., $S/N_o \approx 36$ db, loop noise bandwidth ≈ 100 Hz, the carrier track loop operates as a linear device and the rms frequency tracking error is given by

$$\sigma = \frac{1}{2\pi} \ \frac{1}{\sqrt{2 \ S/N_o \ B_L}} \tag{284}$$

where

N_o = one sided noise density
B_L = one sided noise bandwidth
S = average signal power

Since the actual measurement is a difference measurement between two independent sources, the rms difference error is $\sqrt{2}$ times the error for one loop. For the typical 621B carrier tracking loop parameters, $S/N_o = 36$ db, $B_L = 100$ Hz, the rms frequency error is 008 Hz. A .008 Hz error is insignificant compared to the typical .1 Hz desired error. Thus the major contribution to error will be round off error in the frequency counter. The error in frequency contained in the representation in the counter for each of the two independent sources is uniformly distributed between ± 1 count as shown in Figure 7-104.

The probability distribution for the difference count is found from probability theory to be given by

-432-

$$p(\Delta f) = \int_{-\infty}^{\infty} p(\Delta f - f_2) \, p(-f_2) d f_2 \qquad (285)$$

where

$$\Delta f = f_2 - f_1$$
$$f_1 = \text{start count}$$
$$f_2 = \text{stop count}$$

The distribution $p(\Delta f)$ for the difference count is shown in Figure 7-104. The rms difference error is found to be

$$\sigma_{\Delta f} = \left[\int_{-\infty}^{\infty} \Delta f^2 \, p(\Delta f) \, d\Delta f \right]^{1/2}$$

$$= \left[\int_{-2}^{0} \Delta f^2 \left[\frac{\Delta f}{4} + \frac{1}{2} \right] d\Delta f + \int_{0}^{2} \Delta f^2 \left[-\frac{\Delta f}{4} + \frac{1}{2} \right] d\Delta f \right]^{1/2}$$

$$= .8 \text{ count.} \qquad (286)$$

Since it is desirable that the counting error is not greater than 10% of the typical desired accuracy of .1 Hz, each count should represent .01 Hz. Since all zero crossing can be employed, frequency multiplication by a factor of 50 will produce the desired accuracy within a one second measurement interval.
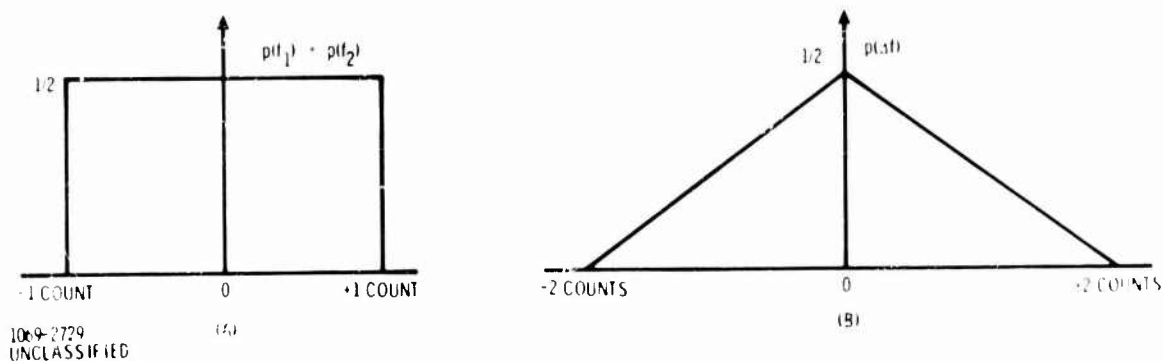
Figure 7-104. Probability Distribution for Start and Stop Count (A) and Probability Distribution for Difference Count, Δf (B)

The preceding discussion assumes that in the case of FH/PN, the receiver local oscillator hops in synchronism with the received signal hop. Non-coherent hopping may be used if the hopping rate is slow enough that the doppler count may be initiated and completed while the system is dwelling on a single frequency slot and that enough time is allotted at the beginning of that frequency slot to allow transients in the carrier loop to die out. The time required for the carrier loop to lock up and settle out at each hop is dependent on the received E/N_o and the loop bandwidth. On the other hand, if coherent hopping is utilized, the doppler measurement procedure is not subject to these restrictions.

** 7.7 (C) NAVIGATION ERROR ANALYSIS

(U) This section presents the results of efforts directed at evaluating the geometrical errors associated with hyperbolic navigation. The error analysis is broken down into separate parts for (1) the enroute case and (2) the terminal landing case. The objectives of the two parts may be summarized as follows:

1. Navigation Error Analysis for Enroute Case

Using the results of the Hughes and TRW 621B (NAVSAT) study programs as a starting point, generate a series of aircraft position and velocity accuracy plots in the required coverage regions for various values of electronic instrumentation accuracy. The 4-satellite range difference position location and range rate difference velocity determination approach as well as the coverage regions considered in the 621B studies will be assumed. The term electronic instrumentation accuracy refers to the range difference and range rate difference measurement accuracies.

2. Navigation Error Analysis for Terminal Landing

Using the results of a document containing landing requirements as a starting point, generate a series of aircraft position and velocity accuracy plots in the required coverage regions for various values of electronic instrumentation accuracy. The range difference position location and range rate difference velocity determination approach will be studied first. For the landing case suitably placed ground terminals in the landing area play the role of the satellites in the enroute case. If the measurement accuracies required to give the needed position and velocity accuracies are too stringent, then a beam-rider type approach is appropriate.

** 7.7.1 (C) NAVIGATION CONSIDERATIONS FOR ENROUTE CASE

(U) This section presents the error analysis for the enroute navigation case, and begins with a description of the 621B parameters that are assumed. The majority of this description was adapted from the Hughes efforts[*] since they appear to be more comprehensive and directly applicable to the CNI program. The parameters presented include those associated with

---

[*] Hughes Aircraft Co. (Space Systems Division); System 621B, Satellite System for Precise Navigation: Final Report SAMST-TR-69-4 (Parts I and II); January 1969.

**Subsections 7.7.1.1 and 7.7.1.2, comprising Volume III, contain the only classified material in Section 7.7 and in this report as a whole.

(1) Satellite geometry.

(2) Satellite orbit determination and satellite-user range
     and range rate measurement methodology.

(3) Modulation.

(4) Frequency selection and power levels.

(5) Types of users and their equipment characteristics.

(6) User position and velocity determination from measured
     range and range rate differences,

(U) The second part of this section presents the aircraft position and velocity accuracy
curves for the parameters in the 621B system which are applicable to a CNI system.

Subsections 7.7.1.1 and 7.7.1.2 , Confidential, have been removed from
Volume II and printed separately as Volume III of this report.

(Pages 437 through 448 deleted, removed to Volume III)

7.7.2 NAVIGATION CONSIDERATIONS FOR THE LANDING MODE

This section presents the efforts conducted relative to hyperbolic navigation in the landing mode of CNI. The material is divided into three parts:

1. Requirements analysis for terminal approach and landing guidance.

2. Derivation of position coordinates of an aircraft for two landing system configurations (the three ground station case where position is determined by using two range differences and aircraft altitude and the four ground station case where position is determined by using three range differences).

3. Summary of required error analysis efforts for the three and four ground station cases.

4. Conflict prediction considerations for aircraft in terminal areas.

7.7.2.1 Accuracy Requirements for Terminal Area Approach and Landing Guidance System

The purpose of this section is to synthesize a set of technical requirements for the terminal area approach and landing guidance system. The published documentation of RTCA Special Committee 117 will be used as a guide. The documentation reviewed included:

1. RTCA Paper 10-69-SC117-6, Tentative Operational Requirements for a New Guidance System for Approach and Landing, January 27, 1969.

2. RTCA Paper 23-69/SC117-47, Tentative Technical Requirements, January 22, 1969.

3. RTCA Paper 24-69/SC117-18, Request for Landing Aid System Concept Descriptions, January 31, 1969.

Following this introductory section, a discussion of operational guidance requirements is given. Subsequently, a set of technical requirements deemed necessary to achieve the operational requirements is presented. The final section provides a preliminary postulated requirements model which will be used for the design of the terminal area approach and landing guidance system. These requirements will be refined and extended as a better understanding of the terminal area problem is developed.

7.7.2.1.1 Operational Requirements

Operational requirements are broken down into five categories:

1. Characteristics of airports at which guidance service must be provided

2. Characteristics of aircraft for which guidance service must be provided

3. Characteristics of approach and landing paths for which guidance service must be provided

4. Particular types of guidance service which must be provided at airports in 1, for aircraft in 2, and for approach and landing paths in 3

5. General miscellaneous requirements.

These are now discussed

7.7.2.1.1.1 Airport Characteristics

1. To meet the growth in the numbers and variety of aircraft operations, the following airport changes are anticipated:

    a. Greater number of parallel and other non-crossing runways

    b. Greater number of special purpose runways and operational areas (for V/STOL aircraft, etc.)

    c. Intensified simultaneous use of runways and special purpose operational areas for takeoffs and landings

    d. Additional reliance on special purpose airports.

    In spite of these changes, a mix of different types of aircraft on many runways is anticipated in the future.

2. The approach and landing guidance system shall not impose limitations on traffic handling capacity.

3. The approach and landing system shall be adaptable to operations and growth patterns at small and intermediate airports, in high density terminal areas, and at military aviation locations.

4. The system must be capable of serving a large range of runway and landing areas and system operation must not be adversely

influenced by airport plant facilities (buildings, runway surfaces, etc.). The types of runways to be considered are:

a. Single runways

b. Crossed multiple runways

c. Parallel runways

d. Uncrossed multiple runways

e. Special purpose landing areas (for V/STOL airciraft, etc.)

d. Combinations of a through e

5. The dimensions of runways or landing areas fall into two categories:

a. Landing areas for helicopters and VTOL

b. 50' by 1500' to 200' by 14,000' runways for V/STOL's and conventional aircraft

7.7.2.1.1.2 Aircraft Characteristics

1. The approach and landing system shall not impose any constraints on participating aircraft.

2. The system performance shall not be affected by propulsion system characteristics.

3. The following classes of aircraft are to be serviced by the system:

a. CLASS I (includes reciprocating engine, turbo-prop, and turbo-jet conventional aircraft)
   - final approach speeds: 60-100 KIAS (knots indicated air speed)
   - descent angle range: 2° to 9°

b. CLASS II
   - final approach speed: 101-135 KIAS
   - descent angle: 2° to 9°

c. CLASS III
   - final approach speed: 136-165 KIAS
   - descent angle range: 2° to 6°

d. CLASS IV
   - final approach speeds: ≥ 166 KIAS
   - descent angle range: 2° to 2.5^o

e. CLASS V (includes helicopter and V/STOL aircraft)
   - final approach angles: 0° to 30°

All descent angle ranges have been optimized for the variety of user aircraft in each class.

7.7.2.1.1.3 Approach and Landing Path Characteristics:

1. The approach path coverages to be specified are intended to accommodate all classes of aircraft and their operating conditions, and the guidance service is to be available everywhere in the coverage region.

2. Horizontal Track Coverage - Service shall be provided out to 20 nmi* from and with 360° coverage around the touchdown area.

3. Horizontal Profiles - Service shall be provided for:

   a. Straight line tracks on the extended runway center line
   b. Other linear tracks (constant angle and multiple angle linear segment relative to runway center line)
   c. Curved tracks (circular - S-shaped, etc.)
   d. Combinations of a, b, and c (i.e., service for multiple aircraft using runway)

4. Vertical Path Coverage - Service shall be provided in the region shown in Figure 7-112.

5. Vertical Profiles - Service shall be provided for:

   a. Constant approach angle paths with and without flare near touchdown
   b. Multiple approach angle paths with and without flare
   c. combinations of a and b (i.e., service for multiple aircraft using same runway)

6. Service shall also be provided for missed approach and climb out as well as roll-out path coverage.

---

* Less range (on the order of 10 nmi) may be acceptable for special operations such as V/STOL aircraft approach and landing.

-452-
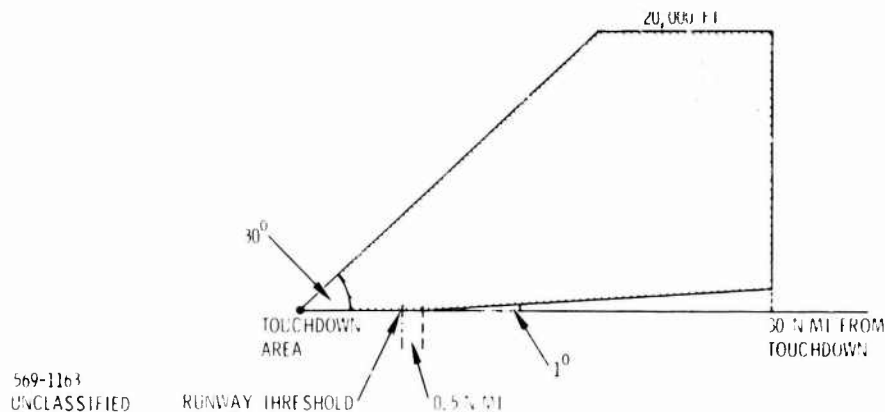
Figure 7-112. Vertical Path Coverage.

7.7.2.1.1.4 Particular Types of Guidance Service

The following classes of guidance service are required. These classes are listed in the order of increasing stringency:

1. Lateral approach guidance down to 150' altitude on a single straight path representing the extended centerline of the landing surface (i.e., proportional deviation from path guidance near path center along with coarse left/right information within at least $\pm 20^\circ$ of the approach path); distance information prior to touchdown optional

2. Lateral approach guidance down to 150' altitude on a single straight path representing the extended centerline of the landing surface: vertical approach guidance down to 150' altitude (i.e., proportional deviation from path guidance near the path's center along with coarse up/down information within vertical path profile defined in Section 7.7.2.1.1.3); distance information prior to touchdown

3. Lateral approach guidance down to 50' altitude (i.e., same lateral service as in 1 and 2 except extended down to 50'); vertical approach guidance down to 50' (i.e., same vertical service as in 2 except extended down to 50'); distance information prior to touchdown

4. Lateral position information, in a sector of at least $\pm 40^\circ$, measured with respect to the touchdown area, about the extended centerline of the landing area (i.e., proportional deviation from path guidance in

-453-

$\pm 40^\circ$ sector) down through touchdown and roll-out (to permit fully automatic landing); vertical position information down through touchdown (i.e., proportional deviation-from-path guidance for vertical profiles defined in Section 7.7.2.1.1.3); distance information above as well as additional information with sufficient accuracy to assess roll-out distance remaining and information for start of turn-off after roll-out; missed approach guidance (lateral and vertical guidance as above but applying to departure and extending up to 5000' altitude)

5. Lateral position information, in a $\pm 90^\circ$ sector, measured with respect to the touchdown area, about the extended centerline of the landing area (i.e., same lateral service as in 4 but extended to a $\pm 90^\circ$ sector) down through touchdown and roll-out; vertical position information through touchdown; distance and missed guidance information described in 4; obstacle warning service defining minimum safe gradient in approach and missed approach areas. (This is the maximum system capability required to provide all needed services.)

7.7.2.1.1.5 General Requirements

1. The above operational requirements have not been tempered by technical feasibility or cost considerations.

2. One system is envisioned to provide all the various classes of guidance service presented in Section 7.7.2.1.1.4.

3. The system shall operate in arctic, tropical, and jungle terrains. The "typical" bad glide slope configuration which is to be used in the system design is shown in Figure 7-113.

4. Rapid simple installation with easily transportable ground units is necessary.

5. System services must not be deteriorated by such influences as near-and-far field terrain effects, airport structures, ground vehicles, and aircraft in air or ground.

6. System services must be available under any weather conditions in which aircraft operations are feasible from an aerodynamic
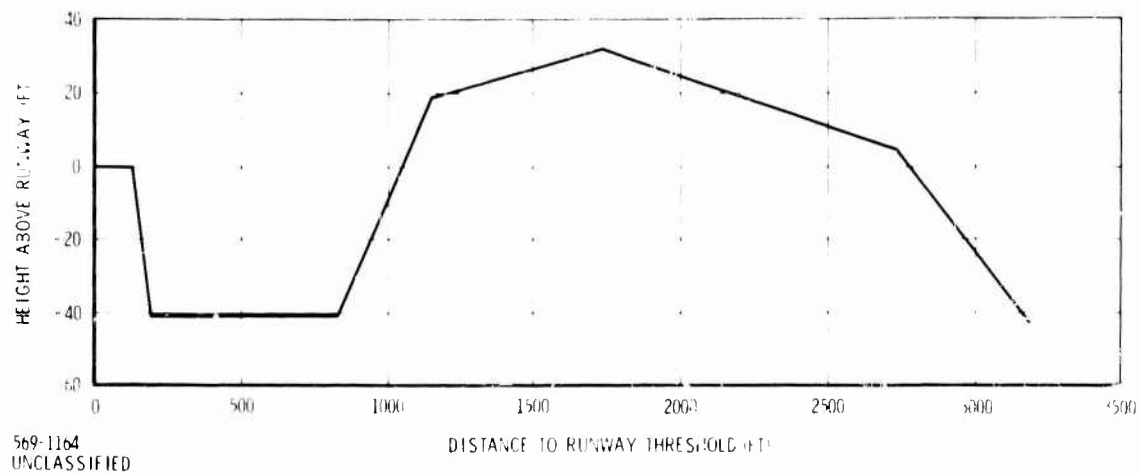
Figure 7-113. Typical "Bad" Glide Slope.

viewpoint. However, the system should not be burdened with rain penetration requirements encountered only rarely or in limited geographical regions.

7. All ground elements should be located on airport real estate.

8. System performance must not be degraded by interfering signals.

7.7.2.1.2 Technical Requirements

RTCA SC-117 has synthesized a set of tentative technical requirements to achieve the operational requirements discussed in Section 7.7.2.1.1. Table 7-21 is a summary of those technical requirements. For each of the particular types of guidance service discussed in Section 7.7.2.1.1.4, a set of tentative requirements is given which is deemed necessary to provide that guidance service.

7.7.2.1.3 Preliminary Postulated Requirements Model for Design of Terminal Area Approach and Landing Guidance System

To execute concept synthesis and detailed system design of the terminal area approach and landing guidance system efficiently, it is necessary to reduce the plethora of operational and technical requirements of Sections 7.7.2.1.1 and 7.7.2.1.2 to a manageable level. It is implicitly assumed that the system must meet the most stringent set of requirements since one system is required to handle the various classes

-455-

Table 7-21. Minimum Performance Requirements

Guidance Requirements		Type of Guidance Service Described in Section				
		2.4 a. i)	2.4 a. ii)	2.4 a. iii)	2.4 a. iv)	2.4 a. v)
Azimuth Accuracy*	Maximum allowable bias relative to true unknown azimuth	$\pm$ 50'	$\pm$ 50'	$\pm$ 32'	$\pm$ 10'	$\pm$ 10'
	Maximum allowable random error (2σ)	26'	26'	11'	9'	9'
Elevation Accuracy*	Maximum allowable bias relative to true unknown elevation	NA	$\pm$ 6'	$\pm$ 1.2'	$\pm$ 1.2'	$\pm$ 1.2'
	Maximum allowable random error (2σ)	NA	7'	1.4'	1.4'	1.4'
Distance Accuracy	Maximum allowable bias relative to true distance	$\pm$ 300'	$\pm$ 100'	$\pm$ 20'	$\pm$ 20'	$\pm$ 20'
	Maximum allowable random error (1σ)	150'	50'	10'	10'	10'
System Capacity (Number of aircraft)		15	15	50	50	50

* These accuracies apply in the coverage region where precise proportional
deviation from path guidance is required.

-456-

of guidance service. A summary of the pertinent requirements for the most stringent class of service required is as follows:

Maximum Allowable Azimuth Bias Error   – $\pm 10'$

Maximum Allowable Azimuth Random Error   – (2σ) $9'$

Maximum Allowable Elevation Bias Error   – $\pm 1.2'$

Maximum Allowable Elevation Random Erro   – (2σ) $1.4'$

Maximum Allowable Distance Bias Error   – $\pm 20'$

Maximum Allowable Distance Random Error   – (1σ) $10'$

System Capacity – 50 aircraft

Coverage Region –

     Horizontal (out to 30 nmi from and with 360° coverage around the touchdown area)

     Vertical – See Figure 7-112.

7.7.2.2 Derviation of Aircraft Position Coordinates for the Three Range Difference and Two Range Difference Plus Altitude Landing System Configurations

This section describes the detailed derivation of the position coordinates for an aircraft for each of the two landing system configurations under investigation:

1.   The three ground station case where position is determined by using two range differences and aircraft altitude.

2.   The four ground station case where position is determined by employing three range differences.

The position coordinates are presented in terms of distance from touchdown. elevation angle above touchdown, and azimuth angle with respect to the extended centerline of the runway. The coordinate system is illustrated in Figure 7-114.

The position coordinates are presented strictly as functions of aircraft altitude, the range differences, and the locations of the individual ground stations. In this form, the desired error analysis can be performed. The objective of the error analysis is to determine – for the given azimuth, elevation, and distance accuracies specified in the preceding section – the maximum allowable range difference errors. The specified accuracies on azimuth, elevation, and distance apply everywhere in the coverage region defined in the aforementioned section. The analysis involves variation of station

d = DISTANCE TO TOUCHDOWN
θ = AZIMUTH ANGLE WITH RESPECT
    TO EXTENDED RUNWAY CENTERLINE
φ = ELEVATION ANGLE ABOVE
    TOUCHDOWN PLANE

669-1531
UNCLASSIFIED
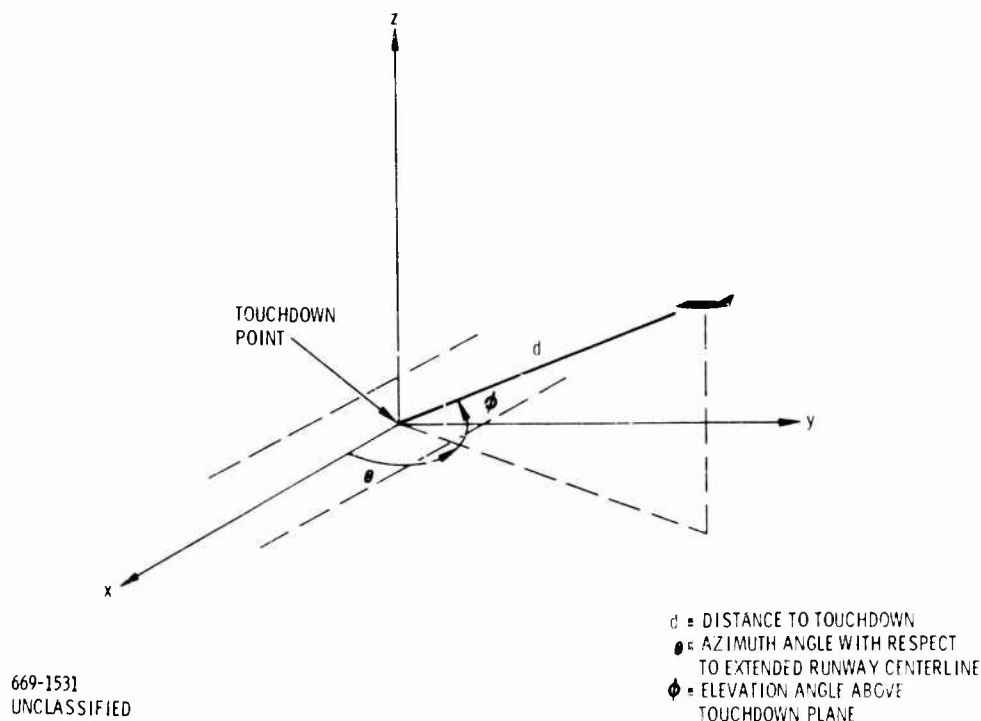
Figure 7-114. Coordinate System for Landing.

geometries to determine that station geometry yielding the maximum allowable range
difference errors.

7.7.2.2.1 Derivation of Aircraft Position for the Two Range Difference
         and Altitude Landing System Configuration

Figure 7-115 depicts the geometry under consideration for the position deter-
mination of the aircraft, where

r_1 = aircraft-station #1 range

d_1 = range difference between station #1 and aircraft
       and station #2 and aircraft

d_2 = range difference between station #1 and aircraft
       and station #3 and aircraft.

The station designated as station #1 is the one common to both range difference
measurements.

-458-
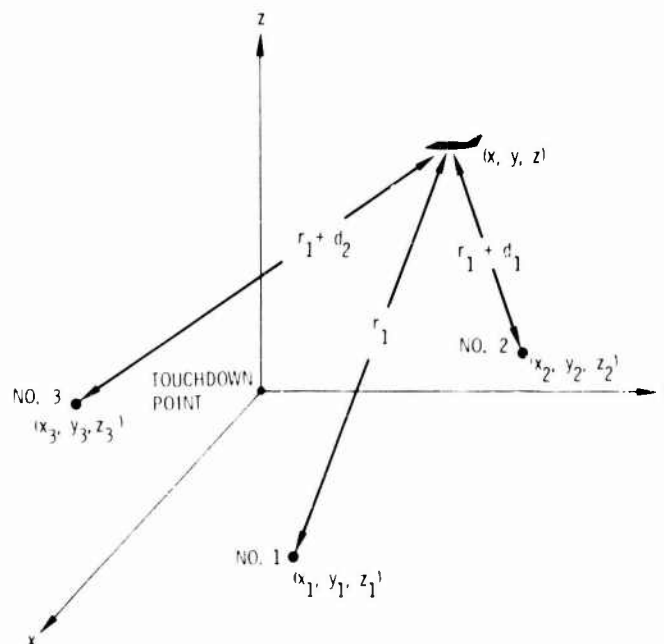
Figure 7-115. Position Geometry for Two-Range Difference
and Altitude Measurement.

Appendix VI contains the detailed derivation of the equations yielding aircraft
position in terms of two range differences and aircraft altitude.

7.7.2.2.2 Derivation of Aircraft Position for the Three Range Difference
System Configuration

Consider Figure 7-116 which is pertinent to the analysis of the three range
difference system configuration, where

r_1 = aircraft range to the master station (called station #1)

d_1 = range difference between station #1 and aircraft
and station #2 and aircraft

d_2 = range difference between station #1 and aircraft
and station #3 and aircraft

d_3 = range difference between station #1 and aircraft
and station #4 and aircraft

Appendix VII gives the derivation of aircraft position from three range difference
measurements.

669-1533
UNCLASSIFIED
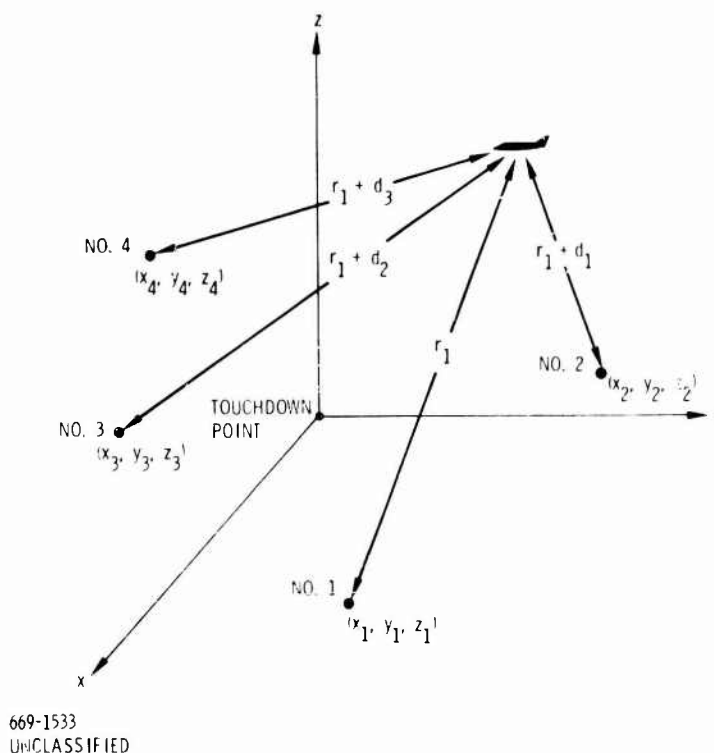
Figure 7-116. Position Geometry of Three Range
Difference Measurement.

7.7.2.3 Error Analysis Efforts on the Three and Four Ground Station Landing System Configurations

The analytical portion of a complete error analysis was conducted for the three and four ground station cases. The objective of the overall (analytical and computer portions) error analysis is to determine, for the given azimuth, elevation, and distance accuracies specified in Section 7.7.2.1, the maximum allowable range difference errors. The specified accuracies on azimuth, elevation, and distance apply everywhere in the coverage region defined. The computer portion of the analysis involves variation of station geometries to determine that station geometry yielding the maximum allowable range difference errors.

The output of the analytical portion of the error analysis was extremely complex expressions for:

- 1σ random distance error
- Distance bias errors

- 2σ random elevation error
- Elevation bias error
- 2σ random azimuth error
- Azimuth bias error

The results are functions of <u>aircraft altitude</u>, <u>range differences</u>, and <u>location of individual ground stations</u>. To complete the computer portion of the error analysis, an extensive computer programming effort is required followed by a large number of computer runs to arrive at maximum allowable range differences for various ground station geometries. This effort must be repeated for the three and four ground station cases. This work is beyond the scope of the present program, since the waveform design has emphasized a beam rider landing mode concept (active ranging with az-el beam coding).

7.7.2.4 Conflict Prediction Considerations

7.7.2.4.1 Required Expressions for Conflict Prediction

This sub-section presents the expressions required for prediction of conflicts among nearby aircraft. What is needed, after altitude sorting is accomplished, is a calculation of <u>distance</u> and <u>relative velocity</u> between pairs of aircraft in each sector controlled by ground stations which provide time of arrival information. It is assumed that each aircraft provides altitude information. The sub-section is organized in three parts:

- Calculation of distance between two aircraft;
- Calculation of relative velocity between two aircraft; and
- Calculation of distance and relative velocity between two airc aircraft under the simplifying assumption that the hyper-boloids obtained from range differences are approximated by planes.

1. Calculation of Distance Between Two Aircraft

The following diagram (Figure 7-117) depicts the geometry under consideration for the position determination of one aircraft:
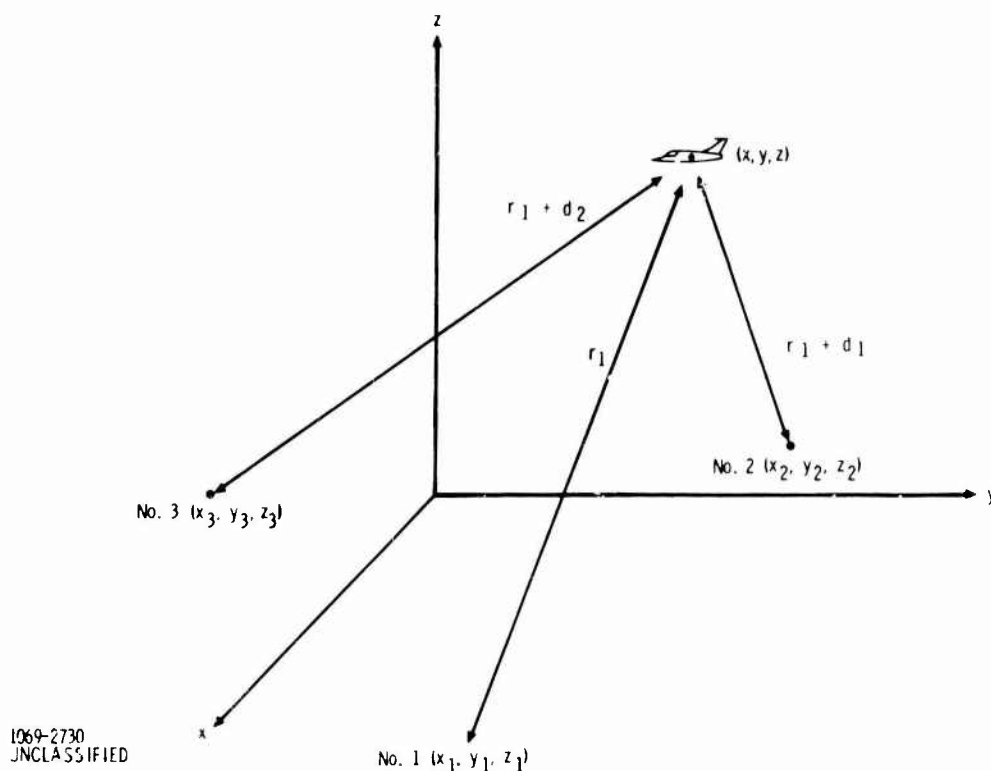
Figure 7-117. Aircraft Position Determination.

where

r_1 = aircraft-station #1 range

d_1 = range difference between station #1 and aircraft and station #2 and aircraft

d_2 = range difference between station #1 and aircraft and station #3 and aircraft

The station designed as station #1 is the one common to both range difference measurements. Calculation of the position of two aircraft permits the determination of distance between two aircraft. The derivation is carried out in Appendix VIII.

2. Calculation of Relative Velocity Between Two Aircraft

In Appendix VIII, the relative velocity along a line connecting two aircraft is derived. In the conflict prediction procedure it is assumed that, after altitude sorting, a distance criteria is employed to determine potential conflicts - that is, $d_{ab} \leq d'$ implies a potential conflict. For those cases such that $d_{ab} \leq d'$ a potential conflict is hypothesized and the next step involves examining relative velocity along a line connecting the aircraft.

-462-

3. Approximation to Conflict Prediction Expressions

For each aircraft we have the following information:

1. Identification (ID) - transmitted by aircraft
2. Altitude (h) - transmitted by aircraft
3. TOA_1 - Time of arrival at sector reporter 1
4. ΔTOA_1 - Difference in time of arrival between one pair of reporters in the sector
5. ΔTOA_2 - Difference in time of arrival between a second pair of reporters in the sector.

We have this information for two different times denoted by subscripts m and n below. Using ΔTOA_1, ΔTOA_2, and h one can derive the position of the aircraft (see Section 1.) and velocity (see above). This information can then be used to determine if a conflict exists. If we assume that the geometry of reporter locations is chosen such that the hyperbolic lines of position (lop) described by the time difference measurements are linear, we may compute the position and velocity of an aircraft in units of lop and lop/second from the raw data. To do this we compute time baseline (Δt) -- in seconds

$$\Delta t \approx \left| TOA_{1_m} - TOA_{1_n} \right|$$

rate of change of altitude (Δh) - in feet

$$\Delta h = h_m - h_n$$

velocity in x_1 direction - in lop/sec

$$v_{x_1} = \frac{(\Delta TOA_{1_m} - \Delta TOA_{1_n})}{\Delta t}$$

velocity in x_2 direction - in lop/sec

$$v_{x_2} = \frac{(\Delta TOA_{2_m} - \Delta TOA_{2_n})}{\Delta t}$$

The current position of the aircraft is $(\Delta TOA_{1_m}, \Delta TOA_{2_m})$ at altitude h_m. Thus for each aircraft we have its position and velocity in three directions and hence may compute relative velocity and distance between aircraft. This is adequate to perform the conflict prediction function.

7.7.2.4.2 Analysis Techniques for Assessment of Accuracy

The purpose of this section is to present analysis techniques which will lead to a realistic assessment of accuracy of distance and relative velocity between two aircraft. Meaningful accuracy information is required to determine conflict prediction performance. The end product is an expresssion for appropriately defined distance and velocity accuracy which is dependent on:

1. The relative geometry of the two aircraft and the reporter stations

2. Survey position errors in reporter stations relative to a surveyed point which serves as a reference for NAMS

3. Random and bias measurement errors in

   a. TOA differences and difference rates

   b. Altitudes and altitude rates of the two aircraft

The accuracy algorithm is developed in a way amenable to numerical analysis by means of a digital computer. Insertion of data regarding the estimated errors in 2. and 3. above will permit the computation of distance and relative velocity accuracy for any relative geometry of reporter stations and aircraft. From these computations accuracy contours can be constructed for various geometries and TOA difference accuracies, thereby providing the rationale for the selection of geometries and TOA difference accuracies which provide desired distance and relative velocity accuracies to meet the conflict prediction performance specifications.

The material in this section is divided into three parts:

1. Development of a meaningful characterization of distance and velocity accuracy

2. Derivation of distance and velocity error equations

3. Derivation of distance and velocity accuracy as a function of system geometry and the statistics of the contributing error sources

1. Characterization of Distance and Velocity Accuracy

The conventional definition of accuracy of distance and velocity is one in which accuracy is specified in terms of the probability of the measured distance and velocity not deviating from the true unknown distance and velocity by more than a certain amount which is called the accuracy. For the application being studied here, a reasonable definition which will be adopted is as follows:

> distance (relative velocity) accuracy of $d(\dot{d})$ meters (meters/sec) is the minimum value of $d(\dot{d})$ such that the probability of the measurement-determined distance (relative velocity) being within $d(\dot{d})$ of the true unknown distance (relative velocity) is 0.95 or greater

The basic problem with this definition and all such probabilistic definitions is that systematic (bias) errors are either neglected or are assumed known and hence removable. In practice, however, bias errors can not be "wished" away; and, in many cases, they are actually the significant contributors to overall distance and velocity error.

Now, an expression is developed for distance (velocity) accuracy. Let the error in distance (velocity) be denoted by $\Delta d_{ab}(\Delta \dot{d}_{ab})$. Thus $d(\dot{d})$ meter (meter/sec) accuracy is given by

$$d(\dot{d}) \text{ meter (meter/sec) accuracy} = \min\, d(\dot{d}) \text{ such that}$$

$$P[\,|\Delta d_{ab}| < d] \geq 0.95 \text{ - distance}$$

$$P[\,|\Delta \dot{d}_{ab}| < \dot{d}] \geq 0.95 \text{ - velocity}$$

where Δd_{ab} and $\Delta \dot{d}_{ab}$ consist of contributions from both random and bias error sources. It is assumed (and will be shown in the last part of this section) that the bias errors, characterized by assignable origin but unknown magnitude, will be modeled as random error sources so that Δd_{ab} and $\Delta \dot{d}_{ab}$ are comprised only of random error contributions and hence are random variables (r.v.'s). The problem therefore is to find

$$\min\, d(\dot{d}) \ni$$

$$P[\,|\Delta d_{ab}| < d] \geq 0.95 \text{ - distance}$$

$$P[\,|\Delta \dot{d}_{ab}| < \dot{d}] \geq 0.95 \text{ - velocity} \tag{287}$$

where Δd_{ab} $(\Delta \dot{d}_{ab})$ is a univariate. Previous studies have always assumed that the univariate has the normal (Gaussian) distribution. However this is a risky assumption even in the absence of bias errors since some error sources are clearly not Gaussian distributed. It will be assumed here that the univariate has an unknown functional form, the only constraint being that a finite second moment exists. Under this assumption the following result is obtained:

$$P[|\Delta d_{ab}| < d_m] \geq 1 - \frac{E(\Delta d_{ab}^2)}{d_m^2} \quad - \quad \text{distance}$$

$$P[|\Delta \dot{d}_{ab}| < \dot{d}_m] \geq 1 - \frac{E(\Delta \dot{d}_{ab}^2)}{\dot{d}_m^2} \quad - \quad \text{velocity}$$

where E is the expected value operator. Thus,

$$P[|\Delta d_{ab}| < d_m] \geq 0.95 \Rightarrow d_m = \sqrt{20} \ [E(\Delta d_{ab}^2)]^{\frac{1}{2}} \quad - \quad \text{distance}$$

$$P[|\Delta \dot{d}_{ab}| < \dot{d}_m] \geq 0.95 \Rightarrow \dot{d}_m = \sqrt{20} \ [E(\Delta \dot{d}_{ab}^2)]^{\frac{1}{2}} \quad - \quad \text{velocity}$$

It is easy to show that $d_m (\dot{d}_m)$ is indeed the minimum value of $d(\dot{d})$ in inequality

This "distribution-free" technique thus yields the result that the least upper bound on distance and velocity accuracy over all possible probability distributions of the univariate is given by $d_m (\dot{d}_m)$. In terms of means and variances we obtain

$$d_m = \sqrt{20} \left(\mu_{\Delta d_{ab}}^2 + \sigma_{\Delta d_{ab}}^2 \right)^{\frac{1}{2}} \quad - \quad \text{distance}$$

$$\dot{d}_m = \sqrt{20} \left(\mu_{\Delta \dot{d}_{ab}}^2 + \sigma_{\Delta \dot{d}_{ab}}^2 \right)^{\frac{1}{2}} \quad - \quad \text{velocity} \quad\quad (288)$$

where μ denotes mean and σ^2 is variance. The least upper bound will be defined as distance (velocity) accuracy when the distribution is unknown and will be called the "distribution-free" accuracy.

The significance of the "distribution-free" accuracy is that it gives a much more realistic evaluation of accuracy since, in general, the distribution of error is unknown. The implications of a possible overestimation of accuracy using the normal assumption are clear.

The method for treating the bias errors is now presented. Assume an error model can be constructed which linearly relates the errors Δd_{ab} and $\Delta \dot{d}_{ab}$ to the various error sources. For example,

$$\Delta d_{ab} = \ldots + a_u u + a_v v + a_w w + \ldots$$

$$\Delta \dot{d}_{ab} = \ldots + b_u u + b_v v + b_w w + \ldots$$

Geometrical effects are manifested by the a's and b's. Using these expressions, it can be demonstrated that the "distribution-free" accuracy is a function of the <u>means</u> and <u>variances</u> of the error sources and the correlation coeffic'ents between them.

The first step in the procedure for including bias errors is to consider each of the system error sources as the sum of a finite number of random and functionally independent systematic components. Let v and w be two of these error sources. Mathematically, v and w can be expressed as

$$v = \sum_{i=1}^{k_1} v_{r_i} + \sum_{j=1}^{k_2} v_{s_j}$$

$$w = \sum_{i=1}^{k_3} w_{r_i} + \sum_{j=1}^{k_4} w_{s_j}$$

where v_{r_i} and w_{r_i} are the ith random components of v and w and v_{s_j} and w_{s_j} are the jth bias components of v and w. The next step is to determine bounds for each v_{s_j} and w_{s_j} based on an assessment of the extremes of their expected variations. Then probability distributions over the bounded intervals are assigned in such a way as to represent the anticipated behavior of the bias components within the bounds. The functionally

independent systematic error components are thus modeled by statistically independent r. v. 's. The mean and variance of v and w and the correlation coefficient between v and w can then be computed and are given by

$$\mu_v = \sum_{j=1}^{k_2} \mu_{v_{s_j}} \; ; \quad \mu_w = \sum_{j=1}^{k_4} \mu_{w_{s_j}} \tag{289a}$$

$$\sigma_v^2 = \sum_{i=1}^{k_1} \sigma_{v_{r_i}}^2 + \sum_{j=1}^{k_2} \sigma_{v_{s_j}}^2 + \sum_{\substack{i=1 \\ i \neq j}}^{k_1} \sum_{j=1}^{k_1} \rho_{v_{r_i} v_{r_j}} \sigma_{v_{r_i}} \sigma_{v_{r_j}} \tag{289b}$$

$$\sigma_w^2 = \sum_{i=1}^{k_3} \sigma_{w_{r_i}}^2 + \sum_{j=1}^{k_4} \sigma_{w_{s_j}}^2 + \sum_{\substack{i=1 \\ i \neq j}}^{k_3} \sum_{j=1}^{k_3} \rho_{w_{r_i} w_{r_j}} \sigma_{w_{r_i}} \sigma_{w_{r_j}} \tag{289c}$$

$$\rho_{vw} = \frac{E(vw) - \mu_v \mu_w}{\sigma_v \sigma_w} \tag{289d}$$

where

$$E(vw) = \sum_{i=1}^{k_1} \sum_{j=1}^{k_3} \rho_{v_{r_i} w_{r_j}} \sigma_{v_{r_i}} \sigma_{w_{r_j}} +$$

$$\sum_{i=1}^{k_2} \sum_{j=1}^{k_4} \rho_{v_{s_i} w_{s_j}} \sigma_{v_{s_i}} \sigma_{w_{s_j}}$$

The notational definitions should be obvious. If, after establishing the bounds and assigning the probability distributions, non-zero means of the systematic components result, they can be subtracted out as a correction.

2. Derivation of Distance and Velocity Error Equations

The error equations are now derived for Δd_{ab} and $\Delta \dot{d}_{ab}$ as a function of system geometry, survey position errors in (x_1, y_1, z_1) (denoted by Δx_i, Δy_i, Δz_i say), errors in TOA (range) differences (denoted by Δd_1, Δd_2 say), errors in TOA (range) rate differences (denoted by $\Delta \dot{d}_1$, $\Delta \dot{d}_2$ say), errors in aircraft altitudes (denoted by Δh_a and Δh_b say), and errors in altitude rates (denoted by $\Delta \dot{h}_a$ and $\Delta \dot{h}_b$ say).

Applying the Taylor series expansion for several independent variables to (16) and (17) in in Appendix VIII yields

$$\Delta d_{ab} \approx \sum_{i=1}^{3} \left(\frac{\partial d_{ab}}{\partial x_i} \Delta x_i + \frac{\partial d_{ab}}{\partial y_i} \Delta y_i + \frac{\partial d_{ab}}{\partial z_i} \Delta z_i \right)$$

$$+ \frac{\partial d_{ab}}{\partial d_{a1}} \Delta d_{a1} + \frac{\partial d_{ab}}{\partial d_{a2}} \Delta d_{a2} + \frac{\partial d_{ab}}{\partial d_{b1}} \Delta d_{b1} + \frac{\partial d_{ab}}{\partial d_{b2}} \Delta d_{b2}$$

$$+ \frac{\partial d_{ab}}{\partial h_a} \Delta h_a + \frac{\partial d_{ab}}{\partial h_b} \Delta h_b \qquad\qquad (290a)$$

$$\Delta \dot{d}_{ab} \approx \sum_{i=1}^{3} \left(\frac{\partial \dot{d}_{ab}}{\partial x_i} \Delta x_i + \frac{\partial \dot{d}_{ab}}{\partial y_i} \Delta y_i + \frac{\partial \dot{d}_{ab}}{\partial z_i} \Delta z_i \right)$$

$$+ \frac{\partial \dot{d}_{ab}}{\partial d_{a1}} \Delta d_{a1} + \frac{\partial \dot{d}_{ab}}{\partial \dot{d}_{a1}} \Delta \dot{d}_{a1} + \frac{\partial \dot{d}_{ab}}{\partial d_{a2}} \Delta d_{a2} + \frac{\partial \dot{d}_{ab}}{\partial \dot{d}_{a2}} \Delta \dot{d}_{a2}$$

$$+ \frac{\partial \dot{d}_{ab}}{\partial d_{b1}} \Delta d_{b1} + \frac{\partial \dot{d}_{ab}}{\partial \dot{d}_{b1}} \Delta \dot{d}_{b1} + \frac{\partial \dot{d}_{ab}}{\partial d_{b2}} \Delta d_{b2}$$

$$+ \frac{\partial \dot{d}_{ab}}{\partial \dot{d}_{b2}} \Delta \dot{d}_{b2} + \frac{\partial \dot{d}_{ab}}{\partial h_{a}} \Delta h_{a} + \frac{\partial \dot{d}_{ab}}{\partial \dot{h}_{a}} \Delta \dot{h}_{a}$$

$$+ \frac{\partial \dot{d}_{ab}}{\partial h_{b}} \Delta h_{b} + \frac{\partial \dot{d}_{ab}}{\partial \dot{h}_{b}} \Delta \dot{h}_{b} \qquad (290b)$$

where the partials are tedious functions of x_i, y_i, z_i, h_a, h_b, $\dot{h}_a$, $\dot{h}_b$, d_{a1}, $\dot{d}_{a1}$, d_{a2}, $\dot{d}_{a2}$, d_{b1}, $\dot{d}_{b1}$, d_{b2}, and $\dot{d}_{b2}$.

3. Derivation of Distance and Velocity Accuracy

In this section distance and velocity accuracy is given as a function of system geometry and the statistics of the contributing error sources.

After applying any mean corrections that arise, accuracy is

$$d_m = \sqrt{20} \; \sigma_{\Delta d_{ab}} \qquad \text{- distance}$$

$$\dot{d}_m = \sqrt{20} \; \sigma_{\Delta \dot{d}_{ab}} \qquad \text{- velocity}$$

Let

$$\eta_1 \equiv \Delta x_1 \qquad\qquad \eta_{11} \equiv \Delta d_{a2}$$

$$\eta_2 \equiv \Delta x_2 \qquad\qquad \eta_{12} \equiv \Delta d_{b1}$$

$$\eta_3 \equiv \Delta x_3 \qquad\qquad \eta_{13} \equiv \Delta d_{b2}$$

$$\eta_4 \equiv \Delta y_1 \qquad\qquad \eta_{14} \equiv \Delta h_a$$

$$\eta_5 \equiv \Delta y_2 \qquad\qquad \eta_{15} \equiv \Delta h_b$$

$$\eta_6 \equiv \Delta y_3 \qquad\qquad \eta_{16} \equiv \Delta \dot{d}_{a1}$$

$$\eta_7 \equiv \Delta z_1 \qquad\qquad \eta_{17} \equiv \Delta \dot{d}_{a2}$$

$$\eta_8 \equiv \Delta z_2 \qquad\qquad \eta_{18} \equiv \Delta \dot{d}_{b1}$$

$$\eta_9 \equiv \Delta z_3 \qquad\qquad \eta_{19} \equiv \Delta \dot{d}_{b2}$$

$$\eta_{10} \equiv \Delta d_{a1} \qquad\qquad \eta_{20} \equiv \Delta h_a$$

$$\eta_{21} \equiv \Delta \dot{h}_b$$

Thus, (289a) and (289b) become

$$\Delta d_{ab} = \sum_{i=1}^{15} a_i \eta_i \qquad\qquad \Delta \dot{d}_{ab} = \sum_{i=1}^{21} b_i \eta_i$$

where a_i and b_i are the partial derivatives. A straightforward exercise in the algebra of expectations yields

$$\sigma^2_{\Delta d_{ab}} = \sum_{i=1}^{15} a_i^2 \sigma_i^2 + \sum_{i=1}^{15}\sum_{\substack{j=1 \\ i \neq j}}^{15} a_i a_j \rho_{ij} \sigma_i \sigma_j$$

$$\sigma^2_{\Delta \dot{d}_{ab}} = \sum_{i=1}^{21} b_i^2 \sigma_i^2 + \sum_{i=1}^{21}\sum_{\substack{j=1 \\ i \neq j}}^{21} b_i b_j \rho_{ij} \sigma_i \sigma_j$$

where σ_i^2 = variance of η_i

$\rho_{ij} \equiv$ correlation coefficient between η_i and η_j

The results in (289b), (289c), (289d) can then be applied to obtain expressions for d_m and $\dot{d}_m$ strictly as a function of system geometry and the statistics of contributing error sources.

7.8 ACCURACY STUDY OF COMBINED INERTIAL NAVIGATION - CNI SYSTEM

This section presents a parametric analysis of the potential advantages of a low-cost, low-accuracy inertial system combined with the CNI system in terms of navigational accuracy. The object is to derive parametric tradeoffs and not to design an optimum interface between the CNI and inertial systems. A representative inertial system with typical inertial system error sources is analyzed to determine the effects on system performance of position fix frequency and fix accuracy over a range of values representative of expected CNI system performance.

This type of combined system represents one of the simplest forms of integrated CNI-inertial navigation systems in that the CNI navigation information is used merely to reset the outputs of the inertial system. There is no attempt at either optimum combination of CNI and inertial system data nor is there any attempt to utilize the error divergence between the two systems to estimate any of the error parameters of either system. The development of these types of more sophisticated systems integration is more properly a part of a systems design effort and depends in part on the particular hardware and configuration chosen for the system.

Nevertheless, the results to be obtained by analysis of the behavior of this simple system's combination are indicative of the expected performance of combined CNI-inertial systems.

7.8.1 INERTIAL NAVIGATION SYSTEM ERROR MODEL

The inertial navigation system error model used in this study is for a locally-level inertial navigation platform with the level axes maintained in a north-east coordinate reference frame. This type of system mechanization, although not the only one possible, is typical of inertial systems utilized in aircraft and provides navigation data (position, velocity and acceleration) in a north-east-vertical coordinate frame, making it readily useable for aircraft navigation and auxiliary calculations.

This type of system has three accelerometers whose inputs are along the north-east, and vertical axes and three gyros whose inputs are with respect to the same axes. For aircraft applications, the inherent instability in the vertical accelerometer channel is controlled by using external altitude information from either a radar or barometric altimeter to damp the vertical channel. As a result, the vertical channel position errors are constrained to errors in the external altitude data source. The primary

-472-

reason for utilizing the vertical accelerometer channel is to provide high-quality vertical velocity information.

An error block diagram of such an inertial navigation system is shown in Figure 7-118. In arriving at the Locally Level Inertial Navigation System Error Block Diagram, several simplifying assumptions have been made. These are:

- The time variable terms and the cross-coupling terms (with the exception of the azimuth misalignment $(\emptyset_z)$ cross coupling terms) have been neglected.

- Error propagation effects which have periods greater than the Schuler period (84 min.) have been neglected.

These simplying assumptions are justified by the fact that typically, these terms and effects are significantly smaller than the error effects modeled, particularly for the relatively short periods of operation (< 2-3 hours or so) of the inertial system for typical aircraft operations of interest.

The inertial navigation system error sources whose effects will be modeled in this study, along with representative values of these error sources, are given in Table 7-22. For typical aircraft inertial navigation systems and operations profiles, these error sources represent the main contributors to inertial navigation system error.

The error propagation effects of each of these error sources is dependent on the particular method of alignment of the system. For example, if the inertial platform is leveled using the level axes accelerometer outputs as the level error signal, then the accelerometer biases result in a correlated level alignment error such that (in a 1 g field) the subsequent error propagation of the accelerometer biases cancels that of the level alignment errors. Similarly, if the east gyro is used to sense the azimuth alignment error of the platform and to correct for it, then while navigating the east gyro drift rate and the azimuth alignment error are correlated.

The particular alignment and calibration techniques to be used for a given inertial navigation system would be determined in a detailed system mechanization design which would depend on the specific hardware and peripheral equipment to be used on the aircraft. This type of design effort is beyond the intent of this study. For

-473-
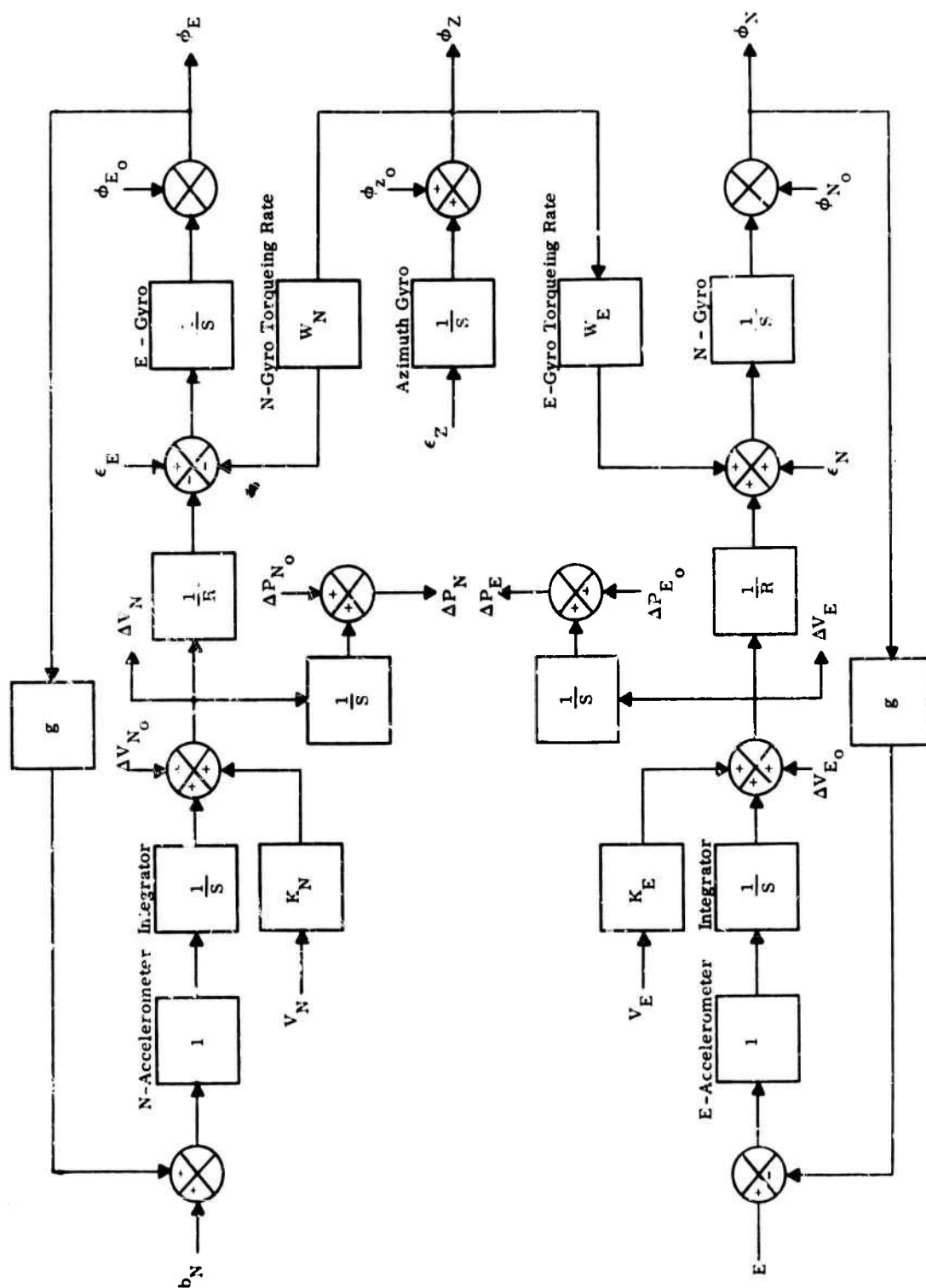
Figure 7-118. Error Block Diagram - Locally Level Inertial Navigation System.

Table 7-22. Representative Inertial Navigation System Error Sources

Error Source	Standard Deviation (1σ)
Accelerometer Bias (b_N, b_E)	67 μg
Accelerometer Scale Factors (K_N, K_E)	400 ppm.
Gyro Drift Rates $(\epsilon_E, \epsilon_N, \epsilon_Z)$	.03 deg/hour
Initial Level Misalignments $(\emptyset_{N_0}, \emptyset_{E_0})$	2 arc-min
Initial Azimuth Misalignments $(\emptyset_{Z_0})$	10 arc-min
Initial Position Error	10-500 ft[*]
Initial Velocity Error	1-10 ft/sec[*]

[*] These initial position and velocity errors are the result of the navigation errors of the CNI system. They will be parametrized over these ranges as part of this study.

the purposes of this study, it is reasonable to assume that the platform is aligned and calibrated using external sources of data. As a result, the error propagation due to each of the above tabulated error sources can be considered as correlated.

Based on the above assumptions, the error propagation equations for a locally-level inertial navigation system can be shown, from the error block diagram, to be given by the equations of Table 7-23. In this table,

ΔP_E = error in east position

ΔP_N = error in north position

ΔV_E = error in east velocity

ΔV_N = error in north velocity

ω_s = Schuler frequency = $\sqrt{g/R}$

g = value of gravity

R = radius of the earth

Ω = earth rotation rate

V_E = east velocity component of aircraft velocity

V_N = north velocity component of aircraft velocity

λ = aircraft latitude

The error propagation equations shown in Table 7-23 represent the inertial navigation system error model being utilized in this parametric study.

Table 7-23. Error Propagation Equations – Locally Level Inertial Navigation System.

Error Source	Symbols	Position Error Propagation	Velocity Error Propagation
East Accelerometer Bias	b_E	$\Delta P_E = \dfrac{b_E}{\omega_s^2}(1 - \cos\omega_s t)$	$\Delta V_E = \dfrac{b_E}{\omega_s}\sin\omega_s t$
North Accelerometer Bias	b_N	$\Delta P_N = \dfrac{b_N}{\omega_s^2}(1 - \cos\omega_s t)$	$\Delta V_N = \dfrac{b_N}{\omega_s}\sin\omega_s t$
East Accelerometer Scale Factor	K_E	$\Delta P_E = K_E\dfrac{V_E}{\omega_s}\sin\omega_s t$	$\Delta V_E = K_E V_E\cos\omega_s t$
North Accelerometer Scale Factor	K_N	$\Delta P_N = \dfrac{V_N}{\omega_s}\sin\omega_s t$	$\Delta V_N = K_N V_N\cos\omega_s t$
East Gyro Drift Rate	ϵ_E	$\Delta P_N = \epsilon_E R(t - \dfrac{1}{\omega_s}\sin\omega_s t)$	$\Delta V_N = \epsilon_E R(1 - \cos\omega_s t)$
North Gyro Drift Rate	ϵ_N	$\Delta P_E = -\epsilon_N R(t - \dfrac{1}{\omega_s}\sin\omega_s t)$	$\Delta V_E = -\epsilon_N R(1 - \cos\omega_s t)$
Azimuth Gyro Drift Rate	ϵ_z	$\Delta P_N = -\epsilon_z(R\Omega\cos\lambda + V_E)\left[\dfrac{t^2}{2} - \dfrac{1}{\omega_s^2}(1 - \cos\omega_s t)\right]$ $\Delta P_E = \epsilon_z V_N\left[\dfrac{t^2}{2} - \dfrac{1}{\omega_s^2}(1 - \cos\omega_s t)\right]$	$\Delta V_N = -\epsilon_z(R\Omega\cos\lambda + V_E)(t - \dfrac{1}{\omega_s}\sin\omega_s t)$ $\Delta V_E = \epsilon_z V_N(t - \dfrac{1}{\omega_s}\sin\omega_s t)$
Initial Level Misalignment (North)	ϕ_{N_0}	$\Delta P_E = -\phi_{N_0} R(1 - \cos\omega_s t)$	$\Delta V_E = -\phi_{N_0}\omega_s R\sin\omega_s t$
Initial Level Misalignment (East)	ϕ_{E_0}	$\Delta P_N = \phi_{E_0} R(1 - \cos\omega_s t)$	$\Delta V_N = \phi_{E_0}\omega_s R\sin\omega_s t$
Initial Azimuth Misalignment	ϕ_{z_0}	$\Delta P_E = \phi_{z_0} V_N(t - \dfrac{1}{\omega_s}\sin\omega_s t)$ $\Delta P_N = -\phi_{z_0}(R\Omega\cos\lambda + V_E)(t - \dfrac{1}{\omega_s}\sin\omega_s t)$	$\Delta V_E = \phi_{z_0} V_N(1 - \cos\omega_s t)$ $\Delta V_N = -\phi_{z_0}(R\Omega\cos\lambda + V_E)(1 - \cos\omega_s t)$
Initial Position Error (North)	ΔP_{N_0}	$\Delta P_N = \Delta P_{N_0}$	---
Initial Position Error (East)	ΔP_{E_0}	$\Delta P_E = \Delta P_{E_0}$	---
Initial Velocity Error (North)	ΔV_{N_0}	$\Delta P_N = \Delta V_{N_0}\dfrac{1}{\omega_s}\sin\omega_s t$	$\Delta V_N = \Delta V_{N_0}\cos\omega_s t$
Initial Velocity Error (East)	ΔV_{E_0}	$\Delta P_E = \Delta V_{E_0}\dfrac{1}{\omega_s}\sin\omega_s t$	$\Delta V_E = \Delta V_{E_0}\cos\omega_s t$

7.8.2 SIMULATION DESCRIPTION

The inertial navigation system error sources which are incorporated into the simulation model are accelerometer bias, accelerometer scale factor, level and azimuth gyro-drift rates, and initial level and azimuth misalignment. In addition, the effect of initialization errors in position and velocity are modeled.

Two methods of updating the inertial navigation system are utilized in this simulation. In one, the discrete position determinations of the CNI equipment is utilized to reset (correct) the position outputs of the inertial system. There is no attempt to utilize CNI-derived velocity data to update the inertial system velocity, and there is no attempt either to optimally combined CNI and inertial system data or to utilize the error buildup between updates to estimate any of the error parameters of the CNI or Inertial Navigation Systems. In the second updating method, both position and velocity data as determined from the CNI equipment is used to update the inertial systems. Again for this update method, no attempt has been made to either optimally combined CNI and inertial navigation data, or to use the divergence between these two systems to attempt to estimate the error parameters of either system.

Thus, the results obtained by use of this simulation are pessimistic, since in an actual system integration of CNI and Inertial Navigation a more sophisticated Kalman filter approach would be used. This would provide an optimal combination of CNI and Inertial Navigation System data and a sequential estimation and correction procedure to estimate the error parameters in the integrated CNI insertial system and correct for them to reduce the error buildup between CNI updates.

7.8.3 RESULTS

The cases considered show the effects of CNI position update accuracy, velocity, initialization, update rate and velocity update accuracy on combined system accuracy, for a given aircraft flight profile and duration. The aircraft flight profile was that of an aircraft flying at approximately 1000 miles an hour and 45 degrees heading at approximately 30 degrees latitude. The flight duration considered was 1 hour.

7.8.3.1 Effects of Position Update Accuracy

In order to determine the effects of position update accuracy on a combined CNI-Inertial Navigation System, simulations were run, using the aircraft flight profile

described above, in which CNI updates to the inertial navigation derived position were assumed to be obtained every 10 minutes. The initial velocity error assumed for the inertial system was 10 feet per second. This number is representative of a poor velocity initialization, such as might be obtained by an in-flight alignment without the use of Doppler radar, CNI-derived velocity or some other such accurate velocity reference. The ten-minute interval between position updates approximates worst case, in that it is anticipated that CNI updates will be available much more frequently. Nevertheless, this serves to show the effects of position update accurate on combined system accuracy.

A range of CNI position accuracies from one foot to 500 feet (1σ) were considered Because the results obtained were so similar, only the two extreme cases; namely, the one for one-foot update errors, and the one for 500-foot update errors are presented.

The results obtained from this case are shown in Figures 7-119 and 7-120. The effects of the position update in resulting position error are apparent from the figures. The velocity error growth is unaffected by the position error reset and, hence, does not show any difference between the one foot update accuracy and the 500-foot update accuracy. The large growth in position error following an update is due primarily to the effects of both the ten-foot-per-second initial velocity errors and the inertial navigation system hardware error sources propagating over the 10-minute intervals between updates. This position error growth tends to make the difference in position reset accuracy insignificant rather quickly following each update.

7.8.3.2 Effects of Initial Velocity Errors

Figures 7-121 and 7-122 present the results of varying the initial velocity error upon the combined system accuracy. These results are the case in which position updates occur every 10 minutes and have an accuracy of 250 feet (1σ). The curves corresponding to the 10 fps initial velocity error are essentially the same as those shown in Figures 7-119 and 7-120. Reducing the velocity initialization error to 0.1 fps from 10 fps has a noticeable effect in reducing both the position and velocity error propagation. This is because the position and velocity error contribution of the initial velocity errors is significantly reduced.
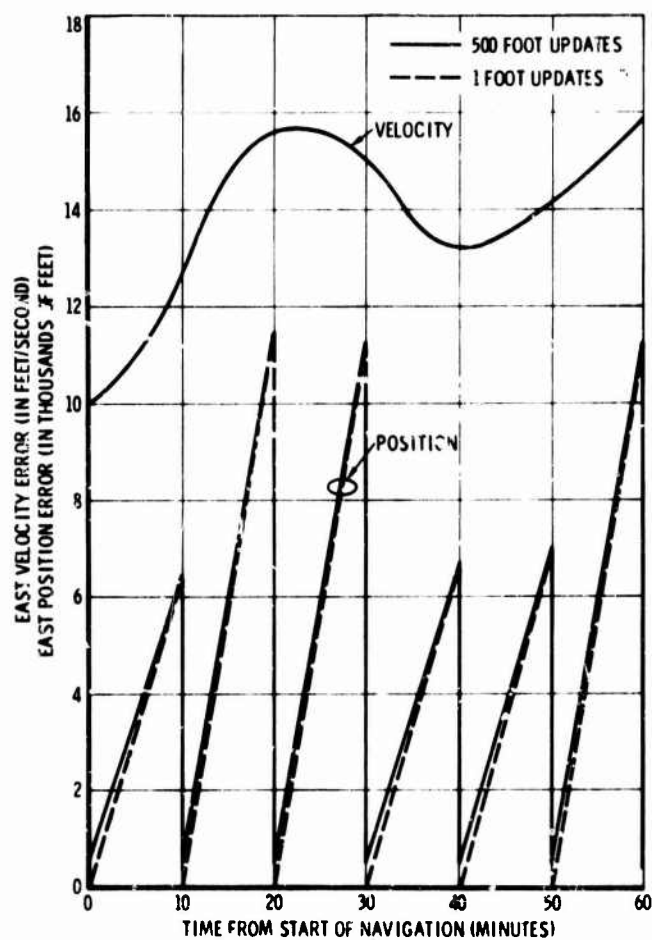
Figure 7-119. East Position and Velocity Errors for Combined CNI -Inertial Navigation System (Position Updates Every 10 Minutes).
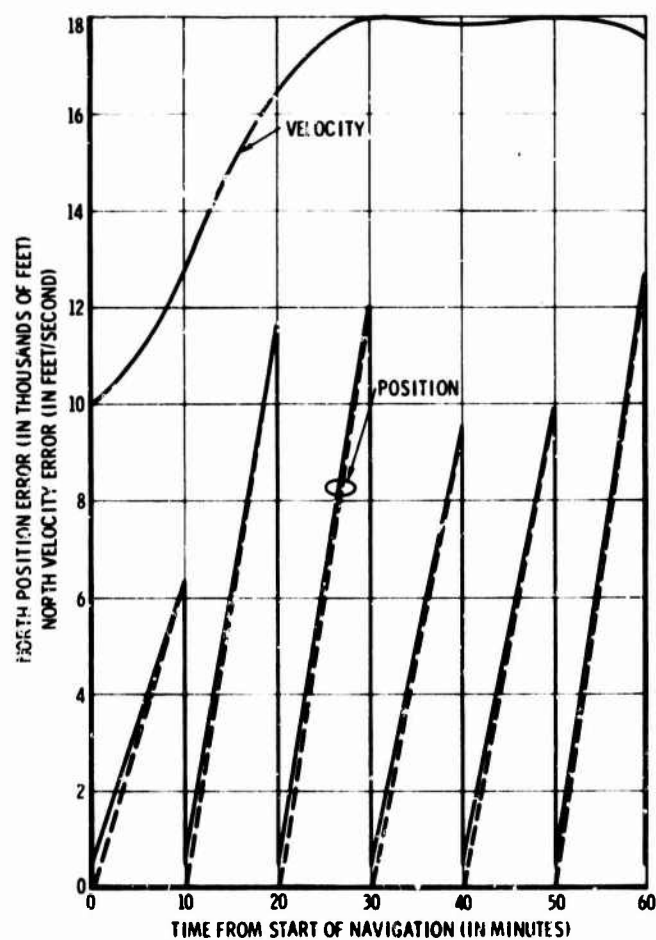
Figure 7-120. North Position and Velocity Errors for Combined CNI
– Inertial Navigation System (Position Updates Every 10 Minutes).

-480-
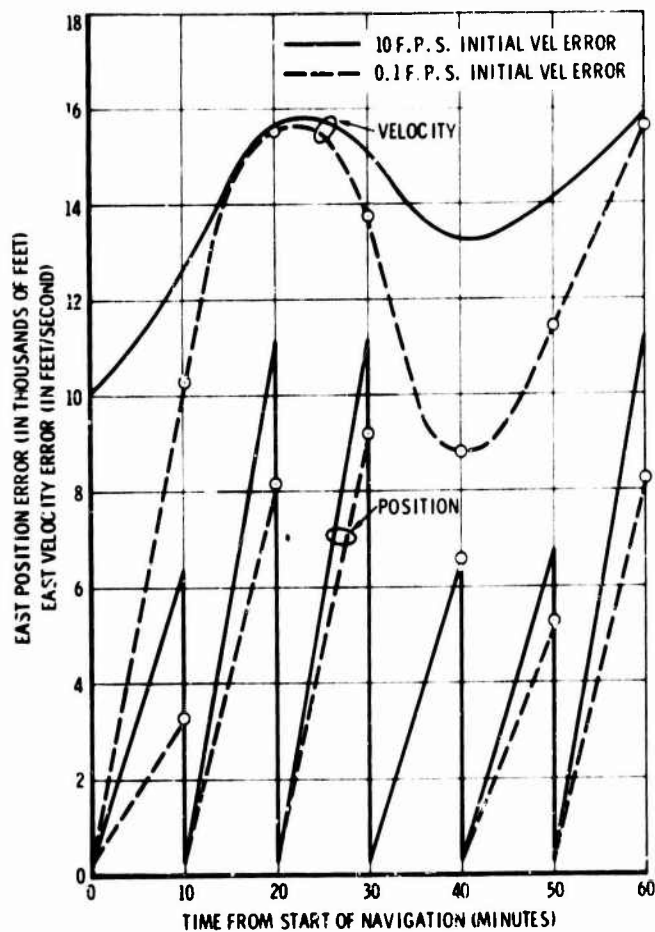
Figure 7-121. Effect of Initial Velocity Error - East Position and Velocity
Errors for Combined CNI - Inertial Navigation System
(Position Updates Every 10 Minutes).
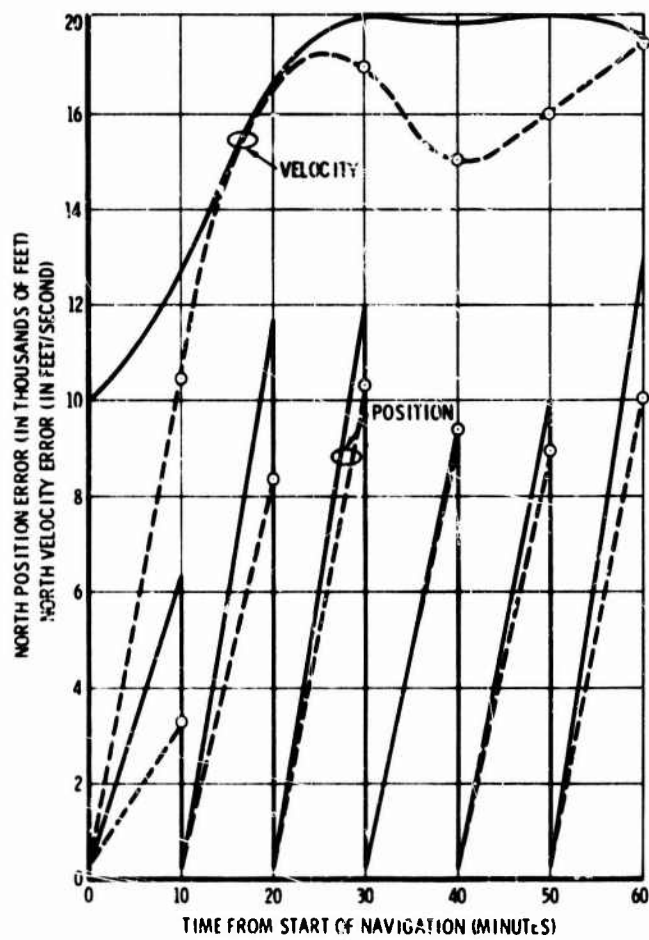
Figure 7-122. Effect of Initial Velocity Error - North Position and Velocity
Errors for Combined CNI - Inertial Navigation System
(Position Updates Every 10 Minutes).

7.8.3.3 Effects of More Frequent Position Updates

Figures 7-123 and 7-124 present the effects of increasing the frequency of position updates. The 10-minute position update period considered in the previous sections is a worst case and it would be more likely that updates would occur much more frequently. Having position updates every minute, as shown in the figures, produces a drastic reduction in the overall combined system position errors, in that it corrects position error buildup before it can build up to a significant value.

More frequent position updates, similar to more accurate position updates, (as shown in Figures 7-119 and 7-120) have no effect on the velocity error buildup. The velocity errors for Figures 7-123 and 7-124 would be identical to those of Figures 7-121 and 7-122.

7.8.3.4 Effects of Velocity Updates

If, in addition to the frequency position updates (once every minute), the CNI system provides velocity data which can be used to correct or update the velocity outputs of the inertial system, a significant reduction in the velocity error buildup will result. Figures 7-125 and 7-126 present the resulting velocity errors when velocity updates (0.3 fps - 1σ) are used to correct the velocity outputs of the inertial system. A comparison of Figures 7-125 and 7-126 with Figures 7-121 and 7-122 indicates the significance of the velocity error reductions.

1069-2718
UNCLASSIFIED
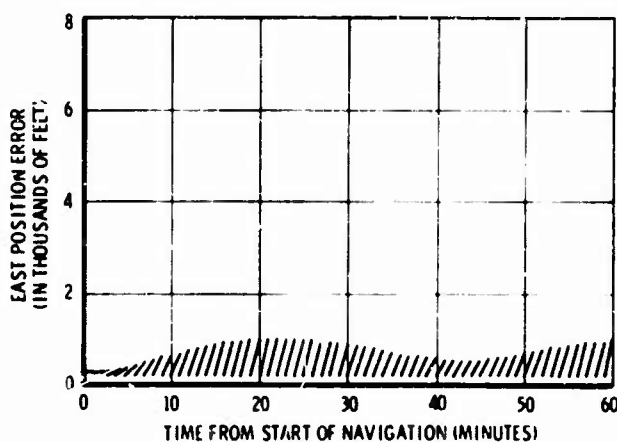
Figure 7-123. Effect of More Frequent Position Updates - East Position Error for Combined CNI-Inertial Navigation System (Position Updates Every Minute)

-482-
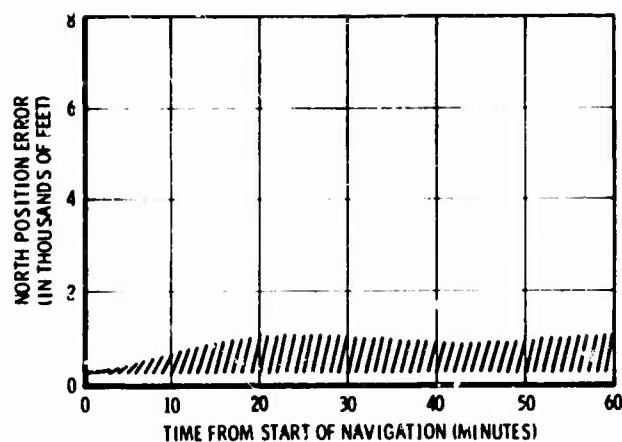
Figure 7-124. Effect of More Frequency Position Updates - North Position
Error for Combined-Inertial Navigation System
(Position Updates Every Minute).
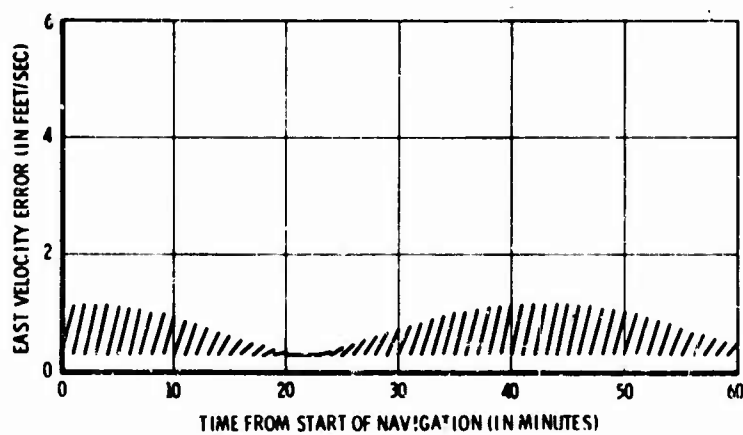
Figure 7-125. Effect of Velocity Updates - East Velocity Errors for
Combined CNI-Inertial Navigation System
(3 fps Velocity Updates Every Minute)

-484-
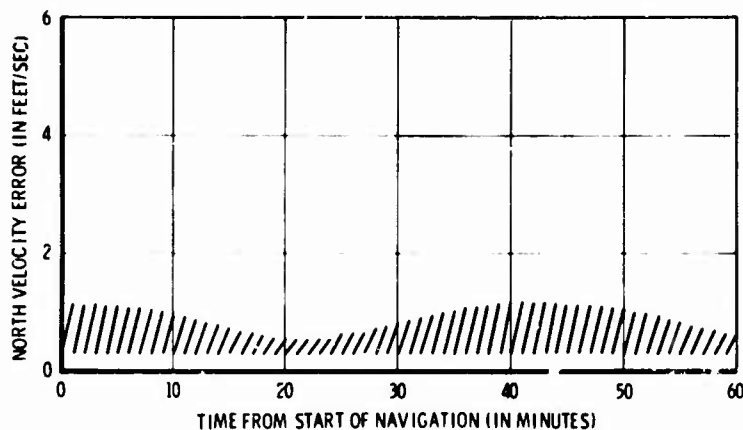
Figure 7-126. Effect of Velocity Updates - North Velocity Errors for
Combined CNI-Inertial Navigation System
(0.3 fps Velocity Updates Every Minute).

7.3.3.5 Conclusions

From these results, it appears that several things can be done to improve
combined system accuracy. First, the frequency of CNI position updates can be
increased so that the position error is reset before it has a chance to build up to the
large values seen in Figures 7-119 and 7-120. This will improve the position error
performance but will have no effect on the velocity errors. Second, the initial velocity
error can be reduced. As discussed above, the ten-foot-per-second assumed initial
velocity error is representative of a poor quality velocity initialization (such as might
be obtained in an in-flight alignment using an air-data computer). Improved in-flight
velocity initialization such as might be obtained from using doppler-radar information,
or CNI-derived velocity data, or initialization while on the ground prior to takeoff
would provide initial velocity errors of the order of one foot per second or less. This
would not only reduce the rate of position error buildup between updates, but would
also reduce the velocity error propagation. Third, in-flight CNI-derived velocity data
can be used to update the inertial-system-derived velocity. This would serve pri-
marily to correct for the velocity error growth.

7.9 COMPUTER REQUIREMENTS

This section discusses some of the functions that will or might be performed by the computer in the areas of integration (transceiver control), COM, NAV and IFF. The type of analysis required to investigate the requirements placed on the computer by any function is demonstrated using the position location function for the 621B (range difference) and all range system.

The general conclusions are that a 32-bit word is required in the computer system, and multiple computers, one for each of the integration, COM, NAV and IFF functions, is a reasonable configuration where these computers and also on-board sensors may be switched to other of the computers in the event of failure. The integration computer will require a multichannel priority interrupt system and a high-speed buffered I/O and a high-speed arithmetic unit. The COM computer requires a single channel interrupt system and medium speed I/O. The IFF computer is the simplest, requiring single-channel interrupt and low-speed I/O.

The best computer configuration for the CNI system can not be decided upon until all system parameters are set and a philosophy on failure protection (multiple back-up) and self test has been established.

7.9.1 INTRODUCTION

Although the study does not specifically call for a detailed analysis of the computer requirements for a CNI system, it was felt that some general requirements ought to be studied. The requirements which will or may be delegated to the computer in the areas of integration, communication, navigation, and identification are discussed with varying amount of detail for each requirement in each area. In doing this the philosophy was to carry out some detailed analysis in areas where the computer functions are defined, such as position location using NAVSAT, and in other areas to give indications of the type of functions which might be incorporated into the computer in a full system implementation. In order for the results arrived at to have some concrete meaning, the Magnavox APUP (Airborne Programmable Utility Processor), which is designed for military airborne application and occupies approximately two cubic feet, is used to demonstrate how the general results arrived at can be applied to a particular computer. Under the identification discussion is also included the requirements for collision avoidance both in and out of CONUS.

-486-

This section does not attempt to list every possible computer requirement and, having listed some, does not attempt to pursue all the detailed analysis required to come up with firm computer requirements. This is merely a recognition of most of the requirements, a statement of the general type of computer required, and an indication of the type of analysis which will be necessary to pinpoint the specific computer necessary to operate a CNI system.

7.9.2 INTEGRATION

The philosophy of an integrated CNI system will place a large burden on the processor to provide command and control to the various system components and route data to and from the appropriate points in this sytem. The waveform chosen is such that many of the transceiver components may be time shared to produce the various COM, NAV, and IFF functions. The coordination of the time sharing of the equipment will be the job of the computer portion of the processor. The control, synchronization and allocation of the time slots will also be directed by the computer. For this function, the buffering necessary to stack the COM and IFF data will be accomplished by computer memory. The formatting/conversion of raw NAV, COM, and IFF data at the transceiver will also be a computer function.

The computer portion of the processor will also be required to monitor the state of the processor to determine proper operation. It should be capable of self testing the transceiver portion of the system and determining where failures have occurred. It should also be in communication with other portions of the aircraft's computer system so that it may be possible to allocate portions of this system, in the event of failure, to other jobs. Another possibility is to replace some of the boxes in the transceiver with software. This is a further step in the evolution from analog circuitry to digital circuitry and finally into software. This step requires A/C converters at appropriate points (preceding the box to be replaced), replacing the function of the box either by a direct simulation, such as a digital circuitry approach, or by functional equivalents and a D/A converter, when appropriate, to the output of the replaced box. Some of the possible applications of this technique are:

DPSK demodulation
Encrypting/Decrypting
Error Correction Encoder/Decoder
Digital Matched Filter

The specifying of which functions should be done analog, which digital and which in software is beyond the scope of this study; however, it should be thoroughly investigated as it will have a significant bearing on the hardware design and in particular the specification of the computer requirements for the CNI system.

The type computer necessary to handle the tasks envisioned for the integration function must have a high-speed buffered i/O capability so that the commands and controls can be exchanged at a high enough rate to handle the processor. If blocks of the transceiver are to be replaced it should also have a high-speed arithmetic capability in order to perform the simulations in real or new real time. It should also have a multichannel priority interrupt system to handle all its data and control lines.

7.9.3 COMMUNICATIONS

The integration function described previously will provide and receive digital data via computer memory. This data will be exchanged with COM equipments. The COM equipment will contain a computer to perform the routing of signals between the various COM equipments and the processor.

This COM computer will be used to keep track of the data link messages that may be in need of passing from the aircraft to the ground such as:

> Aircraft status
> Emergency conditions
> Target data

This will require interface to the NAV equipments probably via NAV computer memory and also other aircraft indicators such as fuel consumptions, power status, and weapon status from the weapon system. It will also automatically notify the processor when it has this data for transmission and will provide the necessary conversion to processor compatible coding

In the receiver mode it will examine the received data and will perform the necessary conversion for use by the COM equipment. The types of data received will be:

Vectoring information

Alerts

Computer data such as radar tracks

The routing of these signals may be simply to display or to other computers such as a weapon systems for the radar tracks.

In the voice communications mode, the COM computer will interface with the voice coding device whether it be a direct transform such as PCM or the output of a channel vocoder (restructured speech). The computer interface may be at the output of such a device and will be used to control the device. Depending on the type of vocoder used, the computer may be capable of performing some of the parameter extraction using software.

The computer required to perform the COM function will require medium-speed I/O capability. It will require an A/D ard D/A conversion system with multi-plexing controls. Unless vocoder simulation is required, no high-speed arithmetic functions are required. Single channel interrupt will be sufficient for the COM computer.

7.9.4 NAVIGATION

The integration function described previously will receive NAV signals from the NAVSAT system in the enroute case and from ILS in the terminal case. The NAV computer will also be in touch with the COM system described above via memory transfer. The NAV computer's function will be to recognize the NAV data, from the satellites as well as via COM links, and use this along with on-board sensor information, also interfaced to the NAV computer, to compute current position and also to compute range and bearing navigation information.

The NAV computer will also provide various driving function for aircraft displays and be capable of accepting manual inputs.

A detailed analysis of some of the computer requirements for position location was carried out. Both a range difference system (621B enroute and perhaps ground-based in the terminal case) and an all-range system (passive using synchronized clocks in the landing area) were considered. The solution of the equations was carried out (see Appendix IX) and a program in a universal-type assembly language written (see Appendix X). Memory requirements for each system are stated and the necessary computing time for each of the systems under various assumptions is given as a function of the standard commands assumed in the program. A computer may now be chosen and the required computing time determined by inserting the time required for each command into the time equation.

The language used in this section assumes a computer with the following instruction capability:

Instruction	Explanation
LOAD	An instruction to fetch information from bulk storage into a register (which we will call accumulator) where it can be operated upon.
STORE	The reverse of LOAD. Puts information from the accumulator into bulk storage.
ADD	Fetch information from bulk storage, add it to that in the accumulator, and leave the results in the accumulator.
SUB	Fetch information from bulk storage, subtract it from that in the accumulator, and leave the results in the accumulator.
MUL	Fetch information from bulk storage, multiply it by that in the accumulator, and leave the results in the accumulator (usually extended).
DIV	Fetch information from bulk storage, divide it into the accumulator contents, (usually extended) and leave the quotient in the accumulator.

Instruction	Explanation
NORM	The operation necessary after a MUL and before a DIV to get the extended accumulator contents into the proper bit positions. (On some machines this is not required.)
NEGATE	An operation to change the sign of the accumulator contents.
SHIFT	Shifting the bits in the accumulator right one position. Equivalent to divide by 2.
JUMP	Transfer of program sequence to the address specified by the JUMP.
SKIP	The next instruction in sequence is skipped if the condition specified by the SKIP is met.

The programs presented are very straightforward and are efficient under the above constraints on the computer capability. It is assumed that the LOAD and STORE commands take the same amount of time to execute, and that ADD and SUB similarly take the same amount of time.

The results were:

A. RANGE DIFFERENCE - 478 Memory Locations

Time Requirements

Instruction	No Reference Update	Reference Update
LOAD/STORE	122	173
ADD/SUB	65	90
MUL	40	52
DIV	23	31
NORM	63	83
SHIFT	4	4
JUMP	11	11
SKIP	15	15
NEGATE	26	31

B. ALL RANGE - 302 Memory Locations

Time Requirements

Instruction	No Reference Update	Reference Update
LOAD/STORE	87	121
ADD/SUB	49	66
MUL	27	37
DIV	12	17
NORM	39	54
SHIFT	3	3
JUMP·	11	11
SKIP	15	15
NEGATE	16	18

Assuming the use of an APUP (Airborne Programable Utility Process) computer whose instruction-execution times are summarized below:

APUP Times

LOAD/STORE	-	4 usec
ADD/SUB	-	4 usec
MUL	-	12 usec
DIV	-	12 usec
NORM	-	5 usec
SHIFT	-	2 usec
JUMP	-	2 usec
SICIP	-	2 usec
NEGATE	-	4 usec

The time to compute position, assuming no reference update, using the Range Difference system is:

$$\text{Time} = 122 \otimes 4 + 65 \otimes 4 + 40 \otimes 12 + 23 \otimes 12$$
$$+ 63 \otimes 5 + 4 \otimes 2 + 11 \otimes 2 + 15 \otimes 2 + 26 \otimes 4$$

$$\text{Time} = 1.983 \text{ msec}$$

The NAV computer must have a medium-speed I/O capability, A/D and D/A for driving, and a high-speed arithmetic unit; a single-channel interrupt capability would be sufficient. A 32-bit computer would be of appropriate size for the required NAV functions.

7.9.5 IDENTIFICATION

The integrated function described previously will exchange data between the IFF equipment and the processor. This data will be in the form of responses to queries or acceptance of responses to generated queries. The IFF equipment is responsible for:

> Friend from foe identification
> Recognition of friend from foe
> Data Link

In addition, the collision-avoidance function is incorporated in this section as an adding of velocity information to the replies and challenges would perhaps implement a collision avoidance system.

Most of the function with the exception of collision avoidance could be handled without a computer. The addition of a computer, however, would ease the system implementation and also give the collision-avoidance capability.

7.9.5.1 Collision Avoidance

A military aircraft is constantly in situations where collision avoidance is a major problem. In the CONUS, projections have shown that in the 1980 time frame aircraft densities will increase tenfold. The aircraft must be capable of participation

in ATC functions either actively or passively. In tactical situations the aircraft may or may not wish to avoid a collision course depending on whether the aircraft is friend or foe and upon his mission. Each of these situations is discussed and the burden placed on the computer and, to some extent, the additional equipment required is examined.

7.9.5.1.1 Conus ATC Systems

7.9.5.1.1.1 <u>Background</u>. Recently the Department of Transportation received a report from the Goldmuntz Committee which recommended a course of action to handle the ground based air traffic control function in the 1975-1990 time frame. The type of systems studied was a synchronous range ordered call system using a trilateration range system. This system results in the ground based computer center (ARTCC) knowing the location and velocity of every aircraft in its control area and checking to determine if they will conflict in the future. If a conflict exists, the information regarding the aircrafts in conflict is passed to a controller who instructs the aircrafts via voice link to perform the necessary avoidance maneuvers. Future systems will do some of this conflict avoidance automatically by instructing the aircraft via UP, DOWN, LEFT, RIGHT, etc, command indicators. The same system will be used in both enroute and terminal areas with increased interrogation rates in the terminal approach cases.

7.9.5.1.1.2 <u>Aircraft Participation</u>. The aircraft equipped with a CNI capability may participate actively by the addition of a receiver-transponder in the range-ordered system. When the aircraft takes off, his ID is introduced into the system, or he may use the voice link to enter into the system. The system automatically interrogates him and the aircraft receiver recognizes his ID, adds his altitude to the message and transmits it back to the stations.

The aircraft may wish to participate passively. In this case, the collision avoidance function must be done in the airborne computer. The aircraft will know its position from the 621B NAV computation and its velocity from onboard sensors in addition to successive position fixes. The location and velocity of aircraft in the area will be obtained by using the aircraft's radar and IFF responses. Given this information, the airborne computer can perform the conflict prediction function and inform the pilot of possible conflicts.

-494-

7.9.5.1.2 Tactical Environment

In a tactical environment the aircraft would be operating in a passive situation as described above. The other source of information may be via ground based radar which are tracking aircraft within the area. The airborne computer will perform the conflict prediction and this information could be used by the pilot to avoid or close on another aircraft.

7.9.5.1.3 Conflict Prediction

The problem of conflict prediction involves computing the distance between two aircraft, assuming they continue on their same courses for a period of time, say the next 30 seconds. If, at any time in the 30 seconds, this distance is less than some minimum miss distance, usually 2000 feet, a conflict is predicted. In the CONUS ATC system the controller notifies the aircraft of the potential conflict and advises as to actions to avoid. Later systems have proposed automatic resolution and instruction to the aircraft via a data link.

7.9.5.1.4 Conflict Prediction Algorithm

The steps in checking for a potential conflict vary slightly depending on the system of position location in use. Normally a system converts to coordinates such that you have available, x, y, h, x, y, h that is x, y and altitude coordinates along with velocities in each direction. A straightforward algorithm would be as follows:

a.   Check if altitudes cross in next 30 seconds (using $h, \dot{h}$)

b.   Check if aircraft are diverging (using $x, y, \dot{x}, \dot{y}$)

c.   Check if aircraft will cross (within miss distance) in the x direction in next 30 seconds (using $x, \dot{x}$)

d.   Check if aircraft will cross (within miss distance) in the y direction in next 30 seconds (using $y, \dot{y}$).

Using this type of algorithm, in CONUS, conservative studies have shown that:

a.   80 percent of the aircraft will be eliminated at Step 1.

b.   10 percent of the aircraft will be eliminated at Step 2.

c.   5 percent of the aircraft will be removed at Step 3.

d.   4 percent of the aircraft will be removed at Step 4.

-495-

In other words, roughly 1 percent of the aircraft will be in conflict. In a tactical situation the numbers would be more like:

a.   70 percent removed in Step 1.

b.   10 percent removed in Step 2.

c.   5 percent removed in Step 3.

d.   5 percent removed in Step 4.

In other words, 10 percent of the aircraft in an area will be in conflict.

7.9.5.1.5 Computer Speed Requirements

7.9.5.1.5.1 Conflict Prediction Algorithm in CONUS. If we assume our universal computer with the standard instruction set described in 1.3 then the required operations would be:

$$M1 = 0.75(4)P+0.5(53)P+0.10(8)P+0.05(36)P+0.04(40)P+0.01(5)P$$

$$M1 = 12.6P \text{ operations/conflict check where there are } P \text{ aircraft in the area.}$$

If we check every 3 seconds for a conflict, then the required operations/seconds are:

$$M' = 12.6P/3$$
$$M' = 4.2P \text{ operations/second}$$

7.9.5.1.5.2 Conflict Prediction Tactical Situation. The computation for M1 is:

$$M1 = 0.50(4)P+0.20(53)P+0.10(8)P+0.5(36)P+0.5(40)P+0.10(5)P$$
$$M1 = 51.9P \text{ operations/conflict check}$$

In a tactical situation we would require more frequent checks because of speeds and situations which may arise; we will assume a check every second:

$$M' = 51.9P \text{ operations/second}$$

7.9.5.1.6 Storage

To store the necessary information for collision avoidance requires the following information for each aircraft:

a.	IB ----------------	21 bits
b.	Altitude -----------	16 bits
c.	X Position ---------	20 bits
d.	Y Position ---------	20 bits
e.	Δ Altitude --------	16 bits
f.	X ----------------	16 bits
g.	Y ----------------	16 bits
h.	Control ----------	3 bits
		128 bits/aircraft

The program requires about 500 memory locations. If we assume a 32-bit word then we need:

$$C = 500 + \frac{128}{32} P$$

$$C = 500 + 4P \text{ memory locations}$$

7.9.5.1.7 Summary

7.9.5.1.7.1 CONUS. Active (Ground-based collision aviodance).

Requires addition of transceiver if range-ordered system used and no additional computer load.

Passive

Requires no additional equipment but computer load increased. In 1990 time frame computer requirement would be:

$C \approx 8,000$ memory locations (32-bit words)

$M \approx 8 \times 10^3$ operations/second

7.9.5.2 Identification Summary

The identification function requires a minimal computer configuration, if any, to perform the simple IFF function. In order to do collision avoidance a computer with low-speed arithmetic capabilities is required. In addition low-speed I/O capability and single-channel interrupt is sufficient.

7.9.6 CONFIGURATION

A type of configuration is shown in Figure 7-127. The Gate Control allows data to be passed between all four computers and can be controlled by any of the computers. Similarly all of the external sensor and displays shown could be handled the same way and hence data could go from transceiver to any sensors via any computer. The NAV computer could be designed as the Integration Computer backup. COM and NAV could back up each other and IFF could be handled simultaneously by either COM or NAV. This is not put forth as the optimum solution but only as a type of configuration which should be further studied when implementation stage is reached and waveform and system operations finalized.

7.9.7 CONCLUSIONS

The conclusions in the computer requirements area are expressable in general terms only. The word length for the computer system should be 32-bits. The various computer capabilities required are:

Function	I/O Capability	Interrupt Capability	Arithmetic Unit
Integration	High Speed Buffered	Multi-channel priority	Low Speed (High Speed to replace transceiver boxes)
COMM	Medium Speed Buffered	Single Channel	Low Speed (High Speed to do vocoder functions)
	Medium Speed Buffered	Single Channel	High Speed
Identification	Low Speed Buffered	Single Channel	Low Speed

-498-
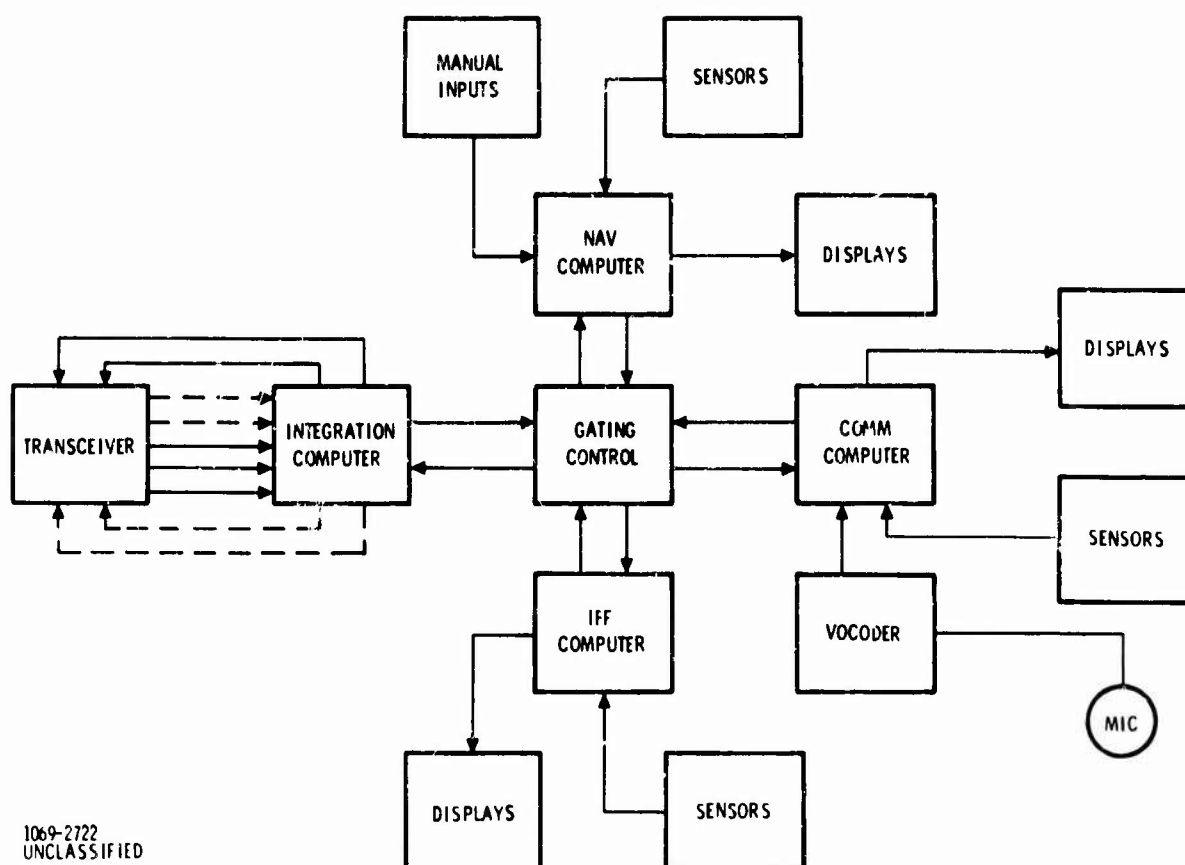
Figure 7-127. Computer Configuration

-499-

APPENDIX I

SEQUENTIAL DECODER ALGORITHMS

Just as the particular characteristics of the convolutional systematic rate one-half code allowed specialization in the memory, similar improvements can be made in the decoding algorithm. The fact that the code to be used is rate 1/2 allows a particularly simple mechanization of the computations for a hard decision channel. Because of the simplicity, computations can be made across a span of several nodes simultaneously. The reason for considering using the parallel procedures is that the sequential decoder will be rate limited by the ability to shift the encoder. Thus, the more information that can be gained at a particular encoder setting, the faster the overall speed factor of the machine will become.

Two unique sequential decoding algorithms are presented that utilize parallel procedures. The first algorithm is the Fano threshold[*] algorithm. This algorithm uses the familiar threshold tightening-loosening scheme, but in addition, has many stored procedures, both in the forward search and in the back search, that allow moves between nonadjacent nodes. The second algorithm is the modified threshold algorithm that utilizes a new threshold scheme that proposes to minimize long back searches. Both of these algorithms also introduce a new concept in their back search. This concept is to limit the back search to a given number of nodes behind the most advanced point the decoder has reached. When the decoder reaches this limit, the decoder is turned around similar to the decoder backing up to the origin of the code tree. This limited back search allows for a sequential decoder design that must only store a small number of nodes to decode. In addition to the algorithms used during normal decoding a tail algorithm utilizing parallel procedures is presented for use with block resynchronization.

The next section provides the necessary background material into the specific code properties used by the algorithms and illustrates the generation of the required information from the hypothesis bits and the error syndrome to allow the parallel procedures.

---

[*] J. Wozencraft and I. Jacobs, Principles of Communication Engineering, John Wiley, 1965, pp 431-439.

I-1 VARIABLE GENERATION

Figure I-1 shows a typical rate 1/2 systematic code encoder that would be used in association with the proposed algorithms. As shown in the figure, the information bit is transmitted without modulo-2 combination with any other of the bits in the encoder. the check bit, however, is a function of not only the present information bit but of k - 1 previous information bits, where k is the constraint length of the encoder.

An encoder like the one shown in Figure I-1 generates the tree code shown in Figure I-2. Several features of the code are worth noting since they will be used in the subsequent logic in the decoder. First, we require that there be a connection to the check bit from the first stage of the shift register; that is, the check bit is a function of the present information bit. This requirement assures that the two branches leaving a node are complements of one another, thus providing a maximum distance between these two adjacent branches. This concept is carried a step further by requiring that the second stage of the shift register also be connected to the modulo-2 adder to generate the check bit. This requirement assures that similar branches leaving the nodes

INFORMATION BIT   CHECK BIT

Figure I-1. Encoder

-501-
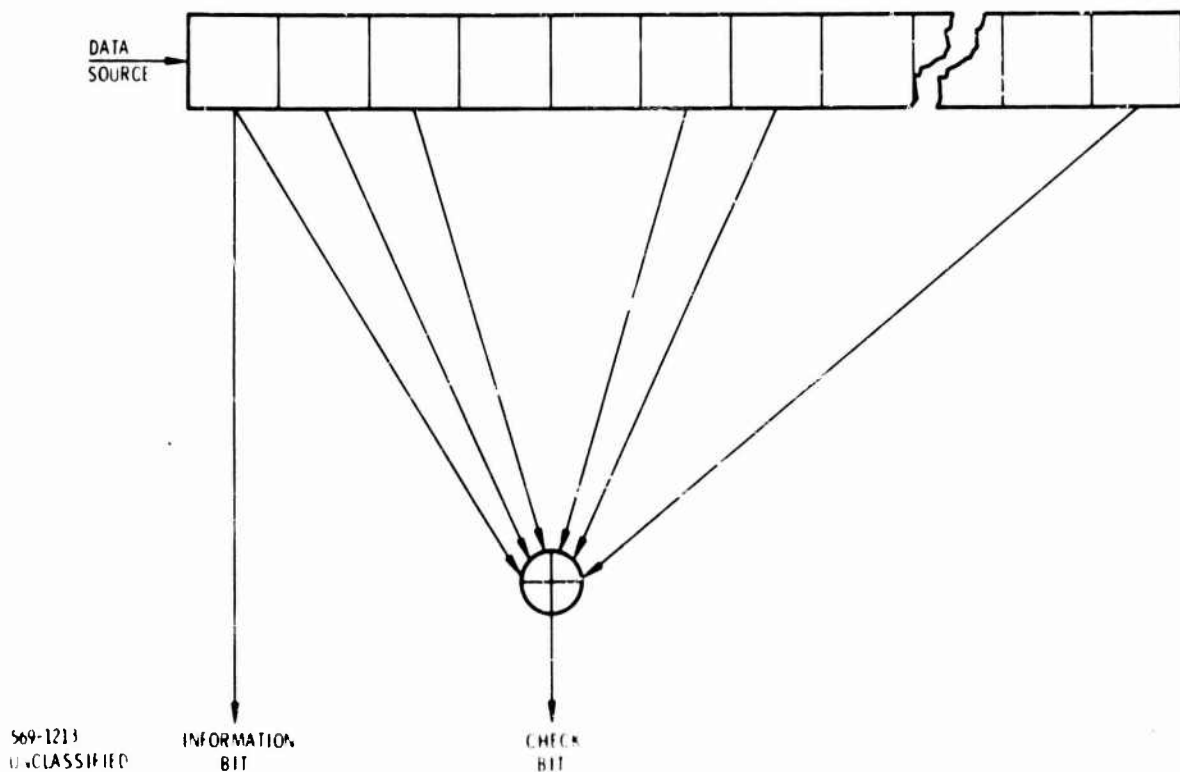
reached by complementary decisions at the previous node have complementary check bits. This can be seen in Figure I-2 if the two branches leaving the node marked "present search node" are considered. The zero information bit branches one node deeper into the tree, terminate at points 1 and 2, and the check bits in the branches leading to these nodes are complements of one another. Finally, the encoder shown in Figure I-1 carries this complementary concept one step further by connecting the third stage to the modulo-2 adder. This produces complementary check bits two nodes deep is used in the decoding algorithm logic to provide transition logic over a tree span of four best branches.

Figure I-3 shows another encoder mechanization where the modulo-2 adders mechanize the impulse response of the encoder of Figure I-1. The impulse response is simply the check bit sequence resulting with the Figure I-1 encoder, having been set to the all zeros state, has a one followed by k - 1 zeros shifted into the register. The encoder shown in Figure I-3 will produce a check bit sequence identical to the one produced by the encoder in Figure I-1; the advantage in the new mechanization is that only one level of modulo-2 adding is required rather than the large number associated with the longer constraint length codes for the configuration shown in Figure I-1.
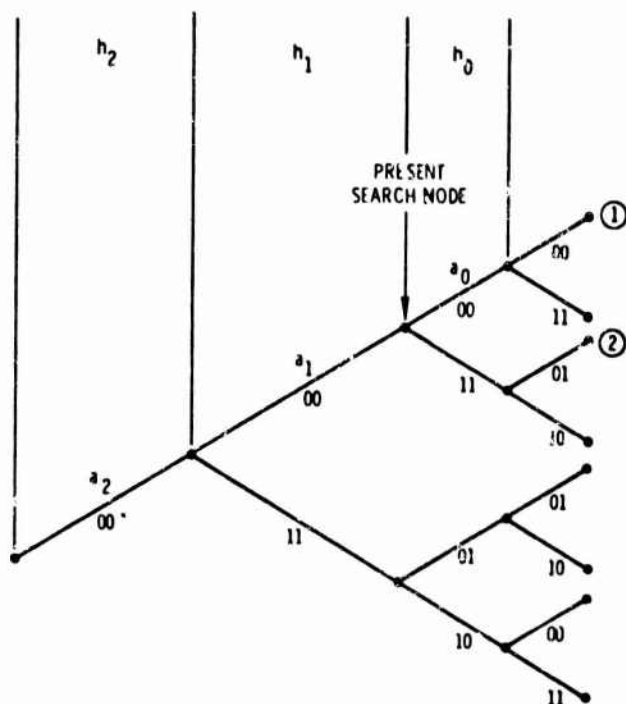
Figure I-2. Tree Diagram

-502-

This reduction in logic levels greatly increases the possible rate of shifting the encoder. Since this shifting rate will limit the decoder speed factor, an encoder like the one in Figure I-3 will be used.

A consequence of the impulse response mechanization is that it is not actually the hypothesized bits that are stored in the decoder hypothesis memory, but the modulo-2 sum of the impulse responses of the hypothesized bits. This will affect the logic of the algorithm described subsequently.

There is nomenclature in Figure I-2 that has not been explained as yet. The "a" and "h" variables, and the concept of the present search node require some explanation. This explanation is made simpler through the use of Figure I-4 showing a hypothesis encoder. This encoder is identical to the encoder shown in Figure I-1 except that it is a composite encoder and the first tap connections are deleted. While the configuration shown in Figure I-1 is not the one to be implemented, the generation of the "a" variables is easier to see than in the impulse response encoder. The desired variables are generated for three different one bit shifts of the hypothesized information. One further variation occurs: any new bit shifted into the hypothesized encoder is a zero. This means that the first stage of the encoder is not actually required and is shown in dashed lines in Figure I-4. Two new stages are required to provide for the added delays but the initial stage is missing so that the total shift register length is k + 1 bits.
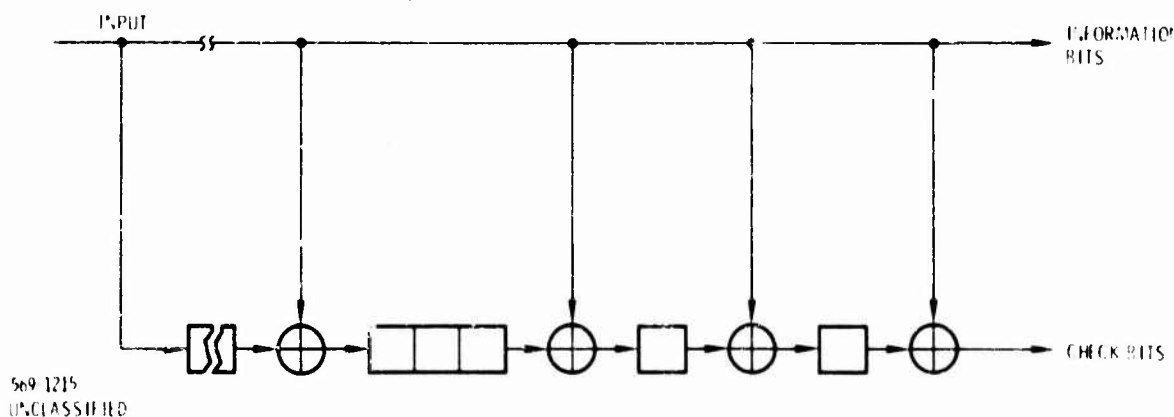
Figure I-3. Impulse Response Mechanization of Encoder

The check bit memory shown in Figure I-4 is the storage of the R sequences of the syndrome calculation. The bit r_0 corresponds to the stored check bit associated with the branch immediately ahead of the node marked "present search node" in Figure I. Thus, the variable a_0 represents the modulo-2 sum of this stored check bit r_0 the check bit generated for the zero branch leaving the present search node. In an identical manner, the variables a_1 and a_2 represent comparisons of the stored check bits with the check bits generated for the zero branches leaving the two nodes hypothesized immediately prior to the present one.

One further point is worthy of note. If the hypothesized bit h_1 is complemented, the variable a_0 is complemented. This can be seen by examining the tree diagram in Figure I-2. Complementing h_1 (making it a 1 instead of 0 in this instance) takes you from the upper branch leaving the node immediately behind the present search node to the lower branch. This complementing of h_1, however, also complements the check bit associated with hypothesis h_0 and thus produces the complement of the output variable a_0 for the branch ahead of the search node. Thus, if a_0 had been a 1 with a hypothesized h_1 equal to 0, then complementing h_1 would have caused a_0 to be equal to 0. Complementing h_1 has no effect on the variable a_1, however, since a_1 is a function of the node from which h_1 emanates but not of h_1 itself.
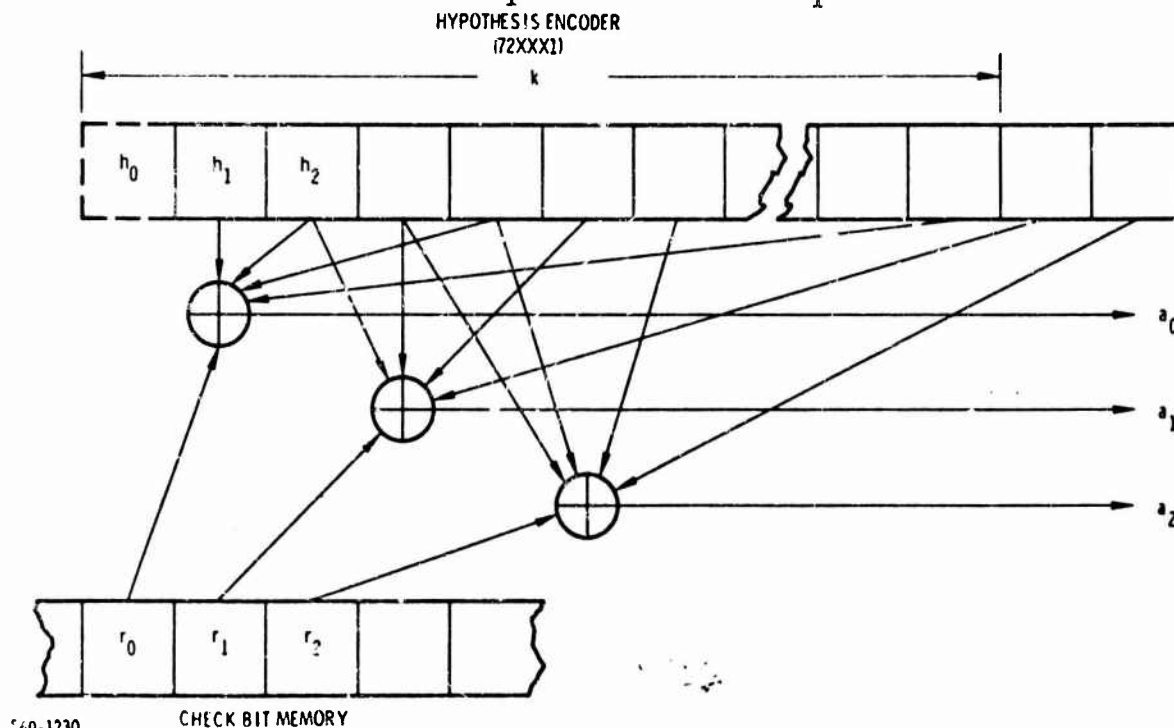
Figure I-4. Decoder Distance Variable Generator

As discussed previously, the actual encoder will have the form of the one shown in Figure I-3 rather than that of Figure I-1. Figure I-5 shows a block diagram of the encoder, "hypothesis memory," and variable generator to be employed. In the shift forward mode h_1 is hypothesized to be one whenever the algorithm set c equal to one during a forward shift. In a manner identical to the deletion of the first tap connection previously, the first bit of the impulse response is deleted. Figure I-6 shows the effect of the hypothesis complementing variables c and c'. As stated, the variable c controls the hypothesis h_1 for the branch leading to the present search node. Similarly, c' controls hypothesis h_2 for the branch leading to the previous node. All complementing is accomplished on a forward step and the new hypothesis h_0 is always zero. This leads to the forward step alternatives shown in Figure I-6. Because the memory contains the summed impulse responses and not the hypotheses, this must be taken into account when shifting hypotheses out of the memory. This accounts for the modulo-2 summations that are functions of a constraint length of the last bits (newest or oldest) in the hypothesis memory, as shown in Figure I-5. The modulo-2 summations on the newest bits take care of the backing up of the decoder and the modulo-2 summations on the oldest bits take care of the output stream used to correct errors in the information sequence. Note that using this load and unload technique, the end bits in the memory actually are the hypotheses for bits in these positions - no other impulse responses are summed in with the bits in these positions. This means that the hypothesis h (previously called h_1) shown in Figure I-3, I-5 and I-6 is simply the value of the first stage of the encoder shown in Figure I-1.

The variables a_0, a_1 and a_2 are the results of modulo-2 summing of stored check bits of the zero branch alternatives leaving the present and two previous hypothesized nodes. Figure 5 shows the taps in the hypothesis memory to obtain the required information directly. Thus, the "a" variables discussed in the previous section are directly available in the impulse response encoder. The algorithm uses only the h_1 shift of the hypotheses. For this reason the subscript is dropped and the variable h is available in the first stage of the hypotheses memory.

I-2 FANO THRESHOLD ALGORITHM

With the above preliminaries, the logic used in the Fano threshold algorithm can be described in detail. The logic employed is shown in the flow diagram of Figure I-7. Figures I-8 and I-9 consist of individual diagrams of the received distance trees for each case in the forward and back search routines. Several additional

variables are employed in the logic presented; these will be discussed briefly prior to a step-by-step description of the logical steps.

The variable M is the metric accumulator. This variable represents the accumulation of the tilted distance function minus threshold tightenings and is used to decide whether the encoder is traversing the correct path. The variable θ indicates whether a threshold tightening is allowed. The variable Δ is the increment of threshold release or tightening.

Two variables employed in this algorithm that are not used explicitly in previous algorithms are the variables Φ and FLAG. Φ is a variable used to indicate whether the algorithm is in the forward or backward search mode (0 in the forward search and 1 in the back search). The variable FLAG is used to denote the beginning of a two node move forward. When the variable $a_0 = 1$, the decoder is moved forward and FLAG is set equal to one. This indicates that on the next move the hypothesis h must be chosen such that a_0 will be zero.

Finally, the metric increments used in the algorithm are 1, α, and β. When an agreement path is followed, 1 is added to the metric. When a double disagreement path is followed β is subtracted from the metric, and when a tie branch is followed α is subtracted from the metric accumulator. A final set of variables is used in the flow diagram pictured in Figure 1-7 to denote the depth into the tree. The variable n is an index of tree depth associated with the present search node. The variable KBACK is used to indicate the maximum allowed backup. It is updated during a move forward to a new depth into the tree. KBACK is then a constant distance behind the node of deepest penetration. If the decode backs up to KBACK, Φ is set equal to zero, the accumulator is increased by Δ and forward search is begun. Initially, KBACK is set equal to zero and is not updated until the depth of penetration reaches a distance such that KBACK should be increased.

The algorithm begins with all the variables including the accumulated M set equal to zero. The hypothesis memory is also zero set at the beginning of a block search. The process shown as $n = n + 1$ or $n = n - 1$ in the flow diagram of Figure 1-7 represents shifting the contents of the registers shown in Figure 1-5 either to the right or to the left depending upon whether the step is forward or backward.
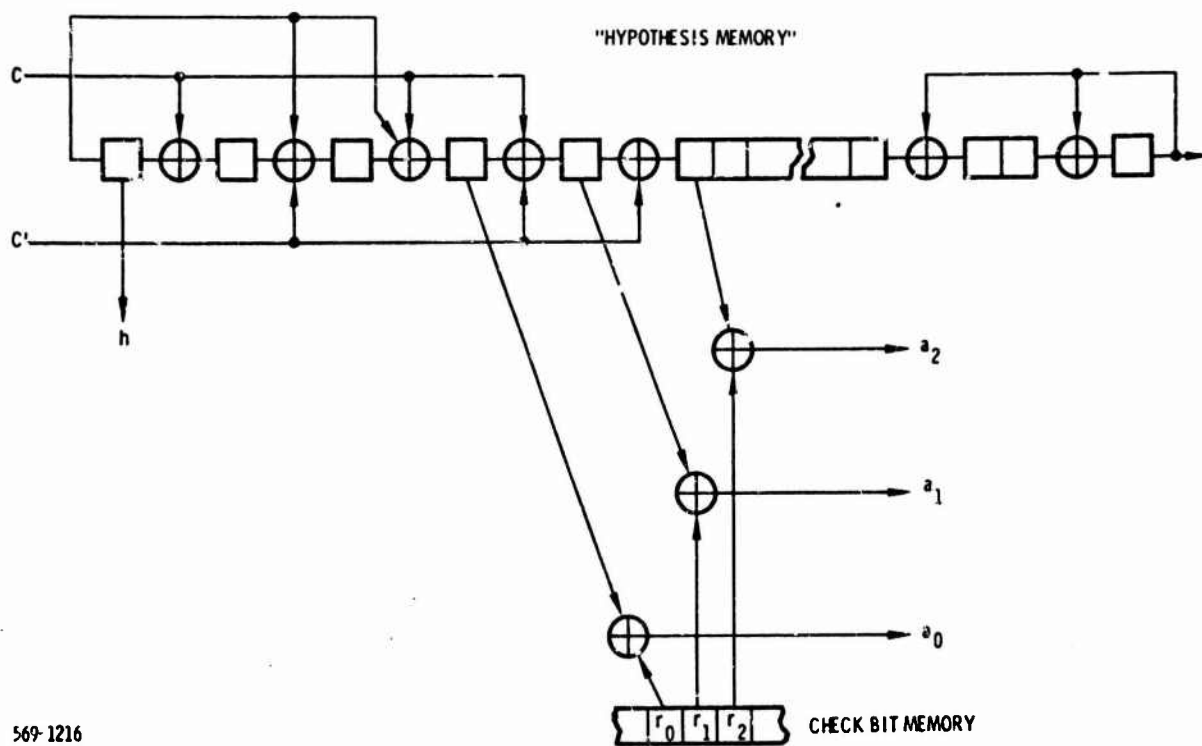
Figure I-5. Hypothesis Memory
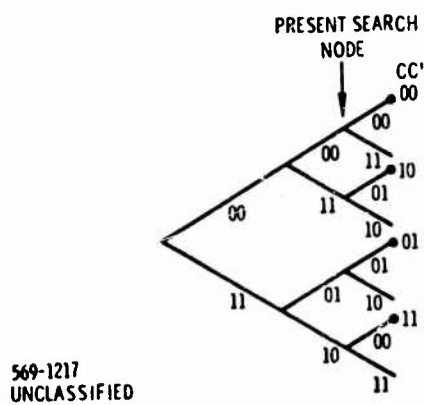
Figure I-6. Tree Diagram of Forward Step Alternatives

-507-

I-2.1 FORWARD SEARCH

In the forward search, indicated by $\Phi = 0$, there are two major logical distinctions as shown in Figure I-7, $a_0 = 0$ and $a_0 = 1$. The flow diagram is simple in the forward search but each case is described in the following. Figure I-8 shows the received distance tree diagrams for the cases individually. The initial cases are simple but the responses to the latter cases are not obvious. The convention followed in Figure I-8 and I-9 is to use upward pointing arrows for the present search node and downward pointing arrows to represent the node reached as a result of the indicated response.

Case F1 represents a condition illustrated in Figure I-8. The node search pointer is presently pointing at a node whose metric is less than the threshold established at $\Delta - 1$ and, since the variable a_0 is zero, the best path increment is indicated. The search pointer advances one node while incrementing the metric accumulator by one. Since the metric increments are always integers, this requires that the metric value at the end of the forward step equal to or less than $\Delta - 1$. In Figure I-8 the increment on the branch immediately prior to the present search node is shown as a one also. This will be true since all forward search steps terminate on a best branch node.

Case F2 shown in Figure I-8 illustrates a threshold tightening. Since a_0 is zero, the best path increment is indicated but M is not allowed to be Δ or greater as long as $\theta = 0$. Hence, when M is equal to $\Delta - 1$ at the beginning of case F1, the search pointer advances one node while incrementing M by one but tightening by Δ making M = 0. Note that threshold tightening necessarily sets M = 0.

When θ is equal to 1 and a_0 is equal to 0, you have case F3 represented in Figure I-8. In this instance, since no threshold tightening is allowed because θ is equal to 1, the metric accumulator is increased by one and a forward shift is indicated. This exhausts possibilities for the condition that a_0 is equal to 0 in the forward search.

When a_0 is equal to 1 in the forward search, there are two cases to be dealt with. The metric accumulator compared with α discriminates between these cases. Case F5 is the case of $a_0 = 1$ occurring when $M \geq \alpha$. Since $M \geq \alpha$ a forward step is allowed causing a decrease in the metric by α. Because of the complementary nature of the encoder discussed previously, it will always be possible to follow a tie metric
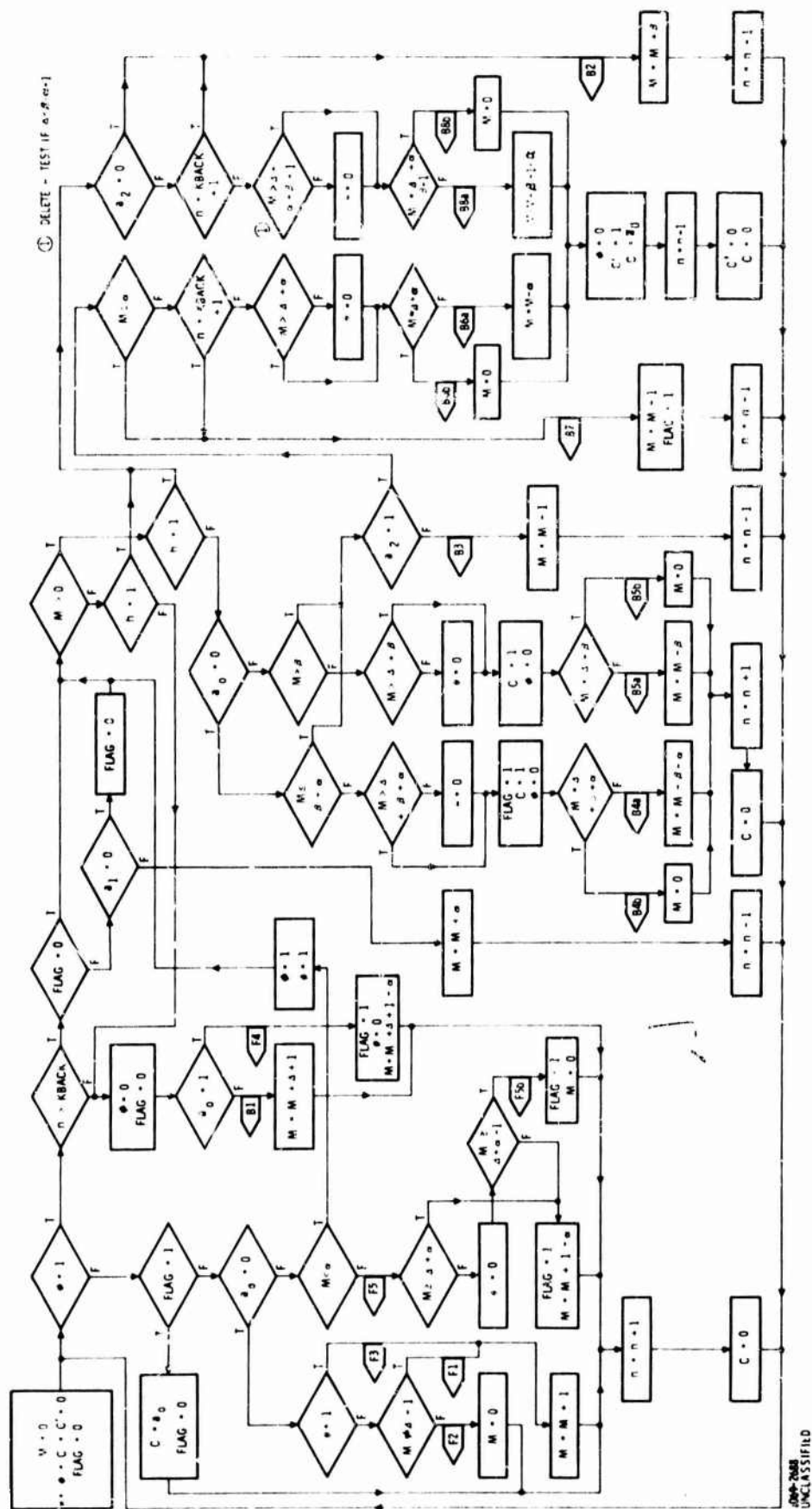
Figure I-7. Flow Diagram - Fano Threshold Algorithm
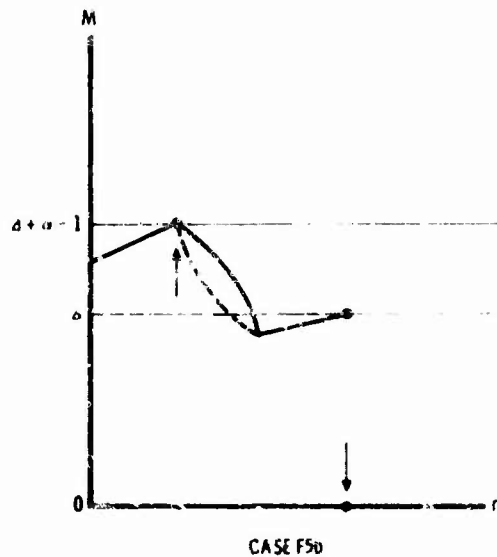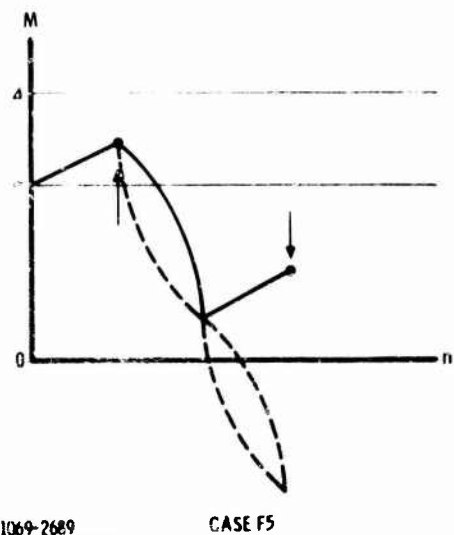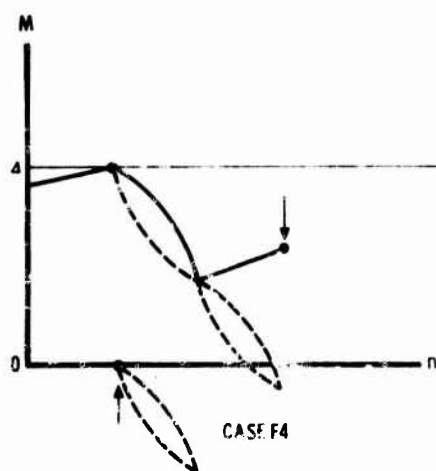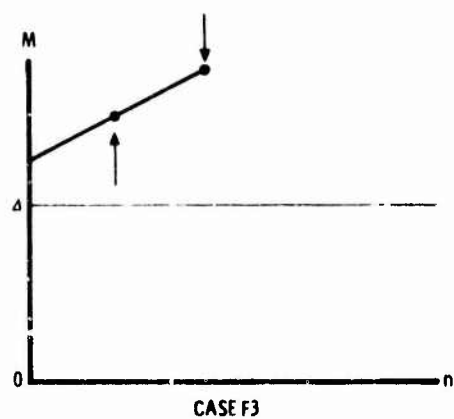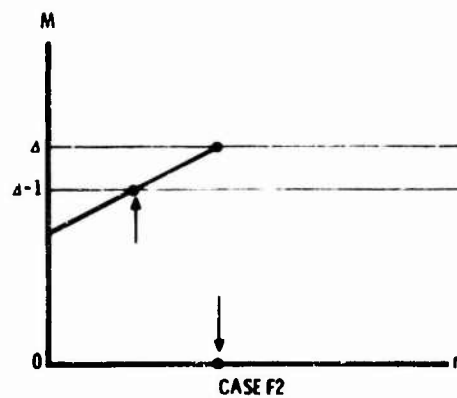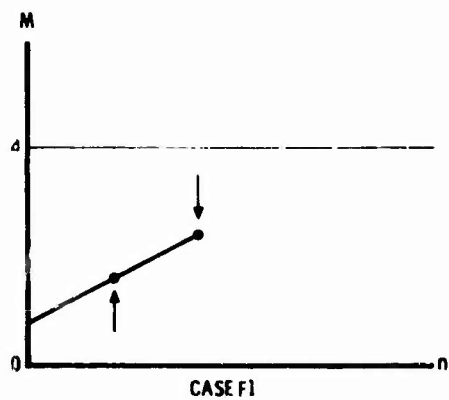
Figure I-8. Forward Distance Diagrams for Fano Threshold Algorithm

-510-

decrease by a best branch increment. Proper selection of the tie path allows this. This case is a two node move forward and the two possible moves depending on the selection of the tie path are illustrated in Figure I-8.

The procedure for making the advance is as follows (see Figure I-7). When the conditions of $a_0 = 1$, $M \geq \alpha$ are detected in the forward mode, M is tested to see if θ can be set equal to 0 as a result of the forward steps. Following this, the variable FLAG is set equal to one and M is adjusted for the entire forward sequence; a single forward step follows. The FLAG variable is detected on the next cycle, and complementing variable c is set equal to a_0, and FLAG is cleared. The subsequent forward step completes the process. Note if $M = \Delta + \alpha - 1$ at the beginning of the sequence of two moves, a threshold tightening is necessary. Hence, M is adjusted to zero for the two forward move sequence. This case is F5b and is shown in Figure I-8.

The second case occurs when the metric accumulator is less than α. Since $a_0 = 1$, the subtraction of α from the metric accumulator is required to proceed ahead. Since M is not great enough to permit this, we are forced to initiate a back search unless $M = 0$. If indeed $M = 0$, then this is case F4. Since all forward search steps terminate on a best branch node, M can only be equal to zero due to a threshold tightening. Thus, M may be increased by Δ and the forward search mode is continued with a procedure similar to case F5. When M is not equal to zero and a back search is to be initiated, θ and the back search variable ϕ are set to one. It should be noted that back search is only initiated due to this condition: $a_0 = 1$, $a_1 = 0$ and $0 < M \leq \alpha$.

I-2.2 BACK SEARCH

In the back search mode most cases are turn around cases. That is, the move originates in the back search mode and terminates in the forward search mode. This accounts for the fact that the final node is often ahead of the initiating node. The first test to be performed in back search mode is the test for maximum allowed backup. If the index of tree depth n is equal to the maximum allowed backup KBACK (this could be the origin of the tree for initial back searches), then M is increased by Δ and the forward search is begun. This backup barrier can be thought of as a reflecting wall. When the decoder backs up to KBACK, the decoder is sent forward on the same paths it backed up on but with the metric increased by Δ. This use of KBACK allows for a design that must only store a number of nodes equal to KBACK in order to decode. Hence, the amount of rapid access storage is minimized and the need for transfer of data from the slow access bulk storage is unnecessary during back search.

After testing for n > KBACK, if test is true, the variable FLAG is tested. The results of this test pertain to the multiple node back search sequence case B7 and will be discussed later. The next test is for $M > 0$. If this test is false, three possible moves can be made depending on hypothesis h made at the node behind the present node. If $h = 0$, then case B1, shown in Figure I-9, is encountered. In this case, $M = 0$ resulted from a threshold tightening. Therefore, M is incremented by $\Delta + 1$ and the decoder advances one node along the best branch node. If $h = 1$, then the path immediately behind the present node must have been along a double disagreement. The two possibilities are case B2 if $a_2 = 0$ and case B8 if $a_2 = 1$. Case B2 in Figure I-9, results because no alternate path exists since $h = 1$ indicates that the better path has already been tried and is found not to satisfy the existing threshold. Hence, β is added to the metric accumulator and the decoder is stepped back.

Case B8 involves a turn around, a change of a hypothesis and a selection of a second tie hypothesis to assure a good branch on the forward step. Since $a_2 = 1$, the node prior to the present node is reached as the result of a tie decision. If, however, the present node is equal to KBACK + 1, this move cannot be performed as that would require the change of hypothesis behind KBACK and no hypotheses are stored farther back than KBACK. Hence, under this condition, case B2 must be performed instead of case B8. After testing to determine the case, the metric is tested to decide whether θ is to be set to zero and whether the result of the move will require a threshold tightening (case B8b). The complementing and path selection are accomplished by setting $c' = 1$, $c = \bar{a}_0$. Since a_0 is a function of the complementing, $\bar{a}_0$ is used. The forward step accomplishes the required branch selection and the c and c' variables are cleared.

If the test $M > 0$ is found to be true, the hypothesis h is again tested. Again cases B2 or B8 result if $h = 1$. If $h = 0$, then the remaining cases B3 through B7 are possible. Case B3 represents an instance when M is too small to allow cases B4 or B5 and $a_2 = 0$ so cases B6 or B7 are not possible. Thus, there is no alternative available to switch forward, so the metric increment one is subtracted from the accumulator and the decoder is shifted back one step.

Cases B4 and B5 are instances in which the accumulator value is sufficiently large to permit the selection of a worst case path. The difference between the cases is the value of a_0 and, thus the path to be followed on the step forward. The Figure I-9 illustrating cases B4 and B5 show different values of a_2, but this does not enter into the
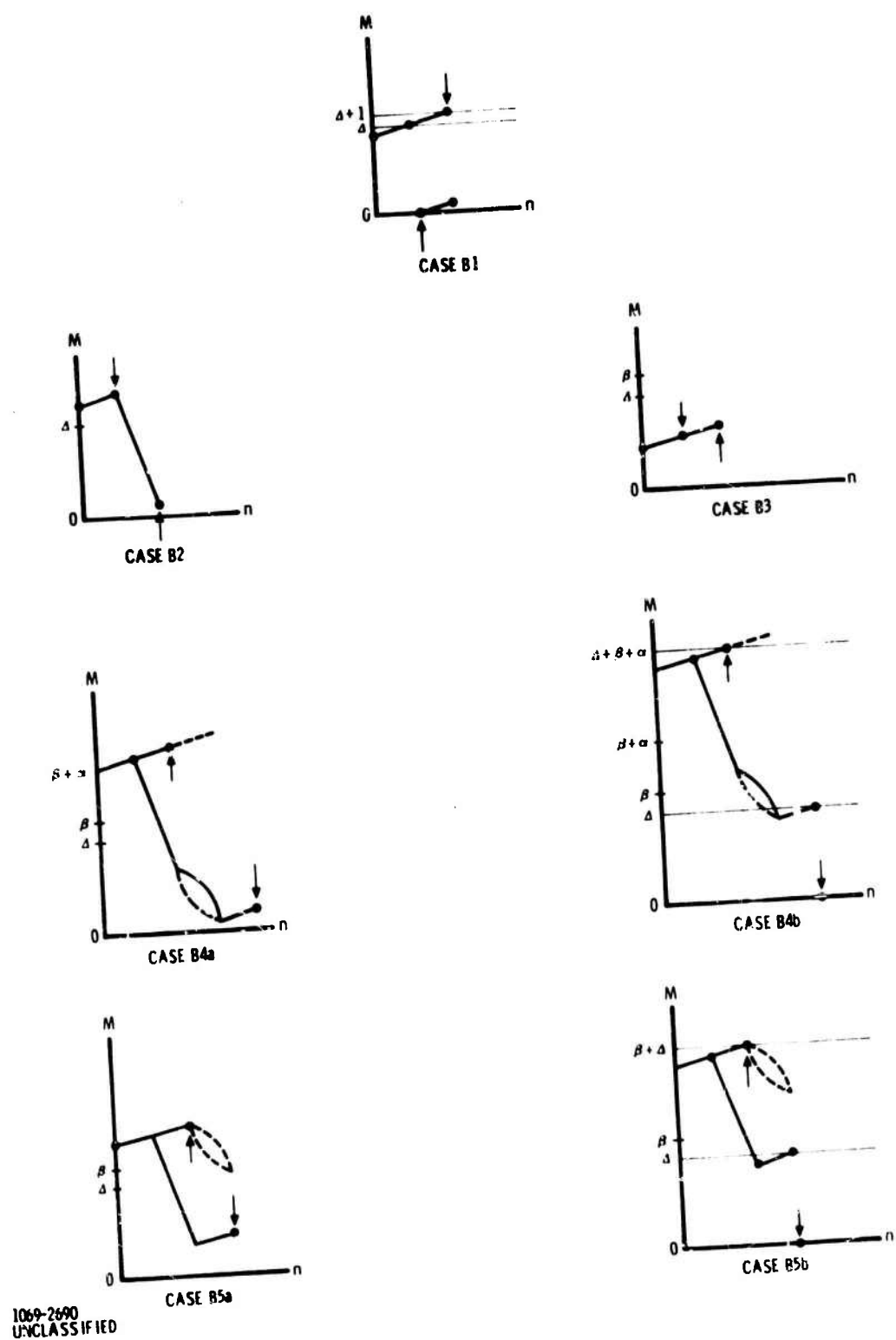
Figure I-9. Back Search Distance Diagrams for Fano Threshold Algorithm
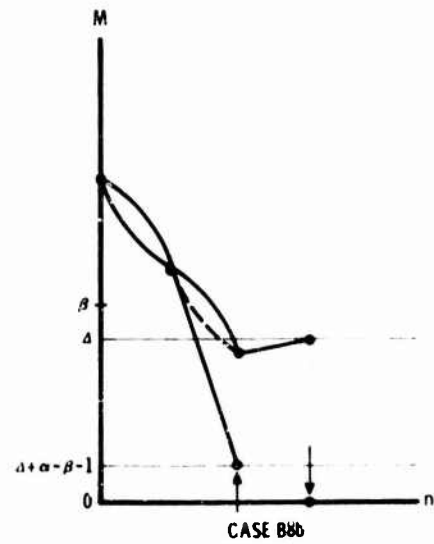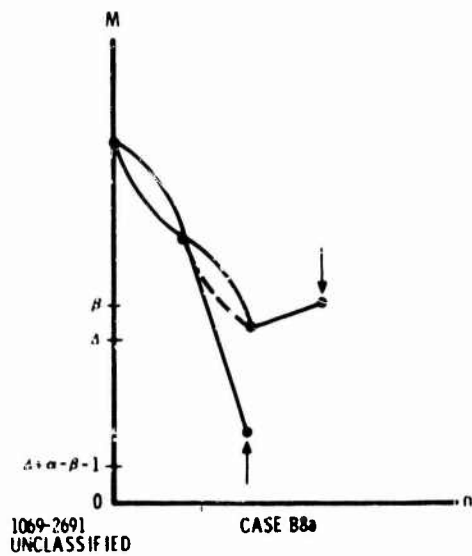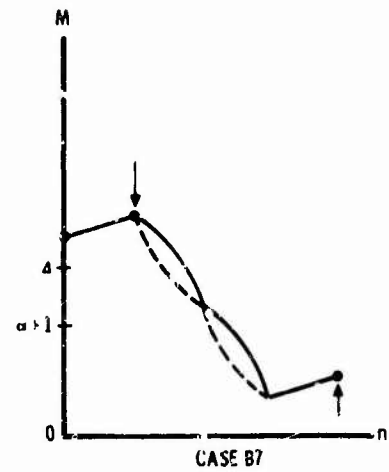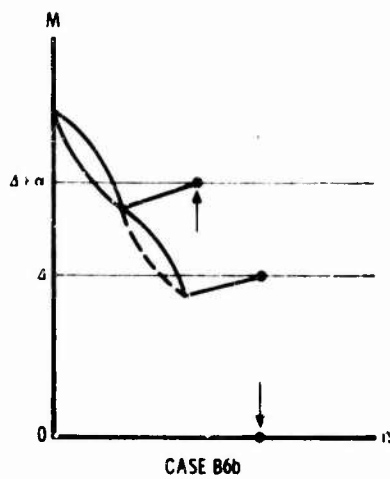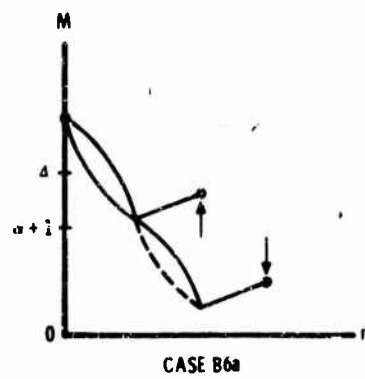
Figure I-9. Back Search Distance Diagrams for Fano Threshold Algorithm (Continued)

-511-

logic of the cases. The cases B4b and B5b are performed when a threshold will be necessary as a result of the move. In case B4, since $a_0 = 0$ for the present search node a_0 will be one when the hypothesis h is changed. This will allow a forward step identical to F5 after the complementing of h.

Case B5 shows that since $a_0 = 1$ at the present search node it will be equal zero after the complementing of h. Therefore, the direct single step move shown is initiated.

The remaining cases represent instances in which a_2 is equal to one. That is, the node prior to the one being examined is reached as the result of a tie decision. Cases B4 and B5 represented instances where the accumulator value permitted the selection of a worst path. When the accumulator is less than $\beta + 1$, however, cases B6 or B7 are encountered.

If the metric is $\alpha < M < \beta + 1$, then case B6 results. Case B6 involves a turn around, a change of a hypothesis and a selection of a second tie hypothesis to assure a good branch on the forward step. As in case B8, if the present node is equal to KBACK + 1, this move cannot be performed since that would require the change of hypothesis behind KBACK. Hence, instead case B7 is used to back up to KBACK. After testing to determine the case, the metric is tested to decide whether θ is to be set to zero and whether the result of the move will require a threshold tightening (Case B6b). The complementing and path selection are accomplished by setting c' = 1 and $c = \bar{a}_0$. Since a_0 is a function of the complementing, $\bar{a}_0$ is used. The forward step accomplishes the required branch selection and c and c' variables are cleared.

If $M \leq \alpha$ then case B6 cannot be performed and the decoder must be backed up along at least one and maybe a multiplicity of tie branches. This one or a multiplicity of the branches is handled by the logic shown for case B7. The move always begins on a good node and continues until another good node is reached. This is accomplished by the FLAG being set to one. The test for FLAG = 1 is the first test after testing for the decoder backing up to KBACK. As long as $a_1 = 1$ during the backup, FLAG = 1 and the metric is incremented by α as the decoder steps back. When a node is found where $a_1 = 0$, indicating a good branch selection, FLAG is set equal to zero and normal backup is resumed. This case concludes the search logic for the Fano threshold algorithm.

-515-

I-3.1 MODIFIED THRESHOLD ALGORITHM

One of the major disadvantages of the Fano threshold algorithm is the occurrence of extremely long back searches necessary if several threshold loosenings are required. This case occurs when a path through an error pattern consisting of a large number of errors must be found. Therefore, a modified threshold algorithm was proposed to minimize these long back searches. In this algorithm the threshold increments were made small to detect an error pattern quickly that was causing the metric to decrease. However, it is not desirable to back up for every single disagreement ($a_0 = 1$) as the condition will occur occasionally due to a check bit error. Since the threshold increments were small, the metric was allowed to build up to 2α due to double agreement paths ($a_0 = 0$) and the threshold tightening was chosen equal to one. Thus, after the metric built up to 2α due to $a_0 = 0$ paths, additional $a_0 = 0$ paths will result in threshold tightenings keeping the metric at 2α since the increase in the metric due to an $a_0 = 0$ path is also equal to one. The value 2α was chosen because this allows a maximum of two $a_0 = 1$ paths consecutively but a double disagreement path requires a threshold release since $\beta > 2\alpha$. The threshold release increment Δ is a variable that can be changed to optimize performance. However, simulations indicate that $\Delta = 1$ gives optimum performance.

In the Fano threshold algorithm, threshold tightenings can be detecting during backup when $M = 0$ is tested and $h = 0$. In the modified threshold algorithm, there are numerous possible moves to arrive at $M = 2\alpha$ and it is impossible to detect a threshold tightening during backup. Thus, a new variable Λ must be added to indicate threshold tightening. This variable represents an added bit of storage that is employed to maintain this memory. The extra bit of storage is associated with a hypothesized path and is required over the span of the allowed back search.

I-3.2 FORWARD SEARCH

The logic used in the algorithm is shown in the flow diagram of Figure I-10. The moves are identical to the ones used in the Fano threshold algorithm except those involving threshold tightenings and releases. The algorithm begins with the variables θ, ϕ, c, c', FLAG, KBACK, and n set equal to zero. The metric accumulator M is set equal to 2α. The initial tightening memory bit $\Lambda(0)$ is permanently set equal to one, the remaining bits in this memory are set to zero. The hypothesis memory is also set to zero at the beginning of a block search.
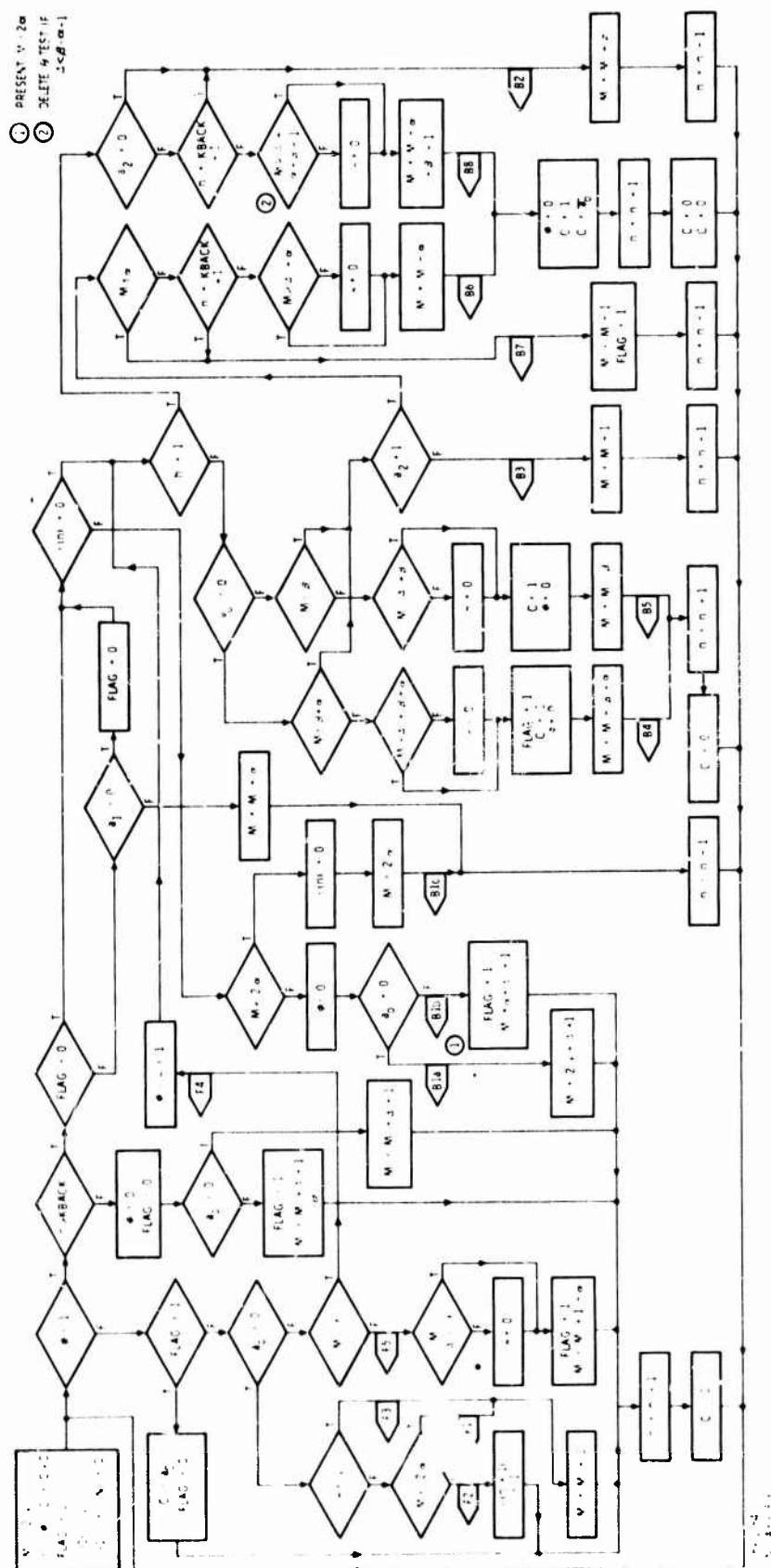
Figure I-10. Flow Diagram – Modified Threshold Algorithm

In the forward search, indicated by $\Phi = 0$, cases F1 and F3 shown in Figure I-11 are identical to the corresponding cases in the Fano threshold algorithm except that the decision between F1 and F3 is at $M < 2\,\alpha$ instead of $M < \Delta$. Case F2 occurs when the forward search has reached the maximum threshold gap and no further increase is allowed while θ is equal to zero. This instance really represents the increasing of the metric by 1 and a subsequent tightening of the metric by 1; thus, no change in metric results. The variable $\Lambda\,(n+1)$ is set equal to one to indicate that a threshold tightening has occurred at this step. The dashed lines show the two possible paths followed by get to the present search node in this case. Again, they must be best branches, the difference is whether a threshold tightening occurred.

When a_0 is equal to 1 in the forward search, either case F4 or F5 is encountered. Case F4 is the case in which $M < \alpha$. Since $a_0 = 1$, the subtraction of α from the metric accumulator is required to proceed ahead. However, M is not great enough to permit this and back search is initiated. The action that is required is that θ and the back search variable Φ be set equal to 1. The reason that there is no alternative in this case,

CASE F1   CASF F2   CASE F3

CASE F4   CASE F5
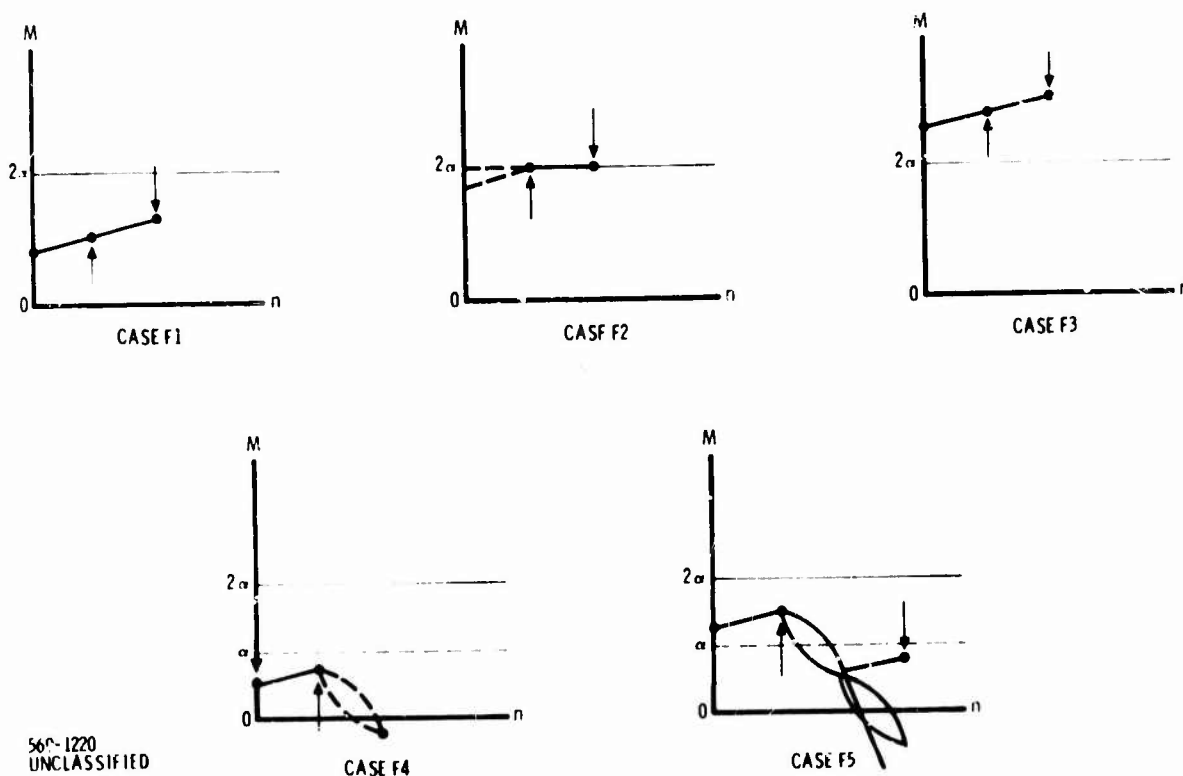
Figure I-11. Forward Search Distance Diagrams
for Modified Threshold Algorithm

-518-

is that because of the forward search logic employed, a_1 must always be equal to zero in this case. Therefore, to complement this hypothesis and thus allow a zero at a_0 would cause a decrease in the metric by $\beta - 1$ which would also violate the threshold condition. It should be noted that case F4 is the only condition that initiated a back search.

Case F4 is shown in the logic diagram (Figure I-10) by the line leaving the $M < \alpha$ test in the forward search and transferring to the back search mode. Entrance to the back search at the point indicated is allowed because the FLAG test has already been performed and $M < \alpha$ implies $\Lambda(n) = 0$.

The second case of $a_0 = 1$ is F5 and occurs when $M \geq \alpha$ (the value of θ is immaterial). Case F5 is similar to case F5 of the Fano threshold algorithm without the possibility of case F5b. Since $M \geq \alpha$ a forward step is allowed causing a decrease in the metric by α. Proper selection of the tie path allows the second move of this two sequence to be along a double agreement path. The procedure for making the necessary advance in case F5 was described for the case in the Fano threshold algorithm.

I-3.3 BACK SEARCH

As in the Fano threshold algorithm, the first test to be performed in the back search is to test for maximum backup. If the index of the tree depth, n, is equal to KBACK, then M is increased by Δ and the forward search is begun.

After testing for $n > $ KBACK, if this test is true, the variable FLAG is tested. As before, this test pertains to the multiple node back search sequence case B7. The next test to be performed in the look-back mode is the test of $\Lambda(n)$. If $\Lambda(n)$ equals one for the present search node a threshold tightening occurred at this node in the forward search. If $\Lambda(n)$ equals one, three different reactions take place as noted by cases B1a, B1b, B1c in Figure I-12.

The first time the search returns to a node where the threshold was tightened, the value of the accumulator will be 2α. When this occurs, cases B1a and B1b result. Briefly, the threshold is released by an increment Δ and a forward search is initiated. The two cases result from test of a_0. For these cases, the $\Lambda(n)$ variable is not reset so that memory is retained of the threshold tightening.

-519-
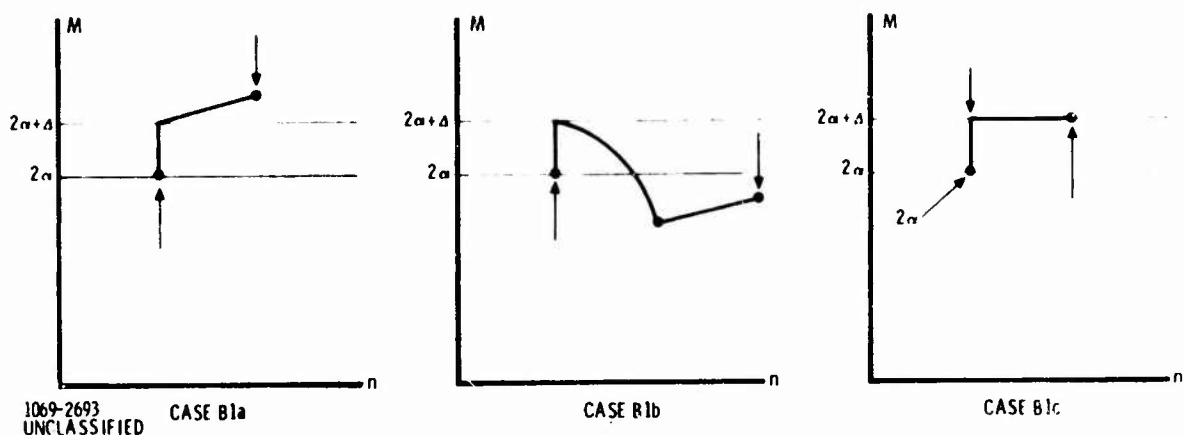
Figure I-12. Back Search Distance Diagrams
for Modified Threshold Algorithm

If the search returns to a tightened node again, the value of the accumulator
will be $2\alpha + \Delta$. When this occurs, case B1c results. The algorithm now makes new
paths available for the decoder to search by stepping back one node. The accumulator
is compensated for the threshold changes by subtracting $(\Delta - 1)$. Further, $\Lambda(n)$ is set
equal to zero for the present search node and the back search node continued. This
exhausts the alternatives when $\Lambda(n) = 1$.

For $\Lambda(n) = 0$, the cases B2 through B8 are possible. Since none of these cases
involve threshold tightenings, they are identical to the previously described back
search cases B2, B3, B4a, B5a, B6a, B7, and B8a of the Fano threshold algorithm
which also involve no threshold tightenings. In the Fano threshold algorithm, cases
B4b, B5b, B6b, and B8b provided the necessary threshold tightenings in the back
search for that algorithm.

I-4.1 BLOCK RESYNCHRONIZATION TAIL ALGORITHM

When block resynchronization is used instead of statistical resynchronization,
special attention must be given to the moves into and inside the tail sequence. Inside
the tail sequence, there are no threshold tightenings and the decoder must hypothesize
zeros for the tail sequence since the present decoder structure calculates a syndrome
from the incoming data stream. Therefore, the basic tail algorithm consists of two
forward search moves and two back search moves. The forward search moves depend
on a_0. For $a_0 = 0$, the move is to add one to the metric accumulator and advance one
node. If the correct hypotheses were made before the tail sequence, $a_0 = 1$ can only

-520-

occur due to an error in the check bit. Thus, if $a_0 = 1$ occurs too often, an incorrect hypothesis must have been made previous to entering tail and the decoder should back out of the tail. For $a_0 = 1$, the move is to subtract α from the metric accumulator if $M \geq \alpha$ and advance one node. However, if $M < \alpha$ the decoder should initiate the back search. Since the decoder cannot change the hypotheses from zero within the tail, the decoder should back all the way out of the tail. Therefore, the two back search moves are the counterpart of the forward moves. During the backup of each node, a one is subtracted from the metric accumulator for $a_1 = 0$, and $\sim$ is added to the metric accumulator for $a_1 = 1$.

While the basic tail algorithm is quite simple, the algorithm becomes complicated by the transition between the normal algorithm and the tail algorithm. The flow diagram for complete tail algorithm is shown in Figures I-13a and I-13b. The basic algorithm consists of case F1 and F2 for the forward search and cases B3 and B7a for the back search. As mentioned, there are no threshold tightenings within the tail sequence. However, at n = ITAIL (the beginning of the tail sequence), the normal algorithm could have caused a threshold tightening. Therefore, it is necessary to test for $M = 0$ in the Fano threshold algorithm shown in Figure I-13a or to test for $\Lambda(n) = 1$ in the modified threshold algorithm shown in Figure I-14 as a replacement set of moves.

Figure I-15 illustrates the two basic forward search moves, Cases F1 and F2. Case F3 in Figure I-15 can occur at n = ITAIL when the Fano algorithm is used. In this case $M = 0$, $a_0 = 1$, $a_1 = 0$ and $h = 0$. Therefore, a threshold tightening must have occurred. The move is to add $\Delta - \alpha$ to the metric accumulator and move forward.

Case B1 shown in Figure I-13a occurs in the Fano threshold algorithm when the decoder backs up to n = ITAIL with $M = 0$, $h = 0$, $a_1 = 0$ and $a_0 = 0$. In this case, M is incremented by Δ and the decoder moves forward along the double agreement path. This case is identical with the Case B1 of the normal Fano threshold algorithm. Likewise, cases B1a, B1b, and B1c occurring due to a threshold tightening at n = ITAIL by the modified threshold algorithm are identical to the cases B1a, B1b, and B1c of the normal backup outside the tail for this algorithm.

Cases B2, B5, B7 and B8 can only occur at n = ITAIL and are identical with the corresponding cases B2, B5, B7 and B8 in the normal algorithms. Cases B3, B3a and B3b are really identical cases occurring at different places in the tail. Case B3,

Figure I-13a. Flow Diagram – Block Resynchronization Algorithm

1069-2694
UNCLASSIFIED
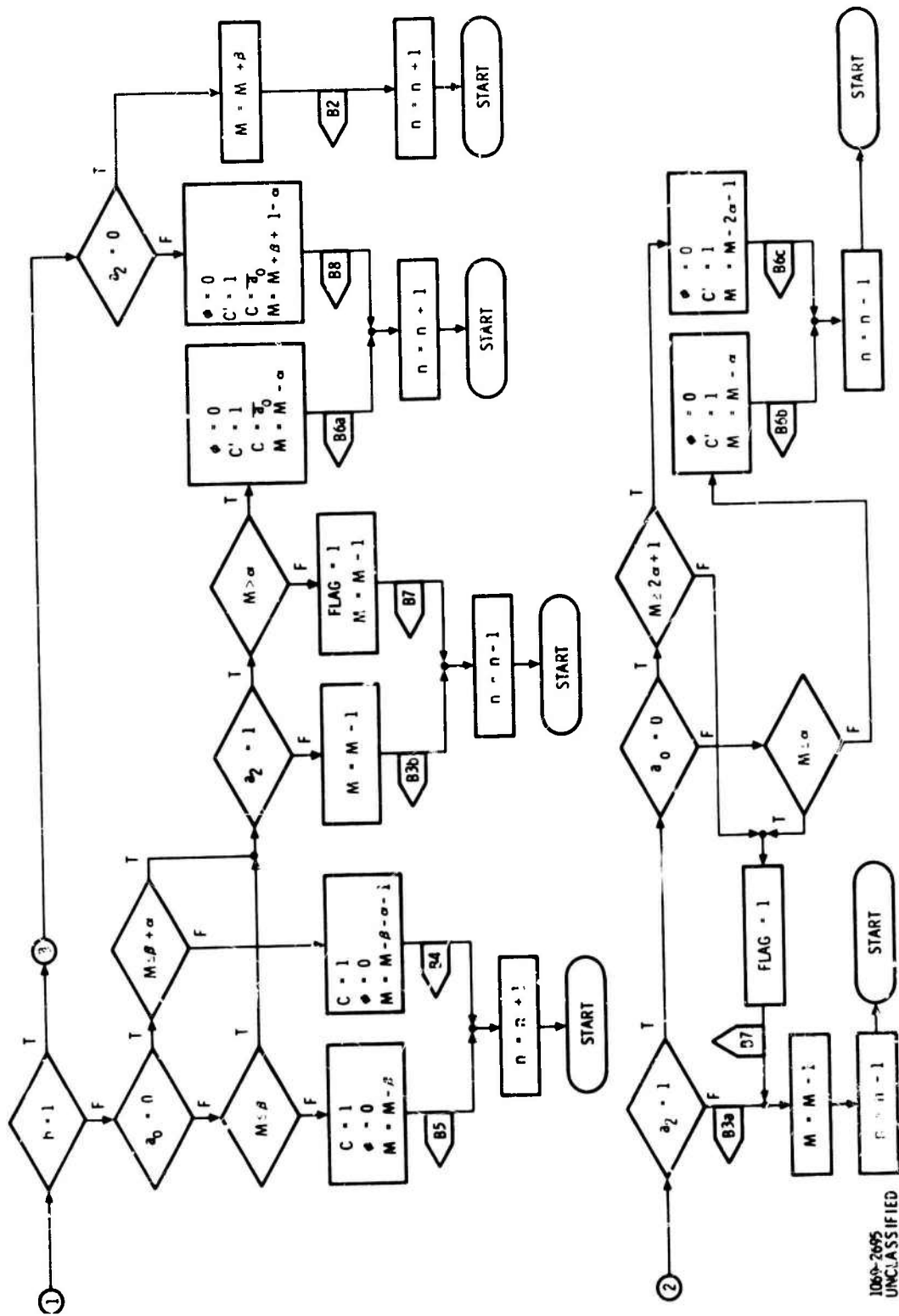
Figure I-13b. Flow Diagram – Block Resynchronization Algorithm

-523-
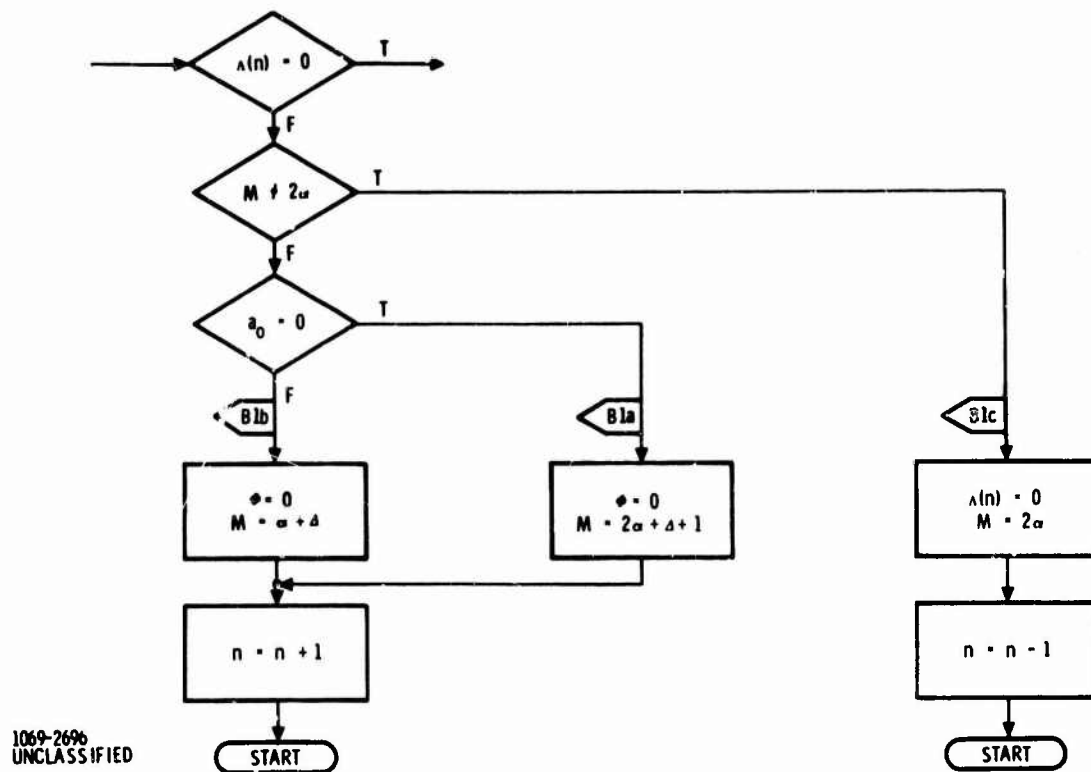
Figure I-14. Flow Diagram - Modified Threshold Algorithm at ITAIL
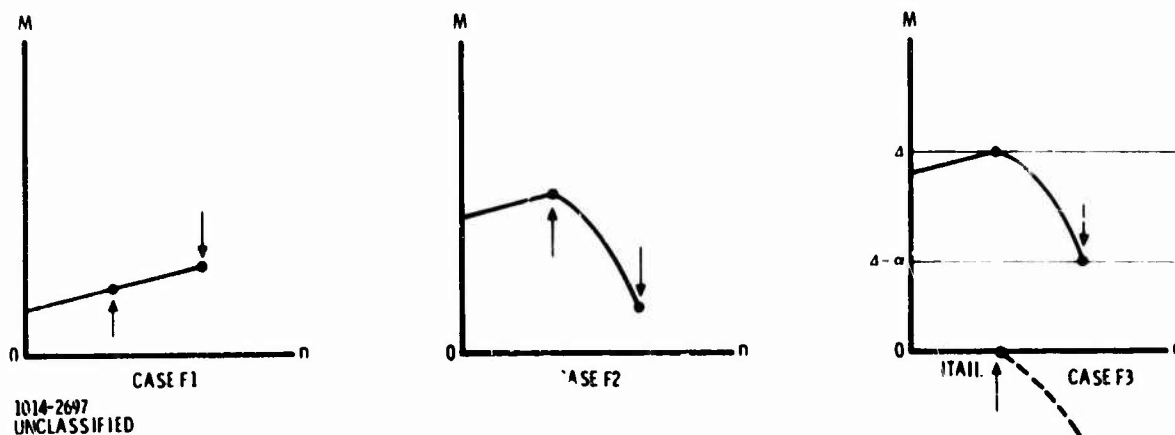
Figure I-15. TAIL Forward Search Distance Diagrams

-524-

as shown in Figure I-16, occurs inside the tail and the move consists of subtracting one from the metric accumulator and stepping back one node regardless of whether $a_2 = 0$ or 1. Cases B3a and B3b are essentially the same case but starting from ITAIL + 1 and ITAIL, respectively. Both cases occur only when $a_1 = 0$, $a_2 = 0$, and h = 0.

Case B4 shown in Figure I-16 is a shortened version of the normal case B4. The shortening results from the requirement that all hypotheses within the tail must be zero. Thus, the move begins by hypothesizing a one for the branch behind ITAIL. Since $a_0 = 0$ before h was set to one, the move forward is moved along a tie branch but the next hypothesis must be zero and therefore the decoder cannot select the tie branch that would be followed by a $a_0 = 0$ path. Hence, the move is ended after advancing along the tie branch instead of advancing along the selected proper tie branch and continuing along the double agreement path as is done in the normal case B4.
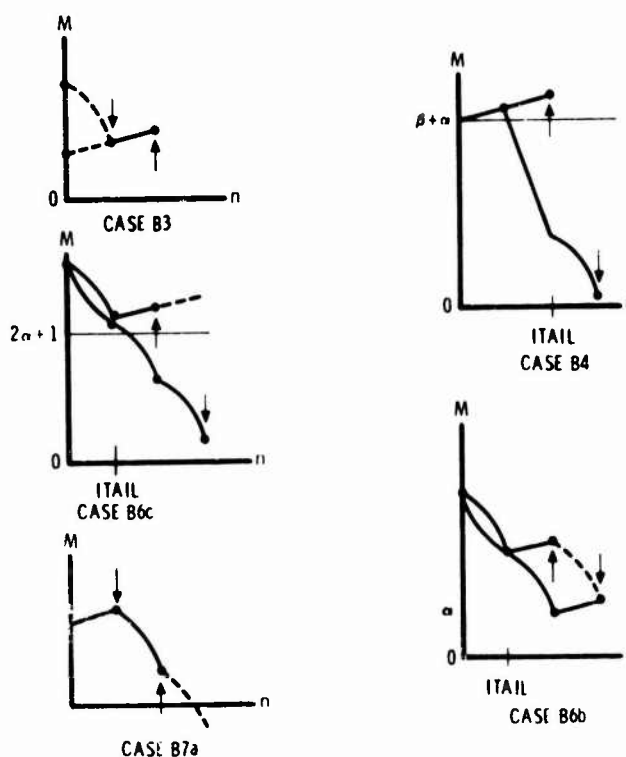
Figure I-16. Tail Back Search Distance Diagrams

Case B6a occurs at $n = $ ITAIL and is identical with case B6 of the normal algorithms. If $a_0 = 1$, then a similar case can also occur at $n = $ ITAIL $+ 1$. Since $a_0 = 1$, then if the hypothesis behind ITAIL is set to one, the required choice of the $h = 0$ tie branch leads to a $a_0 = 0$ path. Hence, case B6b is identical with the normal case B6 with the exception that $a_0 = 1$ is required and it is not necessary to make a selection on the final tie branch. If $a_0 = 0$, then case B6c is possible when $M \geq 2\alpha + 1$. Since $a_0 = 1$ after the complementing, the $h = 0$ tie branch leads to another tie branch. Therefore, the move consists of making the hypothesis behind ITAIL equal to one, selecting the $h = 0$ of the second tie branch and advancing along the third $h = 0$ tie branch. The metric accumulator is then decreased by $2\alpha + 1$. If M is too small to allow the B6 cases, then the decoder must continue to back up along a normal B7 case. The final case to consider is Case B7a. This case is one of the back search cases of the basic tail algorithm. It is a single move back along a tie branch. If a series of these Case B7a cases occur as the decoder backs up to $n = $ ITAIL $+ 1$, it is necessary to switch from case B7a to case B7 by setting FLAG $= 1$. This is necessary since within the tail it is possible to end a forward move with $a_1 = 1$ which is not possible outside the tail. Therefore, the decoder cannot back up along a tie branch outside the tail unless FLAG $= 1$.

This completes the description of the tail algorithm and the normal decoding algorithms necessary to the sequential decoder design.

APPENDIX II

RANDOM NUMBER GENERATOR PERFORMANCE

Upon investigation of the random number generator used for the initial sequential decoder simulations, it was found that the generator had dependency between generated numbers. The program for testing the dependency in the generator is presented here, along with dependency that was found. Using this test program, a random number generator with satisfactory statistics was found for a computer with 24-bit words.

The sequential decoder is operated assuming that the transmitted data is all zeros. Thus, an error produced by the channel is indicated by a one. A random number generator used for simulation of the channel is required to first produce numbers between zero and one that are samples from a uniform distribution. To produce a one for an error using samples from a uniform distribution, an interval equal in magnitude to the probability of error is assigned. Then, if the sample falls in this interval, the received digit is a one; otherwise, the received digit is a zero. However, the channel simulation scheme used for the initial results generated two received digits from each sample of the uniform distribution. In this case, the interval from zero to one is divided into four subintervals, corresponding to the probability of a double error, the probability of only an error in the first digit, the probability of only an error in the second digit, and the probability of two correct digits.

To test for dependency between the generated digits, a number of digits equal to ICON were generated. The number of ones in the set of ICON digits was recorded and another digit was generated. Taking this digit and the ICON-1 previously generated digits, the number of ones in this set of ICON digits was recorded and the process is repeated. Thus, examining each set of ICON digits by replacing the oldest digit with the newly generated digit (sliding aperture) each pattern of ones and zeros is recorded. For example, suppose ICON equals 2 and the pattern 0 1 1 0 0 0 1 1 was generated. By the scheme described, the event of 0 0 occurs twice, the event 0 1 occurs twice, the event 1 0 occurs twice, and the event 1 1 occurs twice. Notice the event 1 1 only is recorded once if the first set of two digits is examined, then the third and fourth digits, etc. Thus, not all possible dependency between digits may be detected without the sliding aperture scheme.

The dependency between digits is found by comparing the statistics obtained from the sliding aperture measurements and the theoretical probability of each event assuming a binomial distribution of the digits. The FORTRAN program that makes the sliding aperture measurements and computes the theoretical probability of each event is presented in Table II-1. The random number generator presented in Table II-1 is the generator used in the initial simulations. By generating 400,000 digits, Table II-2 compares the dependency measurements with the theoretical expectations at probability of error equal to 0.04.

Table II-1. FORTRAN Program to Test Dependency
of Random Number Generators

```
DIMENSIØN P(50),PM(50),IPS(50)
TYPE 101
101 FØRMAT($PRØB,ICØN,NRAN,IRAN$/)
ACCEPT 100,PRØB,ICØN,NRAN,IRAN
100 FØRMAT(F7.4,3I9/)
Q=1.-PRØB
ICØN1=ICØN+1
DØ 1 I=1,ICØN1
IS=I-1
1 P(I)=B(IS,ICØN)*PRØB**IS*Q**(ICØN-IS)
TYPE 103
103 FØRMAT(/$CALCULATED ERRØR PRØBABILITIES$//)
TYPE 102,(P(I),I=1,ICØN1)
102 FØRMAT(4E15.7/)
DØ 2 I=1,ICØN1
PM(I)=0
2 IPS(I)=0
PRØB1=PRØB**2
PRØB3=1.-PRØB+PRØB1
DØ 3 I=1,NRAN
C: BEGINNING ØF RANDØM NUMBER GENERATØR TØ BE TESTED
IRAN=IRAN*4097+5033325
IF(IRAN) 375,375,376
375 IRAN=IRAN+8388607+1
376 RND=IRAN
RND=RND/8388607.
INFØ=1
ICHCK=1
IF(RND-PRØB1) 106,107,107
107 ICHCK=0
IF(RND-PRØB) 106,108,108
108 INFØ=0
IF(RND-PRØB3) 106,109,109
109 ICHCK=1
```

Table II-1 (continued)

```
C: END OF RANDOM NUMBER GENERATOR TO BE TESTED
106 JMOD=MOD(I-1,ICON)+1
IPS(JMOD)=INFO
IM=1
DO 4 J=1,ICON
4 IM=IM+IPS(J)
PM(IM)=PM(IM)+1.
JMOD=MOD(I,ICON)+1
IPS(JMOD)=ICHCK
IM=1
DO 5 J=1,ICON
5 IM=IM+IPS(J)
3 PM(IM)=PM(IM)+1.
COUNT=2*NRAN
DO 6 I=1,ICON1
6 PM(I)=PM(I)/COUNT
TYPE 104
104 FORMAT(/$MEASURED ERROR PROBABILITIES$//)
TYPE 105,(PM(I),I=1,ICON1)
105 FORMAT(4E15.7/)
END
FUNCTION B(I,N)
B=1.
IF(I) 502,502,501
501 DO 500 J=1,I
500 B=B*(N-I+J)/J
502 RETURN
END
```

Notice that the measured probability of three errors in an aperture of four or five is about twice the probability predicted by theory. In an attempt to decrease the dependency, the random number generator was modified such that only one digit was generated at a time. Also of importance is where the subinterval of the uniform distribution corresponding to choosing the digit equal to one is placed. For generators of the form

$$X_{i+1} = aX_i + C \ (\text{Mod } M) \tag{1}$$

where $M = 2^k$, only the most significant bit of the binary representation of the generated number has the maximum period. The other bit periods decrease with bit position until

Table II-2. Performance of the Original Random Number Generator

ICON		Number of Errors in Aperture ICON					
		0	1	2	3	4	5
2	Theoretical	0.9216	0.0768	1.6×10^{-3}			
	Measured	0.9214	0.0769	1.73×10^{-3}			
3	Theoretical	0.8847	0.1106	4.6×10^{-3}	6.4×10^{-5}		
	Measured	0.8844	0.1107	4.8×10^{-3}	4.5×10^{-5}		
4	Theoretical	0.8493	0.1416	8.847×10^{-3}	2.458×10^{-4}	2.56×10^{-5}	
	Measured	0.8486	0.1427	8.238×10^{-3}	4.925×10^{-4}	0	
5	Theoretical	0.8154	0.1699	1.416×10^{-2}	5.898×10^{-3}	1.229×10^{-5}	1.024×10^{-7}
	Measured	0.8137	0.1733	1.152×10^{-2}	1.343×10^{-2}	8.75×10^{-5}	C

the last bit is always 1.[*] To decrease dependency resulting from the short periods of the least significant bits of the generated numbers, the subinterval corresponding to the choice of a one was chosen to be dependent only on the most significant bits of the generated numbers. Thus, if the sample falls in the subinterval nearest one, an

Table II-3. Program for Modified Random Number Generator

```
IRAN=IRAN*4097+5033325
IF(IRAN) 375,376,376
375 IRAN=IRAN+8388607+1
376 RND=IRAN
RND=RND/8388607.
INF0=0
IF(RND-Q) 106,107,107
107 INF0=1
106 IRAN=IRAN*4097+5033325
IF(IRAN) 475,476,476
475 IRAN=IRAN+8388607+1
476 RND=IRAN
RND=RND/8388607.
ICHCK=0
IF(RND-Q) 108,109,109
109 ICHCK=1
```

[*] "Random Number Generating and Testing," Reference Manual C20-8011, IBM Corp , New York, N.Y., 1959.
Barnett, V. D., "The Behavior of Pseudo-random Sequences Generated on Computers by Multiplicative Congruential Method, "Math Comput., Vol. 16, pp. 63-69, 1962

Table II-4. Performance of the Modified Random Number Generator

ICON		Number of Errors in Aperture ICON				
		0	1	2	3	4
2	Theoretical	0.9216	0.0768	1.6×10^{-3}		
	Measured	0.9217	0.0766	1.63×10^{-3}		
3	Theoretical	0.8847	0.1106	4.608×10^{-3}	6.4×10^{-5}	
	Measured	0.8848	0.1108	4.16×10^{-3}	2.22×10^{-4}	
4	Theoretical	0.8493	0.1416	8.847×10^{-3}	2.458×10^{-4}	2.56×10^{-6}
	Measured	0.8498	0.1411	8.96×10^{-3}	2.3×10^{-4}	0

error is indicated by choosing the digit equal to one. Table II-3 presents the FORTRAN
program of the random number generator to be tested Q in the program is equal to
one minus the probability of error Table II-4 compares the dependency measurements
at a probability of error equal to 0.04 Notice that for this generator the measured
probability of three errors in an aperture of three is about 3.5 times the probability
predicted by theory. Hence, it was decided that this generator was not adequate even
when modified.

After examining numerous random number generators, the generator presented
in Table II-5 seemed to give the required independency between generated digits within
the accuracy obtained by generating 400,000 digits. Table II-6 presents the results of
dependency measurements at a probability of error equal to 0.04.

Table II-5. Program for Chosen Random Number Generator

```
IRAN=IRAN*2051
IRAN=IRAN-(IRAN/4194304)*4194304
IF(IRAN) 375,376,375
375 IRAN=-IRAN
376 RND=IRAN
RND=RND/4194303.
INF0=0
IF(RND-Q) 106,107,107
107 INF0=1
106 IRAN=IRAN*2051
IRAN=IRAN-(IRAN/4194304)*4194304
IF(IRAN) 475,476,476
475 IRAN=-IRAN
476 RND=IRAN
RND=RND/4194303.
ICHCK=0
IF(RND-Q) 108,109,109
109 ICHCK=1
```

Table II-6. Performance of Chosen Random Number Generator

ICON		Number of Errors in Aperture ICON					
		0	1	2	3	4	5
2	Theoretical	0.9216	0.0768	1.6×10^{-3}			
	Measured	0.9211	0.0773	1.54×10^{-3}			
3	Theoretical	0.8847	0.1106	4.608×10^{-3}	6.4×10^{-5}		
	Measured	0.8841	0.1113	4.54×10^{-3}	6.0×10^{-5}		
4	Theoretical	0.8493	0.1416	8.847×10^{-3}	2.458×10^{-4}	2.56×10^{-6}	
	Measured	0.8486	0.1424	8.825×10^{-3}	2.325×10^{-4}	5.0×10^{-6}	
5	Theoretical	0.8154	0.1699	0.01416	5.898×10^{-4}	1.29×10^{-5}	1.024×10^{-7}
	Measured	0.8143	0.1710	0.01417	5.225×10^{-4}	2.25×10^{-5}	0

APPENDIX III
S/N LOSS IN A LOW-PASS CLIPPER -CORRELATOR

Digital computation of the correlation between a received signal plus noise and the replica signal can be performed after time sampling and amplitude quantizing. For the present discussion, the replica signal when sampled is represented by a sequence of random binary digits (± 1). The noise will be presumed to be independent for each sample and described by a probability density p(x) with average power (second moment) equal to σ^2. The sampled received amplitude is

$$v = \pm 1 + x \tag{1}$$

depending on the polarity of the signal.

If an infinite clipper is utilized, the amplitude v is quantized to one of two allowed values, represented as ± 1. Then, the correlator output for that sample is

$$\text{Correlator amplitude} = \pm \text{polarity} (\pm 1 + x) \tag{2}$$

where the sign is used depending on the polarity of the signal. The signal-to-noise ratio (S/N) after summing over many samples is a measure of signal detectability, and is of interest here. Compared with a linear (unquantized) correlation, the S/N loss is well known to be $2/\pi$, or 2 db, if x is Gaussian distributed with zero mean, and σ^2 is large.[*]

Since the average correlator output is required to compute S/N, Equation (2) may be averaged to obtain

$$\text{Average correlator amplitude} = 1 - 2P \tag{3}$$

where P = average probability of error in quantizing the received amplitude on the basis of polarity.

---

[*] M. Kanefsky, "Detection of Weak Signals with Polarity Coincidence Arrays," I.E.E.E. Trans. on Information Theory, Vol. IT-12, pp. 260-268; April 1966.

While the S/N loss for Gaussian noise is relatively small, there exists no guarantee against complete loss of correlation. For example, suppose that x is itself a random binary waveform of amplitude exceeding unity, so that the polarity of v is dominated by the polarity of x. This loss of correlation can be prevented by adding a noise perturbation prior to the clipping process. Alternatively, this may be viewed as shifting the threshold away from the zero level[**]. The problem is to select a distribution for the threshold shift which optimizes performance.

Let the threshold shift be denoted by β, with the probability density $g(\beta)$. For a particular β, the probability of error averaged over the two signal polarities can be written as

$$P = \frac{1}{2} \text{ Prob } (x + \beta > 1) + \frac{1}{2} \text{ Prob. } (x + \beta < -1)$$

$$= \frac{1}{2} - \frac{1}{2} \text{ Prob } (-1 < x + \beta < 1) \tag{4}$$

The average probability of error averaged over all allowed β is

$$P = \frac{1}{2} - \frac{1}{2} \int_{-\infty}^{\infty} g(\beta) \, d\beta \int_{-1}^{1} p(y + \beta) \, dy \tag{5}$$

If the noise probability density $p(x)$ is known, the probability of error is minimized by setting β so that

$$\int_{-1}^{1} p(y + \beta) \, dy = \text{Maximum} \tag{6}$$

and

$$P = \frac{1}{2} - \frac{1}{2} \left[\int_{-1}^{1} p(y + \beta) \, dy \right]_{\text{max over } \beta} \tag{7}$$

It is seen that a probability density which tends to a maximum at zero will call for a threshold setting at $\beta = 0$. As a simple generalization, Gaussian noise with a non-zero mean calls for β to be set at the mean in order to maximize the correlation.

[**] W. L. Root, "Communications Through Unspecified Additive Noise," Information and Control, Vol. 4, pp. 15-29; 1961.

If the noise distribution is unknown, a minimax (game theory) concept may be utilized. Here the threshold shift is selected in accordance with a probability density $g(\beta)$ which is defined to minimize the probability of error for the worst noise distribution. Equation (7) gives a lower bound for the worst case probability of error, since the threshold shift density $g(\beta)$ was selected to combat a specific noise density $p(x)$. In order to obtain the greatest lower bound, a $p(x)$ is to be found which yields

$$\text{Minimum} \left\{ \int_{-1}^{1} p(y + \beta) \, dy \right\}_{\text{max over } \beta} \tag{8}$$

The minimum value which has been found occurs for a uniform distribution satisfying the average power constraint, or

$$p(x) = \frac{1}{2 \sqrt{3} \sigma}, \quad - \sqrt{3} \sigma < x < \sqrt{3} \sigma \tag{9}$$

From this, one obtains (assuming $\sigma > 1/\sqrt{3}$)

$$\text{Worst case } P \geq \frac{1}{2} - \frac{1}{2 \sqrt{3} \sigma} \tag{10}$$

A corresponding upper bound is to be found next.

The complement of the above procedure is to assume a threshold shift density $g(\beta)$ and compute the worst noise density $p(x)$ which yields an upper bound on probability of error. It is desired to find the least upper bound. This computation yields an upper bound because the best strategy on threshold shift has not necessarily been utilized.

As a first approach, assume $\sigma >> 1$ so that $g(\beta)$ tends to be essentially constant over a region of width 2. Then Equation (5) may be rewritten with the substitution $x = y + \beta$ and approximated

as

$$P = \frac{1}{2} - \frac{1}{2} \int_{-\infty}^{\infty} p(x)\,dx \int_{x-1}^{x+1} g(\beta)\,d\beta$$

(11)

$$\cong \frac{1}{2} - \int_{-\infty}^{\infty} p(x)\,g(x)\,dx$$

To obtain an upper bound on probability of error, let the threshold shift strategy be

$$g(\beta) = \frac{1}{2B} \qquad\qquad -B < \beta < B$$

(12)

This is chosen as minimizing the maximum of $g(\beta)$ when β is confined to a finite range. Using Equation (11), the noise density which yields the maximum probability of error, subject to the average power constraint is easily verified to be

$$p(x) = \frac{\sigma^2}{2B^2}\,\delta(x + B) + \left(1 - \frac{\sigma^2}{B^2}\right)\delta(x) + \frac{\sigma^2}{2B^2}\,\delta(x - B)$$

(13)

if $B \geq \sigma$. In Equation (13) it is presumed that only the impulse at $x = 0$ falls within the range of β given in Equation (12). (If $B < \sigma$, the density $p(x)$ can be chosen to yield $P = 1/2$, and this clearly is not the least upper bound).

Substituting Equation (13) into Equation (11) yields

$$P = \frac{1}{2} - \frac{1}{2B}\left(1 - \frac{\sigma^2}{B^2}\right)$$

(14)

and the least upper bound occurs for

$$B = \sqrt{3}\,\sigma$$

(15)

yielding

$$\text{Minimax P} \leq \frac{1}{2} - \frac{1}{3\sqrt{3\sigma}} \tag{16}$$

This upper bound is slightly higher than the lower bound previously obtained and given in Equation (10). However, a tighter bound can be found by a more general approach using the approximation of Equation (11).

The minimax solution corresponds to selection of non-negative density functions $p(x)$ and $g(x)$ which, respectively, simultaneously minimize and maximize Equation (11), subject to the constraints

$$\int_{-\infty}^{\infty} g(x)\,dx = 1 \tag{17}$$

$$\int_{-\infty}^{\infty} p(x)\,dx = 1 \tag{18}$$

$$\int_{-\infty}^{\infty} x^2 p(x)\,dx \leq \sigma^2 \tag{19}$$

If the Euler equation for a constrained extremal is applied in an attempt to solve the problem, one obtains

$$p(x) - \lambda_1 = 0$$

$$g(x) - \lambda_2 - \lambda_3 x^2 = 0 \tag{20}$$

It will be shown in a direct manner that the form of the solution given in Equation (20) is, in fact, correct when the range of x is restricted to that given in Equation (9).

If the expression for g(x) in Equation (20) is normalized as required by
Equation (17), one obtains

$$\lambda_2 + \lambda_3 \sigma^2 = \frac{1}{2\sqrt{3}\,\sigma} \tag{21}$$

Similarly, Equation (9) gives the normalization for p(x), assuming equality in
Equation (19), and substitution in Equation (11) gives the right side of Equation (10),
as might have been anticipated. This is independent of the specific selection of
λ_2 and λ_3. The density function g(x) is on the boundary of becoming negative for
the choice yielding

$$g(x) = \frac{\sqrt{3}}{4\sigma}\left(1 - \frac{x^2}{3\sigma^2}\right), \quad -\sqrt{3}\,\sigma < x < \sqrt{3}\,\sigma \tag{22}$$

Equation (22) turns out to be the desired minimax probability density of threshold
shift, as will now be demonstrated by considering an arbitrary p(x) satisfying the
constraints, Equations (18) and (19).

The inequality is obtained

$$\int_{-\sqrt{3}\,\sigma}^{\sqrt{3}\,\sigma} x^2 p(x)\,dx \leq \int_{-\infty}^{\infty} x^2 p(x)\,dx - 3\sigma^2\left[1 - \int_{-\sqrt{3}\,\sigma}^{\sqrt{3}\,\sigma} p(x)\,dx\right]$$

$$\leq \sigma^2 - 3\sigma^2 + 3\sigma^2 \int_{-\sqrt{3}\,\sigma}^{\sqrt{3}\,\sigma} p(x)\,dx \tag{23}$$

by noting that the second moment is decreased if the total probability outside
$-\sqrt{3}\,\sigma < x < \sqrt{3}\,\sigma$ is concentrated just outside this range. Then, by substitution
of Equation (23), Equation (11) becomes

$$P = \frac{1}{2} - \frac{\sqrt{3}}{4\sigma} \int_{-\sqrt{3}\,\sigma}^{\sqrt{3}\,\sigma} \left(1 - \frac{x^2}{3\sigma^2}\right) p(x)\,dx$$

$$\leq \frac{1}{2} - \frac{1}{2\sqrt{3}\,\sigma}$$

(24)

which improves on the previous bound of Equation (16) and equals the lower bound of Equation (10). Note, also, that the equality applies for any p(x) totally confined within $-\sqrt{3}\,\sigma < x < \sqrt{3}\,\sigma$ and having the second moment σ^2.

Thus, a direct proof has been given demonstrating the minimax probability of error and defining a threshold shift density function to achieve the minimax against an arbitrary noise of second moment $\leq \sigma^2$. Although the derivation starting with Equation (21) presumes the range $-\sqrt{3}\,\sigma < x < \sqrt{3}\,\sigma$, it can be generalized to an arbitrary range. The initial presumption is then found to yield the least upper bound on probability of error.

For large σ^2, the preceding result can be interpreted in terms of S/N loss, since P⟶0.5, and the variance of the correlator output approaches unity. Hence

$$\left(\frac{S}{N}\right)_{clipped} = (1 - 2P)^2 = \frac{1}{3\sigma^2} = \frac{1}{3}\left(\frac{S}{N}\right)_{input}$$

(25)

Thus, the minimax loss of signal-to-noise ratio is 4.8 db, regardless of the actual distribution of the noise.

The minimax strategy for obtaining the guaranteed loss of Equation (25) may be as shifting the threshold randomly for each sample within the range $-\sqrt{3}\,\sigma < x < \sqrt{3}\,\sigma$ in accordance with the probability density in Equation (22). Note that the range is determined by the desired interference power σ^2 which is to be tolerated.

The above results may also be interpreted directly as probability of error for a binary communication channel. Against the worst case interference of specified average power, the probability of error is guaranteed to be bounded, and there is a loss of 2.8 db compared with performance optimized against Gaussian noise of the same average power.

APPENDIX IV

DIGITAL MATCHED FILTER FOR QUADRIPHASE AND
DOPPLER SHIFTED SIGNALS

In Section 7.5.2, a concept of a digital matched filter for synchronization is described with reference to a biphase modulated signal. The discussion presumed the carrier frequency to be known exactly (i.e., within a maximum allowable offset error depending on the duration of integration). Thus, the simplest case has been presented. The actual problem may require the matched filter to handle quadriphase modulated signals and signals with a carrier offset due to Doppler and oscillator instability. Extension of the basic approach to these cases is now described; however, without further discussion of quantization effects.

For reference, the basic digital matched filter for a biphase signal is shown again in simplified form in Figure IV-1. The pseudorandom binary sequence is represented by $A(t)$, and the unknown carrier phase error is θ. The function Φ_A is intended to represent the correlation between the received sequence and the replica sequence stored in the matched filter. Interference is present but not shown.

When a carrier frequency offset is introduced on the signal and the local oscillator remains fixed, the received signal may be written in the form

$$s(t) = A(t) \cos (\omega_c t + \omega_D t + \theta) \tag{1}$$

The quadrature components from the two produce detectors are

$$\text{Inphase} = A(t) \cos \omega_D t \cos \theta - A(t) \sin \omega_D t \sin \theta$$

$$\text{Quad} = A(t) \sin \omega_D t \cos \theta + A(t) \cos \omega_D t \sin \theta \tag{2}$$

Hence, a match to the offset signal requires replicas for both $A(t) \cos \omega_D t$ and $A(t) \sin \omega_D t$. Figure IV-2 shows the digital matched filter for this case. It is, of course, necessary to store quantized versions of these two functions, and as mentioned above the effects of such quantization will be ignored for this discussion. In a binary matched filter, these functions can be infinitely clipped to retain only polarity information.

To cover a given frequency uncertainity, the matched filter can be postulated as using a set of discrete values of ω_D. The allowable separation depends on the duration T of integration. A reasonable specification is roughly $1/2T$. Since the

-540-
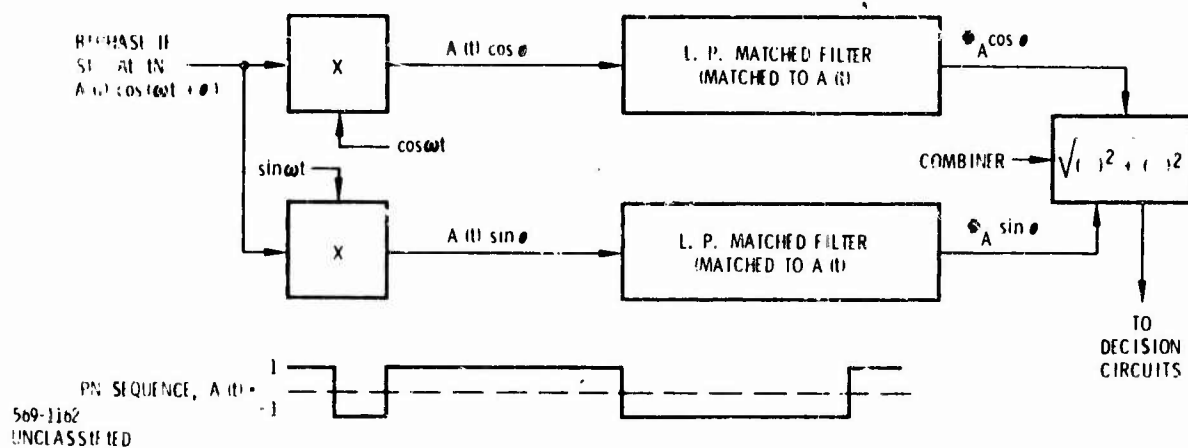
Figure IV-1. Complete Low Pass Matched Filter for
Biphase Signal No Doppler.
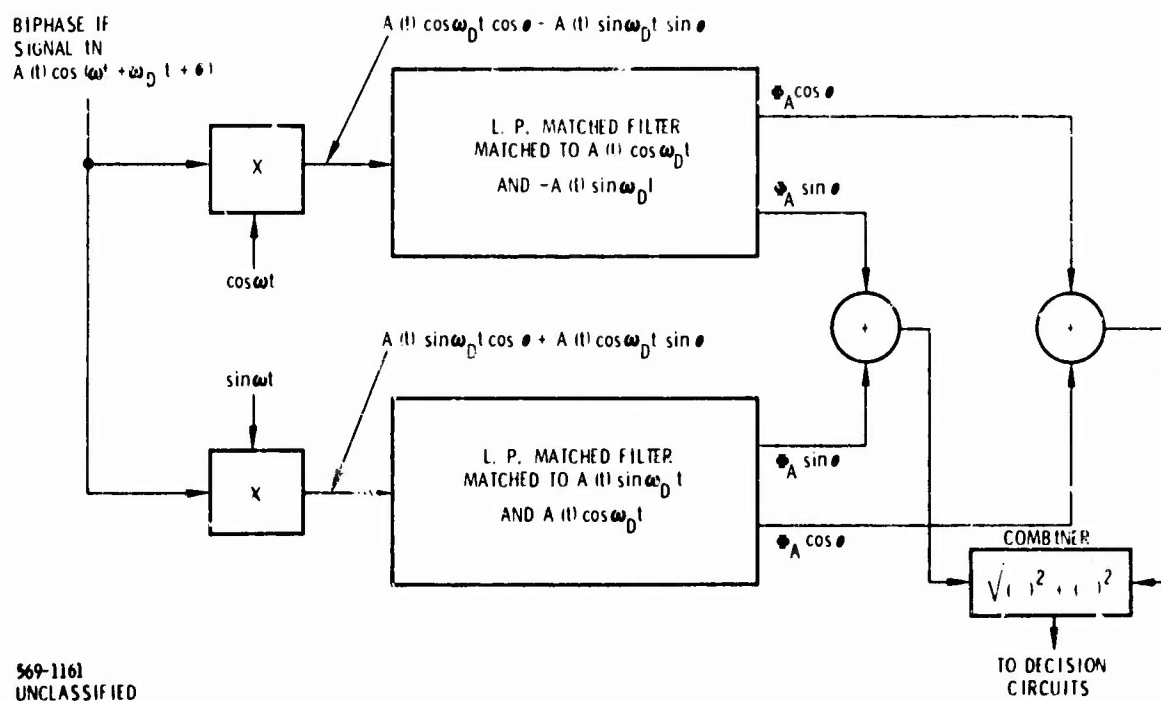
Figure IV-2. Complete Low Pass Matched Filter for
Biphase Signal with Doppler

-541-

phase change is π over the duration of integration for this maximum spacing, the worst-case integration loss is approximately $20 \log_{10} [\sin (\pi/2)/(\pi/2)]$, or 4 db.

A quadriphase modulated signal may be viewed as the quadrature sum of two independent biphase signals. Assuming no carrier frequency error, the quadriphase signal may be written as

$$s(t) = A(t) \cos (\omega_c t + \theta) + B(t) \sin (\omega_c t + \theta) \tag{3}$$

where $A(t)$ and $B(t)$ represent the two independent pseudorandom binary sequences resulting in four possible phases. The quadrature components then are

$$\begin{aligned} \text{In-Phase} &= A(t) \cos \theta + B(t) \sin \theta \\ \text{Quadrature} &= B(t) \cos \theta - A(t) \sin \theta \end{aligned} \tag{4}$$

The similarity of Equation (4) with Equation (2) for the case of an offset frequency with a biphase modulated signal may be noted. Figure IV-3 shows the matched filter configuration for this case. Here, Φ_A and Φ_B denote the correlation functions for $A(t)$ and $B(t)$ with their respective replica waveforms.
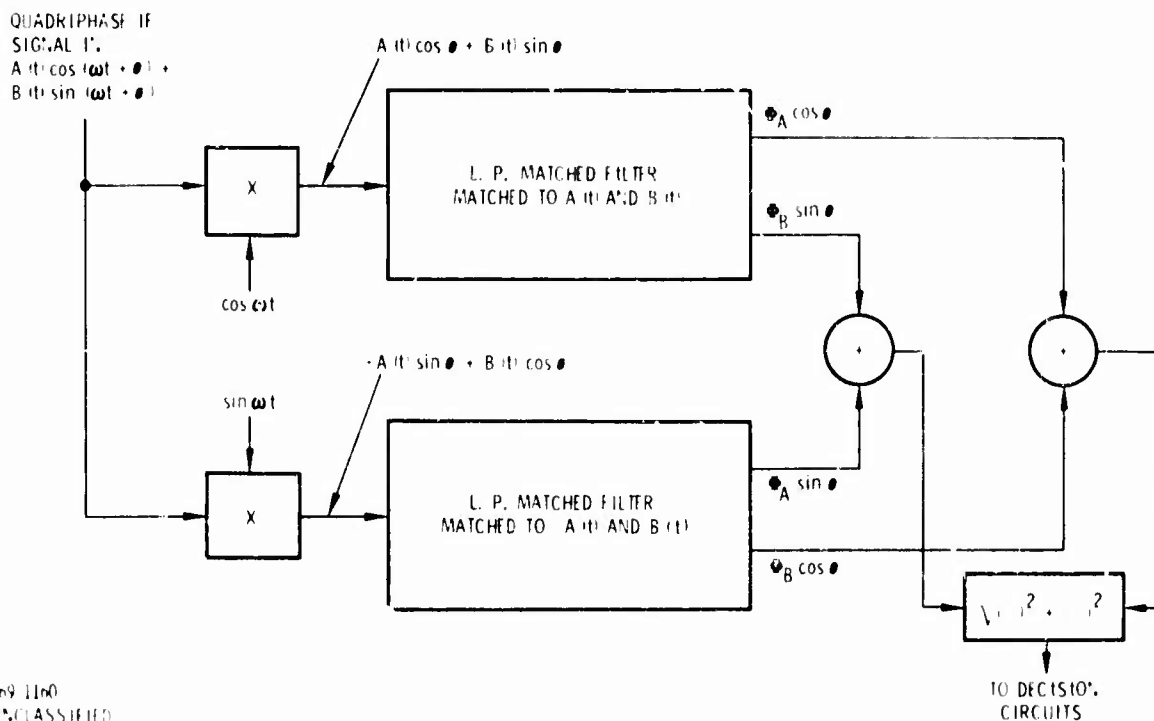
Figure IV-3. Complete Low Pass Matched Filter for
Quadriphase Signal No Doppler.

-542-

Finally, when frequency uncertainties are present, the received signal is of the form

$$s(t) = A(t) \cos (\omega_c t + \omega_D t + \theta) + B(t) \sin (\omega_c t + \omega_D t + \theta) \qquad (5)$$

and the quadrature components are

$$\text{In-Phase} \quad [A(t) \cos \omega_D t + B(t) \sin \omega_D t] \cos \theta$$
$$- [A(t) \sin \omega_D t - B(t) \cos \omega_D t] \sin \theta$$

$$\qquad (6)$$

$$\text{Quadrature} = [B(t) \cos \omega_D t - A(t) \sin \omega_D t] \cos \theta$$
$$- [B(t) \sin \omega_D t + A(t) \cos \omega_D t] \sin \theta$$

which requires matched filters for the four functions $A(t) \cos \omega_D t$, $A(t) \sin \omega_D t$, $B(t) \cos \omega_D t$, and $B(t) \sin \omega_D t$. Figure IV-4 shows the matched filter configuration for this case.

Since the complexity of the matched filter for either biphase or quadriphase is doubled by a requirement to accommodate a frequency offset, a system design which does not display Doppler offsets outside the maximum frequency error $(\pm 1/2T)$ is desirable. A system involving burst transmissions is one such example, since the speed up for the burst gives a corresponding reduction in Doppler sensitivity.

QUADRIPHASE IF
SIGNAL IN
A (t) cos $(\omega t + \omega_D t + \theta)$ +

B (t) sin $(\omega t + \omega_D t + \theta)$

X

cos ω t

sin ω t

X

L. P. MATCHED FILTER
MATCHED TO A (t) cos ω_D t,
- A (t) sin ω_D t, B (t) cos ω_D t
AND B (t) sin ω_D t

A (t) cos ω_D t cos θ - A (t) sin ω_D t sin θ +
B (t) cos ω_D t cos θ + B (t) sin ω_D t sin θ

L. P. MATCHED FILTER
MATCHED TO - A (t) cos ω_D t,
- A (t) sin ω_D t, B (t) cos ω_D t
AND - B (t) sin ω_D t

B (t) cos ω_D t cos θ - B (t) sin ω_D t sin θ
- A (t) sin ω_D t cos θ - A (t) cos ω_D t sin θ

Φ_A cos θ
Φ_B cos θ
Φ_A sin θ
Φ_B sin θ

Φ_A sin θ
Φ_B sin θ
Φ_A cos θ
Φ_B cos θ

+

+

COMBINER

$\sqrt{(\ )^2 + (\ )^2}$

TO DECISION CIRCUITS
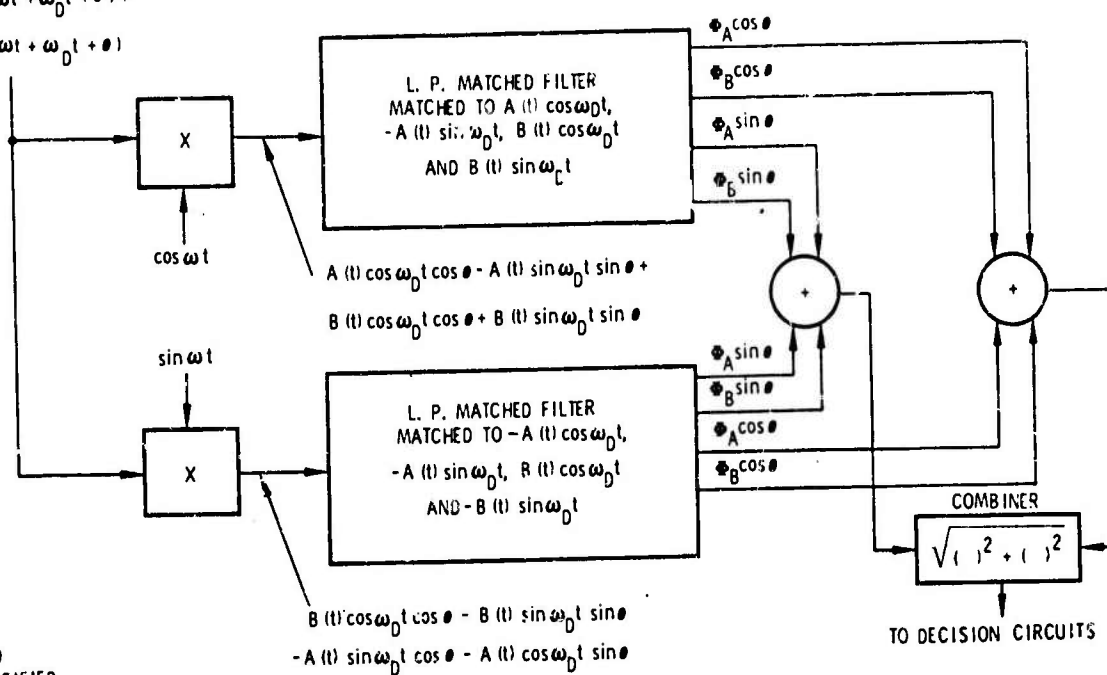
569-1159
UNCLASSIFIED

Figure IV-4. Complete Low Pass Filter for Quadriphase
Signal with Doppler

APPENDIX V
OPTIMUM SPACING FOR DELAY LOCK TRACKING

In the analysis of delay lock tracking presented in Section 7.6.1.4 an expression for the mean square error was derived. This result is based on a linearized model in which the rms error is small compared with the region of linearity for the error characteristic. Application of maximum likelihood estimation principles leads to a configuration having a linear range which approaches zero; hence, the previous conclusion that the optimum correlator spacing for delay lock is zero (leading to correlation with the derivative of the waveform) is valid only in the limit of signal-to-noise ratio approaching ∞. The threshold region must still be further investigated.

In this discussion, a finite spacing is presumed for the delay lock tracking with an unfiltered signal having the ideal triangular autocorrelation function. Figure V-1 shows the error characteristic for a typical spacing $2\tau_d$ where the signal power is S and the PN clock interval is T_c. The output noise density for the delay lock tracker is given by Equation (217) of Section 7.6.1.4, and for the case of no filtering reduces to

$$N_o^{(out)} = 4N_o\tau_d/T_c \tag{1}$$

where N_o is the received noise density (one sided). Since the slope of the error characteristic in the vicinity of zero error is

$$\text{Error slope} = \frac{\sqrt{S}\,2\tau_d/T_c}{\tau_d} = 2\sqrt{S}/T_c \tag{2}$$

the mean square tracking error is

$$\tau_{\Delta\tau}^2 = \frac{N_o^{(out)}B_L}{[\text{Slope}]^2} = \frac{N_o B_L}{S}\,\tau_d T_c \tag{3}$$

where B_L is the noise bandwidth of the linearized tracking loop. Equation (231) of Section 7.6.1.4 reduces to Equation (3) for the same assumptions.
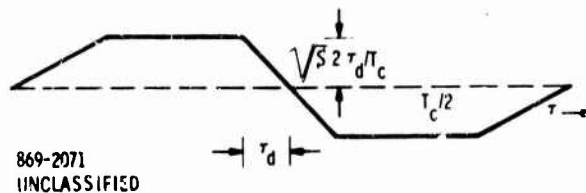
Figure V-1. Error Characteristic for Delay Lock Tracking

The problem is now evident that a threshold exists. Note from Figure V-1 that τ_d is the limit of linearity, while Equation (3) shows the rms time error due to noise is proportional to $\sqrt{\tau_d}$, other parameters being fixed. Although Equation (3) predicts a constantly decreasing error as τ_d is decreases, the region of linearity will be exceeded at some value of τ_d. Hence, an optimum choice τ_d may be expected.

As an approximate first analysis, consider the quasi-linearization approach[*] which has been applied to demonstrate threshold in a phase lock loop. This approach replaces the nonlinear error characteristic by an equivalent gain (i.e., slope) for a linearized model, given by

$$\text{Equivalent slope} = \int_{-\infty}^{\infty} h'(\tau) p(\tau) d\tau \qquad (4)$$

where

$h(\tau)$ = error characteristic

$p(\tau)$ = probability density of the time error, assumed to be Gaussian distributed.

With this equivalent slope, the closed loop bandwidth B_L can still be defined meaningfully. For the case of zero mean error and a variance $\sigma^2_{\Delta\tau}$, Equation (4) is evaluated for the characteristic of Figure V-1 to be

$$\text{Equivalent Gain} \approx \int_{-\tau_d}^{\tau_d} (\sqrt{S}\, 2/T_c) \frac{1}{\sqrt{2\pi}\,\sigma_{\Delta\tau}} e^{-\tau^2/2\sigma^2_{\Delta\tau}} d\tau$$

$$= \frac{\sqrt{S}\,2}{T_c} \left[\Phi(\tau_d/\sigma_{\Delta\tau}) - \Phi(-\tau_d/\sigma_{\Delta\tau}) \right] \qquad (5)$$

[*] J.A. Develet, Jr., "A Threshold Criterion for Phase-Lock Demodulation," Proc. of IRE, Vol. 51, pp. 349-356, February 1963.

considering, for simplicity, only the central portion of the error characteristic as significant. For $\sigma_{\Delta\tau} \rightarrow 0$, the expression reduces to the slope at τ 0. For larger $\sigma_{\Delta\tau}$, the equivalent slope is reduced, which increases the error using Equation (3) with the equivalent slope substituted. This becomes

$$\sigma^2_{\Delta\tau} \cong \left(\frac{N_o B_L}{S}\right) \frac{\tau_d T_c}{\left[\Phi(\tau_d/\sigma_{\Delta\tau}) - \Phi(-\tau_d/\sigma_{\Delta\tau})\right]^2} \tag{6}$$

Minimization of Equation (6) by varying τ_d is now to be carried out. In normalized form, this is equivalent to maximizing the function

$$f(x) - [\Phi(x) - \Phi(-x)]^2/x \tag{7}$$

which occurs at $x = 1.4$. Thus, the optimum τ_d satisfies

$$\frac{\tau_d}{\sigma_{\Delta\tau}} = 1.4 \tag{8}$$

which relates the optimum spacing to the tracking error, and the minimum rms error is computed to be

$$\left.\frac{\sigma_{\Delta\tau}}{T_c}\right]_{min} \cong 2\frac{N_o B_L}{S} \tag{9}$$

for the optimum τ_d given by Equation (8). Equation (9) reflects the decrease in optimum τ_d as $S/N_o B_L$ increases.

As an illustration, if $S/N_o B_L = 20$ db, the theoretical minimum tracking error is 0.02 of the PN bit interval, and the optimum separation is $\tau_d = 0.024$ of the PN bit interval. Referring to Figure 7-81, this result indicates a minimum actually will occur in the curve marked $B = \infty$, when the saturation effect is taken into account.

In the bandlimited case, also illustrated in Figure 7-81, the performance varied much less (essentially not at all for $B = 1.5\pi$) with the separation τ_d. Thus, considering practical filtering requirements, the choice of delay lock separation is not critical. With saturation brought in again, the design tendency should be towards larger τ_d.

As a somewhat more sophisticated analysis leading to a similar conclusion, consider the following criterion of estimation:

Select time delay τ for maximum total likelihood within interval of width $2\sigma_{\Delta\tau}$ (10)

This should be contrasted with the estimator previously described in Section 7.6.1.2, which selected τ to maximize likelihood at one value of time. Using Equation (200) of that section, the proposed criterion may be expressed as

$$\tau_0 = \underset{\tau}{\text{Max}} \int_{\tau-\sigma_{\Delta\tau}}^{\tau+\sigma_{\Delta\tau}} dx \exp\left\{ \frac{2}{N_0} \int_{-T/2}^{T/2} r(t)\, s(t-x)\, dt \right\}$$ (11)

where

$r(t)$ — received signal plus noise

$s(t)$ — known waveform

T — smoothing interval

The maximum is obtained as a solution to the equation setting the derivative equal to zero. Differentiating with respect to τ, which appears only in the limits of integration, gives

$$0 = \exp\left\{ \frac{2}{N_0} \int_{-T/2}^{T/2} r(t)\, s(t-\tau_0-\sigma_{\Delta\tau})\, dt \right\} - \exp\left\{ \frac{2}{N_0} \int_{-T/2}^{T/2} r(t)\, s(t-\tau_0+\sigma_{\Delta\tau})\, dt \right\}$$ (12)

It is observed that the criterion leads to a nonlinear processing; however, the operation of creating an error by correlating with finite separation of the replica waveform again suggests the delay lock configuration with a finite spacing equal to the width accepted for error.

APPENDIX VI

TWO RANGE DIFFERENCE AND ALTITUDE LANDING CONFIGURATION

This appendix derives the aircraft position from the indicated measurements. The following equations apply:

$$(x-x_1)^2+(y-y_1)^2+(z-z_1)^2=r_1^2 \tag{1}$$

$$(x-x_2)^2+(y-y_2)^2+(z-z_2)^2=(r_1+d_1)^2 \tag{2}$$

$$(x-x_3)^2+(y-y_3)^2+(z-z_3)^2=(r_1+d_2)^2 \tag{3}$$

$$z=h \tag{4}$$

A flat earth, which is assumed in order to get (4), is a valid approximation for the coverage regions under consideration (about 20 nmi distances from touchdown point). Subtracting Equation (2) from (1) and (3) from (1) yields

$$x+y\frac{(y_2-y_1)}{x_2-x_1}+z\frac{(z_2-z_1)}{x_2-x_1}+r_1\frac{d_1}{x_2-x_1}=\frac{x_2^2+y_2^2+z_2^2-x_1^2-y_1^2-z_1^2-d_1^2}{2(x_2-x_1)}$$

$$x+y\frac{(y_3-y_1)}{x_3-x_1}+z\frac{(z_3-z_1)}{x_3-x_1}+r_1\frac{d_2}{x_3-x_1}=\frac{x_3^2+y_3^2+z_3^2-x_1^2-y_1^2-z_1^2-d_2^2}{2(x_3-x_1)}$$

Now let

$$X_i=x_i-x_1; \qquad Y_i=y_i-y_1; \qquad Z_i=z_i-z_1;$$

$$D_i=\frac{x_i^2+y_i^2+z_i^2-x_1^2-y_1^2-z_1^2-d_{i-1}^2}{2}$$

and we obtain

$$x+y\frac{Y_2}{X_2}+z\frac{Z_2}{X_2}+\frac{r_1 d_1}{X_2}=\frac{D_2}{X_2} \tag{5}$$

$$x+y\frac{Y_3}{X_3}+z\frac{Z_3}{X_3}+\frac{r_1 d_2}{X_3}=\frac{D_3}{X_3} \tag{6}$$

Subtracting (6) from (5) and using (4) yields

$$y\left(\frac{Y_2}{X_2}-\frac{Y_3}{X_3}\right)+h\left(\frac{Z_2}{X_2}-\frac{Z_3}{X_3}\right)+r_1\left(\frac{d_1}{X_2}-\frac{d_2}{X_3}\right)=\frac{D_2}{X_2}-\frac{D_3}{X_3}$$

or

$$y+h\frac{\left(\dfrac{Z_2}{X_2}-\dfrac{Z_3}{X_3}\right)}{\left(\dfrac{Y_2}{X_2}-\dfrac{Y_3}{X_3}\right)}+r_1\frac{\left(\dfrac{d_1}{X_2}-\dfrac{d_2}{X_3}\right)}{\left(\dfrac{Y_2}{X_2}-\dfrac{Y_3}{X_3}\right)}=\frac{\left(\dfrac{D_2}{X_2}-\dfrac{D_3}{X_3}\right)}{\left(\dfrac{Y_2}{X_2}-\dfrac{Y_3}{X_3}\right)} \tag{7}$$

Let

$$A_i=\frac{Y_i}{X_i};\qquad B_i=\frac{Z_i}{X_i};\qquad C_i=\frac{d_{i-1}}{X_i};\qquad E_i=\frac{D_i}{X_i}.$$

Then, (7) becomes

$$y+h\frac{B_2-B_3}{A_2-A_3}+r_1\frac{C_2-C_3}{A_2-A_3}=\frac{E_2-E_3}{A_2-A_3}$$

or

$$y=\frac{E_2-E_3-h(B_2-B_3)}{A_2-A_3}-r_1\frac{C_2-C_3}{A_2-A_3} \tag{8}$$

Let

$$H_1=\frac{E_2-E_3-h(B_2-B_3)}{A_2-A_3}$$

and

$$H_2=\frac{C_2-C_3}{A_2-A_3}$$

Then, (8) becomes

$$y=H_1-r_1H_2 \tag{9}$$

Substituting A_3, B_3, C_3, and D_3 into (6) with $z=h$ yields

$$x+yA_3+hB_3+r_1C_3=E_3 \tag{10}$$

Putting (9) into (10) yields

$$x+A_3(H_1-r_1H_2)+hB_3+r_1C_3=E_3$$

or

$$x+A_3H_1+hB_3+r_1(C_3-A_3H_2)=E_3$$

from which

$$x=E_3-A_3H_1-hB_3-r_1(C_3-A_3H_2)$$

-550-

Let

$$H_3 = E_3 - A_3 H_1 - h B_3$$

and

$$H_4 = G_3 - A_3 H_2$$

Then

$$x = H_3 - r_1 H_4 \tag{11}$$

Now, putting (9) and (11) into (1) with $z = h$ gives

$$(H_3 - r_1 H_4 - x_1)^2 + (H_1 - r_1 H_2 - y_1)^2 + (h - z_1)^2 = r_1^2$$

or

$$[(H_3 - x_1) - r_1 H_4]^2 + [(H_1 - y_1) - r_1 H_2]^2 + (h - z_1)^2 = r_1^2$$

or

$$(H_3 - x_1)^2 + r_1^2 H_4^2 - 2 r_1 H_4 (H_3 - x_1) + (H_1 - y_1)^2 + r_1^2 H_2^2 - 2 r_1 H_2 (H_1 - y_1) + (h - z_1)^2 = r_1^2$$

Let

$$J_1 = H_3 - x_1; \qquad J_2 = H_1 - y_1; \qquad J_3 = h - z_1$$

Thus,

$$r_1^2 [H_2^2 + H_4^2 - 1] - 2 r_1 (H_4 J_1 + H_2 J_2) + J_1^2 + J_2^2 + J_3^2 = 0$$

Let

$$A = H_2^2 + H_4^2 - 1; \qquad B = H_4 J_1 + H_2 J_2; \qquad C = J_1^2 + J_2^2 + J_3^2$$

Thus the x and y coordinates of the aircraft are:

$$x = H_3 - r_1 H_4 \tag{12}$$

$$y = H_1 - r_1 H_2 \tag{13}$$

where

$$r_1 = \frac{+B \pm \sqrt{B^2 - AC}}{A}$$

$$A = H_2^2 + H_4 - 1; \qquad B = H_4 J_1 + H_2 J_2; \qquad C = J_1^2 + J_2^2 + J_3^2$$

$$J_1 = H_3 - x_1; \qquad J_2 = H_1 - y_1; \qquad J_3 = h - z_1$$

$$H_1 = \frac{D_2X_3 - D_3X_2 - z(Z_2X_3 - Z_3X_2)}{Y_2X_3 - Y_3X_2}$$

$$H_2 = \frac{d_1X_3 - d_2X_2}{Y_2X_3 - Y_3X_2}$$

$$H_3 = \frac{D_3Y_2 - D_2Y_3 - z(Y_2Z_3 - Y_3Z_2)}{Y_2X_3 - Y_3X_2}$$

$$H_4 = \frac{d_2Y_2 - d_1Y_3}{Y_2X_3 - Y_3X_2}$$

$$X_i = x_i - x_1; \qquad Y_i = y_i - y_1; \qquad Z_i = z_i - z_1$$

$$D_i = \frac{x_i^2 + y_i^2 + z_i^2 - x_1^2 - y_1^2 - z_1^2 - d_{i-1}^2}{2}$$

The next step in the analysis is to compute the x and y coordinates of the aircraft by substituting the above expressions into equations (12) and (13). This will then yield the position of the aircraft in cartesian coordinates (x and y) as functions of the location of the three ground stations (x_i, y_i, z_i), time of arrival information (d_1, d_2), and the altitude of the aircraft, h.

Thus looking at (13)

$$y = H_1 - r_1 H_2$$

$$y = H_1 - H_2 \left[\frac{(H_4 J_1 + H_2 J_2) \pm \sqrt{(H_4 J_1 + H_2 J_2)^2 - (H_2^2 + H_4^2 - 1)(J_1^2 + J_2^2 + J_3^2)}}{H_2^2 + H_4^2 - 1} \right]$$

(13a)

Solving for the terms in this expression

$$H_2^2 + H_4^2 - 1 = \left(\frac{d_1X_3 - d_2X_2}{Y_2X_3 - Y_3X_2} \right)^2 + \left(\frac{d_2Y_2 - d_1Y_3}{Y_2X_3 - Y_3X_2} \right)^2 - 1$$

$$H_2^2 + H_4^2 - 1 = \frac{d_1^2(X_3^2 + Y_3^2) + d_2^2(X_2^2 + Y_2^2) - 2d_1d_2(X_2X_3 + Y_2Y_3)}{(Y_2X_3 - Y_3X_2)^2} - 1$$

$$H_2{}^2 + H_4{}^2 - 1 = \frac{d_1{}^2(X_3{}^2 + Y_3{}^2) + d_2{}^2(X_2{}^2 + Y_2{}^2) - 2d_1 d_2(X_2 X_3 + Y_2 Y_3) - (Y_2 X_3 - Y_3 X_2)^2}{(Y_2 X_3 - Y_3 X_2)^2}$$

(14)

Now

$$H_4 J_1 + H_2 J_2 = \frac{d_2 Y_2 - d_1 Y_3}{Y_2 X_3 - Y_3 X_2}(H_3 - x_1) + \frac{d_1 X_3 - d_2 X_2}{Y_2 X_3 - Y_3 X_2}(H_1 - y_1)$$

$$= \frac{d_2 Y_2 - d_1 Y_3}{Y_2 X_3 - Y_3 X_2}\left(\frac{D_3 Y_2 - D_2 Y_3 - h(Y_2 Z_3 - Y_3 Z_2)}{Y_2 X_3 - Y_3 X_2} - x_1\right)$$

$$+ \frac{d_1 X_3 - d_2 X_2}{Y_2 X_3 - Y_3 X_2}\left(\frac{D_2 X_3 - D_3 X_2 - h(Z_2 X_3 - Z_3 X_2)}{Y_2 X_3 - Y_3 X_2} - y_1\right)$$

$$= \frac{1}{(Y_2 X_3 - Y_3 X_2)^2}\left[d_2 D_3 Y_2{}^2 - d_2 D_2 Y_2 Y_3 - d_2 Y_2 h(Y_2 Z_3 - Y_3 Z_2) - d_1 D_3 Y_2 Y_3 \right.$$

$$+ d_1 D_2 Y_3{}^2 + d_1 Y_3 h(Y_2 Z_3 - Y_3 Z_2) + d_1 D_2 X_3{}^2 - d_1 D_3 X_2 X_3$$

$$\left. - d_1 X_3 h(Z_2 X_3 - Z_3 X_2) - d_2 D_2 X_2 X_3 + d_2 D_3 X_2{}^2 + d_2 X_2 h(Z_2 X_3 - Z_3 X_2) \right]$$

$$+ \frac{d_1 Y_3 x_1 - d_2 Y_2 x_1 + d_2 X_2 y_1 - d_1 X_3 y_1}{Y_2 X_3 - Y_3 X_2}$$

$$= \frac{1}{(Y_2 X_3 - Y_3 X_2)^2}\left[d_2 D_3(X_2 + Y_2) + d_1 D_2(X_3 + Y_3) - d_2 D_2(X_2 X_3 + Y_2 Y_3) \right.$$

$$- d_1 D_3(X_2 X_3 + Y_2 Y_3) + d_1[Y_3 h(Y_2 Z_3 - Y_3 Z_2) - X_3 h(Z_2 X_3 - Z_3 X_2)]$$

$$+ d_2[X_2 h(Z_2 X_3 - Z_3 X_2) - Y_2 h(Y_2 Z_3 - Y_3 Z_2)]$$

$$\left. + d_1(Y_3 x_1 - X_3 y_1)(Y_2 X_3 - Y_3 X_2) + d_2(X_2 y_1 - Y_2 x_1)(Y_2 X_3 - Y_3 X_2) \right]$$

-553-

$$H_4 J_1 + H_2 J_2 =$$

$$\frac{1}{(Y_2 X_3 - Y_3 X_2)^2} \left[d_2 D_3 (X_2{}^2 + Y_2{}^2) + d_1 D_2 (X_3{}^2 + Y_3{}^2) - (X_2 X_3 + Y_2 Y_3)(d_2 D_2 + d_1 D_3) \right.$$

$$+ d_1 [Y_3 h (Y_2 Z_3 - Y_3 Z_2) + X_3 h (X_2 Z_3 - X_3 Z_2) + (Y_3 x_1 - X_3 y_1)(Y_2 X_3 - Y_3 X_2)]$$

$$\left. - d_2 [Y_2 h (Y_2 Z_3 - Y_3 Z_2) + X_2 h (X_2 Z_3 - X_3 Z_2) + (Y_2 x_1 - X_2 y_1)(Y_2 X_3 - Y_3 X_2)] \right]$$

$$(15)$$

The rational part of

$$y = H_1 - H_2 \frac{(H_4 J_1 + H_2 J_2)}{H_2{}^2 + H_4{}^2 - 1}$$

$$= H_1 - \frac{(d_1 X_3 - d_2 X_2) M}{(Y_2 X_3 - Y_3 X_2)(d_1^2 (X_3^2 + Y_3^2) + d_2^2 (X_2^2 + Y_2^2) - 2 d_1 d_2 (X_2 X_3 + Y_2 Y_3) - (Y_2 X_3 - Y_3 X_2)^2}$$

Where

$$M = d_1 D_2 (X_3^2 + Y_3^2) + d_2 D_3 (X_2^2 + Y_2^2)$$

$$- (d_2 D_2 + d_1 D_3)(X_2 X_3 + Y_2 Y_3) + d_1 [X_2 X_3 (Z_3 h + Y_3 y_1) + Y_2 Y_3 (Z_3 h + X_3 x_1)$$

$$- X_3^2 (Z_2 h + Y_2 y_1) - Y_3^2 (Z_2 h + X_2 x_1)]$$

$$+ d_2 [X_2 X_3 (Z_2 h + Y_2 y_1) + Y_2 Y_3 (Z_2 h + X_2 x_1) - X_2^2 (Z_3 h + Y_3 y_1) - Y_2 (Z_3 h + X_3 x_1)]$$

Rational part of $y = \dfrac{D_2 X_3 - D_3 X_2 - h(Z_2 X_3 - Z_3 X_2)}{Y_2 X_3 - Y_3 X_2}$

$$H_2^2 + H_4^2 - 1 = \frac{d_1^2(X_3^2 + Y_3^2) + d_2^2(X_2^2 + Y_2^2) - 2d_1 d_2(X_2 X_3 + Y_2 Y_3) - (Y_2 X_3 - Y_3 X_2)^2}{(Y_2 X_3 - Y_3 X_2)^2}$$

<div align="right">(14)</div>

Now

$$H_4 J_1 + H_2 J_2 = \frac{d_2 Y_2 - d_1 Y_3}{Y_2 X_3 - Y_3 X_2} (H_3 - x_1) + \frac{d_1 X_3 - d_2 X_2}{Y_2 X_3 - Y_3 X_2} (H_1 - y_1)$$

$$= \frac{d_2 Y_2 - d_1 Y_3}{Y_2 X_3 - Y_3 X_2} \left(\frac{D_3 Y_2 - D_2 Y_3 - h(Y_2 Z_3 - Y_3 Z_2)}{Y_2 X_3 - Y_3 X_2} - x_1 \right)$$

$$+ \frac{d_1 X_3 - d_2 X_2}{Y_2 X_3 - Y_3 X_2} \left(\frac{D_2 X_3 - D_3 X_2 - h(Z_2 X_3 - Z_3 X_2)}{Y_2 X_3 - Y_3 X_2} - y_1 \right)$$

$$= \frac{1}{(Y_2 X_3 - Y_3 X_2)^2} \left[d_2 D_3 Y_2^2 - d_2 D_2 Y_2 Y_3 - d_2 Y_2 h(Y_2 Z_3 - Y_3 Z_2) - d_1 D_3 Y_2 Y_3 \right.$$

$$+ d_1 D_2 Y_3^2 + d_1 Y_3 h(Y_2 Z_3 - Y_3 Z_2) + d_1 D_2 X_3^2 - d_1 D_3 X_2 X_3$$

$$\left. - d_1 X_3 h(Z_2 X_3 - Z_3 X_2) - d_2 D_2 X_2 X_3 + d_2 D_3 X_2^2 + d_2 X_2 h(Z_2 X_3 - Z_3 X_2) \right]$$

$$+ \frac{d_1 Y_3 x_1 - d_2 Y_2 x_1 + d_2 X_2 y_1 - d_1 X_3 y_1}{Y_2 X_3 - Y_3 X_2}$$

$$= \frac{1}{(Y_2 X_3 - Y_3 X_2)^2} \left[d_2 D_3 (X_2 + Y_2) + d_1 D_2 (X_3 + Y_3) - d_2 D_2 (X_2 X_3 + Y_2 Y_3) \right.$$

$$- d_1 D_3 (X_2 X_3 + Y_2 Y_3) + d_1 [Y_3 h(Y_2 Z_3 - Y_3 Z_2) - X_3 h(Z_2 X_3 - Z_3 X_2)]$$

$$+ d_2 [X_2 h(Z_2 X_3 - Z_3 X_2) - Y_2 h(Y_2 Z_3 - Y_3 Z_2)]$$

$$\left. + d_1 (Y_3 x_1 - X_3 y_1)(Y_2 X_3 - Y_3 X_2) + d_2 (X_2 y_1 - Y_2 x_1)(Y_2 X_3 - Y_3 X_2) \right]$$

$$H_4J_1 + H_2J_2 =$$

$$\frac{1}{(Y_2X_3 - Y_3X_2)^2} \left[d_2D_3(X_2^2 + Y_2^2) + d_1D_2(X_3^2 + Y_3^2) - (X_2X_3 + Y_2Y_3)(d_2D_2 + d_1D_3) \right.$$

$$+ d_1[Y_3h(Y_2Z_3 - Y_3Z_2) + X_3h(X_2Z_3 - X_3Z_2) + (Y_3x_1 - X_3y_1)(Y_2X_3 - Y_3X_2)]$$

$$\left. - d_2[Y_2h(Y_2Z_3 - Y_3Z_2) + X_2h(X_2Z_3 - X_3Z_2) + (Y_2x_1 - X_2y_1)(Y_2X_3 - Y_3X_2)] \right]$$

$$(15)$$

The rational part of

$$y = H_1 - H_2 \frac{(H_4J_1 + H_2J_2)}{H_2^2 + H_4^2 - 1}$$

$$= H_1 - \frac{(d_1X_3 - d_2X_2)M}{(Y_2X_3 - Y_3X_2)(d_1^2(X_3^2 + Y_3^2) + d_2^2(X_2^2 + Y_2^2) - 2d_1d_2(X_2X_3 + Y_2Y_2) - (Y_2X_3 - Y_3X_2)^2}$$

Where

$$M = d_1D_2(X_3^2 + Y_3^2) + d_2D_3(X_2^2 + Y_2^2)$$

$$- (d_2D_2 + d_1D_3)(X_2X_3 + Y_2Y_3) + d_1[X_2X_3(Z_3h + Y_3y_1) + Y_2Y_3(Z_3h + X_3x_1)$$

$$- X_3^2(Z_2h + Y_2y_1) - Y_3^2(Z_2h + X_2x_1)]$$

$$+ d_2[X_2X_3(Z_2h + Y_2y_1) + Y_2Y_3(Z_2h + X_2x_1) - X_2^2(Z_3h + Y_3y_1) - Y_2(Z_3h + X_3x_1)]$$

Rational part of $y = \dfrac{D_2X_3 - D_3X_2 - h(Z_2X_3 - Z_3X_2)}{Y_2X_3 - Y_3X_2}$

-554-

$$- \frac{(d_1X_3-d_2X_3)M}{(Y_2X_3-Y_3X_2)[d_1^2(X_3^2+Y_3^2)+d_2^2(X_2^2+Y_2^2)-2d_1d_2(X_2X_3+Y_2Y_3)-(Y_2X_3-Y_3X_2)^2]}$$

$$= [X_2(hZ_3-D_3)-X_3(hZ_2-D_2)][d_1^2(X_3^2+Y_3^2)+d_2^2(X_2^2+Y_2^2)-2d_1d_2(X_2X_3+Y_2Y_3)$$

$$\frac{-(Y_2X_3-Y_3X_2)^2]-(d_1X_3-d_2X_3)M}{(Y_2X_3-Y_3X_2)[d_1^2(X_3^2+Y_3^2)+d_2^2(X_2^2+Y_2^2)-2d_1d_2(X_2X_3+Y_2Y_3)-(Y_2X_3-Y_3X_2)^2]}$$

(16)

Looking back at (13a), the irrational part of

$$y = \frac{\mp H_2}{h_2^2+H_4^2-1} \quad (J_1+J_2H_4)(J_1-J_2H_4)+(J_2+J_1H_2)(J_2-J_1H_2)+2H_2H_4J_1J_2$$

$$-J_3^2(H_2^2+H_4^2-1)]^{\frac{1}{2}}$$

Looking at parts of this expression

$$\frac{\mp H_2}{H_2^2+H_4^2-1} = \mp \frac{(d_1X_3-d_2X_2)(Y_2X_3-Y_3X_2)}{d_1^2(X_3^2+Y_3^2)+d_2^2(X_2^2+Y_2^2)-2d_1d_2(X_2X_3+Y_2Y_3)-(Y_2X_3-Y_3X_2)^2}$$

$$= \mp \frac{d_1X_3^2Y_2-d_1X_3X_2Y_3-d_2X_2X_3Y_2+d_2X_2^2Y_3}{\text{Denom}}$$

$$= \mp \frac{X_3Y_2(d_1X_3-d_2X_2)+X_2Y_3(d_2X_2-d_1X_3)}{\text{Denom}}$$

$$\frac{\mp H_2}{H_2^2+H_4^2-1} = \pm \frac{(d_2X_2-d_1X_3)(X_3Y_2-X_2Y_3)}{d_1^2(X_3^2+Y_3^2)+d_2^2(X_2^2+Y_2^2)-2d_1d_2(X_2X_3+Y_2Y_3)-(Y_2X_3-Y_3X_2)^2}$$

(17)

Looking inside the radical at the various terms

$$J_1+J_2H_4 = H_3-x_1+(H_1-y_1)H_4$$

$$= \frac{D_3Y_2-D_2Y_3-h(Y_2Z_3-Y_3Z_2)}{Y_2X_3-Y_3X_2} -x_1+ \frac{d_2Y_2-d_1Y_3}{Y_2X_3-Y_3X_2} \left[\frac{D_2X_3-D_3X_2-h(Z_2X_3-Z_3X_2)}{Y_2X_3-Y_3X_2} -y_1 \right]$$

-555-

$$= D_3 X_3 Y_2^2 - D_2 X_3 Y_2 Y_3 - D_3 X_2 Y_2 Y_3 + D_2 X_2 Y_3^2 - h(X_3 Y_2^2 Z_3 - X_3 Y_3 Y_2 Z_2 - X_2 Y_2 Y_3 Z_3 + X_2 Y_3^2 Z_2)$$

$$-x_1(Y_2 X_3 - Y_3 X_2)^2 + d_2 D_2 Y_2 X_3 - d_2 D_3 Y_2 X_2 - d_1 D_2 X_3 Y_3 + d_1 D_3 X_2 Y_3$$

$$\frac{-h(d_2 Y_2 X_3 Z_2 - d_2 Y_2 X_2 Z_3 - d_1 Y_3 X_3 Z_2 + d_1 Y_3 Z_3 X_2) - y_1(Y_2 X_3 - Y_3 Y_2)(d_2 Y_2 - d_1 Y_3)}{(Y_2 X_3 - Y_3 X_2)^2}$$

$$= d_1 X_2 Y_3(D_3 - hZ_3) + d_2 Y_2 X_3(D_2 - hZ_2) - d_1 X_3 Y_3(D_2 - hZ_2) - d_2 Y_2 X_2(D_3 - hZ_3)$$

$$+X_3 Y_2^2(D_3 - hZ_3) + X_2 Y_3^2(D_2 - hZ_2) - X_2 Y_2 Y_3(D_3 - hZ_3) - X_3 Y_2 Y_3(D - hZ_2)$$

$$\frac{-y_1(Y_2 X_3 - Y_3 X_2)(d_2 Y_2 - d_1 Y_3) - x_1(Y_2 X_3 - Y_3 X_2)^2}{(Y_2 X_3 - Y_3 X_2)^2}$$

$$= X_3(D_2 - hZ_2)(d_2 Y_2 - d_1 Y_3)$$
$$+ X_2(D_3 - hZ_3)(d_1 Y_3 - d_2 Y_2)$$
$$+ Y_2(D_3 - hZ_3)(X_3 Y_2 - X_2 Y_3)$$
$$+ Y_3(D_2 - hZ_2)(X_2 Y_3 - X_3 Y_2)$$
$$-y_1(Y_2 X_3 - Y_3 X_2)(d_2 Y_2 - d_1 Y_3)$$
$$\frac{-x_1(Y_2 X_3 - Y_3 X_2)^2}{(Y_2 X_3 - Y_3 X_2)^2}$$

$$J_1 + J_2 H_4 = (d_2 Y_2 - d_1 Y_3)[X_2(hZ_3 - D_3) - X_3(hZ_2 - D_2) - y_1(Y_2 X_3 - Y_3 X_2)]$$
$$\frac{+(Y_2 X_3 - Y_3 X_2)[-Y_2(hZ_3 - D_3) + Y_3(hZ_2 - D_2) - x_1(Y_2 X_3 - Y_3 X_2)]}{(Y_2 X_3 - Y_3 X_2)^2}$$

$$(18)$$

$$J_1 - J_2 H_4 = H_3 - x_1 - H_4(H_1 - y_1)$$

$$= \frac{D_3 Y_2 - D_2 Y_3 - h(Y_2 Z_3 - Y_3 Z_2)}{Y_2 X_3 - Y_3 X_2} - x_1 - \frac{(d_2 Y_2 - d_1 Y_3)}{(Y_2 X_3 - Y_3 X_2)} \left[\frac{D_2 X_3 - D_3 X_2 - h(Z_2 X_3 - Z_3 X_2)}{Y_2 X_3 - Y_3 X_2} - y_1 \right]$$

$$= \frac{\begin{aligned} & D_3 Y_2^2 X_3 - D_3 X_2 Y_2 Y_3 - D_2 X_3 Y_2 Y_3 + D_2 Y_3^2 X_2 - h(X_3 Y_2^2 Z_3 - Y_2 Y_3 X_2 Z_3 - Y_2 Y_3 X_3 Z_2 + Y_3^2 X_2 Z_2) \\ & - x_1(Y_2 X_3 - Y_3 X_2)^2 - d_2 D_2 Y_2 X_3 + d_2 D_3 X_2 Y_2 + d_1 D_2 X_3 Y_3 - d_1 D_3 X_2 Y_3 \\ & + h(d_2 Y_2 Y_3 Z_2 - d_2 Y_2 X_2 Z_3 - d_1 Y_3 X_3 Z_2 + d_1 Y_3 X_2 Z_3) + y_1(d_2 Y_2 - d_1 Y_3)(Y_2 X_3 - Y_3 X_2) \end{aligned}}{(Y_2 X_3 - Y_3 X_2)^2}$$

$$= \frac{\begin{aligned} & d_1 X_2 Y_3(-D_3 + hZ_3) + d_2 Y_2 X_3(-D_2 + hZ_2) + d_1 X_3 Y_3(D_2 - hZ_2) \\ & + d_2 X_2 Y_2(D_3 - hZ_3) + X_3 Y_2^2(D_3 - hZ_3) + X_2 Y_3^2(D_2 - hZ_2) - X_2 Y_2 Y_3(D_3 - hZ_3) \\ & - X_3 Y_2 Y_3(D_2 - hZ_2) - x_1(Y_2 X_3 - Y_3 X_2)^2 + y_1(d_2 Y_2 - d_1 Y_3)(Y_2 X_3 - Y_3 X_2) \end{aligned}}{(Y_2 X_3 - Y_3 X_2)^2}$$

$$= \frac{\begin{aligned} & X_3(D_2 - hZ_2)(d_1 Y_3 - d_2 Y_2) \\ & + X_2(D_3 - hZ_3)(d_2 Y_2 - d_1 Y_3) \\ & - Y_3(D_2 - hZ_2)(Y_2 X_3 - Y_3 X_2) \\ & + Y_2(D_3 - hZ_3)(Y_2 X_3 - X_2 Y_3) \\ & - x_1(Y_2 X_3 - Y_3 X_2)^2 \\ & + y_1(Y_2 X_3 - Y_3 X_2)(d_2 Y_2 - d_1 Y_3) \end{aligned}}{(Y_2 X_3 - Y_3 X_2)^2}$$

$$J_1 - J_2 H_4 = \frac{(d_2 Y_2 - d_1 Y_3)[-X_2(hZ_3 - D_3) + X_3(hZ_2 - D_2) + y_1(Y_2 X_3 - Y_3 X_2)]}{(Y_2 X_3 - Y_3 X_2)^2} $$
$$+ \frac{(Y_2 X_3 - Y_3 X_2)[-Y_2(hZ_3 - D_3) + Y_3(hZ_2 - D_2) - x_1(Y_2 X_3 - Y_3 X_2)]}{(Y_2 X_3 - Y_3 X_2)^2}$$

$$\tag{19}$$

$$J_2+J_1H_2 = H_1-y_1+(H_3-x_1)H_2$$

$$= \frac{D_2X_3-D_3X_2-h(Z_2X_3-Z_3X_2)}{Y_2X_3-Y_3X_2} -y_1+\left(\frac{d_1X_3-d_2X_2}{Y_2X_3-Y_3X_2}\right)\left(\frac{D_3Y_2-D_2Y_3-h(Y_2Z_3-Y_3Z_2)}{Y_2X_3-Y_3X_2} -x_1\right)$$

$$= D_2X_3^2Y_2-D_3X_2X_3Y_2-h(X_3^2Y_2Z_2-X_3Y_3X_2Z_2-X_2X_3Y_2Z_3+X_2^2Y_3Z_3)-D_2X_2X_3Y_3$$

$$+D_3X_2^2Y_3-y_1(Y_2X_3-Y_3X_2)^2+d_1D_3Y_2X_3-d_1D_2X_3Y_3-d_2D_3X_2Y_2+d_2D_2X_2Y_3$$

$$\frac{-hd_1X_3(Y_2Z_3-Y_3Z_2)+hd_2X_2(Y_2Z_3-Y_3Z_2)-x_1(d_1X_3-d_2X_2)(Y_2X_3-Y_3X_2)-y_1(Y_2X_3-Y_3X_2)}{(Y_2X_3-Y_3X_2)^2}$$

$$= \frac{1}{(Y_2X_3-Y_3X_2)^2}[d_1Y_2X_3(D_3-hZ_3)-d_1X_3Y_3(D_2-hZ_2)-d_2X_2Y_2(D_3-hZ_3)$$

$$+d_2X_2Y_3(D_2-hZ_2)+X_2^2Y_3(D_3-hZ_3)-X_2X_3Y_3(D_2-hZ_2)-X_2X_3Y_2(D_3-hZ_3)$$

$$+X_3^2Y_2(D_2-hZ_2)-y_1(Y_2X_3-Y_3X_2)^2-x_1(d_1X_3-d_2X_2)(Y_2X_3-Y_3X_2)]$$

$$= \frac{\begin{aligned}&Y_2(D_3-hZ_3)(d_1X_3-d_2X_2)\\&+Y_3(D_2-hZ_2)(d_2X_2-d_1X_3)\\&-X_2(D_3-hZ_3)(X_3Y_2-X_2Y_3)\\&+X_3(D_2-hZ_2)(X_3Y_2-X_2Y_3)\\&-x_1(Y_2X_3-Y_3X_2)(d_1X_3-d_2X_2)\\&-y_1(Y_2X_3-Y_3X_2)^2\end{aligned}}{(Y_2X_3-Y_3X_2)^2}$$

$$J_2+J_1H_2 = \frac{\begin{aligned}&(d_2X_2-d_1X_3)[Y_2(hZ_3-D_3)-Y_3(hZ_2-D_2)+x_1(Y_2X_3-Y_3X_2)]\\&(Y_2X_3-Y_3X_2)[X_2(hZ_3-D_3)-X_3(hZ_2-D_2)-y_1(Y_2X_3-Y_3X_2)]\end{aligned}}{(Y_2X_3-Y_3X_2)^2} \qquad (20)$$

$$J_2 - J_1 H_2 = H_1 - y_1 - H_2(H_3 - x_1)$$

$$= \frac{D_2 X_3 - D_3 X_2 - h(Z_2 X_3 - Z_3 X_2)}{Y_2 X_3 - Y_3 X_2} - y_1 - \frac{(d_1 X_3 - d_2 X_2)}{(Y_2 X_3 - Y_3 X_2)}\left[-\frac{D_3 Y_2 - D_2 Y_3 - h(Y_2 Z_3 - Y_3 Z_2)}{Y_2 X_3 - Y_3 X_2} - x_1\right]$$

$$= \frac{\begin{array}{l} D_2 X_3^2 Y_2 - D_2 X_2 X_3 Y_3 - D_3 X_2 X_3 Y_2 + D_3 X_2^2 Y_3 - h(X_3^2 Y_2 Z_2 - X_3 Y_3 X_2 Z_2 - X_2 X_3 Y_2 Z_3 + X_2^2 Y_3 Z_3) \\ -y_1(Y_2 X_3 - Y_3 X_2)^2 - d_1 D_3 X_3 Y_2 + d_1 D_2 X_3 Y_3 + d_2 D_3 X_2 Y_2 - d_2 D_2 X_2 Y_3 \\ +h(d_1 X_3 Y_2 Z_3 - d_1 X_3 Y_3 Z_2 - d_2 X_2 Y_2 Z_3 + d_2 X_2 Y_3 Z_2) + x_1(d_1 X_3 - d_2 X_2)(Y_2 X_3 - Y_3 X_2) \end{array}}{(Y_2 X_3 - Y_3 X_2)^2}$$

$$= \frac{\begin{array}{l} d_1 X_3 Y_2(-D_3 + hZ_3) + d_1 X_3 Y_3(D_2 - hZ_z) + d_2 X_2 Y_2(D_3 - hZ_3) - d_2 X_2 Y_3(D_2 - hZ_2) \\ +X_3^2 Y_2(D_2 - hZ_z) + X_2^2 Y_3(D_3 - hZ_3) - X_2 X_3 Y_3(D_2 - hZ_2) - X_2 X_3 Y_2(D_3 - hZ_3) \\ -y_1(Y_2 X_3 - Y_3 X_2)^2 + x_1(d_1 X_3 - d_2 X_2)(Y_2 X_3 - Y_3 X_2) \end{array}}{(Y_2 X_3 - Y_3 X_2)^2}$$

$$= \frac{\begin{array}{l} Y_2(hZ_3 - D_3)(d_1 X_3 - d_2 X_2) \\ +X_2(D_3 - hZ_3)(X_2 Y_3 - X_3 Y_2) \\ +Y_3(D_2 - hZ_2)(d_1 X_3 - d_2 X_2) \\ +X_3(D_2 - hZ_2)(X_3 Y_2 - X_2 Y_3) \\ -y_1(Y_2 X_3 - Y_3 X_2)^2 \\ +x_1(d_1 X_3 - d_2 X_2)(Y_2 X_3 - Y_3 X_2) \end{array}}{(Y_2 X_3 - Y_3 X_2)^2}$$

$$J_2 - J_1 H_2 = \frac{\begin{array}{l} (d_2 X_2 - d_1 X_3)[-Y_2(hZ_3 - D_3) + Y_3(hZ_2 - D_2) - x_1(Y_2 X_3 - Y_3 X_2)] \\ (Y_2 X_3 - Y_3 X_2)[X_2(hZ_3 - D_3) - X_3(hZ_2 - D_2) - y_1(Y_2 X_3 - Y_3 X_2)] \end{array}}{(Y_2 X_3 - Y_3 X_2)^2} \tag{21}$$

$$J_1J_2H_2H_4 = \left[\frac{D_3Y_2-D_2Y_3-h(Y_2Z_3-Y_3Z_2)}{Y_2X_3-Y_3X_2}-x_1\right]\left[\frac{D_2X_3-D_3X_2-h(Z_2X_3-Z_3X_2)}{Y_2X_3-Y_3X_2}-y_1\right]$$

$$\frac{(d_1X_3-d_2X_2)(d_2Y_2-d_1Y_3)}{(Y_2X_3-Y_3X_2)^2}$$

$$= [D_3Y_2-D_2Y_3-h(Y_2Z_3-Y_3Z_2)-x_1(Y_2X_3-Y_3X_2)][D_2X_3-D_3X_2-h(Z_2X_3-Z_3X_2)$$

$$-y_1(Y_2X_3-Y_3X_2)](d_1X_3-d_2X_2)(d_2Y_2-d_1Y_3)$$

$$\overline{\qquad\qquad\qquad (Y_2X_3-Y_3X_2)^4 \qquad\qquad\qquad}$$

$$J_1J_2H_2H_4 = (d_1X_3-d_2X_2)(d_2Y_2-d_1Y_3)[Y_2(D_3-hZ_3)-Y_3(D_2-hZ_3)-x_1(Y_2X_3-Y_3X_2)]$$

$$\frac{[-X_2(D_3-hZ_3)+X_3(D_2-hZ_2)-y_1(Y_2X_3-Y_3X_2)]}{(Y_2X_3-Y_3X_2)^4}$$

$$\tag{22}$$

Let

$$d_2Y_2-d_1Y_3 = A$$

$$d_2X_2-d_1X_3 = B$$

$$X_2(hZ_3-D_3)-X_3(hZ_2-D_2)-y_1(Y_2X_3-Y_3X_2) = C$$

$$-Y_2(hZ_3-D_3)+Y_3(hZ_2-D_2)-x_1(Y_2X_3-Y_3X_2) = D$$

$$d_1^2(X_3^2+Y_3^2)+d_2^2(X_2^2+Y_2^2)-2d_1d_2(X_2X_3+Y_2Y_3) = E$$

$$Y_2X_3-X_3X_2 = F$$

∴ Looking at (17)

$$\frac{\mp H_2}{H_2^2+H_4^2-1} = \frac{\pm BF}{E-F^2}$$

from (18)

$$J_1 J_2 H_4 = \frac{1}{F^2}(AC+FD)$$

-560-

from (19)

$$J_1 - J_2 H_4 = \frac{1}{F^2}(-AC+FD)$$

from (20)

$$J_2 + J_1 H_2 = -\frac{1}{F^2}(-BD+FC)$$

from (21)

$$J_2 - J_1 H_2 = \frac{1}{F^2}(BD+FC)$$

from (22)

$$2J_1 J_2 H_2 H_4 = \frac{2}{F^4}(-ABCD)$$

$\therefore$ the irrational part of $y = Ir(y)$

$$Ir(y) = \frac{\pm BF}{(E-F^2)F^2}[(FD+AC)(FD-AC)+(FC-BD)-2ABCD-(h-z_1)^2(E-F^2)F^2]^{\frac{1}{2}} \quad (23)$$

Earlier we had Equation (16) for the rational part of $y = Ra(y)$. Using Substitutions just shown,

$$Ra(y) = \frac{(C-y_1 F)(E-F^2)+BM}{F(E-F^2)} \quad (24)$$

where

$$A = d_2 Y_2 - d_1 Y_3$$

$$B = d_2 X_2 - d_1 X_3$$

$$C = X_2(hZ_3-D_3)-X_3(hZ_2-D_2)-y_1(Y_2 X_3-Y_3 X_2)$$

$$D = -Y_2(hZ_3-D_3)+Y_3(hZ_2-D_2)-x_1(Y_2 X_3-Y_3 X_2)$$

$$E = d_1^2(X_3^2+Y_3^2)+d_2^2(X_2^2+Y_2^2)-2d_1 d_2(X_2 X_3+Y_2 Y_3)$$

$$F = Y_2 X_3 - Y_3 X_2$$

$$M = d_1 D_2(X_3^2+Y_3^2)+d_2 D_2(X_2^2+Y_2^2)-(d_2 D_2+d_1 D_3)(X_2 X_3+Y_2 Y_3)+d_1[X_2 X_3(Z_3 h+Y_3 y_1)$$
$$+Y_2 Y_3(Z_3 h+X_3 x_1)-X_3^2(Z_2 h+Y_2 y_1)-Y_3^2(Z_2 h+X_2 x_1)]+d_2[X_2 X_3(Z_2 h+Y_2 y_1)$$
$$+Y_2 Y_3(Z_2 h+X_2 x_1)-X_2^2(Z_3 h+Y_3 y_1)-Y_2^2(Z_3 h+X_3 x_1)$$

Now looking back at Equation (12) for x and making the necessary substitutions:

$$x = H_3 - r_1 H_4$$

$$= H_3 - H_4 \left[\frac{H_4 J_1 + H_2 J_2 \pm \sqrt{\begin{array}{c}(J_1 + J_2 H_4)(J_1 - J_2 H_4) + (J_2 + J_1 H_2)(J_2 - J_1 H_2) \\ + 2J_1 J_2 H_2 H_4 - J_3^2 (H_2^2 + H_4^2 - 1)\end{array}}}{H_2^2 + H_4^2 - 1} \right]$$

The rational part of x = Ra(x)

$$Ra(x) = H_3 - H_4 \frac{(H_4 J_1 + H_2 J_2)}{H_2^2 + H_4^2 - 1}$$

$$= \frac{D_3 Y_2 - D_2 Y_3 - h(Y_2 Z_3 - Y_3 Z_2)}{Y_2 X_3 - Y_3 X_2} - \frac{(d_2 Y_2 - d_1 Y_3)M}{(Y_2 X_3 - Y_3 X_2)[d_1^2(X_3^2 + Y_3^2) + d_2^2(X_2^2 + Y_2^2) - 2d_1 d_2(X_2 X_3 + Y_2 Y_3) - (Y_2 X_3 - Y_3 X_2)^2]}$$

$$= \frac{[Y_3(hZ_2 - D_2) - Y_2(hZ_3 - D_2)][d_1^2(X_3 + Y_3^2) + d_2^2(X_2^2 + Y_2^2) - 2d_1 d_2(X_2 X_3 + Y_2 Y_3) - (Y_2 X_3 - Y_3 X_2)^2] - (d_2 Y_2 - d_1 Y_3)M}{(Y_2 X_3 - Y_3 X_2)[d_1^2(X_3^2 + Y_3^2) + d_2^2(X_2^2 + Y_2^2) - 2d_1 d_2(X_2 X_3 + Y_2 Y_3) - (Y_2 X_3 - Y_3 X_2)^2]}$$

$$Ra(x) = \frac{(D - x_1 F)(E - F^2) - AM}{F(E - F^2)} \tag{25}$$

and the irrational part of x = Ir(x)

$$Ir(x) = \frac{\pm H_4 \sqrt{(J_1 + J_2 H_4)(J_1 - J_2 H_4) + (J_2 + J_1 H_2)(J_2 - J_1 H_2) + 2J_1 J_2 H_2 H_4 - J_3^2 (H_2^2 + H_4^2 - 1)}}{H_2^2 + H_4^2 - 1}$$

-562-

$$\frac{H_4}{H_2^2 + H_4^2 - 1} = \frac{(d_2 Y_2 - d_1 Y_3)(Y_2 X_3 - Y_3 X_2)}{d_1^2(X_3^2 + Y_3^2) + d_2^2(X_2^2 + Y_2^2) - 2d_1 d_2(X_2 X_3 + Y_2 Y_3) - (Y_2 X_3 - Y_3 X_2)^2}$$

$$= \frac{d_2 Y_2^2 X_3 - d_2 X_2 Y_2 Y_3 - d_1 Y_2 Y_3 X_3 + d_1 Y_3^2 X_2}{\text{Denom}}$$

$$= \frac{Y_2 X_3 (d_2 Y_2 - d_1 Y_3) + Y_3 X_2 (Y_3 d_1 - d_2 Y_2)}{\text{Denom}}$$

$$= \frac{(d_2 Y_2 - d_1 Y_3)(Y_2 X_3 - Y_3 X_2)}{\text{Denom}}$$

Thus

$$\text{Ir}(x) = \pm \frac{AF}{(E-F^2)(F^2)} \left[(FD+AC)+FC+BD)(FC-BD) - 2ABCD - (h-z_1)(E-F^2)F^2 \right]^{\frac{1}{2}} \quad (26)$$

The final step in the derivation is to transform the (x, y, z: h) coordinates of the aircraft into (d, θ, Φ) coordinates by the use of the following equations.

$$d = \sqrt{x^2 + y^2 + h^2}$$

$$\theta = \text{Arc Tan } \frac{y}{x}$$

$$\phi = \text{Arc Cos } \frac{h}{\sqrt{x^2 + y^2 + h^2}}$$

APPENDIX VII

THREE RANGE DIFFERENCE LANDING CONFIGURATION

This appendix derives the aircraft position from the indicated measurements. The following equations apply:

$$(x-x_1)^2 + (y-y_1)^2 + (z-z_1)^2 = r_1^2 \tag{1}$$

$$(x-x_2)^2 + (y-y_2)^2 + (z-z_2)^2 = (r_1+d_1)^2 \tag{2}$$

$$(x-x_3)^2 + (y-y_3)^2 + (z-z_3)^2 = (r_1+d_2)^2 \tag{3}$$

$$(x-x_4)^2 + (y-y_4)^2 + (z-z_4)^2 = (r_1+d_3)^2 \tag{4}$$

Using Equations (1) - (4), r_1 may be found by writing x as a function of y, z, and r_1, then writing y as a function z and r_1, and finally z to be written as function of r_1. Substitution will allow x, y and z to be written as functions of r_1 and then Equation (1) may be substituted to yield a quadratic in r_1. Back substitution will yield two possible locations for the aircraft. This ambiguity is removed by knowing the approximate aircraft position. The solution of the equations is as follows:

Subtracting (2), (3), and (4) from (1) yields

$$(1) - (2) \qquad x+y\left(\frac{y_2-y_1}{x_2-x_1}\right) + z\left(\frac{z_2-z_1}{x_2-x_1}\right) + r_1\left(\frac{d_1}{x_2-x_1}\right) = \frac{x_2^2+y_2^2+z_2^2-x_1^2-y_1^2-z_1^2-d_1^2}{2(x_2-x_1)}$$

$$(1) - (3) \qquad x+y\left(\frac{y_3-y_1}{x_3-x_1}\right) + z\left(\frac{z_3-z_1}{x_3-x_1}\right) + r_1\left(\frac{d_2}{x_3-x_1}\right) = \frac{x_3^2+y_3^2+z_3^2-x_1^2-y_1^2-z_1^2-d_2^2}{2(x_3-x_1)}$$

$$(1) - (4) \qquad x+y\left(\frac{y_4-y_1}{x_4-x_1}\right) + z\left(\frac{z_4-z_1}{x_4-x_1}\right) + r_1\left(\frac{d_3}{x_4-x_1}\right) = \frac{x_4^2+y_4^2+z_4^2-x_1^2-y_1^2-z_1^2-d_3^2}{2(x_4-x_1)}$$

Let

$$X_i = x_i - x_1, \quad Y_i = y_i - y_1, \quad Z_i = z_i - z_1$$

$$D_i = \frac{x_i^2 + y_i^2 + z_i^2 - x_1^2 - y_1^2 - z_1^2 - d_{i-1}^2}{2}$$

Rewriting (1) – (2), (1) – (3), and (1) – (4) yields:

$$x + y\left(\frac{Y_2}{X_2}\right) + z\left(\frac{Z_2}{X_2}\right) + r_1\left(\frac{d_1}{X_2}\right) = \frac{D_2}{X_2} \tag{5}$$

$$x + y\left(\frac{Y_3}{X_3}\right) + z\left(\frac{Z_3}{X_3}\right) + r_1\left(\frac{d_2}{X_3}\right) = \frac{D_3}{Y} \tag{6}$$

$$x + y\left(\frac{Y_4}{X_4}\right) + z\left(\frac{Z_4}{X_4}\right) + r_1\left(\frac{d_3}{X_4}\right) = \frac{D_4}{X_4} \tag{7}$$

Subtracting (6) and (7) from (5) yields:

$$(5) - (6) \qquad y\left(\frac{\left(\frac{Y_2}{X_2} - \frac{Y_3}{Y_3}\right)}{\left(\frac{Z_2}{X_2} - \frac{Z_3}{X_3}\right)}\right) + z + r_1\left(\frac{\left(\frac{d_1}{X_2} - \frac{d_2}{X_3}\right)}{\left(\frac{Z_2}{X_2} - \frac{Z_3}{X_3}\right)}\right) = \left(\frac{\left(\frac{D_2}{X_2} - \frac{D_3}{X_3}\right)}{\left(\frac{Z_2}{X_2} - \frac{Z_3}{X_3}\right)}\right)$$

$$(5) - (7) \qquad y\left(\frac{\left(\frac{Y_2}{X_2} - \frac{Y_4}{X_4}\right)}{\left(\frac{Z_2}{X_2} - \frac{Z_4}{X_4}\right)}\right) + z + r_1\left(\frac{\left(\frac{d_1}{X_2} - \frac{d_3}{X_4}\right)}{\left(\frac{Z_2}{X_2} - \frac{Z_4}{X_4}\right)}\right) = \left(\frac{\left(\frac{D_2}{X_2} - \frac{D_4}{X_4}\right)}{\left(\frac{Z_2}{X_2} - \frac{Z_4}{X_4}\right)}\right)$$

Let

$$A_i = \frac{Y_i}{X_i}, \quad B_i = \frac{Z_i}{X_i}, \quad C_i = \frac{d_i - 1}{X_i}, \quad E_i = \frac{D_i}{X_i}$$

Rewriting (5) – (6) and (5) – (7), yields:

$$y \left(\frac{A_2-A_3}{B_2-B_3}\right) + z + r_1 \left(\frac{C_2-C_3}{B_2-B_3}\right) = \frac{E_2-E_3}{B_2-B_3} \tag{8}$$

$$y \left(\frac{A_2-A_4}{B_2-B_4}\right) + z + r_1 \left(\frac{C_2-C_4}{B_2-B_4}\right) = \frac{E_2-E_4}{B_2-B_4} \tag{9}$$

Subtracting (9) from (8) yields:

(8) − (9)
$$y = \left(\frac{\dfrac{E_2-E_3}{B_2-B_3} - \dfrac{E_2-E_4}{B_2-B_4}}{\dfrac{A_2-A_3}{B_2-B_3} - \dfrac{A_2-A_4}{B_2-B_4}}\right) - r_1 \left(\frac{\dfrac{C_2-C_3}{B_2-B_3} - \dfrac{C_2-C_4}{B_2-B_4}}{\dfrac{A_2-A_3}{B_2-B_3} - \dfrac{A_2-A_4}{B_2-B_4}}\right)$$

Let

$$H_1 = \left(\frac{\dfrac{E_2-E_3}{B_2-B_3} - \dfrac{E_2-E_4}{B_2-B_4}}{\dfrac{A_2-A_3}{B_2-B_3} - \dfrac{A_2-A_4}{E_2-B_4}}\right), \quad H_2 = \left(\frac{\dfrac{C_2-C_3}{B_2-B_3} - \dfrac{C_2-C_4}{B_2-B_4}}{\dfrac{A_2-A_3}{B_2-B_3} - \dfrac{A_2-A_4}{B_2-B_4}}\right)$$

Rewriting (8) − (9) yields

$$y = H_1 - H_2 r_1 \tag{10}$$

Substituting (10) into (9)

$$(H_1-H_2 r_1)\left(\frac{A_2-A_4}{B_2-B_4}\right) + z + r_1 \left(\frac{C_2-C_4}{B_2-B_4}\right) = \frac{E_2-E_4}{B_2-B_4}$$

$$z = \frac{E_2-E_4}{B_2-B_4} - H_1\left(\frac{A_2-A_4}{B_2-B_4}\right) - r_1\left(\frac{C_2-C_4}{B_2-B_4} - H_2\left(\frac{A_2-A_4}{B_2-B_4}\right)\right)$$

$$z = \frac{E_2-E_4-H_1 A_2+H_1 A_4}{B_2-B_4} - r_1\left(\frac{C_2-C_4-H_2 A_2+H_2 A_4}{B_2-B_4}\right)$$

-566-

Let

$$H_3 = \frac{E_2-E_4-H_1A_2+H_1A_4}{B_2-B_4} \ , \qquad H_4 = \frac{C_2-C_4-H_2A_2+H_2A_4}{B_2-B_4}$$

Then rewriting yields

$$z = H_3 - r_1 H_4 \qquad (11)$$

Substituting (10) and (11) into (7)

$$x + (H_1-H_2r_1)\left(\frac{Y_4}{X_4}\right) + (H_3-H_4r_1)\left(\frac{Z_4}{X_4}\right) + r_1 \ \frac{d_3}{X_4} = \frac{D_4}{X_4}$$

$$x = \frac{D_4}{X_4} - H_1 \frac{Y_4}{X_4} - H_3 \frac{Z_4}{X_4} + r_1\left(\frac{H_2Y_4}{X_4} + \frac{H_4Z_4}{X_4} - \frac{d_3}{X_4}\right)$$

$$x = \frac{D_4-H_1Y_4-H_3Z_4}{X_4} + r_1\left(\frac{H_2Y_4+H_4Z_4-d_3}{X_4}\right)$$

Let

$$H_5 = \frac{D_4-H_1Y_4-H_3Z_4}{X_4} \ , \qquad H_6 = \frac{H_2Y_4+H_4Z_4-d_3}{X_4}$$

Rewriting yields

$$x = H_5 + r_1 H_6 \qquad (12)$$

Substituting (12), (11), and (10) into (1)

$$(H_5+r_1H_6-x_1)^2+(H_1-H_2r_1-y_1)^2+(H_3-r_1H_4-z_1)^2 = r_1^2$$

$$(H_5-x_1)^2+2(H_5-x_1)H_6r_1+H_6^2r_1^2+(H_1-y_1)^2-2(H_1-y_1)H_2r_1+H_2^2r_1^2$$

$$+ (H_3-z_1)^2-2(H_3-z_1)H_4r_1+H_4^2r_1^2 = r_1^2$$

Let

$$J_1 = H_5-x_1 \; ; \quad J_2 = H_1-y_1 \; ; \quad J_3 = H_3-z_1$$

Rewriting yields

$$r_1^2[H_6^2+H_2^2+H_4^2-1]+2r_1[J_1H_6-J_2H_2-J_3H_4]+J_1^2+J_2^2+J_3^2 = 0$$

Let

$$A = H_2^2+H_4^2+H_6^2-1$$

$$B = J_1H_6-J_2H_2-J_3H_4$$

$$C = J_1^2+J_2^2+J_3^2$$

Rewriting (1)

$$Ar_1 +2r_1B+C = 0$$

$$r_1 = \frac{-B\pm\sqrt{B^2-AC}}{A}$$

(13)

To solve x, y, and z, certain terms must be found. Let us find the real and imaginary parts of r, since they will be needed. Real part of $r = \mathrm{Re}(r) = \dfrac{-B}{A}$

$$B = J_1H_6-J_2H_2-J_3H_4$$

$$= H_5H_6-H_1H_2-H_3H_4-x_1H_6+y_1H_2+z_1H_4$$

$$= (H_5-x_1)H_6-H_2(H_1-y_1)-(H_3-z_1)H_4$$

Since the above expression involves H_1, H_2, H_3, H_4, H_5, and H_6, simpler expressions than those shown earlier will be obtained now.

It has been shown that

$$H_1 = \frac{\dfrac{E_2-E_3}{B_2-B_3}-\dfrac{E_2-E_4}{B_2-B_4}}{\dfrac{A_2-A_3}{B_2-B_3}-\dfrac{A_2-A_4}{B_2-B_4}}$$

$$H_1 = \frac{(E_2-E_3)(B_2-B_4)-(E_2-E_4)(B_2-B_3)}{(A_2-A_3)(B_2-B_4)-(A_2-A_4)(B_2-B_3)}$$

$$= \frac{\left(\dfrac{D_2}{X_2} - \dfrac{D_3}{X_3}\right)\left(\dfrac{Z_2}{X_2} - \dfrac{Z_4}{X_4}\right) - \left(\dfrac{D_2}{X_2} - \dfrac{D_4}{X_4}\right)\left(\dfrac{Z_2}{X_2} - \dfrac{Z_3}{X_3}\right)}{\left(\dfrac{Y_2}{X_2} - \dfrac{Y_3}{X_3}\right)\left(\dfrac{Z_2}{X_2} - \dfrac{Z_4}{X_4}\right) - \left(\dfrac{Y_2}{X_2} - \dfrac{Y_4}{X_4}\right)\left(\dfrac{Z_2}{X_2} - \dfrac{Z_3}{X_3}\right)}$$

$$= \frac{\left(\dfrac{D_2X_3-D_3X_2}{X_2X_3}\right)\left(\dfrac{Z_2X_4-Z_4X_2}{X_2X_4}\right) - \left(\dfrac{D_2X_4-D_4X_2}{X_2X_4}\right)\left(\dfrac{Z_2X_3-Z_3X_2}{X_2X_3}\right)}{\left(\dfrac{X_3Y_2-X_2Y_3}{X_2X_3}\right)\left(\dfrac{X_4Z_2-X_2Z_4}{X_2X_4}\right) - \left(\dfrac{X_4Y_2-X_2Y_4}{X_2X_4}\right)\left(\dfrac{Z_2X_3-X_2Z_3}{X_2X_3}\right)}$$

$$= \frac{(D_2X_3-D_3X_2)(X_4Z_2-X_2Z_4)-(D_2X_4-D_4X_2)(X_3Z_2-X_2Z_3)}{(X_3Y_2-X_2Y_3)(X_4Z_2-X_2Z_4)-(X_4Y_2-X_2Y_4)(X_3Z_2-X_2Z_3)}$$

$$= \frac{D_2X_3X_4Z_2-D_2X_2X_3Z_4-D_3X_2X_4Z_2+D_3X_2^2Z_4-D_2X_3X_4Z_2+D_2X_2X_4Z_3+D_4X_2X_3Z_2-D_4X_2^2Z_3}{X_3X_4Y_2Z_2-X_2Y_3Y_2Z_4-X_2X_4Y_3Z_2+X_2^2Y_3Z_4-X_3X_4Y_2Z_2+X_2X_4Y_2Z_3+X_2X_3Y_4Z_2-X_2^2Y_4Z_3}$$

$$H_1 = \frac{X_2^2(D_3Z_4-D_4Z_3)+X_2X_3(D_4Z_2-D_2Z_4)+X_2X_4(D_2Z_3-D_3Z_2)}{X_2^2(Y_3Z_4-Y_4Z_3)+X_2X_3(Y_4Z_2-Y_2Z_4)+X_2X_4(Y_2Z_3-Y_3Z_2)}$$

$$H_1 = \frac{X_2(D_3Z_4-D_4Z_3)+X_3(D_4Z_2-D_2Z_4)+X_4(D_2Z_3-D_3Z_2)}{X_2(Y_3Z_4-Y_4Z_3)+X_3(Y_4Z_2-Y_2Z_4)+X_4(Y_2Z_3-Y_3Z_2)}$$

$$H_1 = \frac{D_2(X_4Z_3-X_3Z_4)+D_3(X_2Z_4-X_4Z_2)+D_4(X_3Z_2-X_2Z_3)}{X_2(Y_3Z_4-Y_4Z_3)+X_3(Y_4Z_2-Y_2Z_4)+X_4(Y_2Z_3-Y_3Z_2)} \tag{14}$$

It has been shown that

$$H_2 = \frac{\dfrac{C_2-C_3}{B_2-B_3} - \dfrac{C_2-C_4}{B_2-B_4}}{\dfrac{A_2-A_3}{B_2-B_3} - \dfrac{A_2-A_4}{B_2-B_4}}$$

Making necessary substitutions:

$$H_2 = \frac{(C_2-C_3)(B_2-B_4)-(C_2-C_4)(B_2-B_3)}{(A_2-A_3)(B_2-B_4)-(A_2-A_4)(B_2-B_3)}$$

$$H_2 = \frac{B_2C_2-B_4C_2-B_2C_3+B_4C_3-B_2C_2+B_3C_2+B_2C_4-B_3C_4}{A_2B_2-A_2B_4-A_3B_2+A_3B_4-A_2B_2+A_2B_3+A_4B_2-A_4B_3}$$

$$\frac{-\dfrac{Z_4}{X_4}\cdot\dfrac{d_1}{X_2} - \dfrac{Z_2}{X_2}\cdot\dfrac{d_2}{X_3} + \dfrac{Z_4}{X_4}\cdot\dfrac{d_2}{X_3} + \dfrac{Z_3}{X_3}\cdot\dfrac{d_1}{X_2} + \dfrac{Z_2}{X_2}\cdot\dfrac{d_3}{X_4} - \dfrac{Z_3}{X_3}\cdot\dfrac{d_3}{X_4}}{-\dfrac{Y_2}{X_2}\cdot\dfrac{Z_4}{X_4} - \dfrac{Y_3}{X_3}\cdot\dfrac{Z_2}{X_2} + \dfrac{Y_3}{X_3}\cdot\dfrac{Z_4}{X_4} + \dfrac{Y_2}{X_2}\cdot\dfrac{Z_3}{X_3} + \dfrac{Y_4}{X_4}\cdot\dfrac{Z_2}{X_2} - \dfrac{Y_4}{X_4}\cdot\dfrac{Z_3}{X_3}}$$

$$= \frac{-d_1X_3Z_4-d_2X_4Z_2+d_2X_2Z_4+d_1X_4Z_3+d_3X_3Z_2-d_3X_2Z_3}{-X_3Y_2Z_4-X_4Y_3Z_2+X_2Y_3Z_4+X_4Y_2Z_3+X_3Y_4Z_2-X_2Y_4Z_3}$$

$$= \frac{X_2(d_2Z_4-d_3Z_3)+X_3(d_3Z_2-d_1Z_4)+X_4(d_1Z_3-d_2Z_2)}{X_2(Y_3Z_4-Y_4Z_3)+X_3(Y_4Z_2-Y_2Z_4)+X_4(Y_2Z_3-Y_3Z_2)}$$

$$\frac{d_2(X_2Z_4-X_4Z_2)+d_3(X_3Z_2-X_2Z_3)+d_1(X_4Z_3-X_3Z_4)}{X_2(Y_3Z_4-Y_4Z_3)+X_3(Y_4Z_2-Y_2Z_4)+X_4(Y_2Z_3-Y_3Z_2)}$$

$$H_2 = \frac{-d_1(X_3Z_4-X_4Z_3)-d_2(X_4Z_2-X_2Z_4)-d_3(X_2Z_3-X_3Z_2)}{X_2(Y_3Z_4-Y_4Z_3)+X_3(Y_4Z_2-Y_2Z_4)+X_4(Y_2Z_3-Y_3Z_2)} \qquad (15)$$

It has been shown that

$$H_3 = \frac{E_2 - E_4 - H_1(A_2 - A_4)}{B_2 - B_4}$$

Making necessary substitutions:

$$H_3 = \frac{\dfrac{D_2}{X_2} - \dfrac{D_4}{X_4} - H_1\left(\dfrac{Y_2}{X_2} - \dfrac{Y_4}{X_4}\right)}{\dfrac{Z_2}{X_2} - \dfrac{Z_4}{X_4}}$$

$$H_3 = \frac{D_2 X_4 - D_4 X_2 - H_1(Y_2 X_4 - Y_4 X_2)}{Z_2 X_4 - Z_4 X_2}$$

$$H_3 = \frac{D_2 X_4 - D_4 X_2}{Z_2 X_4 - Z_4 X_2} - \frac{(Y_2 X_4 - Y_4 X_2)[X_2^2(D_3 Z_4 - D_4 Z_3) + X_2 Y_3(D_4 Z_2 - D_2 Z_4) + X_2 X_4(D_2 Z_3 - D_3 Z_2)]}{(Z_2 X_4 - Z_4 X_2)[X_2^2(Y_3 Z_4 - Y_4 Z_3) + X_2 X_3(Y_4 Z_2 - Y_2 Z_4) + X_2 X_4(Y_2 Z_3 - Y_3 Z_2)]}$$

$$H_3 = \frac{X_2(X_4 Z_2 - X_2 Z_4)[X_4(D_3 Y_2 - D_2 Y_3) - X_3(D_4 Y_2 - D_2 Y_4) + X_2(D_4 Y_3 - D_3 Y_4)]}{X_2(Z_2 X_4 - Z_4 X_2)[X_4(Y_2 Z_3 - Y_3 Z_2) - X_3(Z_4 Y_2 - Z_2 Y_4) + X_2(Y_3 Z_4 - Y_4 Z_3)]}$$

$$H_3 = \frac{X_2(Y_3 D_4 - Y_4 D_3) + X_3(Y_4 D_2 - Y_2 D_4) + X_4(Y_2 D_3 - Y_3 D_2)}{X_2(Y_3 Z_4 - Y_4 Z_3) + X_3(Y_4 Z_2 - Y_2 Z_4) + X_4(Y_2 Z_3 - Y_3 Z_2)} \qquad (16)$$

$$H_3 = \frac{D_2(X_3 Y_4 - X_4 Y_3) + D_3(X_4 Y_2 - X_2 Y_4) + D_4(X_2 Y_3 - X_3 Y_2)}{\text{Denom}}$$

it has been shown that

$$H_4 = \frac{C_2 - C_4 - A_2 H_2 - A_4 H_2}{B_2 - B_4}$$

Making necessary substitutions:

$$H_4 = \frac{C_2 - C_4}{B_2 - B_4} - \frac{(A_2 - A_4)[(C_2 - C_3)(B_2 - B_4) - (C_2 - C_4)(B_2 - B_3)]}{(B_2 - B_4)[(A_2 - A_3)(B_2 - B_4) - (A_2 - A_4)(B_2 - B_3)]}$$

$$= (C_2 - C_4)[(A_2 - A_3)(B_2 - B_4) - (A_2 - A_4)(B_2 - B_3)]$$

$$- \frac{A_2 - A_4[(C_2 - C_3)(B_2 - B_4) - (C_2 - C_4)(B_2 - B_3)]}{(B_2 - B_4)[(A_2 - A_3)(B_2 - B_4) - (A_2 - A_4)(B_2 - B_3)]}$$

$$= \frac{(A_2 - A_3)(C_2 - C_4) - (A_2 - A_4)(C_2 - C_3)}{(A_2 - A_3)(B_2 - B_4) - (A_2 - A_4)(B_2 - B_3)}$$

$$= \frac{A_2 C_2 - A_2 C_4 - A_3 C_2 + A_3 C_4 - A_2 C_2 + A_2 C_3 + A_4 C_2 - A_4 C_3}{\dfrac{X_2(Y_3 Z_4 - Y_4 Z_3) + X_3(Y_4 Z_2 - Y_2 Z_4) + X_4(Y_2 Z_3 - Y_3 Z_2)}{X_2 X_3 X_4}}$$

$$H_4 = \frac{-Y_2}{X_2}\frac{d_3}{X_4} - \frac{Y_3}{X_3}\frac{d_1}{X_2} + \frac{Y_3}{X_3}\frac{d_3}{X_4} + \frac{Y_2}{X_2}\frac{d_2}{X_3} + \frac{Y_4}{X_4}\frac{d_1}{X_2} - \frac{Y_4}{X_4}\frac{d_2}{X_3}$$
$$\overline{} \quad \text{Denom}$$

$$= \frac{-d_3 X_3 Y_2 - d_1 X_4 Y_3 + d_3 X_2 Y_3 + d_2 X_4 Y_2 + d_1 X_3 Y_4 - d_2 X_2 Y_4}{X_2(Y_3 Z_4 - Y_4 Z_3) - X_3(Y_4 Z_2 - Y_2 Z_4) + X_4(Y_2 Z_3 - Y_3 Z_2)}$$

$$= \frac{X_2(d_3 Y_3 - d_2 Y_4) + X_3(d_1 Y_4 - d_3 Y_2) + X_4(d_2 Y_2 - d_1 Y_3)}{X_2(Z_4 Y_3 - Z_3 Y_4) + X_3(Z_2 Y_4 - Z_4 Y_2) + X_4(Z_3 Y_2 - Z_2 Y_3)}$$

$$H_4 = \frac{-d_1(Y_3 X_4 - Y_4 X_3) - d_2(Y_4 X_2 - Y_2 X_4) - d_3(Y_2 X_3 - Y_3 X_2)}{X_2(Y_3 Z_4 - Y_4 Z_3) + X_3(Y_4 Z_2 - Y_2 Z_4) + X_4(Y_2 Z_3 - Y_3 Z_2)} \tag{17}$$

It has been shown that

$$H_5 = \frac{D_4 - H_1 Y_4 - H_3 Z_4}{X_4}$$

Making necessary substitutions:

$$H_5 = \frac{D_4}{X_4} \frac{-X_2 Y_4 (D_3 Z_4 - D_4 Z_3) - X_3 Y_4 (D_4 Z_2 - D_2 Z_4) - X_4 Y_4 (D_2 Z_3 - D_3 Z_2) - X_2 Z_4 (Y_3 D_4 - Y_4 D_3)}{}$$

$$\frac{-X_3 Z_4 (Y_4 D_2 - Y_2 D_4) - X_4 Z_4 (Y_2 D_3 - Y_3 D_2)}{X_2 X_4 (Y_3 Z_4 - Y_4 Z_3) + X_4 X_3 (Y_4 Z_2 - Y_2 Z_4) + X_4^2 (Y_2 Z_3 - Z_2 Y_3)}$$

$$= \frac{D_4 X_4 Y_2 Z_3 - D_4 X_4 Y_3 Z_2 - D_2 X_4 Y_4 Z_3 + D_3 X_4 Y_4 Z_2 - D_3 X_4 Y_2 Z_4 + D_2 X_4 Y_3 Z_4}{Denom}$$

$$H_5 = \frac{D_2 (Y_3 Z_4 - Y_4 Z_3) + D_3 (Y_4 Z_2 - Y_2 Z_4) + D_4 (Y_2 Z_3 - Y_3 Z_2)}{X_2 (X_3 Z_4 - Y_4 Z_3) + X_3 (Y_4 Z_2 - Y_2 Z_4) + X_4 (Y_2 Z_3 - Y_3 Z_2)} \tag{18}$$

It has been shown that

$$H_6 = \frac{H_2 Y_4 - H_4 Z_4 - d_3}{X_4}$$

$$= \frac{X_2 Y_4 (d_2 Z_4 - d_3 Z_3) + X_3 Y_4 (d_3 Z_2 - d_1 Z_4) + X_4 Y_4 (d_1 Z_3 - d_2 Z_2)}{}$$

$$\frac{+X_2 Z_4 (d_3 Y_3 - d_2 Y_4) + X_3 Z_4 (d_1 Y_4 - d_3 Y_2) + X_4 Z_4 (d_2 Y_2 - d_1 Y_3)}{X_2 X_4 (Z_4 Y_3 - Z_3 Y_4) + X_3 Y_4 (Z_2 Y_4 - Z_4 Y_2) + X_4^2 (Z_3 Y_2 - Z_2 Y_3)} - \frac{d_3}{X_4}$$

$$= d_2 X_2 Y_4 Z_4 - d_3 X_2 Y_4 Z_3 + d_3 X_3 Y_4 Z_2 - d_1 X_3 Y_4 Z_4 + d_1 X_4 Y_4 Z_3 - d_2 X_4 Y_4 Z_2$$

$$+ d_3 X_2 Y_3 Z_4 - d_2 X_2 Y_4 Z_4 + d_1 X_3 Y_4 Z_4 - d_3 X_3 Y_2 Z_4 + d_2 X_4 Y_2 Z_4 - d_1 X_4 Y_3 Z_4$$

$$\frac{- d_3 X_2 Y_3 Z_4 + d_3 X_2 Y_4 Z_3 - d_3 X_3 Y_4 Z_2 + d_3 X_3 Y_2 Z_4 - d_3 X_4 Y_2 Z_3 + d_3 X_4 Y_3 Z_2}{X_2 X_4 (Z_4 Y_3 - Z_3 Y_4) + X_3 X_4 (Z_2 Y_4 - Z_4 Y_2) + X_4^2 (Z_3 Y_2 - Z_2 Y_3)}$$

$$= \frac{d_1 X_4 Y_4 Z_3 - d_2 X_4 Y_4 Z_2 + d_2 X_4 Y_2 Z_4 - d_1 X_4 Y_3 Z_4 - d_3 X_4 Y_2 Z_3 + d_3 X_4 Y_3 Z_2}{\text{Denom}}$$

$$H_6 = \frac{-d_1(Y_3 Z_4 - Y_4 Z_3) - d_2(Y_4 Z_2 - Y_2 Z_4) - d_3(Y_2 Z_3 - Y_3 Z_2)}{X_2(Y_3 Z_4 - Y_4 Z_3) + X_3(Y_4 Z_2 - Y_2 Z_4) + X_4(Y_2 Z_3 - Y_3 Z_2)} \tag{19}$$

Let

$$a = X_4 Z_3 - X_3 Z_4$$

$$b = X_2 Z_4 - X_4 Z_2$$

$$c = X_3 Z_2 - X_2 Z_3$$

$$d = X_3 Y_4 - X_4 Y_3$$

$$e = X_4 Y_2 - X_2 Y_4$$

$$f = X_2 Y_3 - X_3 Y_2$$

$$g = Y_3 Z_4 - Y_4 Z_3$$

$$h = Y_4 Z_2 - Y_2 Z_4$$

$$j = Y_2 Z_3 - Y_3 Z_2$$

Then

$$H_1 = \frac{a D_2 + b D_3 + c D_4}{g X_2 + h X_3 + j X_4} \tag{20}$$

$$H_2 = \frac{+a d_1 + b d_2 + c d_3}{g X_2 + h X_2 + g X_4} \tag{21}$$

$$H_3 = \frac{d D_2 + e D_3 + f D_4}{g X_2 + h X_2 + j X_4} \tag{22}$$

$$H_4 = \frac{+d d_1 + e d_2 + f d_3}{g X_2 + h X_3 + j X_4} \tag{23}$$

-574-

$$H_5 = \frac{gD_2 + hD_3 + jD_4}{gX_2 + hX_3 + jX_4} \tag{24}$$

$$H_6 = \frac{-gD_1 - hd_2 - jd_3}{gX_2 + hX_3 + jX_4} \tag{25}$$

$$H_1H_2 = \frac{(aD_2 + bD_3 + cD_4)(ad_1 + bd_2 + cd_3)}{(gX_2 + hX_3 + jX_4)^2}$$

$$= \frac{\begin{array}{c} a^2D_2d_1 + abD_2d_2 + acD_2d_3 + b^2D_3d_2 + bcD_3d_3 \\ + abD_3d_1 + acD_4d_1 \qquad + bcD_4d_2 + c^2D_4d_3 \end{array}}{(gX_2 + hX_3 + jX_4)^2}$$

$$H_1H_2 = \frac{a^2D_2d_1 + b^2D_3d_2 + c^2D_4d_3 + ab(D_2d_2 + D_3d_1) + ac(D_2d_3 + D_4d_1) + bc(D_3d_3 + D_4d_2)}{(gX_2 + hX_3 + jX_4)^2}$$

$$H_3H_4 = \frac{(dD_2 + eD_3 + fD_4)(dd_1 + ed_2 + fd_3)}{(gX_2 + hX_3 + jX_4)^2}$$

$$H_3H_4 = \frac{d^2D_2d_1 + e^2D_3d_2 + f^2D_4d_3 + de(D_2d_2 + D_3d_1) + df(D_4d_1 + D_2d_3) + ef(D_3d_3 + D_4d_2)}{(gX_2 + hX_3 + jX_4)^2}$$

$$H_5H_6 = -\frac{(gD_2 + hD_3 + jD_4)(+gd_1 + hd_2 + jd_3)}{(gX_2 + hX_3 + jX_4)^2}$$

-575-

$$= -[+g^2D_2d_1 + ghD_2d_2 + gjD_2d_3$$
$$ghD_3d_1 \qquad\qquad + h^2D_3d_2 + hjd_3D_3$$
$$gjD_4d_1 \qquad\qquad hjd_2D_4$$
$$\qquad\qquad\qquad\qquad + j^2d_3D_4]$$

$$H_5H_6 = \frac{-[g^2D_2d_1 + h^2D_3d_2 + j^2D_4d_3 + gh(D_2d_2+D_3d_1) + gj(D_2d_3+D_4d_1) + hj(D_3d_3+D_4d_2)]}{(gX_2 + hX_3 + jX_4)^2}$$

We had earlier

$$B = H_5H_6 - H_1H_2 - H_3H_4 - x_1H_6 + y_1H_2 + z_1H_4$$

$$B = \frac{\begin{array}{l} -g^2D_2d_1 - h^2D_3d_2 - j^2D_4d_3 - gh(D_2d_2+D_3d_1) - gj(D_2d_3+D_4d_1) - hj(D_3d_3+D_4d_2) \\ -a^2D_2d_1 - b^2D_3d_2 - c^2D_4d_3 - ab(D_2d_2+D_3d_1) - ac(D_2d_3+D_4d_1) - bc(D_3d_3+D_4d_2) \\ -d^2D_2d_1 - e^2D_3d_2 - f^2D_4d_3 - de(D_2d_2+D_3d_1) - df(D_2d_3+D_4d_1) - ef(D_3d_3+D_4d_2) \end{array}}{(gX_2+hX_3+jX_4)^2}$$

$$+ \frac{x_1(gd_1+hd_2+jd_3) + y_1(ad_1+bd_2+cd_3) + z_1(dd_1+ed_2+fd_3)}{gX_2+hX_3+jX_4}$$

Looking at second term

$$\frac{\begin{array}{l} x_1(gd_1+hd_2+jd_3)(gX_2+hX_3+jX_4) + y_1(ad_1+bd_2+cd_3)(gX_2+hX_3+jX_4) \\ + z_1(dd_1+ed_2+fd_3)(gX_2+hX_2+jX_4) \end{array}}{(gX_2+hX_3+jX_4)^2}$$

$$= x_1[g^2d_1X_2+h^2d_2X_3+j^2d_?X_4+gh(d_1X_3+d_2X_2)+gj(d_1X_4+d_3X_2)+hj(d_2X_4+d_3X_3)]$$

$$+y_1[agd_1X_2+ahd_1X_3+ajd_1X_4+bgd_2X_2+bhd_2X_3+bjd_2X_4+cgd_3X_2+chd_3X_3+cjd_3X_4]$$

$$+z_1[dgd_1X_2+dhd_1X_3+djd_1X_4+egd_2X_2+ehd_2X_3+ejd_2X_4+fjd_3X_2+fhd_3X_3+fjd_3X_4]$$

$$\overline{\hspace{10cm}}$$

$$(gX_2+hX_3+jX_4)^2$$

$$= d_1X_2(g^2x_1+agy_1+dgz_1)+d_2X_3(h^2x_1+bhy_1+ehz_1)+d_3X_4(j^2x_1+cjy_1+fjz_1)$$

$$+d_1X_3(ghx_1+ahy_1+dhz_1)+d_1X_4(gjx_1+ajy_1+djz_1)+d_2X_2(ghx_1+bgy_1+egz_1)$$

$$+d_2X_4(hjx_1+bjy_1+ejz_1)+d_3X_2(gjx_1+cgy_1+fgz_1)+d_3X_3(hjx_1+chy_1+fhz_1)$$

$$\overline{\hspace{10cm}}$$

$$(gX_2+hX_3+jX_4)^2$$

Gathering all terms:

$$B = -d_1D_2(a^2+d^2+g^2)-d_2D_3(b^2+e^2+h^2)-d_3D_4(c^2+f^2+j^2)-(d_2D_2+d_1D_3)(ab+de+gh)$$

$$-(d_3D_2+d_1D_4)(ac+df+gj)-(d_3D_3+d_2D_4)(bc+ef+hj)+d_1X_2g(gx_1+ay_1+dz_1)$$

$$+d_1X_3h(gx_1+ay_1+dz_1)+d_1X_4j(gx_1+ay_1+dz_1)+d_2X_2g(hx_1+by_1+ez_1)$$

$$+d_2X_3h(hx_1+by_1+ez_1)+d_2X_4j(hx_1+by_1+ez_1)+d_3X_2g(jx_1+cy_1+fz_1)$$

$$+d_3X_3h(jx_1+cy_1+fz_1)+d_3X_4j(jx_1+cy_1+fz_1)$$

$$\overline{\hspace{10cm}}$$

$$(gX_2+hX_3+jX_4)^2$$

$$B = d_1(gx_1+ay_1+dz_1)(gX_2+hX_3+jX_4)+d_2(hx_1+by_1+ez_1)(gX_2+hX_3+jX_4)$$

$$+d_3(jx_1+cy_1+fz_1)(gX_2+hX_3+jX_4)-d_1D_2(a^2+d^2+g)-d_2D_3(b^2+e^2+h^2)$$

$$-d_3D_4(c^2+f^2+j^2)-(d_2D_2+d_1D_3)(ab+de+gh)-(d_3D_2+d_1D_4)(ac+df+gj)$$

$$-(d_3D_3+d_2D_4)(bc+ef+hj)$$

$$\overline{\hspace{10cm}}$$

$$(gX_2+hX_3+jX_4)^2$$

$$B = (gX_2+hX_3+jX_4)[d_1(gx_1+ay_1+dz_1)+d_2(hx_1+by_1+ez_1)+d_3(jx_1+cy_1+fz_1)]$$

$$-d_1[D_2(a^2+d^2+g^2)+D_3(ab+dc+gh)+D_4(ac+df+gj)]-d_2[D_2(ab+de+gh)$$

$$+D_3(b^2+e^2+h^2)+D_4(bc+ef+hj)]-d_3(D_2(ac+df+gj)+D_3(bc+ef+hj)$$

$$+D_4(c^2+f^2+j^2)]$$

$$\overline{}$$

$$(gX_2+hX_3+jX_4)^2$$

Now

$$A = H_2^2+H_4^2+H_6^2-1$$

$$= \frac{a^2d_1^2+b^2d_2^2+c^2d_3^2+2abd_1d_2+2acd_1d_3+2bcd_2d_3+d^2d_1^2+e^2d_2^2+f^2d_3^2+2ded_1d_2}{(gX_2+hX_3+jX_4)^2} -1$$

$$\frac{+2dfd_1d_3+2efd_2d_3+g^2d_1^2+h^2d_2^2+j^2d_3^2+2ghd_1d_2+2gjd_1d_3+2hjd_2d_3}{}$$

$$A = \frac{d_1^2(a^2+d^2+g^2)+d_2^2(b^2+e^2+h^2)+d_3^2(c^2+f^2+j^2)+2d_1d_2(ab+de+gh)}{(gX_2+hX_3+jX_4)^2}$$

$$\frac{+2d_1d_3(ac+df+gj)+2d_2d_3(bc+ef+hj)-(gX_2+hX_3+jX_4)^2}{}$$

Now rational part of $r = Ra(r) = \dfrac{-B}{A}$

$$= d_1[D_2(a^2+d^2+g^2)+D_3(ab+de+gh)+D_4(ac+df+gj)]+d_2[D_2(ab+de+gh)$$

$$+D_3(b^2+e^2+h^2)+D_4(bc+ef+hj)]+d_3[D_2(ac+df+gj)+D_3(bc+ef+hj)$$

$$+D_4(c^2+f^2+j^2)]-(gX_2+hX_3+jX_4)[d_1(gx_1+ay_1+dz_1)+d_2(hx_1+by_1+ez_1)$$

$$+d_3(jx_1+cy_1+fz_1)]$$

$$\overline{}$$

$$d_1^2(a^2+d^2+g^2)+d_2^2(b^2+e^2+h^2)+d_3^2(c^2+f^2+j^2)+2d_1d_2(ab+de+gh)$$

$$+2d_1d_3(ac+df+gj)+2d_2d_3(bc+ef+hj)-(gX_2+hX_3+jX_4)^2 \qquad (26)$$

To find irrational part of r   Ir(r)

$$Ir(r) = \frac{\sqrt{B^2-AC}}{A}$$

$$C = J_1^2+J_2^2+J_3^2$$

$$= (H_5-x_1)^2+(H_1-y_1)^2-(H_3+z_1)^2$$

$$= H_1{}^2+H_3{}^2+H_5{}^2+x_1{}^2+y_1{}^2+z_1{}^2-2x_1H_5-2y_1H_1-2z_1H_3$$

Using (20), (22) and (24)

$$C = \frac{(aD_2+bD_3+cD_4)^2+(dD_2+eD_3+fD_4)^2+(gD_2+hD_3+jD_4)^2}{(gX_2+hX_3+jX_4)^2}+x_1{}^2+y_1{}^2+z_1{}^2$$

$$\frac{-2x_1(gD_2+hD_3+jD_4)(gX_2+hX_3+jX_4)-2y_1(aD_2+bD_3+cD_4)(gX_2+hX_3+jX_4)}{-2z_1(gD_2+eD_3+fD_4)(gX_2+hX_3+jX_4)}$$

$$\overline{\qquad\qquad (gX_2+hX_3+jX_4)^2 \qquad\qquad}$$

$$C = \frac{D_2^2(a^2+d^2+g^2)+D_3^2(b^2+e^2+h^2)+D_4^2(e^2+f^2+j^2)}{}$$

$$+2D_2D_3(ab+de+gh)+2D_2D_4(ac+df+gj)+2D_3D_4(bc+ef+hj)$$

$$\frac{-2(gX_2+hX_3+jX_4)[D_2(gx_1+ay_1+dz_1)+D_3(hx_1+by_1+ez_1)+D_4(jx_1+cy_1+fz_1)]}{(gX_2+hX_3+jX_4)^2}$$

$$+x_1{}^2+y_1{}^2+z_1{}^2$$

Let

$$gX_2+hX_3+jX_4 = M$$

and

$$gx_1 + ay_1 + dz_1 = N_1$$

$$hx_1 + by_1 + ez_1 = N_2$$

$$jx_1 + cy_1 + fz_1 = N_3$$

$$a^2 + d^2 + g^2 = R_1$$

$$b^2 + e^2 + h^2 = R_2$$

$$c^2 + f^2 + j^2 = R_3$$

$$ab + de + gh = P_1$$

$$ac + df + gj = P_2$$

$$bc + ef + hj = P_3$$

Therefore:

$$B = \frac{M(d_1 N_1 + d_2 N_2 + d_3 N_3) - d_1(D_2 R_1 + D_3 P_1 + D_4 P_2) - d_2(D_2 P_1 + D_3 R_2 + D_4 P_3) - d_3(D_2 P_2 + D_3 P_3 + D_4 R_3)}{M^2}$$

$$B = \frac{d_1(MN_1 - D_2 R_1 - D_3 P_1 - D_4 P_2) + d_2(MN_2 - D_2 P_1 - D_3 R_2 - D_4 P_3) + d_3(MN_3 - D_2 P_2 - D_3 P_3 - D_4 R_3)}{M^2}$$

$$A = \frac{d_1^2 R_1 + d_2^2 R_2 + d_3^2 R_3 + 2d_1 d_2 P_1 + 2d_1 d_3 P_2 + 2d_2 d_3 P_3 - M^2}{M^2}$$

$$C = \frac{\begin{array}{c} D_2^2 R_1 + D_3^2 R_2 + D_4^2 R_3 + 2D_2 D_3 P_1 + 2D_2 D_4 P_2 + 2D_3 D_4 P_3 \\ -2M(D_2 N_1 + D_3 N_2 + D_4 N_3) + (x_1^2 + y_1^2 + z_1^2)M^2 \end{array}}{M^2}$$

$$B^2 = \frac{\begin{aligned}&d_1^2(MN_1-D_2R_1-D_3P_1-D_4P_2)^2+d_2^2(MN_2-D_2P_1-D_3R_2-D_4P_3)^2+d_3^2(MN_3-D_2P_2-D_3P_3-D_4R_3)^2\\&+2d_1d_2(MN_1-D_2R_1-D_3P_1-D_4P_2)(MN_2-D_2P_1-D_3R_2-D_4P_3)\\&+2d_2d_3(MN_2-D_2P_1-D_3R_2-D_4P_3)(MN_3-D_2P_2-D_3P_3-D_4R_3)\\&+2d_1d_3(MN_1-D_2R_1-D_3P_1-D_4P_2)(MN_3-D_2P_2-D_3P_3-D_4R_3)\end{aligned}}{M^4}$$

$$B^2 = \frac{\begin{aligned}&d_1^2[M^2N_1^2+D_2^2R_1^2+D_3^2P_1^2+D_4^2P_2^2+2D_2D_3P_1R_1+2D_2D_4P_2R_1+2D_3D_4P_1P_2-2MN_1(D_2R_1+D_3P_1+D_4P_2)]\\[6pt]&+d_2^2[M^2N_2^2+D_2^2P_1^2+D_3^2R_2^2+D_4^2P_3^2+2D_2D_3P_1R_2+2D_2D_4P_1P_3+2D_3D_4P_3R_2-2MN_2(D_2P_1+D_3R_2+D_4P_3)]\\[6pt]&+d_3^2[M^2N_3^2+D_2^2P_2^2+D_3^2P_3^2+D_4^2R_3^2+2D_2D_3P_2P_3+2D_2D_4P_2R_3+2D_3D_4P_3R_3-2MN_3(D_2P_2+D_3P_3+D_4R_3)]\\[6pt]&+2d_1d_2[M^2N_1N_2+D_2^2P_1R_1+D_3^2P_1R_2+D_4P_2P_3+D_2D_3(R_1R_2+P_1^2)+D_2D_4(P_3R_1+P_1P_2)\\&\qquad\qquad+D_3D_4(P_1P_3+P_2R_2)-MN_1(D_2P_1+D_3R_2+D_4P_3)-MN_2(D_2R_1+D_3P_1+D_4P_2)]\\[6pt]&+2d_2d_3[M^2N_2N_3+D_2^2P_1P_2+D_3^2P_3R_2+D_4^2P_3R_3+D_2D_3(P_1P_3+P_2R_2)+D_2D_4(P_1R_3+P_2P_3)\\&\qquad\qquad+D_3D_4(R_2R_3+P_3^2)-MN_2(D_2P_2+D_3P_3+D_4R_3)-MN_3(D_2P_1+D_3R_2+D_4P_3)]\\[6pt]&+2d_1d_3[M^2N_1N_3+D_2^2P_2R_1+D_3^2P_1P_3+D_4^2P_2R_3+D_2D_3(P_3R_1+P_1P_2)+D_2D_4(R_3R_1+P_2^2)\\&\qquad\qquad+D_3D_4(P_1R_3+P_2P_3)-MN_1(D_2P_2+D_3P_3+D_4R_3)-MN_3(D_2R_1+D_3P_1-D_4P_2)]\end{aligned}}{M^4}$$

$$AC = d_1^2(R_1^2D_2^2 + D_3^2R_1R_2 + D_4^2R_1R_3 + 2D_2D_3P_1R_1 + 2D_2D_4P_2R_1$$
$$+2D_3D_4P_3R_1 - 2MR_1(D_2N_1 + D_3N_2 + D_4N_3)]$$

$$+d_2^2[D_2^2R_1R_2 + D_3^2R_2^2 + D_4^2R_2R_3 + 2D_2D_3P_1R_2 + 2D_2D_4P_2R_2$$
$$+2D_3D_4P_3R_2 - 2MR_2(D_2N_1 + D_3N_2 + D_4N_3);$$

$$+d_3^2[D_2^2R_1R_3 + D_3^2R_2R_3 + D_4^2R_3^2 + 2D_2D_3P_1R_3 + 2D_2D_4P_2R_3$$
$$+2D_3D_4P_3R_3 - 2MR_3(D_2N_1 + D_3N_2 + D_4N_3)]$$

$$+2d_1d_2[D_2^2P_1R_1 + D_3^2P_1R_2 + D_4^2P_1R_3 + 2D_2D_3P_1^2 + 2D_2D_4P_1P_2$$
$$+2D_3D_4P_1P_3 - 2MP_1(D_2N_1 + D_3N_2 - D_4N_3)]$$

$$+2d_1d_3[D_2^2P_2R_1 + D_3^2P_2R_2 + D_4^2P_2R_3 + 2D_2D_3P_1P_2 + 2D_2D_4P_2^2$$
$$+2D_3D_4P_2P_3 - 2MP_2(D_2N_1 - D_3N_2 - D_4N_3)]$$

$$+2d_2d_3[D_2^2P_3R_1 + D_3^2P_3R_2 + D_4^2P_3R_3 + 2D_2D_3P_1P_3 + 2D_2D_4P_2P_3$$
$$+2D_3D_4P_3^2 - 2MP_3(D_2N_1 + D_3N_2 + D_4N_3)]$$

$$-M^2(D_2^2R_1 + D_3^2R_2 + D_4^2R_3 + 2D_2D_3P_1 + 2D_2D_4P_2 + 2D_3D_4P_3$$
$$-2M(D_2N_1 + D_3N_2 + D_4N_3) + M^2(x_1^2 + y_1^2 + z_1^2)$$

$$M^4$$

$$B^2 - AC = d_1^2[M^2N_1^2+D_3^2(P_1^2-R_1R_2)+D_4^2(P_2^2-R_1R_3)+2D_3D_4(P_1P_2-P_3R_1)$$

$$-2D_3M(P_1N_1-R_1N_2)-2D_4M(P_2N_1-R_1N_3)]$$

$$+d_2^2[M^2N_2^2+ D_2^2(P_1^2-R_1R_2)+D_4^2(P_3^2-R_2R_3)+2D_2D_4(P_1P_3-P_2R_2)$$

$$-2D_2M(P_1N_2-R_2N_1)-2D_4M(P_3N_2-R_2N_3)]$$

$$+d_3^2[M^2N_3^2+D_2^2(P_2^2-R_1R_3)+D_3^2(P_3^2-R_2R_3)+2D_2D_3(P_2P_3-P_1R_3)$$

$$-2D_2M(P_2N_3-R_3N_1)-2D_3M(P_3N_3-R_3N_2)]$$

$$+2d_1d_2[M^2N_1N_2+D_4^2(P_2P_3-P_1R_3)+D_2D_3(R_1R_2-P_1^2)+D_2D_4(P_3R_1-P_1P_2)$$

$$+D_3D_4(P_2R_2-P_1P_3)-MD_2(R_1N_2-P_1N_1)-MD_3(R_2N_1-P_1N_2)-MD_4(P_3N_1+P_2N_2-2P_1N_3)]$$

$$+2d_2d_3[M^2N_2N_3+D_2^2(P_1P_2-P_3R_1)+D_2D_3(P_2R_2-P_1P_3)+D_2D_4(P_1R_3-P_2P_3)$$

$$+D_3D_4(R_2R_3-P_3^2)-MD_2(P_2N_2+P_1N_3-2P_3N_1)-MD_3(R_2N_3-P_3N_2)-MD_4(R_3N_2-P_3N_3)]$$

$$+2d_1d_3[M^2N_1N_3+D_3^2(P_1P_3-P_2R_2)+D_2D_3(P_3R_1-P_1P_2)+D_2D_4(R_1R_3-P_2^2)$$

$$+D_3D_4(P_1R_3-P_2P_3)-MD_2(R_1N_3-P_2N_1)-MD_3(P_3N_1+P_1N_3-2P_2N_2)-MD_4(R_3N_1-P_2N_3)]$$

$$-M^4(x^2+y^2+z^2)$$

$$M^4$$

$$B^2 - AC = \frac{1}{(gX_2+hX_3+jX_4)^4} \left\{ \left\{ \right. \right.$$

$$d_1^2 \left\{ (gX_2+hX_3+jX_4)(gx_1+ay_1+dz_1)^2 \right.$$

$$-D_3^2[ae-bd)^2+(ah-bg)^2+(dh-eg)^2]-D_4^2[(af-cd)^2+(aj-cg)^2+(dj-fg)^2]$$

$$-2D_3D_4[a^2(ef+jh)+d^2(bc+hj)+g^2(bc+ef)-ab(df+gj)-de(ac+gj)$$

$$-gh(ac+df)]+2D_3(gX_2+hX_3+jX_4)[[x_1[h(a^2+d^2)-g(ab+de)]$$

$$+y_1[b(d^2+g^2)-a(de+gh)]+z_1[e(a^2+g^2)-d(ab+gh)]]]$$

$$+D_4(gX_2+hX_3+jX_4)[[x_1[j(a^2+d^2)-g(ac+de)]+y_1[c(d^2+g^2)$$

$$\left. -a(df+gj)]+z_1[f(a^2+g^2)-d(ac+gj)]]] \right\}$$

$$+d_2^2 \left\{ (gX_2+hX_3+jX_4)^2(hx_1+by_1+ez_1)^2 \right.$$

$$-D_2^2[(ae-bd)^2+(ah-bg)^2+(dh-eg)^2]-D_4^2[(ce-bf)^2-(ch-bj)^2-(ef-fh)^2]$$

$$-2D_2D_4[b^2(df+gj)+e^2(ac+gj)+h^2(ac+df)-ab(ef+hj)-de(bc+hj)$$

$$-gh(bc+ef)]+2D_2(gX_2+hX_3+jX_4)[[x_1[g(b^2+e^2)-h(ab+de)]$$

$$+y_1[a(e^2+h^2)-b(de+gh)]+z_1[d(b^2+h^2)-e(ab+gh]]]$$

$$+2D_4(gX_2+hX_3+jX_4)[[x_1[j(b^2+e^2)-h(bc+ef)] +$$

$$\left. +y_1[c(e^2+h^2)-b(ef+hj)]+z_1[f(b^2+h^2)-e(bc+hj)]]] \right\}$$

$$+d_3^2 \left\{ (gX_2+hX_3+jX_4)^2(jx_1+cy_1+fz_1)^2 \right.$$

$$-D_2^2[(af-cd)^2+(aj-cg)^2+(dj-fg)^2]-D_3[(ce-bf)^2+(ch-bj)^2+(ej-fh)^2]$$

$$-2D_2D_3[c^2(de+gh)+f^2(ab+gh)+j^2(ab+de)-ac(ef-hj)$$

$$-df(bc+hj)-gj(bc+ef)]+2D_2(gX_2+hX_3+jX_4)[[x_1[g(c^2+f^2)-j(ac+df)]$$

$$+y_1[a(f^2+j^2)-c(df+gj)]+z_1[d(c^2+j^2)-f(ae+gj)]]]$$

$$+2D_3(gX_2+hX_3+jX_4)[[x_1[h(c^2+f^2)-j(bc+ef)]+y_1[b(f^2+j^2)$$

$$\left. -c(ef+hj)]+z_1[e(c^2+j^2)-f(bc+hj)]]] \right\}$$

$$+2d_1d_2\Big\{(gX_2+hX_3+jX_4)^2(gx_1+ay_1+dz_1)(hx_1+by_1+ez_1)$$

$$-D_2^2[c^2(de+gh)+f^2(ab+gh)+j^2(ab+de)-ac(ef+hj)$$

$$-df(bc+hj)-gj(bc+ef)]+D_2D_3[(ae-bd)^2+(ah-bg)^2+(dh-eg)^2]$$

$$+D_2D_4[a^2(ef+hj)+d^2(bc+hj)+g^2(ef+bc)-ab(df+gj)$$

$$-de(ac+gj)-gh(ac+df)]+D_3D_4[b^2(df+gj)+e^2(ac+gj)$$

$$+h^2(ac+df)-ab(ef+hj)-de(bc+hj)-gh(bc+ef)]$$

$$+D_2(gX_2+hX_3+jX_4)[[x_1[h(a^2+d^2)-g(ab+de)]+y_1[b(d^2+g^2)-a(de+gh)]$$

$$+z_1[e(a^2+g^2)-d(ab+gh)]\ ]]+D_3(gX_2+hX_3+jX_4)[[x_1[g(b^2+e^2)$$

$$-h(ab+de)]+y_1[a(e^2+h^2)-b(de+gh)]+z_1[d(b^2+h^2)-e(ab+gh)]\ ]]$$

$$-D_4(gX_2+hX_3+jX_4)[[x_1[g(bc+ef)+h(ac+df)-2j(ab+de)]$$

$$+y_1[a(ef+hj)+b(df+gj)-2c(de+gh)]$$

$$+z_1[d(bc+hj)+e(ac+gj)-2f(ab+gh)]\ ]]\Big\}$$

$$+2d_2d_3\Big\{(gX_2+hX_3+jX_4)^2(hx_1+by_1+ez_1)(jx_1+cy_1+fz_1)$$

$$-D_2^2[a^2(ef+hj)+d^2(bc+hj)+g^2(bc+ef)-ab(df+gj)$$

$$-de(ac+gj)-gh(ac+df)]$$

$$+D_2D_3[b^2(df+gj)+e^2(ac+gj)+h^2(ac+df)-ab(ef+hj)$$

$$-de(bc+hj)-gh(bc+ef)]+D_2D_4[f^2(ab+gh)+j^2(ab+de)$$

$$+c^2(de+gh)-ac(ef+hj)-df(bc+hj)-gj(bc+ef)]$$

$$+D_3D_4[(ce-bf)^2+(ch-bj)^2+(ej-fh)^2]$$

$$-D_2(gX_2+hX_3+jX_4)[[x_1[h(ac+df)+j(ab+de)-2g(bc+ef)$$

$$+y_1[b(df+gj)+c(de+gh)-2a(ef+hj)]+z_1[e(ac+gj)+f(ab+gh)-2d(bc+hj)]\ ]]$$

$$+D_3(gX_2+hX_3+jX_4)[[x_1[j(b^2+e^2)-h(bc+ef)]+y_1[c(e^2+h^2)-b(ef+hj)]$$

$$+z_1[f(b^2+h^2)-e(bc+hj)]\ ]]\Big\}$$

$$+D_4(gX_2+hX_3+jX_4)[[x_1[h(c^2+f^2)-j\quad \cdot ef)]+y_1[b(f^2+j^2)-c(ef+hj)]$$

$$+z_1[e(c^2+j^2)-f(bc+hj)]\ ]]$$

$$+2d_1d_3\Bigg\{(gX_2+hX_3+jX_4)^2(gx_1+ay_1+dz_1)(jx_1+cy_1+fz_1)$$

$$-D_3^2[b^2(df+gj)+e^2(ac+gj)+h^2(ac+df)-ab(ef+hj)$$

$$-de(bc+hj)-gh(bc+ef)]+D_2D_3[a^2(ef+hj)+d^2(bc+hj)$$

$$+g^2(bc+ef)-ab(df+gj)-de(ac+gj)-gh(ac+df)]$$

$$+D_2D_4[(af-cd)^2+(aj-cg)^2+(dj-fg)^2]$$

$$+D_3D_4[c^2(de+gh)+f^2(ab+gh)+j^2(ab+de)-ac(ef+hj)$$

$$-df(bc+hj)-gj(bc+ef)]$$

$$+D_2(gX_2+hX_3+jX_4)[[x_1[y(a^2+d^2)-g(ac+df)]+y_1[c(d^2+g^2)-a(df+gj)]$$

$$+z_1[f(a^2+g^2)-d(ac+gj)]\ ]]$$

$$-D_3(gX_2+hX_3+jX_4)[[x_1[g(bc+ef)+j(ab+de)-2h(ac+df)]$$

$$+y_1[a(ef+hj)+c(de+gh)-2b(df+gj)]+z_1[d(bc+hj)+f(ab+gh)-2e(ac+gj)]\ ]]$$

$$+D_4(gX_2+hX_3+jX_4)[[x_1[g(c^2+f^2)-j(ac+df)]+y_1[a(f^2+j^2)-c(df+gj)$$

$$+z_1[d(c^2+j^2)-f(ac+gj)]\ ]]-(gX_2+hX_3+jX_4)^4(x_1^2+y_1^2+z_1^2)\Bigg\}\Bigg\}$$

As shown in Equations (10), (11) and (12)

$$y = H_1-H_2r \tag{10}$$

$$z = H_3-r_1H_4 \tag{11}$$

$$x = H_5-r_1H_6 \tag{12}$$

Now

$$y = H_1-H_2r$$

$$= \frac{aD_2+bD_3+cD_4}{gX_2+hX_3+jX_4} -r\left(\frac{ad_1+bd_2+cd_3}{gX_2+hX_3+jX_4}\right)$$

then rational part of y = Ra(y)

$$\frac{aD_2+bD_3+cD_4 - (ad_1'+bd_2+cd_3)[Ra(r)]}{gX_2+hX_3+jX_4}$$

-586-

Irrational part of x   Ir(x)

$$Ir(x) = -\frac{(ad_1+bd_2+cd_3)\,(\pm\sqrt{B^2-AC})}{(gX_2+hX_3+jX_4)\,(A)}$$

Similarly

$$z = H_3 - r_1 H_4$$

$$Ra(z) = \frac{dD_2+eD_3+fD_4-(dd_1+ed_2+fd_3)\,[Ra(r)]}{gX_2+hX_3+jX_4}$$

$$Ir(z) = -\frac{(dd_1+ed_2+fd_3)\,(\pm\sqrt{B^2-AC})}{(gX_2+hX_3+jX_4)\,A}$$

and $x = H_5 - r_1 H_6$

$$Ra(x) = \frac{(gD_2+hD_3+jD_4)+(gd_1+hd_2+jd_3)\,[Ra(r)]}{gX_2+hX_3+jX_4}$$

$$Ir(x) = \frac{(gd_1+hd_2+jd_3)\,(\pm\sqrt{B^2-AC})}{(gX_2+hX_3+jX_4)\,A}$$

APPENDIX VIII

CALCULATION OF DISTANCE AND RELATIVE VELOCITY
BETWEEN TWO AIRCRAFT

This appendix derives the equations for distance and relative velocity between two aircraft for conflict prediction. The following equations apply for calculations of distance:

$$(x-x_1)^2+(y-y_1)^2+(z-z_1)^2=r_1^2 \tag{1}$$

$$(x-x_2)^2+(y-y_2)^2+(z-z_2)^2=(r_1+d_1)^2 \tag{2}$$

$$(x-x_3)^2+(y-y_3)^2+(z-z_3)^2=(r_1+d_2)^2 \tag{3}$$

$$z=h \tag{4}$$

A flat earth, which is assumed in order to get (4), is a valid approximation for the coverage regions under consideration (about 80 miles distance between stations). Subtracting Equation (2) from (1) and (3) from (1) yields

$$x+y\,\frac{(y_2-y_1)}{x_2-x_1}+z\,\frac{(z_2-z_1)}{x_2-x_1}+r_1\,\frac{d_1}{x_2-x_1}=\frac{x_2^2+y_2^2+z_2^2-x_1^2-y_1^2-z_1^2-d_1^2}{2(x_2-x_1)}$$

$$x+y\,\frac{(y_3-y_1)}{x_3-x_1}+z\,\frac{(z_3-z_1)}{x_3-x_1}+r_1\,\frac{d_2}{x_3-x_1}=\frac{x_3^2+y_3^2+z_3^2-x_1^2-y_1^2-z_1^2-d_2^2}{2(x_3-x_1)}$$

Now let

$$X_i=x_i-x_1; \qquad Y_i=y_i-y_1; \qquad Z_i=z_i-z_1;$$

$$D_i=\frac{x_i^2+y_i^2+z_i^2-x_1^2-y_1^2-z_1^2-d_{i-1}^2}{2}$$

and we obtain

$$x+y\,\frac{Y_2}{X_2}+z\,\frac{Z_2}{X_2}+\frac{r_1d_1}{X_2}=\frac{D_2}{X_2} \tag{5}$$

-588-

$$x + y \frac{Y_3}{X_3} + z \frac{Z_3}{X_3} + \frac{r_1 d_2}{X_3} = \frac{D_3}{X_3} \tag{6}$$

Subtracting (6) from (5) and using (4) yields

$$y \left(\frac{Y_2}{X_2} - \frac{Y_3}{X_3} \right) + h \left(\frac{Z_2}{X_2} - \frac{Z_3}{X_3} \right) + r_1 \left(\frac{d_1}{X_2} - \frac{d_2}{X_3} \right) = \frac{D_2}{X_2} - \frac{D_3}{X_3}$$

or

$$y + h \frac{\left(\frac{Z_2}{X_2} - \frac{Z_3}{X_3} \right)}{\left(\frac{Y_2}{X_2} - \frac{Y_3}{X_3} \right)} + r_1 \frac{\left(\frac{d_1}{X_2} - \frac{d_2}{X_3} \right)}{\left(\frac{Y_2}{X_2} - \frac{Y_3}{X_3} \right)} = \frac{\left(\frac{D_2}{X_2} - \frac{D_3}{X_3} \right)}{\left(\frac{Y_2}{X_2} - \frac{Y_3}{X_3} \right)} \tag{7}$$

Let

$$A_i = \frac{Y_i}{X_i} \; ; \qquad B_i = \frac{Z_i}{X_i} \; ; \qquad C_i = \frac{d_{i-1}}{X_i} \; ; \qquad E_i = \frac{D_i}{X_i} \; .$$

Then, (7) becomes

$$y + h \frac{B_2 - B_3}{A_2 - A_3} + r_1 \frac{C_2 - C_3}{A_2 - A_3} = \frac{E_2 - E_3}{A_2 - A_3}$$

or

$$y = \frac{E_2 - E_3 - h(B_2 - B_3)}{A_2 - A_3} - r_1 \frac{C_2 - C_3}{A_2 - A_3} \tag{8}$$

Let

$$H_1 = \frac{E_2 - E_3 - h(B_2 - B_3)}{A_2 - A_3}$$

and

$$H_2 = \frac{C_2 - C_3}{A_2 - A_3}$$

The, (8) becomes

$$y = H_1 - r_1 H_2 \tag{9}$$

Substituting A_3, B_3, C_3, and D_3 into (6) with $z = h$ yields

$$x + y A_3 + h B_3 + r_1 C_3 = E_3 \tag{10}$$

-589-

Putting (9) into (10) yields

$$x + A_3(H_1 - r_1 H_2) + hb_3 + r_1 C_3 = E_3$$

or

$$x + A_3 H_1 + hB_3 + r_1(C_3 - A_3 H_2) = E_3$$

from which

$$x = E_3 - A_3 H_1 - hB_3 - r_1(C_3 - A_3 H_2)$$

Let

$$H_3 = E_3 - A_3 H_1 - hB_3$$

and

$$H_4 = C_3 - A_3 H_2$$

Then

$$x = H_3 \cdot r_1 H_4 \tag{11}$$

Now, putting (9) and (11) into (1) with $z = h$ gives

$$(H_3 - r_1 H_4 - x_1)^2 + (H_1 - r_1 H_2 - y_1)^2 + (h - z_1)^2 = r_1^2$$

or

$$[(H_3 - x_1) - r_1 H_4]^2 + [(H_1 - y_1) - r_1 H_2]^2 + (h - z_1)^2 = r_1^2$$

or

$$(H_3 - x_1)^2 + r_1^2 H_4^2 - 2r_1 H_4(H_3 - x_1) + (H_1 - y_1)^2 + r_1^2 H_2^2 - 2r_1 H_2(H_1 - y_1) + (h - z_1)^2 = r_1^2$$

Let

$$J_1 = H_3 - x_1; \qquad J_2 = H_1 - y_1; \qquad J_3 = h - z_1$$

Thus,

$$r_1^2[H_2^2+H_4^2-1] - 2r_1(H_4J_1+H_2J_2) + J_1^2+J_2^2+J_3^2 = 0$$

Let

$$A = H_2^2+H_4^2-1; \qquad B = H_4J_1+H_2J_2; \qquad C = J_1^2+J_2^2+J_3^2$$

Thus, the x and y coordinates of the aircraft are:

$$x = H_3-r_1H_4 \qquad (12)$$

$$y = H_1-r_1H_2 \qquad (13)$$

where

$$r_1 = \frac{+B\pm\sqrt{B^2-AC}}{A}^{*}$$

$$A = H_2^2+H_4^2-1; \qquad B = H_4J_1+H_2J_2; \qquad C = J_1^2+J_2^2+J_3^2$$

$$J_1 = H_3-x_1; \qquad J_2 = H_1-y_1; \qquad J_3 = h-z_1$$

$$H_3 = \frac{D_3}{X_3} - \frac{Y_3}{X_3}H_1 - h\frac{Z_3}{X_3}$$

$$H_4 = \frac{d_2}{X_3} - \frac{Y_3}{X_3}H_2$$

$$H_1 = \frac{\dfrac{D_2}{X_2} - \dfrac{D_3}{X_3} - h\left(\dfrac{Z_2}{X_2} - \dfrac{Z_3}{X_3}\right)}{\dfrac{Y_2}{X_2} - \dfrac{Y_3}{X_3}}$$

---

*In the actual computation, the past history of the aircraft trajectory will be employed to resolve the ambiguity in r_1.

-591-

$$H_2 = \frac{\dfrac{d_1}{X_2} - \dfrac{d_2}{X_3}}{\dfrac{Y_2}{X_2} - \dfrac{Y_3}{X_3}}$$

$$X_i = x_i - x_1; \qquad Y_i = y_i - y_1; \qquad Z_i = z_i - z_1$$

$$D_i = \frac{x_i^2 + y_i^2 + z_i^2 - x_1^2 - y_1^2 - z_1^2 - d_{i-1}^2}{2}$$

The next step in the analysis is to compute, using (12) and (13), the distance between two aircraft. It was shown in (12) and (13) that the Cartesian coordinates for an aircraft are $x = H_3 - r_1 H_4$ and $7 = H_1 - r_1 H_2$. To study two vehicles (a and b say) requires equations in (x_a, y_a, z_a) and (x_b, y_b, z_b) where z_a and z_b are constant. These equations are expressed as follows:

$$x_a = H_{3a} - r_{1a} H_{4a}; \qquad y_a = H_{1a} - r_{1a} H_{2a}; \qquad z_a = h_a \tag{14}$$

$$x_b = H_{3b} - r_{1b} H_{4b}; \qquad y_b = H_{1b} - r_{1b} H_{2b}; \qquad z_b = h_b \tag{15}$$

These expressions are functions of the coordinate points of each station, the time of arrival information at each station from each aircraft, and aircraft altitudes.

Now the distance d_{ab} between the two aircraft can be expressed in the following manner:

$$d_{ab}^2 = (x_a - x_b)^2 + (y_a - y_b)^2 + (h_a - h_b)^2$$

or

$$d_{ab}^2 = x_a^2 + x_b^2 + y_a^2 + y_b^2 - 2x_a x_b - 2y_a y_b + (h_a - h_b)^2$$

$$= H_{3a}^2 + r_{1a}^2 H_{4a}^2 - 2r_{1a} H_{3a} H_{4a} + H_{3b}^2 + r_{1b}^2 H_{4b}^2 - 2r_{1b} H_{3b} H_{4b}$$

$$+ H_{1a}^2 + r_{1a}^2 H_{2a}^2 - 2r_{1a} H_{1a} H_{2a} + H_{1b}^2 + r_{1b}^2 H_{2b}^2 - 2r_{1b} H_{1b} H_{2b}$$

$$-2(H_{3a}-r_{1a}H_{4a})(H_{3b}-r_{1b}H_{4b})\ 2(H_{1a}-r_{1a}H_{2a})(H_{1b}-r_{1b}H_{2b})+(h_a-h_b)^2$$

$$= H_{1a}^2+H_{1b}^2+H_{3a}^2+H_{3b}^2-2r_{1a}(H_{3a}H_{4a}+H_{1a}H_{2a})-2r_{1b}(H_{1b}H_{2b}+H_{3b}H_{4b})$$

$$+r_{1b}^2H_{4b}^2+r_{1a}^2H_{4a}^2+r_{1a}^2H_{2a}^2+r_{1b}^2H_{2b}^2-2H_{3a}H_{3b}+2r_{1b}H_{3a}H_{4b}$$

$$+2r_{1a}H_{4a}H_{3b}-2r_{1a}r_{1b}H_{4a}H_{4b}-2H_{1a}H_{1b}+2r_{1b}H_{1a}H_{2b}+2r_{1a}H_{1b}H_{2a}-2r_{1a}r_{1b}H_{2a}H_{2b}+(h_a-h_b)^2$$

$$= (H_{1a}-H_{1b})^2+(H_{3a}-H_{3b})^2+(r_{1a}^2H_{2a}^2+r_{1b}^2H_{2b}^2-2r_{1a}r_{1b}H_{2a}H_{2b})$$

$$+(r_{1a}^2H_{4a}^2+r_{1b}^2H_{4b}^2-2r_{1a}r_{1b}H_{4a}H_{4b})-2H_{3a}(r_{1a}H_{4a}-r_{1b}H_{4b})$$

$$-2H_{1a}(r_{1a}H_{2a}-r_{1b}H_{2b})+2H_{3b}(r_{1a}H_{4a}-r_{1b}H_{4b})+2H_{1b}(r_{1a}H_{2a}-r_{1b}H_{2b})+(h_a-h_b)^2$$

from which

$$d_{ab}^2 = (H_{1a}-H_{1b})^2+(H_{3a}-H_{3b})^2+(r_{1a}H_{2a}-r_{1b}H_{2b})^2$$

$$+(r_{1a}H_{4a}-r_{1b}H_{4b})^2-2(r_{1a}H_{4a}-r_{1b}H_{4b})(H_{3a}-H_{3b})$$

$$-2(r_{1a}H_{2a}-r_{1b}H_{2b})(H_{1a}-H_{1b})+(h_a-h_b)^2$$

$$= [(H_{1a}-H_{1b})-(r_{1a}H_{2a}-r_{1b}H_{2b})]^2+[(H_{3a}-H_{3b}-(r_{1a}H_{4a}-r_{1b}H_{4b})]^2+(h_a-h_b)^2$$

$$(H_{1a}-H_{1b}-r_{1a}H_{2a}+r_{1b}H_{2b})^2+(H_{3a}-H_{3b}-r_{1a}H_{4a}+r_{1b}H_{4b})^2+(h_a-h_b)^2$$

from which

$$d_{ab} = \sqrt{(H_{1a}-H_{1b}-r_{1a}H_{2a}+r_{1b}H_{2b})^2+(H_{3a}-H_{3b}-r_{1a}H_{4a}+r_{1b}H_{4b})^2+(h_a-h_b)^2} \qquad (16)$$

The expressions for the r and H terms can be obtained from the relationships following (12) and (13) and are ultimately related to station locations and range differences (and hence time of arrival differences). The results are:

$$r_{1a} = \frac{+B_a \pm \sqrt{B_a^2-A_a C_a}}{A_a}$$

where

$$A_a = H_{2a}^2+H_{4a}^2-1$$

$$B_a = H_{4a}J_{1a}+H_{2a}J_{2a}$$

$$C_a = J_{1a}^2+J_{2a}^2+J_{3a}^2$$

$$J_{1a} = H_{3a}-x_1$$

$$J_{2a} = H_{1a}-y_1$$

$$J_{3a} = h_a-z_1$$

$$r_{1b} = \frac{B_b \pm \sqrt{B_b^2-A_b C_b}}{A_b}$$

$$A_b = H_{2b}^2+H_{4b}^2-1$$

$$B_b = H_{4b}J_{1b}+H_{2b}J_{2b}$$

$$C_b = J_{1b}^2+J_{2b}^2+J_{3b}^2$$

$$J_{1b} = H_{3b}-x_1$$

-594-

$$J_{2b} = H_{1b} - y_1$$

$$J_{3b} = h_b - z_1$$

$$H_{1a} = \frac{D_{2a}X_3 - D_{3a}X_2 - h_a(Z_2X_3 - Z_3X_2)}{Y_2X_3 - Y_3X_2}$$

$$H_{1b} = \frac{D_{2b}X_3 - D_{3b}X_2 - h_b(Z_2X_3 - Z_3X_2)}{Y_2X_3 - Y_3X_2}$$

$$H_{2a} = \frac{d_{1a}X_3 - d_{2a}X_2}{Y_2X_3 - Y_3X_2}$$

$$H_{2b} = \frac{d_{1b}X_3 - d_{2b}X_2}{Y_2X_3 - Y_3X_2}$$

$$H_{3a} = \frac{1}{X_3}\left\{ D_{3a} - h_a Z_3 - \frac{Y_3[D_{2a}X_3 - D_{3a}X_2 - h_a(Z_2X_3 - Z_3X_2)]}{Y_2X_3 - Y_3X_2} \right\}$$

$$H_{3b} = \frac{1}{X_3}\left\{ D_{3b} - h_b Z_3 - \frac{Y_3[D_{2b}X_3 - D_{3b}X_2 - h_b(Z_2X_3 - Z_3X_2)]}{Y_2X_3 - Y_3X_2} \right\}$$

$$H_{4a} = \frac{Y_2 d_{2a} - Y_3 d_{1a}}{Y_2X_3 - Y_3X_2}$$

$$H_{4b} = \frac{Y_2 d_{2b} - Y_3 d_{1b}}{Y_2X_3 - Y_3X_2}$$

$$X_i = x_i - x_1; \qquad Y_i = y_i - y_1; \qquad Z_i = z_i - z_1$$

$$D_{ia} = \frac{x_i^2 + y_i^2 + z_i^2 - x_1^2 - y_1^2 - z_1^2 - d_{a(i-1)}^2}{2}$$

$$D_{ib} = \frac{x_i^2 + y_i^2 + z_i^2 - x_1^2 - y_1^2 - z_1^2 - d_{b(i-1)}^2}{2}$$

The relative velocity is now expressed, using the above information. The derivation begins with the observation that relative velocity is $\dot{d}_{ab}\vec{r}$ where the dot means derivative with respect to time and where $\vec{r}$ is a vector along a line connecting the aircraft and pointing in a direction of increasing separation. To compute $\dot{d}_{ab}$, Equation (16) is differentiated with respect to time. The result is

$$\dot{d}_{ab} = \frac{\begin{aligned}&(H_{1a}-H_{1b}-r_{1a}H_{2a}+r_{1b}H_{2b})(\dot{H}_{1a}-\dot{H}_{1b}-\dot{r}_{1a}H_{2a}-r_{1a}\dot{H}_{2a}+\dot{r}_{1b}H_{2b}+r_{1b}\dot{H}_{2b})\\ &+(H_{3a}-H_{3b}-r_{1a}H_{4a}+r_{1b}H_{4b})(\dot{H}_{3a}-\dot{H}_{3b}-\dot{r}_{1a}H_{4a}-r_{1a}\dot{H}_{4a}+\dot{r}_{1b}H_{4b}+r_{1b}\dot{H}_{4b})+(\dot{h}_a-\dot{h}_b)\end{aligned}}{\sqrt{(H_{1a}-H_{1b}-r_{1a}H_{2a}+r_{1b}H_{2b})^2+(H_{3a}-H_{3b}-r_{1a}H_{4a}+r_{1b}H_{4b})^2+(h_a-h_b)^2}} \quad (17)$$

where H_{1a}, H_{2a}, H_{3a}, H_{4a}, H_{1b}, H_{2b}, H_{3b}, H_{4b}, r_{1a}, r_{2b} are given above and the time derivatives are as follows:

$$\dot{H}_{1a} = \frac{-X_3 d_{1a}\dot{d}_{1a} + X_2 d_{2a}\dot{d}_{2a} - \dot{h}_a(Z_2 X_3 - Z_3 X_2)}{Y_2 X_3 - Y_3 X_2}$$

$$\dot{H}_{1b} = \frac{-X_3 d_{1b}\dot{d}_{1b} + X_2 d_{2b}\dot{d}_{2b} - \dot{h}_b(Z_2 X_3 - Z_3 X_2)}{Y_2 X_3 - Y_3 X_2}$$

$$\dot{H}_{2a} = \frac{\dot{d}_{1a}X_3 - \dot{d}_{2a}X_3}{Y_2 X_3 - Y_3 X_2}$$

$$\dot{H}_{2b} = \frac{\dot{d}_{1b}X_3 - \dot{d}_{2b}X_2}{Y_2 X_3 - Y_3 X_2}$$

$$\dot{H}_{3a} = \frac{1}{X_3}\left\{ -d_{2a}\dot{d}_{2a} - \dot{h}_a Z_3 - \frac{Y_3[-X_3 d_{1a}\dot{d}_{1a} + X_2 \dot{d}_{2a}\dot{d}_{2a} - \dot{h}_a(Z_2 X_3 - Z_3 X_2)]}{Y_2 X_3 - Y_3 X_2} \right\}$$

$$\dot{H}_{3b} = \frac{1}{X_3} \left\{ -d_{2b}\dot{d}_{2b} - \dot{h}_b \dot{Z}_3 - \frac{Y_3[-X_3 d_{1b}\dot{d}_{1b} + X_2 d_{2b}\dot{d}_{2b} - \dot{h}_b(Z_2 X_3 - Z_3 X_2)]}{Y_2 X_3 - Y_3 X_2} \right\}$$

$$\dot{H}_{4a} = \frac{Y_2 \dot{d}_{2a} - Y_3 \dot{d}_{1a}}{Y_2 X_3 - Y_3 X_2}$$

$$\dot{H}_{4b} = \frac{Y_2 \dot{d}_{2b} - Y_3 \dot{d}_{1b}}{Y_2 X_3 - Y_3 X_2}$$

The time derivatives of altitude and range difference can be obtained from averaging altitude and range difference data.

APPENDIX IX

DERIVATION OF POSITION LOCATION EQUATIONS FOR
ALL RANGE AND 621-B RANGE DIFFERENCE SYSTEMS

IX-1 DERIVATION OF POSITION LOCATION EQUATIONS

This Appendix carries out the derivations of both the all-range and 621-B range-difference system equations for position location. Both of the derivations involve the solution of a three-dimensional set equations to determine the position of the aircraft. Both systems require the knowledge of the position of the reference, be they ground based or satellite. In both cases the solution is ambiguous and the correct solution of two must be selected by some knowledge of current position. The derivations were carried out in a straightforward manner with emphasis on making the computer programming of the equations simple to implement. The two-range-difference-plus-altimeter (three satellite constellation) and two-range-plus-altimeter system solutions could be derived in the same manner as follows.

IX-2 COMPUTATION OF AIRCRAFT POSITION USING AN ALL RANGE SYSTEM

The position of an aircraft in a Cartesian coordinate system (x, y, z) may be determined by solution of the equations:

$$(x-x_1)^2+(y-y_1)^2+(z-z_1)^2 = r_1^2 \tag{1}$$

$$(x-x_2)^2+(y-y_2)^2+(z-z_2)^2 = r_2^2 \tag{2}$$

$$(x-x_3)^2+(Y-y_3)^2+(z-z_3)^2 = r_3^2 \tag{3}$$

Where the r_i are the measured ranges from the stations located at (x_i, y_i, z_i) $i = 1,$ 3 respectively. The solution proceeds as follows:

Subtracting (2) and (3) from (1) respectively yields:

$$(1)-(2) \quad x+y\left(\frac{y_2-y_1}{x_2-x_1}\right) + z\left(\frac{z_2-z_1}{x_2-x_1}\right) = \frac{x_2^2+y_2^2+z_2^2-x_1^2-y_1^2-z_1^2+r_1^2-r_2^2}{z(x_2-x_1)}$$

$$(1)-(3) \quad x+y\left(\frac{y_3-y_1}{x_3-x_1}\right) + z\left(\frac{z_3-z_1}{x_3-x_1}\right) = \frac{x_3^2+y_3^2+z_3^2-x_1^2-y_1^2-z_1^2+r_1^2-r_3^2}{2(x_2-x_1)}$$

-598-

Let $X_i = x_i - x_1$, $\quad Y_i = y_i - y_1$, $\quad Z_i = z_i - z_1$

$$S_i = \frac{x_i{}^2 + y_i{}^2 + z_i{}^2 - r_i{}^2 - x_1{}^2 - y_1{}^2 - z_1{}^2 + r_1{}^2}{2}$$

Rewriting (1) $-$ (2) and (1) $-$ (3) yields:

$$x + y\left(\frac{Y_2}{X_2}\right) + z\left(\frac{Z_2}{X_2}\right) = \frac{S_2}{X_2} \tag{4}$$

$$x + y\left(\frac{Y_3}{X_3}\right) + z\left(\frac{Z_3}{X_3}\right) = \frac{S_3}{X_3} \tag{5}$$

Subtracting (5) from (4) yields:

$$(4)-(5) \quad y = \left(\frac{\dfrac{S_2}{X_2} - \dfrac{S_3}{X_3}}{\dfrac{Y_2}{X_2} - \dfrac{Y_3}{X_3}}\right) - z\left(\frac{\dfrac{Z_2}{X_2} - \dfrac{Z_3}{X_3}}{\dfrac{Y_2}{X_2} - \dfrac{Y_3}{X_3}}\right)$$

Let $A_i = \dfrac{Y_i}{X_i}$, $\quad B_i = \dfrac{Z_i}{X_i}$, $\quad F_i = \dfrac{S_i}{X_i}$

Rewriting (4) $-$ (5) yields:

$$y = \left(\frac{F_2 - F_3}{A_2 - A_3}\right) - z\left(\frac{B_2 - B_3}{A_2 - A_3}\right)$$

Let $G_1 = \dfrac{F_2 - F_3}{A_2 - A_3}$, $\quad G_2 = \dfrac{B_2 - B_3}{A_2 - A_3}$

Rewriting yields:

$$y = G_1 - ZG_2 \tag{6}$$

Substituting (6) into (5) yields:

$$x + (G_1 - G_2 Z)\left(\frac{Y_3}{X_3}\right) + z\left(\frac{Z_3}{X_3}\right) = \frac{S_3}{X_3}$$

$$x = \frac{S_3 - G_1 Y_3}{X_3} - Z\left(\frac{Z_3 - G_2 Y_3}{X_3}\right)$$

Let $G_3 = \dfrac{S_3 - G_1 Y_3}{X_3}$, $\quad G_4 = \dfrac{Z_3 - G_2 Y_3}{X_3}$

Rewriting yields:

$$x = G_3 - zG_4 \tag{7}$$

Substituting (6) and (7) into (1) yields:

$$(G_3 - zG_4 - x_1)^2 + (G_1 - zG_2 - y_1)^2 + (z - z_1)^2 = r_1^2$$

$$z^2(G_4^2 + G_2^2 + 1) + 2z\left(G_4(x_1 - G_3) + G_2(y_1 - G_1) - z_1\right)$$

$$+ (x_1 - G_3)^2 + (y_1 - G_1)^2 + z_1^2 - r_1^2 = 0$$

Let $K_1 = x_1 - G_3$, $\quad K_2 = y_1 - G_1$

Rewriting yields:

$$z^2(G_4^2 + G_2^2 + 1) + 2z(G_4 K_1 + G_2 K_2 - z_1) + K_1^2 + K_2^2 + z_1^2 = 0$$

Let $L = G_4^2 + G_2^2 + 1$, $\quad M = G_4 K_1 + G_2 K_2 - z_1$, $\quad N = K_1^2 + K_2^2 + z_1^2$

Rewriting yields:

$$z^2 L + 2zM + N = 0$$

$$z = \frac{-M \pm \sqrt{M^2 - LN}}{L} \tag{8}$$

-600-

Equation (8) yields 2 solutions

$$Z_a = \frac{-M+\sqrt{M^2-LN}}{L} \qquad\qquad Z_b = \frac{-M-\sqrt{M^2-LN}}{L}$$

Substituting each solution into (7) yields

$$x_a = G_3-z_aG_4 \qquad\qquad x_b = G_3-z_bG_4$$

Similarly substituting into (6) yields:

$$y_a = G_1-z_aG_2 \qquad\qquad y_b = G_1-z_bG_2$$

We therefore have two possible locations for the aircraft (x_a, y_a, z_a) and $(x_b, -_b, z_b)$ this ambiguity can be easily resolved by having a rough idea of current position. The quantities are defined as:

$$L = G_4^2+ G_2^2+1$$

$$M = G_4K_1+G_2K_2-z_1$$

$$N = K_1^2+K_2^2+z_1^2$$

$$K_1 = x_1-G_3$$

$$K_2 = y_1-G_1$$

$$G_3 = F_3-G_1A_3$$

$$G_4 = B_3-G_2A_3$$

$$G_1 = \frac{F_2-F_3}{A_2-A_3}$$

$$G_2 = \frac{B_2 - B_3}{A_2 - A_3}$$

$$A_i = \frac{Y_i}{X_i} \qquad B_i = \frac{Z_i}{X_i} \qquad F_i = \frac{S_i}{X_i}$$

$$X_i = x_i - x_1 \qquad Y_i = y_i - y_1 \qquad S_i = \frac{x_i{}^2 + y_i{}^2 + z_i{}^2 - x_1{}^2 - y_1{}^2 - z_1{}^2 + r_1{}^2 - r_i{}^2}{2}$$

IX-3 COMPUTATION OF AIRCRAFT POSITION USING RANGE DIFFERENCE SYSTEM

The procedure followed in this case is to write the equations in the all range form only now having a set of four equations. Once r_1 is determined in the equations below they become simply the all range case.

The position of the aircraft in a Cartesian coordinate system (x, y, z) may be determined using the 4 satellite 621B system by solution of the equations:

$$(x-x_1)^2 + (y-y_1)^2 + (z-z_1)^2 = r_1{}^2 \tag{9}$$

$$(x-x_2)^2 + (y-y_2)^2 + (z-z_2)^2 = (r_1 + d_1)^2 \tag{10}$$

$$(x-x_3)^2 + (y-y_3)^2 + (z-z_3)^2 = (r_1 + d_2)^2 \tag{11}$$

$$(x-x_4)^2 + (y-y_4)^2 + (z-z_4)^2 = (r_1 + d_3)^2 \tag{12}$$

Where r_1 is the range to the master satellite (unknown) and d_1, d_2, d_3 are the measured range differences between master (x_1, y_1, z_1) and the other three satellites at coordinates (x_2, y_2, z_2), (x_3, y_3, z_3) and (x_4, y_4, z_4) respectively. Using equations (9) – (12), r_1 may be found by writing x as a function of y, z and r_1. Then writing y as a function of z and r_1 and finally z as a function of r_1. Substitution will allow x, y and z to be written as functions of r_1 and then equation (9) may be

substituted in to yield a quadratic in r_1. Back substitution will yield two possible locations for the aircraft. This ambiguity is removed by knowing the approximate aircraft position. The solution of the equation is as follows:

Subtracting (10), (11), and (12) from (9) yields

$$(9)-(10) \quad x + y\left(\frac{y_2-y_1}{x_2-x_1}\right) + z\left(\frac{z_2-z_1}{x_2-x_1}\right) + r_1\left(\frac{d_1}{x_2-x_1}\right) = \frac{x_2^2+y_2^2+z_2^2-x_1^2-y_1^2-z_1^2-d_1^2}{2(x_2-x_1)}$$

$$(9)-(11) \quad x + y\left(\frac{y_3-y_1}{x_3-x_1}\right) + z\left(\frac{z_3-z_1}{x_3-x_1}\right) + r_1\left(\frac{d_2}{x_3-x_1}\right) = \frac{x_3^2+y_3^2+z_3^2-x_1^2-y_1^2-z_1^2-d_2^2}{2(x_3-x_1)}$$

$$(9)-(12) \quad x + y\left(\frac{y_4-y_1}{x_4-x_1}\right) + z\left(\frac{z_4-z_1}{x_4-x_1}\right) + r_1\left(\frac{d_3}{x_4-x_1}\right) = \frac{x_4^2+y_4^2+z_4^2-x_1^2-y_1^2-z_1^2-d_3^2}{2(x_4-x_1)}$$

Let $X_i = x_i-x_1$, $Y_i = y_i-y_1$, $Z_i = z_i-z_1$

$$D_i = \frac{x_i^2+y_i^2+z_i^2-x_1^2-y_1^2-z_1^2-d_{i-1}^2}{2}$$

Rewriting (1) − (2), (1) − (3), and (1) − (4) yields

$$x + y\left(\frac{Y_2}{X_2}\right) + z\left(\frac{Z_2}{X_2}\right) + r_1\left(\frac{d_1}{X_2}\right) = \frac{D_2}{X_2} \tag{13}$$

$$x + y\left(\frac{Y_3}{X_3}\right) + z\left(\frac{Z_3}{X_3}\right) + r_1\left(\frac{d_2}{X_3}\right) = \frac{D_3}{X_3} \tag{14}$$

$$x + y\left(\frac{Y_4}{X_4}\right) + z\left(\frac{Z_4}{X_4}\right) + r_1\left(\frac{d_3}{X_4}\right) = \frac{D_4}{X_4} \tag{15}$$

Subtract (14) and (15) from (13) yields

(13)-(14) $\quad y\left(\dfrac{\left(\dfrac{Y_2}{X_2} - \dfrac{Y_3}{X_3}\right)}{\left(\dfrac{Z_2}{X_2} - \dfrac{Z_3}{X_3}\right)}\right) + z + r_1\left(\dfrac{\left(\dfrac{d_1}{X_2} - \dfrac{d_2}{X_3}\right)}{\left(\dfrac{Z_2}{X_2} - \dfrac{Z_3}{X_3}\right)}\right) = \left(\dfrac{\left(\dfrac{D_2}{X_2} - \dfrac{D_3}{X_3}\right)}{\left(\dfrac{Z_2}{X_2} - \dfrac{Z_3}{X_3}\right)}\right)$

(13)-(15) $\quad y\left(\dfrac{\left(\dfrac{Y_2}{X_2} - \dfrac{Y_4}{X_4}\right)}{\left(\dfrac{Z_2}{X_2} - \dfrac{Z_4}{X_4}\right)}\right) + z + r_1\left(\dfrac{\left(\dfrac{d_1}{X_2} - \dfrac{d_3}{X_4}\right)}{\left(\dfrac{Z_2}{X_2} - \dfrac{Z_4}{X_4}\right)}\right) = \left(\dfrac{\left(\dfrac{D_2}{X_2} - \dfrac{D_4}{X_4}\right)}{\left(\dfrac{Z_2}{X_2} - \dfrac{Z_4}{X_4}\right)}\right)$

Let $A_i = \dfrac{Y_i}{X_i}$, $\quad B_i = \dfrac{Z_i}{X_i}$, $\quad C_i = \dfrac{d_i - 1}{X_i}$, $\quad E_i = \dfrac{D_i}{X_i}$

Rewriting (13)-(14), and (12)-(15) yields:

$$y\left(\frac{A_2 - A_3}{B_2 - B_3}\right) + z + r_1\left(\frac{C_2 - C_3}{B_2 - B_3}\right) = \frac{E_2 - E_3}{B_2 - B_3} \tag{16}$$

$$y\left(\frac{A_2 - A_4}{B_2 - B_4}\right) + z + r_1\left(\frac{C_2 - C_4}{B_2 - B_4}\right) = \frac{E_2 - E_4}{B_2 - B_4} \tag{17}$$

Subtracting (9) from (8) yields:

(16)-(17) $\quad y = \left(\dfrac{\dfrac{E_2 - E_3}{B_2 - B_3} - \dfrac{E_2 - E_4}{B_2 - B_4}}{\dfrac{A_2 - A_3}{B_2 - B_3} - \dfrac{A_2 - A_4}{B_2 - B_4}}\right) - r_1\left(\dfrac{\dfrac{C_2 - C_3}{B_2 - B_3} - \dfrac{C_2 - C_4}{B_2 - B_4}}{\dfrac{A_2 - A_3}{B_2 - B_3} - \dfrac{A_2 - A_4}{B_2 - B_4}}\right)$

Let $H_1 = \left(\dfrac{\dfrac{E_2-E_3}{B_2-B_3} - \dfrac{E_2-E_4}{B_2-B_4}}{\dfrac{A_2-A_3}{B_2-B_3} - \dfrac{A_2-A_4}{B_2-B_4}} \right)$, $\qquad H_2 = \left(\dfrac{\dfrac{C_2-C_3}{B_2-B_3} - \dfrac{C_2-C_4}{B_2-B_4}}{\dfrac{A_2-A_3}{B_2-B_3} - \dfrac{A_2-A_4}{B_2-B_4}} \right)$

Rewriting (16)-(17) yields

$$y = H_1 - H_2 r_1 \tag{18}$$

Substituting (18) into (17)

$$\left(H_1 - H_2 r_1 \right) \left(\frac{A_2-A_4}{B_2-B_4} \right) + z + r_1 \left(\frac{C_2-C_4}{B_2-B_4} \right) = \frac{E_2-E_4}{B_2-B_4}$$

$$z = \frac{E_2-E_4}{B_2-B_4} - H_1 \left(\frac{A_2-A_4}{B_2-B_4} \right) - r_1 \left(\frac{C_2-C_4}{B_2-B_4} - H_2 \left(\frac{A_2-A_4}{B_2-B_4} \right) \right)$$

$$z = \frac{E_2-E_4-H_1 A_2+H_1 A_4}{B_2-B_4} - r_1 \left(\frac{C_2-C_4-H_2 A_2+H_2 A_4}{B_2-B_4} \right)$$

Let $H_3 = \dfrac{E_2-E_4-H_1 A_2+H_1 A_4}{B_2-B_4}$, $\qquad H_4 = \dfrac{C_2-C_4-H_2 A_2+H_2 A_4}{B_2-B_4}$

Then rewriting yields

$$z = H_3 - r_1 H_4 \tag{19}$$

Substituting (18) and (19) into (15)

$$x + \left(H_1 - H_2 r_1\right)\left(\frac{Y_4}{X_4}\right) + \left(H_3 - H_4 r_1\right)\left(\frac{Z_4}{X_4}\right) + r_1\,\frac{d_3}{X_4} = \frac{D_4}{X_4}$$

$$x = \frac{D_4}{X_4} - H_1\,\frac{Y_4}{X_4} - H_3\,\frac{Z_4}{X_4} + r_1\left(\frac{H_2 Y_4}{X_4} + \frac{H_4 Z_4}{X_4} - \frac{d_3}{X_4}\right)$$

$$x = \frac{D_4 - H_1 Y_4 - H_3 Z_4}{X_4} + r_1\left(\frac{H_2 Y_4 + H_4 Z_4 - d_3}{X_4}\right)$$

Let $H_5 = \dfrac{D_4 - H_1 Y_4 - H_3 Z_4}{X_4}$, $H_6 = \dfrac{H_2 Y_4 + H_4 Z_4 - d_3}{X_4}$

Rewriting yields

$$x = H_5 + r_1 H_6 \qquad\qquad (20)$$

Substituting (20), (19) and (18) into (1)

$$(H_5 + r_1 H_6 - x_1)^2 + (H_1 - H_2 r_1 - y_1)^2 + (H_3 - r_1 H_4 - z_1)^2 = r_1^2$$

$$(H_5 - x_1)^2 + 2(H_5 - x_1)H_6 r_1 + H_6^2 r_1^2 + (H_1 - y_1)^2 - 2(H_1 - y_1)H_2 r_1 + H_2^2 r_1^2$$

$$+ (H_3 - z_1)^2 - 2(H_3 - z_1)H_4 r_1 + H_4^2 r_1^2 = r_1^2$$

Let $J_1 = H_5 - x_1$ $J_2 = H_1 - y_1$ $J_3 = H_3 - z_1$

Rewriting yields

$$r_1^2\left[H_6^2 + H_2^2 + H_4^2 - 1\right] + 2r_1\left[J_1 H_6 - J_2 H_2 - J_3 H_4\right] + \left[J_1^2 + J_2^2 + J_3^2\right] = 0$$

-606-

Let $A = H_6{}^2 + H_2{}^2 + H_4{}^2 - 1$

$B = J_1 H_6 - J_2 H_2 - J_3 H_4$

$C = J_1{}^2 + J_2{}^2 + J_3{}^2$

Rewriting (1)

$$A r_1{}^2 + 2 r_1 B + C = 0$$

$$r_1 = \frac{-B \pm \sqrt{B^2 - AC}}{A} \tag{21}$$

The system of equation we have are:

(21) $\quad r_a = \dfrac{-B + \sqrt{B^2 - AC}}{A} \qquad\qquad r_b = \dfrac{-B - \sqrt{B^2 - AC}}{A}$

(20) $\quad x_a = H_5 + r_a H_6 \qquad\qquad\qquad x_b = H_5 + r_b H_6$

(19) $\quad z_a = H_3 - r_a H_4 \qquad\qquad\qquad z_b = H_3 - r_b H_4$

(18) $\quad y_a = H_1 - r_a H_2 \qquad\qquad\qquad y_b = H_1 - r_b H_2$

Hence the two possible positions of the aircraft may be calculated by using equations (20), (19) and (18) where the quantities are defined as:

$$A = H_6{}^2 + H_2{}^2 + H_4{}^2 - 1$$

$$B = J_1 H_6 - J_2 H_2 - J_3 H_4$$

$$C = J_1{}^2 + J_2{}^2 + J_3{}^2$$

$$J_1 = H_5 - x_1$$

$$J_2 = H_1 - y_1$$

$$J_3 = H_3 - z_1$$

$$H_5 = E_4 - H_1 A_4 - H_3 B_4$$

$$H_6 = H_2 A_4 + H_4 B_4 - C_4$$

$$H_3 = \frac{E_2 - E_4 - H_1(A_2 - A_4)}{B_2 - B_4}$$

$$H_4 = \frac{C_2 - C_4 - H_2(A_2 - A_4)}{B_2 - B_4}$$

$$H_1 = \frac{\dfrac{E_2 - E_3}{B_2 - B_3} - \dfrac{E_2 - E_4}{B_2 - B_4}}{\dfrac{A_2 - A_3}{B_2 - B_3} - \dfrac{A_2 - A_4}{B_2 - B_4}}$$

$$H_2 = \frac{\dfrac{C_2 - C_3}{B_2 - B_3} - \dfrac{C_2 - C_4}{B_2 - B_4}}{\dfrac{A_2 - A_3}{B_2 - B_3} - \dfrac{A_2 - A_4}{B_2 - B_4}}$$

$$A_i = \frac{Y_i}{X_i}, \quad B_i = \frac{Z_i}{X_i}, \quad C_i = \frac{d_{i-1}}{X_i}, \quad E_i = \frac{D_i}{X_i}$$

$$X_i = x_i - x_1, \quad Y_i = y_i - y_1, \quad Z_i = z_i - z_1 \quad D_i = \frac{x_i^2 + y_i^2 + z_i^2 - x_1^2 - y_1^2 - z_1^2 - d_{i-1}^2}{2}$$

APPENDIX X

POSITION LOCATION PROGRAMS AND THEIR COMPUTER REQUIREMENTS

X-1. POSITION LOCATION PROGRAM USING RANGE DIFFERENCE SYSTEM

The program assumes that the measured range differences d_1, d_2, and d_3 are located in memory locations RD1, RD2 and RD3 respectively when the program is entered.

The program may be entered at two different points:

a. Entry point number 1 is for entering when the reference satellite's position have been updated. The coordinates of the satellites are assumed to be in memory locations X_i, Y_i, Z_i for stations located at (X_i, Y_i, Z_i), i=1, 4 when the program is entered.

b. Entry point number 2 is used when no reference updating is required.

Entry point number 1: Satellite positions updated

ENPT1,	LOAD	Z1
	MUL	Z1
	NORM	
	STORE	Z12
	STORE	SUBE
	LOAD	X1
	MUL	X1
	NORM	
	ADD	SUBE
	STORE	SUBE
	LOAD	Y1
	MUL	Y1
	NORM	
	ADD	SUBE
	STORE	SUBE
	LOAD	X2
	MUL	X2

$/x_1^2 + y_1^2 + z_1^2$

-609-

```
NORM
STORE        D2
LOAD         Y2
MUL          Y2
NORM
ADD          D2
STORE        D2
LOAD         Z2
MUL          Z2
NORM
ADD          D2
SUB          SUBE
STORE        D2          $/x_2^2+y_2^2+z_2^2-x_1^2-y_1^2-z_1^2$
LOAD         X3
MUL          X3
NORM
STORE        D3
LOAD         Y3
MUL          Y3
NORM
ADD          D3
STORE        D3
LOAD         Z3
MUL          Z3
NORM
ADD          D3
SUB          SUBE
STORE        D3          $/x_3^2+y_3^2+z_3^2-x_1^2-y_1^2-z_1^2$
LOAD         X4
MUL          X4
NORM
STORE        D4
LOAD         Y4
```

```
MUL       Y4
NORM
ADD       D4
STORE     D4
LOAD      Z4
MUL       Z4
NORM
ADD       D4
SUB       SUBE
STORE     D4          $/x_4{}^2+y_4{}^2+z_4{}^2-x_1{}^2-y_1{}^2-z_1{}^2$
LOAD      X2
SUB       X1
STORE     X21
LOAD      X3
SUB       X1
STORE     X31
LOAD      X4
SUB       X1
STORE     X41
LOAD      Y2
SUB       Y1
NORM
DIV       X21
STORE     A2
LOAD      Y3
SUB       Y1
NORM
DIV       X31
STORE     A3
NEGATE
ADD       A2
STORE     A23
LOAD      Y4
SUB       Y1
```

```
NORM
DIV       X41
STORE     A4
NEGATE
ADD       A2
STORE     A24
LOAD      Z2
SUB       Z1
NORM
DIV       X21
STORE     B2
LOAD      Z3
SUB       Z1
NORM
DIV       X31
STORE     B3
NEGATE
ADD       B2
STORE     B23
LOAD      Z4
SUB       Z1
NORM
DIV       X41
STORE     B4
NEGATE
ADD       B2
STORE     B24
LOAD      A23
NORM
DIV       B23
STORE     BDEN
LOAD      A24
NORM
DIV       B24
```

```
        NEGATE
        ADD        BDEN
        STORE      BDEN
```

$$\big/\big((A_2-A_3)/(B_2-B_3)\big) - (A_2-A_4)/(B_2-B_4)$$

Entry point number 2: No satellite position updating has occurred

```
ENPT2,  LOAD       RD1
        MUL        RD1
        NORM
        ADD        H1
        NORM
        DIV        BDEN
        STORE      H1
        MUL        A4
        NORM
        NEGATE
        ADD        E4
        STORE      H5
        LOAD       RD1
        NORM
        DIV        X21
        STORE      C2
        LOAD       RD2
        NORM
        DIV        X31
        STORE      C3
        NEGATE
        ADD        C2
        NORM
        DIV        B23
        STORE      H2
        LOAD       RD3
        NORM
        DIV        X41
        STORE      C4
```

```
SUB        C2
NORM
DIV        B24
ADD        H2
NORM
DIV        BDEN
STORE      H2
MUL        A4
NORM
NEGATE
ADD        D2
SHIFT              /Divide by 2
NORM
DIV        X21
STORE      E2
LOAD       RD2
MUL        RD2
NORM
NEGATE
ADD        D3
SHIFT
NORM
DIV        X31
STORE      E3
NEGATE
ADD        E2
NORM
DIV        B23
STORE      H1
LOAD       RD3
MUL        RD3
NORM
NEGATE
ADD        D4
```

```
SHIFT
NORM
DIV         X41
STORE       E4
NEGATE
ADD         E2
STORE       E24
NORM
DIV         B24
NEGATE
SUB         C4
STORE       H6
LOAD        H1
MUL         A24
NEGATE
ADD         E24
NORM
DIV         B24
STORE       H3
MUL         B4
NORM
NEGATE
ADD         H5
STORE       H5
SUB         X1
STORE       J1
MUL         J1
NORM
STORE       C
LOAD        A24
MUL         H2
NORM
NEGATE
ADD         C24
```

```
NORM
DIV        B24
STORE      H4
MUL        H2
NORM
SUB        (1)
STORE      A
LOAD       H4
MUL        B4
NORM
ADD        H6
STORE      H6
MUL        H6
NORM
ADD        A
STORE      A
LOAD       H1
SUB        Y1
STORE      J2
MUL        J2
NORM
ADD        C
STORE      C
LOAD       H3
SUB        Z1
STORE      J3
MUL        J3
NORM
ADD        C
STORE      C
LOAD       J2
MUL        H2
NORM
STORE      B
```

```
        LOAD      J3
        MUL       H4
        NORM
        ADD       B
        STORE     B
        LOAD      J1
        MUL       H6
        NORM
        SUB       B
        STORE     B
        MUL       B
        NORM
        STORE     ROOT
        LOAD      H2
        MUL       H2
        NORM
        ADD       A
        STORE     A
        MUL       C
        NORM
        NEGATE
        ADD       ROOT
    *   SQRT
        STORE     ROOT
        SUB       B
        NORM
        DIV       A
        STORE     RA
        LOAD      ROOT
        ADD       B
        NEGATE
```

*   SQRT is the square root operator either wired in the machine as an instruction or is a subroutine.

```
NORM
DIV        A
STORE      RB
MUL        H2
NORM
NEGATE
ADD        H1
STORE      YB
LOAD       RB
MUL        H4
NORM
NEGATE
ADD        H3
STORE      ZB
LOAD       RB
MUL        H6
NORM
ADD        H5
STORE      XB
LOAD       RA
MUL        H2
NORM
NEGATE
ADD        H1
STORE      YA
LOAD       RA
MUL        H4
NORM
NEGATE
ADD        H3
STORE      ZA
LOAD       RA
MUL        H6
```

```
       NORM
       ADD          H5
       STORE        XA
  **  SELECT
       RETURN
```

** SELECT is a subroutine to pick which of the two solutions is valid (XA,YA,ZA)
    or (XB,YB,ZB) for the (x,y,z) position of the aircraft and places the
    correct answers in memory locations X, Y and Z.

X-2. POSITION LOCATION PROGRAM USING ALL RANGE SYSTEM

The program assumes that the measured ranges r_1, r_2 and r_3 are contained in memory locations R_1, R_2 and R_3 respectively when the program is entered.

The program may be entered at two different points:

a. Entry point number 1 is for entering when the reference stations for the all range computation have been changed since the last computation. These coordinates are assumed to be in memory locations X_i, Y_i, Z_i for stations located at (x_i, y_i, z_i) i=1, 3 when the program is entered.

b. Entry point number 2 is for entering when the reference stations for the all range computation have not changed since the last computation. The coordinates of the stations are assumed to be in X_i, Y_i, Z_i, for stations located at (x_i, y_i, z_i), i=1, 3.

Entry point number 1: Normal Entry When Station Positions Updated

ENTR1,	LOAD	Z1	
	MUL	Z1	
	NORM		
	STORE	Z12	
	STORE	SUBE	
	LOAD	X1	
	MUL	X1	
	NORM		
	ADD	SUBE	
	STORE	SUBE	
	LOAD	Y1	
	MUL	Y1	
	NORM		
	ADD	SUBE	
	STORE	SUBE	$/x_1{}^2 + y_1{}^2 + z_1{}^2$
	LOAD	X2	
	MUL	X2	

```
NORM
STORE      S2
LOAD       Y2
MUL        Y2
NORM
ADD        S2
STORE      S2
LOAD       Z2
MUL        Z2
NORM
ADD        S2
SUB        SUBE
STORE      S2          $/x_2^2+y_2^2+z_2^2-x_1^2-y_1^2-z_1^2$
LOAD       X3
MUL        X3
NORM
STORE      S3
LOAD       Y3
MUL        Y3
NORM
ADD        S3
STORE      S3
LOAD       Z3
MUL        Z3
NORM
ADD        S3
SUB        SUBE
STORE      S3          $/x_3^2+y_3^2+z_3^2-x_1^2-y_1^2-z_1^2$
LOAD       X2
SUB        X1
STORE      X21
LOAD       X3
SUB        X1
STORE      X31
LOAD       Y2
```

```
SUB      Y1
NORM
DIV      X21
STORE    A2
LOAD     Y3
SUB      Y1
NORM
DIV      X31
STORE    A3
NEGATE
ADD      A2
STORE    A23
LOAD     Z3
SUB      Z1
NORM
DIV      X31
STORE    B3
LOAD     Z2
SUB      Z1
NORM
DIV      X21
SUB      B3
STORE    B23
NORM
DIV      A23
STORE    G2
MUL      A3
NORM
NEGATE
ADD      B3
STORE    G4
```

Entry point number 2: Normal entry when no station updating needed

```
ENTR2,   LOAD      R1
         MUL       R1
         NORM
         STORE     R12
         LOAD      R3
         MUL       R3
         NORM
         NEGATE
         ADD       R12
         ADD       S3
         SHIFT
         NORM
         DIV       X31
         STORE     F3
         LOAD      R2
         MUL       R2
         NORM
         NEGATE
         ADD       R12
         ADD       S2
         SHIFT
         NORM
         DIV       X21
         SUB       F3
         NORM
         DIV       A23
         STORE     G1
         MUL       A3
         NORM
         NEGATE
         ADD       F3
```

```
STORE       G3
LOAD        X1
SUB         G3
STORE       K1
MUL         K1
NORM
STORE       N
LOAD        Y1
SUB         G1
STORE       K2
MUL         K2
NORM
ADD         Z12
ADD         N
STORE       N
LOAD        K1
MUL         G4
NORM
STORE       M
LOAD        G2
MUL         K2
NORM
ADD         M
SUB         Z1
STORE       M
MUL         M
NORM
STORE       ROOT
LOAD        G4
MUL         G4
NORM
ADD         (1)
STORE       L
LOAD        G2
```

```
        MUL         G2
        NORM
        ADD         L
        STORE       L
        MUL         N
        NORM
        NEGATE
        ADD         ROOT
   *  SQRT
        STORE       ROOT
        SUB         M
        NORM
        DIV         L
        STORE       ZA
        MUL         G4
        NORM
        NEGATE
        ADD         G3
        STORE       XA
        LOAD        ZA
        MUL         G2
        NORM
        NEGATE
        ADD         G1
        STORE       YA
        LOAD        M
        NEGATE
        SUB         ROOT
        NORM
```

* SQRT is either the square root function if implemented on the machine
being used or else a sub-routine to find the square root of the quantity
in ROOT

```
      DIV      L
      STORE    ZB
      MUL      G4
      NEGATE
**    SELECT
      RETURN
      ADD      G3
      STORE    XB
      LOAD     ZB
      MUL      G2
      NORM
      NEGATE
      ADD      G1
      STORE    YB
```

** SELECT is a subroutine to pick which of the two solutions is valid
    (XA,YA,ZA) or (XB,YB,ZB) for the (x,y,z) position of the aircraft and
    places tne correct answer in memory locations X, Y and Z

X-3. TIME REQUIREMENTS

The following time equations are derived from the programs for each system.

X-3.1 RANGE DIFFERENCE

a. No Reference Updating

Time = 67 (LOAD/STORE)+37(ADD/SUB)+29(MUL)

+16(DIV)+45(NORM)+19(NEGATE)+3(SHIFT)

+1(SQRT)+1(SELECT)

b. Reference Updating

Time = 118(LOAD/STORE)+52(ADD/SUB)+41(MUL)

+24(DIV)+65(NORM)+24(NEGATE)+3(SHIFT)

+1(SQRT)+1(SELECT)

X-3.2 ALL RANGE

a. No Reference Updating

Time = 32(LOAD/STORE)+21(ADD/SUB)+16(MUL)

+5(DIV)+21(NORM)+9(NEGATE)+2(SHIFT)

+1(SQRT)+1(SELECT)

b. Reference Updating

Time = 66(LOAD/STORE)+38(ADD/SUB)+26(MUL)

+10(DIV)+36(NORM)+11(NEGATE)+2(SHIFT)

+1(SQRT)+1(SELECT)

X-4. <u>MEMORY REQUIREMENTS</u>

X-4.1 RANGE DIFFERENCE

340 – Main Program

67 – Variable Storage

1 – Constant Storage

408   Memory Locations + SQRT + SELECT

X-4.2 ALL RANGE

189 – Main Program

42 – Variable Storage

1 – Constant Storage

232   Memory Locations + SQRT + SELECT

X-5. <u>SELECT SUBROUTINE</u>

The following is a possible method of selecting the proper coordinates of the two available. It simply picks those coordinates which minimize the distance traveled in the x-y plane since the last fix. That is:

$$\min \left\{ \sqrt{(XA-X)^2+(YA-Y)^2} \; , \;\; \sqrt{(XB-X)^2+(YB-Y)^2} \right\}$$

determines whether (XA, YA, ZA) or (XB, YB, ZB) are the correct coordinates. The subroutine actually takes the minimum of the squares of the quantities to avoid the square rooting.

X-5.1 SELECT SUBROUTINE PROGRAM

```
LOAD      XA
SUB       X
STORE     T1
MUL       T1
NORM
STORE     ADIS
LOAD      YA
```

```
            SUB     Y
            STORE   T1
            MUL     T1
            NORM
            ADD     ADIS
            STORE   ADIS        · /(XA-X)²+(YA-Y)²
            LOAD    XB
            SUB     X
            STORE   T1
            MUL     T1
            NORM
            STORE   BDIS
            LOAD    YB
            SUB     Y
            STORE   T1
            MUL     T1
            NORM
            ADD     BDIS        /(XB-X)²+(YB-Y)²
            SUB     ADIS
            SKIP    ≥0
            JUMP    OTHER
            LOAD    XA          /(XA-X)²+(YA-Y)²  is smaller
            STORE   X
            LOAD    YA
            STORE   Y
            LOAD    ZA
            STORE   Z
            RETURN
OTHER,      LOAD    XB          /(XB-X)²+(YB-Y)²  is smaller
            STORE   X
            LOAD    YB
            STORE   Y
            LOAD    ZB
            STORE   Z
            RETURN
```

X-5.2   SELECT TIME REQUIREMENTS

Time = 24 (LOAD/STORE)+7(ADD/SUB)+4(MUL)+4(NORM)+1(SKIP)+2(JUMP)

X-5.3   SELECT MEMORY REQUIREMENT

42 - Main Program

3 - Variable Storage

45   Memory Locations

X-6.   SQRT SUBROUTINE

Many possible techniques exist for finding the square root of a quantity.
Perhaps the most famous and simplest is the Newton-Raphson method:

$$x_{i+1} = x_i - \frac{f(x_i)}{f'(x_i)}$$

$$\text{where} \quad f(x_i) = x_i^2 - P$$

$$x_{i+1} = x_i - \frac{x_i^2 - P}{2x_i}$$

$$x_{i+1} = \frac{1}{2}\left(x_i + \frac{P}{x_i}\right)$$

This technique is an iterative technique and is terminated when
$|x_m^2 - P| < \epsilon$ where ϵ is the allowable error.

X-6.1 SQRT SUBROUTINE PROGRAM

Assumes value to be rooted is in the accumulator upon entry into subroutine.

```
        STORE      P
        SHIFT
LOOP,   STORE      XI        /Use 1/2 the value as initial guess
        LOAD       P
```

```
        NORM
        DIV       XI
        ADD       XI
        SHIFT
        STORE     XNEW
        MUL       XNEW
        NORM
        SUB       P
        SKIP      ≥0              /Absolute value
        NEGATE
        SUB       EPSILON
        SKIP      >0
        JUMP      DONE
        LOAD      XNEW
        JUMP      LOOP
DONE,   LOAD      XNEW
        RETURN
```

X-6.2 SQRT TIME REQUIREMENTS

Since the program is an iterative process the time will be given as the fixed time plus time per iteration. Normally seven iterations starting at $x_0 = p/2$ yields 10 significant digits

Time = 3(LOAD/STORE)+1(SHIFT)+2(JUMP)

+N[4(LOAD/STORE)+3(ADD/SUB)+1(MUL)

+1(DIV)+2(NORM)+2(SKIP)+1(NEGATE)+1(JUMP)]

Where N is the number of iterations

Hence for seven iterations we would have:

Time = 31 (LOAD/STORE)+21(ADD/SUB)+7(MUL)

+7(DIV)+14(NORM)+1(SHIFT)+7(NEGATE)

+14(SKIP)+9(JUMP)

X-6.3 SQRT MEMORY REQUIREMENTS

21 - Main Program

3 - Variable Storage

1 - Constant Storage

25   Memory Locations

SECTION VIII

OPERATIONAL ANALYSIS

8.1 INTRODUCTION

The objective of this analysis is to model an Integrated Communication, Navigation, and identification user environment in order to estimate the multiple access requirements which a CNI waveform would be expected to accommodate.

8.2 METHOD

One of the projected uses of a system utilizing an integrated CNI waveform is to improve upon present CNI methods in order to bring about more effective utilization of airspace and aeronautical ground facilities by all users of the Federal Airways System in the post-1975 period. Therefore, the problem of air traffic control on the Federal Airways will be addressed in this analysis. As will be shown in Section 8.3.2, the air traffic control environment is the "worst case" representative of the situations in which a CNI system could be implemented. Within the limited scope of bit capacity and dynamic range requirements (security, and low detectability requirements are not addressed here), development of a CNI waveform compatible with air traffic control (ATC) environment should yield a waveform amenable to any other projected environment for a CNI system. Therefore, a representative ATC environment will be modelled, in which the origins, destinations, frequencies of occurrence, durations, contents and link lengths of message transmissions required by and for ATC of various classes of aircraft are defined. When these data are combined with certain design data, e.g., placement of emitters in the environment, and choice of error-correcting codes, the multiple access requirements can be determined.

The modeled environment will utilize a scenario incorporating peak air traffic loading in a high-traffic-density terminal area and the adjacent enroute airspace. Each airport within this terminal area will be treated as a "source" and a "sink" for aircraft. A method will be developed to define the maximum possible inflow and outflow rates for airports in this terminal area as functions of aircraft class. The proportional mix of aircraft classes in the airspace will be projected from FAA estimates of future air traffic. The data exchange requirements for each class of aircraft will be developed as a function of flight phase using FAA voice transmission data.

-633-

Modifications involving an effective mix of voice and data link exchanges will also be discussed. Message requirements will be defined for the following flight phases:

1. Pre-takeoff including taxi.
2. Takeoff departure and transition to enroute.
3. Enroute between high traffic density terminal areas on the Federal Airways System.
4. Arrival, approach and landing within high traffic density terminal areas from enroute.
5. Post-landing including taxi.

When the data requirements per flight and number of flights per airport are defined, only the number and geographical disposition of airports in the terminal need be defined to obtain the total CNI message traffic volume in the scenario airspace. Multiple access requirements and near/far power level approximations can be made only after intelligent placement of transmitter/receiver sites within the scenario area.

The number of airports and their disposition in the scenario area will be an average of six high traffic density terminal areas in the United States: Boston, New York, Chicago, Los Angeles, San Francisco, and Seattle. The resulting representative terminal area will contain airports of the following types: military, commercial, municipal, and private. Their spacing and disposition is the result of topographically averaging the six sample areas in a composite area (See Appendix I).[*]

8.3 RATIONALE

The analysis is limited to the Air Traffic Control (ATC) environment within the continental United States for the following reasons.

8.3.1 EQUIPMENT COMPATIBILITY

One of the principal desired results of implementing a CNI system is a significant reduction in the number of "black boxes" required in aircraft. However, all classes of aircraft (military, commercial and general aviation) travel on the Federal Airways and are subject to the legal requirement for carrying airborne electronic equipment compatible with the ground electronic equipment of the ATC system. Therefore,

---

[*] Area Charts - U.S., U.S. Dept. of Commerce, Environmental Science Services Administration, Coast and Geodetic Survey, Washington, D.C., 1 May 1969.

implementation of CNI in another environment such as a specialized military situation would in no way reduce the airborne black box count but would increase it because of the requirement to carry separate equipments for the ATC and military environments. Clearly CNI must be implemented in the ATC environment if a significant reduction in airborne black boxes is to result.

8.3.2 WORST CASE DESIGN

Preliminary examination of specialized military environments and the civil ATC environment shows the latter to contain the most stringent CNI requirements. In comparison with the CNI requirements of military missions such as air superiority, close air support, interdiction, reconnaissance, strategic bor' ing, antisubmarine warfare, amphibious assult, search and rescue, etc., the ATC environment is characterized by:

1. Higher traffic density.
2. Greater dependence on external aid to navigation.
3. Greater proportion of inexperienced pilots requiring monitoring and vectoring or other assistance.
4. Less acceptable risk.
5. Greater variety of aircraft characteristics.
6. Less coordination between airspace/facility users and airspace/ facility controllers.
7. Virtual continuous loading (24 hours per day) on system.

Because of these factors, a CNI system design that proves effective in the ATC environment should operate at least as well in specialized military situations. It is recognized that a CNI system operated in a military environment will require certain features, such as security, not required for ATC. However, these features are expected to have little impact on the primary subject addressed in this analysis, i.e., multiple access and data loading on the system.

8.3.3 COMMONALITY

A CNI system design based on the requirements developed for a specific military situation stands the chance of proving inadequate in other military situations or the ATC environment. Development of a CNI system capable of meeting the needs of ATC will provide a common system with the access capacity for functioning in other environments.

8.4 BACKGROUND MATERIAL

Considerable study effort has already been expended toward developing future ATC system requirements.[*] This material provides a starting point for developing CNI requirements. However, complete dependence on the data developed in this material would lead to erroneous requirements for the following reasons.

8.4.1 DATA LINKS

The present ATC environment is essentially devoid of data links. Air/Ground/ Air Communications are conducted entirely by voice except for a small percentage of Morse code communications for transocean flights. It is not reasonable to expect complete dependence on voice and code to continue in the time frame of CNI impelmentation since the majority of present A/G/A communication messages are of a stylized nature, amenable to canning, and more efficiently transmitted by data link. Since the message content of a typical voice transmission of several seconds length can be data linked in a few milliseconds, the inclusion of data link formats in a CNI system has considerable impact on its access capacity. Therefore, extrapolation of future CNI requirements based entirely on present voice channel loading would be an erroneous procedure.

8.4.2 AIR TRAFFIC CONTROL RADAR BEACON SYSTEM

Present ATC planning and past ATC communication studies treat the Air Traffic Control Radar Beacon System (ATCRBS) as a separate (non-integrated) system from communication systems. However, a CNI system will, by definition, include the functions presently accomplished by the ATCRBS while obviating the need for certain communications traffic associated with its operation. Again, CNI channel loading that is partly based on loading requirements imposed by a non-integrated ATCRBS would lead to erroneous conclusions.

8.4.3 AUTOMATION

Certain air traffic controller functions now implemented by means of voice communication channels will be automated in the time frame of CNI causing an uncertain impact on access loading. This impact can be accessed by proper analysis

---

[*] 'Future Air-Ground-Air Communication Subsystem Investigation," FAA Report No. RD-66-16. Communication Systems, Inc., Paramus, New Jersey. July 1966.

but would be unaccounted for in an analysis predicated on extrapolation from present methods. An example of access loading changes brought about by automation can be seen for the case of Track Handover. As an aircraft proceeds from the jurisdiction of one controller to that of another, present methods require a minimum of three voice message transmissions. These are a ground initiated call-up from the present controller directing the pilot to switch to the succeeding controller's frequency, a pilot acknowledgement that may be made but is not required, a pilot initiated check-in with the succeeding controller on the new frequency, and an acknowledgement by the succeeding controller. None of these transmissions need be made in an automated system in which the aircraft is continuously tracked and its position coordinates and discrete identity are passed on from controller to controller by means of its multiple access address. One implementation would be the use of a common calling channel on which aircraft in a given sector are roll-called. The roll-call would include data link coded instructions that cause the aircraft's transponding equipment to automatically switch to the new channel and reply with its position coordinates upon receiving its discrete address code. More details of the impact of automated functions in an CNI system will be presented in succeeding paragraphs.

8.5 SCENARIO RULES

The following paragraphs explain the procedural rules to be applied to the ATC scenario in order to obtain the multiple access requirements in a systematic way. Implicit in these rules are certain design requirements of a CNI system. All such requirements are predicated on goals set for the air traffic control system by the FAA and the Radio Technical Commission for Aeronautics (RTCA).[*]

8.5.1 ROUTE STRUCTURE

The present system of high altitude Jet Routes and low altitude "Victor" Airways will be retained. These routes and airways will retain the present basic characteristic of radiating, spoke-like, from the terminal area. However, they need not necessarily converge over navigational emitter sites. Parallel routes and airways will be permitted.

[*] Universal Air-Ground Digital Communication System Standards, Radio Technical Commission for Aeronautics, Washington, D.C., 7 March 1968.

8.5.2 CONTINUOUS FLIGHT FOLLOWING

All CNI equipped aircraft will be tracked by ground facilities within all portions of the terminal area and on all jet routes. Information continuously available at the ground tracking facilities will be:

a. Aircraft flight number, registration number or side number (19 bits).

b. Aircraft type designation (12 bits).

c. Aircraft address code (12 bits).

d. Aircraft X/Y/h coordinates (22/22/11 bits).

e. Georeference of $X_o/Y_o/h_o$ (22/22/11 bits).

f. Aircraft present velocity vector (18 bits).

g. Aircraft present maneuver; e.g., cruising, holding, descending, etc. (4 vits).

8.5.3 CONTINUOUS BROADCASTS

All portions of the terminal area and adjacent enroute airspace will have available a continuous transcribed voice broadcast of present and forecast weather and winds aloft, applicable to the terminal area, adjacent terminal areas, and the intervening enroute airspace. All airports served by a control tower will have a continuous voice broadcast containing the information presently carried on Automatic Terminal Information Service (ATIS) channels.

8.5.4 INSTRUMENT APPROACH AND LANDING

Each airport will be served by a system enabling area navigation from the airport surface to at least a 20 nmi radius of the airport. In addition, each airport that is served by a control tower will be served by a system enabling accurate azimuth guidance along the landing runway centerline and at least 1 nmi of its upwind and downwind extensions, and accurate vertical guidance along pilot selectable glide-slopes having vertical angles between 2 degrees and 30 degrees. The glideslope signal will be available in at least an eighty-degree azimuth sector centered on the downwind runway centerline extension.

8.5.5 RUNWAY OCCUPANCY

The time separation between successive aircraft using the same runway is the key parameter in establishing the traffic density in the terminal area. That is due to the assumption that traffic delays presently caused by inadequacies of present CNI methods will be eliminated by an integrated waveform system leaving only the factor of safety, as regards the spacing of landing and departing aircraft, as a criterion for assigning a numerical value for flow rate to a given runway. It is assumed that system will retain the present practice of not releasing an aircraft from its departure point until there is a time slot available for it to land around its ETA at its point of intended landing. Thus with a smoothly functioning traffic control system, there should be no more aircraft in the air than there are runway time slots available for an orderly flow of traffic. According to the FAA Airman's Information Manual, the present ATC methods permit aircraft to be released and accepted at two-minute intervals if a functioning ILS is available. The same reference indicates that ten or more minutes separation is required between aircraft making instrument approaches without an ILS. It has been indicated that twenty to thirty seconds should be adequate separation with a functioning advanced instrument landing aid (such as might be incorporated in CNI). * However, Special Committee 117 which wrote this opinion based it on braking deceleration characteristics but not airborne deceleration on glide path. Also, the committee did not take into account the hazard introduced by the wingtip vortices of heavy aircraft. Longer delay is advisable before landing behind such aircraft to allow the vortices to dissipate to a less hazardous strength. Unfortunately, the stable air conditions that prevail when an instrument landing aid obtains its greatest use are also the conditions that inhibit the dissipation of wingtip vortices. No hard data is available on dissipation times, some people claiming a few seconds, while others are claiming up to one-half hour.

* 24-69/SC-117-48, Radio Technical Commission for Aeronautics, Washington, D.C., 31 January 1969.

Actual measurement of separation between aircraft and VFR conditions at three high density terminals in the Los Angeles area showed that controllers tended to space the aircraft so that approaching aircraft passed through 200 feet a.g.l. on glide path at the moment the preceding aircraft vacated the runway and such that departing aircraft were released at the moment the preceding aircraft reached 200 feet a.g.l. on takeoff. Elapsed times between aircraft passing the runway midpoint varied from fifteen to sixty seconds, with an average of forty-five seconds.[**]

Consideration of the above suggests that the RTCA figures are accurate for actual "wheels on the runway" occupancy time but that the actual figures used should include the air time required from decision height to landing and from takeoff to an altitude of 200 feet a.g.l.

8.5.6 APPROACH SPACING

The time separation between aircraft using the same runway will be such that approaching aircraft reach decision height or minimum descent altitude at the moment the landing aircraft that immediately preceded them clears the runway (has turned onto a taxiway), or at the moment the departing aircraft that immediately preceded them reaches 200 feet a.g.l. The time separations used were obtained by actual measurement (see Table 8-1).

8.5.7 TAKEOFF SPACING

The time separation between aircraft using the same runway shall be such that aircraft taking off will start rolling at the moment the landing aircraft that immediately preceded them clears the runway or at the moment the departing aircraft that immediately preceded them reaches 200 feet a.g.l. The time separations used were obtained by actual measurement (see Table 8-1).

8.5.8 ARRIVAL SPACING

The approach and departure spacing specified in paragraphs 8.5.6 and 8.5.7 above represents the maximum or saturation level for any given runway. It will be assumed that during the sample time period used in this analysis, those runways located on airports serving the Air Carrier user class (the largest percentage of traffic) will be

[**] observed May 1969

operated at this maximum possible level. Aircraft entering the terminal area from the adjacent enroute airspace will arrive at the same rate as the absorption rate of the airport complex. This entry rate will be maintained by issuance of computer generated speed commands for speed control of arriving aircraft penetrating the terminal area from the adjacent enroute airspace. Lateral spacing between arriving aircraft in the terminal area will be set by the number of airways into the area. This number will be set at a value representative of the Jet Routes and Low Altitude Airways entering the six sample terminal areas.

8.5.9 DEPARTURE SPACING

Aircraft transitioning from field patterns to airways in the enroute airspace will utilize the same airways set in paragraph 8.5.8 but will occupy altitude levels different from the levels of arrival air traffic. The parting aircraft will be shunted to these airways so as to be uniformly distributed among them.

8.5.10 HOLDING

If the rules detailed above are adhered to, there should be no requirement for holding since the traffic arrival rate never exceeds the handling capacity of the airport complex. Therefore, the communication traffic associated with holding in the scenario volume will be omitted.

8.5.11 FLIGHT RULES AND PLANS

All present air traffic operates in one of three ways; i.e., with a VFR (Visual Flight Rules) flight plan filed with ATC, with an IFR (Instrument Flight Rules) flight plan filed with ATC, or with no filed flight plan (necessarily under VFR conditions since flight under IFR conditions without a flight plan filed is illegal). It will be assumed that IFR conditions prevail in the scenario volume. This assumption eliminates flights such as local landing practice, sightseeing, and sport flying. Such flights place essentially no load on navigational and identification facilities and minimal loading on communication facilities. The assumption of IFR traffic places maximum loading on all facilities.

8.6 DETAILED SCENARIO DATA

8.6.1 ANTICIPATED PROPORTIONAL MIX OF AIRCRAFT TYPES

Aircraft types have been generalized and categorized by user class as is traditionally in studies on air traffic. The user classes are: Military, Commercial, and General Aviation. Representative aircraft types are shown in Figure 8-1. The future air traffic distribution data that follow were derived from FAA Report No. RD-66-16-IV, and data obtained from the FAA Air Route Traffic Control Center at Palmdale, California.[*]

Type Traffic	Percent of Total In Terminal Area	Percent of Type In Enroute Transit
Military	13.8%	25%
Air Carrier	51.7%	25%
General Aviation	34.5%	25%

8.6.2 NUMBER OF AIRPORTS AND AIRWAYS

The average number for each type of airport and through airway in the scenario area was derived from examination of instrument area navigation charts of the six sample areas. Only IFR rate fields are counted.

Airports	No.	Airways	No.
Military	9	High Altitude	4
Commercial	5	Low Altitude	5
Municipal	9		

---

[*] Peak Day Report, Los Angeles Air Route Traffic Control Center. FAA, 1968.
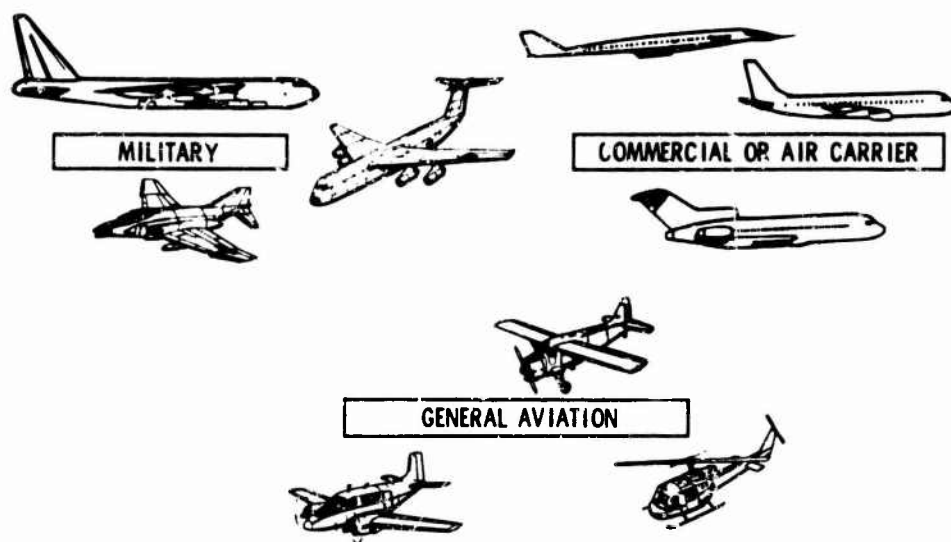
- THESE USER CATEGORIES HAVE DIFFERING VOICE TRANSMISSION REQUIREMENTS. HOWEVER, ALL MUST OPERATE COMPATIBLY IN AN AIR TRAFFIC CONTROL ENVIRONMENT
- VOICE MESSAGE SEQUENCES HAVE BEEN MODELED FOR EACH CATEGORY BASED UPON FAA SUPPLIED DATA, PREVIOUS ATC STUDY REPORTS AND FIELD MONITORING OF ATC VOICE CHANNELS.

769-1746
UNCLASSIFIED

Figure 8-1. Airborne Communicator Categories.

8.6.3 FLIGHT PROFILES

The message demand and message spacing of each aircraft is affected by its altitude/speed profile during its departure, enroute, and arrival phases. These profiles are determined by the aircraft characteristics. The aircraft characteristics shown in Table 8-1 will be assumed for the three principal categories of aircraft users. These characteristics are not based on the maximum capabilities of the aircraft but rather on their average manner of operation while on The Federal Airways System. Military and Commercial aircraft categories will be assumed to consist entirely of turbojet and turboprop aircraft, while The General Aviation category will be assumed to consist of a mix single and twin engine reciprocating engine types with no greater than 700 horsepower. Note that in accordance with Federal Aviation Regulations, all aircraft must not exceed 250 kts when below 10,000 feet altitude, and when in traffic areas, jet aircraft must not exceed 200 kts while propeller aircraft must not exceed 156 kts.[*]

---

[*] Part 91, General Operating and Flight Rules, Federal Aviation Regulations. Federal Aviation Agency, Washington, D.C., 1969.

-643-

Table 8-1. Flight Profiles

	Military	Air Carrier	General Aviation
Land and Takeoff Spacing			
Takeoff minimum	20 sec	20 sec	15 sec
Takeoff average	45 sec	45 sec	45 sec
Landing minimum	20 sec	20 sec	15 sec
Landing average	--	45 sec	--
Vertical Speed			
Climbout	+2000 ft/min	+1000 ft/min	+750 ft/min
Departure Transition	+3000 ft/min	+2000 ft/min	+500 ft/min
Initial Approach	-5000 ft/min	-1000 ft/min	-500 ft/min
Final Approach	-500 ft /min	-500 ft/min	-500 ft/min
Ground Speed			
Climbout	200 kts	200 kts	100 kts
Departure Transition	250 kts	250 kts	110 kts
Initial Approach	250 kts	250 kts	160 kts
Final Approach	150 kts	150 kts	100 kts
Enroute	500 kts	500 kts	160 kts
Type of Departure	MID	SID	Radar Vector
Type of Initial Approach	Penetration	Straight In	Radar Vector
Percent with G to A Data Link	100%	100%	0%
Percent with Hard Copy DL Readout	50%	100%	0%
Average Enroute Altitude	30,000 ft	30,000 ft	8,000 ft
Average distance from airport of first enroute compulsory reporting point	150 nmi	150 nmi	75 nmi

8.6.4 AVERAGE TIME IN TERMINAL AREA

Time in the terminal area for departing and arriving aircraft is defined as airborne time between the first enroute compulsory reporting point on departure, or last enroute compulsory reporting point on arrival, and contact with the airport runway surface. For aircraft in transit, it is the time from the entry reporting point to the departure reporting point.

A summary of the above terminal area transit times is shown in Table 8-2. These times will be used to calculate the population density of aircraft in the terminal area. Details of the elapsed-time calculations are contained in the following paragraphs.

Table 8-2. Terminal Area Flight Times

Flight Phase	Military	Air Carrier	General Aviation
Departure	T_{MD} = 27 min.	T_{CD} = 30 min.	T_{GD} = 66.5 min
Arrival	T_{MA} = 24.4 min.	T_{CA} = 25.5 min.	T_{GA} = 66 min.
Enroute Transit	T_{ME} = 18 min.	T_{CE} = 18 min.	T_{GE} = 49.3 min.

8.6.4.1 Military*

Departure - After takeoff, climb at 2000 ft/min and 200 kts for 20 nmi. Distance from airport assumed zero at this point since turns are made in climb. Elapsed time is six minutes, altitude reached is 12,000 feet. Then climb to 30,000 feet at 250 kts and 3000 ft/min. Elapsed time is six minutes and distance covered is 25 nmi. Cruise at 500 kts the remaining 125 nmi to the first compulsory enroute reporting point. Elapsed time is fifteen minutes. Total military departure time (T_{MD}) is 6 + 6 + 15 = 27 min.

Arrival - After arrival at last compulsory enroute reporting point, proceed inbound 150 nmi to the approach fix at enroute cruising speed. Elapsed time is eighteen minutes. Commence penetration from 30,000 feet to 1,500 foot glide path interception at 5000 ft/min rate of descent holding 250 kts to 10,000 feet and 200 kts below 10,000 feet. Elapsed time is 144 seconds. Total military arrival time (T_{MA}) is (18 + 6) min + (144) sec = 24 minutes, 24 seconds.

8.6.4.2 Air Carriers **

For commercial air carrier aircraft, the time adds as follows:

Departure - After takeoff, climb at 1000 ft/min and 200 kts for 20 nmi maneuvering as described for military aircraft. Elapsed time is six minutes, altitude reached is 6000 feet. Then climb to 30,000 feet at 250 kts and 2000 ft/min. Elapsed time is twelve minutes and distance covered is 50 nmi. Cruise at 500 kts the remaining 100 nmi to the first compulsory enroute reporting point. Elapsed time is twelve minutes. Total air carrier departure time (T_{CD}) is 6 + 12 + 12 = 30 minutes.

Arrival - After arrival at the last enroute reporting point, proceed inbound at cruising speed for 90 nmi while descending to 15,000 feet at 2,000 ft/min. Elapsed time is 7.5 minutes. Decelerate to 250 kts and continue descent at 1,000 ft/min to

---

*Instrument Flying. Air Force Manual No. 51-37, Department of the Air Force, Washington, 20 January 1966.

**U.S. Government Standard Instrument Arrivals and Departures for Civil Aerodromes, Coast and Geodetic Survey, Environmental Science Services Administration, Rockville, Md., 1969.

glideslope interception at 4000 feet. Elapsed time is eleven minutes and distance covered is 45 nmi. Decelerate to 150 kts and proceed inbound on glideslope at 500 ft/min rate of descent. Elapsed time is eight minutes and distance covered is the remaining 25 nmi to the airport. Total air carrier arrival time (T_{CA}) is 7.5 + 11 + 8 = 26 min 30 sec.

8.6.4.3 General Aviation*

For general aviation aircraft, the time adds as follows:

Departure - After takeoff, climb at 750 ft/min and 100 kts while being radar vectored to 4000 feet. Elapsed time is 5.5 minutes and distance covered is 9 nmi. However, assume zero distance from airport due to turns. Continue climb at 500 ft/min and 110 kts to 8000 feet. Elapsed time is sixteen minutes and distance covered is 29 nmi. Proceed 46 nmi to first compulsory reporting point at 160 kts. Elapsed time is seventeen minutes. Proceed 75 nmi to terminal area boundry at 160 kts. Elapsed time is twenty-eight minutes. Total general aviation departure time (T_{GD}) is 5.5 + 16 + 17 + 28 = 68 min 30 sec.

Arrival - After arrival at the terminal area boundry, proceed 75 nmi to last enroute reporting point at 160 kts. Elapsed time is twenty-eight minutes. Commence series of altitude transitions and radar vectored turns to a position on the glideslope 10 nmi from the runway threshold. 160 kts is maintained for 75 nmi distance. Elapsed time is twenty-eight minutes. Proceed inbound on glideslope at 100 kts to runway. Elapsed time is ten minutes. Total time for general aviation arrival (T_{GA}) is 28 + 28 + 10 = 66 minutes.

8.6.5 ENROUTE TRANSIT TIMES

8.6.5.1 Military and Air Carriers

Examination of enroute navigation charts for the sample terminal areas shows that the high altitude airways, or Jet Routes, converge essentially at the center of the terminal areas. Thus, the military and air carrier traffic transmitting on these airways travel a distance of essentially one diameter (150 nmi) of the terminal area. Therefore, military and air carrier enroute elapsed times $(T_{ME}$ and $T_{AE})$ at the ground speeds shown in Table 8-1 are 18 minutes.

---

* Instrument Flying Handbook, Federal Aviation Agency Flight Standards Service, Washington, D.C., 1966.

8.6.5.2 General Aviation

The average low altitude airways structure can be represented by five parallel airways with equidistant spacing (25 nmi) across the terminal area distance. If the general aviation aircraft transmitting the terminal area are assumed to be uniformly distributed on these airways, then the average distance each travels is 131.28 nmi for an elapsed time (T_{GE}) of 49.3 minutes.

8.6.6 GROUND COMMUNICATOR CATEGORIES (See Figure 8-2)

The following paragraphs describe the terminal points and data originators with which pilots communicate in the course of a flight.[*] We are not concerned here with the actual transmitting sites, but rather the functional character of the various transmissions. These transmissions may be carried on dedicated voice channels, superimposed on a navigational channel, or simultaneously carried by both. The order that the ground stations are presented here approximates the chronological order in which they would be encountered during a typical flight. Sections marked (#) (*) are for information only and will not be included in the CNI scenario.

8.6.6.1 Automatic Terminal Information Service (ATIS)[#]

Data that must be repeated often by the tower personnel to departing and arriving aircraft will be recorded on an endless tape and continuously broadcast. The tape will be edited and updated whenever necessary to accommodate changed conditions. Typical broadcast data are barometer setting, temperature, runway in use, traffic pattern procedures, visibility, correct address for tower and ground control, etc. At high density terminals, two dedicated channels for ATIS will be provided. The information on one will be tailored to the needs of departing aircraft while the other will service approaching aircraft. The present use of ATIS has greatly reduced the work load of tower personnel and reduced queueing on the tower channels.

8.6.6.2 Ground Control (GC)

At high-density municipal and military airports, one or more channels will be dedicated for control of taxiing aircraft. Requests for permission to taxi and for specific instructions to reach specific destinations each as a runway or terminal building are made by pilots and, in turn, answered by a ground controller. The controller may have Airport Surface Detection Equipment (ASDE) such as high resolution radar, ground

---

[*] Airman's Information Manual, Department of Transportation, Federal Aviation Administration, National Flight Center, AT-430, Washington, D.C., 1969.

TRANS-OCEAN TRAFFIC CONTROL (HF)
AIR ROUTE TRAFFIC CONTROL
LOCAL CONTROL (TOWER)
APPROACH CONTROL
DEPARTURE CONTROL
GROUND CONTROL
CLEARANCE DELIVERY
AUTOMATIC TERMINAL INFO. SERV.
COMPANY RADIO OR
SQUADRON OPERATIONS
UNICOM

DIRECT MODE NAV.
FACILITIES WITH
VOICE CAPABILITY
(VHF, UHF, LF,
AND L-BAND)

LONG RANGE
NAV.
FACILITIES
(LF, VLF,
AND HF)

FLIGHT
SERVICE
STATION
MULTICOM

869-1892 UNCLASSIFIED

Figure 8-2. Present Ground Communicator Categories.

emplaced proximity sensors or CNI position location equipment, and appropriate read-
outs such as CRT or status board displays to aid him in his task. Also, he will occupy
an elevated position on the airport, such as the tower, to control traffic visually. When
more than one ground control channel is used, each channel will be dedicated to seg-
ments of ground traffic that do not interfere such as separate halves of an airport, two
simultaneously used runways, or departing and just landed aircraft. In locations that
do not have a dedicated clearance delivery channel, its functions will be handled on a
ground control channel.

8.6.6.3 Clearance Delivery (CD)

A dedicated channel for pilot requests for and subsequent transmittal of ATC
flight clearances. The time on-the-air required for a single voice two-way exchange
can be from 10 to 15 seconds for uncomplicated clearances to times in excess of one
minute for more complicated clearances. These times are in sharp contrast to the
terse, less-than-a-second to 10 second messages and acknowledgements typical on other
airport channels and could cause intolerable queueing on tower or ground control channel

if special clearance delivery channels were not provided. A hard-copy print-out of data received on this channel would be desireable in all aircraft and is considered practical in large commercial and military aircraft and some business aircraft.

8.6.6.4 Squadron Operations or Company Dispatch (CR)

A private two-way voice channel would be used for the issuance of instructions from the ground, transmission of status reports and requests from aircraft. Messages are between the aircraft and its owner or the owner's agent. Such communication is not concerned with the public matter of air traffic control but is rather the private concern of the parties involved. Typical transmissions might concern military mission instructions, passenger manifestos, and maintenance reports.

8.6.6.5 Local Control (TW)

Control tower personnel are responsible for expediting the flow of air traffic onto and off of the airport runway(s) and for maintaining safe separation between aircraft in this process. To accomplish this, two-way voice communications are required between tower and aircraft for the following typical message types.

a.   Aircraft, whether airborne or on airport taxiway. inform tower of their positions, intentions.

b.   Tower informs aircraft of airport traffic conditions and runway weather conditions, and directs aircraft to follow some specific procedure, such as taxi onto a runway, enter the traffic pattern, fly to and report over a checkpoint, hold position, go-around, takeoff, land, etc.

c.   Just landed aircraft are directed off the active runway and then directed to switch to a ground control channel.

d.   Aircraft just departing the airport traffic pattern are directed to switch to a departure control or enroute channel.

The tower may exercise emergency authority by directing all aircraft to maintain present position or altitude, depart the pattern, orbit the field, clear the runway, etc. In this instance, the tower is functioning in a broadcast mode rather than a discrete simplex mode. At airports that do not have any or all of the stations described in sections 8.6.1 through 8.6.4, their functions are handled on the tower channels. A

tower may have two or more channels, regardless of whether ATIS and ground control are provided, to simultaneously but separately control several runways, or arriving or departing aircraft.

8.6.6.6 Departure Control (DP)

Departure controllers are responsible for expediting the flow of air traffic from airport traffic patterns to the primary air route (enroute) structure while maintaining safe separation between aircraft. Surveillance radar, ICNI outputs and/or reliance on pilot position/heading/speed/altitude reports will be used to track the aircraft. The departure may be conducted by adherence to a pre-planned set of departure instructions, by vectoring, or by a combination of these. If a pre-planned departure is used, the pilot may be required to report arrival at and departure from position fix points and altitudes. These reports will then be acknowledged by the controller. If vectoring is used, the controller will direct the aircraft when to change heading and/or altitude and indicate the magnitude of the change. These directions will then be acknowledged by the pilot. During the course of these two-way communications, acknowledgements will often take the form of a verbatim repeat of the received message and subsequent listening for corrections to ensure that no misunderstandings have taken place. Upon arrival over the first fix point of the enroute portion of the flight, the pilot will be directed to switch to an enroute communication channel.

In most locations, the departure controller will have assigned to him several aircraft for simultaneous control in his area of jurisdiction. For example, all aircraft departing Northwest may be assigned one controller while another controls aircraft departing Northeast. Up to seven individual aircraft may be time shared by a single controller. The limitation on number of aircraft per controller is a function of both the queuing of voice message exchanges and the mental capacity of a single controller for handling multiple aircraft.

8.6.6.7 Air Route Traffic Control Center (RC)

Air route traffic controllers will be responsible for tracking the progress of aircraft on the primary air route structure in order to maintain safe separation between aircraft, and provide assistance to aircraft. In all instances, the aircraft flight plan will be available in the ARTCC and the traffic controller will merely acknowledge position reports from aircraft. He may also direct aircraft to make minor deviations to their flight plans, such as altitude changes, or pass approval on requests for such

deviations from the aircraft. In each case an acknowledgement is required by the pilot or traffic controller as appropriate, and occasionally, advisory information will be included such as reports of turbulence or other weather conditions by the pilot and reports of current barometer setting and pertinent traffic information by the controller. The controller will keep the aircraft advised of pertinent traffic and weather, and may vector the aircraft around other traffic or hazardous conditions. The ARTCC's area of jurisdiction will be divided into sectors, and several controllers will be allocated to each sector as necessary.

8.6.6.8# Flight Service Station (FSS)

Flight service stations will have a broad area of responsibility covering many functions not directly concerned with air/ground communication links. The following listing is limited to functions that will be implemented directly with air/ground radio.

a.   Enroute communication with aircraft on VFR flight plans. Includes acceptance of position reports, acceptance and answering of requests for weather and traffic information, and vectoring assistance to VFR aircraft in hazardous or congested areas.

b.   Enroute communications with aircraft on IFR flight plans. Includes acceptance approval and readback of major changes to IFR flight plans, IFR flight plans filed by aircraft already airborne on VFR or no flight plan, requests for cancellation of flight plans.

c.   Communications with aircraft on and in the vicinity of airports not served by towers. Includes all the functions described for Ground Control, Clearance Delivery and Local Control. However, since the FSS personnel will seldom be in visual contact with the airport ground traffic or air traffic pattern, the service will function in an advisory capacity only rather than a control capacity and will rely on pilot reports of position and intention for the data base of its advisory service with regard to traffic. Complete pilot weather briefing will also be provided on request.

d.   Assistance to los VFR aircraft. Includes two-way
     communications as necessary to "talk" a lost pilot into a
     position where he regains his bearings, radar vectoring
     of lost aircraft, and coordination of airborne search and
     rescue operations.

e.   Broadcast of weather reports, forecasts and airport
     advisory data.

All Flight Service Stations will have a common calling address for establishment of
original contact. Due to the nature of the two-way exchanges with a FSS, such
exchanges may be several minutes in duration if conducted by voice.

8.6.6.9 Enroute Company Radio or Enroute Military Radio (CR)

These stations serve the same functions and represent the same agents
described for Squadron Operations and Company Dispatch in Section 8.6.4. However,
they are concerned with aircraft enroute rather than at the terminal points. Also, they
may serve most of the functions described for FSS's through land line or microwave
link with FSS's and ARTCC's. Revision to flight plans and inflight filing of flight plans
will be relayed through these stations to the appropriate ARTCC's. These stations
accept and transmit data link messages whose content is the private concern of the
parties involved and is not the concern of ATC.

8.6.6.10# Transcribed Weather

Continuous voice and/or data broadcast from endless tape giving weather con-
ditions, forecasts and notices of hazardous or other unusual conditions of interest to
airmen.

8.6.6.11# Scheduled Weather Station

Voice broadcasts of approximately 5 to 15 minutes duration occurring 15 and 45
minutes past each hour. Could be supplemented with data link broadcasts of shorter
duration.

8.6.6.12# Emergency Radar Advisory Station

Radar advisory service and navigational assistance provided by communication
with picket ships of the Seaward Extension of the Contiguous Radar Warning System.

8.6.6.13# Unicom

Several public discrete air/ground voice communication channels will be allocated to ground stations at airports not served by control towers and to stations on the airport that are not reachable through the tower. These stations are for advisory and information services only and not for traffic control purposes. For example, pilots will call Unicom when approaching a non-tower airport to apprise that airport of their intentions, or student pilots may call the Unicom station assigned to their flight school for various requests and advisories. The Unicom stations will, in turn, answer requests and provide data on weather, traffic. and facilities available at the field.

8.6.6.14# Multicom

Several public discrete air/ground voice communication channels will be allocated for mobile ground stations used for providing advisory service between aircraft and ground for special purposes such as firefighting, crop dusting, and ranching.

8.6.6.15 Approach Control (AP)

Approach controllers will be responsible for expediting the flow of air traffic from the enroute route structure to the airport traffic pattern while maintaining safe separation between aircraft. The procedures. communications and personnel required for approach control will be essentially the same as those described for departure control. Upon arrival within 5 to 8 miles of the airport, the aircraft may be directed to switch to a final controller discrete channel or a control tower channel.

8.6.6.16# Final Controller

If a Ground Controlled Approach (GCA) is to be made using Precision Approach Radar (PAR). or equivalent CNI mechanization, the final vectoring of the aircraft to the runway threshold will be done by a final controller. Once initial contact has been made between the aircraft and the final controller, the controller operates in a broadcast mode and his vectoring instructions need not be acknowledged by the pilot. After the aircraft passes the point of touchdown on the runway, the final controller will continue to provide information to help the pilot maintain alignment with the runway centerline until it is clear to the controller that the aircraft is slowing to a stop or slowing for

turnoff on the runway, or that the aircraft is executing a missed approach and "going around." At this point, the final controller will advise the pilot to contact ground control, the tower, or approach control as appropriate.

8.6.7 CALCULATED SCENARIO DATA

The data presented in the previous paragraphs were obtained from literature search and actual measurement in the field. These data enable calculation of total aircraft in the scenario volume and air traffic movement rates for each user class and aircraft flight phase. A summary of these calculated data, along with some pertinent previous data, is presented in Table 8-3. There are two principal factors that control the outcome of all calculated data. The first is the fact that the greatest percentage of air traffic (the air carriers) must transit the least number of airports. The second is the percentage mix of aircraft in each user class established by FAA future traffic predictions. These factors force the peak traffic volume to be determined by the maximum aircraft processing rate of the five commercial airports. This processing rate will be defined as the average landing and take-off spacing for air carriers. It will be assumed that the airport taxiway complex and the ATC complex are efficient enough to supply aircraft to and remove aircraft from the runways at this maximum rate.

Details of the calculations are contained in the following subparagraphs. Variables, Constants, and Subscripts used are:

a.   Variables and Constants

A = number of airports

N = number of aircraft

V = number of airways or jet routes

T = time in minutes

S = time in seconds

K = percentage of aircraft

r = rate in aircraft per hour per airport

R = rate in aircraft per hour

D = distance in nautical miles

b. Subscripts

C = commercial or air carrier
M = military
G = general aviation
D = departures
A = arrivals
E = enroute transit
T = total
H = high altitude or jet route
L = low altitude route

Table 8.3. Summary of Scenario Data

	Military	Air Carrier	General Aviation	Total
Percent aircraft airborne in terminal area	13.8%	51.7%	34.5%	100%
Percent of each category transiting term. area	25%	25%	25%	25%
Number of aircraft departing	26	100	62	188
Number of aircraft arriving	24	88	62	171
Number of aircraft transiting	17	62	41	120
Departure rate	58 acft/hr	200 acft/hr	56 acft/hr	314
Arrival rate	58 acft/hr	200 acft/hr	56 acft/hr	314
Transit rate	263.3 acft/hr		50 acft/hr	313
Departure rate per airport	6.43 acft/hr	40 acft/hr	6.22 acft/hr	–
Transit rate per airway	65.8 acft/hr		10 acft/hr	–
Number of airways across term. area	4		5	9
Number of airports in term. area	9	5	9	23
Departure spacing per airport	560 sec	90 sec	578 sec	–
Operation spacing per airport	280 sec	45 sec	289 sec	–
Aircraft time separation on airways	0.911 min		6 min	–
Aircraft distance spacing on airways	7.6 nmi		16 nmi	–
Time to depart	27 min	30 min	66.5 min	–
Time to arrive	24.4 min	25.5	66 min	–
Time to transit	18 min	18 min	49.3 min	–

8.6.7.1 Air Carrier Calculations

The following calculations establish air carrier and total traffic data.

$$r_D = r_A = \frac{3600 \text{ sec/hr}}{S_A \text{ sec/arrival}} \tag{1}$$

$$r_{CD} = r_{CA} = \frac{3600}{S_{CA}} = \frac{3600}{90} = 40 \text{ aircraft/hour/airport}$$

$$R_D = R_A = r_D \cdot A \tag{2}$$

$$R_{CD} = R_{CA} = r_{CD} \cdot A_C = 40 \cdot 5 = 200 \text{ aircraft/hour}$$

$$N_D = \frac{T_D \text{ min (60 sec/min) A airports}}{S_D \text{ sec/aircraft/airport}} \tag{3}$$

$$N_{CD} = \left(\frac{T_{AD} \cdot 60}{S_{CD}} \right) A = \left(\frac{30 \cdot 60}{90} \right) 5 = 100 \text{ aircraft}$$

$$N_A = \left(\frac{T_A \cdot 60}{S_A} \right) A \tag{3.1}$$

$$N_{CA} = \left(\frac{T_{CA} \cdot 60}{S_{CA}} \right) A_A = \left(\frac{26.5 \cdot 60}{90} \right) 5 = 88 \text{ aircraft}$$

$$N_E = \frac{K_E \left(N_D + N_A \right)}{1 - K_E} \tag{4}$$

$$N_{CE} = \frac{K_{CE} \left(N_{CD} + N_{CA} \right)}{1 - K_{CE}} = \frac{0.25 \, (100 + 85)}{1 - 0.25} = 61.7 \approx 62 \text{ aircraft}$$

$$N_T = \frac{N_{CD} + N_{CA} + N_{CE}}{K_C} \tag{5}$$

$$N_T = \frac{100 + 85 + 62}{0.517} = \frac{247}{0.517} = 478 \text{ aircraft}$$

8.6.7.2 Military and General Aviation Calculations

The following calculations establish military and general aviation traffic data.

$$N_{MT} = K_M \cdot N_T \tag{6}$$

$$N_{MT} = 0.138 \cdot 478 = 66 \text{ aircraft}$$

$$N_{GT} = K_G \cdot N_T \tag{6.1}$$

$$N_{GT} = 0.345 \cdot 478 = 165 \text{ aircraft}$$

$$N_{MT} = N_{MA} + M_{MD} + N_{ME} \tag{7}$$

$$N_{ME} = K_{ME} \cdot N_{MT} \tag{8}$$

Combining Equations (7) and (8):

$$N_{MA} + N_{MD} = N_{MT} - K_{ME} N_{MT} = N_{MT}\left(1 - K_{ME}\right) \tag{9}$$

From Equations (3) and (3.1):

$$N_{MA} + N_{MD} = \frac{T_{MA}}{S_M} 60 A_M + \frac{T_{MD}}{S_M} 60 A_M \tag{10}$$

$$N_{MA} + N_{MD} = \frac{60 A_M}{S_M} \left(T_{MA} + T_{MD}\right) \tag{10.1}$$

Combining Equations (9) and (10.1):

$$N_{MT}\left(1 - K_{ME}\right) = \frac{60 A_M}{S_M} \left(T_{MA} + T_{MD}\right) \tag{11}$$

$$S_M = \frac{60 A_M \left(T_{MA} + T_{MD}\right)}{N_{MT}\left(1 - K_{ME}\right)} \tag{11.1}$$

-657-

$$S_M = \frac{60 \cdot 9 (24.4 + 27)}{66 (1 - 0.25)} = \frac{60 \cdot 9 \cdot 51.4}{66 \cdot 0.75} = 560 \text{ seconds}$$

From Equation (3):

$$N_{MD} = \frac{T_{MD} \cdot 60 \cdot A_M}{S_M} = \frac{27 \cdot 60 \cdot 9}{560} = 26 \text{ aircraft}$$

From Equation (3.1):

$$N_{MA} = \frac{T_{MA} \cdot 60 \cdot A_M}{S_M} = \frac{24.4 \cdot 60 \cdot 9}{560} = 23.54 \approx 24 \text{ aircraft}$$

From Equation (4):

$$N_{ME} = \frac{K_{ME} \left(N_{MD} + N_{MA} \right)}{1 - K_{ME}} = \frac{0.25 (26 + 24)}{1 - 0.25} = 16.66 \approx 17 \text{ aircraft}$$

From Equation (11.1):

$$S_G = \frac{60 \, A_G \left(T_{GA} + T_{GD} \right)}{N_{GT} \left(1 - K_{GE} \right)} = \frac{60 \cdot 9 (66 + 66.5)}{165 (1 - 0.25)} = 579 \text{ seconds}$$

$$N_{GD} = \frac{T_{GD} \cdot 60 \cdot A_G}{S_G} = \frac{66.5 \cdot 60 \cdot 9}{579} = 62 \text{ aircraft}$$

$$N_{GA} = \frac{T_{GA} \cdot 60 \cdot A_G}{S_G} = \frac{66.5 \cdot 60 \cdot 9}{579} = 61.6 \approx 62 \text{ aircraft}$$

$$N_{GE} = \frac{K_{GE} \left(N_{GD} + N_{GD} \right)}{1 - K_{GE}} = \frac{0.25 (62 + 61.7)}{1 - 0.25} = 41.2 \approx 41 \text{ aircraft}$$

From Equation (1):

$$r_{MD} = r_{MA} = \frac{3600}{S_M} = \frac{3600}{560} = 6.43 \text{ aircraft/hour/airport}$$

$$r_{GD} = r_{GA} = \frac{3600}{S_G} = \frac{3600}{579} = 6.22 \text{ aircraft/hour/airport}$$

From Equation (2):

$$R_{MD} = R_{MA} = r_{MD} \cdot A_M = 6.43 \cdot 9 = 58 \text{ aircraft/hour}$$

$$R_{GD} = R_{GA} = r_{GD} \, A_G = 6.22 \cdot 9 = 56 \text{ aircraft/hour}$$

-658-

8.6.7.3 Enroute Calculations

The following calculations establish enroute traffic data for all user classes.

$$\frac{N_E}{V} = N_V \text{ aircraft enroute/airway} \tag{12}$$

$$N = \frac{N_{ME} + N_E}{V_H} = \frac{17 + 62}{4} = 19.75 \text{ aircraft/airway}$$

$$\frac{T_E}{N_V} = S_E \text{ minutes/aircraft/airway} \tag{13}$$

$$S_{MAE} = \frac{T_{MCE}}{N_{MCV}} = \frac{18}{19.75} = 0.911 \text{ min/aircraft/airway}$$

$$R_E = \frac{60 \text{ min/hour}}{S_E \text{ min/aircraft/airway}} \tag{14}$$

$$R_{MCE} = \frac{60}{S_{MCE}} = \frac{60}{0.911} = 65.8 \text{ aircraft/hour/airway}$$

$$r_E = R_E V \tag{15}$$

$$r_{MCE} = R_{MCE} V_H = 65.8 \cdot 4 = 263.2 \text{ aircraft/hour}$$

From Equation (12):

$$N_{GV} = \frac{N_{GE}}{V_L} = \frac{41}{5} = 8.2 \text{ aircraft/airway}$$

From Equation (13):

$$S_{GE} = \frac{T_{GE}}{N_{GV}} = \frac{49.3}{8.2} \approx 6.01 \text{ min/aircraft/airway}$$

From Equation (14):

$$R_{GE} = \frac{60}{S_{GE}} = \frac{60}{6.01} \approx 10 \text{ aircraft/hour/airway}$$

From Equation (15):

$$r_{GE} = R_{GE} V_L = 10.5 = 50 \text{ aircraft/hour}$$

Distance between transiting aircraft on same airway:

$$D = (\text{ground speed})(\text{interval time})/(60 \text{ min/hour})$$

$$D_{MA} = 500 \cdot 0.911/60 = 7.6 \text{ nmi}$$

$$D_{G} = 160 \cdot 6.01/60 \approx 16 \text{ nmi}$$

8.7 MESSAGE SEQUENCES

The term "message sequence" as used herein denotes an histogram of voice conversations between an aircraft and the various ground stations with which it must communicate during the course of its flight. Three basic message sequences arise due to the differing requirements of the three basic flight phases:

a. Those generated during the departure of an aircraft from its airport of origin to the periphery of the terminal area.

b. Those generated during the arrival of an aircraft from its point of entry at the periphery of the terminal area to its airport of destination.

c. Those generated during the transit of an aircraft through the terminal area while enroute between two other terminal areas.

For any given airport/terminal area situation these message sequences become quite stylized, almost to the point of complete predictability in practice, and vary mainly as a function of the flight profile of the aircraft involved. The flight profile can be reasonably predicted by specifying the aircraft user category. In this analysis, three user categories are specified: Military, Commercial, and General Aviation.

The three-by-three combination of basic message sequences and user categories results in nine distinct message sequences. Each of these sequences is a representative model of the voice traffic that would result when an individual aircraft of a specified user category maneuvers in a specified flight phase. In this analysis, the nine message sequences are respectively identified by a two-letter code as shown in Table 8-4 under the string variable P.

Table 8-4. Computer File Codes

String Variable	Code
T1 or R1: Transmitter or Receiver Type	CD: Clearance Delivery GC: Ground Control TW: Local Control (Tower) CR: Company Radio or Squadron Operations DP: Departure Control AP: Approach Control RC: Air Route Traffic Control Center AF: Aircraft
T2 or R4: Transmitter or Receiver User Category	C: Commercial or Air Carrier M: Military G: General Aviation or Municipal N: Not Applicable
T3 or R3: Transmitter or Receiver Number	0: Not Applicable 1 through 9: Number Identification
P: Message Sequence Identification	DC: Departure, Commercial DG: Departure, General Aviation DM: Departure, Military AM: Arrival, Military AG: Arrival, General Aviation AC: Arrival, Commercial EC: Enroute, Commercial EG: Enroute, General Aviation EM: Enroute, Military
F: Transmission Start Time	(Time in Seconds)
G: Transmission End Time	(Time in Seconds)
S: Interval Spacing	(Time in Seconds)
Z: Transmission Number	(File Line Number)

The essential data required for complete specification of a sequence are:

1.   The time a voice message started

2.   The time the message ended

3.   The sender's identification.

4.   The intended receiver's identification.

These data have been hand generated, tabulated, and stored in a computer file designated ALPHA. Figure 8-3 is a print-out of a portion of this file showing the complete message sequence generated during the departure of a commercial aircraft. The

T1	T2	T3	R1	R2	R3	P	Z	F	G	S
AF	C	0	CD	C	0	DC	101	0	5	90
CD	C	0	AF	C	0	DC	102	5	10	90
AF	C	0	CD	C	0	DC	103	10	12	90
AF	C	0	CR	C	0	DC	104	60	63	90
CR	C	0	AF	C	0	DC	105	63	90	90
AF	C	0	CR	C	0	DC	106	90	94	90
CR	C	0	AF	C	0	DC	107	94	95	90
CD	C	0	AF	C	0	DC	108	240	246	90
AF	C	0	CD	C	0	DC	109	246	248	90
CD	C	0	AF	C	0	DC	110	248	285	90
AF	C	0	CD	C	0	DC	111	285	322	90
CD	C	0	AF	C	0	DC	112	322	326	90
AF	C	0	CD	C	0	DC	113	326	327	90
AF	C	0	GC	C	0	DC	114	420	426	90
GC	C	0	AF	C	0	DC	115	426	428	90
AF	C	0	GC	C	0	DC	116	428	431	90
AF	C	0	TW	C	0	DC	117	600	603	90
TW	C	0	AF	C	0	DC	118	603	607	90
AF	C	0	TW	C	0	DC	119	607	608	90
TW	C	0	AF	C	0	DC	120	630	638	90
AF	C	0	TW	C	0	DC	121	638	639	90
AF	C	0	TW	C	0	DC	122	675	681	90
TW	C	0	AF	C	0	DC	123	681	683	90
AF	C	0	CR	C	0	DC	124	687	702	90
CR	C	0	AF	C	0	DC	125	702	704	90
AF	C	0	DP	N	0	DC	126	705	712	90
DP	N	0	AF	C	0	DC	127	712	714	90
AF	C	0	DP	N	1	DC	128	714	717	90
DP	N	1	AF	C	0	DC	129	843	856	90
AF	C	0	DP	N	1	DC	130	856	869	90
AF	C	0	DP	N	2	DC	131	1023	1027	90
DP	N	2	AF	C	0	DC	132	1027	1040	90
DP	N	2	AF	C	0	DC	133	1203	1211	90
AF	C	0	DP	N	2	DC	134	1211	1219	90
AF	C	0	RC	N	1	DC	135	1323	1329	90
RC	N	1	AF	C	0	DC	136	1329	1331	90
AF	C	0	RC	N	1	DC	137	1331	1334	90
RC	N	1	AF	C	0	DC	138	1335	1342	90
AF	C	0	RC	N	1	DC	139	1342	1349	90
AF	C	0	RC	N	1	DC	140	1350	1353	90
RC	N	1	AF	C	0	DC	141	1353	1354	90
AF	C	0	RC	N	1	DC	142	1530	1533	90
RC	N	1	AF	C	0	DC	143	1533	1534	90
AF	C	0	RC	N	1	DC	144	1710	1713	90
RC	N	1	AF	C	0	DC	145	1713	1714	90
RC	N	1	AF	C	0	DC	146	2250	2255	90
AF	C	0	RC	N	1	DC	147	2255	2260	90
AF	C	0	RC	N	2	DC	148	2490	2499	90
RC	N	2	AF	C	0	DC	149	2499	2500	90

Figure 8-3. A Portion of Message Sequence Computer File ALPHA

transmission start and end times (F&G) shown are with respect to an arbitrary zero reference at the start of the first message. In the computer simulation to be described, these zero references (and, consequently, all sequence times) will be converted to new values in a common simulation reference time frame. The message number Z is an identifying number whose most significant figure enables the computer to determine the message sequence code. The various sequences are assigned number blocks as follows:

Sequence Code	Number Block
DC	101 - 199
AC	201 - 299
DM	301 - 399
AM	401 - 499
DG	501 - 599
AG	601 - 699
EC	701 - 799
EM	801 - 899
EG	901 - 999

The decade and ones figures enable the programmer to rapidly access specific messages in a sequence that has been filtered by the computer. This computer filtering is described in Section 8.8.1.

The Interval Spacing, S, specifies the recurrence time for identical messages (Z numbers) generated by the traffic concerned with any specific airport or airway. It has been tacitly assumed that all aircraft of a given user class in a similar flight phase will generate identical message sequences. Therefore, the time spacings between take-offs and between landings and between airway penetrations are also the respective spacings between identical messages of a given flight-phase/user-class combination. This assumption of identical message sequences for identical flight-phase/user-class combinations is a key simplifying factor that enables the construction of this simulation. This assumption is based upon impressions gained through many hours of monitoring air traffic control voice channels as well as through examination of previous studies conducted for the FAA in this area.[*] It should be noted here that although this assumption results in an orderly and completely predictable message flow as concerns a single airport or airway, the total message traffic is statistical in nature due to the random interval spacing between operations at different airports and on different airways. This randomness is discussed more in Section 5.5.2.4.

---

[*] Observed May 1969.

The transmitter and receiver identification code columns, T1 through R3 in Figure 8-3, are described in Table 8-4; complete description of each transmitter-receiver type identified by these codes was covered in Section 8.6.6. It will be noted that in addition to the type and user codes (T1, R1 and T2, R2) that two columns of number codes T3, R3 have been listed. Thus far these number codes have not been utilized in any significant way. However, they were included on the contingency that in future studies, it may be desirable to derive the traffic through individual terminals of the same type, e.g., near, medium range, and long range Air Route Traffic Control Centers.

Figure 8-4 indicates the nature of voice traffic in a typical message sequence. Figures such as this one have not been constructed for all of the other sequences since they are of no practical value in the simulation. This one figure was constructed solely for use as an aid to the reader in understanding the simulation. The actual raw input data used in the simulation is shown in Appendices I through IV. The sections of Appendix IV are the component sections of the previously mentioned ALPHA file.

8.8 SIMULATION DESCRIPTION

The basic output of this simulation is a "boxcar" function in which the ordinate represents time stepped in one second increments, and the abcisca represents a number of simultaneous voice transmissions. A two-step process involving two computer programs is utilized. It is recognized that both programs could be combined and that data input/output involving the computer operator could be made less cumbersome through use of a "commands" file. However, this procedure is only a nicety that, in no way, alters the results. Incidently, the names used to designate the computer programs and files were obtained from the International Phocnctic Alphabet since they alphabetically indicate the order of operations in the simulation. The first step is to process the ALPHA file in order to create a new file called CHARLIE. This processing is accomplished by a program called BRAVO. The purpose of this processing is to reduce the ALPHA file data such that they represent only those transmitter/receiver pairings or radio links for which further analysis is desired. If all links are desired, then the CHARLIE file becomes essentially a reprint of the ALPHA file.

The second step is to process the CHARLIE file in a program called DELTA in order to obtain the final readout.
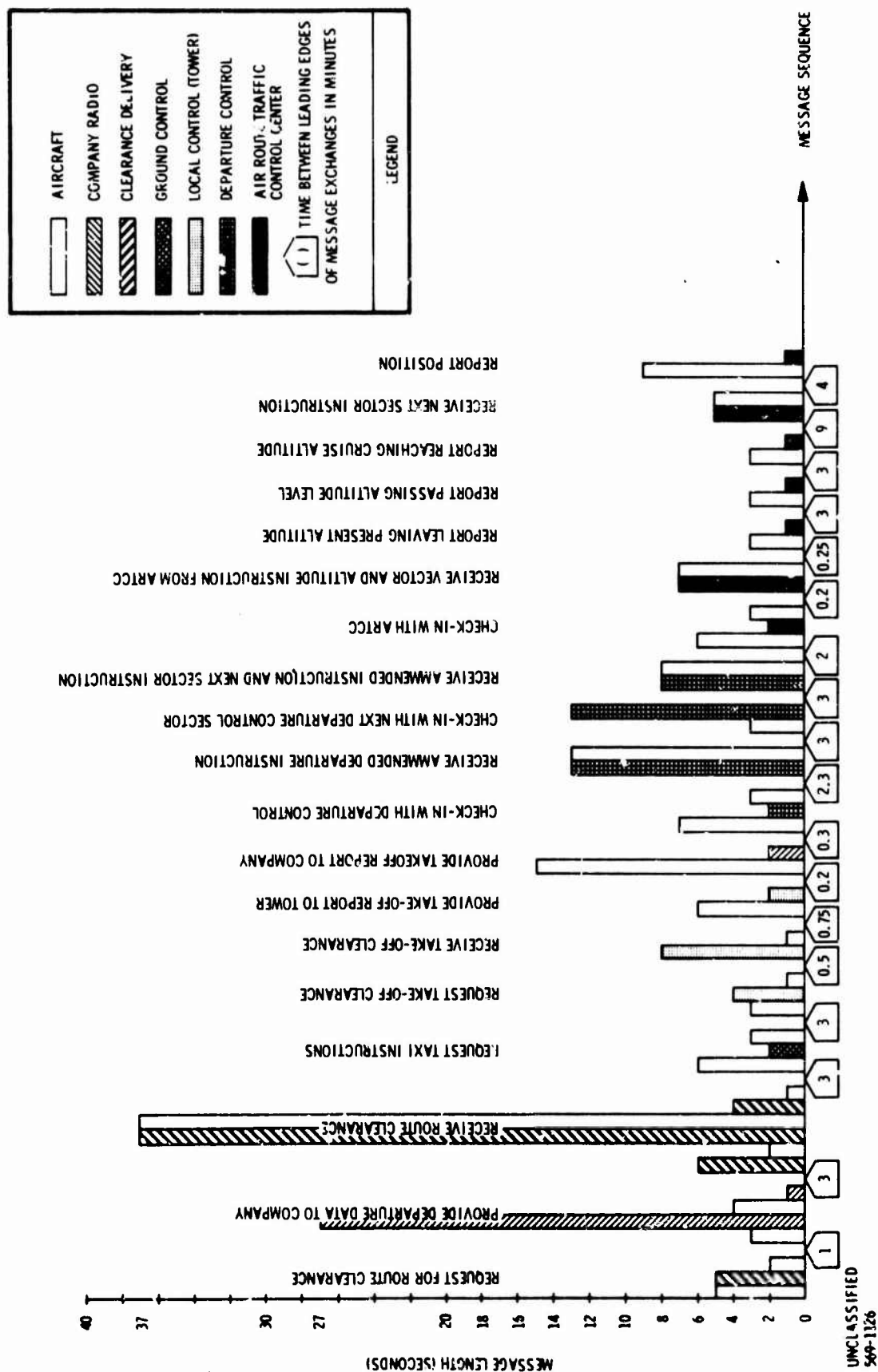
Figure 8-4. Voice Channel Loading, Air Carrier Departure.

8.8.1 THE BRAVO PROGRAM (Refer to Figure 8-5)

This program is written in the SUPER BASIC computer language because of the particular power of this language for manipulating data "strings" in the most economical way. Each line in the ALPHA file is considered to consist of a LEFT data string, and a RIGHT data string with nine data SUBSTRINGS between them. Each total line contains spaces for 41 characters including blanks. Any set of contiguous characters and/or blanks, from among tne 41, can be designated a data string and isolated from the rest of the line by calling out the number of the first position it occupies in the line (counting by ones from left to right) and then the total number of positions it occupies. A data string thus designated is called a SUBSTRING. For convenience, the left-most and right-most data strings can be designated by simply calling out LEFT or RIGHT and the respective numbers of total positions occupied.

The significant statements in the BRAVO program for filtering out desired transmitter/receiver links are found on lines 510, 540, 610, and 640. Line 510 designates the left-most 2 positions on any line in the ALPHA file as T1 for transmitter identification. Line 540 designated 2 positions beginning with position 9, on any line

```
200 AS ="4%2B5%2B5%2B5%2B4%/"
300   TEXT A:253,1):41
400   J=1
410   OPEN/CHARLIE/,OUTPUT,3
420   OPEN/ALPHA/,INPUT,2
430   FOR I=1 TO 253
440   INPUT FROM 2:A(I,1)
510   T1=LEFT(A(I,1),2)
520   T2=SUBSTR(A(I,1),4,1)
530   T3=SUBSTR(A(I,1),6,1)
540   R1=SUBSTR(A(I,1),9,2)
550   R2=SUBSTR(A(I,1),12,1)
560   R3=SUBSTR(A(I,1),14,1)
570   P=SUBSTR(A(I,1),17,2)
580   F=SUBSTR(A(I,1),25,5)
590   G=SUBSTR(A(I,1),31,5)
594   S=RIGHT(A(I,1),5)
598   Z=SUBSTR(A(I,1),20,4)
610 IF T1="CR"OR T1="TW"OR T1="DP"OR T1="RC"OR T1="AF"
OR T1="AP" THEN 640 ELSE 800
640 IF R1="CR"OR R1="TW"OR R1="DP"OR R1="RC"OR R1="AF"
OR R1="AP" THEN 700 ELSE 800
700 WRITE ON 3 IN FORM AS: J,F,G,S,Z
710 WRITE IN FORM AS: J,F,G,S,Z
720   J=J+1
800   NEXT I
```

Figure 8-5. Computer Program BRAVO.

in the ALPHA file, as R1 for receiver identification. Lines 610 and 640, respectively, designate the specific codes for those transmitters and receivers that the analyst desired to use in the simulation. In the example shown in Figure 5, the analyst has elected to study, in the simulation, only those transmitter/receiver links involving Company Radios, Towers, Departure Controllers, Air Route Traffic Controllers, Approach Controllers and Aircraft. He has done this by designating CR, TW, DP, RC, AP, and AF as allowed codes for T1 and R1 in lines 610 and 640. As a result, only those data lines from the ALPHA file that contain these desired radio links will be output to the CHARLIE file. The CHARLIE file will, in turn, be accessed by the simulation program (DELTA). Note that any number of logic statemements of the general form shown in lines 610 and 640 may be inserted between lines 598 and 700 to designate a specific radio link or combination of links for further analysis. The designation may be detailed down to specific flight phases and aircraft numbers through use of the various substrings shown in lines 510 through 598. It should also be mentioned that the number "253" appearing in lines 300 and 430 is the total number of data lines in the ALPHA file. Therefore, if the ALPHA file is ever altered in length through future additions or deletions, the number 253 in lines 300 and 430 should be similarly altered.

Figure 8-6 shows a portion of the CHARLIE file output by the previously discussed BRAVO program. Each data line of this file gives the parameters of a specific voice message required in the simulation. Comparison between the messages in the CHARLIE and ALPHA files can be made with the Message Number (parameter 'Z"). Note that the messages have also been renumbered with the parameter "J" in the CHARLIE file. The "J" parameter designates their order of processing in the DELTA simulation program.

8.8.2 DELTA PROGRAM

The final step in the simulation is running the actual simulation program. This program is written in the FORTRAN IV computer language because this language has a greater power for manipulating arithmetic expressions.

The program is named "DELTA" and is discussed in detail in the following paragraphs. To understand the operation of this program we should first recall some items previously presented.

J	F	G	S	Z
1	60	63	90	104
2	63	90	90	105
3	90	94	90	106
4	94	95	90	107
5	600	603	90	117
6	603	607	90	118
7	607	608	90	119
8	630	638	90	120
9	638	639	90	121
10	675	651	90	122
11	68:	683	90	123
12	687	702	90	124
13	702	704	90	125
14	705	712	90	126
15	712	714	90	127
16	714	717	90	128
17	843	856	90	129
18	856	869	90	130
19	1023	1027	90	131
20	1027	1040	90	132
21	1203	1211	90	133
22	1211	1219	90	134
23	1323	1329	90	135
24	1329	1331	90	136
25	1331	1334	90	137
26	1335	1342	90	138
27	1342	1349	90	139
28	1350	1353	90	140
29	1353	1354	90	141
30	1530	1533	90	142
31	1533	1534	90	143
32	1710	1713	90	144
33	1713	1714	90	145
34	2250	2255	90	146
35	2255	2260	90	147
36	2490	2499	90	148
37	2499	2500	90	149
33	0	9	90	201
39	9	24	90	202
40	24	39	90	203
41	143	151	90	204
42	151	152	90	205
43	257	260	90	206
44	260	275	90	207
45	275	305	90	208
46	366	369	90	209
47	369	378	90	210
48	378	387	90	211
49	474	483	90	212

Figure 8-6. A Portion of Computer File CHARLIE.

Section 8.7 described nine separate message sequences having their zero time references as their respective start times. It was shown in Section 8.6.7 that in any given time interval, several of each kind of sequence would be present in the scenario volume. For example, there would be 26 military aircraft departure sequences. 24 military aircraft arrival sequences. etc. (see Table 8-3) for a total of 479 sequences in the volume. In order for all of these sequences to be properly placed in time, their zero reference times must be offset with respect to the zero reference time of the simulation. This latter zero reference time is taken as the start of the period-of-observation or "look window". The basic function of the DELTA program is to compute the proper values of offset-time for each message sequence and. in effect, stack the sequences in the time frame of the simulation.

The result can be visualized as the stepped sequence stacking shown in Figure 8-7. Once this chronological offsetting is accomplished, the total message traffic in the scenario volume is defined over the time span of the look window. This look window can then be analyzed second-by-second (or any other time increment desired) to determine the loading imposed on any particular channel, group of channels, or the total communications requirement of the ICNI system. In addition to these basic functions, the simulation program necessarily performs certain administrative functions such as opening and closing the correct file for input data, formatting the output data. etc.

The above description is functionally accurate. However, performing the simulation such that the computations literally translate sequence times to simulation time. as is suggested by the above, would result in an excessive number of iterative computations. It is more economical, to perform the following·

1. Assign each sequence a number.
2. Compute the offset-time for each numbered sequence.
3. Using this offset time. convert simulation time to sequence time for each sequence.

This procedure reduces the number of required computations by half. Regardless of which method is used. the essential step in the simulation is to detect coincidences between simulation time and transmitter on time in the various sequences. The number of coincidence detections is then recorded for each increment of time in the "look window". The computer causes this number along with its time of occurrence to be

-669-

MESSAGE SEQUENCES HAVE RANDOM STARTING TIMES (R) BUT CONSTANT
INTERVAL SPACING (S) BASED UPON MAXIMUM AIRPORT CAPACITY
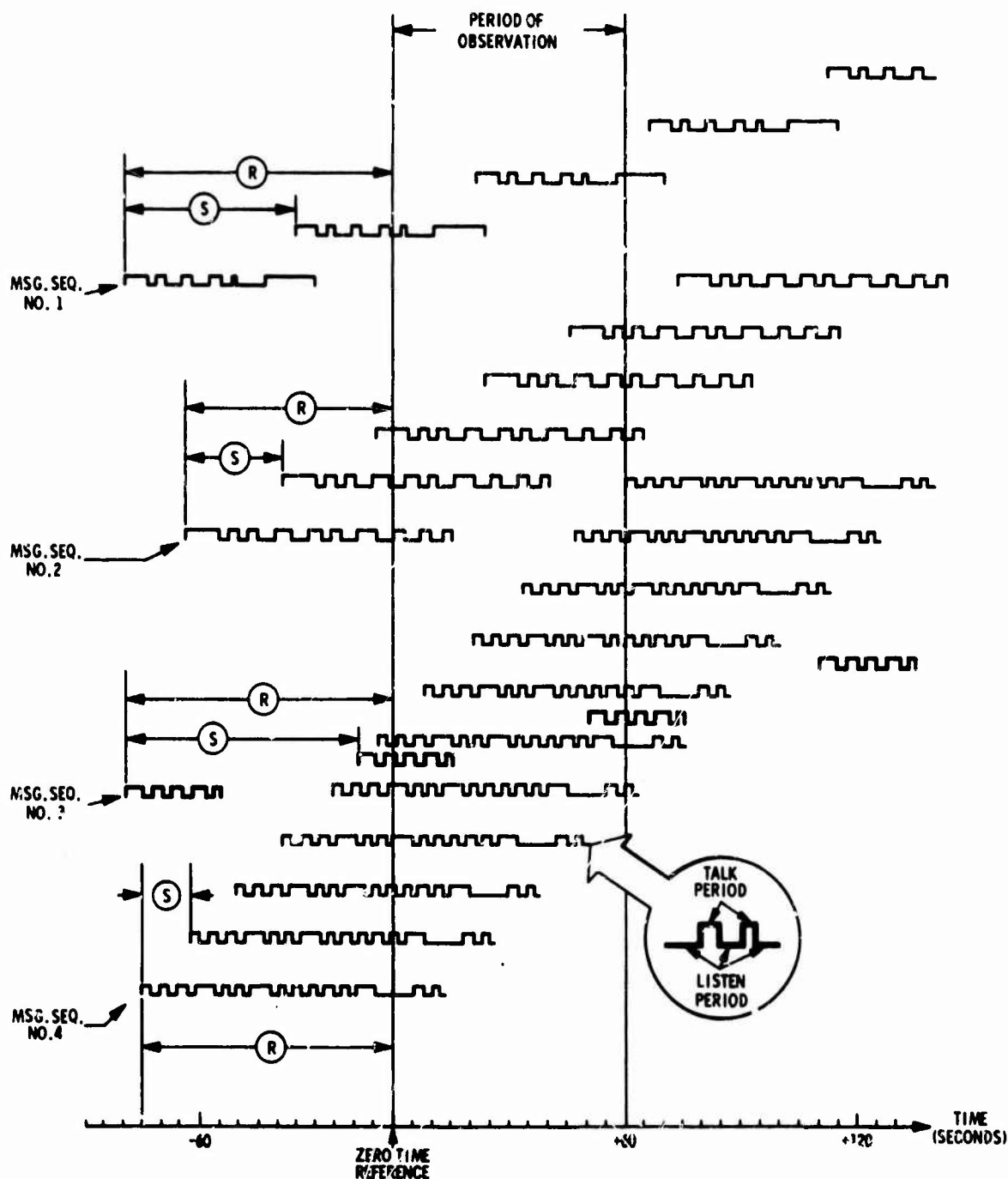
OUTPUT OF SIMULATION MODEL IS NUMBER OF SIMULTANEOUS VOICE TRANS-
MISSIONS IN EACH ONE SECOND INCREMENT OF THE OBSERVATION PERIOD

Figure 8-7.   Computer Simulation of ATC Voice Communications Environment.

-670-

printed out for the start and end times of the look window, and only when a change in the number of coincidence detections occurs between these times.

The following is a detailed description of the simulation computer program DELTA. The line numbers refer to Figures 8-8 through 8-15. The computer program is shown in Appendix VIII. This description should enable anyone to duplicate and run the program on a computer compatible with FORTRAN IV.

8.8.2.1 Lines 1 through 12 and 57 through 60 (See Figure 8-8)

These lines supply the initial numerical data required for the computations by opening and reading-in the CHARLIE file and accepting certain data directly from the programmer.

Notes:

1. The total number of lines in the CHARLIE file should appear in the spaces filled by the number 210 in lines 1 and 4.

2. A number greater than or equal to the total number of lines in the CHARLIE file should appear in the spaces filled by the number 800 in line 5.

3. The codes used in lines 7 through 12, and 58 through 61 have the following meanings. The associated numbers may be changed at the discretion of the analyst.

LAC	=	number of commercial airports in scenario
LAM	=	number of military airports in scenario
LAG	=	number of municipal airports in scenario
LVH	=	number of high altitude airways in scenario
LVL	=	number of low altitude airways in scenario
TW	=	length of look window in seconds
KE	=	number of the first time increment examined in the look window
U	=	initializing value for number of simultaneous transmissions in an increment
R	=	same as U but designated for printout.

```
1.          DI MENSI ON F(210),G(210),S(210),Z(210)
2.          IPITIA,/CHARLY3/,INPUT1
3.          DATA ',/FROU13/, OUTPUT1
4.          DO 90 J=1,210
5.          READ(4,100)J,F(J),G(J),S(J),Z(J)
6.     100  FORMAT(I4,2Y,I5,2Y,I5,2Y,I5,2Y,I5)
7.      90  CONTINUE
8.          LAC=5
9.          LAJ=9
10.         LOC=9
11.         LVM=4
12.         LVL=5
52.         TM=2500
53.         YT=0
54.         IT=0
61.    100   J=0
```

Figure 8-8. Computer Program "DELTA", Lines 1-12, 58-60.

8.8.2.2 Lines 13 through 57 (See Figure 8-9)

These lines comprise a DO LOOP that causes the computer to search through the CHARLIE file and find the line number JS, for the start of each basic sequence and the line number JF, for the end of each basic sequence. In this process, specific values of JS and JF are recorded for each basic sequence. For example, JSDM and JFDM refer to the Start and Finish line number in the message sequence of a Departing Military aircraft.

8.8.2.3 Lines 62 through 131 (See Figure 8-10)

These lines comprise a set of commands that cause the computer to follow the following order of events:

a. Process the Commercial Departure sequences for Airport No. 1.

b. Process the Commercial Arrival sequences for Airport No. 2.

c. Repeat a and b for airports 2, 3, 4, etc., until the number of airports specified in line 7 is reached.

d. Process the Military Departure sequences for base No. 1.

e. Process the Military Arrival sequences for base No. 2.

f. Repeat d and e for bases 2, 3, 4, etc., until the number of bases specified in line 8 is reached.

g. Process the General Aviation Departure sequences for field No. 1.

h. Process the General Aviation Arrival sequences for field No. 2.

-672-

```
13.          DO 500 J=1,43
14.          JF=J
15.          NXTJS=J+1
16.          IX=Z(J)/100.
17.     480  IY=Z(J+1)/100.
18.          IF(IX.NE.IY) GO TO (1,2,3,4,5,6,7,8,9)IX
19.          GO TO 500
20.       1  JSDC=1
21.          JFDC=JF
22.          SPAC1 =S(J)
23.          GO TO 490
24.       2  JSAC=JS
25.          JFAC=JF
26.          SPAC1=S(J)
27.          GO TO 490
28.       3  JSDM=JS
29.          JFDM=JF
30.          SPAC2=S(J)
31.          GO TO 490
32.       4  JSAM=JS
33.          JFAM=JF
34.          SPAC2=S(J)
35.          GO TO 490
36.       5  JSDG=JS
37.          JFDG=JF
38.          SPAC3=S(J)
39.          GO TO 490
40.       6  JSAG=JS
41.          JFAG=JF
42.          SPAC3=S(J)
43.          GO TO 490
44.       7  JSEC=JS
45.          JFEC=JF
46.          SPAC4=S(J)
47.          GO TO 490
48.       8  JSEM=JS
49.          JFEM=JF
50.          SPAC4=S(J)
51.          GO TO 490
52.       9  JSEG=JS
53.          JFEG=JF
54.          SPAC5=S(J)
55.          GO TO 500
56.     490  JS=NXTJS
57.     500  CONTINUE
```

Figure 8-9. Computer Program "DELTA", Lines 12-57.

```
62.             L=0
63.      470 L=L+1
64.             JS=JSDC
65.             JF=JFDC
66.             SPACE=SPAC1
67.             DEL=0
68.             ASSIGN 510 TO LINEX
69.             GO TO 160
70.      510 JS=JSAC
71.             JF=JFAC
72.             SPACE=SPAC1
73.             DEL=(SPACE/2)-1006
74.             ASSIGN 520 TO LINEX
75.             GO TO 190
76.      520 IF(L .NE. LAC) GO TO 470
77.             L=0
78.      515 L=L+1
79.             JS=JSDM
80.             JF=JFDM
81.             SPACE=SPAC2
82.             DEL=0
83.             ASSIGN 530 TO LINEX
84.             GO TO 160
85.      530 JS=JSAM
86.             JF=JFAM
87.             SPACE=SPAC2
88.             DEL=(SPACE/2)-946
89.             ASSIGN 540 TO LINEX
90.             GO TO 190
91.      540 IF(L .NE. LAM) GO TO 515
92.             L=0
93.      545 L=L+1
94.             JS=JSDG
95.             JF=JFDG
96.             SPACE=SPAC3
97.             DEL=0
98.             ASSIGN 550 TO LINEX
99.             GO TO 160
100.     550 JS=JSAG
101.            JF=JFAG
102.            SPACE=SPAC3
103.            DEL=(SPACE/2)-2542
104.            ASSIGN 560 TO LINEX
105.            GO TO 190
```

Figure 8-10. Computer Program "DELTA",
Lines 62-131.

```
106.      560 IF(L .NE. LAG) GØ TØ 545
107.          L=0
108.      565 L=L+1
109.          JS=JSEC
110.          JF=JFEC
111.          SPACE=SPAC4
112.          DEL=0
113.          ASSIGN 570 TØ LINEX
114.          GØ TØ 170
115.      570 JS=JSEM
116.          JF=JFEM
117.          SPACE=SPAC4
118.          DEL=0
119.          ASSIGN 580 TØ LINEX
120.          GØ TØ 190
121.      58C IF(L .NE. LVH) GØ TØ 565
122.          L=0
123.      585 L=L+1
124.          JS=JSEG
125.          JF=JFEG
126.          SPACE=SPAC5
127.          DEL=0
128.          ASSIGN 590 TØ LINEX
129.          GØ TØ 170
130.      590 IF(L.GE.LVL) GØ TØ 300
131.          Go to 585
```

Figure 8-10. Computer Program "DELTA" (Cont.)

i.   Repeat g and h for fields 2, 3, 4, etc., until the number of fields specified in line 9 is reached.

j.   Process the Commercial Enroute sequences for jet route No. 1.

k.   Process the Military Enroute sequences for jet route No. 1.

l.   Repeat j and k for jet routes 2, 3, 4, etc., until the number of high altitude airways specified in line 10 is reached.

m.   Process the General Aviation Enroute sequences for airway No. 1.

n.   Repeat m for airways 2, 3, 4, etc., until the number of low altitude airways specified in line 11 is reached.

Note: The numbers 1006, 946, and 2542, respectively, appearing in lines 73, 88, and 103 are correction factors to their respective arrival sequences. They ensure that the actual spacing, in seconds, between adjacent arrivals and departures using the same runway are equal to one-half the interval spacing (S) called out in the sequence files. These correction factors are necessary because the zero reference times of the sequences do not coincide with takeoffs and

-675-

landings but rather with the first voice transmission. In the case of departing aircraft, this first transmission occurs before it even taxis For arrival aircraft, it occurs just prior to penetration of the terminal area boundry.

8.8.2.4 **Lines 132 through 137 and 175 through 182** (See Figure 8-11)

These lines generate and scale the time separations between operations reference times at different airports, fields, bases and airways. These times are randomly selected by the random number generator in the subroutine of lines 175 through 182. This generator may be reinitiated by inserting any seven digit number for "IRAN" in line 135.

Figure 8-11. Computer Program "DELTA", Lines 132-182.

8.8.2.5 **Lines 138 and 139** (See Figure 8-12)

These lines cause the computer to record numerical values for the maximum length, in seconds, of each sequence; and to skip over that sequence; i.e., do not attempt to process, if its length is zero.

Figure 8-12. Computer Program "DELTA", Lines 138-139.

-676-

Note: If an entire sequence is removed from the CHARLIE file, a dummy
line should be inserted in its place to preserve the proper order of events
in the program. This dummy line should contain all zeros except for the
first and last number groups. The first number group should be an
appropriate consecutive line number; i.e., "J" number. The last should
contain the most significant (hundreds) figure of the Z numbers of the
sequence it replaces. Such a dummy line must also be included, and can
be seen in the example, at the end of the CHARLIE file to properly ter-
minate the program. A revised version of the BRAVO program, shown
in Figure 8-5, has been generated to insert these dummy lines automatically.
This revised program is included as Appendix V.

8.8.2.6 <u>Lines 140 through 167</u> (Refer to Figures 8-13 and 8-14)

These lines comprise the major computation task in which simulation time is
converted to sequence time, each sequence is searched to determine if it has an active
transmitter, and the number of active transmitters is totaled for printout. The process
is begun by initializing the dummy variable for number of simultaneous transmissions

```
140·            M=0
141·            N=0
142·       210  IF((KR+N*SPACE).GE.KE) GO TO 220
143·            N=N+1
144·            GO TO 210
145·       220  NMAX=N
146·       230  IF((KR+N*SPACE+TA).LE.KE) GO TO 240
147·            N=N-1
148·            GO TO 230
149·       240  NMIN=N
150·            N=NMIN
151·       250  TN=KE-KR-N*SPACE
152·            J=JS
153·       260  IF((TN.GE.F(J)).AND.(TN.LT.G(J))) GO TO 280
154·       270  J=J+1
155·            IF(J.LE.JF) GO TO 260
156·            N=N+1
157·            IF(N.LE.NMAX) GO TO 250
158·            GO TO 290
159·       280  M=M+1
160·            GO TO 270
161·       290  R=R+M
162·       295  GO TO LINEX
163·       300  IF(R.EQ.U) GO TO 700
164·            WRITE(1,600) KE,R
165·            WRITE(2,600) KE,R
166·       600  FORMAT(F5.,3X,F5.)
167·       700  U=R
```

Figure 8-13. Computer Program "DELTA", Lines 140-167.
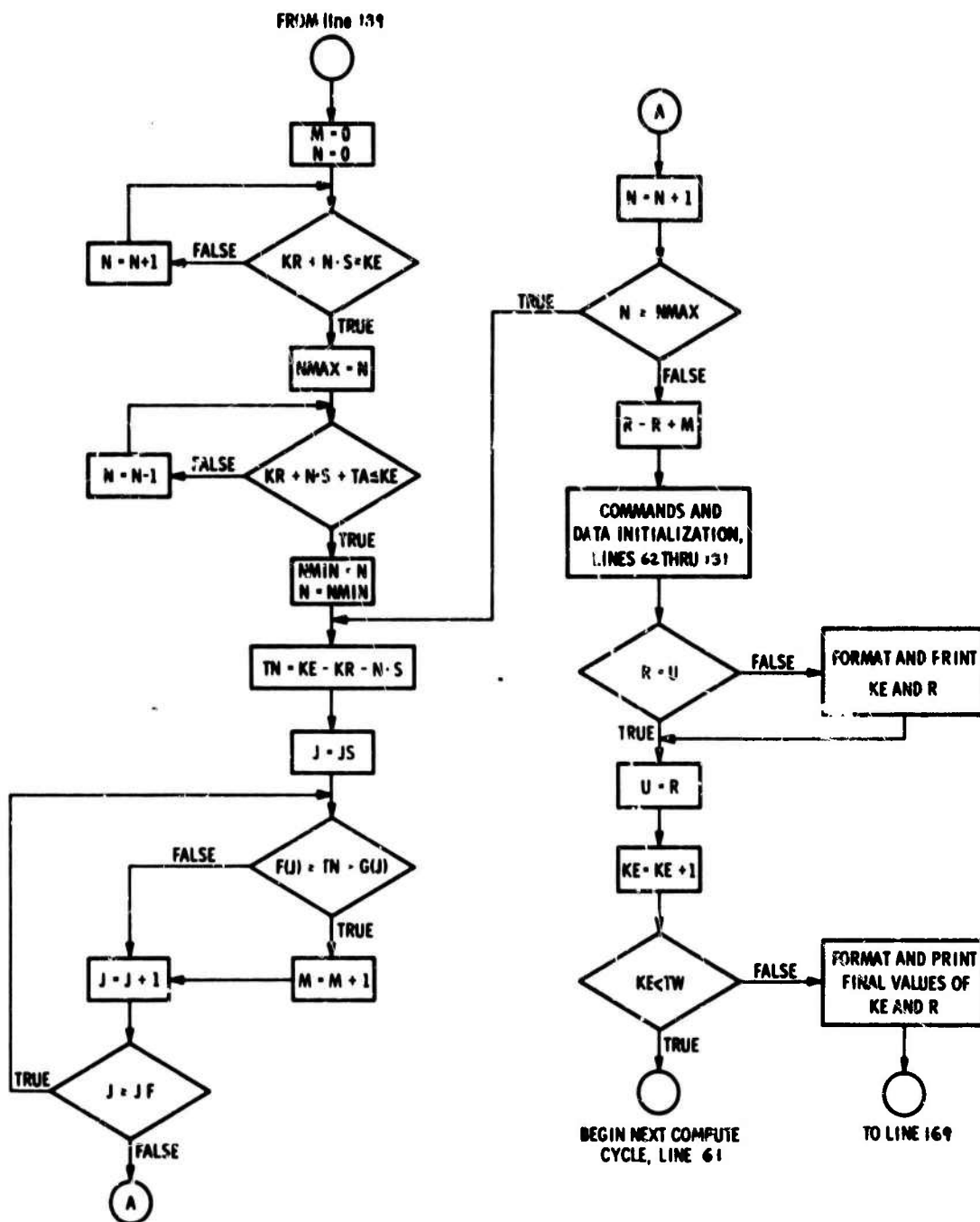
Figure 8-14. Flow Diagram for Lines 140 through 168.

-678-

M at zero in line 140. The next nine lines comprise a logical computation to determine the number of sequences that actually overlap the simulation time increment under investigation. The number of the first of these is assigned the designation NMIN while the last is assigned NMAX. There are other sequences that lie within the look period and either precede NMIN or follow NMAX. However, by computing the values for NMIN and NMAX, the succeeding computations are constrained to process only those sequences that lie between these two values, thus saving considerable computation time that might be wasted on searching through irrelevant message sequences.

Line 150 sets the number designator of the first sequence to be investigated as NMIN. Then line 151 converts simulation time KE to sequence time TN using the previously calculated value for the interval time between the prime sequence zero reference and the simulation zero reference (the random number KR), as well as the sequence number designator N, and the interval spacing between identical messages S obtained from the CHARLIE file. With this accomplished, the CHARLIE file line number J of the first message to be examined is set at the previously set START value JS in line 152.

At this point, the program enters an iterative loop consisting of lines 153 through 160. The previously converted value of simulation time TN is checked by the logic equation in line 153 to determine if it lies between the transmission start and end times, F(J) and G(J), respectively, that appear on line number J in the CHARLIE file. If it does, the dummy variable M is increased by one. If it does not, M remains unchanged from its previous value. In either case, the line number J is increased by one in order to evaluate the next line in the CHARLIE file. However, before the next evaluation takes place, the value of J is checked in line 155 to determine whether it has reached the previously computed number of the FINISH line JF of the sequence under investigation. If it has not, lines 153 through 155 are repeated until it does, thus examining all lines in the sequence. If the value of J has reached JF, the dummy variable for the sequence number N is increased in line 156, by one in order to start examination of the next sequence. However, before this occurs, the value of N is checked to determine if it has reached the previously computed value for the last sequence number NMAX. If it has not, lines 151 through 156 are repeated until all sequences have been examined. If N has reached NMAX, the number of simultaneous transmissions is recorded as R in line 161.

Note: If it were not for the special timing relationship between arrivals and departures at the same airport, the value M could be recorded directly as the number of simultaneous transmissions. However, since arrivals and departures at the same airport are time separated by a constant, and are subject to the same random number (KRAN, see line 136), the value M must be computed twice for the same time increment investigated, i.e., once for departures, and again for arrivals. Therefore, the dummay variable R is initialized at zero and then equated to M when the departure sequence examinations are completed. At this point M is reset to zero and the arrival sequence examinations are started. When these are complete, the resulting new value of M is added to the previous value (now recorded as R) to create a new R that is the sum of all simultaneous transmissions in arrivals and departures. The assigned "go to" statement in line 162 and the commands discussed in paragraph 8.8.2.3 then continue cycling the program until R represents the sum of all the M's for sequences of all user classes including those for the enroute flight phase as well as for departures and arrivals.

The value of U in line 163 was initialized at zero in line 60. However, as soon as the first time increment has been investigated, U represents the value of R for the previous time increment. In line 163, U is checked for equality with R in the present sequence. If U does not equal R, the value of R is printed out along with the simulation time increment KE by lines 164 and 166.

8.8.2.7 Lines 168 through 171 (See Figure 15)

Continuing the above explanation, if U does equal R, i.e., no change in the number of simultaneous transmissions has taken place since the previous time increment, no print out is made. Instead, the program is cycled to the next time increment (by raising the value of KE by one in line 168 in preparation for repeating the next computation of R. However, before proceeding with the next cycle, the value of KE is checked in line 169 to determine if the end of the "look window" has been reached. If it has, the final values of KE and R are printed out, the CHARLIE file is closed, and the program is ended.

```
168.          KE=KE+1
169.          IF(KE.LT.TW) GO TO 100
170.          WRITE(1,600) KE,R
171.          CLOSE(4)
```

Figure 8-15. Computer Program "DELTA", Lines 168-171.

8.9 PRESENTATION AND DISCUSSION OF RESULTS

The output file generated in simulation run No. 2 is shown in Appendix IX.
Thus far, three runs have been made to examine the following situations:

a.   All accesses available (no filtering by the BRAVO program).

b.   All accesses except Ground Control and Clearance Delivery
      available.

c.   Only Ground Control, Clearance Delivery and Aircraft
      accesses available.

This series was chosen to evaluate the impact on the total multiple access problem of
those accesses used exclusively by aircraft on airport surfaces. Presumably, if it
became necessary to limit the number of active accesses due to other waveform design
considerations, these surface accesses could be handled differently than those required
for airborne aircraft. They could be handled differently because; transceivers operating
in these accesses need not radiate beyond the boundaries of airports, and it is reason-
able to assume that in most cases, potential interferers at different airports will never
be in radio line-of-sight of each other.

All three runs are plotted in Figure 8-16. It can be seen that the ground control
and clearance delivery channels do have considerable impact on the total user traffic.
This was anticipated because of the lengthy transmissions that occur on the clearance
delivery channel. However, the potential queueing of users is considerably less than
anticipated. The following data was obtained from the simulation run results.

Run No.	Accesses	Number of Simultaneous Users			
		Maximum	Minimum	Mean	Variance
1	All	87	24	55.1	202.8
2	All but GC CD	75	15	41.5	176.1
3	GC, CD AF only	33	0	13.5	64.1

These results characterize the multiple access situation in the 150 nautical mile
diameter circular ground projection of the scenario air space. The 479 aircraft in
this area individually occupy, on the average, 36.89 square miles, resulting in an
average spacing of each aircraft from its closest neighbors of 6.07 nmi. However,
as was shown in Section 8.6.7, the actual average spacing on high altitude airways
(jet routes) would be 16 nmi, while on low altitude airways it would be 7.6 nmi. In
airport approach and departure patterns spacing would be down to one nmi. On airport
surfaces, actively transmitting aircraft may be within a wingspan of each other.

682
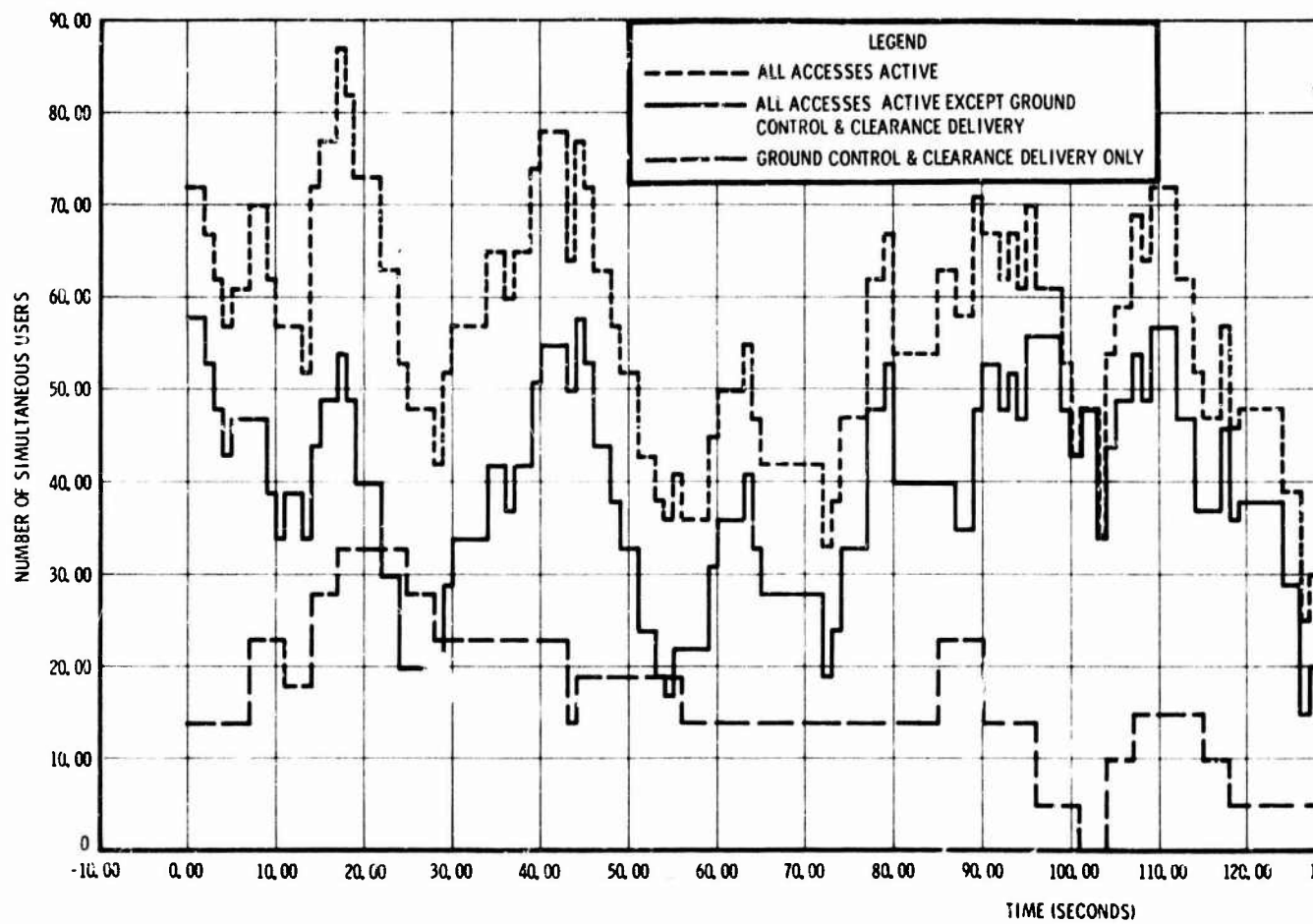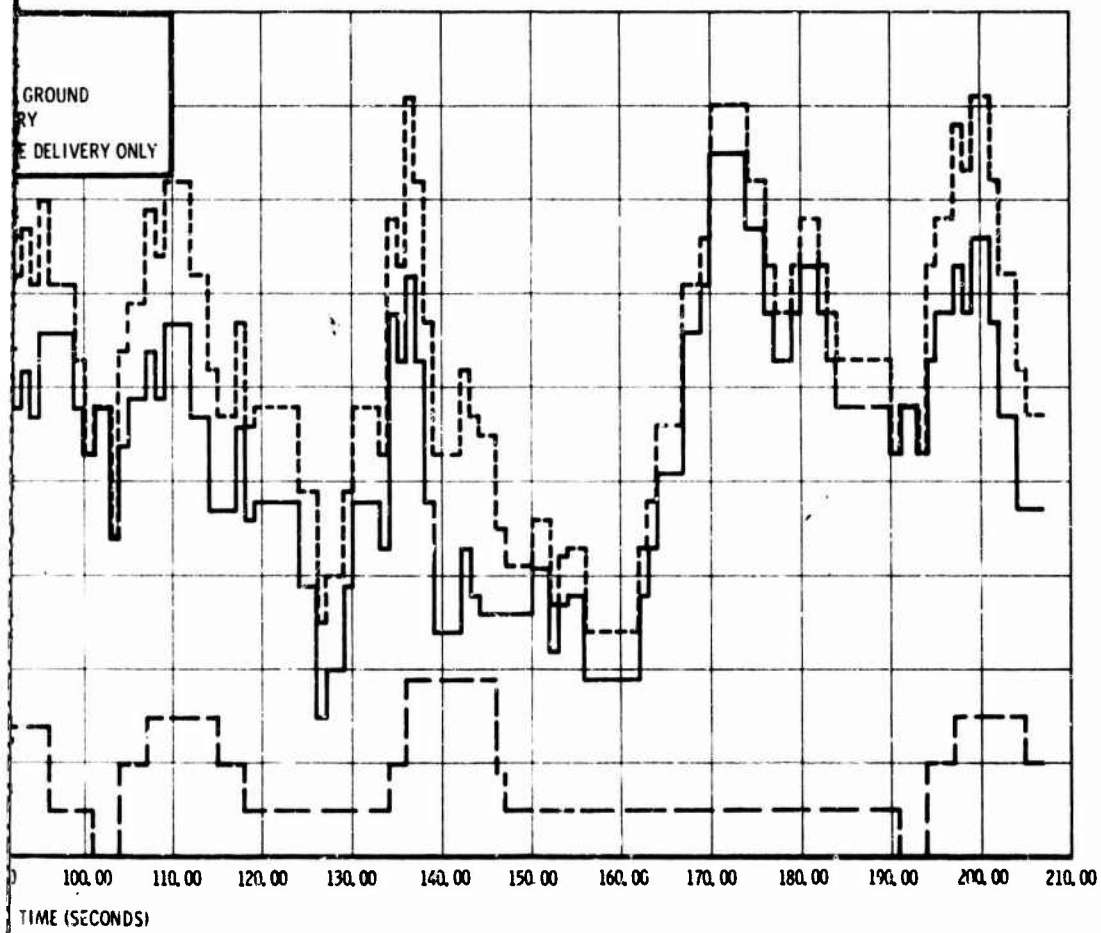
Figure 8-16. User Queuing Versus Simulation Time

It should be recalled that the aircraft density producing the above results is based on a saturated condition at the commercial airports. That is, these airports cannot accept or release aircraft at a faster rate than that presumed in the simulation. The only ways of increasing the population density of aircraft would be the inclusion of more commercial airports or parallel runways, increasing the relative proportions of military or general aviation aircraft, or increasing the proportion of enroute aircraft of all classes. At present, there is no evidence to support doing any of these things as the data used includes future expansion factors.

Scenario areas described as 250 and 500 nmi diameter circles are frequently mentioned in connection with CNI studies. This is probably due to the 250 nmi line-of-sight radio/radar range typical of high altitude aircraft. If the population density of aircraft in the ATC scenario were projected to fill these 250 and 500 mi circles, then they would enclose 1,331 and 5,332 aircraft respectively. However, this simple projection of the same density into a larger area is not considered realistic because it is more likely that the peripheral areas would be much less densely populated than the center area. Reasonable approximations to the traffic density in these extended areas and the resulting impact on multiple access can be made by finding the typical density in the peipheral areas and adding this to the results already obtained. For example, the 250 mi and 500 mi areas would result in the respective additions of 400 nmi and 1400 nmi of high altitude airways. Maintaining the same separation of aircraft on airways already developed would result in the respective additions of 53 and 189 additional enroute jet aircraft to be added to those already present. This one factor alone would raise the total aircraft in the scenario volumes to 532 and 663 respectively. Other factors to be considered are the low altitude airways, outlying airfields and adjacent traffic control centers.

Note: These results are based on simulation runs equivalent to periods of observation (look window widths) of only 205 seconds. It is believed that simulation runs equivalent to look windows of 580 seconds will reveal all the essential data that can be obtained from the simulation. This is because the longest interval spacing (the parameter S) in the input data is 579 seconds and, therefore, the output data should become essentially cyclic, with minor randomness, after this length of time. However, thus far computer runs longer than those presented in Figure 8-15 have not been made due to the extended computer time required for this program.

8.10 DATA LINKS

The baseband information transmitted via a CNI waveform may be categorized
as follows:

1. Information required on a routine or cyclic basis such as:
   - Data required for an aircraft to determine its own
     navigational position.
   - Data required by traffic or tactical control facilities
     to track the aircraft and label its "blip" on dynamic
     situation displays.
   - Routine tactical or flight information data exhcange
     between aircraft and ground.
2. Information required on demand such as:
   - Identification of an unknown target by interceptors
     or other weapon control facilities, and traffic
     control facilities.
   - Voice traffic.

Information in Category 1 is amenable to organization schemes involving coordination
between users and repetitive sequential data transfer in order to maintain orthogonality
and avoid mutual interference. Information in Category 2 is difficult to organize and
subject to periods when the data transfer demand may exceed the data rate of the CNI
waveform (queueing). Thus far, the analysis has addressed voice traffic, and it has
been presumed that all voice traffic falls in the "on demand" category. Much of this
voice traffic and, consequently, the multiple access problems it causes could be
eliminated by isolating those voice messages that are concerned with transferring
Category 1 type data and transmitting them on an organized data link net. The most
immediately apparent types of messages that can be isolated for data link transmission
are those concerned with transferring the data required for flight following and hand-
off from one traffic control unit to the next. These data requirements were listed in
Section 8.5.2. When these data are transferred by voice link, 30 to 45 percent of
the required transmission time is wasted in establishing initial contact and in self-
identification. For example, consider the following sequence:

1. Air Force 4-1-1-9-5, This is New York Radio, over.
2. New York, Air Force 4-1-1-9-5, go ahead.
3. Air Force 1-9-5, New York, request your present position, over.

-684-

4. New York, 1-9-5, crossing Hampton VORTAC at one-zero thousand, over.

5. 1-9-5, New York, roger. contact Boston Radio on one-three-two point four at Montauk intersection, over.

6. Air Force 1-9-5, roger out. Note: At this point, Air Force 195 may repeat part or all of Transmission 5 at his discretion for New York's approval to be certain he has copied it correctly. Upon reaching Montauk, Air Force 195 manually switches from New York's frequency to Boston's (132.4 MHz) and calls Boston.

7. Boston Radio, this is Air Force 4-1-1-9-5, Montauk intersection, one-zero thousand, over.

8. Air Force 4-1-1-9-5, Boston, roger, squawk mode 3, code one-one, over.

9. 1-9-5 roger, squawking mode 3, code one-one, over.
   195, Boston, have you in radar contact, contact Boston Approach Control on one-two-four point four at Providence, over.

Note: At Providence, Air Force 195 will again manually change frequency and another round of alerting and identifying transmissions will ensue. The same thing will happen again when 195 switches from Boston Approach Control to Hanscom Tower (L. G. Hansom Field has been assumed as the aircraft's destination in this hypothetical example).

Transmission series such as this account for 22 percent of all transmissions in the enroute flight phase, 10 percent in the arrival phase and 20 percent in the departure, ground, and local control phases. These are the transmissions concerned only with tracking and identifying the aircraft during its progress along its route. If data items a, b, c, d, f, and g shown in Section 8.5.2 were routinely exchanged between aircraft and ground stations on a coordinated data link net, virtually all transmission series of the above type could be eliminated. With a data transmission rate of 2400 bits per second, each aircraft could provide ground stations with all the data necessary for tracking and identification in a 50 millisecond transmission burst. Burst's could be transmitted on a cyclic basis according to some coordination scheme, or they could be triggered by interrogation from the ground. In either case, it seems reasonable to have the various ground stations along an aircraft's flight path automatically access the aircraft's address rather than continue the present practice of manual frequency changes by the pilots to access the various ground stations. This

point becomes particularly pertinent in the case of SST's. Such aircraft will fly from one ground station's area of jurisdiction to another's more quickly than the present voice report-in, beacon control, hand-off, and manual frequency change procedures will permit.

Another important area for consideration of data links is in the delivery of flight clearances. It was shown in Section 8.9 that considerable queueing occurs due to the longer than average length of these transmissions. If some form of data buffering and a readout device are provided in aircraft, clearances could be data linked with considerable reduction in channel queueing. For example, consider the following typical clearance:

> ATC clears Air Force 41195 to the Tulsa Airport via Victor 14. Turn right after departure, proceed direct to the Oklahoma City Vortac. Maintain three thousand to the Oklahoma City Vortac. Hold West on the Oklahoma City 277 radial. Climb to five thousand in the holding pattern before proceeding on course. Maintain five thousand until crossing the Ponca City 167 Radial. Climb to and maintain seven thousand. Departure control frequency will be 121.1. [*]

This clearance takes approximately 35 seconds to transmit at average speed by voice, not including prefixes and suffixes required by radio procedures. If data linked at 2400 bits per second, it would require 1.068 seconds to transmit, assuming 6 bits per alphanumeric character. If hard-copy readout is provided in the aircraft, the additional time required for pilot readback would also be eliminated.

Finally, standardized instructions such as "climb to (altitude), descend to and maintain (altitude)", etc. could be data linked and displayed in the cockpit rather than accepted by voice. Displays such as the one shown in Figure 8-17 have been proposed for this purpose. Their stylized nature enables data linking with greater bit-economy than plain English text.

_____

[*] Pilot's Radio Handbook, Federal Aviation Agency, Washington, D.C., 1962.

Display Readout	Interpretation

Descend to 6000 feet.
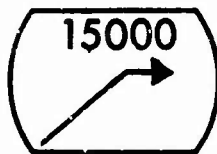
Climb to and maintain 15000 feet

Report reaching Oklahoma City VORTAC.

Figure 8-17. Data Link Displays

8.11 IDENTIFICATION

8.11.1 COORDINATED IDENTIFICATION

Many of the problems of the current IFF system arise because of the lack of coordination among interrogators and the lack of selectivity in interrogations, i.e., each interrogation elicits many replies in addition to the desired one. In an effort to reduce the proliferation of responses, methods of coordinating the identification system are worthy of consideration.

8.11.2 SPONTANEOUS REPLIES

In this approach, each aircraft is given an assigned slot position in a TDMA channel. Each time its slot comes up, the aircraft broadcasts an identity/position report. All would-be interrogators monitor this channel, selecting, by identity or position, those messages that are of interest for further display, computation or other action. The position data contained within these messages could be in a common grid coordinate system, derived from the ICNI navigation subsystem. The required

-687-

data was presented in Section 8.5.2. This method of spontaneous replies is useful for flight following and collision avoidance as well as identification. The disadvantage of this scheme is the necessity of allocating the slots to aircraft on a dynamic basis in order to obtain reasonable efficiency in the use of the channel.

8.11.3 COORDINATED INTERROGATION

It might be somewhat easier administratively to organize the interrogators rather than the responders. In this approach, each interrogator would be assigned a slot in a TDMA frame. In this frame it would transmit a short message requesting either an identity reply from an aircraft to a stated location, or alternatively a position report from a given aircraft. Thus, an aircraft would receive interrogations in non-overlapping sequence and the replies would then organize similarly.

APPENDIX I
AIRPORT DISTRIBUTION IN HIGH DENSITY TRAFFIC AREAS
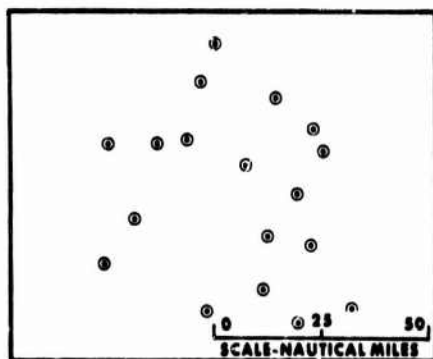
BOSTON
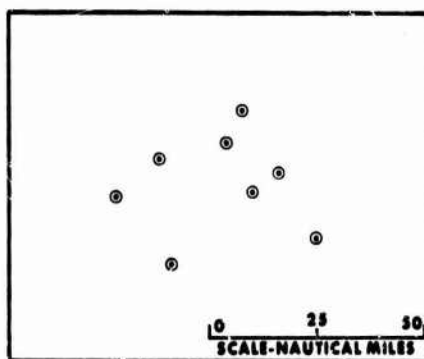
CHICAGO
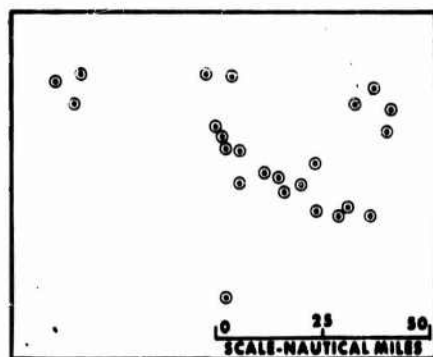
LOS ANGELES
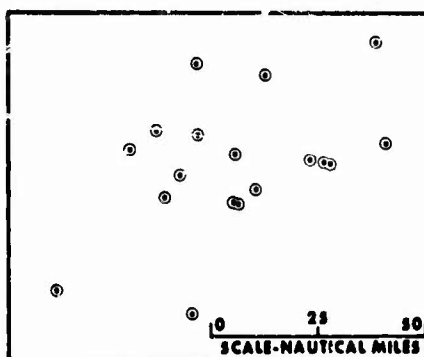
NEW YORK
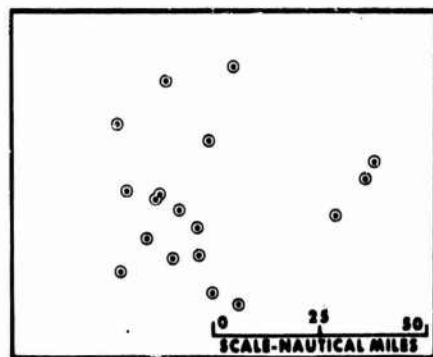
SAN FRANCISCO
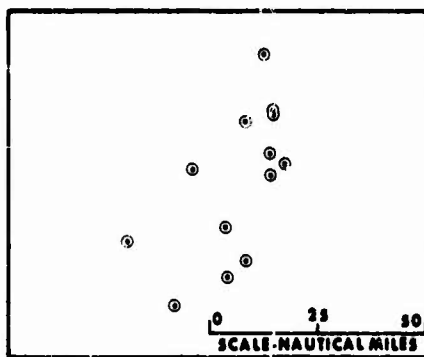
SEATTLE (not used)
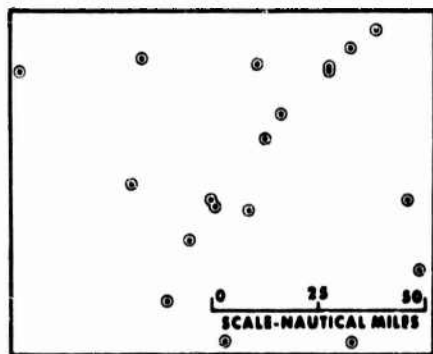
WASHINGTON D.C.

COMPOSITE

SCALE-NAUTICAL MILES

-689-
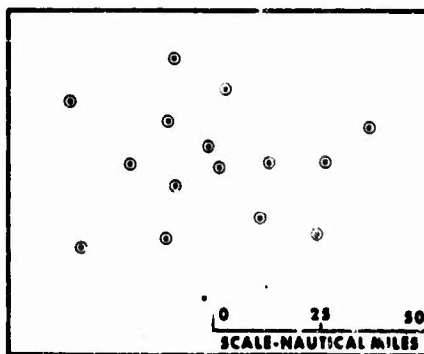
APPENDIX II

VOICE MESSAGE TEXT CATEGORIES

1. Clearances:	Route Ammended Route Taxi Takeoff Hold Approach Land Altitude Change Speed Change Cancellation Expect Further Clearance Per Request
2. Instructions:	Taxi Departure Route Approach Altitude Change Heading Change (Vector) To Report Read Back To Acknowledge Go-around
3. Routine Reports:	Reaching) Leaving } Altitude Passing) Entering } Departing } Holding Entering } Departing } Traffic Pattern Commencing Approach Out of; e.g., Procedure Turn Executing; e.g., Missed Approach
4. Status Reports:	Pattern or Area Position Overland Position Ocean Position Configuration (fuel, gear, flaps, persons aboard, etc.) Present Heading Present Speed

5. Special Reports:	PIREPS POMAR CIRVIS Near Miss Lost Failure Accident Emergency Unusual Event
6. Advisories:	Traffic Present Weather Forecast Weather Winds Aloft Unusual Condition Cautionary Facilities Status Notice of Intentions Notice to Standby
7. Requests:	Clearances Instructions Reports Advisories Assistance Supports Services
8. Supports:	Call-up Acknowledgement Report-In Hand-Off
9. Amplifying Remarks	
10. Miscellaneous	Beacon Control Commands and Responses

APPENDIX III

TYPICAL MESSAGE SEQUENCE
DEPARTURE – ENROUTE – ARRIVAL

Aircraft Message	Ground Message
START 1. Call CD, Request Clearance 3. Acknowledge 4. Call FSS, Request Weather Data 6. Acknowledge 7. Call CR 9. Acknowledge and Exchange Data 11. Monitor ATIS	 2. CD Says Standby 5. FSS Responds with Weather 8. CR Acknowledges with Data 10. CR Acknowledge
WAIT 2. Inform CD of Rediness to Copy Clearance 4. Readback Clearance to CD 6. Acknowledge	 1. CD Calls 3. CD Reads Clearance 5. CD Acknowledges and Amplifies
WAIT 1. Call GC, State Position and Intentions 3. Acknowledge	 2. GC Provides Instructions
TAXI 1. Monitor ATIS and NAV 2. Call TW with Position and Intentions 4. Acknowledge	 3. TW Issues Taxi and Hold Instruction
TAKE-OFF 2. Acknowledge 3. Call TW When Airborne	 1. TW Issues Take-Off Clearance and Instruction for Hand-Off to DP. 4. TW Acknowledge

Aircraft Message	Ground Message
TAKE-OFF (Continued) 5. Call CR with Time Off, Fuel Status, Gross Weight, Passenger Data and FTA 7. Call DP with Position and Status 9. Acknowledge and Comply	 6. CR Acknowledge 8. DP Acknowledge with Ident. Instr.
DEPARTURE 2. Acknowledge with Readback 3. Call DP with Position (check in with new sector) 5. Acknowledge with Readback	 1. DP Calls with Nav. Instr. and Sector Hand-off 4. DP Calls with NAV. Instr. and Hand Off to ARTCC
ENROUTE 1. Call ARTCC with Position 3. Acknowledge and Comply 5. Supply Heading Data 7. Acknowledge Readback and Comply	 2. ARTCC Acknowledge with Ident. Instr 4. ARTCC Requests Heading 6. ARTCC Issues Turn Instruction
CRUISE 1. Request Altitude Change 3. Acknowledge with Readback 4. Report Leaving Present Altitude 6. Report Passing Altitude Level Called Out in Instructions 8. Report Reaching Altitude 11. Acknowledge with Readback	 2. ARTCC Issues Altitude Change Instr. 5. ARTCC Acknowledge 7. ARTCC Acknowledge 9. ARTCC Acknowledge 10. ARTCC Calls with Hand Off to Next Center
CRUISE 1. Call ARTCC with Position 3. Call CR, Request Weather Data	 2. ARTCC Acknowledge 4. CR Supplies Weather Data

Aircraft Message	Ground Message
CRUISE (Continued) 5. .cknowledge 6. Call ARTCC, Request Weather Data 8. Acknowledge	 7. ARTCC Supplies Weather Data
CRUISE 1. Call ARTCC 3. Give Position Report to ARTCC 5. Call CR 7. Give Maintenance Report, ETA and Request Gate Assignment 10. Acknowledge 12. Acknowledge with Readback 13. Report Leaving Present Altitude 15. Report Passing Altitude Level Called in Instruction 17. Report Reaching Altitude	 2. ARTCC Acknowledge 4. ARTCC Acknowledge with Data 6. CR Acknowledge 8. CR Acknowledge and Supply Data 9. ARTCC Calls 11. ARTCC Issues Altitude Change Instruction 14. ARTCC Acknowledge 16. ARTCC Acknowledge 18. ARTCC Acknowledge
ARRIVAL 1. Call ARTCC with Position 3. Acknowledge with Readback and Report Leaving Altitude	 2. ARTCC Acknowledge with Altitude Change, NAV Instruction and Hand-Off to Next Sector
DESCEND 1. Report Passing Intersection with Altitude 3. Call ARTCC with Position 5. Acknowledge with Readback and Report Leaving 6. Monitor ATIS	 2. ARTCC Acknowledge 4. ARTCC Acknowledge with Altitude Change, NAV Instruction and Hand-Off to Next Sector

Aircraft Message	Ground Message
DESCEND (Continued) 7. Report Passing Intersection with Altitude 9. Acknowledge with Readback 10. Call AP with Position and Altitude 12. Acknowledge with Readback and Comply	 8. ARTCC Acknowledge with Hand-Off to AP 11. AP Acknowledge with Vector and Altitude Instruction
APPROACH 1. Call AP with Position and Altitude 3. Acknowledge with Readback and Comply 5. Acknowledge with Readback 6. Call TW with Position 8. Acknowledge	 2. AP Acknowledge with Vector and Altitude Instruction 4. AP Calls with NAV Data and Hand-Off to TW 7. TW Acknowledges with Data
LAND 1. Call TW with Position 3. Call CR with Time On and Maintenance Data	 2. TW Acknowledges with Landing Clearance 4. CR Acknowledges and Verifies Gate Assignment
TAXI 2. Call GC with Position and Intentions 4. Acknowledge	 1. TW Calls with Hand-Off to GC 3. GC Acknowledge with Instruction
TAXI AND SHUT-DOWN	

APPENDIX IV

ALPHA FILE

This file comprises the primary input data for the simulation program   Key to file codes may be found in Table 8-4.

Table IV-1. ALPHA File, Commercial Departures.

1,49

AF	C	0	CD	C	0	DC	101	0	5	90
CD	C	0	AF	C	0	DC	102	5	10	90
AF	C	0	CD	C	0	DC	103	10	12	90
AF	C	0	CR	C	0	DC	104	60	63	90
CR	C	0	AF	C	0	DC	105	63	90	90
AF	C	0	CR	C	0	DC	106	90	94	90
CR	C	0	AF	C	0	DC	107	94	95	90
CD	C	0	AF	C	0	DC	108	240	246	90
AF	C	0	CD	C	0	DC	109	246	248	90
CD	C	0	AF	C	0	DC	110	248	285	90
AF	C	0	CD	C	0	DC	111	285	322	90
CD	C	0	AF	C	0	DC	112	322	326	90
AF	C	0	CD	C	0	DC	113	326	327	90
AF	C	0	GC	C	0	DC	114	420	426	90
GC	C	0	AF	C	0	DC	115	426	428	90
AF	C	0	GC	C	0	DC	116	428	431	90
AF	C	0	TW	C	0	DC	117	600	603	90
TW	C	0	AF	C	0	DC	118	603	607	90
AF	C	0	TW	C	0	DC	119	607	608	90
TW	C	0	AF	C	0	DC	120	630	638	90
AF	C	0	TW	C	0	DC	121	638	639	90
AF	C	0	TW	C	0	DC	122	675	681	90
TW	C	0	AF	C	0	DC	123	681	683	90
AF	C	0	CR	C	0	DC	124	687	702	90
CR	C	0	AF	C	0	DC	125	702	704	90
AF	C	0	DP	N	1	DC	126	705	712	90
DP	N	1	AF	C	0	DC	127	712	714	90
AF	C	0	DP	N	1	DC	128	714	717	90
DP	N	1	AF	C	0	DC	129	843	856	90
AF	C	0	DP	N	1	DC	130	856	869	90
AF	C	0	RC	N	1	DC	131	1023	1027	90
RC	N	1	AF	C	0	DC	132	1027	1040	90
RC	N	1	AF	C	0	DC	133	1203	1211	90
AF	C	0	RC	N	1	DC	134	1211	1219	90
AF	C	0	RC	N	1	DC	135	1323	1329	90
RC	N	2	AF	C	0	DC	136	1329	1331	90
AF	C	0	RC	N	2	DC	137	1331	1334	90
RC	N	2	AF	C	0	DC	138	1335	1342	90
AF	C	0	RC	N	2	DC	139	1342	1349	90
AF	C	0	RC	N	2	DC	140	1350	1353	90
RC	N	2	AF	C	0	DC	141	1353	1354	90
AF	C	0	RC	N	2	DC	142	1530	1533	90
RC	N	2	AF	C	0	DC	143	1533	1534	90
AF	C	0	RC	N	2	DC	144	1710	1713	90
RC	N	2	AF	C	0	DC	145	1713	1714	90
RC	N	2	AF	C	0	DC	146	2250	2255	90
AF	C	0	RC	N	2	DC	147	2255	2260	90
AF	C	0	RC	N	3	DC	148	2490	2499	90
RC	N	3	AF	C	0	DC	149	2499	2500	90

Table   IV-2.   ALPHA File, Commercial Arrivals

```
50,79
AF C 0   RC N 3   AC   801      0      9    90
RC N 3   AF C 0   AC   2C2      9     24    90
AF C 0   RC N 3   AC   203     24     39    90
AF C 0   RC N 3   AC   204    148    151    90
RC N 3   AF C 0   AC   205    151    152    90
AF C 0   RC N 3   AC   206    257    260    90
RC N 3   AF C 0   AC   207    260    275    90
AF C 0   RC N 3   AC   208    275    305    90
AF C 0   RC N 3   AC   309    366    369    90
RC N 3   AF C 0   AC   210    369    378    90
AF C 0   RC N 3   AC   211    378    387    90
AF C 0   RC N 2   AC   212    474    483    90
RC N 2   AF C 0   AC   213    483    493    90
AF C 0   RC N 2   AC   214    493    503    90
AF C 0   AP N 1   AC   215    710    719    90
AP N 1   AF C 0   AC   216    719    729    90
AF C 0   AP N 1   AC   217    729    739    90
AP N 0   AF C 0   AC   218    917    921    90
AF C 0   AP N 1   AC   219    921    924    90
AF C 0   TW C 0   AC   220   1134   1140    90
TW C 0   AF C 0   AC   221   1140   1150    90
AF C 0   TW C 0   AC   222   1150   1151    90
AF C 0   TW C 0   AC   223   1382   1388    90
TW C 0   AF C 0   AC   224   1388   1391    90
AF C 0   CR C 0   AC   225   3005   1627    90
CR C 0   AF C 0   AC   226   1627   1634    90
TW C 0   AF C 0   AC   227   1644   1651    90
AF C 0   GC C 0   AC   228   1654   1658    90
GC C 0   AF C 0   AC   229   1658   1663    90
AF C 0   GC C 0   AC   230   1663   1665    90
```

Table IV-3. ALPHA File, Military Departures

```
80,118
AF  M  0   CD  M  0   DM   301      0      5    560
CD  M  0   AF  M  0   DM   302      5     10    560
AF  M  0   CD  M  0   DM   303     10     12    560
CD  M  0   AF  M  0   DM   304    240    246    560
AF  M  0   CD  M  0   DM   305    246    248    560
CD  M  0   AF  M  0   DM   306    248    285    560
AF  M  0   CD  M  0   DM   307    285    322    560
CD  M  0   AF  M  0   DM   308    322    326    560
AF  M  0   CD  M  0   DM   309    326    327    560
AF  M  0   GC  M  0   DM   310    420    426    560
GC  M  0   AF  M  0   DM   311    426    428    560
AF  M  0   GC  M  0   DM   312    428    431    560
AF  M  0   TW  M  0   DM   313    600    603    560
TW  M  0   AF  M  0   DM   314    603    607    560
AF  M  0   TW  M  0   DM   315    607    608    560
TW  M  0   AF  M  0   DM   316    630    638    560
AF  M  0   TW  M  0   DM   317    638    639    560
AF  M  0   TW  M  0   DM   318    675    681    560
TW  M  0   AF  M  0   DM   319    681    683    560
AF  M  0   DP  N  1   DM   320    705    712    560
DP  N  1   AF  M  0   DM   321    712    714    560
AF  M  0   DP  N  1   DM   322    714    717    560
AF  M  0   DP  N  1   DM   323    818    825    560
DP  N  1   AF  M  0   DM   324    825    833    560
AF  M  0   RC  N  1   DM   325    998   1002    560
RC  N  1   AF  M  0   DM   326   1002   1015    560
AF  M  0   RC  N  0   DM   327   1015   1020    560
AF  M  0   RC  N  1   DM   328   1178   1191    560
RC  N  1   AF  0  0   DM   329   1191   1199    560
AF  M  0   RC  N  1   DM   330   1199   1207    560
AF  M  0   RC  N  2   DM   331   1358   1361    560
RC  N  2   AF  M  0   DM   332   1361   1362    560
AF  M  0   RC  N  2   DM   333   1808   1814    560
RC  N  2   AF  M  0   DM   334   1814   1816    560
AF  M  0   RC  N  2   DM   335   1816   1819    560
RC  N  2   AF  M  0   DM   336   2023   2036    560
AF  M  0   RC  N  2   DM   337   2036   2044    560
AF  M  0   RC  N  3   DM   338   2258   2265    560
RC  N  3   AF  M  0   DM   339   2265   2268    560
```

Table IV-4. ALPHA File, Military Arrivals

119,148

AF	M	0	RC	N	3	AM	401	0	9	560
RC	N	3	AF	M	0	AM	402	9	24	560
AF	M	0	RC	N	3	AM	403	24	39	560
AF	M	0	RC	N	3	AM	404	552	561	560
RC	N	3	AF	M	0	AM	405	561	576	560
AF	M	0	RC	N	3	AM	406	576	591	560
AF	M	0	RC	N	2	AM	407	816	825	560
RC	N	2	AF	M	0	AM	408	825	840	560
AF	M	0	RC	N	2	AM	409	840	855	560
AF	M	0	AP	N	1	AM	410	1080	1084	560
AP	N	1	AF	M	0	AM	411	1084	1088	560
AF	M	0	AP	N	1	AM	412	1088	1089	560
AF	M	0	AP	N	1	AM	413	1200	1203	560
AP	N	1	AF	M	0	AM	414	1203	1204	560
AF	M	0	AP	M	1	AM	415	1260	1263	560
AP	N	1	AF	M	0	AM	416	1263	1264	560
AF	M	0	AP	N	1	AM	417	1320	1323	560
AP	N	1	AF	M	0	AM	418	1323	1326	560
AF	M	0	AP	N	1	AM	419	1440	1443	560
AP	N	1	AF	M	0	AM	420	1443	1449	560
AF	M	0	AP	N	1	AM	421	1449	1450	560
AF	M	0	TW	M	0	AM	422	1451	1454	560
TW	M	0	AF	M	0	AM	423	1454	1457	560
AF	M	0	TW	M	0	AM	424	1457	1458	560
AF	M	0	TW	M	0	AM	425	1550	1553	560
TW	M	0	AF	M	0	AM	426	1553	1554	560
TW	M	0	AF	M	0	AM	427	1584	1590	560
AF	M	0	GC	M	0	AM	428	1595	1599	560
GC	M	0	AF	M	0	AM	429	1599	1604	560
AF	M	0	GC	M	0	AM	430	1604	1606	560

Table IV-5. ALPHA File, General Aviation Departures

149,194

AF	G	0	CD	G	0	GD	501	0	5	578
CD	G	0	AF	G	0	GD	502	5	10	578
AF	G	0	CD	G	0	GD	503	10	12	578
AF	G	0	GC	G	0	GD	504	22	28	578
GC	G	0	AF	G	0	GD	505	28	34	578
CD	G	0	AF	G	0	GD	506	300	303	578
AF	G	0	CD	G	0	GD	507	303	305	578
CD	G	0	AF	G	0	GD	508	305	342	578
AF	G	0	CD	G	0	GD	509	342	379	578
CD	G	0	AF	G	0	GD	510	379	383	578
AF	G	0	TW	G	0	GD	511	388	391	578
TW	G	0	AF	G	0	GD	512	391	395	578
AF	G	0	TW	G	0	GD	513	395	396	578
TW	G	0	AF	G	0	GD	514	410	418	578
AF	G	0	TW	G	0	GD	515	418	419	578
AF	G	0	TW	G	0	GD	516	429	435	578
TW	G	0	AF	G	0	GD	517	435	437	578
AF	G	0	DP	N	1	GD	518	437	444	578
DP	N	1	AF	G	0	GD	519	444	447	578
AF	G	0	DP	N	1	GD	520	447	449	578
AF	G	0	DP	N	1	GD	521	598	601	578
DP	N	1	AF	G	0	GD	522	601	602	578
AF	G	0	DP	N	1	GD	523	718	721	578
DP	N	1	AF	G	0	GD	524	721	729	578
AF	G	0	DP	N	1	GD	525	729	737	578
AF	G	0	DP	N	1	GD	526	1198	1201	578
DP	N	1	AF	G	0	GD	527	1201	1202	578
AF	G	0	DP	N	1	GD	528	1678	1681	578
DP	N	1	AF	G	0	GD	529	1681	1689	578
AF	G	0	DP	N	1	GD	530	1689	1697	578
AF	G	0	RC	N	1	GD	531	1700	1704	578
RC	N	1	AF	G	0	GD	532	1704	1711	578
AF	G	0	RC	N	1	GD	533	1711	1718	578
RC	N	1	AF	G	0	GD	534	2032	2039	578
AF	G	0	RC	N	1	GD	535	2039	2046	578
RC	N	0	AF	G	0	GD	536	2364	2371	578
AF	G	0	RC	N	1	GD	537	2371	2378	578
AF	G	0	RC	N	1	GD	538	2698	2702	578
RC	N	1	AF	G	0	GD	539	2702	2715	578
AF	G	0	RC	N	1	GD	540	2715	2728	578
RC	N	1	AF	G	0	GD	541	2728	2729	578
AF	G	0	RC	N	3	GD	542	2734	2738	578
RC	N	2	AF	G	0	GD	543	2738	2741	578
AF	G	0	RC	N	2	GD	544	2741	2742	578
AF	G	0	RC	N	3	GD	545	4378	4382	578
RC	N	3	AF	G	0	GD	546	4382	4385	578

Table IV-6. ALPHA File, General Aviation Arrivals

195.824

AF	G	0	RC	N	3	GA	601	0	4	578
RC	N	3	AF	G	0	GA	602	4	7	578
AF	G	0	RC	N	2	GA	603	840	843	578
RC	N	2	AF	G	0	GA	604	843	844	578
AF	G	0	RC	N	2	GA	605	844	848	578
RC	N	2	AF	G	0	GA	606	848	861	578
AF	G	0	RC	N	2	GA	607	861	863	578
AF	G	0	RC	N	2	GA	608	1680	1684	578
RC	N	2	AF	G	0	GA	609	1684	1697	578
AF	G	0	RC	N	2	GA	610	1697	1705	578
AF	G	0	RC	N	1	GA	611	2016	2019	578
RC	N	1	AF	G	0	CA	612	2019	2032	578
AF	G	0	RC	N	1	GA	613	2032	2040	578
AF	G	0	RC	N	1	GA	614	2352	2355	578
RC	N	1	AF	G	0	GA	615	2355	2358	578
AF	G	0	RC	N	1	GA	616	2358	2361	578
AF	G	0	AP	N	1	GA	617	2688	2692	578
AP	N	1	AF	G	0	GA	618	2692	2695	578
AF	G	0	AP	N	1	GA	619	2695	2698	578
AF	G	0	AP	N	1	GA	620	3024	3027	578
AP	N	1	AF	G	0	GA	621	3027	3030	578
AF	G	0	AP	N	1	GA	622	3030	3033	578
AF	G	0	TW	G	0	GA	623	3360	3366	578
TW	G	0	AF	G	0	GA	624	3366	3376	578
AF	G	0	TW	G	0	GA	625	3945	3948	578
TW	G	0	AF	G	0	GA	626	3948	3951	578
TW	G	0	AF	G	0	GA	627	3960	3967	578
AF	G	0	GC	G	0	GA	628	3977	3981	578
GC	G	0	AF	G	0	GA	629	3981	3986	578
AF	G	0	GC	G	0	GA	630	3986	3988	578

Table IV-7. ALPHA File, Enroute Traffic

225,232

AF	C	0	RC	N	3	EC	701	0	3	55
RC	N	3	AF	C	0	EC	702	3	5	55
AF	C	0	RC	N	3	EC	703	5	9	55
RC	N	3	AF	C	0	EC	704	9	10	55
AF	C	0	RC	N	2	AC	705	1080	1083	55
RC	N	2	AF	C	0	EC	706	1083	1085	55
AF	C	0	RC	N	2	EC	707	1085	1089	55
RC	N	2	AF	C	0	EC	708	1089	1090	55

233,240

AF	M	0	RC	N	2	EM	801	0	3	55
RC	N	2	AF	M	0	EM	802	3	5	55
AF	M	0	RC	N	2	EM	803	5	9	55
RC	N	2	AF	M	0	EM	804	9	10	55
AF	M	0	RC	N	3	EM	805	1080	1083	55
RC	N	3	AF	M	0	EM	806	1083	1085	55
AF	M	0	RC	N	3	EM	807	1085	1089	55
RC	N	3	AF	M	0	EM	808	1089	1090	55

241,253

AF	G	0	RC	N	3	EG	901	0	3	360
RC	N	3	AF	G	0	EG	902	3	5	360
AF	G	0	RC	N	3	EG	903	5	9	360
RC	N	3	AF	G	0	EG	904	9	10	360
AF	G	0	RC	N	1	EG	905	1475	1478	360
RC	N	1	AF	G	0	EG	906	1478	1480	360
AF	G	0	RC	N	1	EG	907	1480	1484	360
RC	N	1	AF	G	0	EG	908	1484	1485	360
AF	G	0	RC	N	2	EG	909	2940	2943	360
RC	N	2	AF	G	0	EG	910	2943	2945	360
AF	G	0	RC	N	2	EG	911	2945	2949	360
RC	N	2	AF	G	0	EG	912	2949	2950	360
00	0	0	00	0	0	00	1000	0000	0000	0000

APPENDIX V

REVISED BRAVO PROGRAM[*]

```
100    A$="4%2B5%2B5%2B5%2B4%/"
220    J=1
230    Q=1
240    W=0
300    D1="00000"
310    D2="00000"
320    D3="00000"
408    TEXT A(253,1):41
410    OPEN/CHARLY3/ ,OUTPUT,3
420    OPEN/ALPHA/,INPUT,2
430    FOR I=1 TO 253
440    INPUT FROM 2:A(I,1)
442    D4=VAL(SUBSTR(A(I,1),20,2))
444    X=D4-Q
446    IF X=0 THEN 510 ELSE 448
448    IF W=0 THEN 450 ELSE 490
450    D5=Q*100
452    D6=D5+99
454    WRITE ON 3 IN FORM A$:J,D1,D2,D3,D5
455    WRITE        IN FORM A$:J,D1,D2,D3,D5
456    J=J+1
458    WRITE ON 3 IN FORM A$:J,D1,D2,D3,D6
459    WRITE        IN FORM A$:J,D1,D2,D3,D6
460    J=J+1
461    IF D4=10    THEN 462 ELSE 500
462    D7=D4*100
470    WRITE ON 3 IN FORM A$:J,D1,D2,D3,D7
471    WRITE        IN FORM A$:J,D1,D2,D3,D7
480    GO TO 860
490    W=0
500    Q=Q+1
510    T1=LEFT(A(I,1),2)
520    T2=SUBSTR(A(I,1),4,1)
530    T3=SUBSTR(A(I,1),6,1)
540    R1=SUBSTR(A(I,1),9,2)
550    R2=SUBSTR(A(I,1),12,1)
560    R3=SUBSTR(A(I,1),14,1)
570    P=SUBSTR(A(I,1),17,2)
580    F=SUBSTR(A(I,1),25,5)
590    G=SUBSTR(A(I,1),31,5)
594    S=RIGHT(A(I,1),5)
598    Z=SUBSTR(A(I,1),20,4)
610    IF T1="CD" OR T1="GC" OR T1="AF" THEN 640 ELSE 850
640    IF R1="CD" OR R1="GC" OR R1="AF" THEN 800 ELSE 850
800    WRITE ON 3 IN FORM A$: J,F,G,S,Z
801    WRITE        IN FORM A$: J,F,G,S,Z
820    W=1                                    850   NEXT I
840    J=J+1                                  860   CLOSE 2,3
                                              890   WRITE:"END"
                                              900   END
```

---

[*] See note to Section 8.8.2.5 for explanation and Appendix XVI for a flow diagram.

APPENDIX VI

FLOW DIAGRAM OF REVISED BRAVO PROGRAM
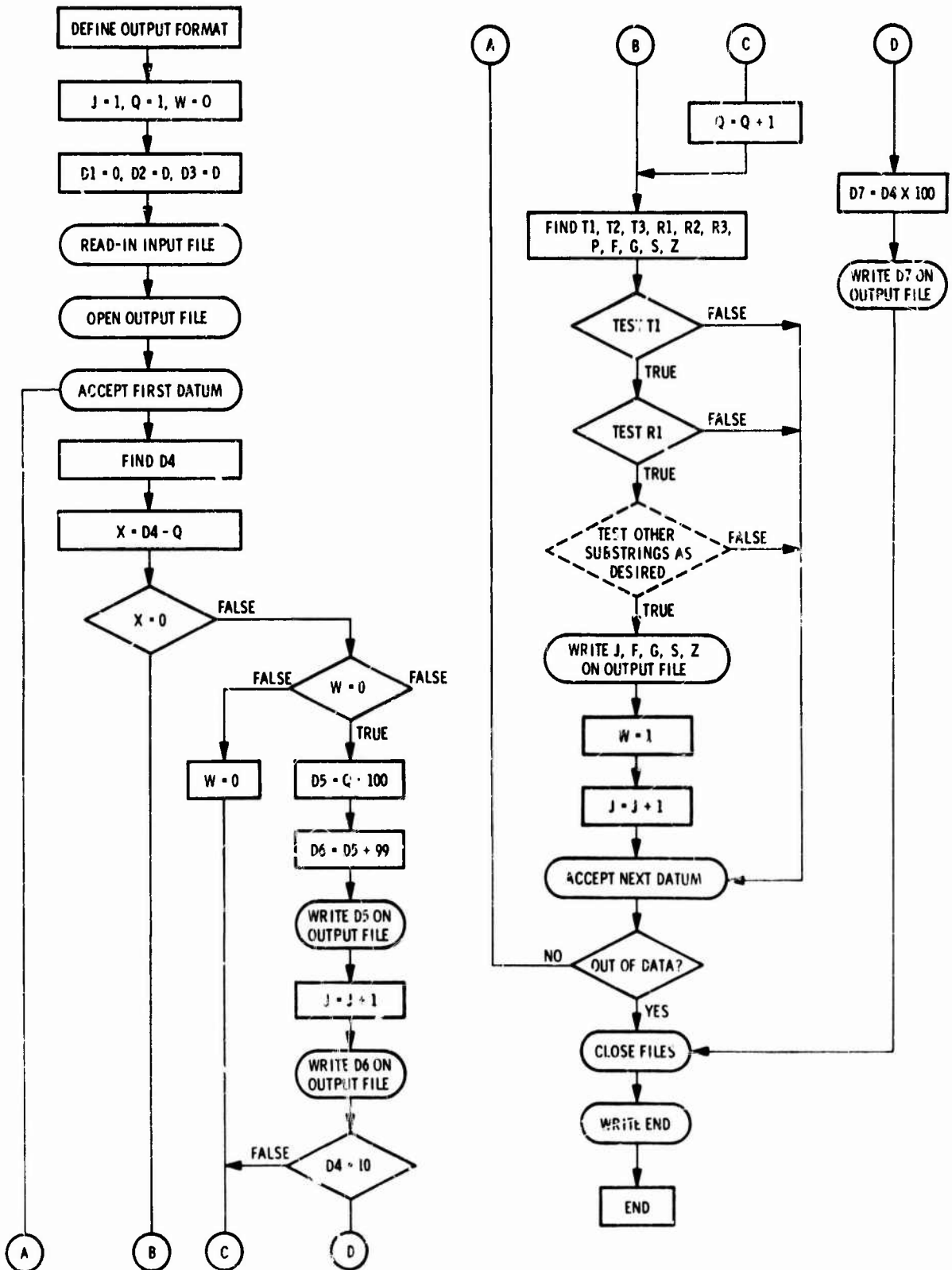
APPENDIX VII.   CHARLIE File

1,53

1	60	63	90	104
2	63	90	90	105
3	90	94	90	106
4	94	95	90	107
5	600	603	90	117
6	603	607	90	118
7	607	608	90	119
8	630	638	90	120
9	638	639	90	121
10	675	681	90	122
11	681	683	90	123
12	687	702	90	124
13	702	704	90	125
14	705	712	90	126
15	712	714	90	127
16	714	717	90	128
17	843	856	90	129
18	856	869	90	130
19	1023	1027	90	131
20	1027	1040	90	132
21	1203	1211	90	133
22	1211	1219	90	134
23	1323	1329	90	135
24	1329	1331	90	136
25	1331	1334	90	137
26	1335	1342	90	138
27	1342	1349	90	139
28	1350	1353	90	140
29	1353	1354	90	141
30	1530	1533	90	142
31	1533	1534	90	143
32	1710	1713	90	144
33	1713	1714	90	145
34	2250	2255	90	146
35	2255	2260	90	147
36	2490	2499	90	148
37	2499	2500	90	149
38	0	9	90	201
39	9	24	90	202
40	24	39	90	203
41	148	151	90	204
42	151	152	90	205
43	257	260	90	206
44	260	275	90	207
45	275	305	90	208
46	366	369	90	209
47	369	378	90	210
48	378	387	90	211
49	474	483	90	212
50	483	493	90	213
51	493	503	90	214
52	710	719	90	215
53	719	729	90	216

53,106

53	719	729	90	216
54	729	739	90	217
55	917	921	90	218
56	921	924	90	219
57	1134	1140	90	220
58	1140	1150	90	221
59	1150	1151	90	222
60	1382	1388	90	223
61	1388	1391	90	224
62	3005	1627	90	225
63	1627	1634	90	226
64	1644	1651	90	227
65	600	603	560	313
66	603	607	560	314
67	607	608	560	315
68	630	638	560	316
69	638	639	560	317
70	675	681	560	318
71	681	683	560	319
72	705	712	560	320
73	712	714	560	321
74	714	717	560	322
75	818	825	560	323
76	825	833	560	324
77	998	1002	560	325
78	1002	1015	560	326
79	1015	1020	560	327
80	1178	1191	560	328
81	1191	1199	560	329
82	1199	1207	560	330
83	1358	1361	560	331
84	1361	1362	560	332
85	1808	1814	560	333
86	1814	1816	560	334
87	1816	1819	560	335
88	2023	2036	560	336
89	2036	2044	560	337
90	2258	2265	560	338
91	2265	2268	560	339
92	0	9	560	401
93	9	24	560	402
94	24	39	560	403
95	552	561	560	404
96	561	576	560	405
97	576	591	560	406
98	816	825	560	407
99	825	840	560	408
100	840	855	560	409
101	1080	1084	560	410
102	1084	1088	560	411
103	1088	1089	560	412
104	1200	1203	560	413
105	1203	1204	560	414
106	1260	1263	560	415

106, 159

106	1260	1263	560	415
107	1263	1264	560	416
108	1320	1323	560	417
109	1323	1326	560	418
110	1440	1443	560	419
111	1443	1449	560	420
112	1449	1450	560	421
113	1451	1454	560	422
114	1454	1457	560	423
115	1457	1453	560	424
116	1550	1553	560	425
117	1553	1554	560	426
118	1584	1590	560	427
119	388	391	578	511
120	391	395	573	512
121	395	396	578	513
122	410	418	578	514
123	418	419	578	515
124	429	435	578	516
125	435	437	578	517
126	437	444	578	518
127	444	447	578	519
128	447	449	578	520
129	598	601	578	521
130	601	602	578	522
131	718	721	578	523
132	721	729	578	524
133	729	737	578	525
134	1198	1201	578	526
135	1201	1202	578	527
136	1678	1681	578	528
137	1681	1689	578	529
138	1689	1697	578	530
139	1700	1704	578	531
140	1704	1711	578	532
141	1711	1718	578	533
142	2032	2039	578	534
143	2039	2046	578	535
144	2364	2371	578	536
145	2371	2378	578	537
146	2698	2702	578	538
147	2702	2715	578	539
148	2715	2728	578	540
149	2728	2729	578	541
150	2734	2738	578	542
151	2738	2741	578	543
152	2741	2742	578	541
153	4378	4382	578	545
154	4382	4385	578	546
155	0	4	578	601
156	4	7	578	602
157	840	843	578	603
158	843	844	578	604
159	844	848	578	605

159, 210

159	844	848	578	605
160	848	861	578	606
161	861	863	578	607
162	1680	1684	578	608
163	1684	1697	578	609
164	1697	1705	578	610
165	2016	2019	578	611
166	2019	2032	578	612
167	2032	2040	578	613
168	2352	2355	578	614
169	2355	2358	578	615
170	2358	2361	578	616
171	2688	2692	578	617
172	2692	2695	578	618
173	2695	2698	578	619
174	3024	3027	578	620
175	3027	3030	578	621
176	3030	3033	578	622
177	3360	3366	578	623
178	3366	3376	578	624
179	3945	3948	578	625
180	3948	3951	578	626
181	3960	3967	578	627
182	0	3	55	701
183	3	5	55	702
184	5	9	55	703
185	9	10	55	704
186	1080	1083	55	705
187	1083	1085	55	706
188	1085	1089	55	707
189	1089	1090	55	708
190	0	3	55	801
191	3	5	55	802
192	5	9	55	803
193	9	10	55	804
194	1080	1083	55	805
195	1083	1085	55	806
196	1085	1089	55	807
197	1089	1090	55	808
198	0	3	360	901
199	3	5	360	902
200	5	9	360	903
201	9	10	360	904
202	1475	1478	360	905
203	1478	1480	360	906
204	1480	1484	360	907
205	1484	1485	360	908
206	2940	2943	360	909
207	2943	2945	360	910
208	2945	2949	360	911
209	2949	2950	360	912
210	0	0	0	1000

APPENDIX VIII

COMPUTER PROGRAM "DELTA"

```
 1.            DIMENSION F(210),G(210),S(210),Z(210)
 2.            OPEN[4,/CHARLIE /,INPUT]
 3.            OPEN[2,/ECHO /,OUTPUT]
 4.            DO 20 J=1,210
 5.            READ(4,800)J,F(J),G(J),S(J),Z(J)
 6.        800 FORMAT(I4,2X,I5,2X,I5,2X,I5,2X,I4)
 7.         20 CONTINUE
 8.            LAC=5
 9.            LAM=9
10.            LAG=9
11.            LVH=4
12.            LVL=5
13.            DO 500 J=1,209
14.            JF=J
15.            NXTJS=J+1
16.            IX=Z(J)/100.
17.        480 IY=Z(J+1)/100.
18.            IF(IX.NE.IY) GO TO (1,2,3,4,5,6,7,8,9)IX
19.            GO TO 500
20.          1 JSDC=1
21.            JFDC=JF
22.            SPAC1 =S(J)
23.            GO TO 490
24.          2 JSAC=JS
25.            JFAC=JF
26.            SPAC1=S(J)
27.            GO TO 490
28.          3 JSDM=JS
29.            JFDM=JF
30.            SPAC2=S(J)
31.            GO TO 490
32.          4 JSAM=JS
33.            JFAM=JF
34.            SPAC2=S(J)
35.            GO TO 490
36.          5 JSDG=JS
37.            JFDG=JF
38.            SPAC3=S(J)
39.            GO TO 490
40.          6 JSAG=JS
41.            JFAG=JF
42.            SPAC3=S(J)
43.            GO TO 490
44.          7 JSEC=JS
45.            JFEC=JF
46.            SPAC4=S(J)
47.            GO TO 490
48.          8 JSEM=JS
```

```
49.             JFEM=JF
50.             SPAC4=S(J)
51.             GO TO 490
52.         9 JSEG=JS
53.             JFEG=JF
54.             SPAC5=S(J)
55.             GO TO 500
56.       490 JS=NXTJS
57.       500 CONTINUE
58.             TW=3600
59.             KE=0
60.             U=0
61.       100 R=0
62.         '   L=0
63.       470 L=L+1
64.             JS=JSDC
65.             JF=JFDC
66.             SPACE=SPAC1
67.             DEL=0
68.             ASSIGN 510 TO LINEX
69.             GO TO 160
70.       510 JS=JSAC
71.             JF=JFAC
72.             SPACE=SPAC1
73.             DEL=(SPACE/2)-1006
74.             ASSIGN 520 TO LINEX
75.             GO TO 190
76.       520 IF(L .NE. LAC) GO TO 470
77.             L=0
78.       515 L=L+1
79.             JS=JSDM
80.             JF=JFDM
81.             SPACE=SPAC2
82.             DEL=0
83.             ASSIGN 530 TO LINEX
84.             GO TO 160
85.       530 JS=JSAM
86.             JF=JFAM
87.             SPACE=SPAC2
88.             DEL=(SPACE/2)-946
89.             ASSIGN 540 TO LINEX
90.             GO TO 190
91.       540 IF(L .NE. LAM) GO TO 5:5
92.             L=0
93.       545 L=L+1
94.             JS=JSDG
95.             JF=JFDG
96.             SPACE=SPAC3
```

```
 97.          DEL=0
 98.          ASSIGN 550 TO LINEX
 99.          GO TO 160
100.     550 JS=JSAG
101.          JF=JFAG
102.          SPACE=SPAC3
103.          DEL=(SPACE/2)-2542
104.          ASSIGN 560 TO LINEX
105.          GO TO 190
106.     560 IF(L .NE. LAG) GO TO 545
107.          L=0
108.     565 L=L+1
109.          JS=JSEC
110.          JF=JFEC
111.          SPACE=SPAC4
112.          DEL=0
113.          ASSIGN 570 TO LINEX
114.          GO TO 170
115.     570 JS=JSEM
116.          JF=JFEM
117.          SPACE=SPAC4
118.          DEL=0
119.          ASSIGN 580 TO LINEX
120.          GO TO 190
121.     580 IF(L .NE. LVH) GO TO 565
122.          L=0
123.     585 L=L+1
124.          JS=JSEG
125.          JF=JFEG
126.          SPACE=SPAC5
127.          DEL=0
128.          ASSIGN 590 TO LINEX
129.          GO TO 170
130.     590 IF(L.GE.LVL) GO TO 300
131.          GO TO 585
132.     160 ISCAL=SPACE/2
133.          GO TO 180
134.     170 ISCAL=SPACE
135.     180 IRAN   00001
136.          KRAN   ORNRT[IRAN]*ISCAL
137.     190 KR=KRAN+DEL
138.          TA=G(JF)
139.          IF(TA .EQ. 0) GO TO LINEX
140.          M=0
141.          N=0
142.     210 IF((KR+N*SPACE).GE.KE) GO TO 220
143.          N=N+1
144.          GO TO 210
```

```
145.        220 NMAX=N
146.        230 IF((KR+N*SPACE+TA).LE.KE) GO TO 240
147.            N=N-1
148.            GO TO 230
149.        240 NMIN=N
150.            N=NMIN
151.        250 TN=KE-KR-N*SPACE
152.            J=JS
153.        260 IF((TN.GE.F(J)).AND.(TN.LT.G(J))) GO TO 280
154.        270 J=J+1
155.            IF(J.LE.JF) GO TO 260
156.            N=N+1
157.            IF(N.LE.NMAX) GO TO 250
158.            GO TO 290
159.        280 M=M+1
160.            GO TO 270
161.        290 R=R+M
162.        295 GO TO LINEX
163.        300 IF(R.EQ.U) GO TO 700
164.            WRITE(1,600) KE,R
165.            WRITE(2,600) KE,R
166.        600 FORMAT(F5.,3X,F5.)
167.        700 U=R
168.            KE=KE+1
169.            IF(KE.LT.TW) GO TO 100
170.            WRITE(1,600) KE,R
171.            CLOSE(4)
172.            CLOSE (2)
173.            DISPLAY "END"
174.            END


175.            FUNCTION UDRNRT[J]
176.            JRAN=J
177.            JRAN=JRAN*2051
178.            JRAN=JRAN-(JRAN/4194304)*4194304
179.            J=JRAN
180.            U-JRAN
181.            Y=U/4194303.0
182.            UDRNRT=Y
183.            RETURN
184.            END
```

APPENDIX IX

ECHO FILE

(Printout of DELTA Program)

T	N	T	N	T	N
0	58	64	33	136	62
2	53	65	28	137	53
3	48	72	19	138	38
4	43	73	24	139	28
5	47	74	39	142	33
9	39	77	48	143	28
10	34	79	53	144	26
11	39	80	40	150	31
13	34	87	35	152	22
14	44	89	48	153	27
15	49	90	53	154	23
17	54	92	48	156	19
18	49	93	52	162	28
19	40	94	47	163	33
22	30	95	56	164	41
24	20	99	48	167	56
28	19	100	43	169	61
29	29	101	48	170	75
30	34	103	34	174	67
34	42	104	44	176	58
36	37	105	49	177	53
37	42	107	54	179	58
39	51	108	49	180	63
40	55	109	57	182	58
43	50	112	47	183	53
44	58	114	37	184	48
45	53	117	46	190	43
46	44	118	36	191	48
48	38	119	38	193	43
49	33	124	29	194	53
51	24	126	15	195	58
53	19	127	20	197	63
54	17	129	29	198	58
55	22	130	38	199	66
59	31	133	33	201	57
60	36	134	58	202	47
63	41	135	53	204	37

T = Seconds past simulation start time.

N = Number of simultaneous voice transmissions.

-714-

DOCUMENT CONTROL DATA - R & D

(Security classification of title, body of abstract and indexing annotation must be entered when the overall report is classified)

1. ORIGINATING ACTIVITY (Corporate author)	2a. REPORT SECURITY CLASSIFICATION
Magnavox Research Laboratories 2829 Maricopa Street Torrence, California 90503	UNCLASSIFIED
	2b. GROUP N/A

3. REPORT TITLE

INTEGRATED FUNCTION (CNI) WAVEFORM STUDY
Volume II

4. DESCRIPTIVE NOTES (Type of report and inclusive dates)
Final Report

5. AUTHOR(S) (First name, middle initial, last name)
Charles R. Cahn
Stanley E. Kosowski

6. REPORT DATE	7a. TOTAL NO. OF PAGES	7b. NO. OF REFS
January 1970	502	43

8a. CONTRACT OR GRANT NO. F30602-69-C-0186	9a. ORIGINATOR'S REPORT NUMBER(S)
b. PROJECT NO 4519	MRL Report R-1959
c. Task 451911	9b. OTHER REPORT NO(S) (Any other numbers that may be assigned this report) RADC-TR-69-424, Volume II (of 3)
d.	

10. DISTRIBUTION STATEMENT

This document is subject to special export controls and each transmittal to foreign governments or foreign nationals may be made only with prior approval of RADC (EMCRC), Griffiss AFB, NY 13440.

11. SUPPLEMENTARY NOTES	12. SPONSORING MILITARY ACTIVITY
	Rome Air Development Center (EMCRC) Griffiss Air Force Base, New York 13440

13. ABSTRACT

This Final Report, presented in three volumes, describes a comparison of candidate spread spectrum waveforms and the selection of a preferred waveform to perform integrated communication, navigation, and identification (CNI) functions. Satellites are presumed available in appropriate orbits for global communication and navigation. A coordinated frequency hop/pseudonoise/time hop (FH/PN/TH) waveform is made considering such factors as efficient use of satellite ERP in the remote mode, multiple access of wide dynamic range signals in the direct mode, range and range rate measurement accuracy, initial synchronization, and equipment complexity for full capacity implementation in a nominal 100 MHz bandwidth. Since CNI system requirements are not presently known, the waveform choice has been made considering a postulated worst case environment based on future air traffic control requirements. Implementation of the preferred CNI waveform will depend on certain technology developments particularly in the areas of wide dynamic range receivers, phase coherent frequency hopping, high peak power pulse transmitters, and LSI digital devices. However, a demonstration concept can be advanced within the present state-of-the-art to illustrate the preferred waveform with scaled parameters. Volume I covers the concept formulation studies leading to the preferred waveform and demonstration concept while Volume II summarizes the detailed performance and operational analysis. Volume III presents navigation considerations for the enroute case.

14. KEY WORDS	LINK A		LINK B		LINK C	
	ROLE	WT	ROLE	WT	ROLE	WT
Waveform study						
Satellite communications						
CNI						
Navigation performance analysis						